



**London  
South Bank  
University**

# Determining Safety Parameters for Small Scale Passive Hydrogen Venting Schemes [Fuel Cell and Nuclear Enclosures]

**Tara Singh Ghatauray**

<https://orcid.org/0000-0003-1863-4039>

A thesis submitted in partial fulfilment of the requirements at  
London South Bank University  
For the award of the degree of Doctor of Philosophy in  
Chemical, Process and Energy Engineering

A jointly funded research project supported by  
Sellafield Ltd. and London South Bank University and in collaboration with BOC  
Ltd.

© Copyright Tara Singh Ghatauray, London South Bank University  
and Sellafield Ltd. All rights reserved.

April 2019

## Acknowledgements

I would like to thank my supervisors at London South Bank University (LSBU), Dr James Ingram and Dr Paul Holborn for their support with this research project. I would further like to thank Dr Martin Fairclough and his colleagues at Sellafield Ltd. for their co-sponsorship of this project and the provision of support funds. I am similarly grateful to LSBU for sponsoring this project.

I would like to acknowledge BOC Ltd. (Linde Group), for creating the opportunity to investigate passive hydrogen venting in fuel cell enclosures. BOC Ltd. provided the funding for training in SolidWorks Flow Simulation CFD along with access to the software at their Guildford HQ. My thanks go to Stewart Dow, Head of UK Fuel Cell Marketing for making this possible.

I would also like to praise the technical talents of Steven Jones and Chris Merridan for assistance with rig development and the mechanical engineering workshop technicians for their technical advice and support. I also thank Professor David Mba (Dean of the School of Engineering) for agreeing match funding which helped to resolve difficulties that could have stalled progress.

The assistance of these people has allowed me to consolidate years of investigative research and personal and professional development and pave the way to the successful conclusion of this project.



## **Academic Declaration**

I declare that this Ph. D thesis has been written by myself with the professional support of my supervision team. It is submitted for examination for the award of the higher degree of Doctor of Philosophy in Chemical, Process and Energy Engineering. This thesis is the outcome of my personal efforts and has not been submitted for any other degree or professional qualification. Great care has been taken to ensure that this work is original and does not breach the intellectual property rights of any other party. All sources of supporting literature are cited and fully referenced.

## **Contribution to Knowledge**

The efficient use and management of hydrogen are important safety engineering priorities in the nuclear and fuel cell industries. In both fields the safe dispersion of leaked hydrogen through passive ventilation is a prime objective. Hydrogen fuel cells are a major element in the structure of a hydrogen economy. Low power fuel cells housed in protective enclosures will become widely used, but hydrogen has the potential to leak from the system into the enclosure. In nuclear waste storage installations, hydrogen leaks from stacked storage boxes into confined areas between. Hydrogen leaks in both scenarios can lead to flammable mixtures forming in the confined space, with passive hydrogen venting the preferred means for managing concentrations. However datasets for a range of passive ventilation scenarios at this scale have not been available to design engineers. This thesis adds knowledge by presenting new empirical and numerical (CFD) datasets and analysis.

## **Dedication**

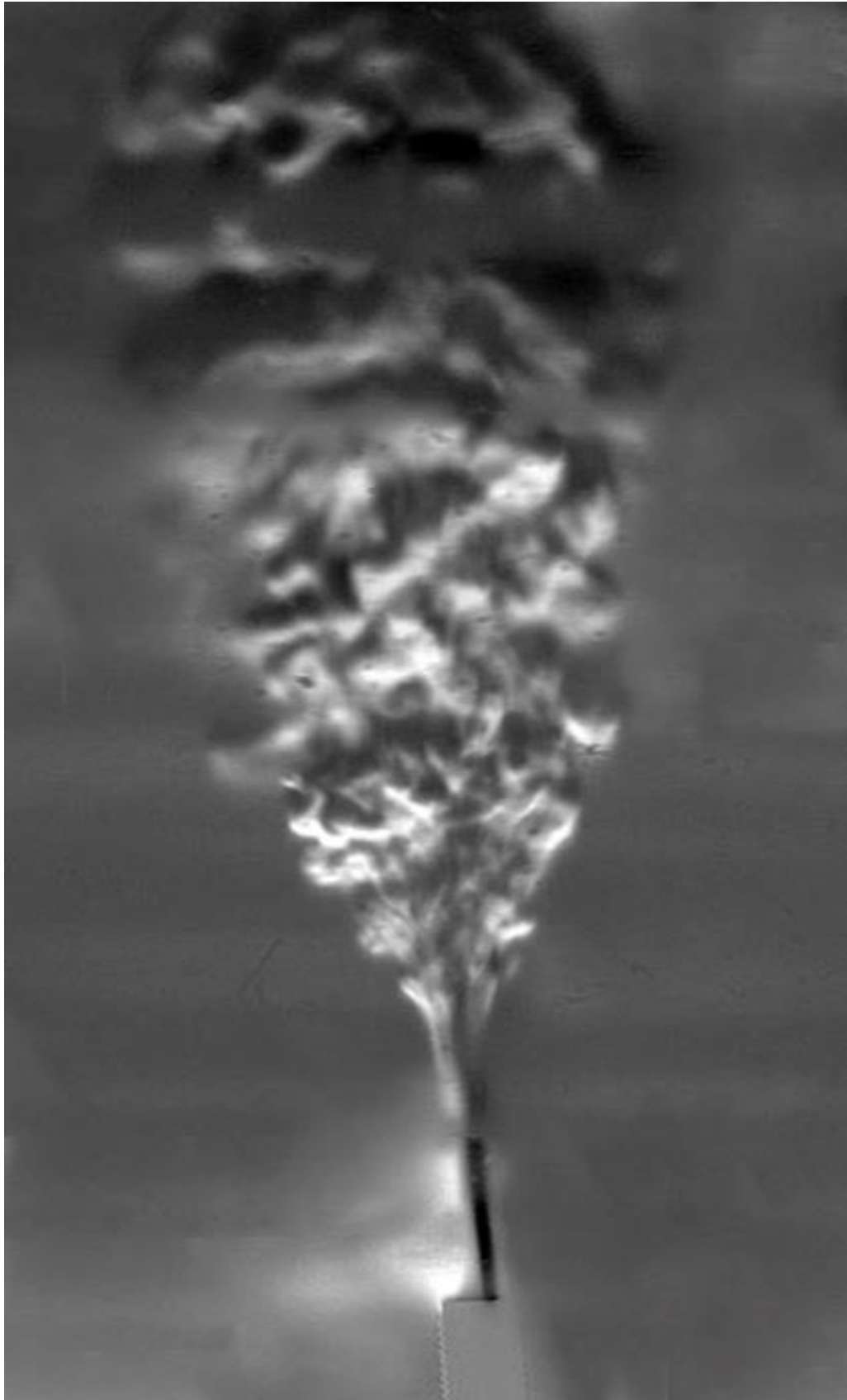
I would like to dedicate this work to my family,  
my wife Sally for supporting this endeavour and  
my children Truly, Rory and Jack who inspire  
me to strive for success.

## Abstract

**Introduction:** A hydrogen economy is proposed to mitigate the effects of climate change, using hydrogen fuel cells (housed in enclosures for protection) to generate heat and energy. There is the potential though for hydrogen leaks to develop in the enclosure. Nuclear waste stored in stacked boxes produces hydrogen as a by-product of water decomposition (through corrosion and radiolysis). Hydrogen is a buoyant gas with a flammable range of 4 to 75 % in air. In both cases, leaked hydrogen can build up in confined spaces, with fuel cells the protective enclosure and with nuclear waste boxes in the spaces between the stacked boxes. To prevent flammable mixtures forming, ventilation schemes are used to disperse the hydrogen. Fail-safe passive ventilation schemes are preferred to mechanical systems that are vulnerable to power outages.

**Thesis:** This thesis supports the development of small fuel cell systems by investigating buoyant gas removal from a small enclosure. The thesis hypothesis is that; *'Safe, passive ventilation parameters can be determined that will manage hydrogen concentrations below the lower flammable limit, for hydrogen leak rates at or below 10 litres per minute in a passively ventilated 0.144m<sup>3</sup> hydrogen fuel cell enclosure'*. [A 0.144 m<sup>3</sup> enclosure houses the BOC Ltd. Hymera small fuel cell environmental unit]. To obtain new data sets the thesis hypothesis, passive ventilation experimental tests using displacement or mixing regimes were undertaken. The tests studied the effects of plain, louvre, chimney and flue ventilation openings applied to the enclosure test rig. Helium was used as a safe analogue for hydrogen in the tests.

**Findings:** The displacement passive ventilation regimes were more effective than the mixing regimes and managed helium concentrations at or below 4 %, but at a leak rate limit of 4 lpm. Louvre vents applied to the enclosure increased flow resistance compared to plain vents increasing enclosure concentrations. Tall chimneys enhanced flow through the enclosure, reducing concentrations compared to shorter chimneys. Horizontal flues can be useful for transporting gas away from the enclosure [through a building wall]. The experimental data was used to validate a series of SolidWorks Flow Simulation CFD models with a good correlation found between the experimental and CFD data sets, supporting its use in enclosure design. The thesis response is that this thesis presents a range of new experimental datasets for passive ventilation in a 0.144 m<sup>3</sup> fuel cell enclosure, setting out hydrogen LFL safety limits. In some scenarios, the LFL is breached at a very low leak rate, demonstrating the importance of this safety investigation, as minor leaks can lead to devastating consequences.



**Schlieren image of helium gas leaving a nozzle in the 0.144 m<sup>3</sup> enclosure (Section 4.11)**

## Contents

<b>Acknowledgements</b> .....	<b>ii</b>
<b>Academic Declaration</b> .....	<b>iii</b>
<b>Contribution to Knowledge</b> .....	<b>iii</b>
<b>Dedication</b> .....	<b>iii</b>
<b>Abstract</b> .....	<b>iv</b>
<b>List of abbreviations and symbols: Nomenclature</b> .....	<b>x</b>
<b>List of Figures</b> .....	<b>xi</b>
<b>Chapter 1: Introduction</b> .....	<b>1</b>
<b>1.0 Motivation for this research</b> .....	<b>1</b>
<b>1.1 The energy trilemma</b> .....	<b>2</b>
<b>1.2 Managing the energy baseload</b> .....	<b>3</b>
<b>1.3 The Hydrogen Economy – the energy solution</b> .....	<b>5</b>
<b>1.4 Hydrogen fuel cells</b> .....	<b>6</b>
<b>1.5 Hydrogen Safety</b> .....	<b>8</b>
<b>1.6 Small hydrogen fuel cell enclosures</b> .....	<b>10</b>
<b>1.7 Passive ventilation of enclosures</b> .....	<b>11</b>
<b>1.8 Computational Fluid Dynamics (CFD) modelling</b> .....	<b>12</b>
<b>1.9 Economic and social benefits of this research</b> .....	<b>12</b>
<b>1.10 Research hypothesis</b> .....	<b>14</b>
<b>1.11 Research aims and objectives</b> .....	<b>14</b>
<b>1.12 Thesis structure</b> .....	<b>15</b>
<b>1.13 Conclusion</b> .....	<b>17</b>
<b>Chapter 2 Literature Review</b> .....	<b>18</b>
<b>2.0 Introduction</b> .....	<b>18</b>
<b>2.1 Hydrogen</b> .....	<b>20</b>
<b>2.1.1 Hydrogen economy generated research</b> .....	<b>20</b>
<b>2.1.2 Hydrogen fuel cell deployment</b> .....	<b>26</b>
<b>2.1.3 Hydrogen safety</b> .....	<b>27</b>
<b>2.2 Enclosures: Enclosure hydrogen confinement ventilation research</b> .....	<b>33</b>
<b>2.2.1 Large scale enclosures (garage scale and above)</b> .....	<b>37</b>
<b>2.2.2 Small scale enclosure (sub kW fuel cell installations)</b> .....	<b>47</b>
<b>2.3 Natural and passive ventilation in enclosures</b> .....	<b>53</b>
<b>2.4 Ventilation openings</b> .....	<b>59</b>
<b>2.5 Flow impact factors and dimensionless parameters</b> .....	<b>61</b>
<b>2.6 Data Collection</b> .....	<b>68</b>

2.6.1 Experimental Rig design .....	68
2.6.2 Computational Fluid Dynamics (CFD) Modelling.....	69
2.6.3 CFD Modelling approach .....	74
2.7 Knowledge gaps.....	77
Chapter 3 Methodology .....	79
3.0 Introduction.....	79
3.1 Experimental set-up background .....	80
3.2 Passive hydrogen venting scoping exercise .....	81
3.3 Initial laboratory test rig.....	85
3.3.1 Helium gas delivery .....	85
3.3.2 Brooks GF125 Digital Thermal Mass Flow Controller .....	85
3.3.3 Xensor – XEN-TCG3880 MEMS Thermal Conductivity Helium Sensors .....	87
3.4 Initial laboratory test rig experiments .....	90
3.5 Final experimental test rig. ....	92
3.5.1 Plywood helium permeation test .....	93
3.5.2 Sensors:.....	98
3.6 Ventilation configurations.....	99
3.6.1 Plain vents .....	100
3.6.2 Simple louvre vents.....	101
3.6.3 Pressed aluminium louvre vents.....	101
3.6.4 Chimney vents.....	101
3.6.5 Chimney vents with obstruction.....	102
3.6.6 Flues.....	102
3.6.7 Snorkel vent .....	102
3.7 Schlieren System – Visualising helium flow in the enclosure .....	102
3.8 Environmental parameters .....	104
3.9 Computational Fluid Dynamics (CFD): Methodology .....	104
3.9.1 Governing equations .....	104
3.9.2 Mesh.....	106
3.9.3 Mesh sensitivity.....	106
3.9.4 The CFD Process .....	109
3.9.5 SolidWorks Flow Simulation (2017): CFD.....	111
3.9.6 ANSYS: Fluent (19.2): CFD .....	116
3.10 Statistical Performance Indicators .....	120
3.11 Conclusion .....	122
Chapter 4 Results and Analysis: Experimental tests .....	123
4.0 Introduction.....	123

4.1 BOC Ltd. scoping exercise (hydrogen tests) .....	123
4.1.1 Analysis.....	125
4.2 Initial test rig: High-level ventilation openings .....	128
4.2.1 Analysis.....	131
4.3 Developed Test Rig: Plain ventilation openings – Control test .....	133
4.3.1 Analysis: Plain Vents-Frame sensors.....	135
4.3.2 Plain Vents-Stacked sensors .....	135
4.4 Paper louvres (same opening area as plain vents section 4.3) .....	136
4.4.1 Analysis: Louvre Vents-Frame sensors .....	138
4.4.2 Louvre Vent-Stacked sensors .....	138
4.4.3 Helium sensor deployment.....	140
4.5 Plain vent tests [same opening area as aluminium louvres section 4.6] .....	140
4.5.1 Analysis.....	141
4.6 Aluminium louvre vents [1-12 louvres].....	145
4.6.1 Analysis.....	145
4.6.2 High level louvre vents only .....	149
4.7 Chimney ventilation [Roof mounted various heights] .....	151
4.7.1 Analysis.....	153
4.7.2 Effect of a tall chimney.....	158
4.8 Chimney test with internal obstruction [Simulated fuel cell].....	159
4.9 Flue ventilation [Tubular side vent] .....	161
4.9.1 Analysis.....	162
4.10 Snorkel ventilation [Inverted tubular side flue] .....	165
4.10.1 Analysis.....	166
4.11 Schlieren imaging: Helium release in the enclosure .....	167
4.11.1 Analysis.....	169
4.12 Conclusion .....	172
Chapter 5 Results and Analysis: CFD simulations.....	173
5.0 Introduction.....	173
5.1 Initial test rig (four sensor positions) .....	175
5.2 Final test rig (eight sensors) simple plain vents (BOC Ltd enclosure) .....	178
5.2.1 Plain Vents-Frame sensors .....	179
5.2.2 Plain Vents-Stacked sensors .....	180
5.3 Simple louvre tests – horizontal louvre extensions.....	182
5.3.1 Louvre Vents-Frame sensors .....	183
5.3.2 Louvre vents-stacked sensors .....	184
5.4 Plain vents (equivalent opening area to aluminium vents).....	186



5.4.1 Analysis: 3400 mm <sup>2</sup> opening area .....	187
5.4.2 Analysis 10200 mm <sup>2</sup> opening area [388,916 cells in mesh] .....	189
5.5 Aluminium louvre vents [4 and 12 louvres] .....	191
5.5.1 Analysis 4 louvres .....	192
5.5.2 Analysis 12 louvres .....	195
5.6 Chimney ventilation [Roof mounted various heights] .....	197
5.6.1 Analysis 420 mm chimney .....	198
5.6.2 Analysis 840 mm chimney .....	201
5.6.3 Analysis 1680 mm chimney .....	202
5.7 Flue ventilation [Tubular side vent / T Flue / Snorkel Flue] .....	205
5.7.1 Analysis standard enclosure with 110 mm straight flue no inlet .....	206
5.7.2 Analysis: enclosure with 110 mm straight flue and 3200/6400/9600 mm <sup>2</sup> inlet .....	207
5.7.3 Analysis standard enclosure 330 mm straight flue and 9600/6400 mm <sup>2</sup> inlet .....	208
5.7.4 Analysis: Standard enclosure 'T' flue with 3200 mm <sup>2</sup> inlet .....	210
5.7.5 Analysis: Standard enclosure with snorkel vent [Inverted tubular side flue] .....	212
5.8 Internal obstruction [Simulated fuel cell] .....	214
5.8.1 Analysis: Internal obstruction .....	214
5.9 ANSYS: Fluent comparison study .....	216
5.10 Conclusion .....	221
Chapter 6 Discussion .....	222
6.0 Introduction .....	222
6.1 Small enclosure test performance .....	224
6.2 Passive ventilation performance .....	229
6.3 Safety guidance .....	233
6.4 Factors affecting enclosure performance .....	236
6.5 CFD and empirical data analytical comparison .....	238
6.6 Experimental Error .....	243
6.7 Computational fluid dynamics comment .....	244
6.8 Small enclosure design safety .....	252
6.9 Conclusion .....	254
Chapter 7 Conclusion .....	255
7.0 Introduction .....	255
7.1 Overview .....	255
7.2 Conclusion .....	256
Chapter 8 Recommendations for Future Work .....	257
8.0 Introduction .....	257
8.1 Ideas for further research .....	257

8.2 Conclusion .....	258
References .....	259
Appendix A: Posters and Publications [Front page only].....	267
Appendix B: Helium Sensor Manufacturers Calibration Data.....	279
Appendix C: Schlieren image thumbnails (unprocessed) .....	280
Appendix D Aluminium vent data .....	281
Appendix E CFD Configuration Comparison Table.....	282

### List of abbreviations and symbols: Nomenclature

Symbol or Abbreviation	Meaning	Symbol or Abbreviation	Meaning	Symbol or Abbreviation	Meaning
%	Percentage	IPG	Installation permitting guidance	PPM	Parts Per Million
% (v/v)	Percentage volume for volume	J	Joule	PV	Passive ventilation
A	Enclosure surface area	k-ε	kappa epsilon (kinetic energy dissipation)	Q	Volume flow rate
ATEX	Appareils destines a etre utilises en ATmospheres Explosibles: EC directive on explosive atmospheres	kg/h	kilogram per hour	Q <sub>v</sub>	Heat per unit volume
BS	British Standard	kPa	Kilopascal	R	Universal gas constant
C <sub>d</sub>	Discharge coefficient	l/h	litre per hour	RAC	Royal Automobile Club
CE	Conformite Europeene	L/min	Litre per minute	RNG	Renormalisation Group
CEA	Alternative energies and atomic energy commission (France)	LFL	Lower Flammable Limit	s	Second
CFD	Computational Fluid Dynamics	lpm	Litre per minute	slpm	Standard litre per minute
CHP	Combined Heat and Power	LSBU	London South Bank University	Solar PV	Solar photo voltaic
CO <sub>2</sub>	Carbon Dioxide	m	Metre	SO <sub>x</sub>	Sulphur Oxides
CPP	Clean Power Plan	m <sup>3</sup>	Cubic metre	SST	Shear Stress Transport
CVE	Chamber view explosion	MEA	Membrane Electrode Assembly	STP	Standard temperature and pressure
D <sub>e</sub>	Diffusion coefficient	MEMS	Micro electro mechanical systems	T	Enclosure temperature
D <sub>e</sub>	nozzle diameter	MFC	Mass Flow Controller	T	Temperature Degrees Celsius
E	Energy per unit mass of fluid	mm	Millimetre	TCG	Thermal conductivity guage
e <sup>-</sup>	Electron	mol	Mole	toe	tonnes of oil equivalent
EIA	Energy Information Agency (US)	NDA	Nuclear decommissioning Authority	u, v, w	velocity
EJ	Exajoules	N <sub>f</sub>	Helium molar flow rate	UFL	Upper Flammable Limit
g	Gravitational acceleration	NL/min	Normal litre per minute	UNIPI	Universita di Pisa
Gt	Gigaton	nlpm	Normal litre per minute	USB	Universal serial bus
h	Hour	NO <sub>x</sub>	Nitrogen Oxides	v	Volume
H <sub>2</sub>	Hydrogen	O <sub>2</sub>	Oxygen	w	Watt
H <sub>2</sub> O	Water	P	Enclosure presue	y <sub>ss</sub>	Enclosure mole (He) fraction at steady state
He	Helium	p	Pressure	δ	Thickness of plywood panel
HFC	Hydrogen Fuel Cell	Pa	Pascal	μ	Coefficient of dynamic viscosity
H <sub>r</sub>	Humidity (Relative)	PEM	Proton Exchange Membrane	ρ	Fluid density
HSE	Health and Safety Executive	PIRT	Phenomena Identification and Ranking Table		
HSL	Health and Safety Laboratory	PIV	Particle image velocimetry		

## List of Figures

	<b>Figure</b>	<b>Page</b>
<i>Chapter One</i>		
Figure 1.1 The ‘Energy Trilemma		2
Figure 1.2 World energy consumption by energy source, 1991-2040 (© EIA 2016)		2
Figure 1.3 Renewable energy use 1960 to 2015 [thousand toe] (© OECD 2016)		3
Figure 1.4 Net base load electricity generation (© California ISO-2012)		4
Figure 1.5 Hydrogen economy schematic		6
Figure 1.6 Hydrogen (PEM) Fuel Cell Schematic		7
Figure 1.7 The Hindenburg explodes on landing in New Jersey 1937 (airships.net)		8
Figure 1.8 Fuel Cell Enclosures (Barilo. N 2013)		10
<i>Chapter Two</i>		
Figure 2.1 Literature review roadmap		19
Figure 2.2 HFCs MW shipped (a) by application (b) by region (E4tech, 2017)		26
Figure 2.3 Cumulative number of fuel cell micro-CHP systems (Dodds 2014)		26
Figure 2.4 CEA GAMELAN facility and schematic (Bernard-Michel et al. (2016))		30
Figure 2.5 Richardson numbers (Bernard-Michel et al (2016))		31
Figure 2.6 Comparison of Helium and hydrogen concentrations – 2m <sup>3</sup> single vent enclosure (Bernard-Michel et al (2016))		31
Figure 2.7 presents the helium velocity for a given leak rate at the nozzle		32
Figure 2.8 Iranian Badgir ‘wind catcher’/schematic (flickr.com-2016)		33
Figure 2.9 (a) Comparison of CFD and helium test concentrations, (b) Comparison of CFD results for helium and hydrogen, (Barley and Gawlik 2009)		39
Figure 2.10 Pre-test and post-test photos of damage to the vehicle caused by an internal hydrogen–air deflagration (Merilo et al 2011).		43
Figure 2.11 Enclosure schematic showing dimensions and sensor positions (Cariteau 2011)		44
Figure 2.12 Large scale test rig at HSL (Hedley 2014)		45
Figure 2.13 CEA GAMELAN facility schematic (Deri et al 2010)		48
Figure 2.14 Experimental set-up (Cariteau et al 2012)		49
Figure 2.15 Synthetic Schlieren images 5mm nozzle at 5 NLPM (Cariteau 2012)		50
Figure 2.16 GAMELAN Set-Up showing vent position (Cariteau 2013)		50
Figure 2.17 Steady state vertical distribution of the volume fraction (Cariteau 2013)		51
Figure 2.18 Enclosure with single vent, showing two-way flow about the neutral plane.		54
Figure 2.19 Enclosure with single vent and with a buoyant gas mixture in the enclosure, showing two-way flow about the ‘lower’ neutral plane.		54
Figure 2.20 Engineering nomogram for graphical calculation of hydrogen leak mass flow rate in an enclosure with one vent, which leads to 100% of hydrogen concentration, by the vent height and width.		56

Figure 2.21 hydrogen volume fraction in enclosure as a function of neutral plane height fraction (Molkov 2014)	58
Figure 2.22 Enclosure geometry – Chimney and obstructions (Friedrich 2011) IKET	61
Figure 2.23 Five ventilation plate configurations used in CFD exercise.	62
Figure 2.24 Hydrogen contours on symmetry plane for left ‘dry air’ and right ‘humid air’	64
Figure 2.25 Concentration distribution Fluent 3.03 (Swain 1996)	71
Figure 2.26 (a) CFD graphic of helium mole fraction and (b) Comparison of CFD and test data (Barley and Gawlik 1996)	71
Figure 2.27 (a) CFD Graphic of hydrogen distribution in containment and (b) A comparison of CFD and test data hydrogen concentrations (Visser et al).	72
Figure 2.28 Comparison of CFD and empirical data (Srinivasa 2014)	73
Figure 2.29 Comparison of CFD and empirical data (Giannissi 2014)	73
Figure 2.30 Proposed CFD methodology for the safe design of confined spaces exposed to a hydrogen release (Dadashzadeh 2016)	76

### ***Chapter Three***

Figure 3.1 Workflow Process Map	79
Figure 3.2 IP-2 ISO Nuclear waste storage container	80
Figure 3.3 (a) Hymera environmental enclosure (b) Experimental enclosure	80
Figure 3.4 BOC Genie hydrogen cylinder and Hymera unit (BOC 2016)	81
Figure 3.5 BOC Ltd scoping exercise	82
Figure 3.6 Ion Science Gas Check 3000 handheld Hydrogen sensor (IonScience.com)	82
Figure 3.7 BOC Ltd Hydrogen HFC Enclosure Tests all tests run at 1 L/min	83
Figure 3.8 SolidWorks Flow Simulation CFD images of BOC model	84
Figure 3.9 Initial laboratory experimental test rig	85
Figure 3.10 Brooks GF125 High Purity Digital Thermal Mass Flow Device	86
Figure 3.11 Brooks GF125 Operating principles (Brooks 2015)	87
Figure 3.12 (a) Xensor XEN3880 Helium sensor (b) USB hub and sensors	88
Figure 3.13 Comparison of Xensor (Xensor Ltd 2016) and LSBU calibration tests (trend line equation added)	89
Figure 3.14 Experimental set up for the calibration test	89
Figure 3.15 Comparison of Xensor and LSBU calibration tests (trend line equation added)	90
Figure 3.16 Schematic for the initial enclosure test rig	91
Figure 3.17 Final experimental test rig	92
Figure 3.18 Schematic diagram of the final test rig	93
Figure 3.19 The final enclosure sealed for the permeation test	94
Figure 3.20 Schematic of experimental test	94
Figure 3.21 Helium permeation test: Helium concentration against sensor time step	95
Figure 3.22 Diffusion test: Helium concentration – average of all sensors- against seconds [Inset concentration against time (hours)]	96

Figure 3.23 Graph of diffusion coefficient against enclosure helium mole fraction	97
Figure 3.24 (a) Frame sensor arrangement; (b) frame installed in enclosure	98
Figure 3.25 (a) Frame sensors; (b) frame installed in enclosure; (c) Sensor height	99
Figure 3.26 Experimental scheme, showing the position of helium sensors	99
Figure 3.27 Example ventilation scheme configurations	100
Figure 3.28 Schlieren system to visualise helium in the HFC enclosure (Ingram J 2015)	103
Figure 3.29 a) Meshed containment b) Section c) Four meshes (Visser et al 2016)	107
Figure 3.30 Mesh data comparison with experimental data (Visser et al 2016)	107
Figure 2.31 Simulation methodology (Dadashzadeh 2016)	108
Figure 2.32 (a) Six mesh levels (b) Comparison with experimental data (Driss 2014)	108
Figure 3.33 CFD process map SolidWorks Flow Simulation and ANSYS: Fluent	110
Figure 3.34 (a) Initial Mesh (b) With geometry added to create a Local Initial Mesh	114
Figure 3.35 Fluid Flow (Fluent) Analysis System	117
Figure 3.36 (a) Geometry, (b) Fluid volume preparation, (c) Fluid volume	117
Figure 3.37 Meshed geometry: (a) Simple tetrahedral mesh (b) Complex, but poorly refined mesh (c) Polygonal mesh	118
Figure 3.38 ANSYS Fluent application screen	118
Figure 3.39 Fluent turbulence model menu	119
 <b>Chapter Four</b>	
Figure 4.1 BOC Ltd. Rig showing vent and sensor positions	124
Figure 4.2 BOC results: Tests 1-6 H <sub>2</sub> % (v/v) versus enclosure height	125
Figure 4.3 (a) Celotex enclosure with door vent (b) Position of sensor holes in door	126
Figure 4.4 Test 7 results: H <sub>2</sub> % (v/v) versus leak rate	127
Figure 4.5 Experimental schematic, showing sensor and vent position	128
Figure 4.6 Crossflow test: Lower inlet on the left and upper outlet on the right: Increasing leak rate from (a) to (e)	130
Figure 4.7 Average <u>vertical</u> helium concentration (Vol %) versus leak rate (LPM) at sensor stack positions of 100, 200, 300, 400 and 500mm across the enclosure.	130
Figure 4.8 Average <u>horizontal</u> helium concentrations (Vol %) for each sensor height across four stack positions, versus leak rate (LPM), for each scenario test	130
Figure 4.9 Experimental schematic showing vent and sensor position	133
Figure 4.10 Sensor results for a full test run with frame sensors	134
Figure 4.11 Frame sensor helium concentrations (a) all sensors (b) the 555 mm level	135
Figure 4.12 Stacked sensor helium concentrations against height (a) Plain vents (b) Louvre vents	136
Figure 4.13 Developed test rig with paper louvres applied to the openings	137
Figure 4.14 Louvre vent design specification	137

Figure 4.15 Frame sensor helium concentrations (a) all sensors (b) the 555 mm level	138
Figure 4.16 Comparison of plain (P) and louvre (L) vent (stacked sensor) concentrations at (a) 1 lpm, (b) 2 lpm, (c) 4 and 10 lpm and (d) Frame sensor concentrations at sensor 1 (Peak concentrations shown on graphs)	139
Figure 4.17 Test rig with (a) rectangular plain vent and (b) aluminium louvre vent	140
Figure 4.18 Plain vent opening results all twelve vent areas	143
Figure 4.19 Plain vent results at 10 lpm for all opening sizes	144
Figure 4.20 Comparison of wide plain vent and plain vent opening at 10 lpm	144
Figure 4.21 Comparison of wide plain vent and plain vent opening at 10 lpm	146
Figure 4.22 Louvre vent results at 10 lpm for all opening sizes	148
Figure 4.23 Comparison plain and louvre vent concentrations at 10 lpm-850 mm <sup>2</sup>	148
Figure 4.24 Top louvre vent only results for 3400 mm <sup>2</sup> vent opening area	149
Figure 4.25 Helium concentration with time-top louvre vents 3400mm <sup>2</sup> at 1 lpm	150
Figure 4.26 Comparison two and four vent schemes (3400 mm <sup>2</sup> ) at 1 and 10 lpm	151
Figure 4.27 Chimney schematic showing flat and china caps [not to scale]	152
Figure 4.28 Test 1: Single 110 mm chimney, no rain cap, at 1 lpm leak rate	153
Figure 4.29 Test 2: Single chimney, no rain cap, 1 lpm, sensors adjacent to opening	154
Figure 4.30 Schematic showing two-way flow and recirculation with single chimney	155
Figure 4.31 Tests 3 and 4 two chimneys, with and without flat lids at 1lpm	155
Figure 4.32 Schematic showing displacement ventilation and recirculation with double chimney arrangement [not to scale]	156
Figure 4.33 Test 5 two chimneys, flat lids and 15 mm gap at 1lpm	156
Figure 4.34 Test 6 two chimneys, china hat lids, 15mm gap at 1lpm	157
Figure 4.35 Comparison of tests 3, 4, 5 and 6 at 1 lpm	157
Figure 4.36 Flow through chimney with flat lid and china cap [not to scale]	158
Figure 4.37 Tests 7 to 12: Increasing chimney height at 2 lpm	159
Figure 4.38 Enclosure containing fuel cell box [not to scale]	160
Figure 4.39 Chimney x2 china cap with and without obstruction at 2 lpm.	160
Figure 4.40 Enclosure with flue [Not to scale]	161
Figure 4.41 Enclosure with T flue [not to scale]	162
Figure 4.42 Test 1 64 mm flue with no inlet at 0.5 lpm	162
Figure 4.43 Results of tests 2, 3 and 4: 110 mm flue with increasing inlet size	163
Figure 4.44 Comparison of 4 lpm results for test 2, 3 and 4	164
Figure 4.45 Result of test 5: 330 mm long flue	164
Figure 4.46 Results of test 6: T flue test	165
Figure 4.47 Schematic of snorkel enclosure (not to scale)	165
Figure 4.48 Results of the snorkel test	166
Figure 4.49 Schlieren equipment laid out in the laboratory for the test	168
Figure 4.50 Schlieren image lens contamination and glass irregularities.	168
Figure 4.51 Composite Schlieren helium plume in the enclosure at 10 lpm	170

Figure 4.52 Schlieren image helium emerging from plain vent at 10lpm	171
Figure 4.53 Schlieren image of helium near the ceiling	171
<b>Chapter five</b>	
Figure 5.1 SolidWorks CAD model	175
Figure 5.2 SolidWorks CFD data for the five scenarios tested	175
Figure 5.3 Average helium concentration (all sensor positions) vs leak rate (CFD and experimental data comparison)	176
Figure 5.4 SolidWorks cut plane images of steady state helium concentrations (0-4% v/v range) for each scenario at 1 to 5 lpm leak rates	177
Figure 5.5 Helium sensor positions (stacked and frame sensors)	178
Figure 5.6 Frame sensor helium concentrations (a) all sensors (b) at the 555 mm level	179
Figure 5.7 Stacked sensor helium concentrations against height	180
Figure 5.8 Comparison of experimental, adjusted experimental and CFD at 10 lpm	180
Figure 5.9 Simple plain vent CFD cut plane of initial mesh with 318589 cells	181
Figure 5.10 Cut plane CFD image through the plume and vents at 5 lpm	181
Figure 5.11 SolidWorks (a) Enclosure and computational domain (b) louvres	182
Figure 5.12 Frame sensor helium concentrations (a) all sensors (b) at 555 mm	182
Figure 5.13 A comparison of CFD, experimental and adjusted data at sensor 4	183
Figure 5.14 A comparison of CFD plain and louvre vent data at sensor 4	183
Figure 5.15 Stacked sensor helium concentrations against height-louvre vent	184
Figure 5.16 Stacked sensor plain and louvre CFD data at 10 lpm	184
Figure 5.17 Comparison of stacked plain and louvre CFD and adj. Exp, @ 10 lpm	185
Figure 5.18 Plain vent enclosure showing mesh refinement 382,077 cells	186
Figure 5.19 Cut-plane concentration contour image of plain vent 3400mm <sup>2</sup> @ 10lpm	186
Figure 5.20 Combined iso-surface/lines 0-4 % helium at 10 lpm 3400mm <sup>2</sup> plain vent	187
Figure 5.21 Comparison of experimental and CFD 3400 mm <sup>2</sup> plain vent @ 10lpm	187
Figure 5.22 Combined iso-surface/lines 0-4 % helium at 1 lpm 3200mm <sup>2</sup> plain vent	188
Figure 5.23 Comparison of experimental and CFD 3400 mm <sup>2</sup> plain vent @ 1 lpm	188
Figure 5.24 Iso-surface/lines 0-4% helium at 10 lpm 10200 mm <sup>2</sup> side view	189
Figure 5.25 Iso-surface/lines 0-4% helium at 10 lpm 10200 mm <sup>2</sup> isometric view	189
Figure 5.26 Comparison of experimental and CFD 10200 mm <sup>2</sup> plain vent @ 10 lpm	190
Figure 5.27 Combined iso-surface/lines 0-4 % helium at 1 lpm 10200mm <sup>2</sup> plain vent	190
Figure 5.28 Comparison of experimental and CFD 10200 mm <sup>2</sup> plain vent @ 1 lpm	191
Figure 5.29 SW simplified louvre vent CAD design (a) Acute (b) obtuse	191

Figure 5.30 Four louvre initial mesh (acute louvres) (334,230 cells)	192
Figure 5.31 Four louvre (acute) cut plane concentration contour 0-4 %	192
Figure 5.32 Iso-surface at 4 % (10 lpm) acute louvre vents	193
Figure 5.33 Streamlines at top left louvre vent, showing backed up flow at 10 lpm	193
Figure 5.34 Comparison of CFD and experimental data; 4 louvre vent at 10lpm	194
Figure 5.35 CFD comparisons of 4 louvre and 3400 mm <sup>2</sup> plain vent data; @ 10 lpm	194
Figure 5.36 Comparison of CFD and experimental data; 4 louvre vent at 1 lpm	195
Figure 5.37 CFD comparison of louvre and 3400 mm <sup>2</sup> plain vent data, @ 1 lpm	195
Figure 5.38 12 louvre initial mesh (422,456 cells: additional louvre refinement)	196
Figure 5.39 Concentration contour images 12 louvre enclosure (a) 10 lpm (b) 1 lpm	196
Figure 5.40 12 louvre and 10200 mm <sup>2</sup> plain vent results 10 lpm: CFD and Exp.	196
Figure 5.41 Twelve louvre and 10200 mm <sup>2</sup> plain vent results 1 lpm	197
Figure 5.42 (a) Meshed 420 mm CAD model (241,334 cells) (b) chimney vent with lid	198
Figure 5.43 CFD data for the 420 mm chimney compared with Adj. Exp. data	198
Figure 5.44 420 mm chimney CFD cut-plane images at 1, 2, 4 and 10 lpm	199
Figure 5.45 Cut-plane image with velocity vectors describing enclosure circulation	200
Figure 5.46 840 mm chimney cut-plane images at 2 and 4 lpm	201
Figure 5.47 CFD data for the 840 mm chimney compared with Adj. Exp. data	202
Figure 5.48 Meshed 1680 mm chimney enclosure CAD model (514,899 cells)	202
Figure 5.49 CFD data for the 1680 mm chimney compared with Adj. Exp. data	203
Figure 5.50 1680 mm chimney cut-plane images at 2 and 4 lpm	203
Figure 5.51 Cut-plane image with velocity vectors describing enclosure circulation	204
Figure 5.52 Comparison 420, 840 and 1681 mm chimney height CFD results (4LPM)	204
Figure 5.53 Cut-plane concentration contour and iso vectors Chinese cap	205
Figure 5.54 Meshed 110 mm flue enclosure without inlet (355925 cells)	206
Figure 5.55 Comparison of CFD and exp. data for 110 mm straight flu-no inlet	206
Figure 5.56 Comparison: CFD and exp. data for 110 mm straight flu/ 3200mm inlet	207
Figure 5.57 Comparison: CFD and exp. data for 110 mm straight flu/ 9600mm <sup>2</sup> inlet	207
Figure 5.58 CFD data for the 330mm flue with the 9600 mm <sup>2</sup> inlet	208
Figure 5.59 Comparison: CFD and exp. data for 3300 mm straight flu/ 6400mm inlet	209
Figure 5.60 Comparison of flue cut-plane images	209
Figure 5.61 CAD model of the T flue design	210
Figure 5.62 Comparison of experimental and CFD T Flue data at 1 and 4 lpm	210
Figure 5.63 (a) T Flue meshed CAD model (290,330 cells) (b) Cut plane 4 lpm @ 4%	211



Figure 5.64 Comparison of 110mm flue and T flue at 4lpm leak rate	211
Figure 5.65 CAD models showing Snorkel design and enclosure configuration	212
Figure 5.66 Meshed CAD model and cut planes at 1 and 4 lpm @ 4% concentration	212
Figure 5.67 Comparison of experimental and CFD snorkel data at 1 and 4 lpm	213
Figure 5.68 Flow lines in snorkel	213
Figure 5.69 Obstruction test cut-plane images at 1lpm	214
Figure 5.70 Obstruction tests cut-plane images at 4 lpm	215
Figure 5.71 Enclosure with HFC obstruction showing flow paths at 4lpm	215
Figure 5.72 Comparison of experimental and CFD snorkel data at 1 and 4 lpm	216
Figure 5.73 ANSYS: Meshing: Mesh of computational domain (511363 cells)	217
Figure 5.74 ANSYS: Fluent cut-plane $K\epsilon$ std, std. wall, std. buoyancy @ 4 lpm	218
Figure 5.75 ANSYS: Fluent-simulation predictions (with SW and empirical results)	218
Figure 5.76 ANSYS: Fluent cut-plane image. 4 lpm leak rate and 4 % range	219
Figure 5.77 ANSYS: Fluent-LES simulation predictions	220
Figure 5.78 ANSYS: Meshing at 6.1 million cells equivalent-small domain	220
Figure 5.79 ANSYS: DES cut-plane contour image at 4 lpm (4 % conc. range)	221

### ***Chapter Six***

Figure 6.1 Leak rate at which hydrogen LFL (4%) was achieved for selected scenarios	226
Figure 6.2 Leak rate at which hydrogen LFL (4%) was achieved with initial test rig	227
Figure 6.3 Initial enclosure with two top vents at 5 lpm compared with the BOC plain vent enclosure at 5 lpm: Concentration against time	228
Figure 6.4 Scatter plot: Total vent area vs. peak conc. at 4 lpm for plain and louvre vents	231
Figure 6.5 Scatter plot: Vent area vs. peak concentration for three regimes at 4 lpm	231
Figure 6.6 Total vent area vs peak concentration for the rectangular plain vents with BOC wide plain vents overlaid; leak rates from 1 to 5 lpm.	232
Figure 6.7 Safety guidance: Decision tree: std. 0.144 m <sup>3</sup> enclosure deployment	235
Figure 6.8 Structure of the model evaluation protocol (HYMEP)(Baraldi 2016)	236
Figure 6.9 BOC Plain vent test helium concentration and temperature vs time	237
Figure 6.10 BOC Plain vent test helium concentration and humidity vs time	238
Figure 6.11 Fraction bias test results	240
Figure 6.12 Normalised mean square error results	240
Figure 6.13 Geometric mean bias results	241
Figure 6.14 Geometric mean variance results	241
Figure 6.15 Scatter plot of the observed versus the predicted peak enclosure concentrations for all the models tested in this section.	242
Figure 6.16 CFD validation and verification process (Meroney et al (2016))	244
Figure 6.17 CFD comparison of helium and hydrogen-ANSYS: Fluent [WM LES]	248

Figure 6.18 ANSYS: Fluent (a) WM LES [hydrogen] (b) DES SST k- $\omega$ [hydrogen]	248
Figure 6.19 CFD comparison helium and hydrogen-ANSYS: Fluent [DES SST k- $\omega$ ]	249
Figure 6.20 Ratio of helium and hydrogen values against height	249
Figure 6.21 CFD Comparison helium and hydrogen-SolidWorks [k- $\epsilon$ ]	250
Figure 6.22 SolidWorks cut-plane image at 4 lpm	250
Figure 6.23 SolidWorks mesh sensitivity study	251
Figure 6.24 Leak rate prediction analysis	253
Figure 6.25 Enclosure surface area/vent area against helium % at 5 lpm	254

## List of Tables

Table	Page
<b>Chapter One</b>	
Table 1.1 Global final energy consumption in buildings 2011 (IEA (2014))	13
<b>Chapter Two</b>	
Table 2.1 Recent literature examining hydrogen dispersal in enclosures	25
Table 2.2 Some of the turbulence models available	74
Table 2.3 Simulation intent (Nolan 2015)	75
<b>Chapter Three</b>	
Table 3.1 Results of helium sensor calibration tests conducted at LSBU	90
Table 3.2 Initial ‘base-case’ experimental rig test scenarios	91
Table 3.3 Range of turbulence models available in SolidWorks and ANSYS	109
Table 3.4 Example Flow Simulation configuration settings	112
Table 3.5 Statistical performance indicators	122
<b>Chapter Four</b>	
Table 4.1 Experimental configurations	124
Table 4.2 Test 7 results	127
Table 4.3 Experimental configurations	129
Table 4.4 Louvre and plain vent opening areas	141
Table 4.5 Chimney vent configurations: Various arrangements	152
Table 4.6 Chimney vent configurations: Increasing chimney height/obstruction	153
Table 4.7 Flue tests	161
<b>Chapter Five</b>	
Table 5.1 SolidWorks Flow Simulation studies CFD approach	174
Table 5.2 Initial test rig configurations	175
<b>Chapter Six</b>	
Table 6.1 Analysis results-empirical and SolidWorks data sets	239
Table 6.2 Example experimental error calculations	243

## **Chapter 1: Introduction**

### **1.0 Motivation for this research**

This research investigation is supporting the global move away from fossil fuel dependence and its replacement with a distributed energy system using renewable sources of energy. A 'Hydrogen Economy' is being promoted as a transition measure that will support a new energy infrastructure based upon renewables. The hydrogen economy will only succeed if issues around hydrogen production, storage, transportation and safety in use are resolved. This thesis extends safety knowledge in support of this endeavour.

Hydrogen fuel cells (HFC), a key part of the Hydrogen Economy initiative, will be used at a variety of scales to provide distributed power. Low power units in small protective enclosures will become widely used. Domestic and commercial combined heat and power (CHP) applications are popular in Korea, Japan and California (Staffell, I 2013). The fuel cell enclosures are a hydrogen confinement hazard. Hydrogen's wide flammable range (4-75% in air) needs effective ventilation to maintain safe concentrations. Confidence in fuel cell safety will support their use and progression to wider use of renewable energy.

A connected hydrogen safety concern relates to the nuclear decommissioning industry. Large amounts of nuclear waste (high, medium and low grade) has been accrued through the running and decommissioning of nuclear installations. This waste is held in storage facilities. However, through either radiolysis or corrosion processes it can produce a steady stream of hydrogen. This hydrogen must be safely vented from the installation to prevent the formation of flammable atmospheres that could lead to a devastating explosion. Nuclear waste storage boxes are packed tightly in the containment facility, with small spaces left between them. Hydrogen that diffuses through filters on the top of the boxes could potentially accumulate in these spaces if ventilation is not adequate to clear it. Effective passive hydrogen venting is therefore required.

The management of hydrogen concentrations in small enclosures and confined spaces using passive ventilation is highly relevant to the safety cases in both instances. This introduction outlines the need to transition to renewable forms of energy, issues of baseload management, how hydrogen and fuel cells can help and the need for effective

passive ventilation of hydrogen in confined spaces that also affects nuclear waste storage. The thesis hypothesis, aims and objectives and the thesis structure are also presented.

## 1.1 The energy trilemma

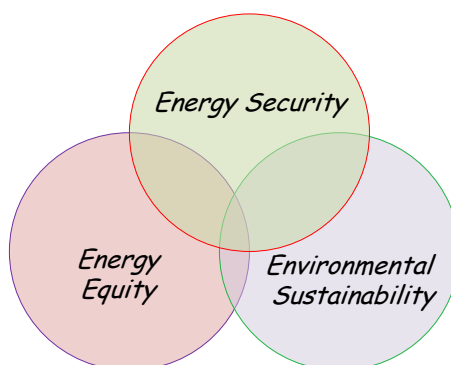


**Figure 1.1 The ‘Energy Trilemma’**

The world is facing an energy crisis, with economic, social and environmental challenges. High rates of population growth, resource depletion, climatic change and pollution are producing instabilities and inequalities in the human population. The World Energy Council specifically focuses upon the core issues of ‘energy security’, ‘energy equity’ and ‘environmental sustainability’, referred to as the ‘Energy Trilemma’ (Wyman 2016). The uppermost anthropogenic threat, linked to the trilemma (Figure 1.1), is global warming and climate change, significantly caused by energy dependence on and overuse of fossil fuels since the industrial revolution.

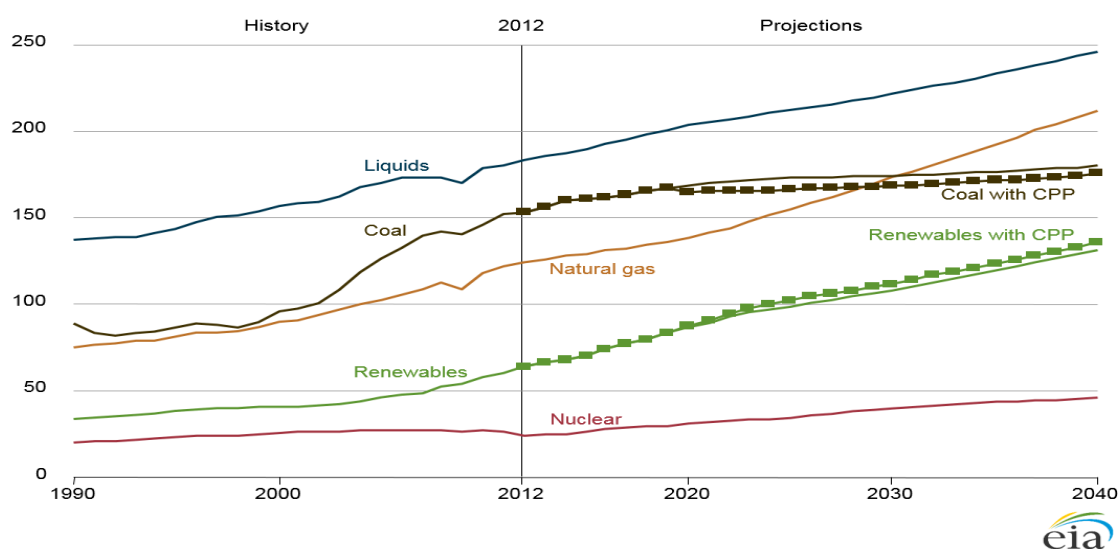


**Figure 1.2 World energy consumption by energy source, 1991-2040 (© EIA 2016)**

It is of interest that fossil fuel stocks (although still significant) are depleting, whilst their global use is increasing and predicted to continue to rise (Figure 1.2 US Energy Information Administration (2016) [CPP is the Clean Power Plan introduced by President Obama to combat anthropogenic climate change and global warming but now repealed by President Trump. Public discussions on its replacement are ongoing]). This growth in fossil fuel use is attributed mainly to developing non-OECD (Organisation for Economic Cooperation and Development) nations with a predicted 71 % increase by 2040, whereas mature energy-consuming and slower-growing OECD economies rise by only 18 % (US Energy Information Administration (2016)).

### 1.2 Managing the energy baseload

The ongoing use of fossil fuel to meet our energy needs will further increase CO<sub>2</sub> levels in the atmosphere, increasing global temperatures and exacerbating energy trilemma instabilities. Amongst many fossil fuel harms, air pollution is adversely affecting human health and has been linked to many deaths. Fossil fuel needs to quickly be replaced by low carbon renewable sources of energy that sustainably reduce CO<sub>2</sub> levels, improve air quality and provide energy security. The intermittent generation of some technologies (e.g. wind and solar) though, poses new questions for effective energy management.

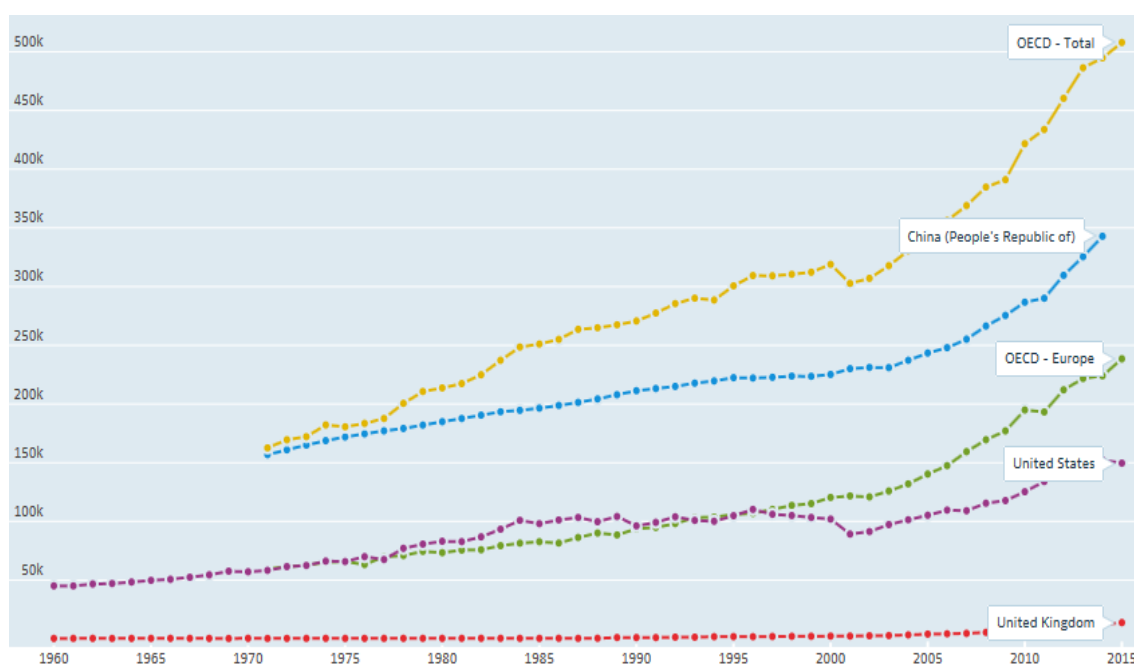


**Figure 1.3 Renewable energy use 1960 to 2015 [thousand toe] (© OECD 2016)**

Renewable energy is available in a wide variety of technologies e.g. wind, solar Photovoltaic (PV) and hydroelectric, with their adoption increasing noticeably in recent years (Figure 1.3 IEA (2016)). These increases, although welcome, are only the start and more needs to be done to drive their uptake. Renewable energy technologies are maturing and becoming more efficient, producing growing amounts of electricity.

However, the intermittent nature of some renewable energies means that peak production does not necessarily coincide with peak energy demand, particularly with solar, which is predicted to become the primary renewable component. As renewable energy production and use increases, a significant problem of oversupply arises.

Due to the way that coal fired power stations operate (needing to stay running because of long start up times) the fossil fuel power generation ‘base-load’ cannot be reduced. During the day when solar renewables are at peak production, their output, plus the coal base-load will exceed demand and ultimately waste energy (Figure 1.3; Rothleder, Mark (2017)). An effective solution for managing and balancing energy supply and demand is required if the transition from fossil fuels is to be successful and cost effective.

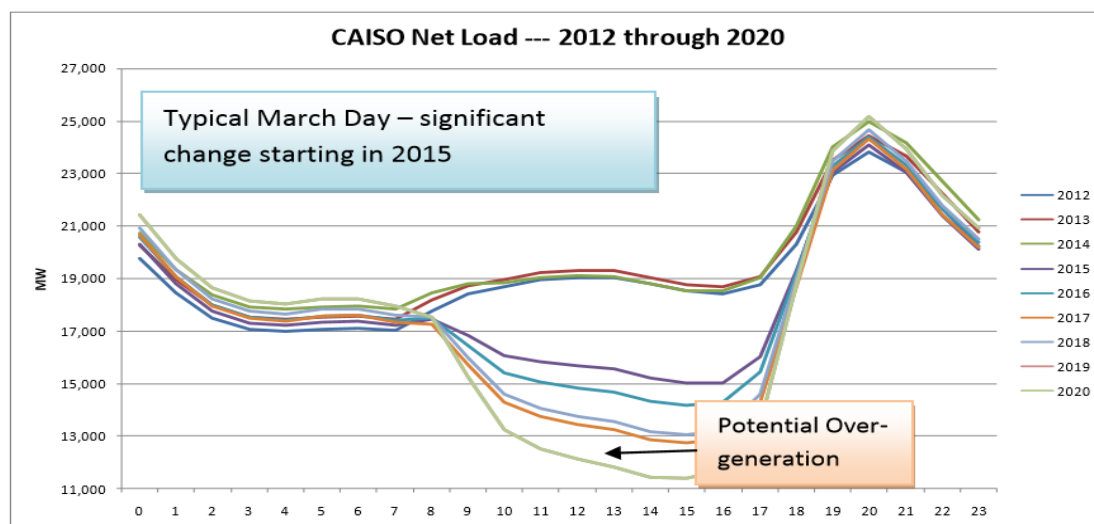


**Figure 1.4 Net base load electricity generation (© California ISO-2012)**

A solution to the base-load problem is to find an effective way of storing surplus off peak energy so that it can be used at peak demand. In conjunction with this there also needs to

be an evolution in how energy is produced, with more distributed local/onsite generation together with on demand production. Battery storage of surplus energy is an option. Batteries are improving in terms of capacity and life, but they are also resource and cost expensive. Pumped hydro-electricity has restrictions due to geological limits. An alternative approach is to use surplus generation to produce hydrogen for later use.

Hydrogen is a versatile ‘energy carrier’, storing energy generated by other means and releasing it as needed through chemical processes. It can be mixed with gaseous fuels such as methane to improve combustion and reduce carbon emissions in boilers. It can also be burnt in isolation producing only water as a by-product and heat. Hydrogen fuel cells generate electricity with water and heat as a by-product. HFCs have stationary, transportable and transport power generation applications.

### **1.3 The Hydrogen Economy – the energy solution**

Hydrogen is a by-product in many industrial processes but can also be produced on a large scale through the electrolysis of water or steam reforming of hydrocarbons (with carbon capture and storage (CCS)) until renewables are fully established for hydrogen production. Much research is currently being undertaken to meet the challenge of storing large amounts of hydrogen and make it a viable energy source that can balance the demand issue and reduce carbon emissions. The hydrogen economy concept is the optimal transition route from fossil fuels to ubiquitous renewable energy and reduced carbon emissions. It is also perfectly suited to distributed electricity and heat generation.

Figure 1.5 shows the path from hydrogen production to storage and its final use in fuel cells and for heat. Hydrogen can also be used in internal combustion engines and gas turbines. HFCs will be the primary hydrogen energy converter, particularly with domestic micro-CHP and remote outdoor sites, replacing diesel generators. Commercial properties and vehicles will also be hydrogen powered and heated. Trials are also taking place to introduce hydrogen into the natural gas grid for commercial and domestic applications (Dodds et al 2013), but currently limited to 20 % so that adaptations to burners are not required.

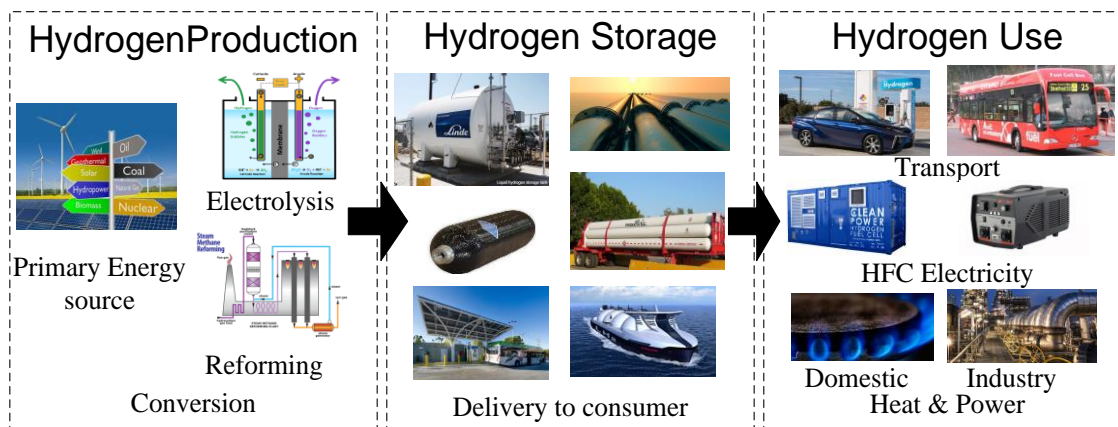


**Figure 1.5 Hydrogen economy schematic for production, storage and use**

### 1.4 Hydrogen fuel cells

Hydrogen fuel cells that produce ‘clean’ energy with no carbon emissions and only water and heat as by-products are pivotal to hydrogen economy success, helping to reduce carbon emissions and create a distributed (grid independent) energy supply structure. Fuel cells are versatile machines, which are scalable to produce greater amounts of electricity. They already power cars, buses and trains and produce heat and power in homes. Small low power hydrogen fuel cells (sub 200W peak power) are becoming popular to replace diesel generators in remote locations for lighting and cellular telephone towers.

A hydrogen fuel cell (Figure 1.6) is a machine that generates electricity through the chemical reaction of hydrogen and oxygen, in the presence of a catalyst, to produce an electric current, water and heat. They are different from batteries, which have a finite amount of reactants. Fuel cells require a continuous supply of hydrogen to sustain the reaction, with oxygen from the air, and can run indefinitely. There are several fuel cell designs, but a popular one is the proton exchange membrane (PEM) used in transport, stationary and transportable applications. PEM technology is at the heart of BOC Ltd.’s, small fuel cell ‘Hymera’ range of low power HFCs (20 to 200W) (BOC Ltd. 2017).

PEM fuel cells are constructed from ‘Membrane Electrode Assemblies’ (MEA). These assemblies include the electrodes, electrolyte, catalysts and gas diffusion layers. The triple phase boundary where electrolyte, catalyst and reactants come together is where the



reactions take place. This membrane must not be electrically conductive, so that the half reactions do not interact.

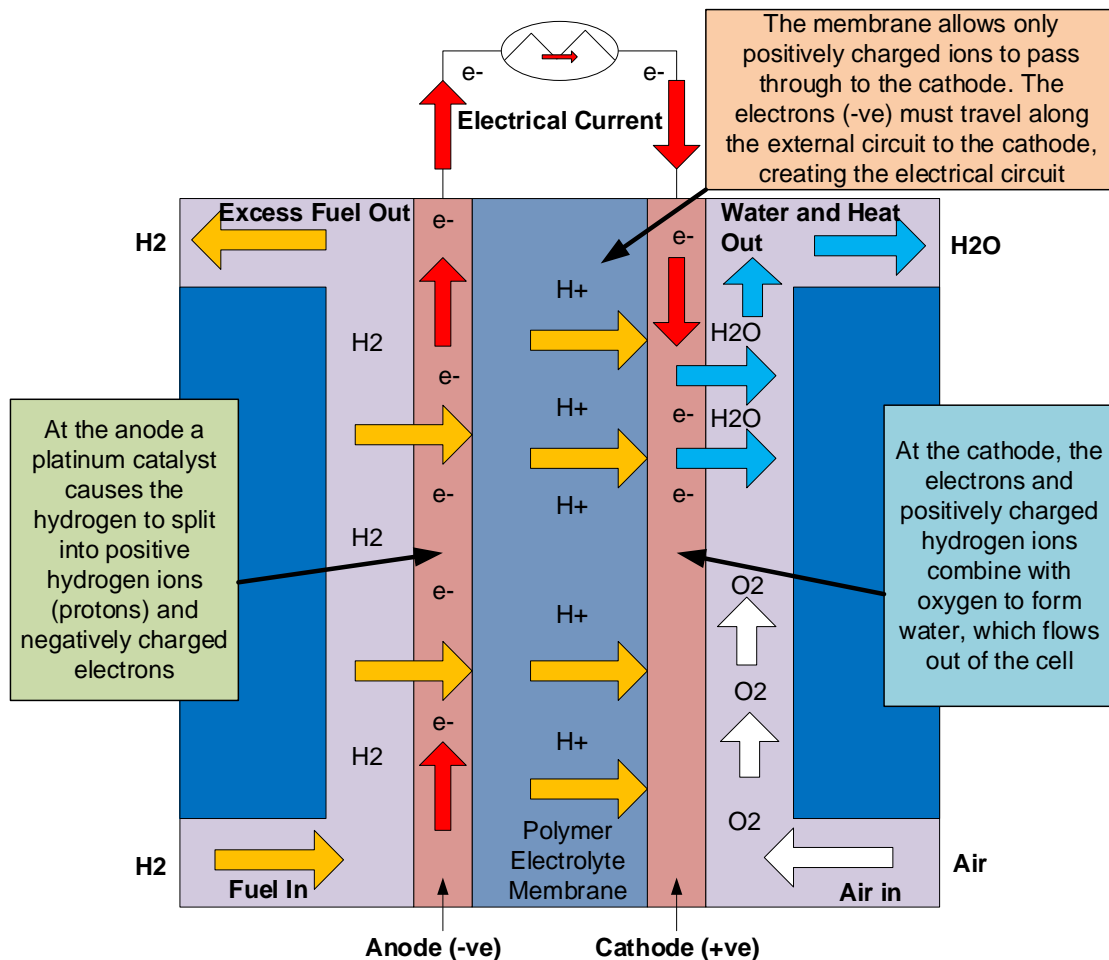


**Figure 1.6 Hydrogen (PEM) Fuel Cell Schematic**

Hydrogen is supplied at the anode where it is catalytically broken down into protons and electrons (equation 1). The protons permeate through the polymer electrolyte membrane to the cathode side, where they combine with oxygen from the atmosphere to form water (equation 2). The electrons travel along an external circuit to the cathode producing the current output.

Reaction at the anode:



Reaction at the cathode:



Some of the unreacted hydrogen can be recovered and resupplied to the anode. The use of a multi-component fuel cell assembly makes the chances of some of the small hydrogen molecules leaking out high, particularly with membrane degradation. Small amounts of hydrogen should be passively vented away safely. In high-load situations or with fatigued or damaged membranes more hydrogen could leak out. Joints in the hydrogen supply system are further weak points for leaks. Hydrogen safety management now becomes important, particularly in small enclosed situations where hydrogen may accumulate.

### 1.5 Hydrogen Safety

High profile accidents early in the 20<sup>th</sup> century where hydrogen air ships caught fire such as the Hindenburg (35 deaths) (Figure 1.7), USS Akron (73 deaths) and the British R101 (48 deaths) (airships.net) are the reason hydrogen has a poor safety reputation. More recently, the explosions at the Fukushima nuclear power plant were primarily due to a ‘loss of coolant’ accident caused by the tsunami flooding and knocking out of the back-up power generation system. This led to overheating of some of the reactor cores and the generation of large volumes of hydrogen, which was then vented into the outer reactor buildings where it built-up and was ignited.



**Figure 1.7 Hindenburg explodes on landing in New Jersey 1937 (© airships.net)**

The main risk associated with the use of hydrogen is the creation of a flammable or detonatable mixture, which leads to fire, deflagration (subsonic combustion propagating through heat transfer and diffusion of free radicals) or detonation (a form of combustion occurring at the interface between supersonic shock waves and the compressing unburned gas, producing a chemical reaction) (NASA 2005).

Hydrogen has a wide flammable range. The flammability limits of hydrogen in dry air at standard temperature and pressure (STP) are 4.1 percent (Lower flammable limit (LFL)) to 74.8 percent (Upper flammable limit (UFL)). In oxygen at STP, they are 4.1 percent (LFL) to 94 percent (UFL). A reduction in pressure below 101.3 kPa narrows the range of flammability, raising the lower limit and lowering the upper limit (NASA 2005).

Detonations are associated with higher hydrogen/air concentrations than for deflagrations and are likely in the 18-55% region. Ignition sources can come from valve operations, electrostatic discharges, catalyst particles and lightning strikes (relevant to outdoors fuel cell installations). If hydrogen is present, there is also always a potential fire hazard. A deflagration can result if a flammable mixture is ignited at a single point and a detonation can occur in a flammable mixture with an appropriate energy source or if it undergoes a 'deflagration to detonation transition' (DTT). A deflagration can become a detonation in confinement (NASA 2005) e.g. an HFC enclosure.

Hydrogen fuel cells have a good safety record, but this is in part due to high levels of engineering, the use of hydrogen sensors and powered ventilation systems. Hydrogen leaks though generally originate from valves, gaskets, seals and fittings (NASA 2005) present in highly engineered fuel cell and supply rig set-ups. Simplification of the design may therefore improve safety. An advantageous property of hydrogen is its buoyancy, which in enclosure situations means the gas will rise towards upper vents and exit to the atmosphere. This property can limit horizontal spread and promotes dispersion but can also produce a high-level concentrated stratified layer in confinement (NASA 2005).

Hydrogen ignition will normally lead to an ordinary deflagration that is less hazardous than if detonation results. In confined or partially confined enclosures, deflagration can

evolve into detonation, with enclosure geometry, gas concentration, flow conditions and turbulence affecting the transition. The shock wave from a detonation has greater potential for causing harm and damage. Small fuel cells in enclosures are therefore a significant risk. Adequate ventilation is key to maintaining concentrations below the LFL. Ventilation schemes must provide adequate air exchange and not allow flow reversal to occur, ideally keeping concentrations to 25% of the LFL (NASA 2005).

Small fuel cells will frequently be housed in an enclosure. Hydrogen's wide flammable range means that even low-level leaks in the enclosure can lead to explosive mixtures forming in confinement with a risk of detonation or deflagration, devastating the enclosure and fuel cell and with the potential for other harm. Forced ventilation can clear the hydrogen but mechanical systems add to costs, drain power and are vulnerable to failure with failsafe passive ventilation systems preferred for such enclosures.

### 1.6 Small hydrogen fuel cell enclosures

Small fuel cells can replace diesel generators and gas boilers and become ubiquitous in the stationary and portable generator markets. They quietly and cleanly produce electricity for extended periods with minimal maintenance. Steel enclosures house the fuel cell equipment, which needs to be ventilated to remove any hydrogen (Figure 1.8). Vents are pressed into the steelwork of these enclosures to enable ventilating airflows to occur through the internal volume.



**Figure 1.8 Fuel Cell Enclosures (Barilo. N 2013)**

To keep costs down, readily available electrical enclosures have been used for housing small fuel cells without adaption. Vent configurations in these enclosures are there for passive thermal management, to maintain optimum operating temperatures. However, the presence of a flammable buoyant gas in a small enclosure presents a more complex

scenario for ventilation and safety management. Ventilation schemes that can effectively clear leaked hydrogen from the enclosure are required. Passive ventilation uses buoyancy and small natural driving forces to move air and hydrogen through the enclosure. The performance of a passive ventilation system is dependent upon the size, shape and position of the ventilation openings on the enclosure as well as local outdoor environmental conditions.

Many small fuel cell deployments will be in the outdoor environment and exposed to nature. Vent design now becomes important, as water must not enter the enclosure. Wind forces can affect passive flow in the enclosure and vents are liable to being blocked by foliage. It may even be necessary to install grills to prevent rodents and insects from gaining access and damaging pipes and circuitry. These interventions affect enclosure ventilation flow, with the potential for flow reversal that can lead to increased hydrogen concentrations. What appears to be a simple ventilation solution therefore requires complex safety considerations and design insight.

### **1.7 Passive ventilation of enclosures**

Hydrogen management through passive venting is viable due to its inherent reliability and suitability as a buoyant gas (Hübert 2011). Passive ventilation schemes for the removal of pollutants from buildings, airflow management and thermal control are well established (Liddament 1996), so there is confidence that the application of these concepts to small fuel cell enclosures can manage concentrations below the LFL (Bachelierie 2003). An extensive review of the conditions responsible for producing natural ventilation found that density differences and buoyancy are the driving forces in scenarios where wind forces are absent (Liddament 1996).

The terms ‘passive ventilation’ and ‘natural ventilation’ have been introduced and are often used interchangeably to denote a naturally driven ventilation system (i.e. one that is passive in nature and not driven by a mechanically forced system). However, in small enclosure ventilation schemes where a buoyant gas flow is introduced, such as with a hydrogen leak, an important distinction has been identified (Molkov et al 2014) with a more precise usage of the terms being defined. For natural ventilation (applicable to the

flow of air), the ‘neutral plane’ (where internal pressure is equal to external air pressure) is assumed to be positioned approximately half-way up the opening (single vent scenarios).

However, under passive ventilation conditions which can occur for lighter than air gases, particularly those capable of filling the entire enclosure such as hydrogen (for a single vent scenario), the neutral plane can be positioned anywhere between the halfway point and the bottom of the ventilation opening. A further factor governing passive ventilation performance is vent design. Experimental investigations have routinely used plain rectangular vertical wall vents whose performance is understood and can be optimised. Their use in outdoor environmental situations though would not protect the enclosure. The performance of vents such as louvres, chimneys and flues intended to provide protection is less clear-cut. It is important to understand how alternative enclosure ventilation schemes perform as enclosure applications and conditions will vary, necessitating efficient ventilation adaptations to be made.

### **1.8 Computational Fluid Dynamics (CFD) modelling**

CFD software codes solve the partial differential equations for the conservation of mass, momentum (Navier-Stokes), energy, chemical concentrations and turbulence quantities. Solutions provide the field distributions of pressure, velocity, temperature, the concentrations of water (relative humidity), gas and contaminants and turbulence parameters. A buoyant gas release in confinement is a complex case to replicate using CFD. Selecting the appropriate turbulence model and boundary conditions is crucial for achieving reliable prediction data. SolidWorks Flow Simulation is the primary CFD tool in this thesis. ANSYS: Fluent is used in a comparison performance study.

### **1.9 Economic and social benefits of this research**

The economic benefits of a hydrogen economy will be significant. Fossil fuel exploitation has caused global problems. Oil rich states have profited economically over the past century, but with dire environmental consequences. Greenhouse gas emissions from fossil fuels are causing climate change, global warming and extreme weather events. Events, such as Hurricane Katrina caused billions of pounds in damages and the loss of lives and livelihoods. The ecological cost of damage from oil spillages, NO<sub>x</sub> and SO<sub>x</sub> emissions,

sulphurisation and non-biodegradable waste is incalculable for now and into the future. Global warming is already leading to premature deaths, migration from uninhabitable areas and shortages of fresh water.

A hydrogen economy will mitigate these effects and ultimately lead to a cleaner and healthier planet. The economic benefits will primarily emerge from the reduced measures needed to tackle climate change, although this will be in the long term. In the short term, the development of a new industry based around hydrogen and fuel cells will create new and more distributed wealth. The hydrogen economy infrastructure will be more efficient and secure. Energy security for a nation is a significant economic strength. With many fuel cells that are marketed needing to be housed in an enclosure, enclosure safety is a significant success factor. Greater confidence in safety will lead to raised consumer confidence and speedier uptake of the technology.

**Table 1.1 Global final energy consumption in buildings 2011 (IEA (2014))**

<b>Energy Source</b>	<b>Residential (EJ)</b>	<b>Commercial (EJ)</b>	<b>Industrial (EJ)</b>	<b>Total (EJ)</b>
<b>Petroleum Products</b>	9	4	14	27
<b>Coal</b>	3	1	31	35
<b>Natural gas</b>	17	7	21	45
<b>Biofuels and waste</b>	35	1	8	44
<b>Electricity</b>	18	15	28	61
<b>Heat (CHP/District heating)</b>	5	1	5	11
<b>Other</b>	0	0	0	0
<b>Total</b>	<b>87</b>	<b>29</b>	<b>107</b>	<b>223</b>

In 2011 the total energy use for heat in buildings was 172 EJ, with 75% generated using fossil fuels (Table 1). This released 10 Gt CO<sub>2</sub> into the atmosphere. Fossil fuel emissions are having a significant effect on air quality, particularly in cities, affecting human health and mortality. More than half of global energy production is used for heat (Dodds et al 2014). Using zero emission [at point of use] hydrogen, will significantly improve air quality. Domestic fuel cell micro CHP will play a key role in this transition, using

hydrogen or natural gas. The social benefits of improved health and quality of life will reduce the burden on health services and create a broadly healthier external environment.

### 1.10 Research hypothesis

There is the potential for a hydrogen leak to occur in the fuel cell or supply system contained within an enclosure. Where lead acid batteries are used to store surplus energy, the battery too can become a source of hydrogen when under charge and a source of ignition. If a catastrophic leak occurs releasing the entire volume of the storage cylinder, the dangers are clear. However, such a release will be rapid and if outside, the hydrogen will quickly disperse through the vents. A more likely scenario though is a persistent low-level leak below 10 litres per minute (lpm). Such a leak can create a persistent flammable atmosphere in an enclosure.

Passive ventilation systems in low-level leak scenarios rely upon small driving forces, with environmental conditions such as wind, temperature and humidity affecting performance. The area, position and design of the ventilation opening(s) on the enclosure will determine the rate of airflow through the enclosure. Vent area must be sufficient to facilitate an air exchange rate that removes hydrogen from the enclosure and keeps concentrations below the LFL. The design of ventilation openings, whether they are holes in the enclosure or chimney arrangements must also afford some protection to the enclosure from the elements. Such restrictions can impede flow.

**Research Hypothesis:** *Safe, passive ventilation parameters can be determined that will manage hydrogen concentrations below the lower flammable limit, for hydrogen leak rates at or below 10 litres per minute in a passively ventilated 0.144m<sup>3</sup> hydrogen fuel cell enclosure.*

### 1.11 Research aims and objectives

This study is motivated by the need to demonstrate passive ventilation schemes for small HFC enclosures that are predictable, reliable and failsafe. The danger of a flammable buoyant gas in confined spaces is not limited to the fuel cell industry, so findings from this study will have engineering applications in many industries, particularly nuclear.



**Research aims are;**

- To investigate passive ventilation capability to manage hydrogen concentrations below the LFL, when applied to a small fuel cell type enclosure containing a hydrogen leak
- To investigate CFD capability to predict the empirical test outcomes

**The project objectives are;**

- To carry out experimental tests and produce data sets for helium concentration variation, in a small hydrogen fuel cell type enclosure containing a helium leak, with a number of ventilation arrangements.
- To obtain data variables through;
  - Construction of a fuel cell enclosure test rig
  - Delivering helium into the enclosure at metered flow rates between 0.5 and 10 lpm and observing how helium concentrations are affected by
    - Vent size, arrangement and use of louvres
    - The use of chimneys and snorkels/flues
    - Leak position/internal obstructions
- To produce datasets from CFD prediction modelling for helium gas concentration variation in a small hydrogen fuel cell type enclosure
- To obtain data variables through
  - CFD modelling of the experimental variations
- Development of buoyant gas passive ventilation guidance

**1.12 Thesis structure**

**Chapter 1 – Introduction to the issues and hypothesis:** An explanation of the need to move away from fossil fuel use and the role of hydrogen and fuel cells in achieving a renewable energy infrastructure. The role of small hydrogen fuel cells housed in enclosures is examined and how safety is paramount to their success. The role of passive ventilation is introduced, relevant to the fuel cell and nuclear decommissioning industries. The hypothesis, aims and objectives of the research project are set out.

**Chapter 2 – Literature review:** A critical review of previous academic literature in this research field to identify knowledge gaps requiring research.

**Chapter 3 – Methodology:** This chapter explains how the empirical and computational research was carried out. The construction of the test rig is described and the experimental method of data collection. The use of CFD to model the experimental scenarios is explained. Techniques to assess numerical model performance are also explained.

**Chapter 4 – Experimental results and analysis: Hydrogen fuel cell enclosures.** A presentation of the experimental results and their analysis;

- BOC Ltd. scoping exercise hydrogen tests
- Base case initial enclosure plain vent tests
- Plain vent and simple louvre tests
- Aluminium louvre vent tests
- Plain vent comparison test
- Chimney-Stack tests
- Flue / snorkel tests
- Internal obstruction tests
- Schlieren system helium visualisation

**Chapter 5 – Computational fluid dynamics modelling results and analysis: Hydrogen fuel cell enclosures.** A presentation of the SolidWorks Flow Simulation numerical modelling results and analysis;

- BOC Ltd. Scoping exercise hydrogen tests
- Base case initial enclosure plain vent tests
- Plain vent and simple louvre tests
- Aluminium louvre vent tests
- Plain vent comparison test
- Chimney-Stack tests
- Flue / snorkel tests
- Internal obstruction tests
- ANSYS: Fluent comparison study

**Chapter 6 – Discussion:** A critical discussion of the empirical and computational results. The discussion includes the CFD validation tests.

**Chapter 7 – Conclusion:** An assessment of the investigation and concluding remarks.

**Chapter 8 – Recommendations for future work:** Further work to develop and extend the findings of this investigation are set out.

**References:** A list of references cited in the thesis.

**Appendices:** Supplementary documents

### **1.13 Conclusion**

This research is motivated by the urgent need to stop fossil fuel exploitation and facilitate the transition to a low/zero carbon future based upon renewable sources of energy. A hydrogen economy is the likely mechanism for this transition. With flammable hydrogen at its heart, it is important that research and development in this field focuses upon safety. Hydrogen safety is also important to other industries, particularly nuclear waste storage and decommissioning.

In both of these fields, it is the effective means of dealing with leaked hydrogen that is an important safety challenge. Passive ventilation techniques are preferred as they are inherently reliable and failsafe. A comparison can also be drawn between the confinement of hydrogen in a small fuel cell enclosure and in the gaps between nuclear waste storage boxes. Passive ventilation is a potential safety solution in both cases, requiring further research to establish safe design parameters.

This thesis presents new datasets for a variety of untested passive ventilation scenarios relevant to buoyant gas removal from confinement. Computational fluid dynamics is an engineering tool used in the design and development of ventilation systems. Its application to buoyant gas venting scenarios is new and similarly empirical datasets for CFD validation are few. This thesis applies a previously untested CFD code (SolidWorks Flow simulation) and presents validation outcomes.

## Chapter 2 Literature Review

### 2.0 Introduction

Chapter 1 has outlined how a ‘Hydrogen Economy’ (Rifkin, 2002) can facilitate the transition from fossil fuel dependence. It is the prospect of a hydrogen economy and the potential to reduce carbon emissions on a global scale that is the catalyst for research into the infrastructure that will support it. This thesis is safety focused and considers passive hydrogen removal from confined spaces, be that a ventilated fuel cell enclosure or the spaces between nuclear storage boxes where gas can become trapped. This research therefore adds to the hydrogen safety knowledge base and supports passive ventilation hydrogen safety in two safety-engineering fields.

This literature review presents a critical assessment of the previous work of academics in and supporting this field of research, establishing the current position of the research space and the knowledge gaps. This review considers hydrogen use, safety issues and background research relating to the nuclear and fuel cell industries. Research into hydrogen releases in enclosures of various scales is considered with a focus on smaller scale enclosures. The difference between *natural ventilation* and *passive ventilation* [involving a buoyant gas in confinement] is outlined followed by an overview of the types of ventilation openings previously tested in this field. Environmental and theoretical factors that influence gas flow in an enclosure are explained.

Computational fluid dynamics (CFD) numerical modelling has been widely used in hydrogen safety research. CFD codes have been used to investigate hydrogen dispersion behaviour in a variety of test scenarios. This review of previous work also looks at how CFD has been used in enclosure research and the modelling of buoyant gas behaviour. ANSYS: Fluent is used routinely in hydrogen research projects. SolidWorks Flow Simulation CFD is untested in the field of hydrogen dispersion from enclosures, other than in this thesis. The assessment of previous CFD studies informs the design of the CFD investigation in this thesis. The broad review of literature presented has pointed towards where the research gaps exist both empirically and with CFD modelling. Figure 2.1 presents a literature review road map presenting the research path that has been taken to identify knowledge gaps and areas for new research.

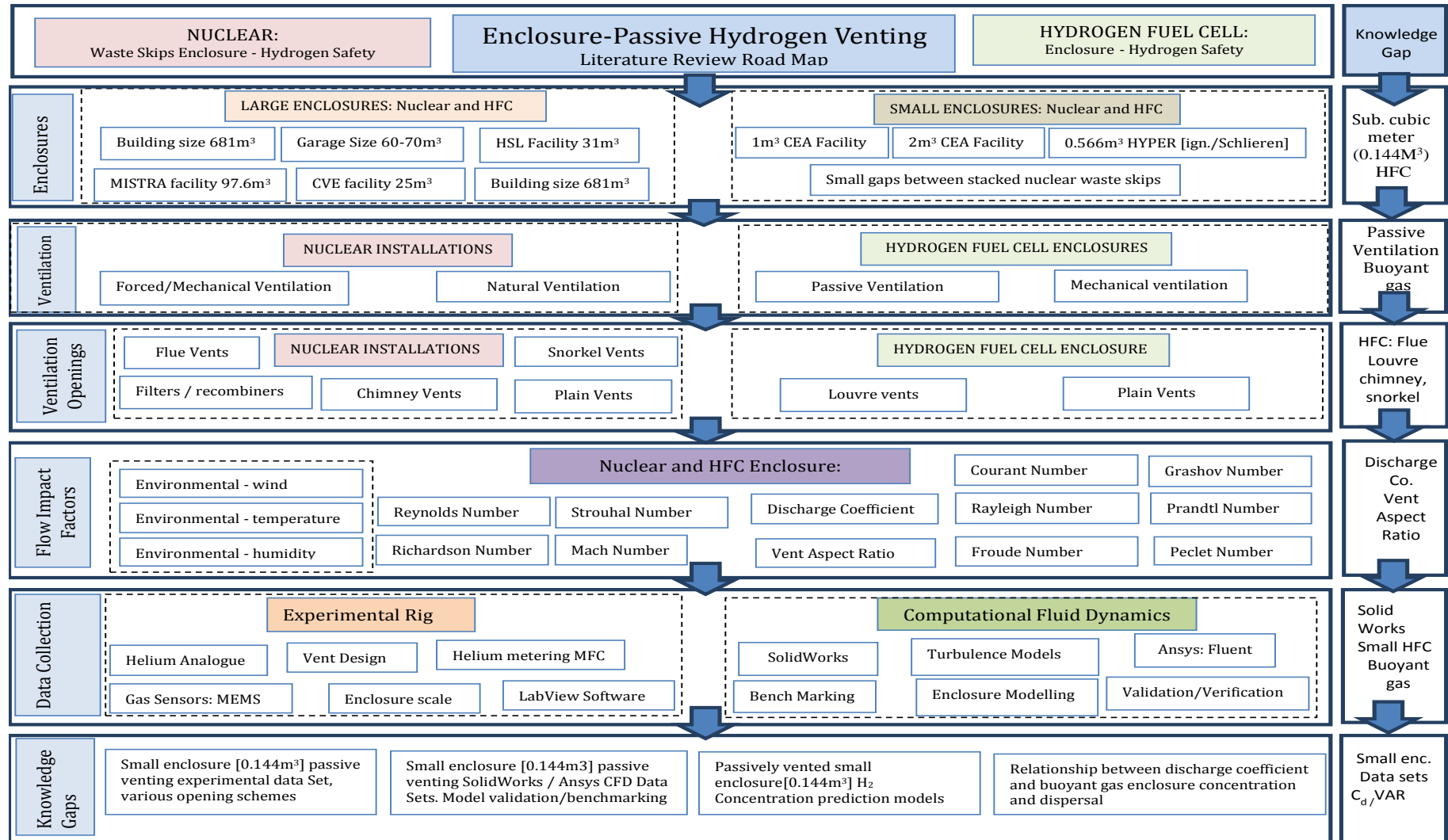


Figure 2.1 Literature review roadmap

## 2.1 Hydrogen

Hydrogen is a non-toxic, colourless and odourless diatomic gas at standard temperature and pressure and is the most abundant element in the universe. On Earth it is rarely found as monatomic elemental hydrogen, since it readily forms compounds with other elements through covalent ‘hydrogen bonds’, such as with oxygen to form water (H<sub>2</sub>O). Hydrogen at a density of 0.0899 kg m<sup>-3</sup> (at STP) is the lightest gas and is significantly lighter than air at 1.225 kg m<sup>-3</sup>. A hydrogen molecule (H<sub>2</sub>) comprises only two protons and two electrons, held together by a covalent bond. The light hydrogen molecules have a higher velocity than any other gas and similarly diffuse faster (at similar temperatures and pressures). Hydrogen, at fourteen times lighter than air will rapidly disperse into the surrounding air should a leak occur. Hydrogen’s wide flammable range (4 – 75 %) means that controlling the accumulation of hydrogen in enclosures is important. Even at low concentrations, buoyant pockets and flows can form which require management (Hawksworth et al. (2014)).

An effective way of dispersing hydrogen is the use of natural ventilation processes. In enclosure scenarios this is referred to as passive ventilation, due to the influence of the buoyant gas on flow conditions. For example, passive ventilation is used in nuclear scenarios to manage nuclear skip ullage hydrogen concentrations at below 25% of the LFL (Hawksworth et al. (2014)). This hydrogen is produced through corrosion processes (metals present in the waste) and/or radiolysis of water present in the skips. It is also applicable to hydrogen leaks from fuel cells housed in enclosures at various scales.

### 2.1.1 Hydrogen economy generated research

The transition towards a ‘Hydrogen Economy’ has been the motivation for an increase in hydrogen research in recent decades. Hydrogen has the potential to meet most of our energy and heat requirements. Intergovernmental pressures and global targets to reduce greenhouse gas emissions to abate climate change have led to significant investment in research and development in alternative sources of energy. Hydrogen is favoured as it is regarded as having the potential to replace oil and gas for heat and transport (Marban 2007). Although not Hydrogen Economy related, hydrogen safety research has also been ongoing in the nuclear industry due to the significant dangers it presents. Using surplus

nuclear energy to generate hydrogen though is a supporting consideration. Nuclear is not sustainable energy but is regarded as low carbon. As such, its use to produce hydrogen is a viable proposition.

Hydrogen fuel cells will play a significant role in this transition. Hydrogen can be produced through electrolysis of water from surplus electricity generated by intermittent renewables, such as solar PV and wind (Ekins 2009). It is also produced commercially from the steam reforming of methane. When required, electricity can be produced again through a chemical process in a hydrogen fuel cell. Hydrogen fuel cells can be scaled from low power transportable units to medium sized domestic CHP units, through to large MW scale commercial generators. They are also now powering cars, buses, trams and trains (Moreno Bonito 2017).

Many hydrogen economy research projects have been run over the past decade. They have focused on research that supports the transition from fossil fuels to renewables using hydrogen as the supporting energy vector. These research projects have covered areas such as hydrogen production and purity, storage, transportation, hydrogen fuel cells, hydrogen for heat and hydrogen safety. Hydrogen safety covers the management of hydrogen in all the above areas, as well as investigations into hydrogen dispersal in enclosures. The following organisations and projects have led on this research;

1. FCH-JU: The Fuel Cells and Hydrogen Joint Undertaking is a European public private partnership supporting research, technological development and demonstration activities in fuel cell and hydrogen energy technologies ([www.fch.europa.eu](http://www.fch.europa.eu)).
2. HYPER (EC Funded (FCH-JU)): A three-year project to develop unique, flexible and fully integrated fuel cell and storage system for portable power applications.
3. SUSANA (SUpport to SAfety aNAlysis of Hydrogen and Fuel Cell Technologies (FCH-JU)): “CFD model evaluation protocol (MEP) for safety analysis of hydrogen and fuel cell technologies”. SUSANA’s remit was to critically review the state-of-the-art in physical and mathematical modelling of phenomena and

scenarios relevant to hydrogen safety, i.e. releases and dispersion, ignitions and fires, deflagrations and detonations, etc.; compile a guide to best practices in use of CFD for safety analysis of FCH systems and infrastructure; update verification and validation procedures; generate database of verification problems; develop model validation database; perform benchmarking; and finally create the CFD model Evaluation Protocol built on these documents and project activities (<http://www.fch.europa.eu/project/support-safety-analysis-hydrogen-and-fuel-cell-technologies>).

4. HYSAFE: The international association for hydrogen safety, which aims to facilitate the international coordination, development and dissemination of hydrogen safety knowledge by being the focal point for hydrogen safety research, education and training. It is a consortium of 25 partners including research organizations, governmental agencies, universities and industry. They run the annual International Conference on Hydrogen Safety (<http://www.hysafe.info>).
5. HySAFER: Hydrogen Safety Engineering and Research: The centre, based at Ulster University, is carrying out research, consultancy, knowledge and technology transfer in the safety of hydrogen as an energy carrier and fuel cell technologies. The group is led by the renowned Professor Vladimir Molkov, an expert in hydrogen and fire safety science ([www.ulster.ac.uk/research/built-environment/hydrogen-safety-engineering](http://www.ulster.ac.uk/research/built-environment/hydrogen-safety-engineering)).
6. H<sub>2</sub>FC – European Research Infrastructure Project: Integrating European Infrastructure to support science and development of Hydrogen- and Fuel Cell Technologies towards European Strategy for Sustainable Competitive and Secure Energy. Finished in 2015 (<http://www.h2fc.eu/portal.html>).
7. H<sub>2</sub>FC Supergen – The Hydrogen and Fuel Cell Research Hub: The hydrogen and fuel cells SUPERGEN is funded by the Research Councils UK Energy Programme, as part of the government’s Sustainable Power Generation and Supply initiative. It was set up in 2012 to address challenges facing the hydrogen and fuel cell sector as it strives to provide cost competitive, low carbon



technologies in a more secure UK energy landscape (<http://www.h2fcsupergen.com/about>).

8. HyIndoor: The HyIndoor project addresses the issue of the safe use of HFC systems. It aims to provide scientific and engineering knowledge for the specification of cost-effective means to control hazards and to develop state of the art guidelines. It aims to specify practical means and strategies that will prevent or mitigate the potential consequences of a hydrogen release indoors (<http://www.hyindoor.eu/>).

Government and EU supported research projects have taken the lead in work that contributes to the transition to more sustainable development in Europe by facilitating the safe introduction of hydrogen technologies and applications (HySafe.org 2017). The EC funded HySafe project endeavoured to draw together knowledge and experience from various research and industrial fields such as gas, oil and nuclear.

Hydrogen safety research has previously centred on mitigation techniques in the nuclear industry but is now confronting issues associated with use by the public (HySafe.org 2017). HySafe has drawn together research organisations, government agencies, universities and industrial partners from around the world to break new ground in the field of hydrogen safety research to increase public acceptability.

To help demonstrate the potential of hydrogen as an energy carrier, with fuel cells as the energy converter, the EU funded 'Fuel cells and hydrogen Joint Undertaking (FCH-JU) started the HYPER project, with the objective to develop to market readiness, by 2020, a portfolio of clean, efficient and affordable hydrogen solutions ([www.fch.europa.eu](http://www.fch.europa.eu) (2015)). The HYPER projects focus was an integrated hydrogen power pack for portable and stationary applications.

Other prominent European projects are HyIndoor (Hydrogen energy applications for use indoors), HySAFER (Hydrogen safety research-Ulster University), H2FC Supergen (A UK research hub connecting industry and academia) and the H2FC European Infrastructure which provided free access to European hydrogen and fuel cell research

centres e.g. The CEA (The French Alternative Energies and Atomic Energy Commission) GEMELAN facility.

N. ERGHY (Research on fuel cells and Hydrogen), represents European Universities and research institutes together with Hydrogen Europe and the European Commission. Other active bodies are the European Hydrogen and Fuel Cell association (EHA), H2FC (Research Councils UK funded) and Hydrogen London, supported by the Mayor for London. As the titles of some of these agencies indicate, safety is a major focus in the development of and transition to a hydrogen economy.

The behaviour of hydrogen in an enclosure has been the subject of several work packages undertaken by the above organisations. Enclosure scenarios are a common theme where hydrogen fuel cells are expected to be present. These include building scale investigations, covering releases in commercial or domestic situations. As fuel cell vehicles are expected to become widespread and potentially housed in a garage, a number of garage scale tests have been conducted.

Smaller scale, 1 cubic meter sized, enclosures have also been investigated, which will house stationary and transportable fuel cells. Table 2.1 provides a summary of recent literature examining hydrogen dispersal in enclosures of various scales. An enclosure of 0.144m<sup>3</sup> scale or similar, used for small hydrogen fuel cells, has not been tested in other hydrogen safety investigations.

**Key points informing this research thesis:**

- Hydrogen dispersal takes places through diffusion and buoyancy, and can also be momentum driven e.g. via the jet from a leak
- Passive ventilation can displace hydrogen from an enclosure, its effectiveness determined by the ventilation scheme applied
- Hydrogen economy has generated new research into hydrogen
- Many investigations into hydrogen dispersal in large-scale confinement
- Passive hydrogen venting from small enclosures is an important research area

**Table 2.1 Recent literature examining hydrogen dispersal in enclosures**

Date	Author	Title	Enclosure
2009	Barley and Gawlick	Buoyancy-driven ventilation of hydrogen from buildings:	Garage scale
2009	Matsuura k	Effects of the geometrical configuration of a ventilation system on leaking hydrogen dispersion and accumulation	Garage scale
2010	Venetsanos et al	Laboratory test and model validation	681m <sup>3</sup>
2010	Zhang, Venetsanos	Numerical studies of dispersion and flammable volume of hydrogen in enclosures	INERIS
2010	Papanikolaou et al	HySafe SBEP-V20: Numerical studies of release experiments inside a naturally ventilated residential garage	Garage
2010	Cerchiara G	Hydrogen and fuel cell stationary applications: Key findings of modelling and experimental work in the HYPER project	CVE Facility
2010	Friedrich A	Hyper experiments on catastrophic hydrogen releases inside a fuel cell enclosure	560l
2010	Prasad. Pitt	Effect of wind and buoyancy on hydrogen release and dispersion in a compartment with vents at multiple levels	108m <sup>3</sup>
2011	Merilo et al	Experimental study of hydrogen release accidents in a vehicle garage	Garage
2011	Bernard-Michel	Helium release in a closed enclosure: Comparison between simple models, CFD calculations and experimental results	Small 1m <sup>3</sup>
2011	Cariteau et al	Experiments on the distribution of concentration due to buoyant gas low flow rate release in an enclosure	Garage size
2011	Cariteau et al	Experimental results on the dispersion of buoyant gas in a full scale garage from a complex source	Garage size
2011	Papanikolaou et al	CFD simulations on small hydrogen releases inside a ventilated facility and assessment of ventilation efficiency [HYPER Project]	CVE Facility
2011	Venetsanos et al	On the use of hydrogen in confined spaces: Results from the internal project InsHyde [HySafe project]	Garage size
2011	Prasad. Pitt	A numerical study of the release and dispersion of a buoyant gas in partially confined spaces	Scaled garage
2011	William M Pitts et al	Helium dispersion following release in a 1/4-scale two-car residential garage	Scaled garage
2012	Visser et al	Validation of a FLUENT CFD model for hydrogen distribution in a containment	THAI Vessel
2012	Cariteau et al	Experimental study of the concentration build-up regimes in an enclosure without ventilation	Small 1m <sup>3</sup>
2013	Cariteau et al	Experimental study of the effects of vent geometry on the dispersion of a buoyant gas in a small enclosure	Small 1m <sup>3</sup>
2014	Srinivasa Rao Ravva	CFD code benchmark against the air/helium tests performed in the MISTRA facility	MISTRA
2014	Hawksworth et al	Large scale passive ventilation trials of hydrogen	40m <sup>3</sup>
2014	Giannissi S	CFD benchmark on hydrogen release and dispersion in confined, naturally ventilated space with one vent [HyIndoor Project]	Small 1m <sup>3</sup>
2014	Molkov et al	Passive ventilation of a sustained gaseous release in an enclosure with one vent	Small 1m <sup>3</sup>
2014	Molkov et al	Numerical and physical requirements to simulation of gas release and dispersion in an enclosure with one vent	Small 1m <sup>3</sup>
2014	Giannissi S	Mitigation of buoyant gas releases in single-vented enclosure exposed to wind: Removing the disrupting wind effect	Small 1m <sup>3</sup>
2015	Yassine Hajji	Natural ventilation of hydrogen during a leak in a residential garage	Garage
2015	Giannissi S	CFD benchmark on hydrogen release and dispersion in a ventilated enclosure: Passive ventilation[H2FC Project]	31 m <sup>3</sup> HSL
2016	Hoyes	CFD modelling of hydrogen stratification in enclosures: Model validation and application to PAR performance	MISTRA test
2016	Bernard-Michel	Comparison of hydrogen and helium releases in 1m <sup>3</sup> and 2m <sup>3</sup> two vent enclosures:	Small 1m <sup>3</sup>
2016	Jiaqing He et al	Assessment of similarity relations using helium for prediction of hydrogen dispersion and safety in an enclosure	Scaled garage
2016	Dadashzadeh	Dispersion modelling and analysis of hydrogen fuel gas released in an enclosed area: A CFD-based approach	Garage size
2016	Aneesh Prabhakar	Experimental investigation on helium distribution and stratification in unventilated vertical cylindrical enclosure –	2m <sup>3</sup>
2017	Baraldi, Molkov	Development of a model evaluation protocol for CFD analysis of hydrogen safety issues the SUSANA project	Small 1m <sup>3</sup>

### 2.1.2 Hydrogen fuel cell deployment

Globally, fuel cell shipments have grown at 15 % by MW and 37 % by unit per year from 2012 to 2017, led by the stationary sector (Figure 2.2(a) (E4tech, 2017)). There have been 230,000 fuel cell micro-CHP installations so far in Japan (Cogen-Europe, 2015), with many more in the USA and South Korea.

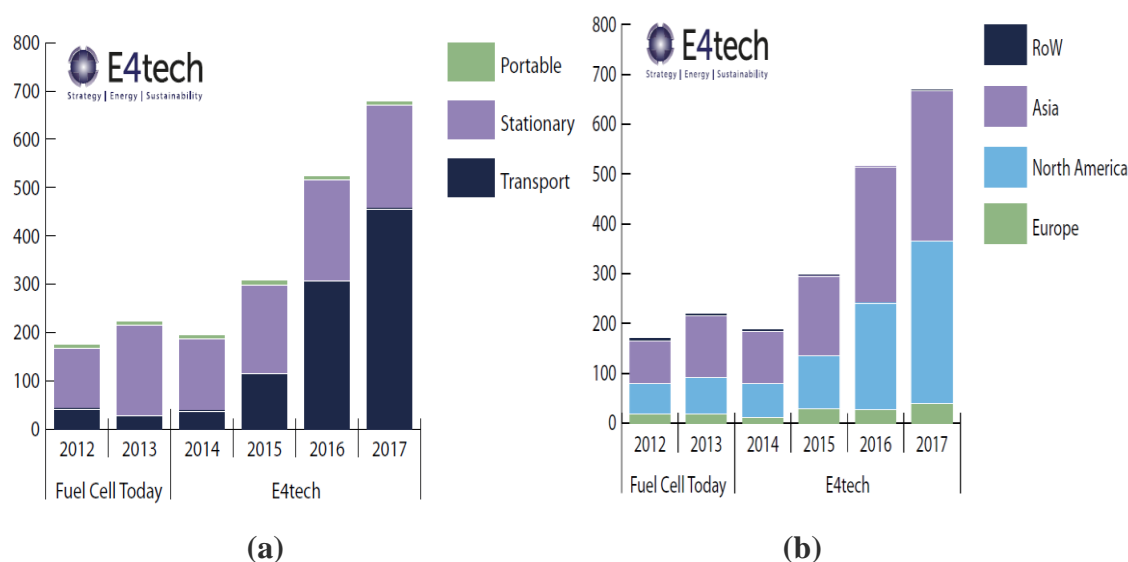


**Figure 2.2 HFCs per MW shipped (a) by application (b) by region (E4tech, 2017)**

This growth is encouraging, but Europe is lagging in delivering this low carbon technology (Figure 2.2 (b)). Micro-CHP units for domestic use have seen significant growth in Japan, with some units also sold in South Korea. Europe though is not achieving significant market diffusion. (Figure 2.3 Dodds et al., 2014).

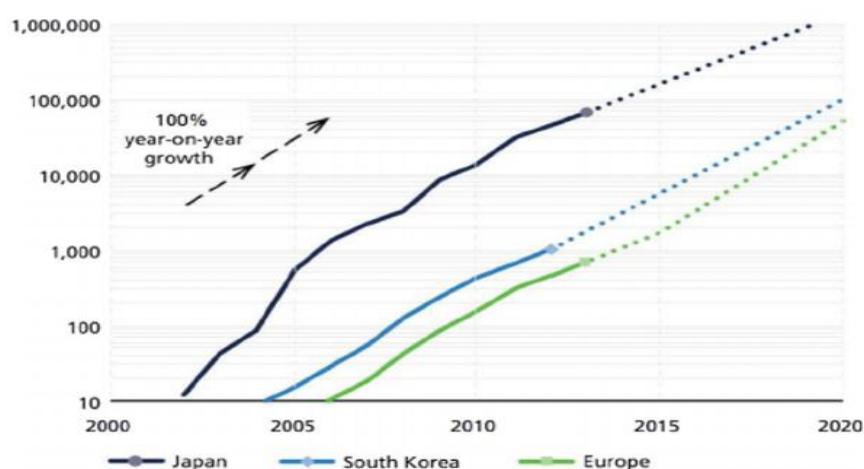


**Figure 2.3 Cumulative number-fuel cell micro-CHP systems deployed (Dodds 2014)**

Portable, small stationary HFCs and domestic CHP units will be housed in small protective enclosures. Figure 2.2(a) shows how small the uptake of portable HFCs has been and Figure 2.2(b) how Europe is trailing the rest of the world. This is partly a reflection on Europe's readiness for hydrogen and on confidence in hydrogen safety. Despite the many European research projects into hydrogen, this is not so far manifesting itself in EU HFC sales. Research that supports fuel cell deployment, raising confidence in hydrogen safety, whether for micro CHP or small portable units, will improve this.

A hydrogen economy will not develop without research that supports it. BOC Ltd. are developing 'portable' sub 200W HFCs that are housed in enclosures, with a view to wider commercialisation. This research investigation supports their objectives and safety case, by testing passive ventilation schemes in a small enclosure to BOC Ltd. specifications (0.144m<sup>3</sup> enclosure). Establishing the safety parameters for their enclosure will support safety certification, and provide confidence in its performance, leading to greater sales.

### 2.1.3 Hydrogen safety

Hydrogen's properties have been described above. Its wide flammable range, buoyant behaviour and diffusive nature make it a very challenging gas to manage in both nuclear and hydrogen fuel cell scenarios.

**Nuclear:** A mature global nuclear energy industry has developed over the past sixty-five years, leaving a legacy of contaminated plant and radioactive waste. Sellafield Ltd. manages the safe decommissioning of the UK's nuclear legacy. Sellafield Ltd. is a co-sponsor of the London South Bank University 'Explosion and Fire Research Group' and also of this research to find new data, on passive hydrogen venting in confinement.

Sellafield Ltd. (now a subsidiary of the Nuclear Decommissioning Authority (NDA)) has responsibility for fuel recycling, specialist waste storage (low, high and intermediate level nuclear waste) and the management of radioactive emissions and potentially explosive hydrogen gas (<https://www.gov.uk/government/organisations/sellafield-ltd> (2018)).

In 1947, Sellafield Ltd. was announced as the new atomic energy site and construction work began on the Windscale nuclear piles with its two air-cooled reactors. By March 1952 the Windscale reactors were operational, producing Plutonium. A plant to separate Uranium and Plutonium from used fuel also became operational. In 1956, the first of four commercial nuclear reactors opened at Calder Hall generating electricity until 2003.

In the 1990s, Sellafield Ltd. began construction of facilities to treat and dispose of waste from commercial and decommissioning operations. The Magnox Encapsulation Plant (MEP) dealing with intermediate level waste and the Waste Encapsulation Plant (WEP) became operational. The 'Vitrification Plant', converts high-level waste into an immobile solid for, long-term storage. In 2011/12 Windscale became the first UK nuclear reactor to be decommissioned and nuclear fuel was retrieved from a legacy storage pond for the first time in over sixty-years.

The management of spent fuel, contaminated plant and treated waste is a major concern for Sellafield Ltd. Hydrogen is continually produced in storage containment and must be removed to stop flammable concentrations forming. Most Sellafield Ltd. installations use mechanical ventilation systems with their associated concerns. Sellafield Ltd. would like to broaden the use of Passive Ventilation schemes, as a resilient back-up system in the event of a power failure on site. However, demonstrating that the predicted flows will occur and persist, in the event of foreseeable changes such as temperature or a combination of diffusion and buoyancy is a concern, with research required to raise confidence in the underpinning knowledge base and available predictive models.

**Hydrogen Fuel cell:** Hydrogen fuel cells produce 'clean' energy with no carbon emissions and only water and heat as by-products. William R Grove first published his fuel cell concept in 1838, using hydrogen and oxygen to produce a voltage (Grove, W. 1838). Although other scientists showed interest in the concept, a hundred years passed before significant steps were made in hydrogen fuel cell development.

The first high profile use of fuel cells was in the U.S.A.'s space program, where they were used to supply electricity and drinking water, the hydrogen and oxygen being sourced

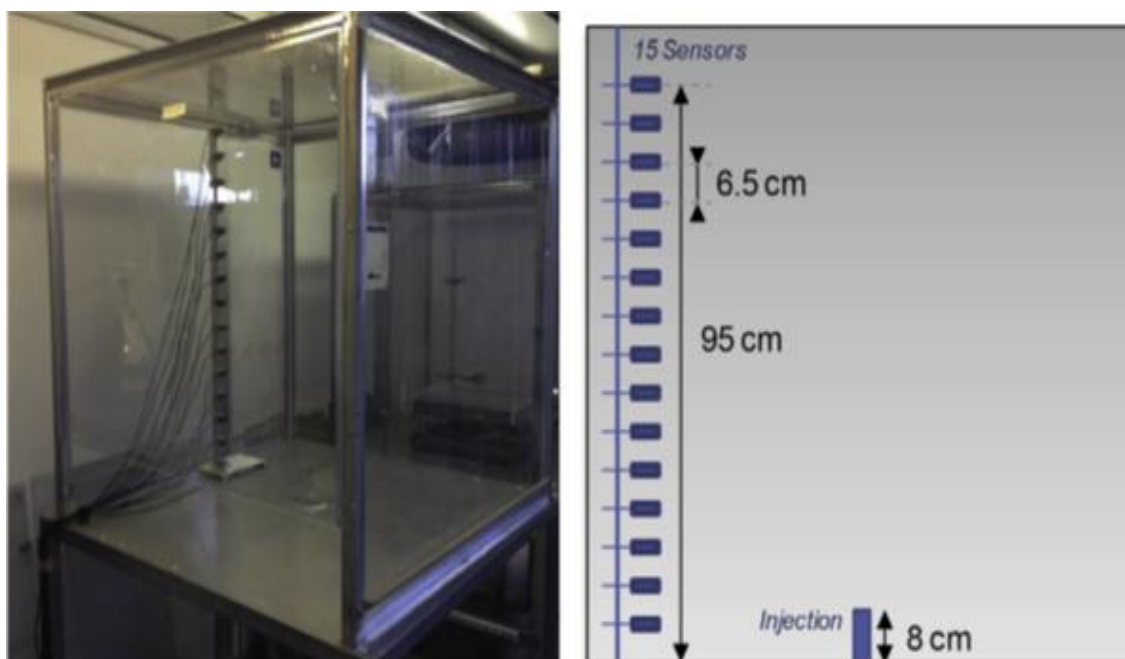
from the fuel tanks ([https://www.nasa.gov/centers/glenn/technology/fuel\\_cells.html](https://www.nasa.gov/centers/glenn/technology/fuel_cells.html)). Recent decades have seen a growth in interest in hydrogen as an energy carrier.

Fuel cells facilitate the electro-chemical conversion of hydrogen and oxygen to produce an electric current. They can operate up to a theoretical efficiency of 80% for electricity and heat, making them highly suitable to CHP applications (Volkart et al. 2017). There are many HFC applications, but this review focuses on those operating in enclosed conditions.

Hydrogen's wide flammable range is a safety concern, from production, storage, transportation through to final use in the fuel cell. The small hydrogen molecule will exploit any weak point, with leaks forming in supply pipework, joints or the fuel cell itself. Leaks can range from small diameter, slow releases from holes in delivery pipes to larger, high-volume releases from breaks in tubing from high-pressure storage tanks. The resulting hydrogen jet and the combustible cloud in the enclosure is a fire and explosion hazard (Schefer et al. 2008).

Batteries are also often present in the enclosure for storage of surplus electricity. When charging, these too can release small amounts of hydrogen (Baer 1996) adding to the dangers of a hydrogen leak. An explosive hydrogen mixture in confinement, as previously explained, has grave consequences should ignition occur. As with the nuclear hydrogen case, passive hydrogen removal is the preferred solution motivated by accident prevention and the need to understand hydrogen's behaviour in hazardous scenarios (Weiner 2014).

**Helium analogue:** For safety reasons it is not practicable to use hydrogen in significant quantities in the laboratory tests in this investigation. Its wide flammable range makes it difficult to manage in the laboratory, particularly in enclosure tests (Prasad et al. 2012). Helium, the next lightest element and a gas at STP, has very similar buoyancy characteristics to hydrogen but none of the safety concerns. As its buoyant behaviour is so close to that of hydrogen it is deemed to be a satisfactory analogue for hydrogen and is used widely in academic investigations, both nuclear and hydrogen fuel cell (See Chapter 3, Section 3.2).



(a) CEA GAMELAN 1m<sup>3</sup> enclosure (b) Enclosure Helium sensor schematic  
**Figure 2.4 CEA GAMELAN facility and schematic (Bernard-Michel et al. (2016))**

Bernard-Michel et al (2016) used the CEA GAMELAN facilities 1 and 2 cubic meter test rigs (Figure 2.4) to compare the behaviour of helium and hydrogen in a small enclosure. They used nozzle leak rates of 5 to 210 NL min<sup>-1</sup> and nozzle diameters of 4 and 27mm for helium and 5.2 NL min<sup>-1</sup> to 128 NL min<sup>-1</sup> for hydrogen. These values correspond to a volume Richardson number range from 800 down to  $1.1 \times 10^{-4}$ , and cover conditions from plume up to a jet release from the nozzle. The volume Richardson number is;

$$R = g'_{0,gas} \frac{H}{U_0^2} \quad [1]$$

*H* is the height of the cavity (m)

*U*<sub>0</sub> is the injection velocity (m s<sup>-1</sup>)

*g'* is reduced gravity (m s<sup>-2</sup>)

Figure 2.5 presents Log<sub>10</sub> (Richardson number) against the leak rate. For a Richardson number below 0.1, the flow rate is almost a pure jet. The transition between a jet and a plume occurs in the Richardson range 0.1 to 10. For numbers above 10 the flow behaves like a pure plume. They inferred that with a (low velocity) plume release helium is a good analogue for hydrogen, which only breaks down when the flow turns into a jet at the nozzle exit.



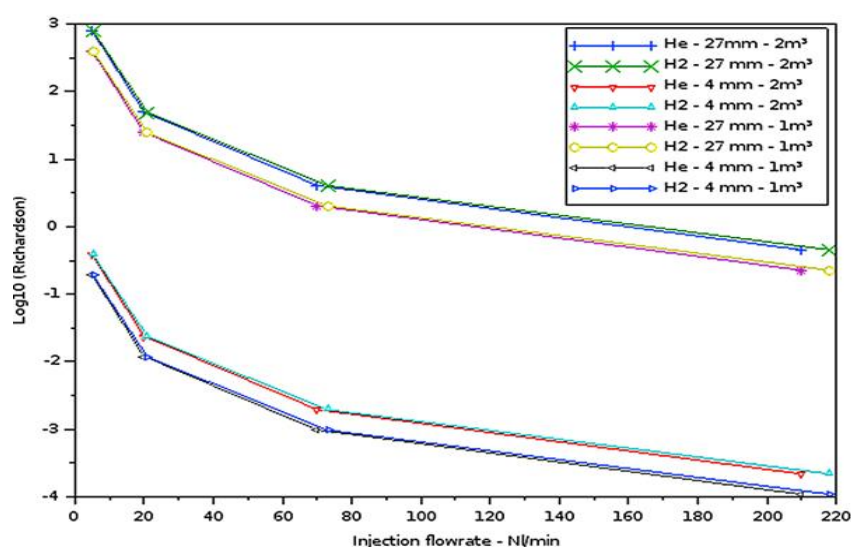


**Figure 2.5 Richardson numbers-Hydrogen and Helium (Bernard-Michel (2016))**

Figure 2.6 shows hydrogen and helium concentrations for the Bernard-Michel tests. The test results are similar but with about a 1 percentage point discrepancy at steady state. Low velocity plume releases provided the best correlation. There is a difference in buoyancy flux between hydrogen and helium for a given flow rate. This was though found only to be an issue at vent openings and the leak source. Many studies, as noted in this review show helium to be a good analogue for hydrogen. This research project will use helium flow rates from 1-10 lpm with a 4 mm nozzle diameter, which equates to nozzle velocities from 1.3 to 13.3 m s<sup>-1</sup>. Figure 2.7 presents the helium velocity range at these leak rates (using equation 2).

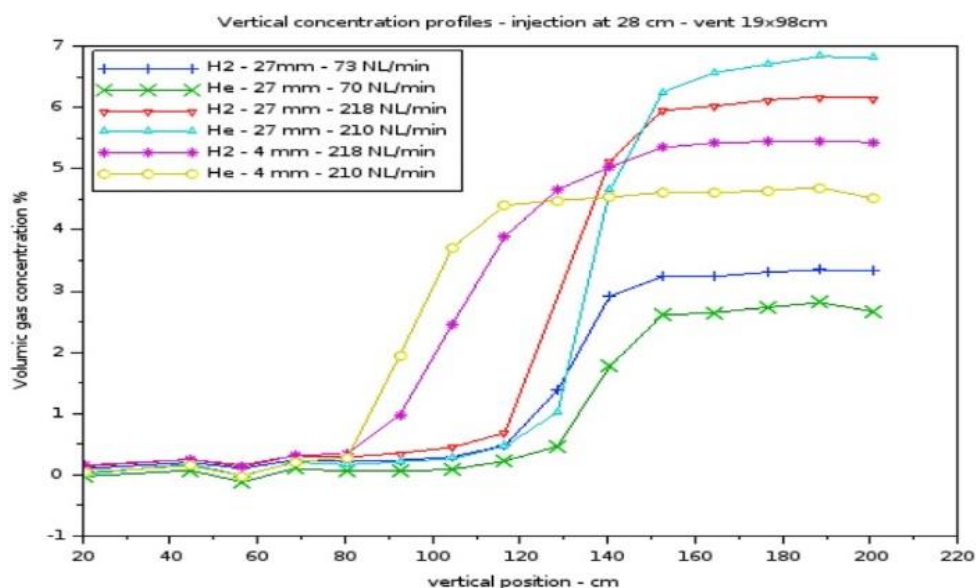


**Figure 2.6 Comparison of Helium and hydrogen concentrations – 2m<sup>3</sup> single vent enclosure (Bernard-Michel et al (2016))**

$$v = \frac{4.Q}{\pi d^2} \quad [2]$$

$v$  is the velocity ( $m s^{-1}$ )

$Q$  is the volume flow rate ( $m^3 s^{-1}$ )

$d$  is the nozzle diameter (mm)

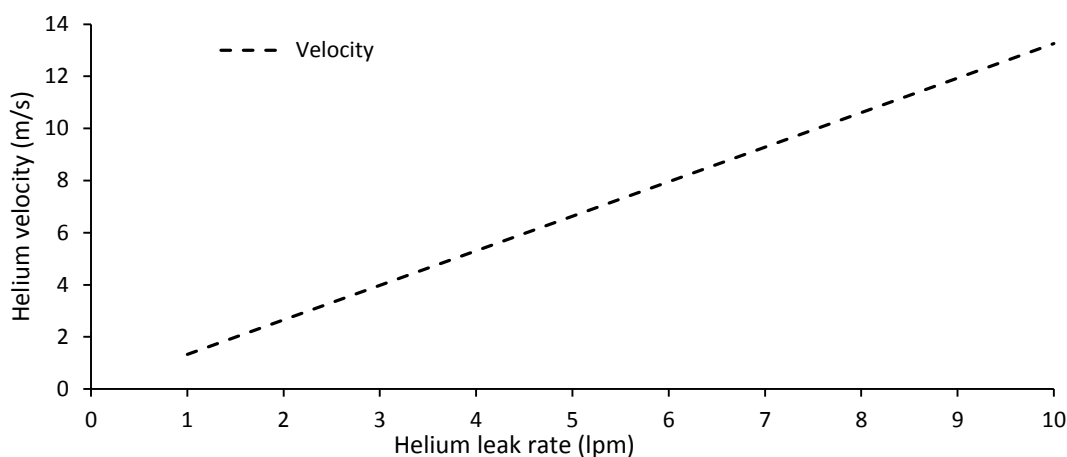


**Figure 2.7 presents the helium velocity for a given leak rate at the nozzle**

Following Bernard-Michel et al., the release characteristics at the lower leak rates will be in jet/plume transition, tending towards a plume. Helium behaviour will be closer to that of hydrogen, further supporting helium's use of in this investigation. This study is looking at the behaviour of a buoyant gas in a passive ventilation scheme in a small enclosure. Helium meets these requirements and is sufficiently close to hydrogen's characteristics to be an effective analogue. Helium has been widely used in enclosure dispersal tests [Swain (2002), Gupta (2009), Cariteau (2010), Papanikolaou (2010), Venetsanos (2010), Cariteau (2011), Prasad (2011), Cariteau (2012), Molkov (2014), Prabhakar (2016) He (2016)] and is in effect now a standard used to replace hydrogen in laboratory testing.

**Key points informing this research thesis:**

- Fuel cell deployment/commercialisation is growing annually
- Europe is lagging behind, particularly in small HFC/micro-CHP market
- Focus of hydrogen safety research has moved to the hydrogen economy
- Helium is a satisfactory analogue for hydrogen in buoyancy/dispersal scenarios

## 2.2 Enclosures: Enclosure hydrogen confinement ventilation research

Natural ventilation has been used for thousands of years to drive the flow of fresh air through buildings to create a safer and healthier internal environment. The displacement of stale and contaminated air with fresh external air was the basis of air management and thermal control in buildings, as demonstrated by the Badgir ‘wind catcher’ shown in figure 2.8. Understanding how the driving forces of wind (positive and negative pressure differentials) and temperature (convective and buoyant flows) affect internal conditions provides an important passive control mechanism for enclosed areas.

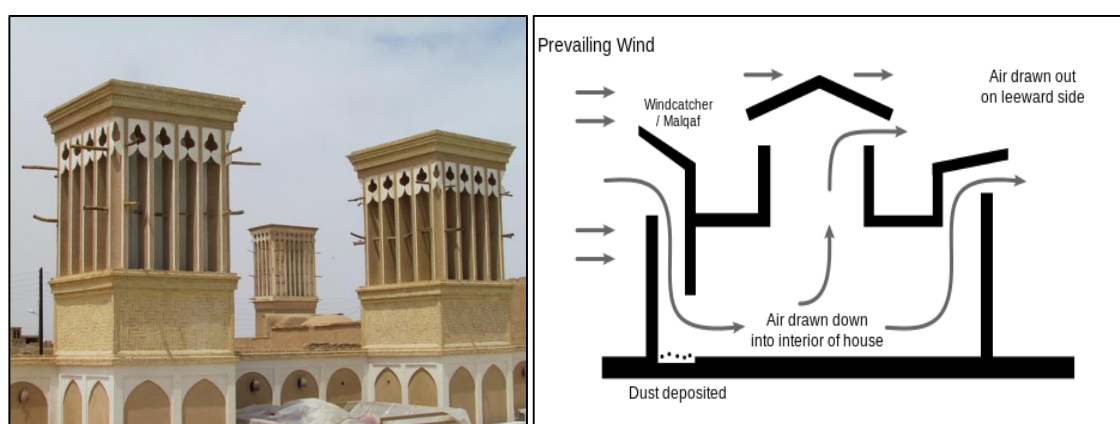


**Figure 2.8 Iranian Badgir ‘wind catcher’/schematic (flickr.com-2016)**

Academic research over the past 50 years has developed the theory of natural ventilation in buildings. As fuel cell research has progressed, these theories have been developed to account for the presence of a buoyant gas in the enclosure. Early work by Brown and Solvason (1962) developed the theory of natural convection across openings in vertical and horizontal partitions to include both heat and mass transfer. Their experiments used large *heat flow* apparatus, with air as the convecting fluid and ventilation openings from 3 to 12 inches long.

Baines and Turner (1969), in their ‘*filling box model*’ experiments, examined the release of a buoyant fluid in an enclosure. Their experimental work consisted of supplying a *salt solution* at a steady rate via a nozzle, just below the surface of an aquarium holding fresh water. Dye was added to identify the plume. Their focus was the behaviour of the turbulent buoyant fluid in a bounded region. They found that a non-turbulent layer formed

at the bottom of the tank (stratification). Openings were not present in these experiments, as their investigation related to wider environmental buoyancy effects.

In the 1980s, Michael Epstein (Fauske and Associates) began a series of investigations into buoyancy-driven exchange (countercurrent) flow through openings in horizontal partitions in a 0.231m<sup>3</sup> water tank, to better understand airflow in buildings. In these *saltwater analogue* experiments, density-driven exchange flow was achieved by using a brine solution above the partition, with fresh water below. In his 1988 paper, he made flow measurements on single and double opening arrangements. With single openings, he identified four flow regimes developing, as the L/D ratio (Length/diameter of opening) increases;

1. Oscillatory exchange flow,
2. Bernoulli flow (Bernoulli's principle shows that, as the speed of fluid flow increases there is a reduction in pressure in the fluid. In Epstein's case (1988), it was derived that the channel fluid speed was determined by the pressure loss at the entrance and exit of the channel.),
3. Turbulent diffusion,
4. Combined Bernoulli flow and turbulent diffusion.

Epstein found that for all practical purposes the exchange flow rate was independent of viscosity in low flow conditions. This enabled a universal correlation between Froude number (dimensionless exchange flow rate) and L/D to be obtained. With two openings, both one way and countercurrent flows were observed.

In their 1989 paper, Kenton and Epstein extended the investigation of flow through horizontal openings, this time now looking at combined, buoyancy-driven and forced exchange flow, through the opening. Interestingly, the motivation of the research was said to be, to assess the movement of toxic gases and smoke through buildings. This time the brine in fresh water would simulate the movement of a light gas moving in a dense gas. The test was used to determine the magnitude of the forced flow required to purge the opening of the oppositely directed buoyant component, overcoming countercurrent flow.

Linden et al (1989) used a similar saltwater analogue 'filling box' methodology to better understand the fluid mechanics of natural ventilation in buildings. He identified two

distinct regimes of ventilation flow where density difference and buoyancy are the driving forces where wind forces are absent; mixing ventilation and displacement ventilation;

1. Mixing ventilation occurs via a single upper vent, with bi-directional flow, where the incoming fluid mixes with the fluid in the space, producing an approximately uniform concentration throughout the interior of the enclosure with little or no stratification present.
2. Displacement ventilation, via two vents, one located near the top and one near the bottom of the enclosure, occurs where the incoming fluid (lower vent) displaces the interior fluid through high-level opening, with one directional flow. Strong stratification is evident, with little mixing of the two fluids.

Linden et al (1999), still using a saltwater analogue, extended the investigation looking at displacement ventilation when buoyancy forces are reinforced by wind forces. Strong stable stratification developed and the rate at which the enclosure drained was increased as the wind induced pressure differential increased.

Swain and Swain (1992) reported a novel investigation into hydrogen safety. They were modelling flammable gas clouds formed by residential gas leaks. Their early use of CFD required the setting of a leak rate boundary condition as the source of the gas cloud. Their interest was hydrogen, but they conducted empirical tests with methane and propane too for comparison. The experimental data was used in the computer model to predict the size and motion of the cloud in residential kitchens. Swain et al continued their work with CFD modelling of hydrogen, set out in section 2.5. This work signaled a connection between hydrogen releases and buildings, relevant to hydrogen economy infrastructure.

Epstein and Burelbach (1999) used a  $0.587\text{m}^3$  water tank to conduct saltwater analogue tests, motivated by flammable gas concerns in the ullage space of certain process waste storage tanks. This was early research into the problem of hydrogen production in nuclear waste storage skips, as Epstein was working with Fauske and Associates Inc, who specialise in nuclear research.

Previous experiments on density-gradient driven vertical mixing had been carried out in high ‘aspect ratio’ tubes or columns. The geometry of the mixing region in the shallow ullage space of the waste tank is of low aspect ratio, so this investigation set out to establish the mixing length in these conditions. It is interesting to note how Epstein’s work developed using the same experimental process, from natural ventilation flows of air in buildings to the movement of toxic gases and smoke through buildings to here looking at hydrogen in confinement in a nuclear scenario. It demonstrates the close link with hydrogen dispersal in the two fields.

There seems to have been a period in the early 2000s where the threat of climate change was becoming more apparent and the need to move away from fossil fuel became more urgent. Nuclear safety research, as stated earlier, had been the main driver for investigating hydrogen behaviour in confinement and passive hydrogen venting. As the possibility of using hydrogen as a new energy vector became more of a reality, research to support its use accelerated. In this period, there was an increase in investment for hydrogen research programmes as noted in section 2.1.1.

These research programmes and others have endeavoured to extend knowledge around hydrogen production, storage, transportation and its final use, either in a fuel cell or in combustion for heat. Safety at all stages of the hydrogen economy support infrastructure has been considered, including CFD modelling of hydrogen dispersion. Reinecke et al (2011) produced a useful review of HySafe experimental facilities and hydrogen safety investigations undertaken up to that point. An outcome was broad interest in the use of mini-katharometer gas sensors for gas concentration recording.

This research investigation neatly supports this international undertaking by researching the behaviour of hydrogen in a 0.144 m<sup>3</sup> passively ventilated fuel cell enclosure, to raise confidence in safety and promote commercialisation of small stationary fuel cells. Enclosure research in this new era of hydrogen fuel cell work has operated at various enclosure scales, which will now be considered. Enclosure scale is an important consideration when dealing with a hydrogen leak as the enclosed volume will influence the hydrogen concentrations achievable.

**Key points informing this research thesis:**

- Development of passive ventilation modelling for buoyant gas
- Definitions of mixing and displacement ventilation
- Small scale enclosure tests (dispersal and single vent)
- Mini-katharometer gas sensors used in tests with helium analogue

**2.2.1 Large scale enclosures (garage scale and above)**

Research into passive hydrogen removal from enclosures is motivated by accident prevention and the need to understand hydrogen's behaviour in hazardous scenarios (Weiner 2014). A hydrogen leak can be followed by the evolution of a hydrogen-air cloud that if within the flammable mixture range has the potential for ignition, fire or deflagration with thermal/pressure effects that can threaten life and property. Confinement scenarios have more serious outcomes since significant explosion overpressures can be developed (Molkov 2012).

Fuel cell enclosure hydrogen leak scenarios are well matched to hydrogen leaks in nuclear enclosure scenarios, in terms of the conditions and likely outcomes. Empirical data and prediction modelling produced for fuel cell enclosures will have relevance to nuclear cases. This review focuses upon the hypothesis that passive ventilation concepts are relevant to hydrogen removal scenarios and its ability to manage gas concentrations. This section of the review will consider literature in the post 2000 period relating to hydrogen releases in larger enclosures.

Swain et al. (2002), continuing their work into hydrogen leaks in simple geometric enclosures, undertook an exercise aimed at the simplification of the hydrogen risk assessment method (HRAM), used to guide venting in buildings containing hydrogen fuelled equipment. The HRAM methodology applies four steps;

1. Simulation of the accident scenario with leaking helium,
2. Verification of a CFD model of the accident scenario using the helium data,
3. Prediction of the behaviour of hydrogen using the CFD model,
4. Determination of the risk from the temporal and spatial distribution of hydrogen.

Their aim was to demonstrate that (for simple enclosures) helium could be used as a direct analogue for hydrogen without the need for CFD. This is an interesting perspective, probably motivated by the computational expense of CFD at the time. CFD is now much more accessible and effective and a primary contemporary engineering tool. Swain modelled a half size garage with a leak rate of 120 lpm. A large vertical vent was modelled along with a 1 foot by 1 foot by 6-foot-tall chimney. They determined that because of the similarity of behaviour of hydrogen and helium in a simple geometry steps 2 and 3 could be replaced with a simplified process.

In 2007, Astbury of the Health and Safety Laboratory, UK, published a critique, considering the venting of low-pressure hydrogen gas. Astbury noted how the use of hydrogen in industrial processes was increasing and would increase further with its potential use as an energy carrier, in a hydrogen economy. Astbury states, “the venting of hydrogen is inevitable for almost all uses, and its propensity to ignite, makes it essential that safe venting regimes are understood”. Astbury’s focus was on ignition of vented hydrogen in proximity to buildings. The review considered ignition avoidance through, inerting, dilution, air purging and deliberate flaring. Astbury cited Swain and Swain (1992, 1996) noting that small leaks of hydrogen are so buoyant that they disperse with minimal flammable volumes even under passive ventilation in enclosed spaces.

In 2009, Barley and Gawlik published their often-cited paper *‘Buoyancy-driven ventilation of hydrogen from buildings: Laboratory test and model validation’*. They considered the effectiveness of using passive buoyancy driven ventilation to limit hydrogen concentrations at a safe level following a gas leak from a hydrogen-powered vehicle in a residential garage. The relationships between leak rates, ventilation design and hydrogen concentration were considered using laboratory tests and mathematical and CFD modelling. The enclosure was garage scale (82.5 m<sup>3</sup>) with helium used in the experimental tests at leak rates ranging from 9 to 50 lpm. Two vent openings were present in one end wall (32.4 cm wide x 24.3 cm high, and 2 metres vertically apart). Concentrations were obtained at 11 points in the enclosure through sampling. Fluent 6.3 CFD (implicit pressure-based solver, first order discretisation, RNG- $k\epsilon$  turbulence model) was used in a validation exercise with the test results. Figure 2.9 (a) provides a



results comparison, with CFD under predicting, but following the dispersal pattern and (b) a hydrogen and helium CFD comparison showing close correlation at low concentrations.

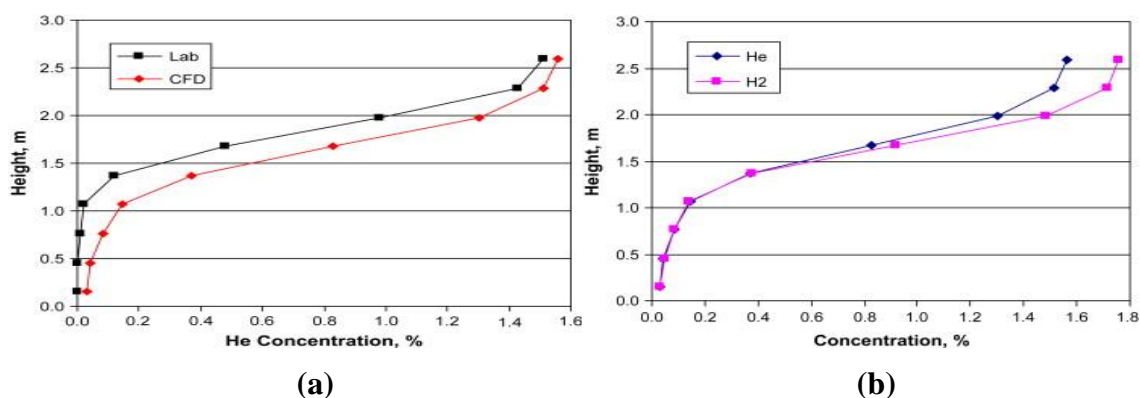


**Figure 2.9 (a) Comparison of CFD and helium test concentrations, (b) Comparison of CFD results for helium and hydrogen, (Barley and Gawlik 2009)**

In 2010, Venetsanos et al., reported on the findings of the InsHyde project (HySafe), which was investigating realistic small to medium sized indoor hydrogen leaks to provide guidance on the safe use and storage of hydrogen indoors. HySafe's 'Phenomena Identification and Ranking Table (PIRT) identified that hydrogen releases, even slow releases with small release rates, in confined or partially confined geometries represent a serious risk countering the earlier Swain and Swain citation. The CEA garage sized installation (78.5 m<sup>3</sup>) was used with helium as the buoyant gas to test leaks without ventilation. The releases were;

- 688 lpm, with a 20.7 mm diameter nozzle for 300 s
- 18 lpm, with a 5 or 29.7mm diameter nozzle for 3740 s

The project also conducted combustion tests and CFD modelling using the INERIS 6C code. These were not passive venting tests but clearly add to the body of knowledge. Their recommendations for further research included;

- Risk assessment studies examining realistic scenarios for a wide range of confined environments using validated CFD tools,

- Further hydrogen/helium dispersion experiments to test a wider range of conditions (release location, strength, direction, ventilation, obstructions, and inclined roof) including the effect of temperature gradients between confined space and outside environment.

In 2010, Venetsanos et al. also conducted helium dispersion experiments at a second CEA garage sized installation (41.2 m<sup>3</sup>). This garage was ventilated with two openings on a back wall. Helium was released from a 70 mm diameter nozzle, 210mm above the ground in a central position. Leak rates of 1 lpm and 0.03 lpm were tested for 8.3 h and 2.3 days. Helium concentrations were monitored using an array of thirty gas sensors (Xensor TCG 3880 mini katharometer), distributed in six vertical lines. Based on their findings they provided a definition of homogenous and stratified conditions. They defined *homogenous* as the condition when the concentration difference between the bottom and the top is much lower than the bottom concentration. If the concentration difference is much higher than the bottom concentration, then conditions would be considered *stratified*. CFD modelling with the ADREA-HF code was also conducted and found to be in good agreement with the helium dispersion experiments, with the only discrepancies found using the 0.03 lpm flow rate.

In 2011, a paper by Papanikolaou and Venetsanos et al., described how the HYPER project aimed to facilitate the safe introduction of stationary hydrogen and fuel cell systems, in various environments, through research and the development of a ‘public harmonised Installation Permitting Guidance (IPG) document. The paper focused upon an ADREA-HF CFD exercise, using data from previous experiments with natural and forced ventilation, carried out by UNIPI using the CVE facility. This facility was a 25 m<sup>3</sup> garage style enclosure with a 4.8 kW fuel cell installed. The leak was assumed at the valve of the inlet gas pipeline, just before the pressure reducer. The tests trialed several ventilation arrangements with the aim of limiting hydrogen concentrations to 50 % of the LFL. The IPG document was published by HSL for the HSE in 2009. A summary of IPG guidance where ‘enclosures’ are mentioned is provided below;

- Rooms or enclosures containing equipment should be fitted with measures to prevent a person from being accidentally trapped within it or, if that is impossible, with a means of summoning help.
- Ensure that any area, enclosure or housing etc. into which hydrogen may leak is designed to prevent the gas becoming trapped and is equipped with effective high and low-level ventilation openings.
- Security barriers, fences, landscaping and other enclosures should not affect the required flow into or exhaust out of the installation;
- For all indoor fuel cell locations, liquefied and gaseous hydrogen storage should either be located outside in the open air, in an appropriate dedicated unoccupied storage building, in an appropriately ventilated enclosure, or in a purpose designed indoor or underground facility, and should conform to recognised guidance.
- If practicable, the installation should be located in a normally unoccupied room built to appropriate fire-resistance standard and within an appropriate fire-resisting and noncombustible enclosure. Congestion, blockages and obstructions should be kept to an absolute minimum in the room as they may enhance flame acceleration in the event of an accident.
- All equipment (electrical or mechanical) within the identified hazardous zone shall be CE certified. Whenever reasonably practicable, the fuel cell and other hydrogen handling equipment shall be located at the highest level within the enclosure and physically isolated from any electrical equipment that is not ATEX-compliant or other potential sources of ignition.
- The forced ventilation of an area may be either general or local and, for both of these, differing degrees of air movement and replacement can be appropriate. Although forced ventilation is mainly applied inside a room or enclosed space, it can also be

applied to situations in the open air to compensate for restricted or impeded natural ventilation due to obstacles.

As in the case of natural ventilation, the dilution air used to artificially ventilate the area should enter at low level and be taken from a safe place. The ventilation outflow should be located at the highest point and discharge to a safe place outdoors. Furthermore, the mechanical means used to ventilate the enclosure should be suitable and, the electrical motor(s) should not be located in the potentially contaminated exhaust air stream.

- Suitable arrangements should be in place to detect when the ventilation system is failing to provide adequate ventilation. This may be based on the measurement of flow or pressure. This should raise an alarm and safely isolate the electricity supply outside the enclosure and the hydrogen supply outside the building with a normally closed (fail-safe) valve. The fuel cell system should shut down safely upon loss of adequate ventilation.
- BS EN 60529 (Degrees of protection provided by enclosures) requires the final manufacturer/installer of an assembly to ensure that after any electrical equipment has been installed within the enclosure, it still meets the required IP rating.

The guidance is helpful for considerations around the siting of hydrogen and fuel cells. It did not however, provide guidance on effective passive ventilation of the enclosure itself. In 2011, Brennan et al published the findings of the HYPER project. In their conclusion, they commented on small foreseeable releases of hydrogen. Their analysis of forced and natural ventilation efficiency suggested the adoption of the safety system in all enclosures where a credible non-catastrophic leakage can occur. They recommended the use of one or more solutions ‘if convenient’ e.g.

1. Reasonably increase the vent areas beyond the minimum value calculated using ATEX (Appareils destinés à être utilisés en ATmosphères EXplosibles: EC directive on explosive atmospheres),

2. Consider the vent areas for a leak flow reasonably bigger than the minimum,
3. Incline the roof making natural ventilation easy and efficient,
4. Install a small fan able to remove the internal mixture from the enclosure (not feasible for the small fuel cells considered in this investigation).

They note that a leakage limit rate of 40 lpm is often referred to with fuel cells for civil use. They suggest that leaks bigger than 90 lpm would amount to a catastrophic leakage.



**Figure 2.10 Pre-test and post-test photos of damage to the vehicle caused by an internal hydrogen–air deflagration (Merilo et al 2011).**

Research on large/garage scale enclosures has been conducted outside of Europe. Merilo et al (2011) conducted tests on a garage scale enclosure ( $60.39 \text{ m}^3$ ), using mechanical and natural ventilation with a release rate of  $9 \text{ kg h}^{-1}$  ( $1666 \text{ lpm}$  of  $\text{H}_2$ ) focusing on ignition and combustion. In their tests, they included a vehicle in the garage to assess the extent of the damage from an explosion (figure 2.10). They determined that internal vehicle geometry needed to be accounted for, when numerically modelling the enclosure.

Cariteau et al. in 2010 produced two papers relating to their work on a garage sized enclosure, at the CEA, with an experimental set up named GARAGE. The first paper detailed an investigation analysing the conditions required to form an explosive atmosphere. The enclosure volume was  $41.3 \text{ m}^3$ , with a full-sized garage door at one end and two circular ventilation openings, 200mm in diameter, at the other (one high and one low) (Figure 2.11). Helium was used as an analogue for hydrogen and TCG 3880 helium sensors were used to determine vertical concentration distribution. A vehicle was parked in the garage and tests at various release locations undertaken. Two leaks rates were tested,  $569 \text{ nlpm}$  and  $19 \text{ nlpm}$ .

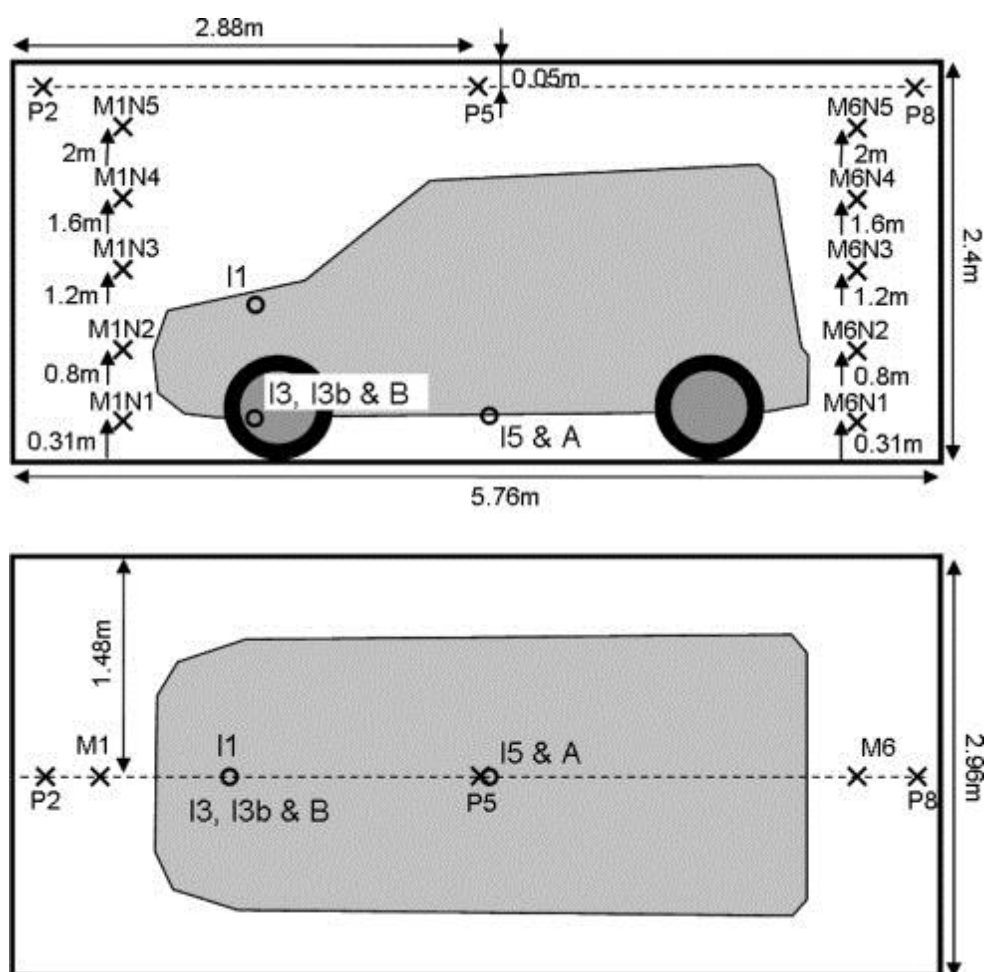


**Figure 2.11 Enclosure schematic showing dimensions and sensor positions (Cariteau 2011)**

The distribution of the buoyant gas in the enclosure depends on the release rate, momentum and buoyancy flux, the volume of the enclosure, the position of the source and the ventilation conditions of the enclosure (Cariteau et al. 2011). The position of the leak (in the vehicle or outside) was found to affect the gas distribution, with flow rate having less influence. Confined diffuse sources led to a stratified environment, whereas impinging jets on the floor produced a near homogenous mixture. The path of the gas exiting the vehicle and the subsequent plume that fills the enclosure appear to be the controlling factor for the vertical distribution of volume fraction. In their second paper, the garage was empty and low leak rates from 0.1 nlpm to 18 nlpm were tested with several ventilation arrangements. A vertical stratification was found to develop for all scenarios at all the leak rates tested. This was weak though for very low leak rates below 3 nlpm.

As well as the garage scale tests, a large-scale test (Figure 2.12) was carried out at the Health and Safety Laboratory (HSL) (Hedley et al 2014). This was an investigation into a passive ventilation solution to manage the hydrogen concentration in the large ullage space (0.9-3m depth) above a liquid of surface area 40 m<sup>2</sup> and containing a hydrogen source. Chimney arrangements were tested to manage the hydrogen concentration below 25 % of the LFL. Although not stated in the text, this is a nuclear scenario. With a release rate of 1.125 m<sup>3</sup> per hour (18.75 lpm) and two 300 mm diameter chimneys, the hydrogen concentrations were kept to about 1% v/v.



**Figure 2.12 Large-scale test rig at HSL (Hedley 2014)**

The research detailed above has looked at dispersal experiments in building size enclosures, often referred to as garage scale. This has been to cover the scenario where a hydrogen fuel cell vehicle will be stored within a building where a hydrogen supply may also be present. The USA has more than 65 million residential garages (Merilo 2011), so with hydrogen fuel cell vehicles on the horizon these are important scenarios. However, in the UK modern cars are rarely stored in garages in residential situations.

In 2010, there were 22.4 million dwellings in England. 40 % of UK dwellings had use of a garage, with houses and bungalows more likely to have a garage than a flat (48 % compared with 9 %). 44 % of suburban dwellings had a garage and 73 % of local authority dwellings rely upon street parking. 23 % of all households do not have a car (DCLG 2010). In 2006, research by the RAC found that only 26% of garages were used for car storage. This percentage is reducing, as larger modern cars will not fit in garages attached

to the older housing stock and the security measures built into new cars mean owners do not feel the need to lock their car away (RAC 2006). In addition, many of the occupied garages will contain one of the 'registered' 540,000 pre-1973 historic vehicles (FBHVC 2006). Other garages will contain post 1973 cherished vehicles and 'un-registered barn-finds'. The storage of a hydrogen fuel cell vehicle in a UK domestic garage is likely to be quite unusual.

Public enclosed car parks are more likely locations for a hydrogen release from an HFC vehicle to be confined but air exchange rates would be very high in such a location, keeping concentrations low. Ignition testing and flame length investigations have also been tested in large enclosure scenarios, but this investigation focuses on buoyant gas dispersion behaviour.

The more likely enclosure scenario that may occur in the UK will be where a small stationary fuel cell is in use in either a domestic or commercial application. In the domestic situation, fuel cell applications will be CHP units that replace the traditional boiler for heat and power or a fuel cell/electrolyser installation working in conjunction with domestic renewables such as solar PV, micro wind or heat pumps (in lieu of battery storage). Commercial applications will see small stationary fuel cells replace diesel generators. For this reason, research into small hydrogen fuel cell enclosure passive ventilation is important for their success.

**Key points informing this research thesis:**

- Large scale (garage size) investigated due to fuel cell vehicle development
- HRAM methodology simplified for tests with helium
- Swain and Swain report that small hydrogen leaks are so buoyant that they disperse quickly
- HySafe reports that small releases in confinement pose a serious risk
- Homogenous and stratified conditions defined (Venetsanos 2010)
- Installation permitting guidance (IPG) (HYPER Project)
- Safety systems in all enclosures where credible non-catastrophic leak can occur
- The distribution of the buoyant gas in the enclosure depends on



- the release rate,
- momentum and buoyancy flux,
- the volume of the enclosure,
- the position of the source and
- the ventilation conditions of the enclosure.

### 2.2.2 Small scale enclosure (sub kW fuel cell installations)

European research into passive hydrogen venting in small enclosures has been centred on the CEA GAMELAN installation in Paris (which became part of the H<sub>2</sub>FC-European Infrastructure Project). The CEA is the French atomic energy agency and the installation was originally constructed for nuclear hydrogen scenarios, in particular, studying jets and stratified layers (Krakovich et al 2015). In 2008, Deri and Cariteau were investigating the stratification of hydrogen in containment. The accumulation of hydrogen in high regions in a nuclear installation is of concern and they were collecting data to refine CFD numerical models.

Their experiments used the CEA GAMELAN facility to conduct fountain tests, where the injection of air at the bottom of the enclosure would break up a stratified buoyant layer of helium at the top. The installation comprised a one cubic meter (0.92 x 0.92 x 1.29 m) Perspex™ enclosure (Figure 2.13). An array of TCG 3880 mini katharometer gas sensors recorded species evolution and Particle Image Velocimetry was used to monitor flow velocity. Helium was used in lieu of hydrogen (Deri et al 2010). They identified three different homogenisation regimes:

- When the injection rate is very small, molecular diffusion dominates the mixing,
- Increasing the fountain flow rate leads to buoyancy dominated mixing, stratification is pushed upwards, stiffened and eroded by entrainment,
- For high momentum injection, the flow regime is momentum dominated and sudden stratification break-up is experienced

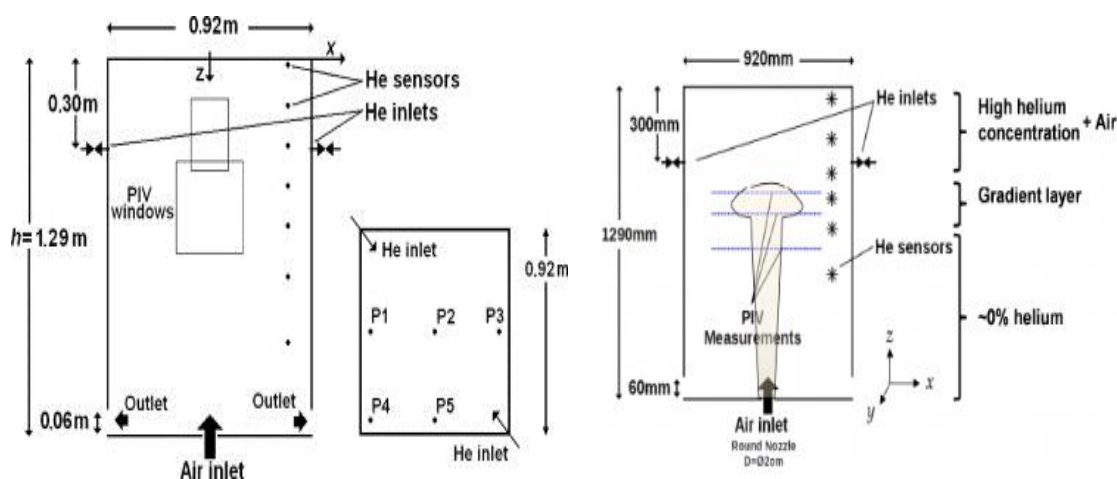


**Figure 2.13** CEA GAMELAN facility schematic (Deri et al 2010)

With the increase in hydrogen economy research, the GAMELAN installation became available for research within the H<sub>2</sub>FC Infrastructure Project. Ulster Universities HySAFER project, led by Professor Molkov, carried out investigations using the GAMELAN facility. A wide range of hydrogen scenarios were tested, with the data subsequently used for CFD validation. Cariteau et al. (2012), who was involved in the fountain tests above at the CEA GAMELAN facility, commenced a series of tests aiming to quantify the effects of a hydrogen leak in a fuel cell system. Cariteau had already conducted garage scale tests at the CEA and was now looking at the smaller enclosure. It is notable how scientists involved in nuclear hydrogen safety have seen the clear links to hydrogen safety in the hydrogen economy and have diversified their interest.

Cariteau et al.'s first investigation (2012) looked at the different concentration build-up regimes encountered during a release of a helium/air mixture into an empty unventilated enclosure. *They suggested the most realistic scenario would be for the enclosure to be crowded with the fuel cell and system parts and a release of varied orientation but considered this too complex to start with and instead chose the empty enclosure as the best first step.* The helium/air mix was injected into the enclosure through a vertical 5 or 20 mm diameter nozzle, located 210 mm above the base of the enclosure. Three compositions of helium/air mix (100 %, 80 %, and 60 % helium volume fraction) were injected into the enclosure. Ten mini-katharometer gas sensors were installed to record the helium concentrations in two vertical arrays (Figure 2.14).

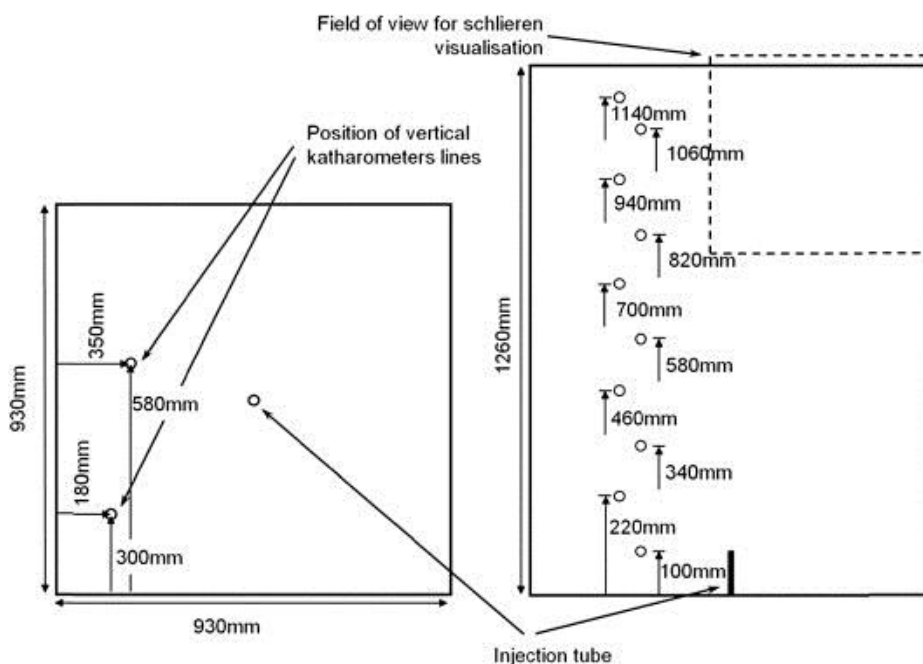


**Figure 2.14 Experimental set-up (Cariteau et al 2012)**

Three distinct regimes were identified in the tests, stratified, stratified with a homogenous layer and homogenous. Stratification was found when buoyancy strongly dominated the dispersion behaviour. Stratification and a homogenous layer was observed where an increased injection rate led to an increase in gas velocity and jet length. The injected momentum was sufficiently large near the enclosure edges near the ceiling, to overturn the buoyant layer, leading to enhanced local mixing and homogeneity lower down.

A homogeneous condition was observed when the previous regime reached a limit, where the injection conditions led to the formation of a homogeneous layer equal to the height of the enclosure. The parameter differentiating the three regimes is the volume Richardson number (see equation [1] page 30) based on the volume of the enclosure. For values greater than 1, the vertical profile of the volume fraction has a regular stratification. The transition to a more homogenous regime occurs for Richardson numbers less than 1. Synthetic Schlieren images were taken of the various regimes (e.g. figure 2.15 shows the helium jet rising to the enclosure ceiling and spreading horizontally to the edge. Schlieren field of view is indicated in figure 2.14). [Synthetic Schlieren is a simplified visualisation system relying on the variable refractive index of a fluid with density fluctuations. It utilises a linear arrangement of a camera the fluid object and a backlit grid (light source). Distortions in the grid are recorded by the camera, which can be enhanced with image processing. The Schlieren system used in this research is explained in section 3.7]

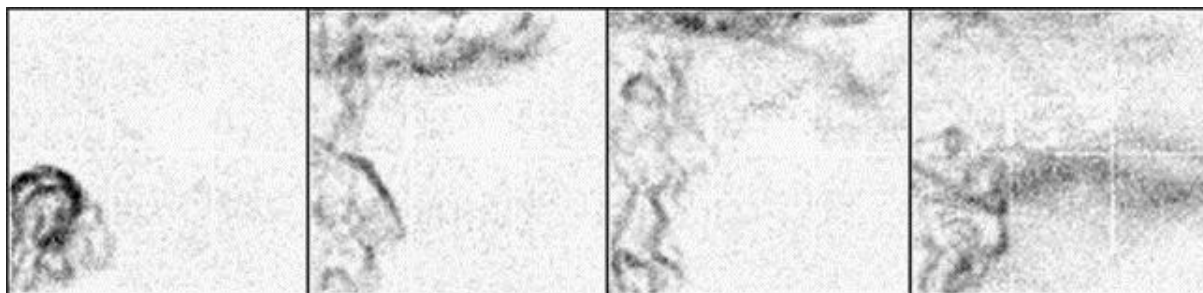


**Figure 2.15 Synthetic Schlieren images 5mm nozzle at 5 NLPM (Cariteau 2012)**

In 2013, Cariteau et al. moved on to study the effects of a single vent on the dispersion of a buoyant gas in the CEA GAMELAN enclosure. Three vent geometries were tested. Cariteau et al. had previously found in vented garage tests the presence of a vertical buoyant gas volume fraction gradient and were investigating parameters leading to the same condition in the GAMELAN enclosure.

For an accidental leak in a small enclosure, the inertial effects of a buoyant jet of high velocity must have a strong influence on the mixing and dispersion behaviour. One vent was added to the enclosure near the ceiling. Helium was injected and the effect of flow rate, injection velocity, vent size and geometry on the vertical volume fraction gradient was assessed (figure 2.16). The vent sizes were 90 cm x 18 cm, 18 cm x 18 cm and 90 cm x 3.5 cm (vent areas, 1620 cm<sup>3</sup>, 325 cm<sup>3</sup>, and 315 cm<sup>3</sup> respectively).

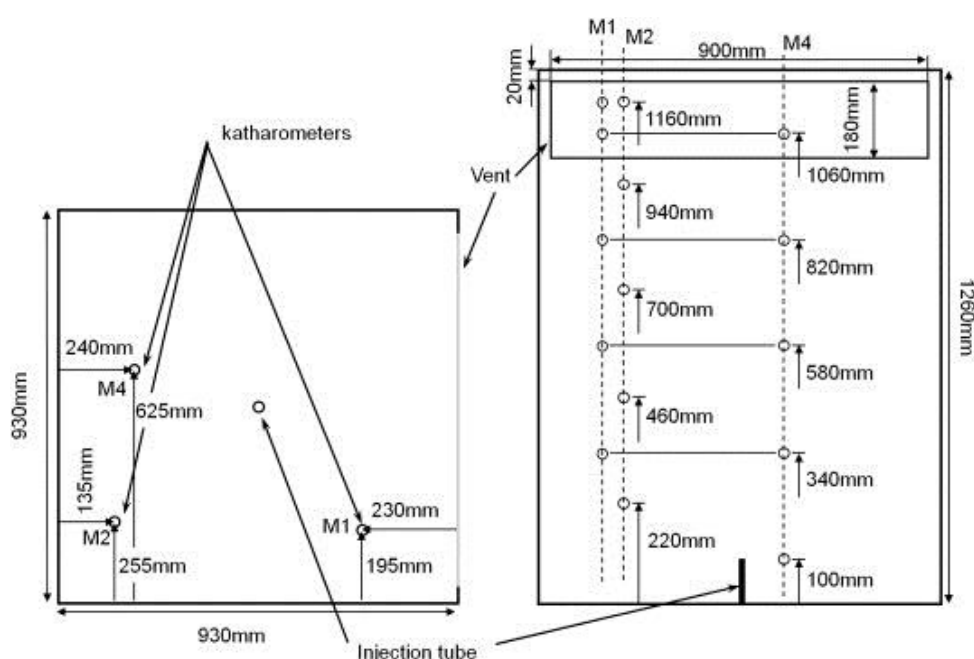


**Figure 2.16 GAMELAN rig showing 900mm x 180 mm top vent (Cariteau 2013)**

In the enclosure, 15 mini katharometer gas sensors were deployed in three vertical arrays of five sensors. Helium was injected into the enclosure via the central nozzle (5 mm or 20 mm), 210mm above the floor at flow rates from 5 to 300 NLPM. Tests were run through transients to reach steady state conditions. Plotted data exhibited small amplitude perturbations, likely due to inhomogeneity in turbulent mixing and to gravity waves that may propagate in a vertically stratified environment. The data was therefore time averaged to minimise this effect (Cariteau et al. 2013).

It was found that in the steady state regime, the helium volume fraction vertical distribution featured a homogenous layer in the upper part of the enclosure. For the vent with the highest vertical extension, the homogenous upper layer formed quickly with a high-density gradient. This prevented recirculation due to fresh air entering the enclosure over its full height. With the wide and narrow vent, a homogenous layer was still present near the ceiling with stratification forming slowly during the test. Fresh air entering the enclosure diluted the bottom area with little homogeneity evident (Cariteau et al. 2013). Figure 2.17 presents the vertical distribution of the helium volume fraction observed for the three vent sizes over a range of different flow rates. Further work in the literature relating to the GAMELAN facility relates to the distinction between natural and passive ventilation (see section 2.3) and extensive CFD modelling (see section 2.4).

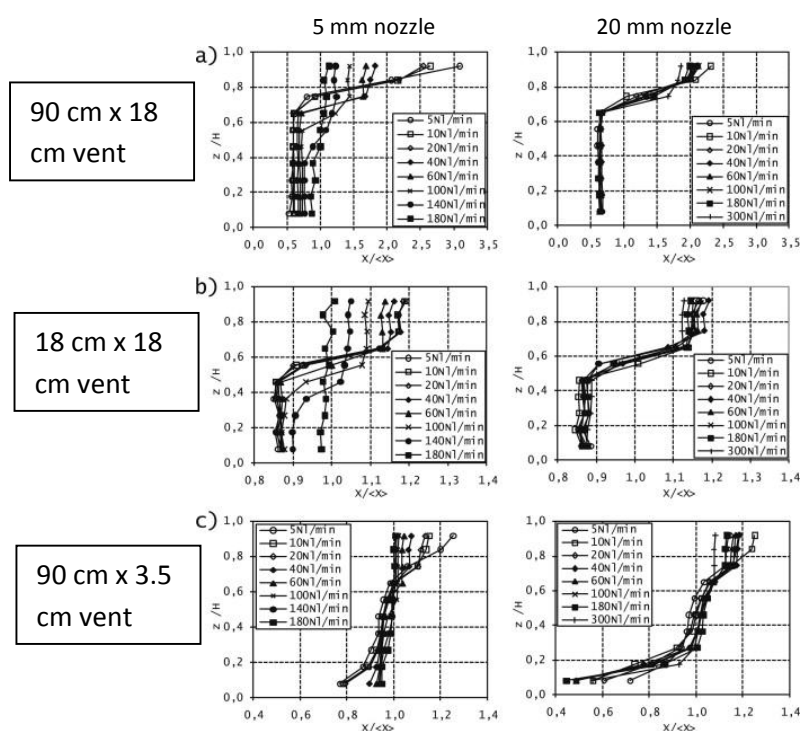


**Figure 2.17 Steady state vertical distribution of the volume fraction (Cariteau 2013)**

Evidence of research into passive ventilation in a small hydrogen fuel cell enclosure is limited in the literature. The CEA facility is ideal for such testing but probably due to its limited availability, other ventilation scenarios were not tested. The Cariteau data has though been used for CFD validation exercises by the HySAFER Project. Small fuel cells such as the Hymera unit will be housed in much smaller enclosures such as the 0.144 m<sup>3</sup> enclosure used in this research investigation.

Although the concepts and theories outlined are relevant, the empirical data for such an enclosure, with a variety of ventilation schemes, does not currently exist. Molkov (2014) (HySAFER) comments on an absence of well-instrumented experiments and that “correct prediction of steady-state concentration of a sustained leak of hydrogen in an enclosure with one vent is not currently possible in a wide range of accident scenarios”. This research sets out to improve this position and develop it with multiple vent arrangements.

**Key points informing this research thesis:**

- Link between nuclear and fuel cell, hydrogen venting scenarios at the small scale
- Small enclosure passive venting research viable and necessary
- Investigations conducted
  - Nuclear fountain tests – Stratification dispersal
  - Helium injection with no ventilation – stratification/homogeneity
  - Helium injection with a single upper vent – concentration gradient
- Distribution regimes identified
  - Stratified
  - Stratified with homogenous upper layer
  - Homogenous
- Volume Richardson number used to differentiate dispersal regimes
- Xensor TCG 3880 mini-katharometer gas sensors becoming standard in this field
- Helium as an analogue for hydrogen now a standard in fuel cell, buoyancy, research
- Schlieren imaging should be possible with helium in a small enclosure

- An application by the author to use the CEA GAMELAN facility was declined
- Absence of passive hydrogen venting small scale empirical data
- Absence of a range of ventilation schemes tested in the literature
- Disagreement in literature over small enclosure risk of explosion

### 2.3 Natural and passive ventilation in enclosures

Passive hydrogen venting is a viable prospect for small enclosures, because of hydrogen's buoyant nature. Liddament's review of natural ventilation (1996), established that density differences and buoyancy are the driving forces for *natural ventilation* (where wind is absent). As previously defined, Linden (1989) identified two distinct regimes of natural ventilation, mixing ventilation and displacement ventilation. Linden was modelling air movement in his work and his definitions referred to the movement of air due to convective forces.

However, the introduction of a buoyant gas, into the enclosure air, has an impact upon the behaviour of the fluid in the enclosure system. Molkov et al (2014) identified that when theoretical 'natural ventilation' models are applied to a 'passive ventilation' enclosure scenarios, they can under predict the lower buoyant gas concentration in the enclosure by up to two times and over predict the higher enclosure concentrations by up to two times. Molkov et al. (2014) noted this distinction and derived a definition for *passive ventilation*.

The presence of a light buoyant gas in the enclosure in mixed conditions will give the internal fluid properties that are at variance with the external ambient air. (A temperature difference between air in the enclosure and the external ambient would also lead to buoyancy differences and convective flow). *Natural ventilation*, involves the flow of air through an enclosure, containing only air. The purpose being to refresh the internal air or manage thermal conditions. As the internal and external fluids are the same, a neutral plane can be identified where internal pressure is equal to external pressure. The neutral plane is important, as an opening below the plane will become an inlet and one above an outlet. Where there is only one ventilation opening, the plane will be at the vertical midpoint, which facilitates two-way flow into and out of the enclosure (Figure 2.18).

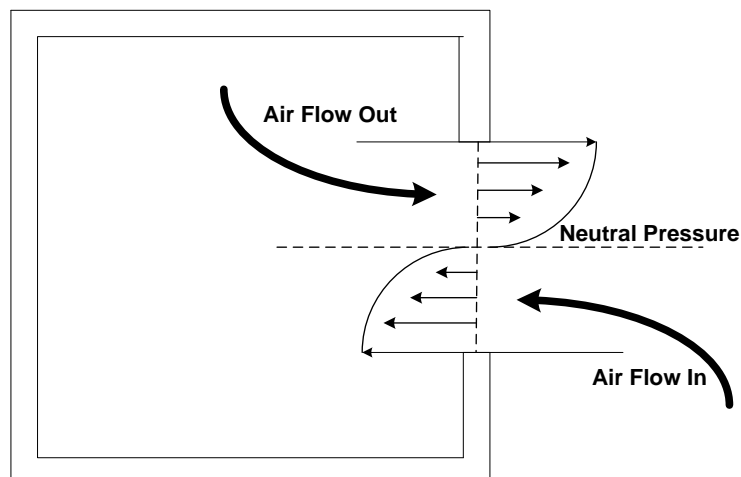


**Figure 2.18** Single vent enclosure, showing two-way flow about the neutral plane.

If a buoyant, lighter than air, gas is present in the single vent enclosure, particularly one capable of filling the entire enclosure (such as hydrogen) the pressure inside the enclosure will change and the neutral plane will be lower. With a single ventilation opening, this will lead to the neutral pressure plane being positioned between the vertical midpoint and the bottom of the opening (Figure 2.19). This phenomenon, termed *passive ventilation*, can have an impact on the rate of flow through the vent and therefore on internal concentration. This distinction allowed the derivation of a generalised expression for the gas concentration for a well-mixed, single upper vent passive ventilation scenario (Molkov 2014). This becomes important for vent positioning and sizing. This research investigation deals with passive ventilation only.

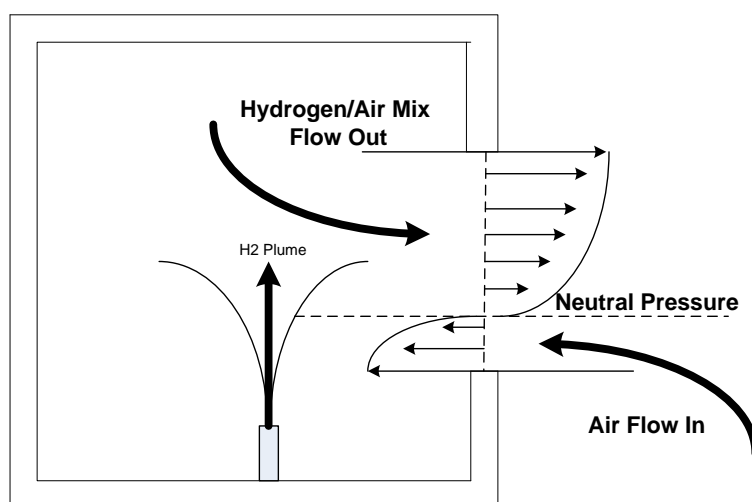


**Figure 2.19** Enclosure with single vent and with a buoyant gas mixture in the enclosure, showing two-way flow about the 'lower' neutral plane.



The GAMELAN single vent tests, described above, although a useful starting point are not truly reflective of a small fuel cell installation. A large open vent on one side of the enclosure is an impractical proposition for real life installation. Smaller plain rectangular vents are more likely to be found often with the addition of louvres (horizontal extensions for environmental protection). Hydrogen fuel cell enclosures, in deployment, may have multiple upper and lower openings, with optional chimneys and flues to optimise flow through the enclosure. The passive ventilation distinction still applies, but the neutral plane will be located at a point in the enclosure between the upper and lower openings, its position dependent upon the enclosure buoyant gas concentration. Ventilation opening design also affects performance e.g. tall versus wide vents and louvres. A literature gap exists for small enclosure passive ventilation data using alternative vent arrangements.

Molkov (2014) noted that the unignited release of flammable gas in an enclosure is a typical scenario that could lead to loss of life and property but that there was a lack of understanding of the underlying phenomena and an absence of validated tools for passive ventilation safety engineering. Linden et al (1999) theory describes the fluid mechanics of natural ventilation by buoyancy driven flow and wind assistance, specifically concerning airflow in buildings. For the reasons that Molkov gives, Linden's theory breaks down due to the presence of a buoyant gas such as hydrogen. Specifically, a buoyant gas leak can lead to single direction outflow, with a transition between two flow regimes. Molkov's motivation was that prediction of steady-state concentration of a sustained hydrogen leak in an enclosure was not currently possible. He hoped to relate leak rate, vent parameters and flammable gas concentration for the single vent enclosure.

A model was developed in the assumption of perfect mixing and results from equations for natural and passive ventilation were compared with empirical data. The passive ventilation model assumes a discharge coefficient  $C_d = 0.60$ , but results were found to be conservative. Best-fit values were achieved using values of  $C_d$  between 0.60 and 0.95. CFD analysis produced a value of 0.85, which is recommended for 100 % hydrogen accumulation. Molkov presented an engineering nomogram (Figure 2.20) to calculate the mass flow rate leading to 100% gas concentration in the enclosure, as a function of vent width and height. Vertically tall vents were established as being more efficient than horizontally wide vents at ventilation performance. A criterion for mixture uniformity (UC) was also suggested (equations 3 and 4) as the product of three dimensionless ratios;

- The ratio of entrainment rate to the mass flow rate of the mixture out of the enclosure,
- The ratio of the enclosure surface area to the vent area,
- The ratio of the release source diameter to the vent height.

$$UC = \frac{V^{2/3} \sqrt{D}}{A \sqrt{H}} \frac{\dot{m}_{ent}(x)}{\dot{m}_{mix}} \quad [3]$$

UC = Uniformity criterion

A = Vent area

H = Vent height

D = Release diameter

$$\dot{m}_{mix} = \dot{m}_{air} + \dot{m}_{H_2}$$

$$\dot{m}_{ent}(x) = K_1 M_0^{1/2} \rho_{mix}^{1/2} x \quad [4]$$

$K_1 = 0.282$

$\rho_{mix}$  = the density of the mixture being entrained into the hydrogen jet

$x$  = The distance from the nozzle to the surface of the impingement (typically distance from floor to ceiling)

$M_0$  = Momentum flux

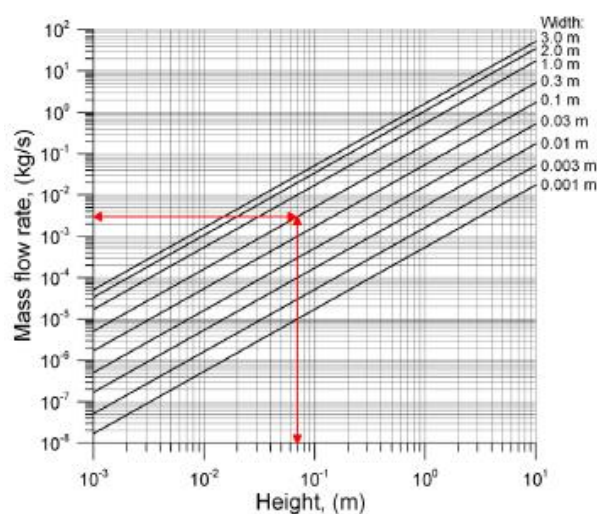


**Figure 2.20 Engineering nomogram for graphical calculation of hydrogen leak mass flow rate in an enclosure with one vent, which leads to 100% of hydrogen concentration, by the vent height and width (Molkov, 2014).**

In developing the equation for this passive ventilation scenario, Molkov first looked at the equation produced by Brown and Solvason (1962) (Eq.5), for volume flow rate through half of a single rectangular vent, of area A and height H, for natural ventilation in a building. The assumption used to derive this equation is the parity of flow into and out of the enclosure, implying that vent area is split equally between inflow and outflow.

$$Q = \frac{1}{3} C_D A \sqrt{g' H} \quad [5]$$

$g' = g(\Delta\rho/\bar{\rho})$ ; is the reduced gravity, where  $g$  is acceleration due to gravity, ( $m s^{-2}$ )

$\Delta\rho = (\rho_{ext} - \rho_{int})$ ; is the density difference, ( $kg m^{-3}$ )

$\bar{\rho} = (\rho_{ext} + \rho_{int})/2$ ; is the average density, ( $kg m^{-3}$ )

$\rho_{ext}$  and  $\rho_{int}$  are the densities of the fluid inside and outside of the enclosure ( $kg m^{-3}$ )

$A$  is the vent area ( $m^2$ )

$H$  is the vent height ( $m$ )

$C_D$  is the discharge coefficient

$Q$  is the volumetric flow rate through the vent ( $m^3 s^{-1}$ )

This equation [5] with the 1/3 comes from the derivation by Brown and Solvason (1962). Shaw and Whyte (1974) and Wilson and Kiel (1990) followed this approach. Dalziel and Lane Serff (1991) removed the 1/3, without explanation with Linden (1999) doing the same. Cariteau et al. (2011) rewrote the equation (Equation 6), again without the 1/3, in terms of the volumetric fraction of hydrogen in air, as part of their investigation into a helium release in an enclosure with one vent. In Molkov's view, this process has placed uncertainty on selection of a suitable discharge coefficient.

$$X = \left[ \frac{Q_0}{C_D A (g' H)^{1/2}} \right]^{2/3} \quad [6]$$

$X$  = The volumetric fraction of hydrogen in air

$Q_0$  = The volumetric flow rate of the release ( $m^3 s^{-1}$ )

$g'$  = reduced gravity =  $g(\rho_{air} - \rho_{hydrogen})/\rho_{air}$  ( $m s^{-2}$ )

The mass flow rate of the hydrogen mixture flowing out of the enclosure is equal to the mass flowrate of air entering the enclosure through the vent, plus the mass flow rate of the hydrogen entering the enclosure from the release source, for steady state conditions ( $\dot{m}_{mix} = \dot{m}_{air} + \dot{m}_{H_2}$ ). The mass flow rate of hydrogen in the hydrogen air mixture flowing out of the vent is equal to the mass flow rate of hydrogen in the release source. The equation for volumetric fraction of hydrogen in the enclosure is:

$$X = \frac{\rho_{air} - \rho_{mix}}{\rho_{air} - \rho_{H_2}} \quad [7]$$

Molkov wrote a new equation for *passive ventilation* (Equation 8), in the style of Cariteau's (equation 6). The function  $f(x)$ , (Equation 9), defines the difference between the approximate solution for volumetric fraction of hydrogen by natural ventilation (Equation 6) and the exact solution of the problem by passive ventilation theory (Equation 8). Equation 8 has been derived on the assumption of mixture uniformity in the enclosure. Experimental tests have shown that non-uniform mixtures are also present in enclosure releases. Molkov determined that the derivation of an analytical model for such conditions was outside of the scope of the 2014 paper.

$$X = f(x) \left[ \frac{Q_0}{C_D A (g' H)^{1/2}} \right]^{2/3} \quad [8]$$

$$\text{Where; } f(x) = \left(\frac{9}{8}\right)^{1/3} \cdot \left\{ \left[ 1 - X \left( 1 - \frac{\rho_{H_2}}{\rho_{air}} \right) \right]^{1/3} + (1 - X)^{2/3} \right\} \quad [9]$$

The important finding here is the distinction that has been made between the two ventilation regimes and the effect that it has on the neutral pressure line. It is likely that many enclosure leaks will lead to non-uniform conditions however, there will still be an effect on enclosure pressure. Figure 2.21 (Molkov 2014) presents the functional dependence between the neutral pressure plane height fraction in a vent and hydrogen mole fraction in the enclosure, assuming uniformity. It shows how for a case of natural ventilation (air), the hydrogen mole fraction would be zero and the neutral plane fraction is 0.5, demonstrating the equal inflow/outflow split at the vent. As the hydrogen mole fraction increases in the enclosure, the neutral plane location gets lower.

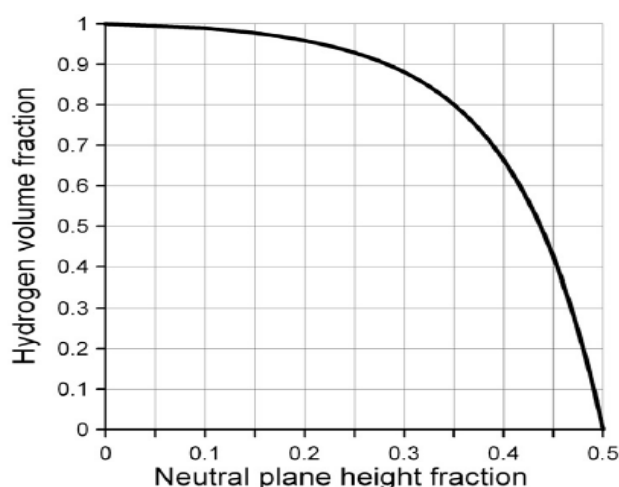


**Figure 2.21 hydrogen volume fraction in enclosure as a function of neutral plane height fraction (Molkov 2014)**

**Key points informing this research thesis:**

- Natural ventilation theory fails to predict concentrations of buoyant gas releases in an enclosure
- Natural ventilation (air) leads to a 50:50 vent opening split
- Distinction between natural and passive ventilation established
- Passive ventilation (buoyant gas), lowers the position of the NP at the vent
- The presence of a buoyant gas in an enclosure lowers the neutral pressure plane, important for vent position
- A gap in knowledge exists with regards to data sets for alternative passive ventilation schemes
- Tall vents are more efficient than wide vents
- Passive ventilation equation derived for uniform mixture
- Equation not available for non-uniform mixtures

## 2.4 Ventilation openings

Ventilation systems require openings to allow the mass transfer of fluids to take place. When designing a natural ventilation system for a building, the sizing of ventilation openings is a straightforward process, based upon the volume of the building, the required air change rate (varies depending upon the use of the volume) and where the opening(s) can be sited. As explained above a new regime, passive ventilation, exists when a buoyant gas is present in the volume, which influences ventilation flow and performance.

A further factor effecting flow is the vent design itself. Tall vents are more effective than wide vents at managing enclosure concentrations as they allow for mixing to occur to a greater depth and height in the enclosure. Cariteau at al. (2011, 2013) found vertically tall vents quickly achieved a homogenous air/helium upper layer, producing a high-density gradient. The type of vent e.g. louvre, will also affect the rate of flow. As shown above with Molkov's deliberations, the discharge coefficient, a measure of vent flow resistance, has a significant impact on equation outputs and is itself difficult to determine. A further way of venting fluid is using chimneys or flues, which can increase the pressure differential between inlet and outlet, enhancing the flow driving force.

### **Plain and Louvre vents**

The vent aspect ratio is a straightforward parameter to determine for plain vents but becomes more troublesome with louvres. Louvres, in most cases, are horizontal or tangential and not vertical and their shape is not rectangular. These characteristics of louver vents increase flow resistance through the vent and affect the flow regime through the enclosure. As such, data obtained for plain vents cannot be simply applied to louver vents with the same opening area. In the literature, passive ventilation investigations have been undertaken using rectangular plain vents. Plain vent performance is understood and they can be optimised and provide simple numbers for the flow equations.

The small enclosures used for hydrogen fuel cells are generally stock electrical enclosures used for thermal management of electronics and are not designed for passive ventilation. They are usually found to have either plain or louver vents or a combination of the two. As such, research to date has not met the needs of small fuel cell businesses and further experimental data is required to characterise the performance of a range of ventilation openings that are more likely to be used. This data should also account for the use of chimneys and flues.

### **Chimneys and Flues**

Fuel cell enclosure passive ventilation with chimneys or flues is not currently evidenced in the literature. Friedrich et al. (2011) undertook ignition and combustion experiments using a 0.56 m<sup>3</sup> fuel cell enclosure and tested multiple vent/chimney arrangements and internal obstructions, as part of the HYPER project. Figure 2.22 shows the enclosure geometry with vent and chimney positions. Also shown are the internal obstructions used, which take up a significant amount of the internal volume.

Friedrich noted when running chimney tests that, with an empty enclosure or a low obstruction, a stack enhanced flow effect was present due to the chimney pressure differential. However, when the upper obstruction was in place, the stack effect was diminished, and internal hydrogen concentrations were high. Friedrich attributed this to partial blocking of the openings. Prasad (2010) reported that obstructions in the enclosure led to turbulent mixing between buoyant hydrogen and the surrounding air, which could

help to reduce concentrations. Clearly, the position of the obstruction and proximity of a vent or chimney opening will determine the extent of mixing that occurs.

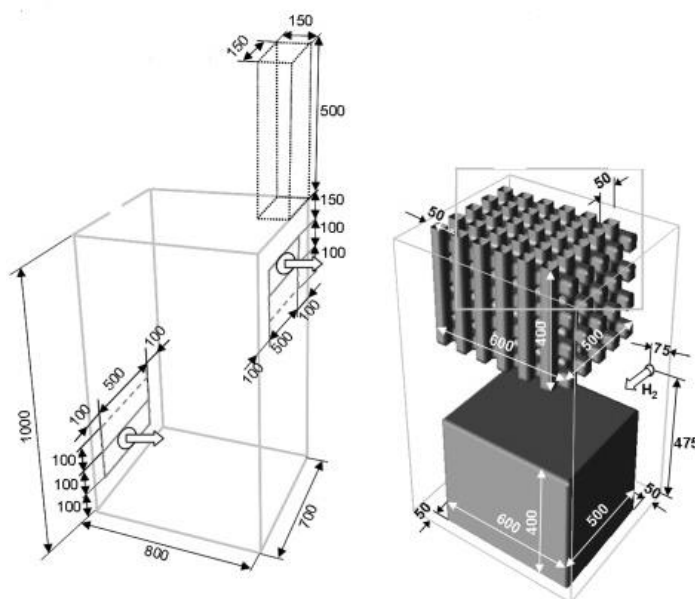


**Figure 2.22 Enclosure geometry – Chimney and obstructions (Friedrich 2011) IKET**

#### Key points informing this research thesis:

- Only plain rectangular and circular openings have been tested in the literature
- Louvre vents may reduce ventilation flow and increase concentration
- Chimneys (except for Swain's (2003) CFD HRAM passive ventilation investigation – garage scale) and flues are untested in the literature for passive ventilation

## 2.5 Flow impact factors and dimensionless parameters

The concept of passive ventilation due to the presence of a buoyant gas in a vented enclosure has been explained. Other factors can affect the flow regime in the enclosure. The environment where the enclosure is situated and the degree of exposure to external forces can have a significant impact on flow behaviour. A fuel cell enclosure situated outside may be exposed to the influence of wind, temperature and humidity variations. Wind forces are important for ventilation performance in externally sited enclosures aiding or opposing those due to buoyancy. Some wind forces can enhance flow in the enclosure, but if the forces are too strong, flow out can be impeded, increasing enclosure concentrations. Methods to minimise these effects are therefore important. Enclosures sited indoors maybe protected from wind but may be prone to variations such as draughts.

## Wind effects

The effect of wind on ventilation in an enclosure was tested by Linden et al (1999) with a *displacement ventilation* scheme (two openings, upper and lower) who found it produced an enhanced flow, when there is an increased pressure differential between the lower windward and upper leeward ventilation openings. Giannissi et al (2015, 2016) undertook an empirical and CFD investigation into the effect of wind on enclosure concentrations, using *mixing ventilation*.

They used the CEA GAMELAN 1 m<sup>3</sup> enclosure with a single vent and low, moderate and high simulated wind forces blowing against the non-ventilated enclosure face. They found that enclosure helium concentrations were 1.25 times greater at the top of the enclosure and 2.5 times greater at the bottom of the enclosure, when compared to tests without wind. This is attributed to turbulent eddies forming in the vent region and disrupting ventilation flow and inhibiting the mixing phenomenon.

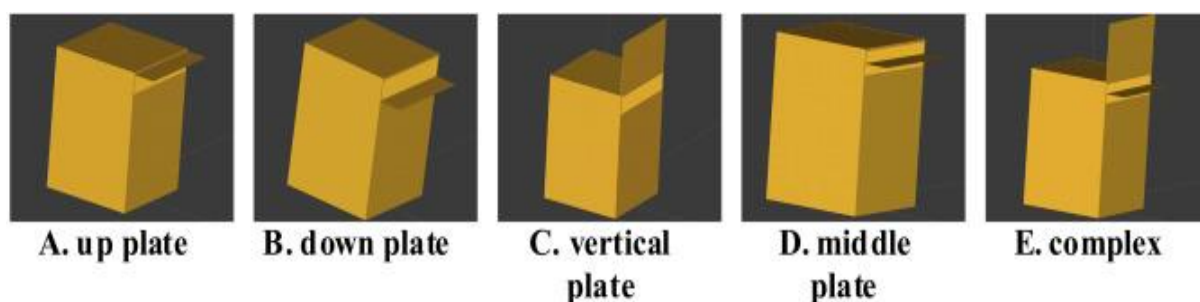


**Figure 2.23 Five ventilation plate configurations used in CFD exercise (Giannissi et al 2015)**

CFD simulations were undertaken using the GAMELAN geometry with plates fixed adjacent to the vent opening (Figure 2.23) to divert the wind flow and reduce the formation of disruptive eddies. Five variations were tested;

- A. Fixing a horizontal plate to the upper horizontal section of the vent,
- B. Fixing a horizontal plate to the lower horizontal section of the vent,
- C. Fixing a vertical plate to the upper horizontal section of the vent,
- D. Fixing a horizontal plate at the vent vertical midpoint,
- E. A combination of arrangement C and D.



Test D was found to be effective at managing enclosure concentrations close to the case without wind. This is believed to be due to the centrally positioned plate aiding separation of inflow and outflow. Positioning the plate exactly at the passive ventilation neutral plane as defined by Molkov (2014), would no doubt enhance this position.

### **Temperature and Humidity**

The Xensor gas sensors used in the experimental test can detect enclosure temperature and relative humidity. Temperature variations will affect convective flow and buoyancy in the enclosure. Externally sited enclosures subject to solar heating for example would experience higher internal temperatures. The fuel cell and associated electronics in the enclosure also produce heat, which will provide convective flow. Humidity variations in the enclosure may impact upon buoyancy. The literature was reviewed, but the only hydrogen humidity paper in this field (Giannissi et al 2018) related to a liquid hydrogen release as opposed to a gas release. The findings are of interest as they present the mechanisms involved in a liquid hydrogen release and the resultant effect on buoyancy. The effect of humidity on a hydrogen gas release would be different.

Giannissi et al demonstrated that humidity has an impact upon buoyancy when liquid hydrogen is released. The CFD investigation used the ADREA-HF code to study the effects of humidity on the buoyant plume. Test 7 of the health and Safety Laboratory experiments (Hooker 2011) was used as the basis for the simulations. This test involved the horizontal spill of liquid hydrogen 860 mm above concrete ground, with a nominal storage pressure of 1 bar and a release flow rate of 60 lpm.

During the liquid hydrogen release, air components, nitrogen and oxygen and ambient humidity in proximity to the release condense and freeze due to the low temperature. This leads to a multi-phase flow condition where air and hydrogen vapour are mixed with liquid and solid particles, with a resultant effect on flow turbulence. Two conflicting effects are now present, a positive buoyancy effect due to heat released from condensation and an increase in density due to the liquid/solid phase now present. Due to water's high heat of vaporisation and that it condenses in an extended area of the release it has a significant effect. The heat liberated can influence the cloud temperature and the hydrogen dispersion.

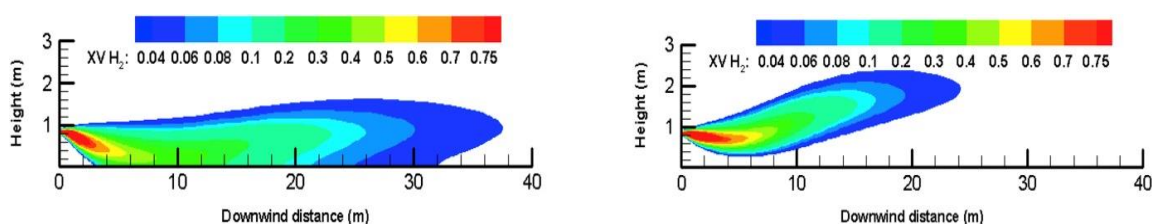


**Figure 2.24 Hydrogen contours on symmetry plane for left ‘dry air’ and right ‘humid air’ (Giannissi et al 2015)**

Giannissi et al concluded that with liquid hydrogen spills, the liquefaction and freezing of nitrogen, oxygen and humidity makes the gas cloud more buoyant and reduces the LFL distance by almost 35% (Figure 2.24). They also advised the use of a humidity model in similar CFD investigations.

### Vent Blockages

Enclosures sited outside may be prone to ventilation openings becoming blocked by foliage, animals, insects or debris (leading to a single vent scenario developing).

### Fluid dynamics governing dimensionless parameters

The following dimensionless parameters determine the flow characteristics of a hydrogen release in air (Agranat et al (2004)); the Reynolds number (Re), the Schmidt number (Sc), the Mach number (Ma), the Richardson number (Ri), the Froude number (Fr) and the density ratio ( $k_p$ ). Other relevant dimensionless numbers are also explained.

#### (i) Reynolds number, Re

The Reynolds number characterises the effect of turbulence and expresses the ratio of inertia to viscous forces (Holborn 2012). The Reynolds number is useful for predicting whether flow will be laminar, turbulent or in transition between the two states and will vary for different flow conditions (such as flow in a pipe). The critical Re value will depend entirely on the flow and can vary from very low numbers (4 or 5 for jet flow [laminar]) to very high values (4000 [turbulent flow]). Flow from a nozzle as in this investigation would see Laminar flow (low Re) from the nozzle breaking down to turbulent (high Re).

$$\text{Re} = \frac{\rho UL}{\mu} = \frac{UL}{\nu} \quad [10]$$

$U$  and  $L$  are the characteristic velocity ( $\text{m s}^{-1}$ ) and length (m) scales,  $\rho$  is the gas density ( $\text{kg m}^{-3}$ ),  $\mu$  is the dynamic viscosity (Pa. s) and  $\nu$  is the kinematic viscosity ( $\text{m}^2 \text{s}^{-1}$ ).

**(ii) Schmidt number, Sc**

The Schmidt number is the ratio of momentum diffusivity to mass diffusivity;

$$Sc = \frac{\nu}{D} \quad [11]$$

$D$  is the mass diffusivity (diffusion coefficient of hydrogen or helium in air ( $m^2 s^{-1}$ ))

**(iii) Mach number, Ma**

The Mach number is the ratio of the fluid velocity  $u$  to the sonic velocity  $V$ . If  $Ma > 1$ , then the flow is supersonic, if  $Ma < 1$ , flow is subsonic.

$$Ma = \frac{U}{V_{sonic}} \quad [12]$$

**(iv) Richardson number, Ri and Froude number, Fr**

The Richardson number characterises the importance of buoyancy in the flow by expressing the ratio of buoyancy forces to inertia

$$Ri = \frac{(\rho_a - \rho_g)gL}{\rho U^2} = \frac{g'L}{U^2} \quad [13]$$

$\rho_a$  is the density of the ambient air ( $kg m^{-3}$ )

$\rho_g$  is the density of the released gas ( $kg m^{-3}$ )

$g'$  is the density modified reduced gravitational acceleration ( $m^2 s^{-1}$ ), defined as

$$g' = \frac{(\rho_a - \rho_g)g}{\rho} \quad [14]$$

$\rho$  is the density characteristic of inertia forces (dependent upon the region of flow). In regions of flow with large concentrations (e.g. Close to the source)  $\rho = \rho_g$ . In regions of flow with the low concentrations (Boussinesq approximation)  $\rho = \rho_a$ .

It is also possible to characterise the importance of buoyancy to the flow by using the densimetric Froude number expressing the ratio between inertia and buoyancy forces. Gas releases that have a high Froude number ( $Fr > 1000$ ) are dominated by the initial momentum of the jet, while releases with low Froude numbers ( $Fr < 10$ ) are dominated by the buoyancy forces generated by the relative density of the gas in the jet and the surrounding air. Gas releases with Froude numbers in the intermediate range ( $10 < Fr < 1000$ ) are influenced by both the initial momentum of the jet and the buoyancy forces (Houf and Schefer (2008)).

$$Fr = \frac{U}{[gL(\rho_a - \rho_g)/\rho]^{1/2}} = \frac{U}{\sqrt{g'L}} \quad [15]$$

The Richardson number is the inverse square of the Froude number.

$$Ri = \frac{1}{Fr^2} \quad [16]$$

(v) **Gas density ratio,  $k_\rho$**

The gas density ratio expresses the ratio of the density of the buoyant gas to the density of the surrounding air

$$k_\rho = \frac{\rho_a}{\rho_g} \quad [17]$$

(vi) **Rayleigh number Ra**

The dimensionless Rayleigh number is used in the calculation of natural convection and represents the ratio of buoyancy and thermal diffusivity. It is the product of the Grashov and Prandtl numbers (described below).

$$Ra = \frac{g\beta\Delta T x^3}{\nu k} = Gr \cdot Pr \quad [18]$$

*Ra is the Rayleigh number for characteristic length  $x$*

*$x$  is the characteristic length*

*$g$  is the acceleration due to gravity*

$\beta$  is the thermal expansion coefficient (is equal to  $1/T$ , for ideal gases, where  $T$  is absolute temperature)

$\Delta T$  is the characteristic temperature difference (e.g. difference between the ambient temperature and the temperature of the flow of gas from the nozzle)

$\nu$  is the kinematic viscosity

$Gr$  is the Grashof number

$Pr$  is the Prandtl number

### (vii) Grashof number $Gr$

The Grashof number  $Gr$ , is the ratio of buoyancy to viscous forces acting on a fluid

$$Gr = \frac{L^3 g \beta \Delta T}{\nu^2} \quad [19]$$

$g$  = acceleration due to gravity,  $m s^{-2}$

$L$  = characteristic length

$\beta$  = coefficient of expansion of the fluid,  $K^{-1}$

$\Delta T$  = temperature difference between the surface and the bulk of the fluid,  $K$

$\nu$  = kinematic viscosity of the fluid,  $m^2 s^{-1}$

### (viii) Prandtl number $Pr$

The Prandtl number is the ratio of momentum diffusivity (kinematic viscosity) to thermal diffusivity.

$$Pr = \frac{\nu}{\alpha} \quad [20]$$

$\nu$  is the momentum diffusivity ( $m^2 s^{-1}$ )

$\alpha$  is the thermal diffusivity ( $m^2 s^{-1}$ )

#### Key points informing this research thesis:

- The effect of external environmental conditions such as rain, sun and wind on enclosure performance is worthy of future research investigation

## 2.6 Data Collection

The collection of data in support of this thesis is naturally an important part of the research investigation. The review of passive ventilation in enclosures has identified the frequently used equipment and research design approach that has proved reliable and relevant to this investigation.

### 2.6.1 Experimental Rig design

**Enclosure:** Many of the large garage scale enclosures are solidly constructed from blockwork or steel to withstand detonations (Merilo 2010). Polycarbonate or Perspex® is also used for enclosures, such as those at CEA. These construction materials are costly and so plywood has been used in this investigation. There is no evidence in the literature of plywood being used for testing passive ventilation schemes in small enclosures. A helium permeation test conducted at LSBU supports the use of plywood at low leak rates (see Chapter 3 section 3.5.1)

**Gas delivery:** Many of the recent cited papers use mass flow controllers to deliver helium to the test rig. Flow ranges and error are reported, but manufacturers are rarely named.

**Gas sensors:** Mini-katharometer gas sensors (description provided in section 3.3.3) have become popular, in experimental tests, to measure flammable gas concentrations in enclosures. They are suitable for binary gas systems and are ideal for use with helium. Venetsanos (2010) in garage scale tests used 30 Xensor TCG3880 sensors in an array to detect helium concentrations. This was followed by Cariteau (2011) who used six columns of five Xensor TCG 3880 sensors in the CEA garage facility to measure vertical concentration gradient.

The CEA GAMELAN one cubic metre facility was built to test post Fukushima nuclear scenarios, studying jets and stratified layers (Krakovich et al 2015). It used TCG 3880 gas sensors. Cariteau (2012) and Molkov (2014) used GAMELAN for dispersion and passive ventilation tests, with ten TCG 3880 sensors in two vertical columns of five. Hedley et al (2014) used the XEN-TCG 3880 sensors in their large-scale hydrogen test rig at The Health and Safety Laboratory (HSL) for nuclear passive ventilation scenarios.

Eight Xensor TCG 3880 pt100 sensors are used in this research investigation, which include a platinum resistance thermometer to account for ambient temperature. A benefit of these sensors is data collection via a USB hub to a PC, running LabView software.

**Key points informing this research thesis:**

- Small enclosure sub-cubic meter scale requires further research– 0.144 m<sup>3</sup>
- Xensor TCG 3880 gas sensors growing in use
- Helium as an analogue for hydrogen in buoyancy cases
- Mass flow controller to deliver measured amounts of gas [low leak rates]
- Lab view software to collect data-via USB to PC
- Plywood enclosure not evidenced in the literature
- Vent arrangements not extensively tested

### 2.6.2 Computational Fluid Dynamics (CFD) Modelling

Computational Fluid Dynamics (CFD) software codes solve the partial differential equations for the conservation of mass, momentum (Navier–Stokes), energy, chemical concentrations, and turbulence quantities. Solutions provide the field distributions of pressure, velocity, temperature, the concentrations of water vapour (relative humidity), gas and contaminants, and turbulence parameters such as:

- Turbulent kinetic energy  $k$ ,
- Turbulence dissipation  $\epsilon$ ,
- Specific turbulence dissipation  $\omega$
- Turbulence intensity,  $Tu$
- Turbulence viscosity ratio  $\mu_t / \mu$
- Turbulence length scale  $Tu_L$

CFD codes hold many modelling uncertainties, requiring modelling assumptions and user interpretation, but are widely used for engineering predictions (Chen, Qingyan 2009). The advantages of CFD are the potential to provide detailed flow patterns and temperature distributions throughout the space and the ability to deal with complex geometry. Chen (2009) used multi-zone CFD models as the main tool for predicting ventilation performance.

Work on hydrogen dynamics in building size spaces is associated with hydrogen economy and nuclear decommissioning safety work. Middha (2009) worked to improve the validation basis of hydrogen dispersion simulations using the CFD code FLACS in garage size spaces, finding some correlation between predicted rates and experiments.

Vudumu (2009) looked at hydrogen dispersion and leak phenomena from one-metre high cylinders into confined areas, considered to be one of the most dangerous scenarios. Vudumu used the ANSYS: Fluent CFD code for numerical modelling, “since accurate predictions are difficult with experiments and theoretical hand calculations”.

Buoyancy driven flows are difficult to model with CFD because of the small driving forces, which can lead to numerical instabilities and uncertainties caused by turbulence and flow modelling (Cook and Lomas 1979). Shravan (2009) though, found ANSYS: Fluent to be suitable for analysing buoyant flows. CFD depends upon computing power and selection and adaption of the most appropriate turbulence model for the scenario under investigation.

CFD modelling of the dispersion behaviour of helium in a small enclosure is a significant part of this research investigation and thesis. CFD can minimise the time and expense involved in experimental work. It facilitates predictions about performance and feasibility of experimental rig design, reducing the number of iterations required (Chen 2007). There are many CFD codes available, both open source and commercial. All have as their basis the Navier Stokes equations but can vary in the choice of turbulence models that have been developed to close the mean flow equations.

A wide range of CFD codes have been tested in the literature in the field of hydrogen safety and passive ventilation. In 1996 Swain used Fluent 3.0.3 (Predates ANSYS: Fluent by 10 years) to investigate passive ventilation of a hydrogen leak in a building. Figure 2.25 shows results from Swains CFD simulation. The data is informative, but primitive compared to modern graphics.



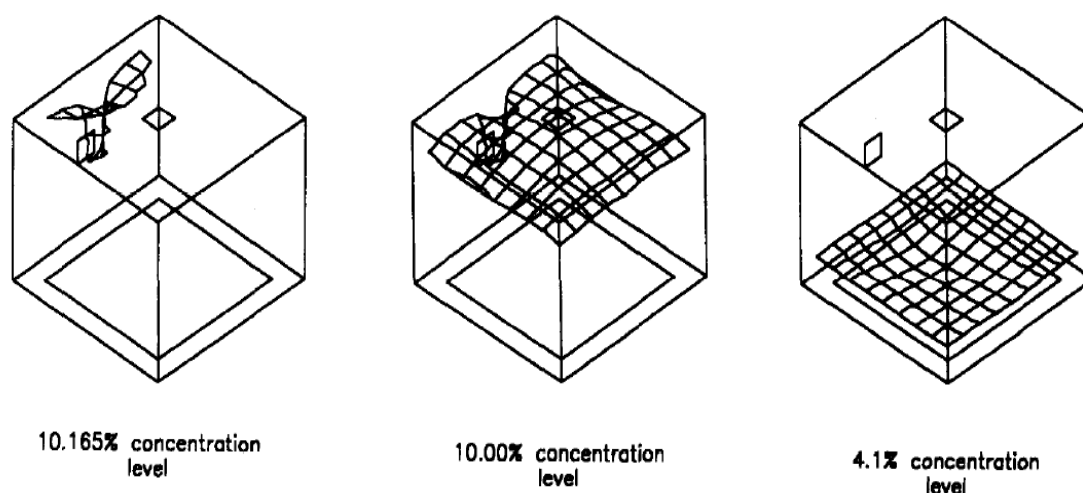


**Figure 2.25 CFD concentration distribution-Fluent 3.03 (Swain 1996)**

In 2009 Barley and Gawlik modelled hydrogen leaking from a vehicle in a garage, using ANSYS Fluent: 6.3.26, with an implicit pressure-based solver and first order discretisation of convection and time for speed and stability (First order will converge quicker but may be less accurate. Second order will take longer but should provide greater accuracy). Renormalisation Group (RNG)  $k-\epsilon$  turbulence model with the differential viscosity was applied as well as a laminar model. Figure 2.26 shows a graphic of mole fraction (Using Fluent 6.3), with improved graphics compared to Fluent 3.0.3 and a graph comparing CFD and test data, with the CFD over predicting helium concentration.

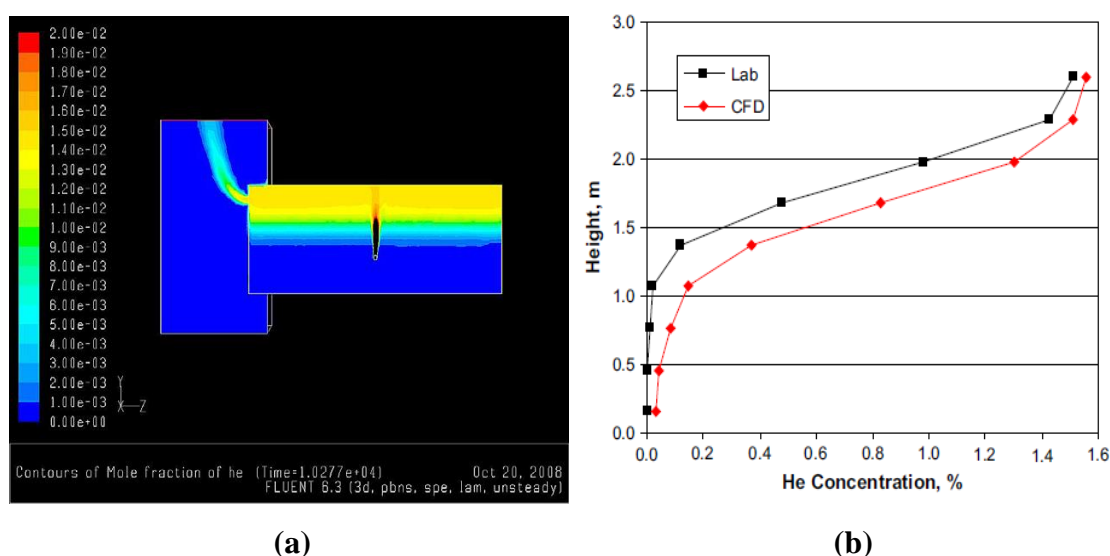


**Figure 2.26 (a) Fluent: 6.3 CFD graphic of helium mole fraction and (b) Comparison of CFD and test data (Barley and Gawlik 1996)**

In 2010, Papanikolaou et al conducted a CFD benchmarking exercise. The experimental investigations, used for the benchmarking, aimed to determine the ventilation requirements for parking a hydrogen-fuelled vehicle in a residential garage. The following CFD codes were tested; ADREA-HF using  $k-\varepsilon$  model, FLACS using  $k-\varepsilon$ , FLUENT using  $k-\varepsilon$  and CFX using laminar and the low-Re number SST. General agreement between CFD predictions and experimental data was good with tendency to overestimate the results of the upper sensors for the small and medium vent sizes and underestimate for the large vent size.

Visser et al (2012) conducted a CFD validation exercise for hydrogen distribution in nuclear containment, looking at accident scenarios using ANSYS: Fluent 6.3. The standard  $k-\varepsilon$  turbulence model with full buoyancy effects was utilized for the analysis. They were pleased with the model's ability to predict the buoyant plume in containment. Figure 2.27 provides an example of (a) a graphical representation of hydrogen distribution in containment and (b) a comparison of CFD and test data. On this occasion the CFD had slightly under predicted concentrations at the higher elevation.

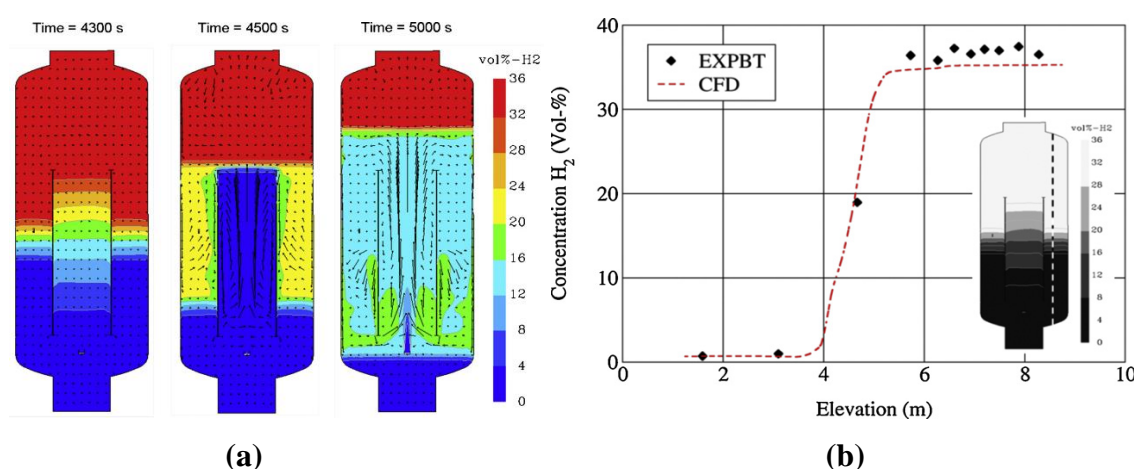


**Figure 2.27 (a) CFD Graphic of hydrogen distribution in containment and (b) A comparison of CFD and test data hydrogen concentrations (Visser et al 2012).**

Srinivasa et al (2014) undertook a validation exercise using ANSYS: Fluent and experimental data taken from tests in the MISTRA (97.6 m<sup>3</sup>) facility on stratification and stratification erosion behaviour. They wanted to select the most appropriate two-equation turbulence model for the analysis. The objective of the turbulence models is to provide closure for the Reynolds stresses in the Reynolds Averaged Navier Stokes (RANS) equations. Three turbulence models were tested, standard  $k-\varepsilon$ , RNG  $k-\varepsilon$  and realizable  $k-$

$\varepsilon$ . Figure 2.28 presents the CFD results against a plot of the experimental data. The realizable  $k-\varepsilon$  turbulence model was considered the best performing and that its predictions were fair (though clearly still not a close correlation).

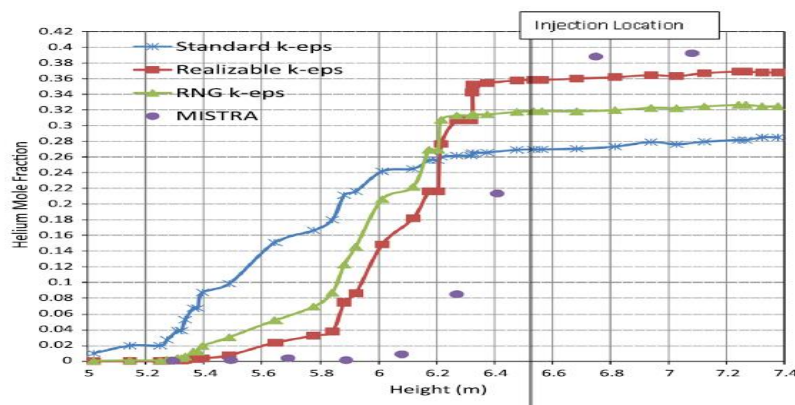


**Figure 2.28 Comparison of CFD and empirical data (Srinivasa et al 2014)**

Giannissi (2014), as part of the HyIndoor project, undertook a CFD benchmarking exercise using data from the dispersion tests conducted at the CEA GAMELAN facility. ANSYS: Fluent 14.5 was tested along with AFREA-HF and ANSYS: CFX 14.0 with the following respective turbulence models' transitional SST, standard  $k-\varepsilon$ , dynamic Smagorinski LES. Generally, good agreement was found between predicted and measured helium concentrations. Vent configuration was found to influence predictions. In the case of the vent with the smallest vertical extension, all the codes overestimated concentrations at the lower part of the enclosure. Figure 2.29 shows a comparison of test and CFD data using the 900mm x 180mm vent opening. SST (ANSYS) was found to over predict, more noticeably at the higher sensor locations.

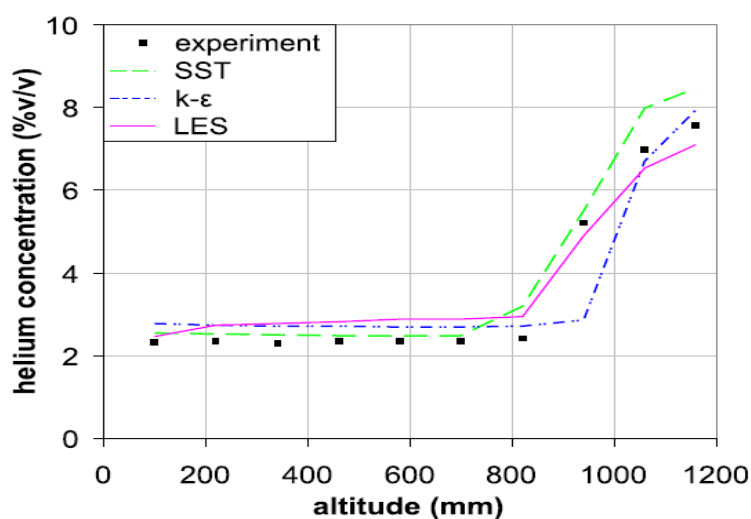


**Figure 2.29 Comparison of CFD and empirical data (Giannissi et al 2014)**

### 2.6.3 CFD Modelling approach

ANSYS: Fluent offers a wide range of turbulence models (Table 2.2) to suit a variety of flow scenarios and is used extensively in academic investigations in this field. Fluent has been tested in the literature for various dispersal and single vent passive ventilation schemes and provides some guidance on model selection. SolidWorks Flow Simulation has evolved from their CAD system and as such is a more limited product. It uses a modified standard  $k-\varepsilon$  turbulence model (see section 6.6) and has the facility to specify values of turbulence intensity and length ( $I$  and  $L$ ). SolidWorks Flow simulation has not been tested in the literature in this field of study, other than with this research project.

Despite having some limitations, the standard  $k-\varepsilon$  two-equation turbulence models are widely used and considered suitable for most industrial CFD simulations (Launder and Spalding 1972). They combine the transport equation for turbulent kinetic energy  $k$  and its rate of dissipation  $\varepsilon$ . The RNG  $k-\varepsilon$  (Renormalisation Group theory model) includes an additional term in the  $\varepsilon$  equation that improves accuracy and accounts for the effect of swirl in turbulence. The RNG model is more accurate for a wider class of flows, including those with low Reynolds numbers (Liu 2009). Jiang and Chen (2003) found in large-scale experiments with single sided ventilation and simple geometry that the Large Eddy Simulation (LES) performed better than the Reynolds Averaged Navier Stokes (RANS) simulation. However, LES is limited by the required computing power for complex geometries and RANS modelling will provide quicker outputs.

**Table 2.2 Some of the turbulence models available SolidWorks and ANSYS**

Turbulence model	CFD Code
Standard $k-\varepsilon$	ANSYS-Fluent
Standard $k-\varepsilon$ ( <i>Favre</i> )	SolidWorks Flow Simulation
I-L Turbulence intensity and length	SolidWorks Flow Simulation
Realizable $k-\varepsilon$	ANSYS-Fluent
RNG $k-\varepsilon$	ANSYS-Fluent
EDC (Eddy dissipation concept)	ANSYS-Fluent
SST (Shear Stress transport)	ANSYS-Fluent
LES (large Eddy Simulation)	ANSYS-Fluent

Dynamic Smagorinski LES	ANSYS-Fluent
LES-RNG (Renormalisation Group)	ANSYS-Fluent

The CFD process starts with a CAD model. Nolan (2015) describes a significant disconnect between the design process and CFD simulation activities. Historically design and simulation were distinct activities carried out by people with different skill sets, requiring analysts to extensively rework models to idealise them. Nolan's concept of 'simulation intent' (Table 2.3) establishes the link between CAD and simulation and creating fit for purpose analysis models.

**Table 2.3 Simulation intent (Nolan 2015)**

<b>Simulation Intent Attribute</b>	<b>Analysis decision</b>	<b>Analysis variables</b>
<i>Dimensionality</i>	3D/2D	Aspect ratio
<i>Boundary conditions</i>	Uniform-pressure /isothermal/adiabatic/flow rates	Volume flow/mass flow/Temperature/pressure
<i>Mesh type</i>	Quad/tri/hex//Linear/quadratic	Mesh parameters/Material properties
<i>Model clean-up</i>	Features removed	Target element size
<i>Solution type</i>	Turbulence model (SST, k-e)	Time step

Simulation intent provides a neat conceptual basis for the simplified approach used in this study. Simplification of the model is important to optimise the computational performance of the simulation, as this depends upon the number and complexity of geometric features (Thakur, 2009). Complex models can lead to ill conditioned meshes that produce inaccurate results (Saad, 2003). The use of a simple cuboid enclosure for the test rig supports this approach.

Hamri (2010) describes the concept of High Level Topology (HLT), which focuses on the key common requirements of CAD and simulation and their integration in a multi-physics approach. The multi-physics approach is becoming popular in commercial CFD

software, providing a smoother experience for the user. SolidWorks has incorporated this ‘manifold modelling environment’ (Nolan 2015) into their CFD offering. ANSYS includes a CAD modeller and now a solid modeller (Space Claim), with an integrated interface to their CFD codes. Importing of CAD files from other providers is possible, but extensive repairs may be required before meshing.

Giannisi and Srinivasa (above) both undertook validation and benchmarking exercises with ANSYS: Fluent. A similar exercise is undertaken with SolidWorks Flow Simulation and Fluent, with the test data from this research study. Dadashzadeh (2016) undertook a CFD modelling exercise of hydrogen dispersal in an enclosed area, producing a methodology (Figure 2.30) for the CFD approach, informing the CFD methodology for this research project.

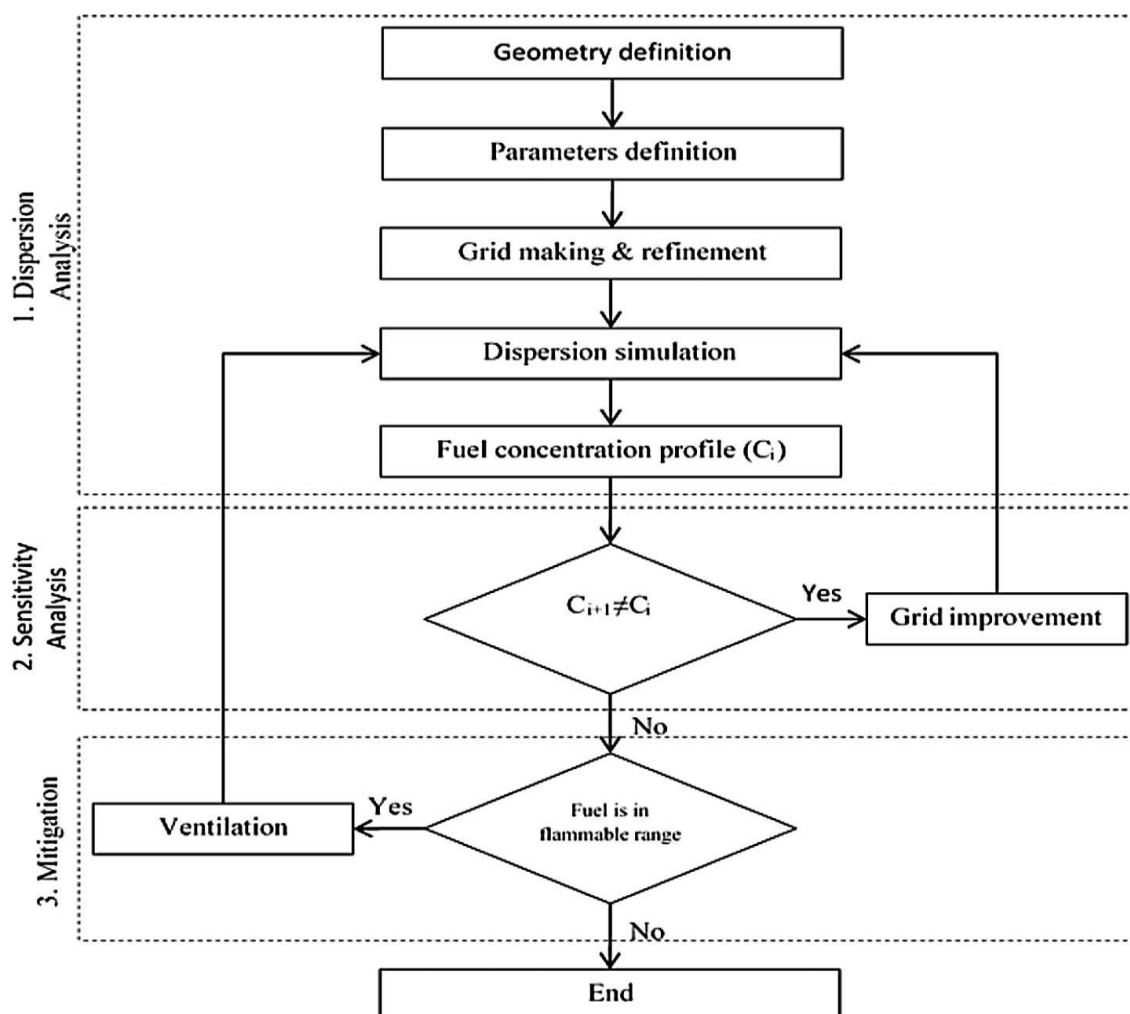


**Figure 2.30 Proposed CFD methodology for the safe design of confined spaces exposed to a hydrogen release (Dadashzadeh 2016)**

**Key points informing this research thesis:**

- CFD: SolidWorks Flow Simulation – Not tested to date
- CFD: ANSYS: Fluent: various turbulence models tested
  - Standard k- $\epsilon$
  - (RNG) k- $\epsilon$  turbulence model with the differential viscosity
  - Realisable k- $\epsilon$
  - k- $\epsilon$  turbulence model with full buoyancy effects
  - SST (Shear stress transport)
  - LES

## 2.7 Knowledge gaps

Small hydrogen fuel cell enclosure empirical research has been limited, primarily to research conducted at CEA GAMELAN facility and more extensive CFD investigations. Only single vent buoyant gas scenarios have been tested at GAMELAN. Large scale, garage size and above tests have been widely covered, but enclosure scale is an important flow parameter and small enclosures will have their own unique properties. An enclosure of 0.144 m<sup>3</sup> or similar has not been tested in the literature for buoyant gas passive hydrogen venting.

For practical applications and deployment of small fuel cells, a wide variety of ventilation options needs to be available, with the safety parameters known. This is not the current position. CFD codes have been used for validation exercises for passive ventilation. ADRENA FX, FDS and ANSYS Fluent/CFX have been tested. SolidWorks Flow simulation has not previously been tested in this field. SolidWorks is a more cost-effective application for organisations to use, with a much simpler graphical user interface (GUI) to negotiate. Validation of the code provides new data on a previously untested CFD system. BOC Ltd. use SolidWorks as their primary engineering design platform. ANSYS: Fluent has been used for comparison and validation of the SolidWorks data.

This research project has therefore investigated the following knowledge gaps;  
Hydrogen dispersal in a small passively ventilated hydrogen fuel cell enclosure

- The effect of multiple plain vent arrangements on dispersal

- The effect of louvre vents on dispersal
- The effect of obstructions in the enclosure
- The effect of flues/snorkels on dispersal
- The effect of chimneys on dispersal
- Schlieren imaging of helium in the enclosure
- SolidWorks Flow Simulation's capability to model the above tests
- ANSYS: Fluent comparison with SolidWorks predictions

**Key points informing this research thesis:**

- Knowledge gaps
  - Data sets for alternative ventilation arrangements
  - Hydrogen dispersal in a 0.144 m<sup>3</sup> passively ventilated hydrogen fuel cell enclosure
  - The effect of multiple plain vent arrangements on dispersal
  - The effect of louvre vents on dispersal
  - The effect of obstructions in the enclosure
  - The effect of chimneys on dispersal
  - The effect of flues/snorkels on dispersal
  - Schlieren imaging of helium in the enclosure
  - SolidWorks Flow Simulation's capability to model the above tests
  - ANSYS Fluent comparison with SolidWorks predictions

## 2.6 Conclusion

This review establishes the research position for small enclosure passive hydrogen venting and its importance, particularly the growth in hydrogen research linked to the hydrogen economy. There are many hydrogen research areas, but safety is crucial to providing confidence in hydrogen's use. This research focuses on hydrogen safety in small enclosures and is relevant to fuel cell and nuclear industries, where there has been limited research. The significant 1 m<sup>3</sup> GAMELAN study led to a definition for 'passive ventilation' but using only single vents. Multi vent research is rare. Much CFD modelling has been undertaken, but a critique is the limited number of empirical datasets available for validation purposes. This research helps address this position for passively ventilated small enclosures and tests SolidWorks CFD in this research area for the first time.



## Chapter 3 Methodology

### 3.0 Introduction

The critical review of academic literature has provided the insight for the design and criteria of this research methodology. It has informed how the empirical data is collected and CFD validation undertaken. Figure 3.1 presents a summary workflow process map of the experimental methodology for this research.

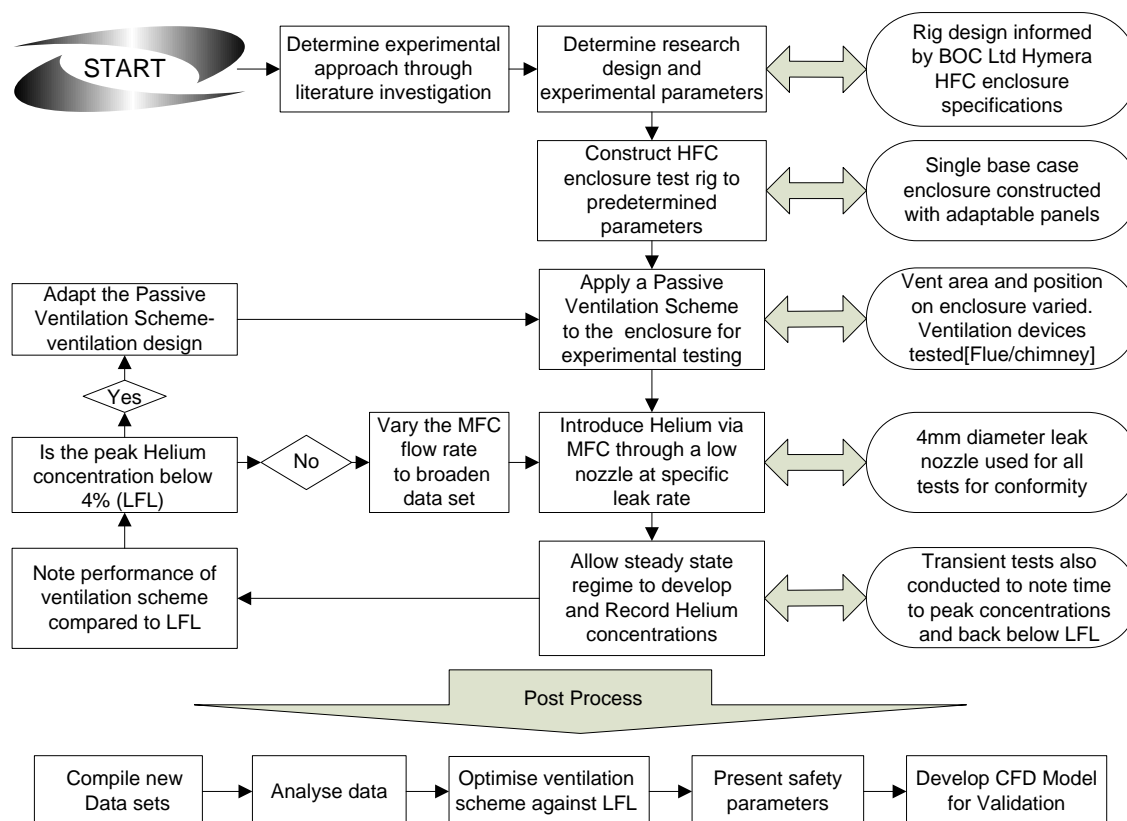


**Figure 3.1 Work Flow Process Map**

The review has identified the knowledge gap relating to passive hydrogen ventilation in small fuel cell enclosures. More specifically, enclosures that will house low power hydrogen fuel cells (HFC) (20 to 200W output) which can potentially leak hydrogen at low release rates. This research is also relevant to the nuclear decommissioning industry, where enclosures are used in nuclear waste management. For example, hydrogen vented from IP-2 ISO storage containers (Figure 3.2), used for transport and storage of nuclear waste, must be passively vented away to maintain safe concentrations. Stacking of containers in storage creates small voids where hydrogen can accumulate if not dispersed.



**Figure 3.2 IP-2 ISO Nuclear waste storage container (Patram2010)**

### 3.1 Experimental set-up background

This investigation uses an enclosure test rig the design of which has been informed by the BOC Ltd. standard Hymera enclosure, which is intended for deployment outside (Figure 3.3 (a)). The experimental enclosure test rig (Figure 3.3 (b)) is similar in size, with the initial experimental tests using a displacement ventilation scheme with opposing upper and lower ventilation openings as seen on the Hymera enclosure to create realistic scenarios.

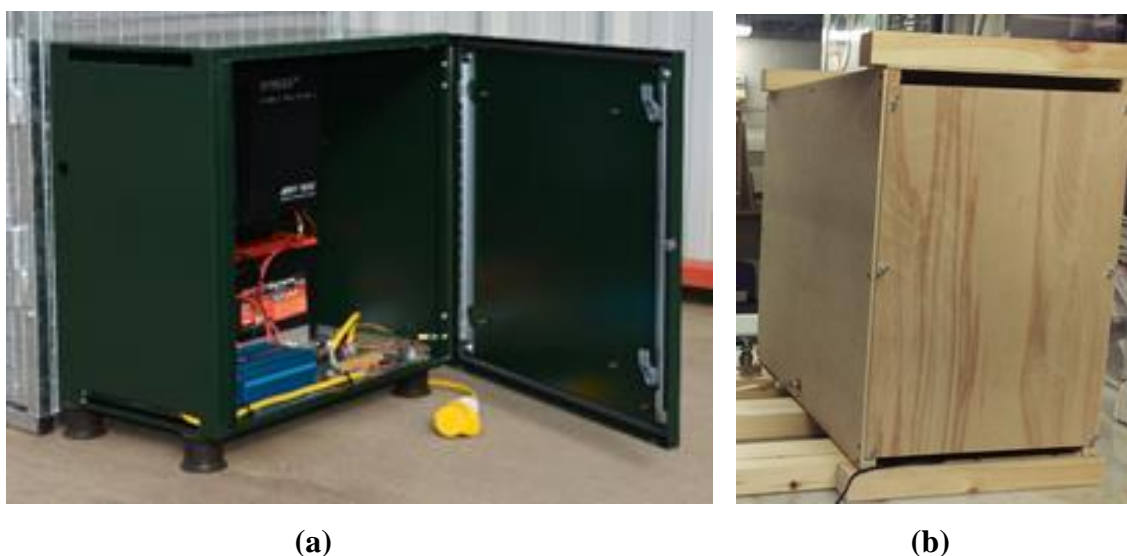


**Figure 3.3 (a) Hymera environmental enclosure (b) Experimental enclosure**

The focus of the experimental tests is on ventilation scheme design and performance. This was to derive data sets for enclosure hydrogen concentrations in certain ventilation configurations. Several ventilation concepts were tested to reflect the variety of real life applications that may be encountered and the potential ventilation arrangements that are employed. The CFD investigation followed the experimental design parameters.

### 3.2 Passive hydrogen venting scoping exercise

Initial scoping for the experimental trials were conducted at BOC Ltd. in association with a BOC Ltd. engineer. BOC Ltd. markets the Hymera range of portable hydrogen fuel cell generators (Figure 3.4) available in 60, 175 and 200W units. The fuel cells are deployed in an enclosure in conjunction with a compact hydrogen cylinder, the Genie unit. The BOC Genie (54 G20) hydrogen gas cylinder (Figure 3.4) is a lightweight alternative to a steel cylinder and holds almost twice as much gas as a steel cylinder of equivalent weight. The Genie has been designed with fuel cell use in mind. It has a wide stable base and carry handles, making it a more practical unit to move and change. It contains 424g @ 300 bar of high purity (99.995%) hydrogen. The unit is 660 mm tall with a base diameter of 325 mm, with a mass of 22.4 kg. It can deliver 7 kWh (electric) assuming a fuel cell efficiency of 50 % (BOC 2016).



**Figure 3.4 BOC Genie hydrogen cylinder and Hymera unit (BOC Ltd. 2016)**

To model the BOC Ltd. enclosure, Celotex® panels were used to quickly create a box 600mm high x 500mm wide x 400mm deep in size. Ventilation openings were cut into

the side panels and refined using masking tape (Figure 3.5). Hydrogen from a ‘Genie’ cylinder was supplied via a rotameter to the enclosure through a 4mm bore plastic pipe. This pipe was fed through a hole at the bottom of the enclosure and taped centrally to the floor, but directed vertically up, to facilitate the hydrogen leak.



**Figure 3.5 BOC Ltd. scoping exercise (a) Enclosure (b) Enclosure outside test**

An Ion Science, Gas Check 3000, hand-held hydrogen sensor (Figure 3.6) with short probe, was used to record the hydrogen concentrations in the enclosure. The device uses a micro thermal conductivity sensor, with a 1 second response time and accuracy of  $\pm 5\%$  (displayed reading), to record gas concentrations. The short probe of the sensor was inserted into holes at various heights, vertically, on the face of the enclosure to take gas samples. The manufacturer's probe extension was not available and tests with 100mm and 200mm lengths of 4mm bore tube proved unsuccessful, with no deep samples taken.

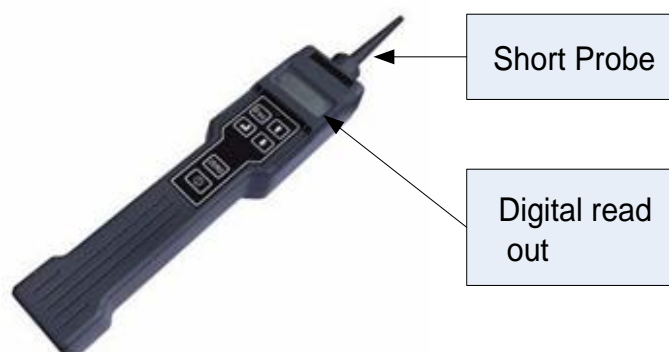


**Figure 3.6 Ion Science Gas Check 3000 handheld Hydrogen Sensor (IonScience.com)**

Tests were conducted with an empty enclosure and an enclosure containing a Hymera fuel cell shell and a battery. The fuel cell, when used was fixed to the rear wall 300 mm from the base. The battery, when used was positioned on the enclosure floor beneath the fuel cell and against the rear wall. Various vent configurations were tested (Exp. 1 was a single upper vent, Exp. 2, 3, and 4 were two vent cross-flow and Exp. 5 and 6 were 4 vent cross-flow). The hydrogen tests were conducted outside for safety, but the moderate wind present that day added some realism to the tests. The handheld sensor was difficult to calibrate needing frequent resetting and allowing only single readings to be recorded.

The short sensor probe was only able to take samples a couple of centimetres past the enclosure wall. This meant that a fuller picture of gas distribution was not possible to achieve. The test results although limited did suggest the viability of the experimental set-up but with further refinement and the need for a more detailed investigation. The graph in figure 3.7 does indicate the difference in concentration distribution between a mixing ventilation (single vent) and displacement ventilation regime. It also shows the effect of wind assistance to flow in the enclosure and the effect of increasing the vent area. These experiments were the basis of a trial SolidWorks CFD modelling project (Figure 3.8).

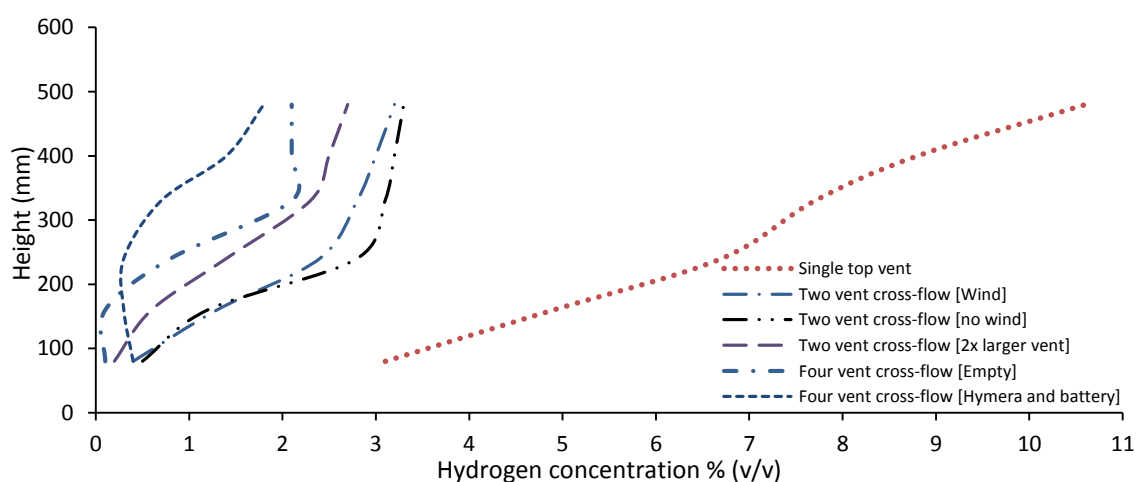


**Figure 3.7 BOC Ltd. HFC enclosure tests using hydrogen. All tests run at 1 lpm**

A number of learning points were taken from this first test. An accurately controllable gas supply is essential, ideally using an electronic mass flow controller. A more robust enclosure is also required. The Celotex enclosure was quick to construct but was leaky and it was difficult to apply accurate vent sizes. It was also unrealistically thick and not readily adaptable for other regimes. Rigid plywood sheets provide a viable alternative,

which is a versatile construction material and allows for iterative rig development. The initial laboratory plywood test rig was lined with aluminium foil and the outside varnished to reduce gas diffusion through the walls. The subsequent plywood test rigs were not lined or varnished, but aluminium tape was used in their construction, particularly to seal panel joints. Due to the short duration of the tests, diffusion through the plywood walls was not a significant factor. A diffusion test, however, was conducted with a fully sealed plywood enclosure following Yang (2013) to obtain a diffusion coefficient (see section 3.5.1).

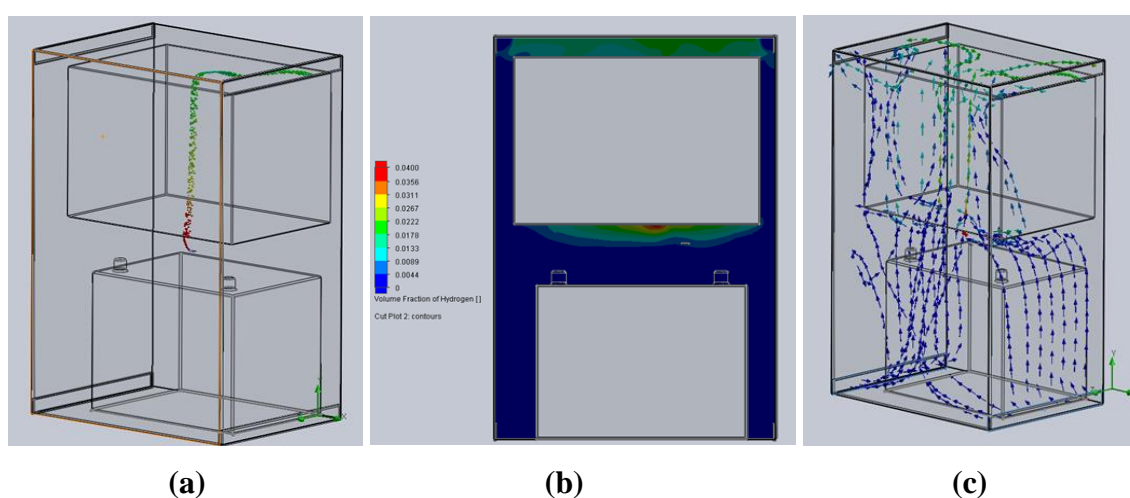


**Figure 3.8 SolidWorks CFD images of BOC Ltd. model (a) Wireframe image showing flow (b) Concentration contours (c) Flow path vectors**

It was also established that effective gas measurement at a range of various locations within the test chamber would be crucial for the investigation. A fixed internal sensor array is preferable, with fast sensor response times. MEMS helium sensors were identified (see section 3.3.3) with USB connectivity and LabView data collection. The sensors are also able to measure temperature (verify isothermal conditions) and humidity providing further useful data relating to conditions within the enclosure.

There were no fume extraction facilities in the laboratory and ventilation was via manual clerestory windows. Due to the dangers of a hydrogen explosion occurring in the enclosure and test chamber, it was decided that helium gas would be used as a safe analogue for hydrogen. Helium has been used as a substitute for hydrogen in many research investigations due to its buoyancy characteristics being close to those of hydrogen. In comparison experimental enclosure tests there has been shown to be a close correlation between the gases for concentration and dispersion behaviour (He et al. 2016).

### 3.3 Initial laboratory test rig

Using the learning from the scoping exercise an initial test rig was built in the laboratory to evaluate the new experimental apparatus. A plywood and Perspex™ enclosure was constructed (Figure 3.9), 600mm x 600mm x 600mm. The side panels were moveable to allow ventilation openings to be added. The test rig was contained within a Perspex™ outer test chamber (2m x 1m x 1m), to reduce the impact of airflow in the laboratory on gas flow in the enclosure. The plywood walls were varnished and lined with aluminium foil because of initial concerns about diffusion, which was subsequently discounted.



**Figure 3.9 Initial laboratory experimental test rig**

#### 3.3.1 Helium gas delivery

High purity A-Grade helium gas supplied from a 9 m<sup>3</sup> capacity (STP) cylinder (BOC Ltd.) located adjacent to the rig was used for all research investigations. A high-pressure Swagelok stainless steel flexible pipe was connected from the cylinder to a Swagelok gas valve, which in turn was connected via speed-fit connectors to a Brooks GF125 mass flow controller (MFC) (Figure 3.10). A further speed-fit pipe connected the MFC to the enclosure. A plastic 4 mm bore tube was then passed through a hole in the base of the enclosure. This 4 mm bore tube acted as the vertical inlet nozzle for the helium leak.

#### 3.3.2 Brooks GF125 Digital Thermal Mass Flow Controller

Gas delivery to the enclosure was in the sub 10 lpm range in accordance with the leak rates anticipated by BOC Ltd. Several MFCs were purchased but the most reliable and versatile was the Brooks GF125 Digital Thermal MFC. This device features (Brooks (2015));

- Sub 1 second settling time for quick start up and very rapid process steps
- MultiFlo™ gas and range configurability enabling reconfiguration without removing device from the gas line
- +/- 1.0 % Flow Accuracy (Set Point) / +/- 0.35 % (Full Scale)
- An independent diagnostic/service port to troubleshoot or change flow conditions without removing the mass flow controller from service
- Long-term stability due to extremely low wetted surface area, and corrosion resistant Hastelloy® sensor and valve seat

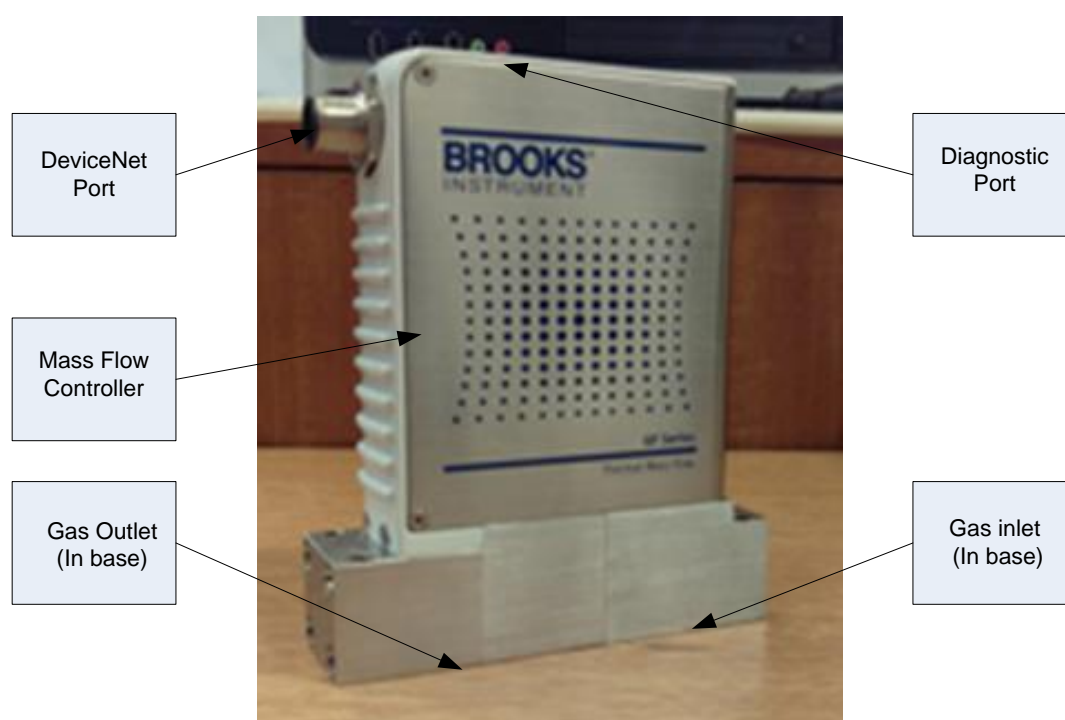


**Figure 3.10 Brooks GF125 High Purity Digital Thermal Mass Flow Device**

### Operating principles

The thermal mass flow measurement system comprises a restrictor and a flow sensor (Figure 3.11). Gas flowing into the MFC is split into two paths, one travelling straight through the restrictor and the other through the flow sensor. During flow conditions, there is a pressure differential across the restrictor, which forces gas to flow through the sensor. The scale flow rate of the device is determined by the selection of an appropriate restrictor when manufactured. The two streams rejoin at the far end of the restrictor.



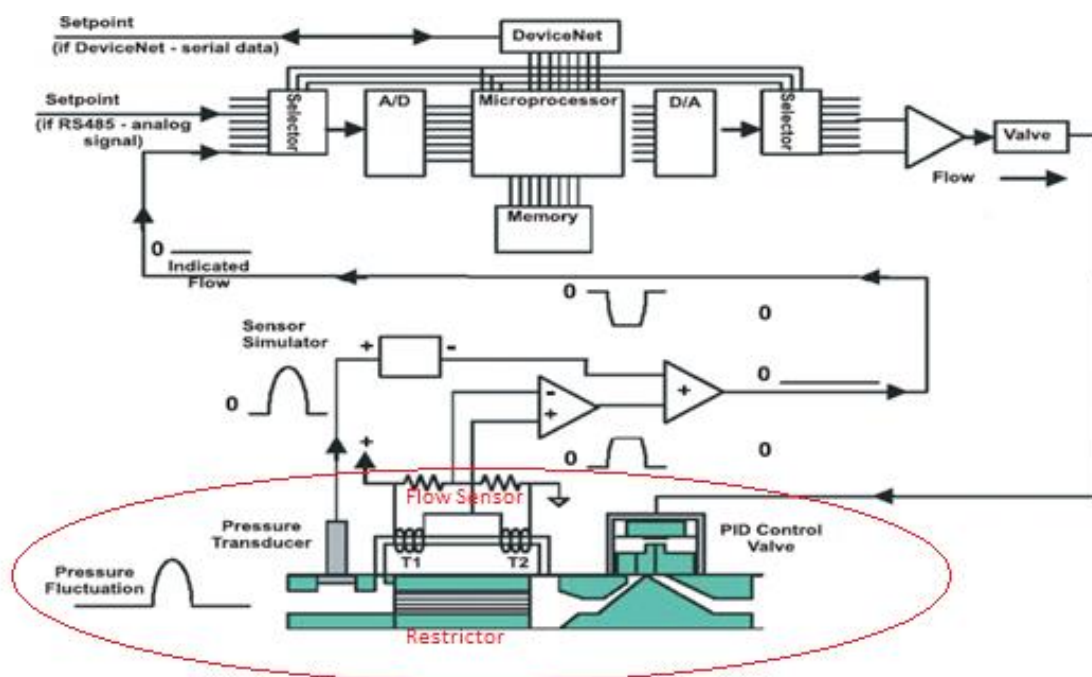


**Figure 3.11 Brooks GF125 Operating principles (Brooks 2015)**

The flow sensor is a very narrow, thin-walled Hastelloy tube. On this tube are upstream and downstream temperature sensing and heating elements (T1 and T2). During no flow conditions, the amount of heat reaching each element is equal so T1 and T2 are equal. Gas travelling in the tube carries heat away from T1 and towards T2. The temperature difference  $T_2 - T_1$  is directly proportional to the gas mass flow. The device was powered via its 'DeviceNet' port from a 5V laboratory power supply unit. The Brooks Expert Service Tool (BEST) software was used to control the device and assign setpoints via a USB link to the diagnostic port on the top of the MFC. Testing was carried out to verify the accuracy and operation of the Brooks mass flow controller for flows up to 10 lpm.

### **3.3.3 Xensor – XEN-TCG3880 MEMS Thermal Conductivity Helium Sensors**

Determining helium gas concentrations in the enclosure is a fundamental part of the research investigation. Accuracy, response time and a wide detection range are all important criteria for the experimental methodology. The sensor also needs to be small and easily positioned within the enclosure. XEN-TCG3880, MEMS (Micro Electro Mechanical Systems) helium sensors (Figure 3.12 (a)) were identified as meeting these requirements. The sensors are supplied as a set of four together with a USB hub (Figure 3.12 (b)), which allow connection to a PC and data collection using LabView software.

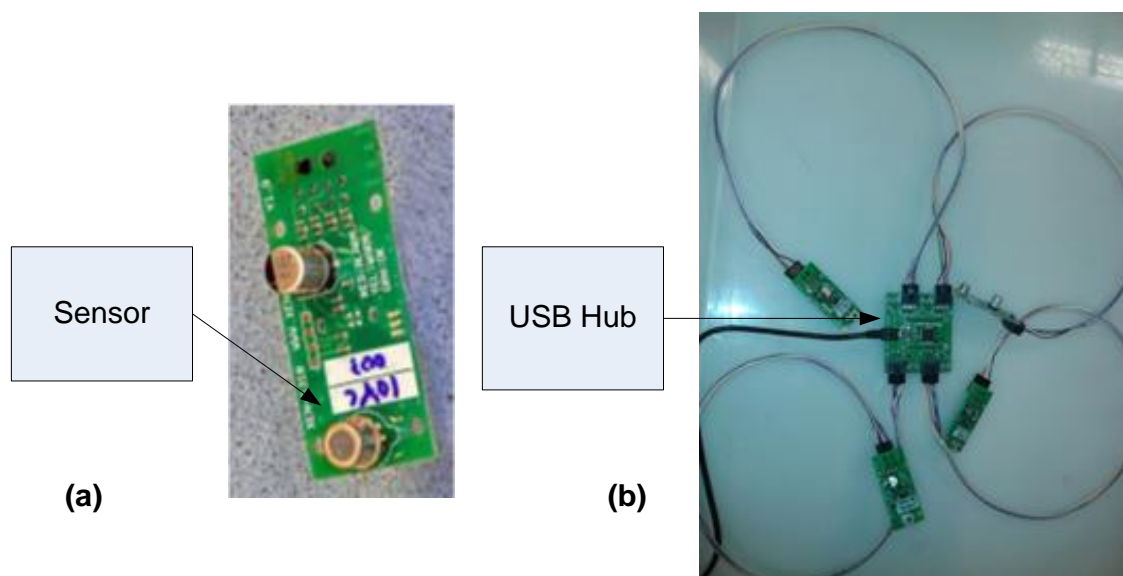


**Figure 3.12 (a) Xensor XEN3880 Helium sensor (b) USB hub and sensors**

### Operating principles

The XEN-TCG3880 thermal conductivity gauge is a thin-film thermopile thermal conductivity sensor, designed with a silicon-nitride closed-membrane structure to provide high sensitivity and resolution. The measurement principle relies on the decrease in effective thermal resistance between the sensitive area of the sensor and the ambient, caused by the thermal conductance of the surrounding gas. The thermal conductivity gauge performs a measurement of the thermal resistance between the hot junctions of its thermopile in the centre of the membrane and the cold junctions on the thick rim of the chip. This is achieved by using a resistor to heat the centre of the membrane, with the thermopile detecting the temperature increase. The actual temperature increase depends on the thermal resistance of the membrane and that of the ambient gas, in this case a helium air mix. [Sensor accuracy: Response time: 1s; Sensitivity: -1.1%/ (signal change for concentration in air); Precision: Inaccuracy He: 1 to 3% Full Scale: (Built in curves)] (Xensor Integration 2017). Recent updates to the sensor include battery power and WIFI, which could eliminate cables (which have a small effect on gas flow) from the test rig.

### Sensor calibration tests

Xensor Ltd. the helium sensor manufacturer advised of an update to the error on the concentration read outs of the XEN TCG 3880. Xensor Ltd. provided data from their own calibration tests. However, their data did not provide any detail around the error below

5% helium delivered by their mass flow controller. The tests in this investigation predominantly consider flow rates up to and around the hydrogen LFL of 4 %, so it would be important to have this information and adjust the data as needed. Also, it appeared from the Xensor Ltd graph (figure 3.13) that the error increased as concentration reduced.

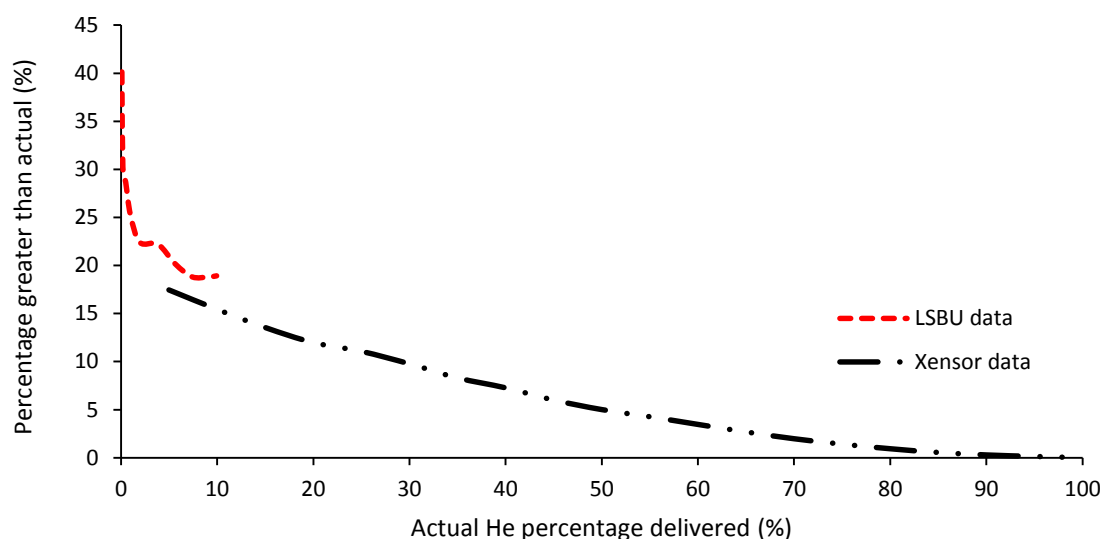


**Figure 3.13 Comparison of Xensor (Xensor Ltd. 2016) and LSBU calibration tests**

To be sure of the performance of the sensors used in these tests a calibration study was undertaken at LSBU using the eight sensors installed in the test rig. A sealable Perspex™ box (Figure 3.14) was prepared in which the eight sensors and two USB hubs were placed. Three MFCs were used to mix helium and air in fixed proportions from 1 to 10 % helium (v/v) and then supplied to the box. A steady state regime was reached in the box and then sensor concentrations noted via the USB readout (see table 3.1).

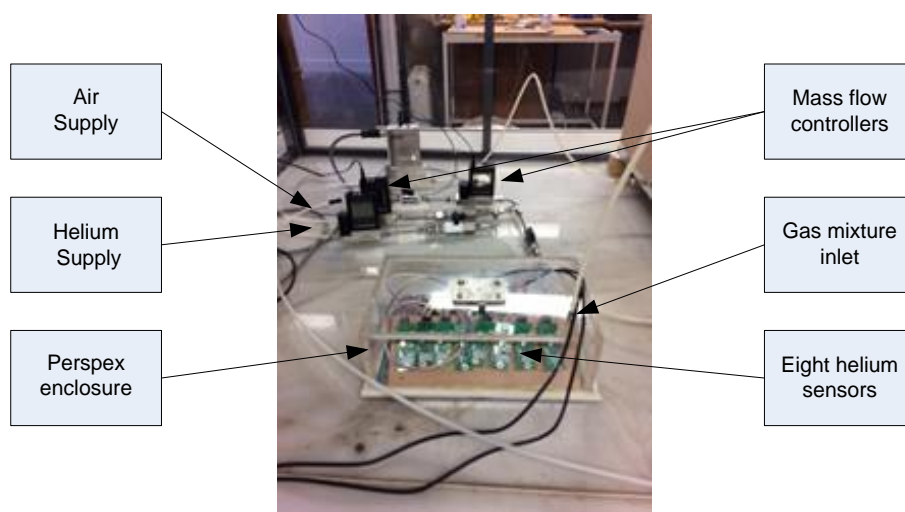


**Figure 3.14 Experimental set up for the calibration test**

**Table 3.1 LSBU Helium sensor calibration test results (Average of all 8 sensors)**

MFC He	MFC Air	Total Mix	He %	Sensor %	Increase	% Increase
5.00	5000.00	5005.00	0.10	0.14	0.04	40.14
10.00	5000.00	5010.00	0.20	0.26	0.06	30.26
25.00	5000.00	5025.00	0.50	0.64	0.14	28.64
50.00	5000.00	5050.00	0.99	1.24	0.25	25.24
100.00	5000.00	5100.00	1.96	2.40	0.44	22.40
200.00	5000.00	5200.00	3.85	4.70	0.85	22.20
300.00	5000.00	5300.00	5.66	6.80	1.14	20.13
400.00	5000.00	5400.00	7.41	8.80	1.39	18.80
500.00	5000.00	5500.00	9.09	10.80	1.71	18.80
BOC Ltd. Calibration gas			9.94	11.82	1.81	18.10

Figure 3.15 presents a graph of the delivered helium concentration (via the MFCs) against the sensor readout concentrations. The graph provided by Xensor Ltd has been added in for comparison (albeit they did not have data below 5 %). Trend line equations have been added. The graphs are similar, particularly at the lower concentrations. This new data will allow for error in the test results to be properly accounted for. Each sensor was calibrated at the commencement of each experimental test as part of the setup procedure and periodic calibration gas checks were also undertaken to check for sensor drift.

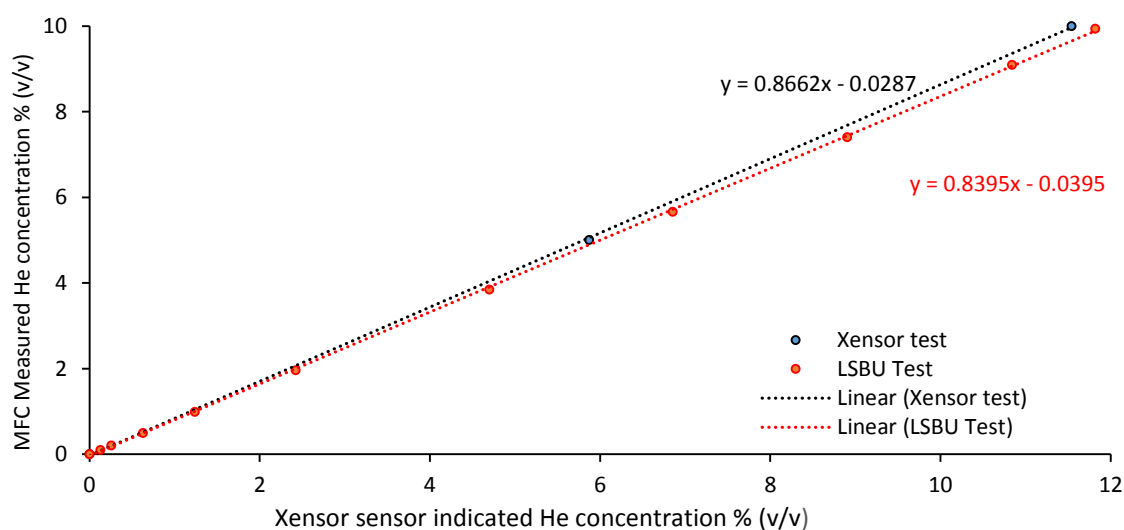


**Figure 3.15 Comparison of Xensor Ltd. and LSBU calibration tests (trend line equation added)**

### 3.4 Initial laboratory test rig experiments

The initial ‘base-case’ experimental rig was used to test the performance of the helium supply, MFC and sensors. A series of experiments to study the dispersion of helium in the enclosure and the effect of different vent arrangements on gas concentrations was

conducted. Figure 3.16 presents a schematic of the test enclosure, showing the position of the helium leak, ventilation openings and the Xensor helium sensors.

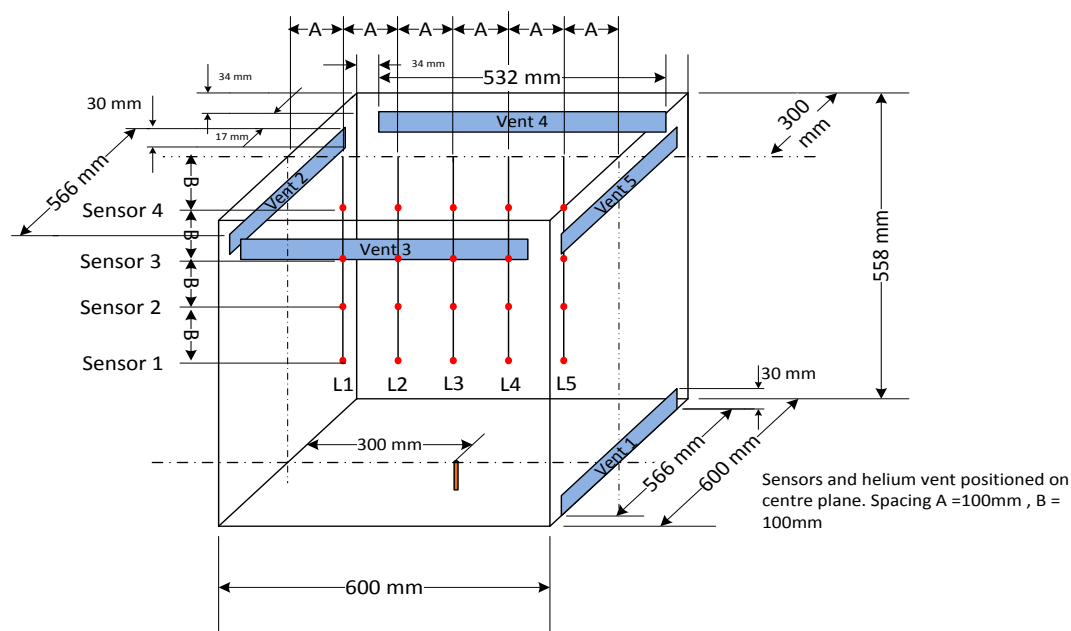


**Figure 3.16 Schematic for the initial enclosure test rig**

The sensors were attached to a rigid wire that was suspended from a rail fixed to the top of the enclosure. The rail allowed the wire to slide laterally across the roof to enable sensor readings to be taken on a plane through the centre of the enclosure. Five scenarios were tested (Table 3.2).

**Table 3.2 Initial ‘base-case’ experimental rig test scenarios**

Scenario	Vent Height (mm)	Vent Width (mm)	Vent Area (mm <sup>2</sup> )	Number of vents	Total Vent Area (mm <sup>2</sup> )
<b>Opposing upper and lower vents</b>	30	566	16980	2	33960
<b>Single upper vent</b>	30	566	16980	1	16980
<b>Two opposing upper vents</b>	30	566	16980	2	33960
<b>Three upper vents</b>	30	566	16980	2	49920
	30	532	15960	1	
<b>Four upper vents</b>	30	566	16980	2	65880
	30	532	15960	2	

Helium leak rates from 1 to 5 lpm were tested. For each test, the helium gas build-up passed through the transient phase to reach a steady state condition. Helium concentration data from the four sensors was retrieved and a time-averaged section (60 data points) of steady state data provided the helium gas concentration. The results of these tests were fully presented in a paper presented at the IChemE Hazards 26 Conference 2016.

The main learning from these tests was that the enclosure would not be versatile enough for future tests. In addition, the sensor ‘sliding rail’ arrangement was found to be too cumbersome and slow for data acquisition. Additional sensors would be the preferred method. The tests also provided the opportunity to test the accuracy of the MFC and determine its maximum accurate flow rate, which proved to be 10 lpm. Software control of the MFC and LabView data collection proved to be successful.

### 3.5 Final experimental test rig.

The base case test rig proved the experimental concept and the parameters within which the research test rig would need to operate. A new plywood enclosure was constructed to the specifications of the BOC Ltd. HFC enclosure. It was 600mm x 600mm x 400mm in size. The opposing end panels were easily removed (secured by bolts and wing nuts) to allow different vent schemes to be tested. The remaining panels were also changeable. The initial end panels installed replicated the BOC Ltd. enclosure vent size.



**Figure 3.17 Final Experimental test rig**

The final experimental rig (Figure 3.17) would now form the basis for all the tests required in this research investigation. The equipment was now optimised and effective.

Figure 3.18 presents a schematic for the final equipment layout. Additional helium sensors were purchased, and a new frame was built to hold them in two arrangements.

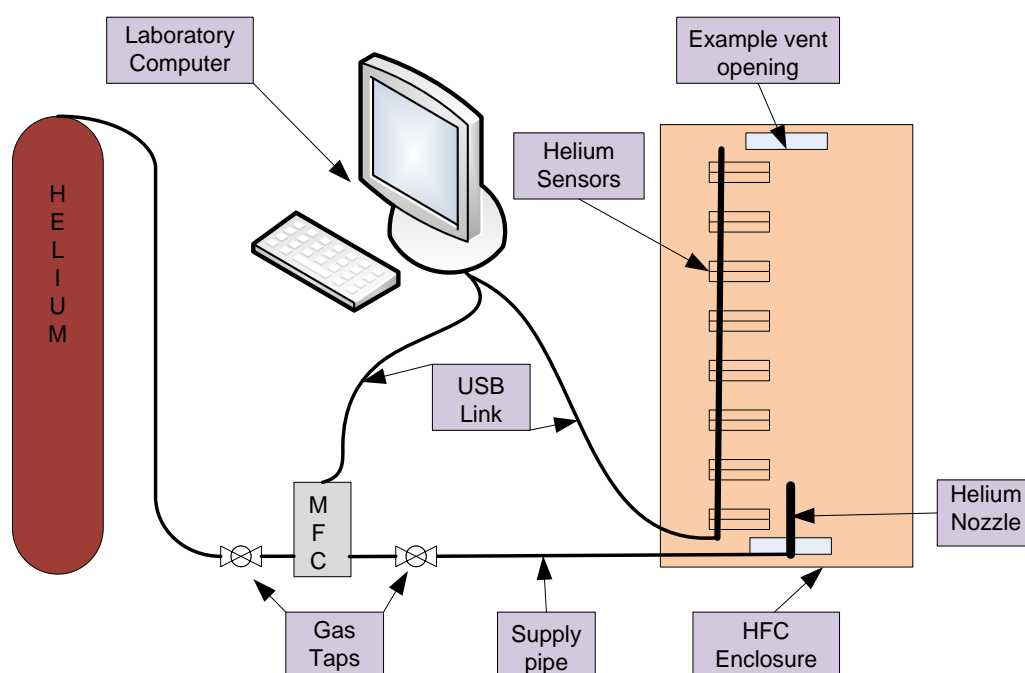


**Figure 3.18 Schematic diagram of the final test rig**

### 3.5.1 Plywood helium permeation test

The use of plywood to construct enclosures for helium passive ventilation experiments is not tested in the literature. As such, there is no data for helium permeation through 5mm plywood and no available diffusion coefficient. Helium like hydrogen is a very small atom and will readily pass through the structures of the materials containing it. Some materials are more resistant than others. Plywood is a strong composite material, but essentially organic in structure and will have a degree of porosity. The plywood used in the enclosure was not treated or coated to reduce this porosity, although aluminium tape was used to cover the end panels in some tests, which would reduce porosity.

**Experimental setup:** The ‘final’ ( $0.144 \text{ m}^3$ ) enclosure was used for this test (Figure 3.19) with the methodology used by Yang (2013) as a guide. The enclosure was sealed at every joint using adhesive aluminium tape. When constructed a silicon bead was added internally to all visible joints. Helium was supplied to the enclosure via a 4 mm nozzle at the centre of the enclosure 100 mm above the floor. A mass flow controller metered the gas supply. Eight sensors in the stack configuration were installed in the enclosure as per

figure 3.25(b). [Sensor number and height: 74-560 mm, 73-520 mm, 31-470 mm, 33-420 mm, 72-320 mm, 71-220 mm, 30-120 mm, 32-40 mm]. The cabling for the sensor USB connectors was passed through a small hole at the base of one of the end panels. This hole would allow air/helium to escape from the enclosure whilst it was filling.

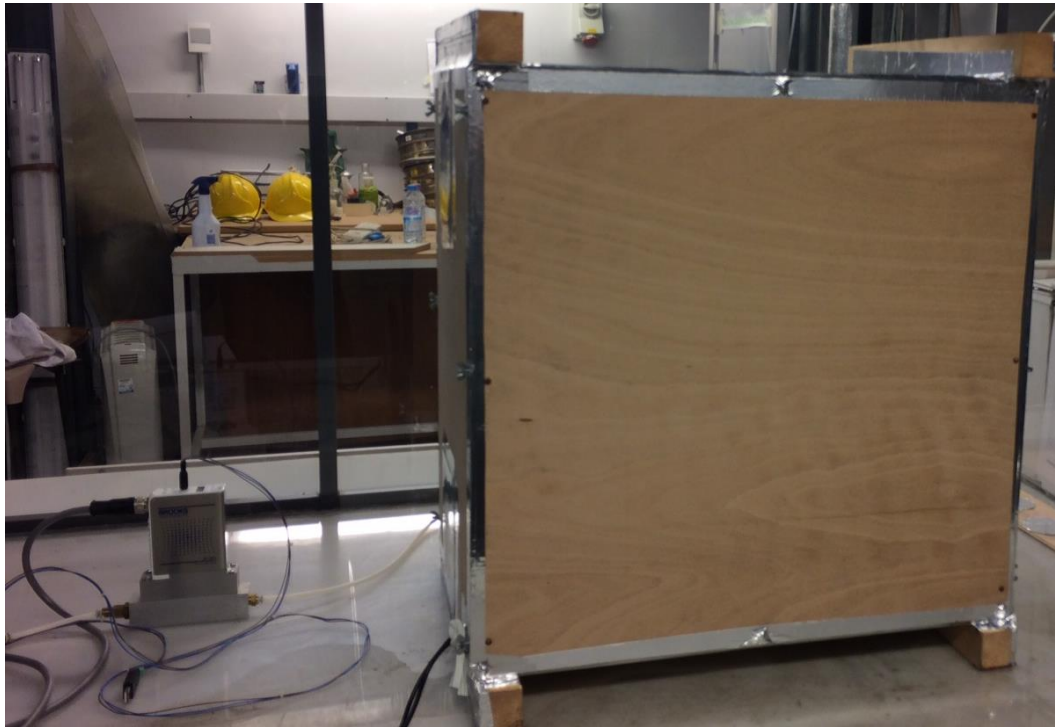


**Figure 3.19** The final enclosure sealed for the permeation test

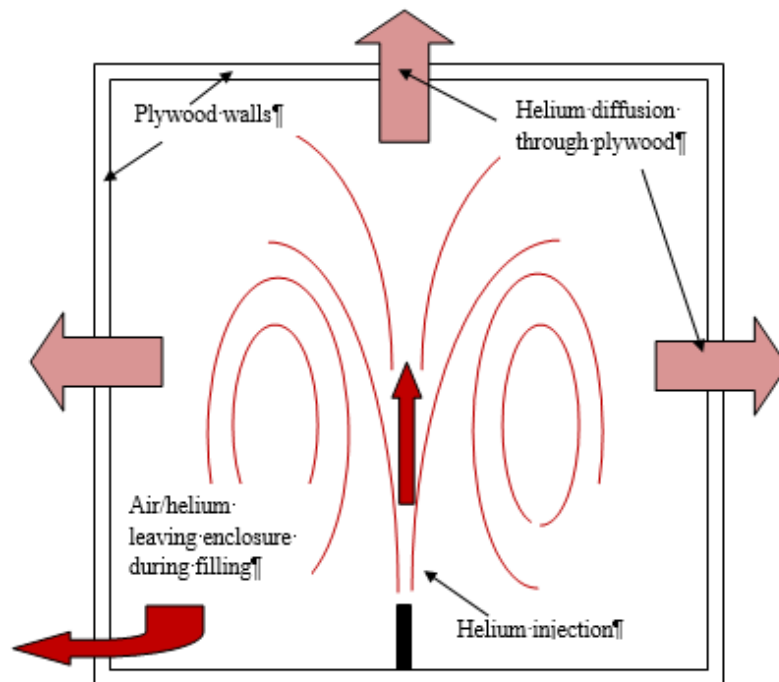


**Figure 3.20** Schematic of experimental test



**Experimental test:** Once the enclosure was sealed and the sensors calibrated, helium was introduced into the enclosure at 10 lpm (Figure 3.20) (also at 0.5 and 0.25 lpm). The helium concentration increased steadily. As the concentration increased it became more uniform vertically in the enclosure. When the concentration reached about 96 % (> 1 hour) a near steady state was apparent. At this point the cable hole was sealed with aluminium tape and the gas supply was halted. The sensors then recorded the slow and steady decline in the internal helium concentration. Over a period of 24 hours the helium diffused through the enclosure structure until an approximately zero helium concentration was reached. Figure 3.21 presents the decay curve showing how the helium concentration decreased with time. The test was repeated at rates of 0.5 lpm and 0.25 lpm.

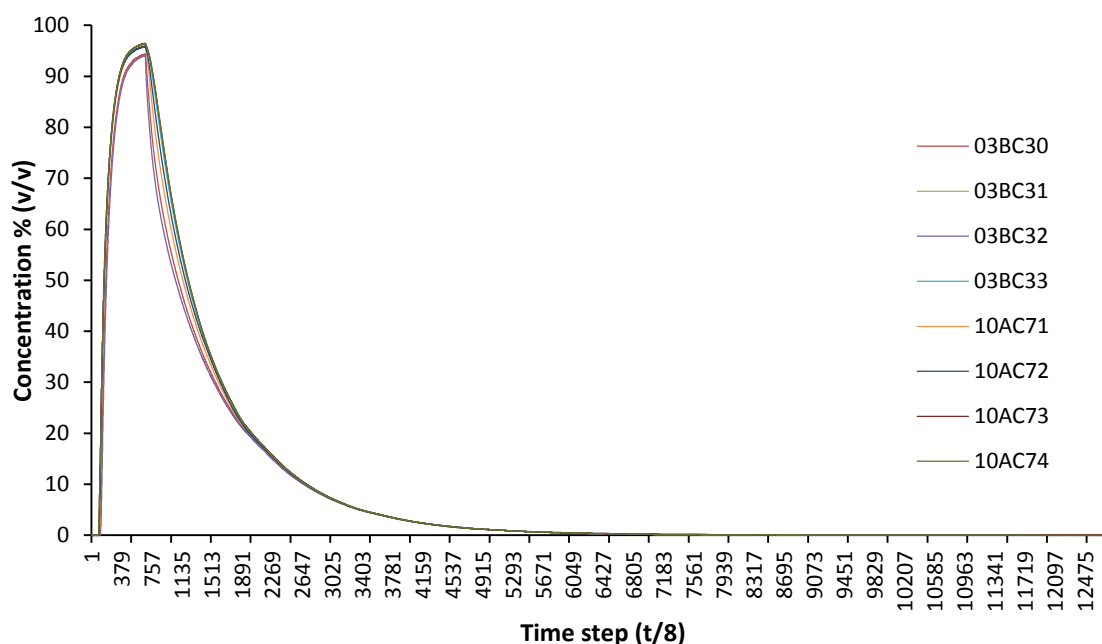


**Figure 3.21 Helium permeation test: Concentration vs sensor time step [8 sensors]**

**Analysis:** Analytical assumptions are that a uniform helium concentration was present in the enclosure, a quasi steady-state concentration gradient is achieved within the plywood, even though the enclosure concentration changes over time and helium is treated as an ideal gas. Yang's equation is then used to calculate a diffusion coefficient for a given enclosure mole fraction. Yang's equation provides a diffusion coefficient for a given steady state condition and mole fraction. As such the diffusion coefficient will vary temporally as the concentration reduces. The concentration was uniform through the enclosure, so an average concentration was used in the calculation. Figure 3.22 presents the average concentration against seconds and inset against hours elapsed.

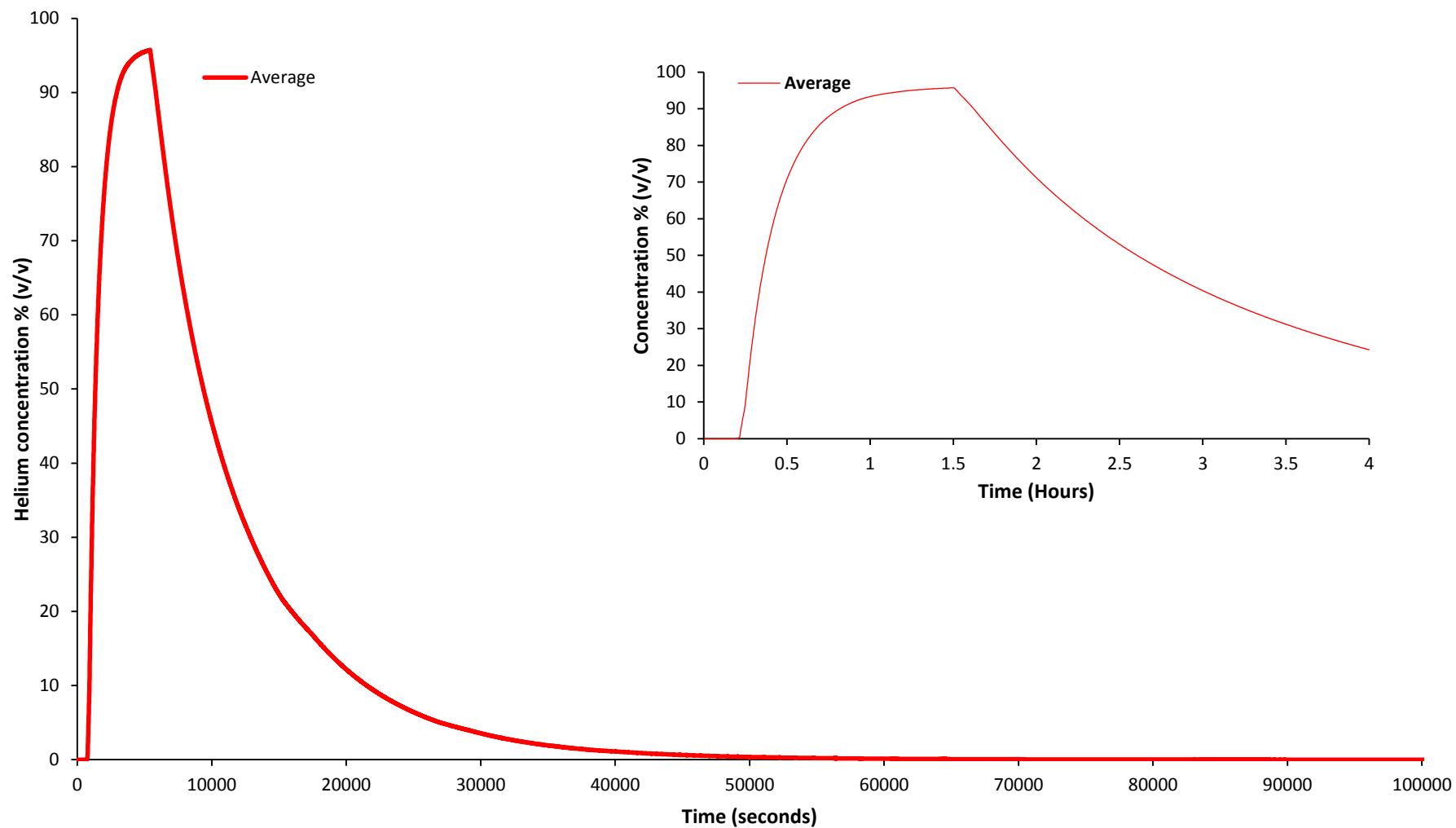


**Figure 3.22 Diffusion test: Helium concentration – average of all sensors- against seconds [Inset concentration against time (hours)]**

**Diffusion coefficient calculation:** Yang's equation [1] was used to calculate a diffusion coefficient at a steady state mole fraction of 0.96 (@ 10 lpm), 0.32 (@ 0.5 lpm) and 0.25 (@ 0.25 lpm) to test the model. A spreadsheet was then used to apply the equation to these values (and average temperature, from the sensors).

$$D_e = \frac{n_f R T \delta}{P A y_{ss}} \quad [1]$$

$D_e$  = Diffusion coefficient

$\delta$  = Thickness of the plywood panel (0.005 m)

$n_f$  = Helium molar flow rate into the enclosure ( $\text{mol s}^{-1}$ )

$P$  = Enclosure pressure (Pa) (Atmospheric 101325 Pa)

$R$  = Universal gas constant ( $8.315 \text{ J mol}^{-1} \text{ K}^{-1}$ )

$T$  = Enclosure temperature (K) ( $273.16 + \text{average enclosure temperature}$ )

$A$  = Enclosure surface area ( $1.68 \text{ m}^2$ )

$Y_{ss}$  = Enclosure helium mole fraction at steady state

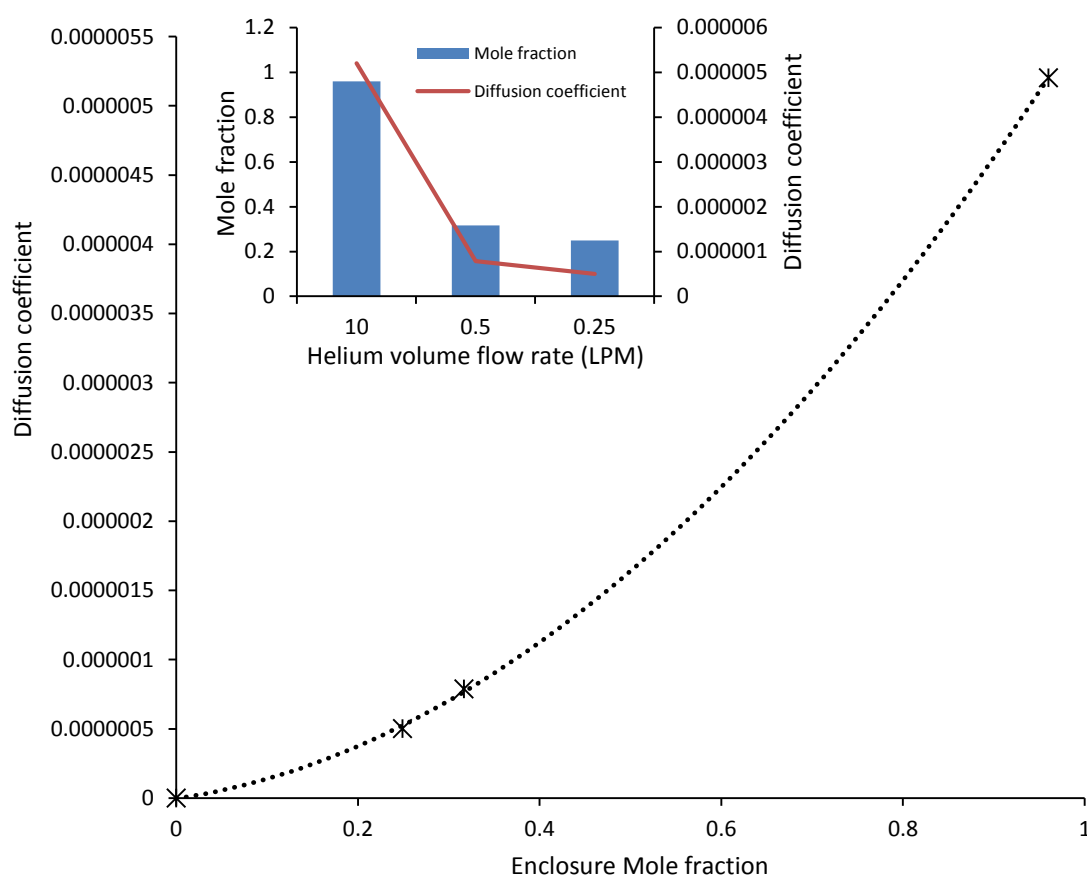


**Figure 3.23 Graph of diffusion coefficient against enclosure helium mole fraction**

At a steady state helium delivery rate of  $0.007 \text{ mol s}^{-1}$  a steady state concentration of 96% was achieved. Yang's equation produces a diffusion coefficient of  $5.24 \times 10^{-7} \text{ m}^2 \text{ s}^{-1}$ . Figure 3.23 presents a graph of diffusion coefficient against enclosure mole fraction, with a plot of mole fraction and diffusion coefficient against helium leak rate inset.

**Conclusion:** Some experimental tests in this investigation have led to enclosure mole fractions that have peaked at about 0.25. Most tests though have resulted in mole fractions less than 0.1, with the majority at levels below 0.04, the hydrogen LFL. At this level, particularly in a ventilated enclosure with driving forces pushing the helium towards a vent as opposed to the wall surface, diffusion through the plywood enclosure is negligible and can be disregarded for ventilation calculations in this thesis.

### 3.5.2 Sensors:

A stainless-steel frame was constructed to hold eight sensors and two USB hubs. The sensors were fitted on two parallel bars (Figure 3.24 (a)), with the hubs on the end supports. The sensors were positioned either side of the helium plume. This arrangement would capture the average concentration of helium in the stratified buoyant layer at the top of the enclosure. The frame was inserted centrally into the enclosure (Figure 3.24 (b)).

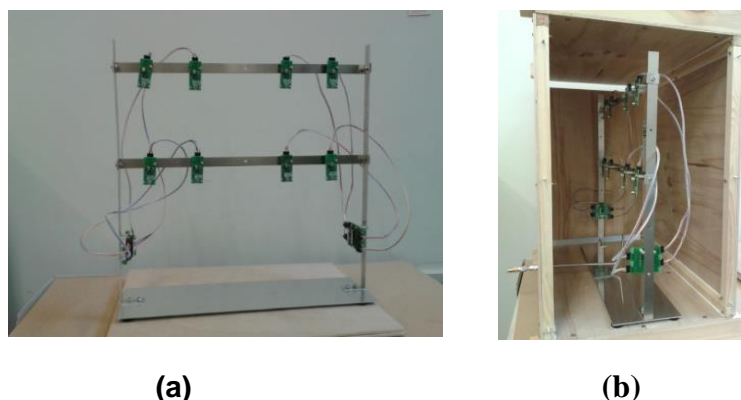


**Figure 3.24 (a) Frame sensor arrangement; (b) frame installed in enclosure**

To obtain more detailed data on concentration distribution in the enclosure, a second sensor arrangement was used. A vertical stack of sensors was created using the frame end support. This would provide an insight into concentration variation vertically in the enclosure. Figure 3.25 (a) shows the sensor stack and Figure 3.25 (b) shows it installed in the enclosure. Figure 3.26 is a schematic of the rig showing the sensor positions and nozzle gas inlet in the enclosure. The new enclosure also contained a stainless steel 4 mm internal diameter nozzle set 100 mm above the base of the enclosure. This nozzle position

is used in the majority of the experimental tests. This approach follows methodologies in the literature, it simplifies transition from study to study and also a low altitude leak has the potential to fill more of the enclosure, providing a more rigorous test. Leak position is important and worthy of further investigation.

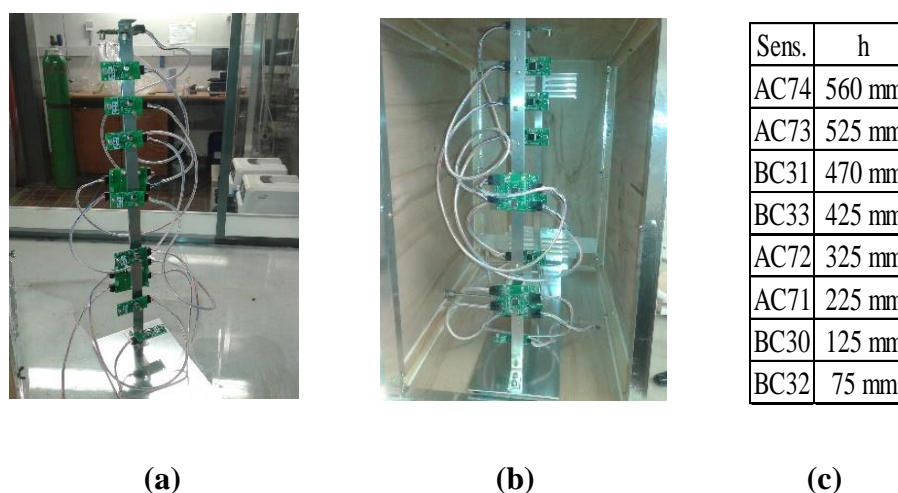


**Figure 3.25 (a) Sensor Stack; (b) Stack installed in enclosure; (c) Sensor height**

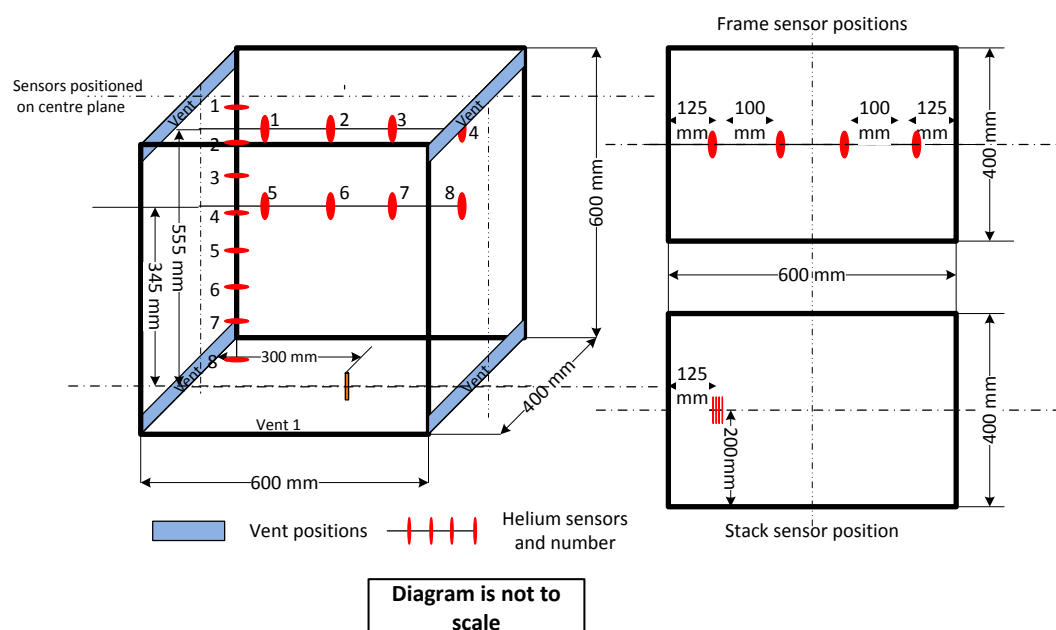


**Figure 3.26 Experimental scheme, showing the position of helium sensors**

### 3.6 Ventilation configurations

The revised enclosure forms the basis for all subsequent experimental tests. A series of iterations have been developed to test the ventilation performance of the enclosure in different scenarios. An operational HFC enclosure may be deployed in a variety of

external environments, so different ventilation options need to be investigated. For all tests, the 4 mm diameter inlet nozzle was used with leaks in the range 0.25 lpm to 10.0 lpm. The following sections outline the ventilation schemes tested.

### 3.6.1 Plain vents

Plain vents in this investigation are simple rectangular vents on the vertical face of the enclosure. Primarily cross flow schemes were tested, with opposing upper and lower ventilation openings. Two series of plain vent tests were conducted:

**Series A:** These tests replicate the openings on the BOC Ltd. environmental enclosure. They are 360 mm wide x 20 mm high and there are opposing upper and lower vents. Leak rates from 1 to 10 lpm were tested (Figure 3.27 (a)).

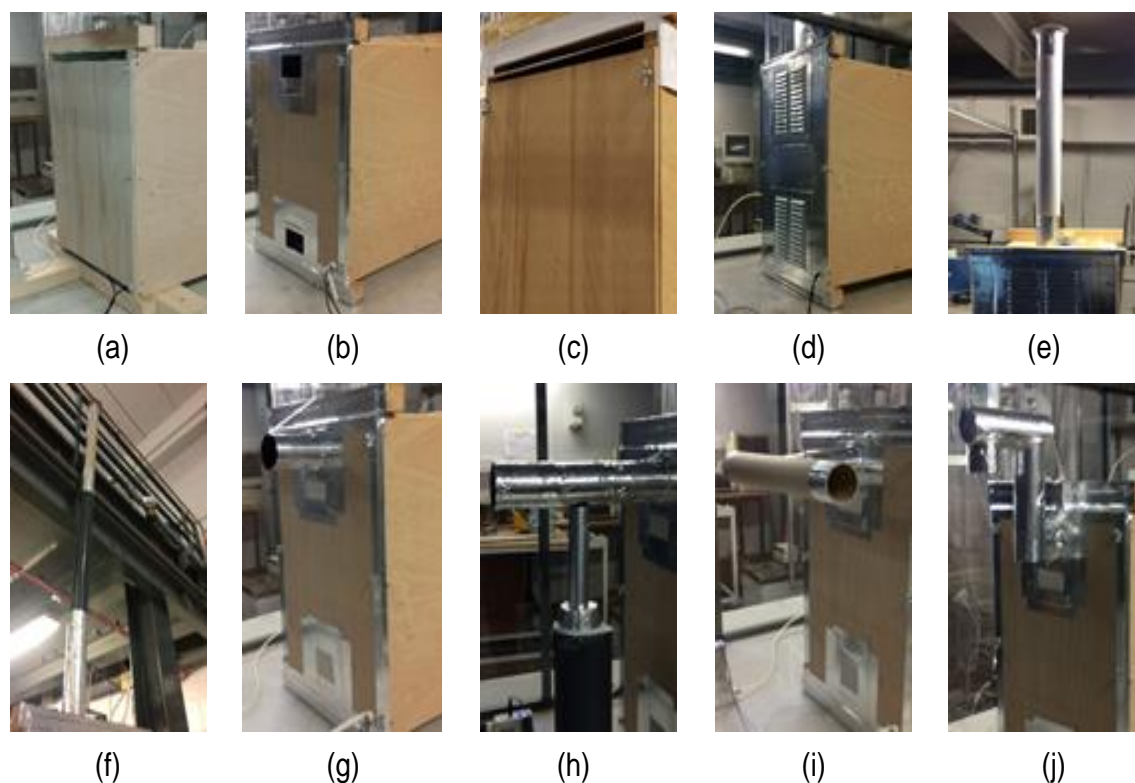


**Figure 3.27 Example ventilation scheme configurations (a) BOC plain vent (b) Same are plain vent (c) Simple louvre vent (d) Aluminium louvre vent (e) Small chimney (f) Tall chimney (g) Short flue (h) Long flue (i) T-flue (j) Snorkel**

**Series B** These tests replicated the opening sizes of the aluminium vent tests. Twelve aluminium louvre vent tests were completed, a test for each row of louvres added. Comparison tests with plain rectangular vents of the same opening area as the louvres

were conducted. Opposing upper and lower vents were used (Figure 3.27 (b)). Leak rates from 1 to 10 lpm were tested.

### **3.6.2 Simple louvre vents**

For these tests the Series A vents were fitted with simple horizontal louvre slats (Figure 3.27 (c)). Leak rates from 1 to 10 lpm were tested. A comparison exercise was then conducted which formed the basis of a paper presented at the HySafe International Conference on Hydrogen Safety 2017 in Hamburg (Ghatauray et al 2017).

### **3.6.3 Pressed aluminium louvre vents**

BOC Ltd. are interested in the use of pressed louvres on their environmental enclosure. Upper and lower sets of one to twelve louvres (Figure 3.27 (d)) were installed on both ends of the enclosure. Leak rates from 1 to 10 lpm were tested. Further tests were conducted using only the upper louvre vents to simulate the case where lower vents may become blocked. Data collected from these tests was used for comparison with the Series B tests.

### **3.6.4 Chimney vents**

Chimney vents are a useful way of increasing the pressure differential between upper and lower ventilation openings (Figure 3.27 (e) and (f)). Chimney stacks can be vulnerable to damage, so it is important to understand the benefits and the effect of stack height on enclosure concentration. Leak rates from 0.5 to 5 lpm were used. Several variations were tested

- Single chimney
- Twin chimneys
- Rain cover chimney
- Height differential (doubling, tripling, quadrupling)

Two of the potential uses of the BOC Ltd. enclosure are for lighting and mobile telecom towers. The telescopic towers used could potentially double as chimney vents.

### **3.6.5 Chimney vents with obstruction**

Most of the tests in this investigation were carried out with an empty enclosure (except for the sensors and frame) for comparative purposes. Some chimney tests have been carried out with a simulated fuel cell obstruction positioned in the top half of the enclosure and attached to a side wall. These tests provided data on how the reduced volume affects helium concentrations. Similar tests were conducted in the scoping exercise.

### **3.6.6 Flues**

Flues are used to remove flammable gas away from an enclosure (Figure 3.27 (g, h and i)). A flue was tested to see whether it improved conditions over a similar area plain vent. Several variations were tested at leak rates from 0.5 to 5 lpm.

- Short flue - no inlet
- Short flue with same area inlet
- Long flue with same area inlet
- Double exit flue

### **3.6.7 Snorkel vent**

The snorkel vent (Figure 3.27 (j)) attempts to add stack height, rain protection and flue distance to the outlet vent. They can potentially meet the environmental protection needs of the enclosure. Leak rates from 1 to 10 lpm were tested and comparisons made with the other schemes tested.

## **3.7 Schlieren System – Visualising helium flow in the enclosure**

Useful qualitative information about buoyant gas behaviour in the HFC enclosure could be obtained if it was possible to view the helium as it emerged from the nozzle and formed a stratified plume. It would also provide information about how it behaved with obstructions in the enclosure and help to inform design developments. The Schlieren system provides a means to visualise gases of different densities and refractive index. As refractive index is proportional to density, helium as a light gas, is well suited to visualisation techniques based upon refractive index, such as Schlieren (Ingram 2015).



Schlieren (streaks) are optical inhomogeneities in transparent media, first observed by Robert Hooke in 1665, using a large convex lens and two candles, to observe warm air rising. The conventional Schlieren technique was developed and named by August Toepler in the 19<sup>th</sup> century, using a point light source to illuminate a test section, containing the schliere. In the conventional Schlieren system, a source of collimated light (parallel light rays) is focused with a converging optical element (curved mirror) with a knife edge placed at the focal point to block out half of the light, uniformly reducing the illumination of the image. A second mirror is used to image the test section onto a screen or camera. (Settles 2001) (Hargather 2012).

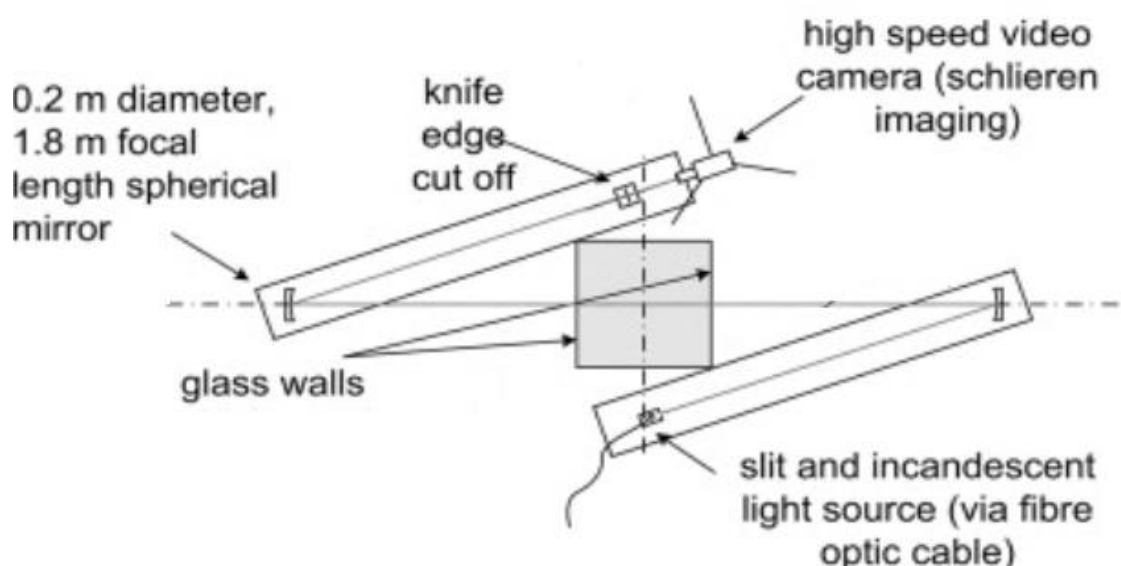


**Figure 3.28 Schlieren system to visualise helium in the enclosure (Ingram J 2015)**

To visualise the helium leak in the HFC enclosure the two 600mm x 600mm plywood side panels, on the enclosure, were replaced with plate glass panels. A general-purpose, 2-mirror, Z-type Schlieren system (Settles 2001) was set up using two high quality ( $\lambda/10$ ), 0.20 m diameter, spherical mirrors of 1.8 m focal length (Figure 3.28). Illumination was provided by a light box masked with a 1 mm by 3 mm slit and an Olympus i-Speed digital camera (with 150 mm lens) was used to record the images.

A knife-edge with adjustable mount provided the optical cut-off necessary for the Schlieren effect to be visualised. Helium emerging from the nozzle and subsequent turbulent plume was filmed, during an experimental test, using the Olympus camera.

Digital images were obtained from the camera using Olympus “De-luxe” i-Speed software (Ingram 2015). Two areas of interest were selected for the Schlieren system visualisations;

1. The helium emerging from the nozzle
2. The behaviour of helium passing through a plain outlet vent and a louvre outlet vent to observe the flow behaviour.

### **3.8 Environmental parameters**

The behaviour of the buoyant gas release can be affected by environmental conditions such as temperature, humidity and wind. The Xensor helium sensors are also able to detect temperature and humidity. The data collected from the various tests was examined to look for the influence of temperature and humidity on enclosure helium concentration.

### **3.9 Computational Fluid Dynamics (CFD): Methodology**

There are significant benefits to the use of computer-based models and simulation techniques to predict fluid flow conditions and behaviour in engineering investigations. Physical modelling can be reduced, saving money and time. That said, computer modelling outcomes are dependent upon the numerical model used, the knowledge and skill of the user and the computing power available. The codes also need to be benchmarked and validated against reliable experimental data, so that their use can be optimised. CFD is a valuable tool for improving experimental rig and ventilation design in this investigation.

#### **3.9.1 Governing equations**

Computational fluid dynamics (CFD) has evolved to become a useful tool for engineers. There are many commercial and open source software codes available, the latter predominantly used in academia. Commercial codes have become user focused and easier to use facilitating learning and practical use. At the heart of all CFD codes though are the differential equations for the conservation of mass, momentum (three equations) and energy, known as the Navier-Stokes equations (equations 2-6).

**Conservation of mass**

$$\frac{d\rho}{dt} + \nabla \cdot \rho \vec{V} = 0 \quad [2]$$

**Conservation of momentum**

$$\rho \left( \frac{\partial u}{\partial t} + u \frac{\partial u}{\partial x} + v \frac{\partial u}{\partial y} + w \frac{\partial u}{\partial z} \right) = \rho g_x - \frac{\partial P}{\partial x} + \mu \left( \frac{\partial^2 u}{\partial x^2} + \frac{\partial^2 u}{\partial y^2} + \frac{\partial^2 u}{\partial z^2} \right) \quad [3]$$

$$\rho \left( \frac{\partial v}{\partial t} + u \frac{\partial v}{\partial x} + v \frac{\partial v}{\partial y} + w \frac{\partial v}{\partial z} \right) = \rho g_y - \frac{\partial P}{\partial y} + \mu \left( \frac{\partial^2 v}{\partial x^2} + \frac{\partial^2 v}{\partial y^2} + \frac{\partial^2 v}{\partial z^2} \right) \quad [4]$$

$$\rho \left( \frac{\partial w}{\partial t} + u \frac{\partial w}{\partial x} + v \frac{\partial w}{\partial y} + w \frac{\partial w}{\partial z} \right) = \rho g_z - \frac{\partial P}{\partial z} + \mu \left( \frac{\partial^2 w}{\partial x^2} + \frac{\partial^2 w}{\partial y^2} + \frac{\partial^2 w}{\partial z^2} \right) \quad [5]$$

**Conservation of energy**

$$\rho \left( \frac{dE}{dt} + u \frac{dE}{dx} + v \frac{dE}{dy} + w \frac{dE}{dz} \right) = \nabla \cdot (k \nabla T) - \nabla \cdot p \vec{V} + Q_v + Q_g \quad [6]$$

$\rho$  = Fluid density (mass per unit volume)

$u, v$  and  $w$  represent velocity ( $m s^{-1}$ )

$g$  = Gravitational acceleration ( $9.81 m s^{-2}$ )

$\mu$  = the coefficient of dynamic viscosity

$E$  = Energy per unit mass of fluid

$\bar{V}$  = Volume (control volume)  $m^3$

$T$  = Temperature (K)

$p$  = Pressure (Pa)

$Q_v$  = heat per unit volume

Additional equations are included to cater for the conditions being examined for example, turbulence, laminar flow or multiple species and this is where individual codes start to

differ. This investigation will use the commercially available codes, SolidWorks Flow Simulation (Dassault Systems 2016) and ANSYS: Fluent (ANSYS Inc. 2018). They have different approaches to running a CFD simulation and this investigation will provide useful comparative data with which to assess their performance.

### **3.9.2 Mesh**

The equations are discretised in the CFD model using the ‘finite volume method’ (FVM). The geometry under consideration is divided into discrete small cells (finite volumes). The equations are solved in a cell and the output is fed to adjacent cells where the next calculation is made and so on. The cell structure created in the model geometry is known as a mesh. There are numerous ways of creating a mesh from simple block to complex polyhedral structures. The different structures have an impact upon computational complexity and simulation output, so much consideration must be given to how the mesh is structured and refined before the simulation takes place.

### **3.9.3 Mesh sensitivity**

The engineering question will usually inform the mesh design with refinement being focused upon areas of interest. For example, if examining buoyant gas stratification in an enclosure with an upper vent, refinement would be appropriate at the top of the enclosure and surrounding the vent. Mesh quality will impact upon the quality of the result and the computational expense. A mesh sensitivity study is undertaken to assess the level of mesh refinement necessary before consistent results are achieved. Mesh refinement refers to the amount of detail in the mesh, such as the number and size of mesh cells. Consistent results are where further refinement does not improve on the numerical outcome. Several levels of mesh refinement are chosen, simulations run and the results compared.

Visser et al (2016) were investigating CFD capability to model hydrogen distribution during the course of a severe accident due to a hydrogen release in nuclear containment. They used the THAI-HM2 experimental investigation as the basis of their study. The THAI-HM2 tests used a cylindrical containment vessel (9.2 m tall, 3.2 m diameter, 60 m<sup>3</sup> volume). Visser et al used ANSYS: Fluent 6.3 to produce a model for CFD analysis and conducted a mesh sensitivity test. Figure 3.29 shows a) the vessel, b) a section through the vessel and c) the four meshes produced for the test ( $y^+ = 1$  mesh, a standard mesh, a

coarse mesh and a fine mesh). Simulations were run with the four meshes and comparison made with the experimental data. Visser et al found that in their investigation the course mesh provided results close enough to the fine mesh. This meant that the coarse mesh could be used, saving computational time. Figure 3.30 compares mesh sensitivity test data with the THAI-HM2 experimental data at four data points as indicated in the figure.

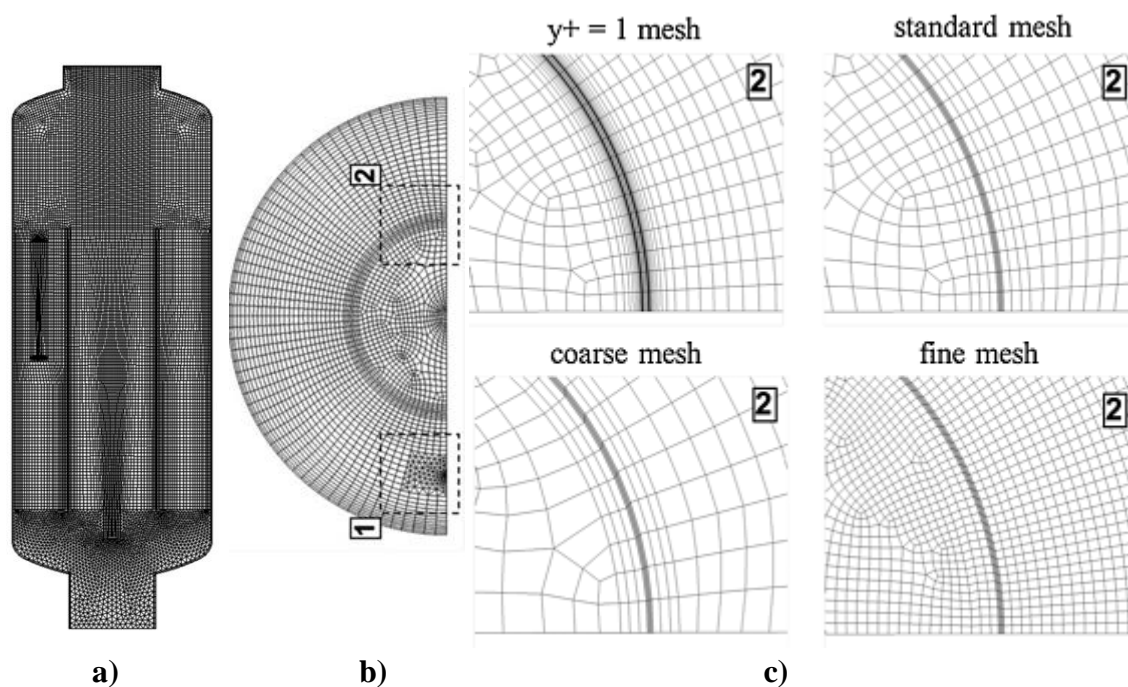


**Figure 3.29 a) Meshed containment b) Section c) Four meshes (Visser et al 2016)**

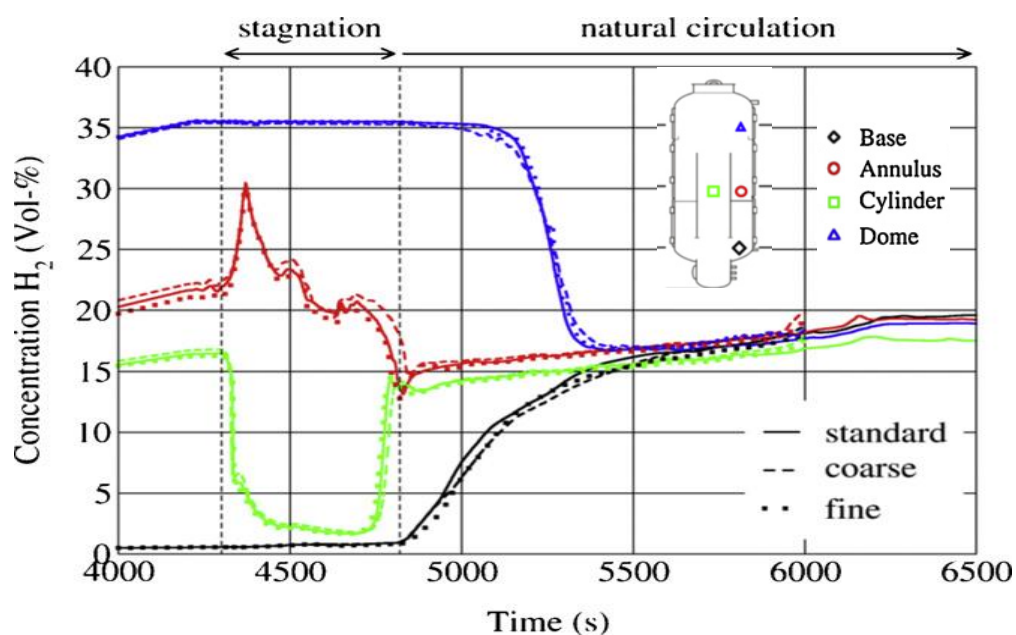


**Figure 3.30 Mesh data comparison with experimental data (Visser et al 2016)**

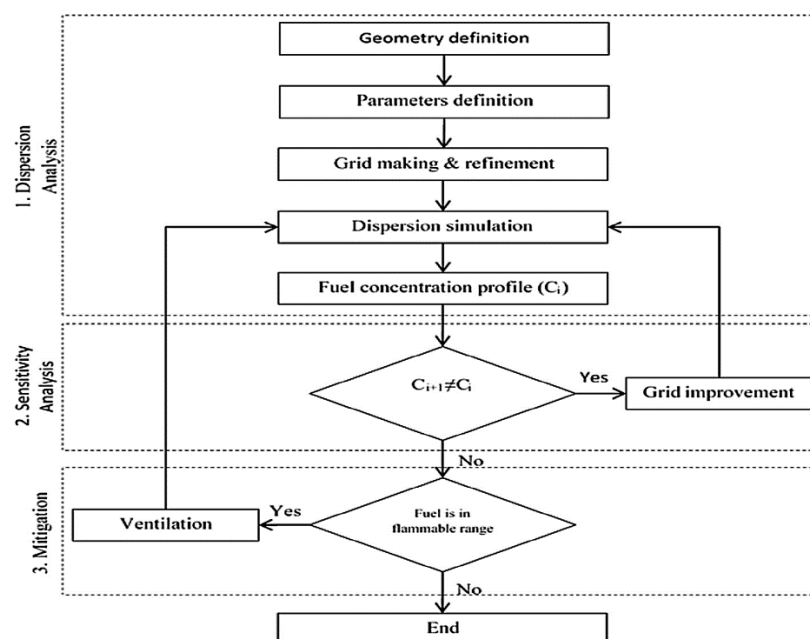


**Figure 2.31 Simulation methodology (Dadashzadeh 2016)**

Dadashzadeh (2016) applied the simulation methodology shown in Figure 2.31. The hydrogen concentration profile was examined and if it did not meet expectations, further refinement was applied. Driss et al (2014) used SolidWorks Flow Simulation to study turbulent flow around a turbine rotor in a wind tunnel. Their mesh sensitivity study used six levels of refinement of the wind tunnel model (Figure 3.32 (a)). The graph in figure 3.32 (b) shows the largest mesh size was a good correlation to the experimental data.

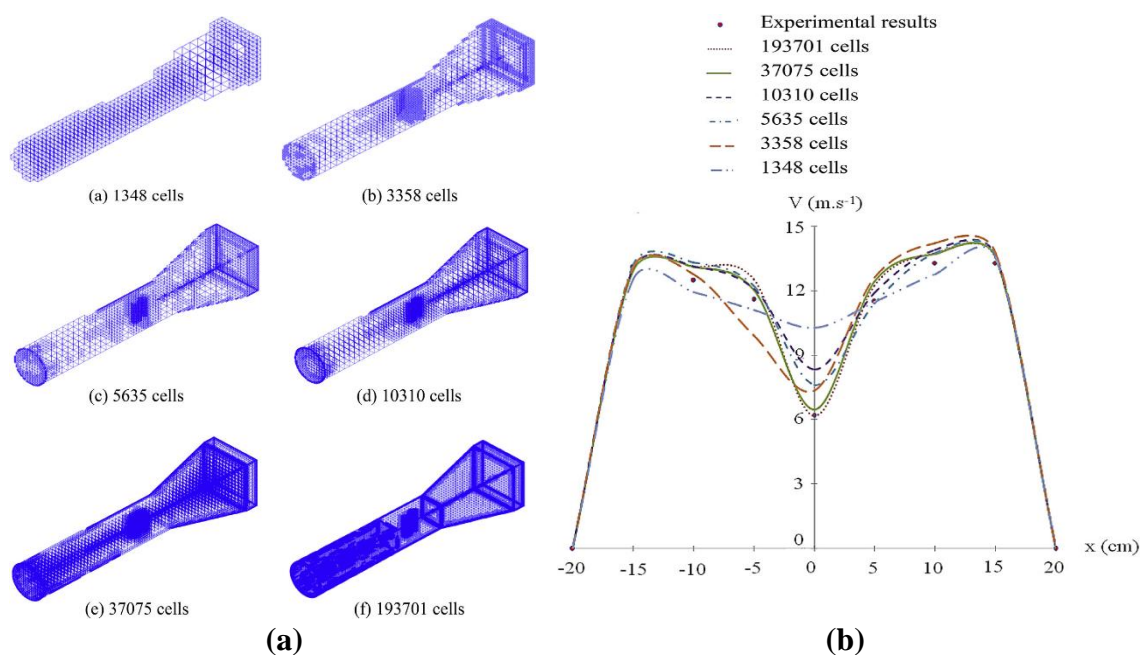


**Figure 2.32 (a) Six mesh levels (b) Comparison with experimental data (Driss 2014)**

### 3.9.4 The CFD Process

The CFD process can be simplified into three components, pre-processing, solver and post-processing. Pre-processing uses an interface for inputting data and defining the engineering problem. The physical geometry with associated fluid or computational domain can be set. The computational mesh is created and refined. Fluids, material, boundary conditions and the initial conditions for the simulation can all be allocated. A turbulence model (Table 3.3) is also applied.

**Table 3.3 Range of turbulence models available in SolidWorks and ANSYS**

Turbulence model	CFD Code
Standard $k-\varepsilon$ ( <i>Favre</i> )	SolidWorks Flow Simulation
I-L Turbulence intensity and length	SolidWorks Flow Simulation
Standard $k-\varepsilon$	ANSYS-Fluent
Realizable $k-\varepsilon$	ANSYS-Fluent
RNG $k-\varepsilon$	ANSYS-Fluent
EDC (Eddy dissipation concept)	ANSYS-Fluent
(Transitional) SST (Shear Stress transport)	ANSYS-Fluent
SAS (Scale Adaptive simulation)	ANSYS-Fluent
LES (large Eddy Simulation)	ANSYS-Fluent
Standard $k-\Omega$	ANSYS-Fluent
E-LES (Embedded LES)	ANSYS-Fluent
WM-LES (Wall model)	ANSYS-Fluent
Dynamic Smagorinski LES	ANSYS-Fluent
LES-RNG (Renormalisation Group)	ANSYS-Fluent
DES (Detached eddy simulation)	ANSYS-Fluent

The solver is responsible for the major computational and numerical solutions. The solver uses a discretisation method to solve the equations. The finite volume method integrates the governing equations in finite (control) volumes, throughout the whole computational domain. The SIMPLE (Semi-Implicit Method for Pressure Linked-Equations) algorithm (Patankar and Spalding 1972) is used to ensure the correct coupling between the pressure and velocity fields. It is an iterative solution method where a guessed pressure field is used to solve the momentum equations and a pressure correction equation is solved to obtain a pressure correction field, used to update the velocity field (Holborn et al 2012).

A solution is delivered when convergence is achieved (arrives at a stable value). The solver output is flow variable values at the mesh nodes. Solutions provide the field

distributions of pressure, velocity, temperature, the concentrations of water vapour (relative humidity), gas and contaminants, and turbulence parameters such as:

- Turbulent kinetic energy  $k$ ,
- Turbulence dissipation  $\varepsilon$ ,
- Specific turbulence dissipation  $\omega$
- Turbulence intensity,  $Tu$
- Turbulence viscosity ratio  $\mu_t / \mu$
- Turbulence length scale  $Tu_L$

The post processor user interface allows the operator to extract the data from the nodes for analysis and present it graphically in several ways. Figure 3.33 presents a process map for SolidWorks Flow Simulation and ANSYS Fluent.

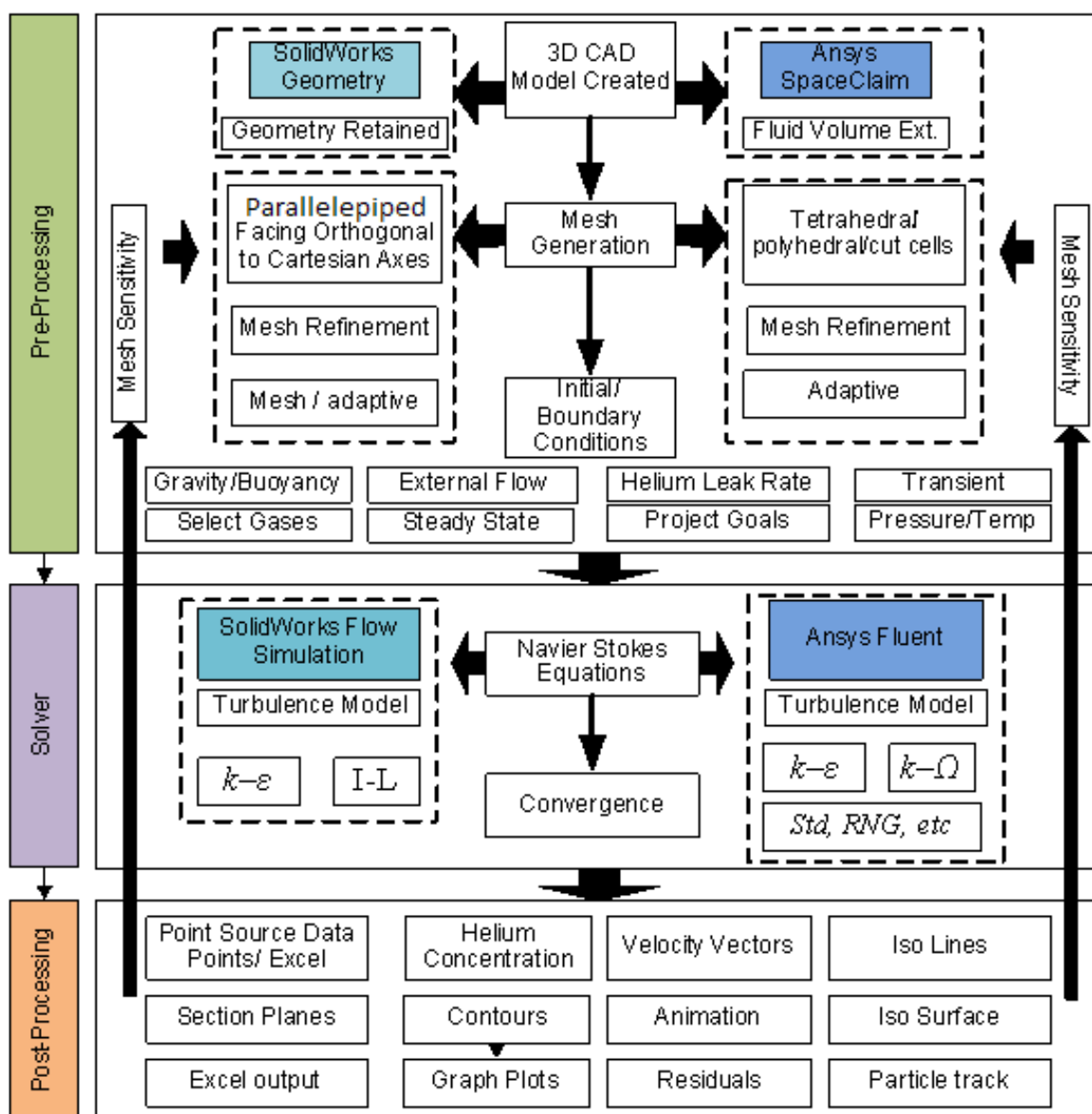


Figure 3.33 CFD process map SolidWorks Flow Simulation and ANSYS: Fluent



### 3.9.5 SolidWorks Flow Simulation (2017): CFD

SolidWorks Flow Simulation solves the Navier Stokes equations for the conservation of mass, momentum and energy for fluid flows. These equations are supplemented by fluid state equations, which define the nature of the fluid with regards to for example, fluid density, viscosity and thermal conductivity. The problem under investigation is quantified by the definition of its geometry, boundary and initial conditions (Dassault Systemes 2015 (a)) Turbulent fluid flows are frequently encountered in engineering and Flow Simulation was developed to study these flows. To predict turbulent flows, Flow Simulation uses the ‘Favre-averaged Navier Stokes equations’ (density weighted averaging), where time averaged effects of the flow parameters are considered. Transport equations for turbulent kinetic energy are used to close the equations (e.g. the  $k$ - $\varepsilon$  transport equation for turbulent kinetic energy and its dissipation rate: Equations 7 and 8 (Launder and Spalding 1974)), with source terms and constant values (equations 9-14). Flow Simulation uses one system of equations to describe both laminar and turbulent flows (Dassault Systemes 2015 (a))

$$\frac{\partial \rho k}{\partial t} + \frac{\partial}{\partial x_i} (\rho u_i k) = \frac{\partial}{\partial x_i} \left( \left( \mu + \frac{\mu_t}{\sigma_k} \right) \frac{\partial k}{\partial x_i} \right) + S_k \quad [7]$$

$$\frac{\partial \rho \varepsilon}{\partial t} + \frac{\partial}{\partial x_i} (\rho u_i \varepsilon) = \frac{\partial}{\partial x_i} \left( \left( \mu + \frac{\mu_t}{\sigma_\varepsilon} \right) \frac{\partial \varepsilon}{\partial x_i} \right) + S_\varepsilon \quad [8]$$

$\mu$  = dynamic viscosity;  $\mu_t$  = turbulent eddy viscosity coefficient;  $k$  = turbulent kinetic energy  
 $S_k$  and  $S_\varepsilon$  are source terms defined as;  $\varepsilon$  = turbulent dissipation

$$S_k = \tau_{ij}^R \frac{\partial u_i}{\partial x_j} - \rho \varepsilon + \mu_t P_B \quad [9]$$

$$S_\varepsilon = C_{\varepsilon 1} \frac{\varepsilon}{k} \left( f_1 \tau_{ij}^R \frac{\partial u_i}{\partial x_j} + \mu_t C_B P_B \right) - C_{\varepsilon 2} f_2 \frac{\rho \varepsilon^2}{k} \quad [10]$$

$$P_B = \frac{G_i}{\sigma_B} \frac{1}{\rho} \frac{\partial p}{\partial x_i} \quad [11]$$

$$\mu_t = f_\mu \frac{C_\mu \rho k^2}{\varepsilon} \quad (\text{Turbulent eddy viscosity}) \quad [12]$$

$$f_\mu = [1 - \exp(-0.0165 R_y)]^2 \cdot \left( 1 + \frac{20.5}{R_T} \right) \quad (\text{Turbulent viscosity factor}) \quad [13]$$

$$\text{Where } R_T = \frac{\rho k^2}{\mu \varepsilon}, \quad R_y = \frac{\rho \sqrt{k} y}{\mu}, \quad f_1 = 1 + \left( \frac{0.05}{f_\mu} \right)^3, \quad f_2 = 1 - \exp(-R_T^2) \quad [14]$$

The constants are  $C_\mu = 0.09$   $C_{\varepsilon 1} = 1.44$   $C_{\varepsilon 2} = 1.92$   $\sigma_\varepsilon = 1.3$   $\sigma_k = 1$ ,  $C_B = 1$  if  $P_B > 0$  and 0 otherwise.

SolidWorks uses a modified  $k-\varepsilon$  turbulence model with damping functions, developed by Lam and Bremhorst (1981), to model the laminar, turbulent and transitional flows of homogenous fluids. The damping functions modify the standard  $k-\varepsilon$  model by decreasing the turbulent viscosity and turbulence energy and increasing turbulent dissipation rate to represent laminar conditions for small Reynolds numbers (based upon average velocity of fluctuations and wall distance (two-scale wall functions)) (Lam and Bremhorst, 1981).

### **Model geometry**

SolidWorks computer aided design (CAD) software is a feature based parametric solid modelling design tool. A solid geometric model contains all the wire frame, surface geometry required to describe the edges and faces of the model (Dassault Systemes 2015 (a)). With design and simulation intent in mind, CAD is used to create the fuel cell enclosure for the CFD simulation study as a basic cuboid structure with simplified vent openings. This allows the engineering objectives of obtaining vertical enclosure helium concentrations to be met.

### **Simulation configuration**

With the model prepared a decision is made on whether to simulate internal or external flow. For internal flow, the enclosure geometry would usually be the entire computational domain. Inlets and outlets in the enclosure, are applied as boundary conditions (specifying pressure or flow rates) at the edge of the domain. For external flow, the model is surrounded by a larger, computational domain. This case allows gas flow through the enclosure vents to be modelled explicitly and provides a more representative simulation.

External flow simulations have been used in this investigation. Simulation configuration parameters are now applied to the project (Table 3.4). This sets the unit system, internal/external analysis, default fluid (air), wall conditions (boundary conditions for flow at the walls), initial conditions (ambient conditions of solids and fluids) and simulation goals. Computational domain size and initial mesh level (see below) are set.

**Table 3.4 Example Flow Simulation configuration settings**

<b>Configuration</b>	<b>Value</b>
<i>Units</i>	SI

<i>Analysis Type</i>	External
<i>Gravity</i>	- 9.81 m s <sup>-2</sup>
<i>Project fluid (Initial condition)</i>	Air – 100%
<i>Project fluid (Initial condition)</i>	Helium – 0%
<i>Wall conditions</i>	Adiabatic/zero roughness
<i>Initial Pressure</i>	101325 Pa
<i>Initial Temperature</i>	293.2 K
<i>Turbulence parameter</i>	Turbulent/Laminar ( $k\varepsilon$ )
<i>Initial mesh level</i>	Setting level 1 to 8
<i>Computational domain</i>	Set input data (1m x 1m x 2m)

### Boundary conditions

Boundary conditions are applied to surfaces that are designated as outlets or inlets. In this modelling exercise the helium nozzle is set as an inlet. A volume flow rate is assigned normal to the nozzle's horizontal top surface. As this is an external analysis with flow through the enclosure into the wider computational domain, boundary conditions are not set at ventilation openings. The solver equations will determine the conditions as the simulation evolves. Environmental conditions are set for the wider domain.

### Engineering goals and convergence

SolidWorks solves the time-dependent set of equations for all problems, including steady-state cases as tested in this investigation. In this case the simulation will be finished when the steady state is attained. SolidWorks also allows the selection of independent finishing conditions to be used to stop the calculation e.g. convergence of pre-set goals;

- maximum number of refinements;
- maximum number of iterations;
- maximum physical time (for time-dependent problems only);
- maximum CPU time;
- maximum number of travels (Travel is the number of iterations required for the propagation of a disturbance over the whole computational domain); (Dassault Systemes 2015(a)) and
- convergence of goals

Engineering goals e.g. mass flow rate, velocity, temperature, species volume flow rate and concentration can be set and used as convergence criteria. Goals have not been used in this research as all simulations were taken to steady conditions (Dassault Systemes (2015 (b))).

### Meshing

When creating the project, a ‘basic’ parallelepiped cuboid mesh, orthogonal to the Cartesian axes, is created in the computational domain, the ‘basic mesh’. Mesh settings can then be applied to the project to improve the basic mesh with refinements in areas of interest. Figure 3.34 (a) shows that the basic mesh has received a low level of refinement at the vent openings to create the ‘initial mesh’. This is the mesh that the calculation will start from unless further refinement is added e.g. ‘*local initial mesh*’ or ‘*solution adaptive meshing*’ is selected. The level of the initial mesh can be set on a sliding scale from 1 to 8. The higher the level the more complex the mesh will be and consequently more computationally expensive.

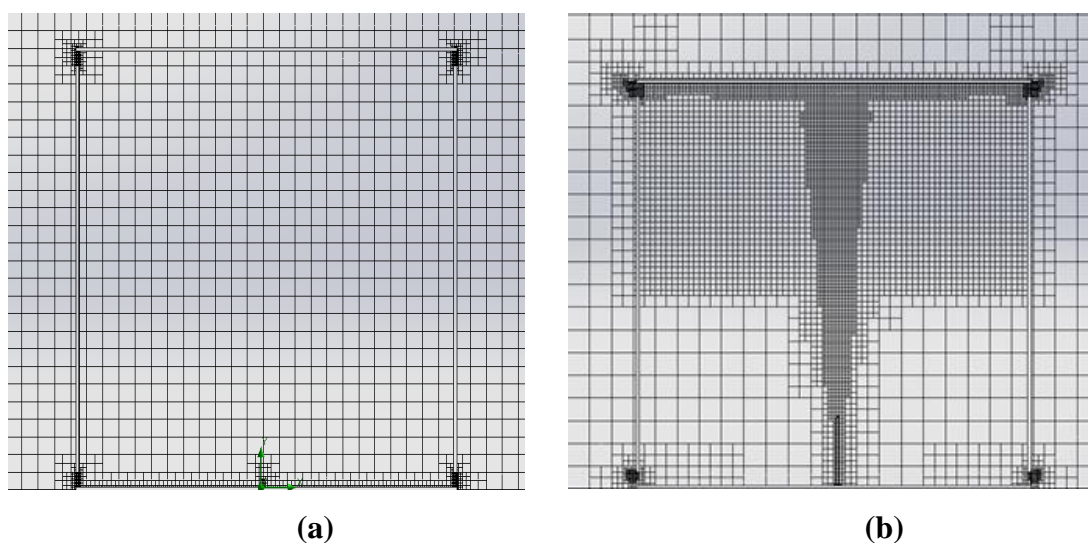


**Figure 3.34 (a) Initial Mesh (b) With geometry added to create a Local Initial Mesh**

In this project, the *local initial mesh* technique is used to add refinement. A solid feature is added to the geometry in the area of interest and then disabled. The re-meshed model will have additional refinement in these volumes. In this study the area of the plume and the stratified zone received refinement with the addition of a cone and a cuboid (Figure

3.34 (b)). *Solution adaptive meshing* is activated if the initial mesh level is set to 6 or higher. Solution adaptive meshing refines the mesh during the calculation. In regions of low gradient cells are merged and in regions of high gradient cells are split. The mesh results summary screen will provide the total number of cells created, the number of fluid and solid cells and partial cells. If adaptive meshing has been chosen, the final mesh can only be inspected once the solution has been achieved.

In this research, the experimental results are known and the CFD simulations are run to validate the capability of the software for the experimental scenario in question. For each modelling exercise, three mesh resolutions are selected with additional refinement in areas of interest (vents, plumes, stratified layer and chimneys). Mesh sensitivity as described in section 3.9.3 is then determined. It is an important consideration in some cases that further mesh refinement may not provide a significant benefit when balanced against the increase in computational expense.

### **Solution**

To run the simulation, select run and check the solve box. The simulation will now find a solution. There is also an opportunity to select the number of processors used in the calculation to manage computer time. The monitor will allow the progress of pre-set goals to be viewed. These are presented graphically. It is also possible to view the progress of the simulation and observe the flow develop in the geometry. When the calculation is complete the monitor window can be closed to return to the project. In the project tree the results can be loaded to allow for analysis to take place.

### **Post processing**

With the simulation results loaded many processing options become available. The sensor point locations are specified and helium concentrations are obtained. This data is downloaded into Excel for further processing outside of Flow Simulation. Within flow simulation there are facilities to represent the numerical solution graphically.

Any area of the geometry can be closely examined for the parameters under investigation. A full qualitative analysis of the simulation output is therefore possible. A cut plot of the

geometry is possible on a plane in any position of interest. Contour plots, iso-lines and velocity vectors are available. Animations are also available.

### **3.9.6 ANSYS: Fluent (19.2): CFD**

ANSYS is a Multiphysics engineering simulation tool. It has been developed over many years from different software packages that have been acquired by ANSYS Inc. The different packages have not been integrated but are linked through a common interface ‘Workbench’, which allows the user to take a systematic approach to engineering simulation. ANSYS is considered a market leader in CFD Multiphysics applications and is widely used in academia and industry.

Its component nature makes it a very different application to SolidWorks. Also, because many of the components have been brought in and ‘made’ to fit, it isn’t always a simple system to use. Each application requires a licence to operate it, so it is not possible, with a single licence, to have two applications open at the same time (e.g. meshing and Fluent). There are also residual elements that have been retained as simulation options, but which in fact are not relevant to many engineering simulations. ANSYS has though been widely validated and its solutions are considered reliable.

#### **WorkBench**

ANSYS provides a range of analysis systems, either preconfigured or in component form for the user to determine their requirements. These components and tools are found in ANSYS: Workbench, the project management interface. Workbench is usually the starting point for a project, although it is possible to use any of the ANSYS software applications, such as Fluent, independently.

Workbench is the logical starting point though, as a sequential workflow is provided, which ensures that each step is correctly completed, before moving to the next. It is also possible to manage multiple projects through Workbench as well as parametric studies. The first step is to open Workbench and select a Fluid Flow (Fluent) ‘Analysis System’ and drag into the ‘Project Schematic’ window (Figure 3.35).

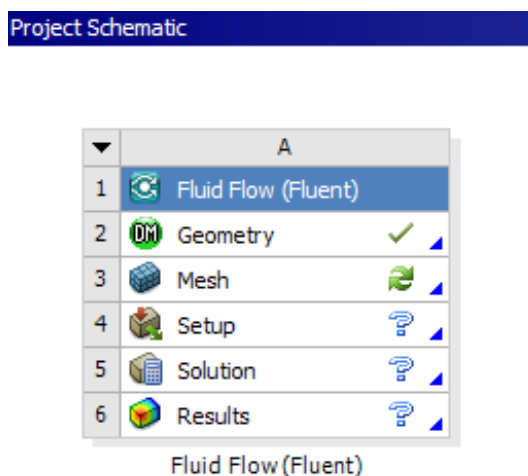


**Figure 3.35 Fluid Flow (Fluent) Analysis System in Workbench**

### Model Geometry

Two CAD applications are available via the Geometry cell, ‘Design Modeller’ and ‘Space Claim’. Space Claim is a modern solid modeller and the recommended CAD package. The CAD model is constructed in Space Claim and when complete, the fluid volume can be extracted (Figure 3.36 (c)) for meshing and simulation. ‘Groups’ can be assigned, which will become named selections in Meshing and Fluent. Groups or named selections are geometry elements that will later have a boundary condition assigned to them, such as inlet or outlet vents. At this point space claim is closed to return to Workbench.

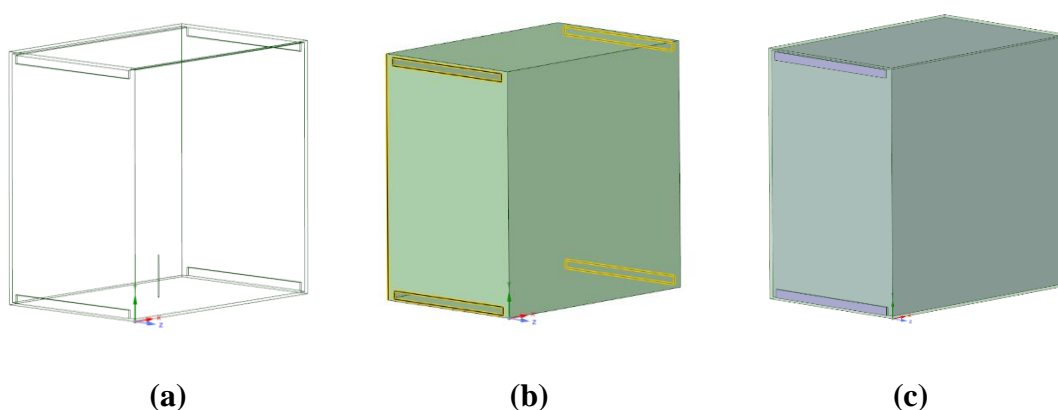


**Figure 3.36 (a) Geometry, (b) Fluid volume preparation, (c) Fluid volume**

### Meshing

ANSYS Meshing is then opened via the Mesh cell. A simple tetrahedral mesh is applied to the fluid volume, when the application opens (Figure 3.37 (a)). The mesh properties can then be examined, and the mesh adapted if required. Figure 3.37 (b) shows a poorly

refined mesh. The auto-mesh has determined that the nozzle, as a small feature, is an area that requires refinement. A dense area of small cells has been created, where there will be little flow activity. There is no refinement in the vent areas. As such the mesh will prove computationally expensive for no benefit. Distinct types of mesh are available too, e.g. polygonal (Figure 3.37 (c)). Once a suitable mesh is achieved, the Meshing application is closed and Fluent can be opened through the ‘Setup cell’ to prepare the model for simulation.

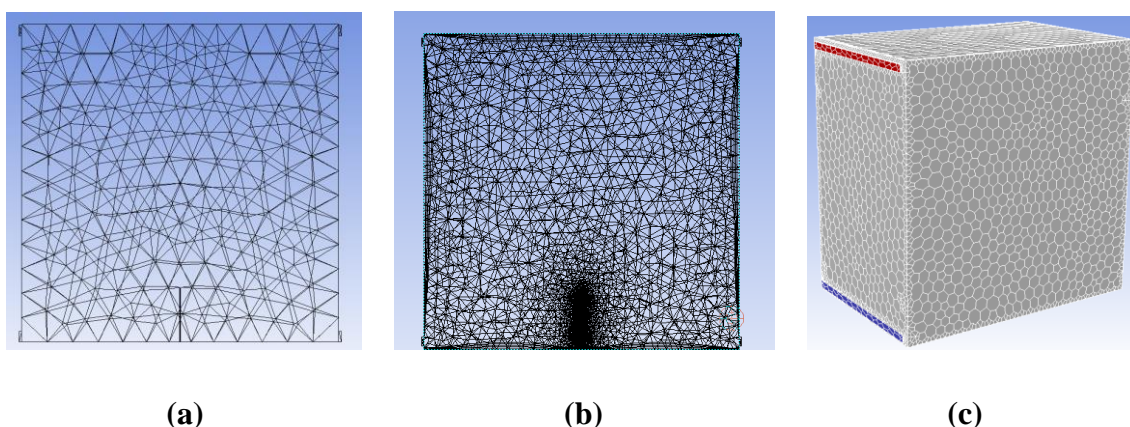


**Figure 3.37 Meshed geometry: (a) Simple tetrahedral mesh (b) Complex, but poorly refined mesh (c) Polygonal mesh**

### Setup

The Fluent application graphical interface is presented as a series of tabs, which represents the logical sequence of operations to prepare the model for a simulation. Under each tab are the various settings available for that operation. (Figure 3.38).

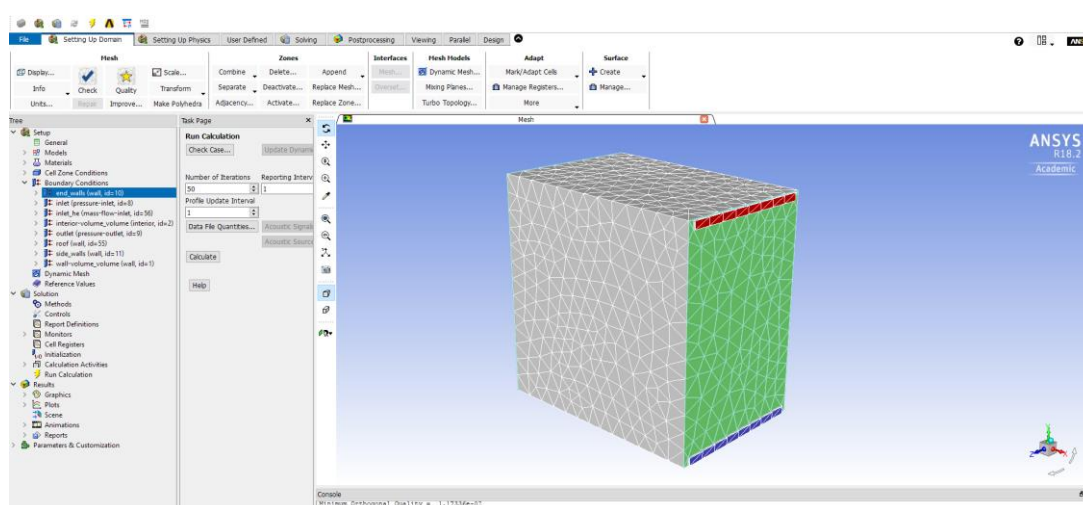


**Figure 3.38 ANSYS Fluent application screen**



The first tab is 'setting up the domain'. Here the mesh is quality checked, and the computational domain determined. The next tab, 'Setting up Physics', allows the user to determine the type of simulation that will be run. The type of solver and turbulence model are set here (Figure 3.39). Operating conditions, gases and boundary conditions are also set. The 'User defined' tab allows for parameterisation and the inclusion of functions in the simulation.

The 'Solving' tab finalises the model for simulation, initialises the model and allows the calculation to take place. During the calculation a 'Residuals monitor' appears which allows the user to track the simulation to convergence. The simulation process is iterative. At each step the calculations taking place in each cell will change in value. When these values achieve a certain level and then become steady, convergence is achieved and indicates that the calculation is complete.

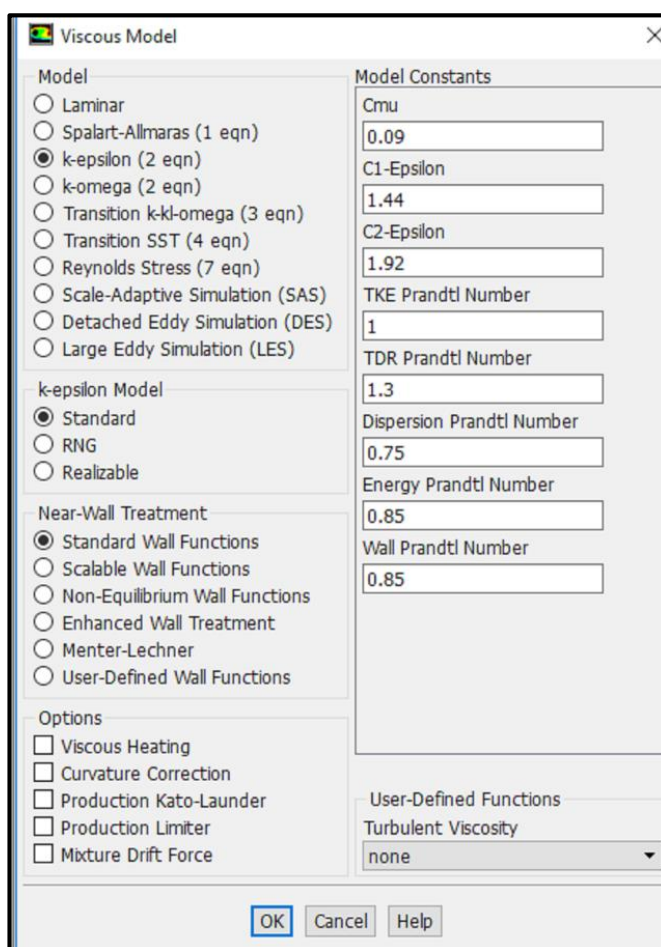


**Figure 3.39 ANSYS: Fluent turbulence model menu**

### Post processing

The Fluent application includes a post processing tab. This provides the facility to graphically present the simulation results. Graphics (e.g. contours, vectors), plots (e.g. graphs), reports and animations can be prepared. However, the recommended analysis path is to use the CFD-Post application, accessed through the 'Results' cell in Workbench. This application is a more comprehensive analysis tool providing better resolution graphics and more data presentation options.

### 3.10 Statistical Performance Indicators

To determine the performance of the numerical prediction modelling against the empirical results statistical analysis tests are applied. Several statistical models are available for investigating dispersion of chemicals in the atmosphere, which are relevant to the enclosure conditions in this research. Two types of model can be applied to evaluate prediction models;

- Measures of difference
- Measures of correlation

Difference measures provide a quantitative estimate of the size of the differences between observed and predicted values. Correlation is the quantitative measure of the association between observed and predicted values. The ratio of  $C_o$  (the observed experimental value) and  $C_p$  (the predicted concentrations) of a good model should not show large deviations from unity. Correlation coefficients are also used to assess model performance. Several tests relevant to actual and predicted gas concentrations are explained below (Toledo.edu (2017), the over-bar stands for the average value over the entire dataset;

#### 1. Model Bias (MB)

This is the mean error, defined as the predicted value of concentration ( $C_p$ ), less the observed value of ( $C_o$ );

$$\text{Model Bias} = \overline{(C_p - C_o)} \quad [9]$$

#### 2. Fractional Bias (FB)

The bias is normalised and varies between +2 and -2, with an ideal value of zero.

$$\mathbf{FB} = 2 \times \left( \frac{\overline{C_o} - \overline{C_p}}{\overline{C_o} + \overline{C_p}} \right) \quad [10]$$

### 3. Normalised Mean Square Error (NMSE)

This test emphasises the scatter in the data set. The normalisation by the product of  $C_p \times C_o$  ensures that the NMSE will not be biased towards models that over or under predict. Smaller values suggest better model performance.

$$\mathbf{NMSE} = \frac{(\overline{C_o} - \overline{C_p})^2}{\overline{C_o} * \overline{C_p}} \quad [11]$$

### 4. Correlation Coefficient (r)

Correlation coefficient (r), provides numerical (quantitative) and graphical (qualitative) analysis output. A value for the correlation coefficient close to unity suggests good model performance.

$$\mathbf{r} = \frac{(\overline{C_o} - \overline{C_o})(\overline{C_p} - \overline{C_p})}{\sigma_{C_p} \sigma_{C_o}} \quad [12]$$

### 5. Geometric Mean Bias (MG)

The geometric mean bias is provided by;

$$\mathbf{MG} = \exp(\overline{\ln C_o} - \overline{\ln C_p}) \quad \text{or} \quad = \exp \left[ \overline{\ln \left( \frac{C_o}{C_p} \right)} \right] \quad [13]$$

### 6. Geometric Mean Variance (VG)

The geometric mean variance is provided by;

$$\mathbf{VG} = \exp \left[ \overline{[\ln C_o - \ln C_p]^2} \right] \quad \text{or} \quad = \exp \left[ \overline{\ln \left( \frac{C_o}{C_p} \right)^2} \right] \quad [14]$$

In this research investigation, analysis is used to compare the experimental results, with the numerically predicted results. Primarily, following the methodology in Baraldi (2016) which relies upon recommendations made by Hanna et al (1993), four methods are applied; fractional bias (FB), normalised mean square error (NMSE), geometric mean

bias (MG) and geometric mean variance (VG). NMSE and VG are measures of scatter, reflecting systematic and unsystematic (random) errors. FB and MG are measures of mean bias and indicate only systematic errors, which lead to always underestimate or overestimate the measured values (Baraldi et al, 2016). Table 3.5 provides performance ranges for the four selected tests.

**Table 3.5 Statistical performance indicators**

Analytical test	Ideal value	Range	
<i>FB</i>	0 (Zero Bias)	-2 (Extreme over prediction)	2 (Extreme under prediction)
<i>NMSE</i>	0	-	$\leq 0.5$
<i>MG</i>	1	0.75	1.25
<i>VG</i>	1	0.75	1.25

### 3.11 Conclusion

The literature review along with the enclosure criteria from BOC Ltd. determined the parameters for the experimental and numerical tests to be conducted in this research investigation. The initial scoping exercise carried out at BOC Ltd. provided insight into the research methodology and the need for effective, accurate and reliable metering and data recording instruments. It also highlighted the need to use helium and not hydrogen in enclosed laboratory conditions for safety reasons.

A test methodology was developed to allow the ventilation performance of a small enclosure at leak rates from 0.5 lpm to 10 lpm to be investigated. Tests could sometimes take a long time to achieve steady state and use a lot of helium in the process. In the name of sustainable and cost-effective research, the test runs that were conducted were kept to the minimum where possible. Several ventilation schemes were incorporated into the enclosure, such as plain rectangular vents, louvre vents, chimneys and flues. An exercise to visualise a helium leak in the enclosure was also undertaken using the Schlieren system. The experimental tests were followed by CFD simulations. CAD models developed from the rig design were used to try to validate numerical models using SolidWorks Flow Simulation and Ansys: Fluent, CFD software. The experimental and numerical results were then compared using statistical tests to determine significance.

## Chapter 4 Results and Analysis: Experimental tests

### 4.0 Introduction

This chapter presents the test results and analysis of the experimental investigation into the performance of a variety of passive ventilation schemes applied to the BOC Ltd. specification fuel cell enclosure. Further analysis is provided later (Chapter 6) to compare the performance of CFD predictions with experimental data. A series of ten experimental setups have been tested. Passive ventilation performance has been investigated and capability to manage helium (used as a hydrogen analogue) concentrations to below the hydrogen lower flammable limit. A Schlieren system test was also conducted to visualise the helium flow in the enclosure. The ten setups were;

- A. BOC Ltd. scoping exercise using hydrogen (Hand-held hydrogen sensor)
- B. Initial test rig (Four Xensor sensors):
  - i. Base case tests – plain vents
- C. Final test rig (Eight Xensor sensors):
  - i. Control tests – plain vents
  - ii. Simple louvre tests – horizontal louvre extensions
  - iii. Aluminium louvre tests – 1 to 12 louvres
  - iv. Chimney-Stack tests – roof mounted chimney
  - v. Internal obstruction test
  - vi. Flue test – side mounted
  - vii. Snorkel tests – side mounted
  - viii. Schlieren system helium visualisation

### 4.1 BOC Ltd. scoping exercise (hydrogen tests)

These experiments were the initial tests undertaken with BOC Ltd. to try and understand the behaviour of hydrogen in their enclosure and the concentration levels achieved at various hydrogen leak rates. The tests were crude, due to the need to do them quickly and the location of the tests, the BOC Ltd. consultant's garage. That said, the specification of the experiments was realistic in terms of the size of the enclosure, vent configurations, the use of Hymera fuel cell shells and using hydrogen gas from a BOC Ltd. Genie bottle. These were the only tests to use hydrogen, subsequent laboratory tests used helium.

Limitations of the experimental rig set up were the leakiness of the enclosure, due to being held together by masking tape, an uncalibrated and uncertified rotameter to supply the hydrogen and a hand-held gas sensor that could only sample a couple of centimetres into the enclosure due to the absence of the probe extension. The Celotex® walls used were 25 mm thick, whereas the steel walls of a real enclosure would be a couple of millimetres. Vent mouths were therefore quite thick and unrealistic. These tests informed the design of the laboratory test rig and instruments. Figure 4.1 is a schematic of the test rig. Seven experimental tests were conducted using the test rig as per Table 4.1.

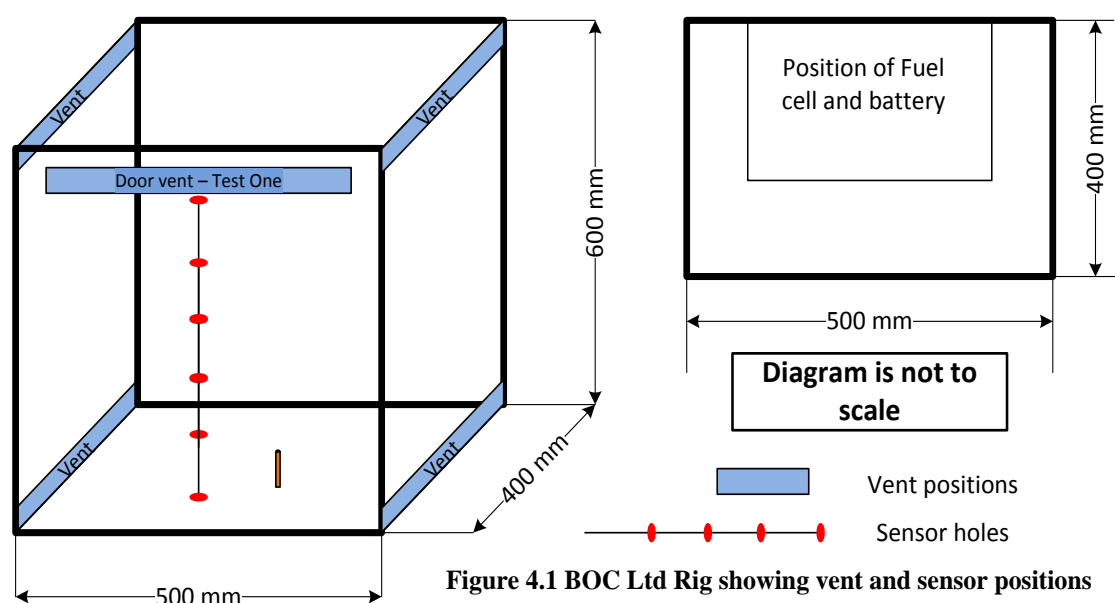
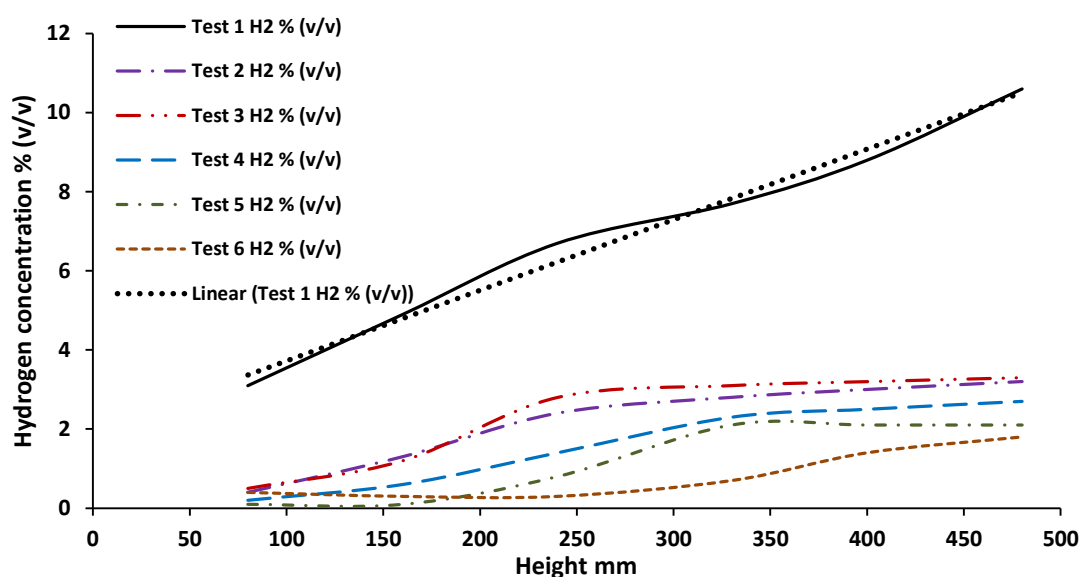


Figure 4.1 BOC Ltd Rig showing vent and sensor positions

Table 4.1 Experimental configurations

Test No.	Experimental Configuration
1	Single vent at the top of the door (exchange flow-poor). Hydrogen leak at the base of the enclosure. (Indoor test)
2	Two vent cross flow (displacement). Low level left. Top level right (with wind). Leak at enclosure base. (Outdoor test)
3	Two vent cross flow. Low level left. Top level right (No wind). Leak at the enclosure base. (Indoor test)
4	Two vent cross flow. Low level left. Top level right (Larger vents x2). Leak at the enclosure base. (Indoor test)
5	Four vent cross flow. Empty enclosure. Leak at the base. (Indoor test)
6	Four vent cross flow. (Battery and Hymera) Leak central at 300 mm height. (Outside-slight breeze)
7	Four vent cross flow. (Battery and Hymera) Leak central at 300 mm. Fixed central sensor point. (Outside-slight breeze/readings fluctuated widely)

The leak rates tested were to the BOC Ltd. specification of 1-10 lpm. Gas was released into the enclosure through the nozzle (positioned either on the enclosure floor or at mid-height) and allowed to settle to as near a steady state condition as possible, subject to the vagaries of the gas sensor. Tests 1 to 6 (Figure 4.2) were all conducted at a leak rate of 1 lpm. This was partly due to the difficulty of controlling the flow through the rotameter but also because the focus of BOC Ltd.'s interests was on low leak rates. It provides a useful comparison of the schemes at the same leak rate. Test 7 attempted to test higher leak rates, but the results were erratic as the sensor could not provide a reliable reading.



**Figure 4.2 BOC Ltd. results: Tests 1-6 H<sub>2</sub> concentration % (v/v) versus sensor height**

#### 4.1.1 Analysis

Test 1 (Table 4.1) used a single upper vent in the front (door) panel of the enclosure and recorded the highest hydrogen concentrations of all seven tests. An almost linear concentration gradient is evident (Figure 4.2). The sensor probe only extended two centimetres into the enclosure, so 'near wall' samples were taken. No clear stratified layer is present and the LFL is exceeded from about 100 mm height. An exchange ventilation regime should be present, which would lead to a well-mixed condition. If the test had been allowed to run for longer, this may well have developed. Exceeding the LFL in this indoor test was a safety concern, so personal protection equipment was worn. The explosion risk was mitigated though by the loose-fitting nature of the structure, made from lightweight foam panels designed to come apart and vent any explosion at very low

overpressures. The explosion risk justified using helium in subsequent laboratory experimental tests.

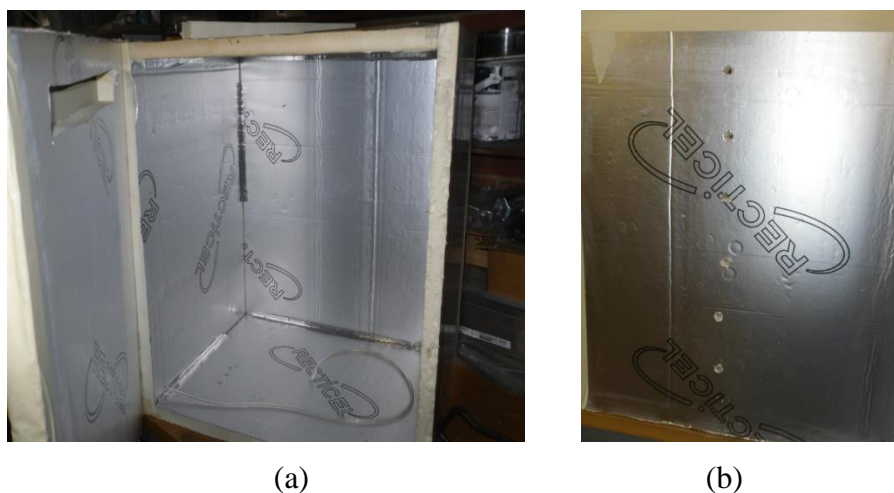


**Figure 4.3 (a) Celotex® enclosure with door vent (b) Position of sensor holes in door**

Tests 2 and 3 (Table 4.1) used the same configuration (a two-vent cross-flow scheme) but test 2 was conducted outside. The graphs for these tests are very close with the inside test showing marginally higher values in the stratified zone above 250 mm. A displacement regime such as this should lead to the formation of a stratified layer, and this has happened. The average hydrogen concentration in the stratified zone is about 3.2 % for test 3 and 3.0 % for test 2. These figures are close to the LFL and a slight increase in the leak rate would breach the LFL. The wind assisted test has led to a lower concentration, likely due to an increased ventilation flow rate.

Test 4 (Table 4.1) employed the same vent configuration as test 3, but with the vents enlarged and the test conducted inside. A stratified layer has formed from about 330mm with an average stratified zone hydrogen concentration of 2.5 %. Increasing the vent size has increased the volume air flow through the enclosure, leading to a higher stratified zone and a lower concentration. Test 5 (Table 4.1) used four vents, two opposing upper and lower. Increased volume air flow would be expected and the further reduction in enclosure concentrations provides evidence of this. The stratified layer is at about 330 mm with a concentration of 2.1 %.

Test 6 (Table 4.1) used the four-vent scheme from test 5, but this time with two Hymera units inside and the hydrogen leak at 300mm, centrally positioned. The internal volume has been significantly reduced and airflow impeded by the Hymera obstructions.



Concentrations below the leak are low at about 0.4 %. Concentrations above the leak are lower than for test five, with no clear evidence of a stratified layer. The presence of the Hymera at the top of the enclosure would make the formation of a stratified zone difficult and with the leak closer to the upper vents' hydrogen can leave the enclosure more quickly. The poor position of the sensor readings will have reduced data resolution.

Test 7 (Table 4.2 and Figure 4.4) repeated the test 6 scenario, but this time it was outside and higher leak rates were tested. The sensor was fixed at the 300 mm position, the same height as the leak. The data appears to be erratic, but some sense can be made of it. The reading of 0.8 % at 1 lpm seems high when compared to the previous test, where the concentration was about 0.5 %. At this leak rate the speed and pressure of the hydrogen release is low. The lower momentum plume may become more dispersed and remain in the mid area of the enclosure for longer, particularly if confined by the obstruction.

As the leak rate increases there is a steady increase in hydrogen concentration up to about the 6 lpm point. After this there is a steady decline. This may be due to the increased speed of the hydrogen jet taking the hydrogen higher into the enclosure and facilitating its removal from the enclosure through the upper vents. The higher release rates in this case may well be leading to lower concentrations lower in the enclosure, but without sensor data, this cannot be substantiated.

**Table 4.2 Test 7 results**

Leak rate lpm	H <sub>2</sub> % (v/v)
1	0.8
2	0.25
3	0.65
4	1.05
6	1.3
10	1
16	0.75

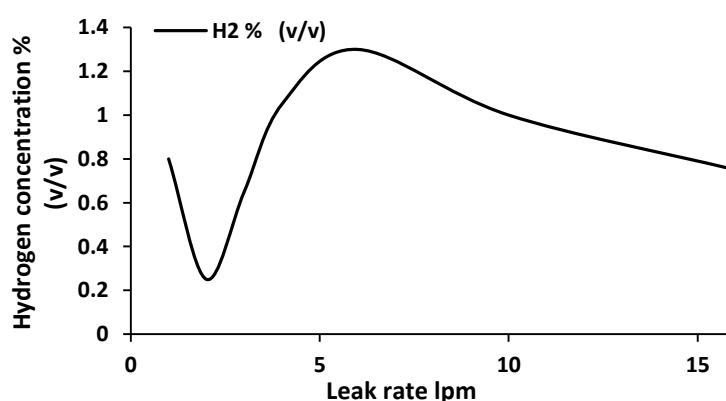


**Figure 4.4 Test 7 results: H<sub>2</sub> % (v/v) versus leak rate**

The analysis of the data from the scoping exercise provided a useful insight into the performance of a small passively ventilated enclosure subject to a buoyant gas release. Despite their crude nature, when tests were repeated results were consistent. Vent position

and size clearly has an effect, as does the position of internal components. Exchange and displacement ventilation mechanisms were apparent. Subsequent tests built on this work.

## 4.2 Initial test rig: High-level ventilation openings

Building on the work of the scoping exercise a new experimental test rig was constructed in the laboratory at LSBU. Designed to represent either a nuclear waste skip liner or fuel cell enclosure, it was used to investigate passive buoyant gas behaviour in a representative small-scale enclosure. The rig consisted of a plywood and Perspex™ cuboid enclosure (0.6 m x 0.6 m x 0.6 m outer dimensions (0.216 m<sup>3</sup> internal volume)) (Figure 4.5), designed so that an upper ventilation opening could be introduced on each wall. The rig was housed in a larger Perspex™ outer chamber (1 m x 1 m x 2 m long) to minimise the effects of drafts. This chamber was vented at either end, but it was found that it was necessary to remove a side panel to prevent the build-up of helium in the chamber, so as not to affect enclosure helium concentrations. In the tests varying numbers of ventilation openings were used along with a control test using one upper and one lower vent.

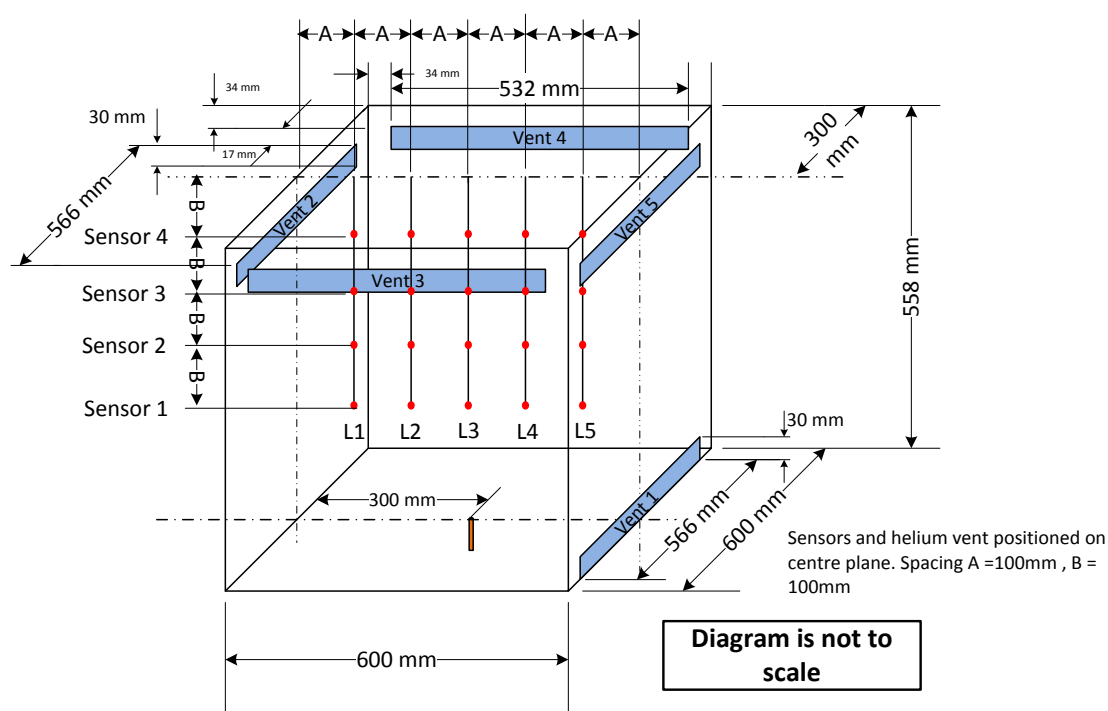


**Figure 4.5** Experimental schematic, showing sensor and vent position

Helium was introduced into the enclosure at gas flow rates of 1, 2, 3, 4 and 5 normal litres per minute through a 4 mm diameter inlet orifice located at the centre of the floor of the

enclosure to simulate a hydrogen leak in a fuel cell enclosure. Four XEN-TCG3880 helium sensors were incorporated into the rig, positioned in a vertical line at heights of 200 mm, 300 mm, 400 mm and 500 mm above the enclosure floor and used to monitor and record variations in helium concentration in the enclosure over time.

The horizontal location of the vertically suspended helium sensor line could also be adjusted to one of five positions across the central plane of the enclosure (100 mm, 200 mm, 300 mm, 400 mm and 500 mm). For each experiment the helium gas build-up was allowed to pass through the transient phase and reach a steady state position for each flow rate. A time-averaged section of steady state data has been used to provide helium concentration results following the approach in Cariteau (2013).

**Table 4.3 Experimental configurations**

No.	Experimental Test	Vent Height (mm)	Vent width (mm)	Vent area (mm <sup>2</sup> )	Number of vents	Total vent area (mm <sup>2</sup> )
1	<i>Opposing upper and lower vents (Crossflow displacement)</i>	30	566	16980	2	33960
2	<i>Single upper vent</i>	30	566	16980	1	16980
3	<i>Two opposing upper vents</i>	30	566	16980	2	33960
4	<i>Three upper vents</i>	30	566	16980	2	49920
		30	532	15960	1	
5	<i>Four upper vents</i>	30	566	16980	2	65880
		30	532	15960	2	

A series of five tests (Table 4.3) were carried out. The first ‘control’ test used a cross flow displacement ventilation set-up for comparison with the subsequent high vent tests. Of interest with this test rig was the effect of different combinations of horizontal ventilation openings, positioned near to the top of the enclosure. Four further tests were carried out, the first with a single upper ventilation opening on one wall with subsequent tests introducing a further high-level opening. Concentration data for each test was taken from the helium sensors at five points across the enclosure and then compared.

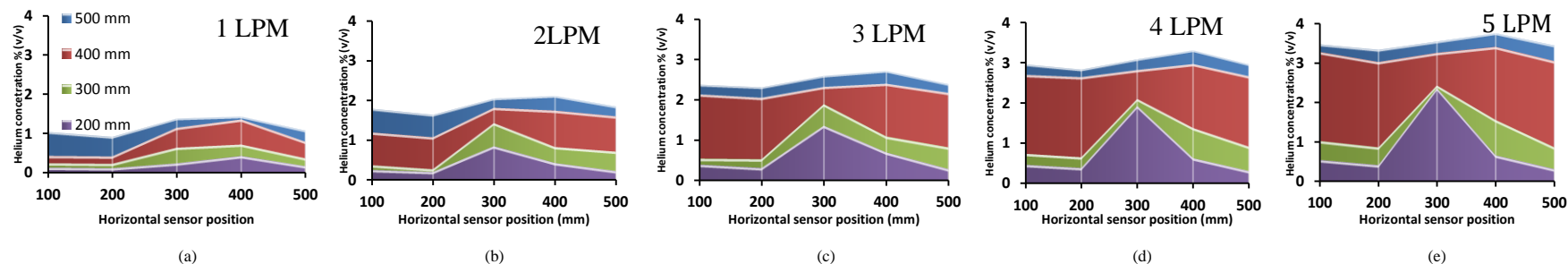


Figure 4.6 Cross-flow test: Lower inlet on the left and upper outlet on the right: Increasing leak rate from (a) to (e) [Colour denotes enclosure height]

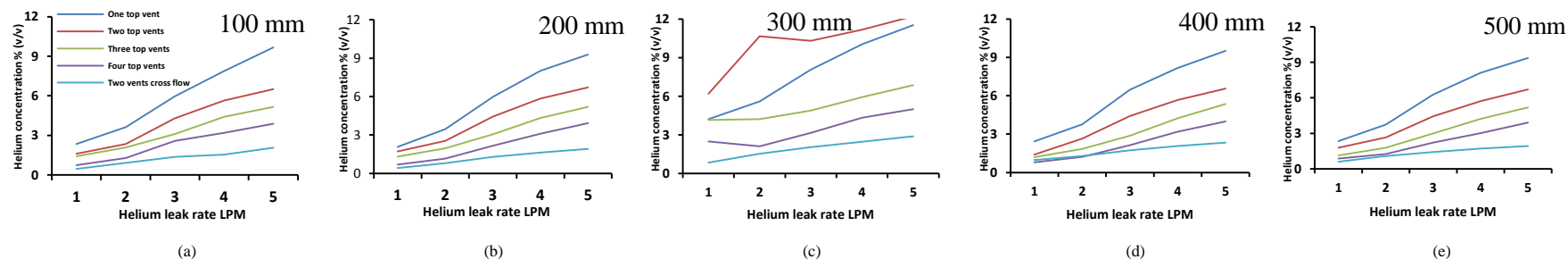


Figure 4.7 Average vertical helium concentration (Vol %) versus leak rate (LPM) at sensor stack positions of 100, 200, 300, 400 and 500mm across the enclosure.

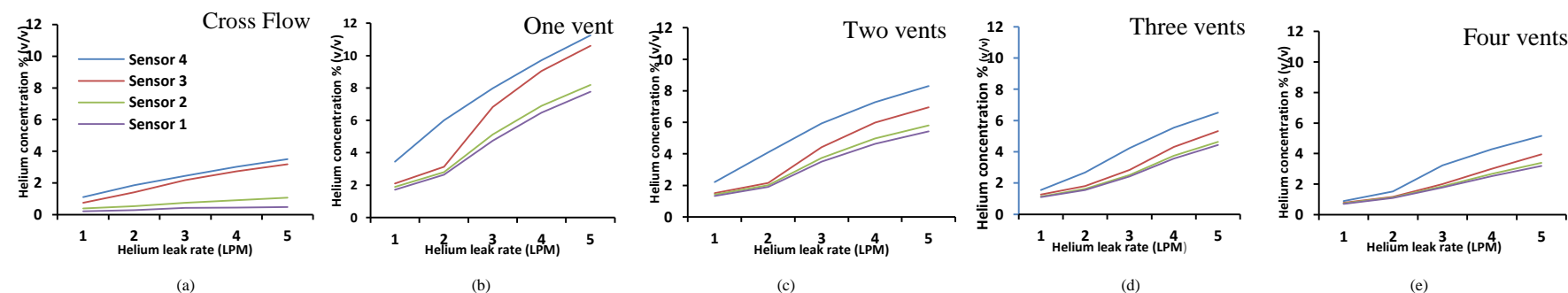


Figure 4.8 Average horizontal helium concentrations (Vol %) for each sensor height across four stack positions, versus leak rate (LPM), for each scenario test

#### 4.2.1 Analysis

**Cross-flow:** The cross-flow test used a displacement ventilation scheme (section 2.2) and maximised the possible pressure differential (driving force) with opposing lower and upper ventilation openings. Figure 4.6 (a) to (e) presents the results of the tests, showing helium concentration against horizontal sensor position for the four sensor heights. The graphs nicely show how the air entering the enclosure at the bottom left ventilation inlet is displacing the gas to the right and up towards the right upper ventilation outlet.

At 1 lpm the helium leak is low velocity and the gas appears displaced to the right. From 2 lpm the jet is becoming stronger and is more obvious at the 300 mm point as a higher concentration spike. As the leak rate increases, the enclosure concentration rises, and a thicker stratified zone develops, as is expected with a displacement ventilation scheme. Concentrations though are kept below the LFL.

**High-level vents:** Figure 4.7(b-e) presents the average vertical helium concentration at each of the sensor stack positions. This provides the average concentration between the 200 mm and 500 mm height sensor points. Apart from graph (c) at 300 mm, average high-level enclosure concentrations decrease with increasing numbers of vents. High-level vents are normally associated with mixing ventilation, where fresh external air is drawn into the enclosure, as the helium-air gas mixture leaves. This will normally lead to a well-mixed condition, as opposed to stratification.

The ventilation openings are at the same height, so there is no air pressure differential between the vents as is the case with vents at different heights. Dense ambient air will pour into the enclosure through the lower part of the vent and travel to the bottom of the enclosure. This heavier air will displace the lighter air/helium mix which leaves through the upper part of the vent. This flow regime will lead to a mixed homogenous condition.

The graphs in figure 4.7 show that the most challenging scenario is the single top vent, where concentrations are only below the LFL at 1 and 2 lpm. This is a useful scenario as it demonstrates what could happen if the lower vent in a cross-flow scheme becomes blocked. The single vent scenario achieves the highest helium concentration at 9.67 % (5

lpm), significantly above the LFL. The highest concentration achieved with the cross-flow regime was 3.79 % at 5 lpm.

Figure 4.8 presents average horizontal helium concentration across all sensor stack positions. Figure 4.8(a) presents data for the cross-flow scheme. There is a clear separation between sensors 2 and 3, which becomes more pronounced with increased flow rate. The concentration values at sensors 1 and 2 and 3 and 4 follow each other closely and separated by about a quarter percentage point. A higher concentration layer is present closer to the enclosure roof and much lower concentrations are found at the mid-level, further evidence of stratification.

The 300 mm stack position is directly in the path of the helium jet. The sensors will be in a region of concentrated flow and report elevated helium levels. Flow may also be more turbulent in this region (as evidenced in the Schlieren system tests (Section 4.12)), leading to noise in the sensor readings and variation in output. This is apparent in Figure 4.7(c) where some data points appear skewed. For average enclosure concentration calculations, the 300 mm sensor position is disregarded.

The graphs in figure 4.8 (b) to (e) present the effect on horizontal enclosure concentration of increasing the number of upper vents. Broadly, enclosure concentration reduces with increasing number of vents. The highest concentrations are recorded at the top of the enclosure at sensor 4. With two, three and four top vents, there is a gap of about one percentage point between sensor three and four above 2 lpm.

As the number of vents increases the concentrations recorded at the lower three sensors get closer, suggesting a more mixed environment as more air can pour into the enclosure. The readings at sensor 4 are noticeably higher, inferring a slim area of stratification, however this could also be the more concentrated mixture being drawn to the vents. It would be interesting to see if higher leak rates resulted in the top sensor readings getting closer to the lower ones.

Cross-flow ventilation was the most effective configuration for managing the enclosure helium concentration. The 500 mm height difference between the vents provides a small air flow driving force, which coupled with the buoyancy of the helium is sufficient to displace it. Mixing ventilation schemes become more effective with increasing vent number but the vent sizes tested were not effective at reducing concentrations below the LFL. Larger vents will increase exchange volume flow and vertically longer vents allow exchange flow across a deeper section creating greater enclosure homogeneity.

### 4.3 Developed Test Rig: Plain ventilation openings – Control test

Experience with the scoping rig and initial rig suggested that improvements were required. Having only four sensors necessitated having to move them and repeat a test to gain cross section data. Four more sensors were purchased. The initial rig also proved less flexible than expected, so a new enclosure was constructed, to the dimensions of the BOC Ltd. specification fuel cell enclosure (Figure 4.9). The panels on this enclosure were designed to be more readily moved to facilitate different vent schemes. A stainless steel nozzle (4 mm diameter) was incorporated to introduce leaking gas into the enclosure at a fixed height of 100 mm in the centre of the enclosure.

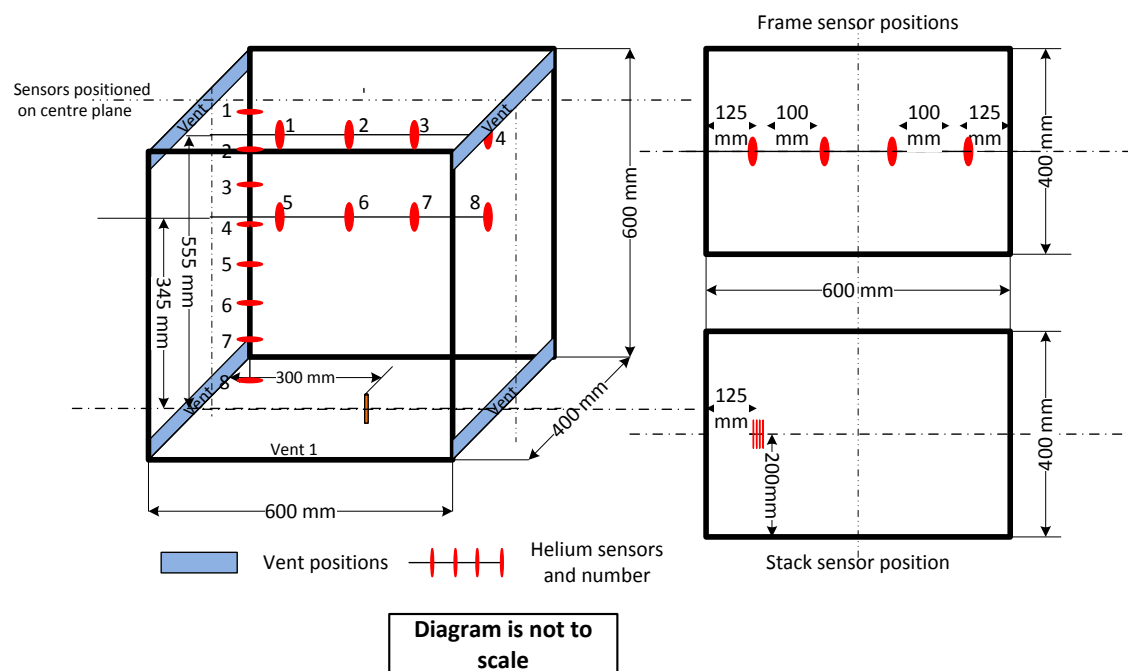


**Figure 4.9 Experimental schematic showing vent and sensor position (with number)**

A displacement ventilation scheme was incorporated into this rig with two lower and two upper opposing ventilation openings. The ‘plain’ ventilation openings were 20 mm high and 360 mm wide (7200 mm<sup>2</sup> area). Helium was introduced into the enclosure at rates from 1 to 10 lpm. Two sensor array configurations were used. The first configuration, referred to as ‘frame sensors’ used two horizontal lines of four sensors in the upper part of the enclosure at heights of 345 mm and 555 mm above the enclosure floor. This arrangement was used to establish an average helium concentration in the upper part of the enclosure. The second configuration, referred to as ‘stacked sensors’, comprised a single vertical column of eight sensors placed centrally near to one of the vented walls at heights of 120, 225, 320, 420, 470, 535, 570 and 590 mm above the enclosure floor. This arrangement provided data on vertical helium concentration gradient and buoyant gas stratification in the enclosure.

For each experiment the helium gas build-up was allowed to pass through the transient phase and reach a steady state. A time averaged section of steady state data was used to provide average helium concentrations. Figure 4.10 is an example of test data using the frame sensor arrangement. It presents a continuous trace showing leak rate progression from 1 to 10 lpm. It is interesting how rapid the transitions are between each level and how quickly steady state is achieved. The higher readings are from the sensors at 555 mm and the lower set of readings are at the 345 mm level. The noise in the graphs can be attributed to flow instabilities local to the sensors and their fast response times (data is logged every eight seconds).

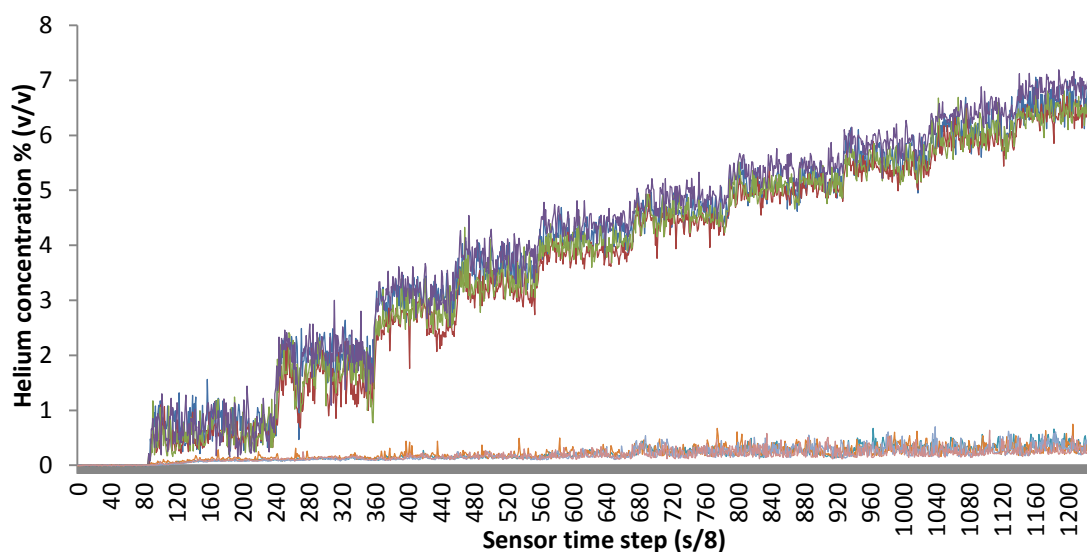


**Figure 4.10** Frame sensor results, showing rate increments from 1 to 10 lpm



### 4.3.1 Analysis: Plain Vents-Frame sensors

The frame sensor results for the plain vent test are shown in figure 4.11. Figure 4.11 (a) shows a distinct difference in concentrations achieved by the sensors on the upper and lower bars of the frame. The lower bar at 345 mm does not exceed 0.41 % at the highest leak rate and the top bar at 555 mm achieves a maximum of 6.87 % at 10 lpm, with the LFL achieved between 4 and 5 lpm. The maximum average concentration of all the sensors is 3.45 % at 10 lpm.

The much higher concentrations present at the top level clearly indicates the buoyant nature of the gas and the build-up of helium in the upper part of the enclosure suggests that stratification may be present. A further point of interest is the change of gradient at 3 lpm in figure 4.11 (a) for sensors 1 to 4 and also in figure 4.11 (b) from 3 lpm, the increase in concentration at each leak rate increase, is much reduced from that found between 1 lpm and 2 lpm and between 2 lpm and 3 lpm. This may be due to the helium leak developing from a weak plume to a stronger plume or more of a jet as the leak velocity increases.

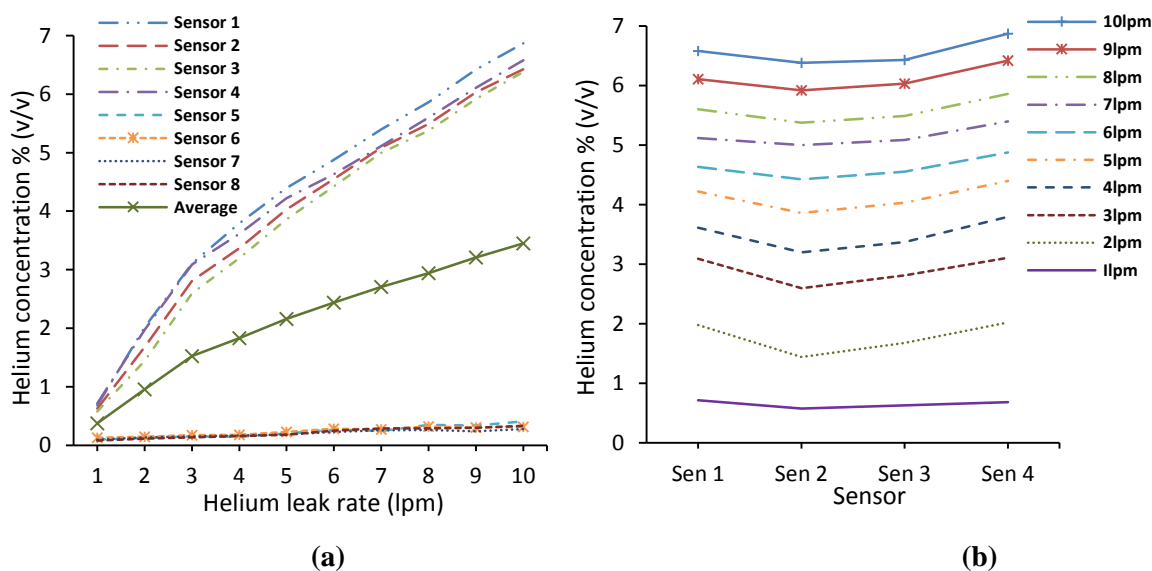


**Figure 4.11** Frame sensor helium concentrations (a) all sensors (b) the 555 mm level

### 4.3.2 Plain Vents-Stacked sensors

Figure 4.12(a) presents the plain vent enclosure results with stacked sensors and Figure 4.12(b) louvre vent stacked sensor results, discussed in section 4.4. The stacked sensor

arrangement provides more information about the concentration gradient in the enclosure and how it changes with height at each leak rate. With plain vents a distinct stratified layer is very evident in the enclosure, particularly from 3 lpm upwards. Concentrations above 4 % (the LFL) are present above about 500mm and from 4 lpm upwards.

The displacement ventilation scheme has created the predicted stratified layer at the top of the enclosure. This layer gradually thickens, and stratified layer concentrations increase as the helium leak rate increases. Of note again is the change in behaviour at 3 lpm. There is a clear development in the regime inside the enclosure with a significant increase in helium concentration in the stratified layer.

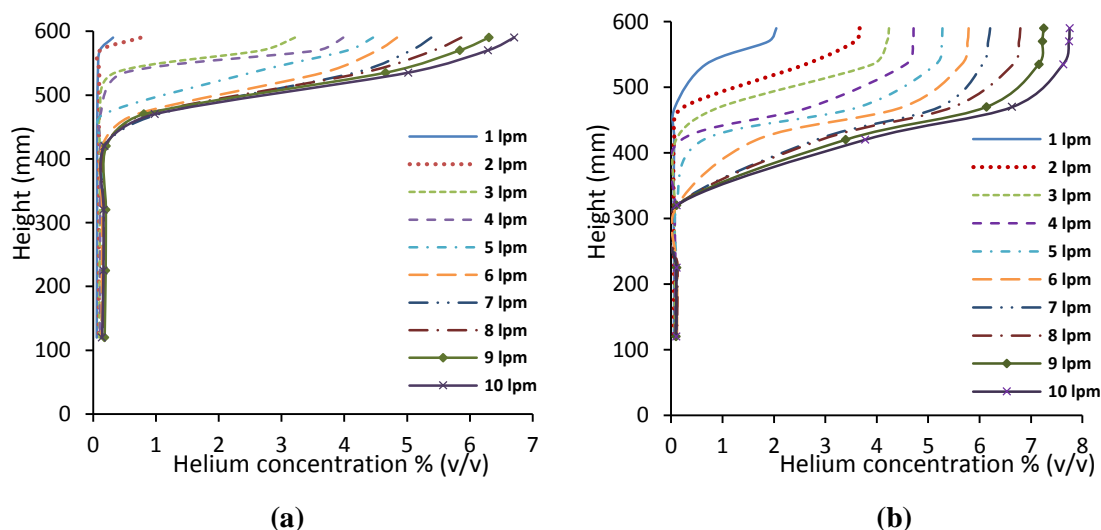


**Figure 4.12 Stacked sensor helium concentrations against height (a) Plain vents (b) Louvre vents**

#### 4.4 Paper louvres (same opening area as plain vents section 4.3)

For this experiment the enclosure set up detailed in section 4.3 was used, but with the addition of horizontal paper louvre extensions as shown in figure 4.13. The same displacement ventilation scheme was incorporated, with two lower and two upper opposing ventilation openings (Figure 4.9). The ventilation openings were 20 mm high and 360 mm wide (7200 mm<sup>2</sup> area), with one horizontal louvre positioned at the vertical midway position and a second upper louvre in line with the top horizontal bar of the opening (see figure 4.14 for specification).



**Figure 4.13** Developed test rig with paper louvres applied to the openings

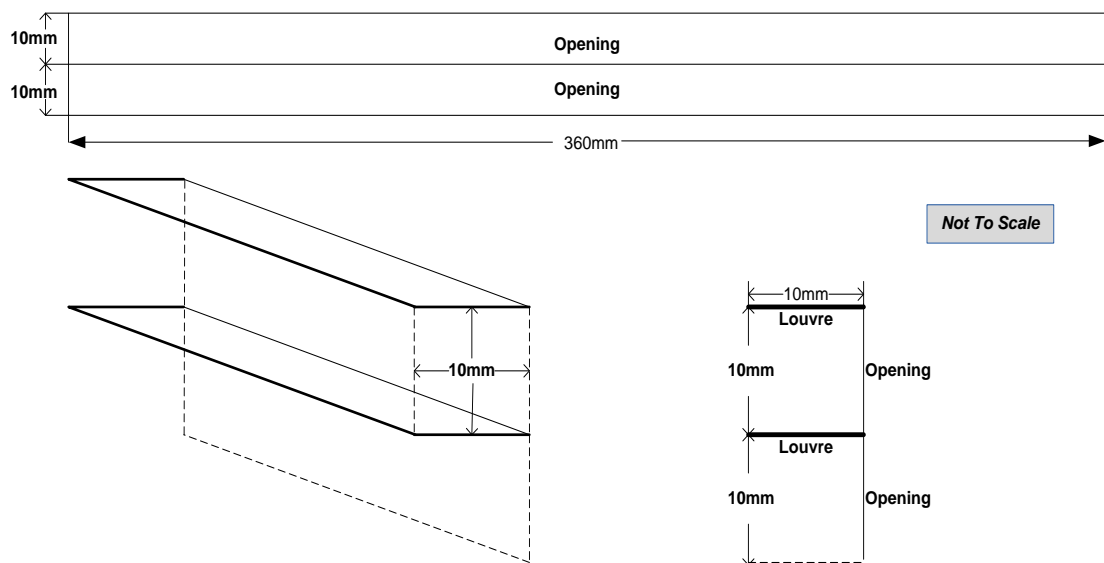


**Figure 4.14** Louvre vent design specification

Helium was released into the enclosure at rates from 1 to 10 lpm. The frame and stack sensor array configurations were used as per the plain vent test. The first configuration used two horizontal lines of four sensors in the upper part of the enclosure at heights of 345mm and 555mm above the enclosure floor, to establish an average helium concentration in the upper part of the enclosure.

The second configuration used the eight vertical sensors in a stack positioned as per figure 4.9 to determine the vertical concentration gradient. For each test helium gas build-up passed through the transient phase to reach a steady state position for each leak rate. A time averaged section of steady state data was used to provide average helium concentrations.

#### 4.4.1 Analysis: Louvre Vents-Frame sensors

Figure 4.15 (a) shows the graph for helium concentration against leak rate for the louvre vented enclosure using frame sensors. The trends presented are similar to those found with the plain vents (Figure 4.11(a)), but the concentrations at the top row of sensors are higher, peaking at 7.23 % at 10 lpm. Sensors 7 and 8 on the lower row have also recorded slightly higher concentrations as the leak rate increases. A change of gradient is again apparent from 3 lpm.

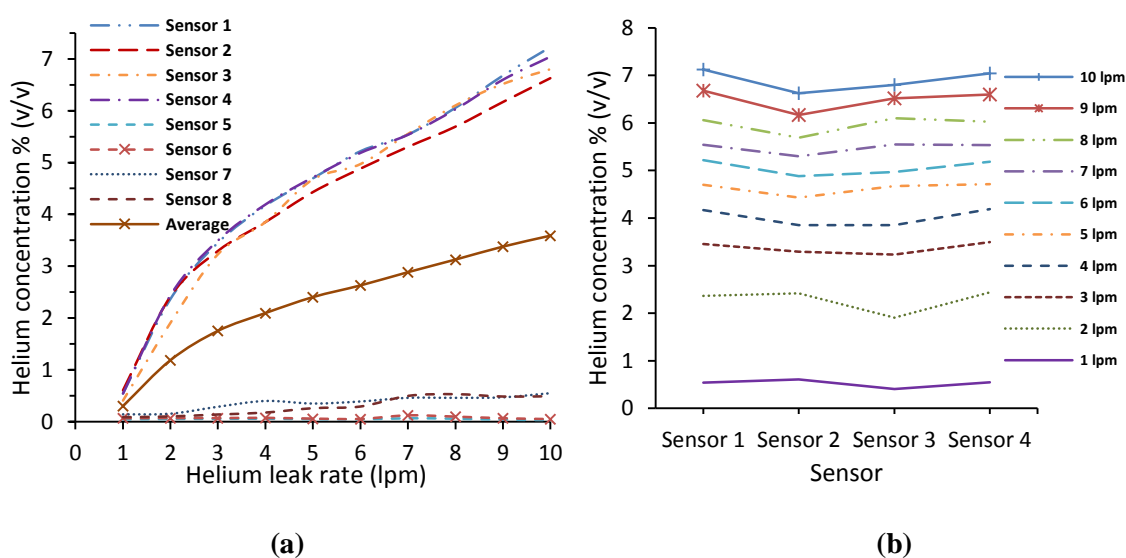


**Figure 4.15** Frame sensor helium concentrations (a) all sensors (b) the 555 mm level

#### 4.4.2 Louvre Vent-Stacked sensors

The results in Figure 4.12 (b) show that a distinct stratified layer is present for all leak rates. The LFL is exceeded at 3 lpm and all leak rates produce concentrations exceeding 25 % of the LFL in the stratified layer. The addition of two horizontal louvres has changed the ventilation regime present in the enclosure. The louvres would appear to be reducing the flow rate through the vents causing the helium to ‘back-up’ and build a thicker layer at the top of the enclosure, than was experienced with plain vents.

Figure 4.16 (a) shows a comparison of stacked sensor readings for plain and louvre vents at 1 lpm and 4.16 (b) at 2 lpm. Although the LFL is not exceeded at these leak rates, the increase in high-level concentration is quite marked with the addition of louvres on the vent opening. At 1 lpm the peak concentration goes from 0.32 to 2.04 % and at 2 lpm the peak concentration jumps from 0.75 to 3.67 % an almost 3 percentage point increase.

Figure 4.16 (c) compares enclosure helium concentrations using plain and louvre vents at 4 and 10 lpm. In both instances the addition of louvres has increased helium concentrations in the stratified layer, by 18.38 % (at 4 lpm) and 15.61 % (at 10 lpm) at sensor 1. Figure 4.16 (d) shows the difference in plain and louvre vent concentrations at frame sensor position 1. From 3 lpm onwards the addition of louvres has led to an increase in helium concentration.

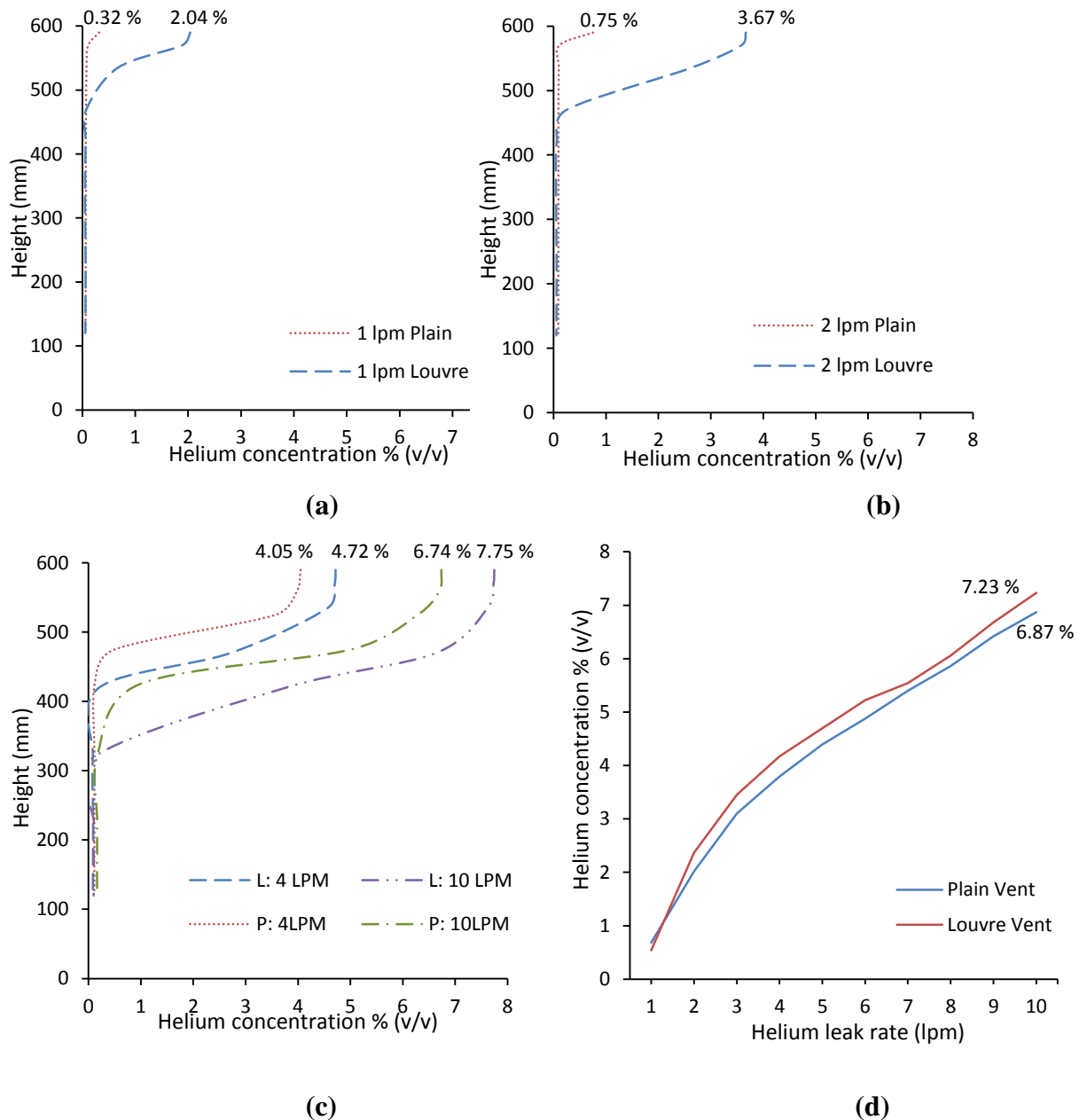


**Figure 4.16 Comparison of plain (P) and louvre (L) vent (stacked sensor) concentrations at (a) 1 lpm, (b) 2 lpm, (c) 4 and 10 lpm and (d) Frame sensor concentrations at sensor 1 (Peak concentrations shown on graphs)**

The ventilation regime within the enclosure has changed with addition of the horizontal louvres. Giannissi et al's (2015, 2016) tests with wind deflectors demonstrated that a centrally positioned horizontal plate (Figure 2.23) (similar to a louvre vent) divides flow equally between in flow and out flow, in a single vent mixing ventilation scheme, effectively managing flow. In the louvre vent displacement flow scheme tested here, one-way flow through the vents is most likely. The addition of louvres has led to an increase in enclosure concentration, suggesting that the louvre extensions are impeding ventilation flow, i.e. increasing vent flow resistance.

#### 4.4.3 Helium sensor deployment

These first tests have shown that the stack sensors arrangement provides more information on buoyant gas distribution than the frame sensors arrangement. The frame sensors were used to try and determine an average concentration in the stratified area. This was not entirely successful as the lower bar was often outside of the stratified zone. In all scenarios tested in this research investigation, a stratified layer should be present in the enclosure and it is the depth of the stratified layer as well as the concentrations achieved that is of interest. If a greater number of sensors was available, then a broader array could be installed to capture concentration data across the enclosure. This was not the case so for the remaining tests only the stacked sensor arrangement was used to collect data. All remaining tests were also run at leaks helium leak rates in the range 1 to 10 lpm.

#### 4.5 Plain vent tests [same opening area as aluminium louvres section 4.6]



(a)



(b)

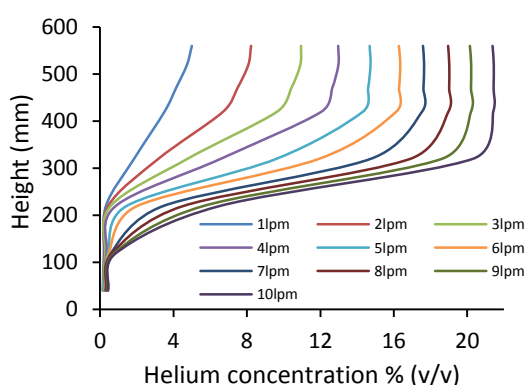
**Figure 4.17 Test rig with (a) rectangular plain vent and (b) aluminium louvre vent**

For this set of experimental tests, the standard enclosure was set up with a cross flow passive ventilation scheme, using opposing upper and lower rectangular plain vent openings (Figure 4.17(a)). The openings were centrally positioned with an opening area equivalent to that of the corresponding aluminium louvre vent (Figure 4.17(b)). Table 4.4 provides information on the vent areas of the aluminium proprietary vents tested later (section 4.6). The rectangular openings were made to an equivalent opening area of the louvre vents. Twelve tests were conducted representing the number of louvre rows.

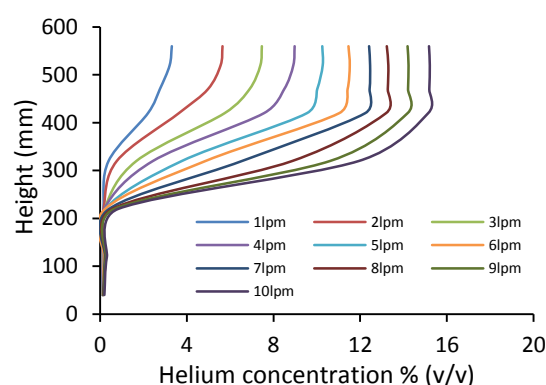
**Table 4.4 Louvre and plain vent opening areas**

Number of louvre rows	Vent area Louvre vent mm <sup>2</sup>	Vent area Plain vent mm <sup>2</sup>	Number of vents	Total vent area mm <sup>2</sup>
1	850	850	4	3400
2	1700	1700	4	6800
3	2550	2550	4	10200
4	3400	3400	4	13600
5	4250	4250	4	17000
6	5100	5100	4	20400
7	5950	5950	4	23800
8	6800	6800	4	27200
9	7650	7650	4	30600
10	8500	8500	4	34000
11	9350	9350	4	37400
12	10200	10200	4	40800

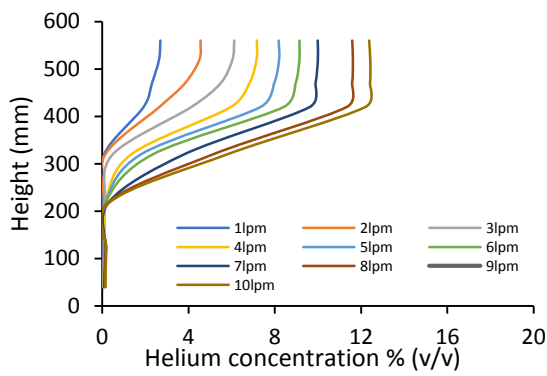
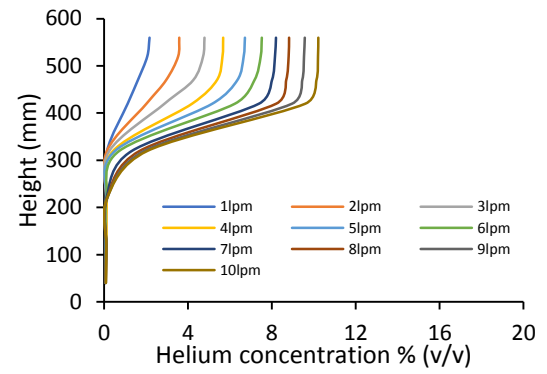
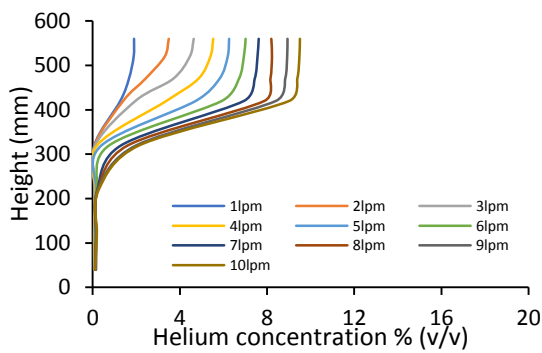
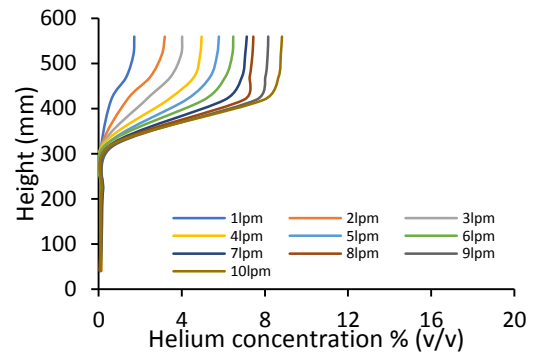
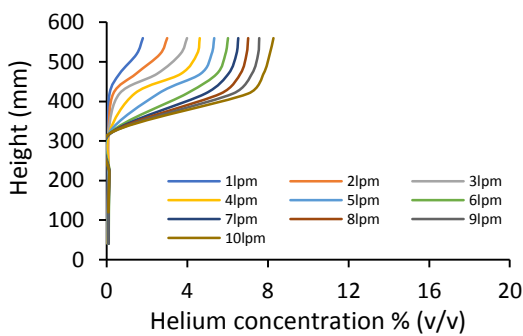
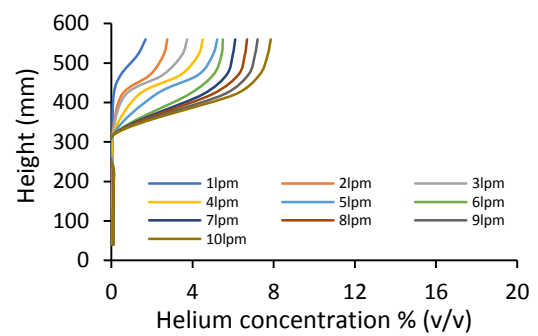
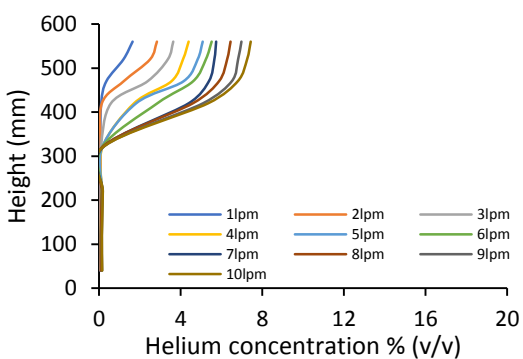
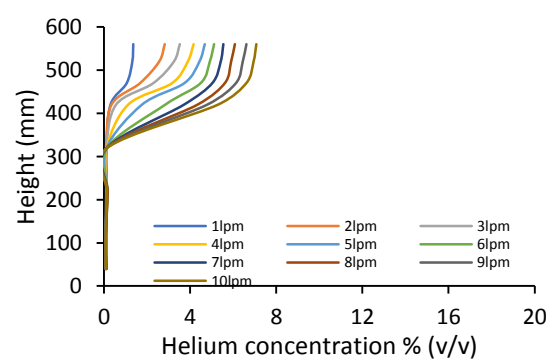
#### 4.5.1 Analysis



(a) 850 mm<sup>2</sup>



(b) 1700 mm<sup>2</sup>

(c) 2550 mm<sup>2</sup>(d) 3400 mm<sup>2</sup>(e) 4250 mm<sup>2</sup>(f) 5100 mm<sup>2</sup>(g) 5950 mm<sup>2</sup>(h) 6800 mm<sup>2</sup>(i) 7650 mm<sup>2</sup>(j) 8500 mm<sup>2</sup>



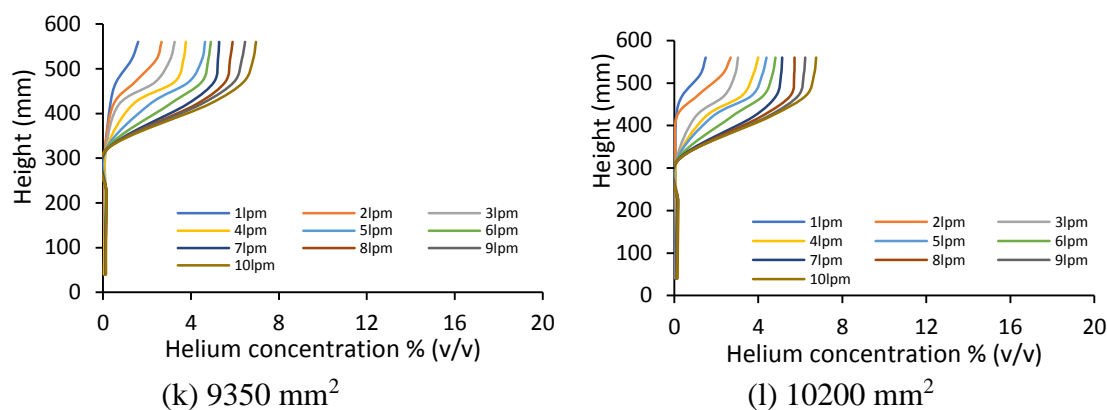


**Figure 4.18 Plain vent opening results for all twelve vent areas**

The graphs in figure 4.18 show that as vent opening area increases, the resultant concentrations in the stratified zone decrease. Also apparent is that stratified zone depth decreases with increasing vent size. In graphs (a) to (f), with the higher leak rates, a layer is present at the top of the stratified zone with a consistent concentration. This is less evident in graphs (g) to (l) where concentration generally increases through the stratified zone. As vent size gets larger, passive ventilation volume flow increases. As a result, more helium is entrained in the flow and removed from the enclosure through the upper vents.

Figure 4.19 provides more detail using the 10 lpm data. There is a significant reduction in the size of the stratified zone and peak concentration achieved when moving from the 850 mm<sup>2</sup> opening to the 1700 mm<sup>2</sup> opening. Each subsequent step increase in area is the equivalent of adding another louvre opening to the vent. At each step as the vent area increases, the impact upon the depth of the stratified layer and the concentration present becomes less.

The graphs for the larger opening areas are very close. This is because the vent area increase becomes proportionally less compared to the previous size, as the vent size increases. Of significance at this leak rate is that the LFL is reached above 400mm in the stratified zone for all vent sizes. With the smallest opening size, half of the enclosure has a concentration in excess of 20%, a very dangerous situation.

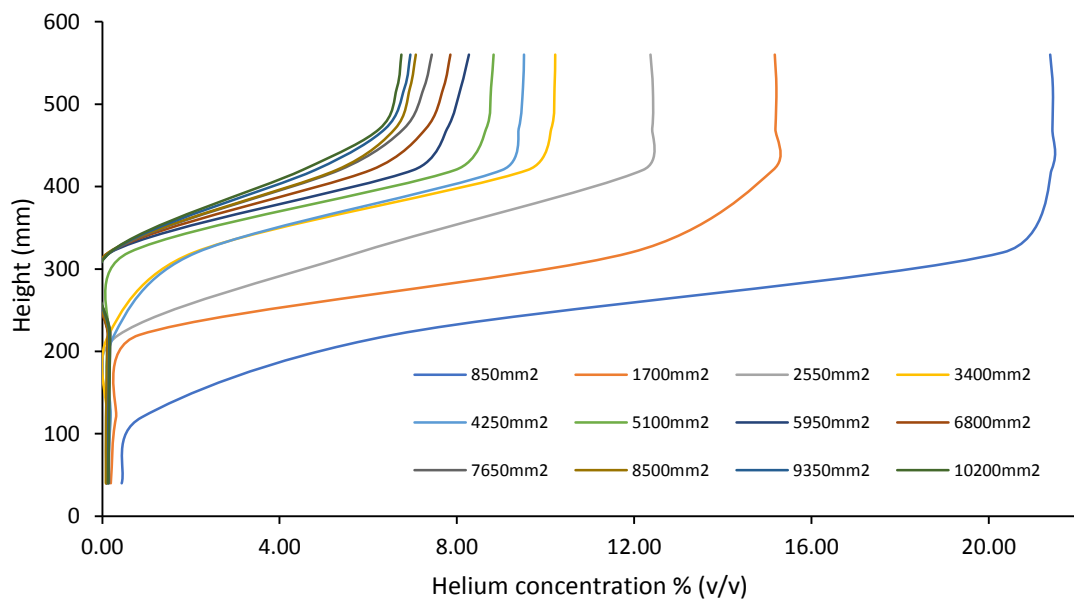


**Figure 4.19 Plain vent results at 10 lpm for all opening sizes**

The wide plain ventilation openings tested in section 4.3 had an opening area of 7200 mm<sup>2</sup>. There is no direct comparison with the tall rectangular vents used in this test, however, the average of 6800 mm<sup>2</sup> and 7650 mm<sup>2</sup> vent areas used in this section, is 7225 mm<sup>2</sup>, which is close to 7200 mm<sup>2</sup>. Figure 4.20 compares the average of the 6800 mm<sup>2</sup> and 7225 mm<sup>2</sup> 10 lpm data sets and the 7200 mm<sup>2</sup> vent 10 lpm data from section 4.3. The tall rectangular vents have led to a higher stratified zone concentration than the wide vents, although the thickness of the stratified zone is similar. The wide vents were positioned further apart though, creating a greater differential pressure.

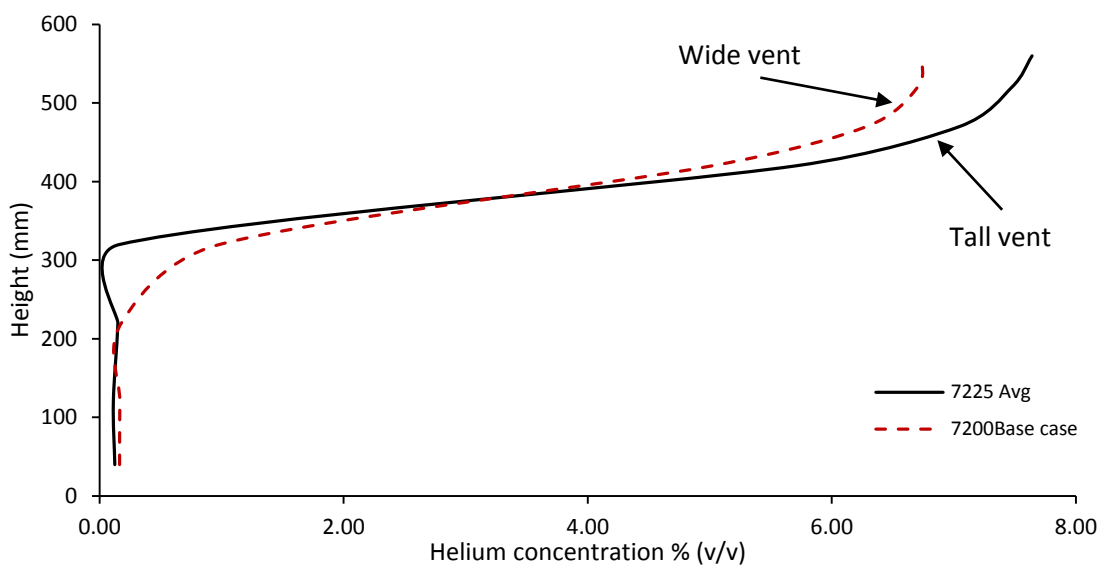


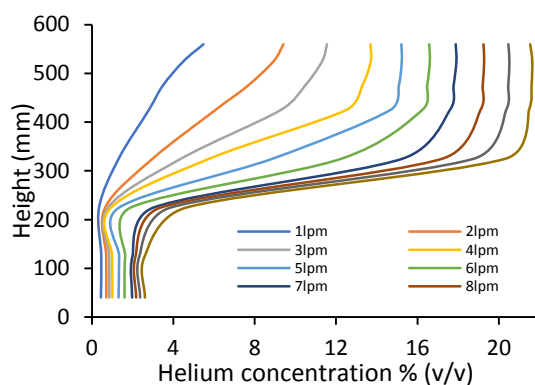
**Figure 4.20 Comparison of wide and tall plain vent openings at 10 lpm**

## 4.6 Aluminium louvre vents [1-12 louvres]

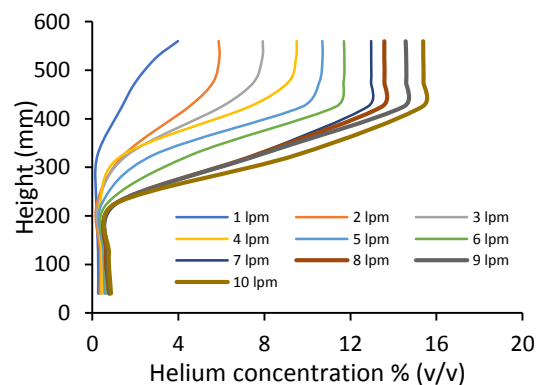
For this set of experimental tests, the standard enclosure was set up with a cross flow passive ventilation scheme, using centrally positioned opposing upper and lower louvre vent openings (Figure 4.17(b)). The louvres were proprietary items available from hardware suppliers (see appendix D), which comprised twelve rows of louvres pressed into an aluminium sheet with downward facing openings. Twelve tests were conducted.

The first test used all twelve louvres. In subsequent tests, louvres were progressively sealed with aluminium adhesive tape, to create the twelve different louvre arrangements tested. The top louvre plate was sealed progressively from the bottom louvre and the bottom louvre plate from the top louvre. This maximised the distance between openings and consequently the differential pressure, to maximise the driving force.

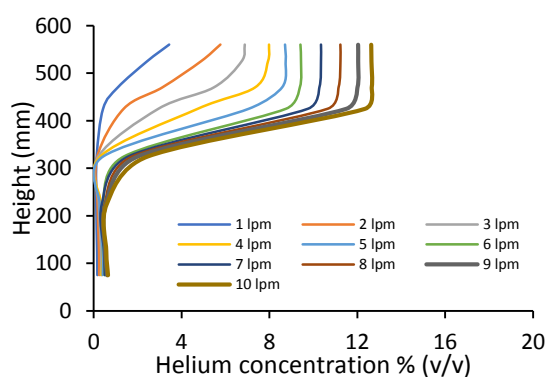
### 4.6.1 Analysis



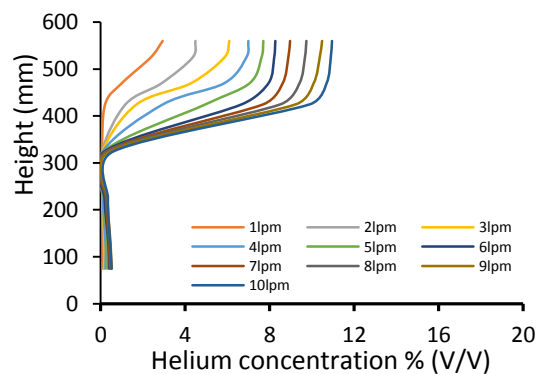
(a) 850 mm<sup>2</sup>



(b) 1700 mm<sup>2</sup>



(c) 2550 mm<sup>2</sup>



(d) 3400 mm<sup>2</sup>

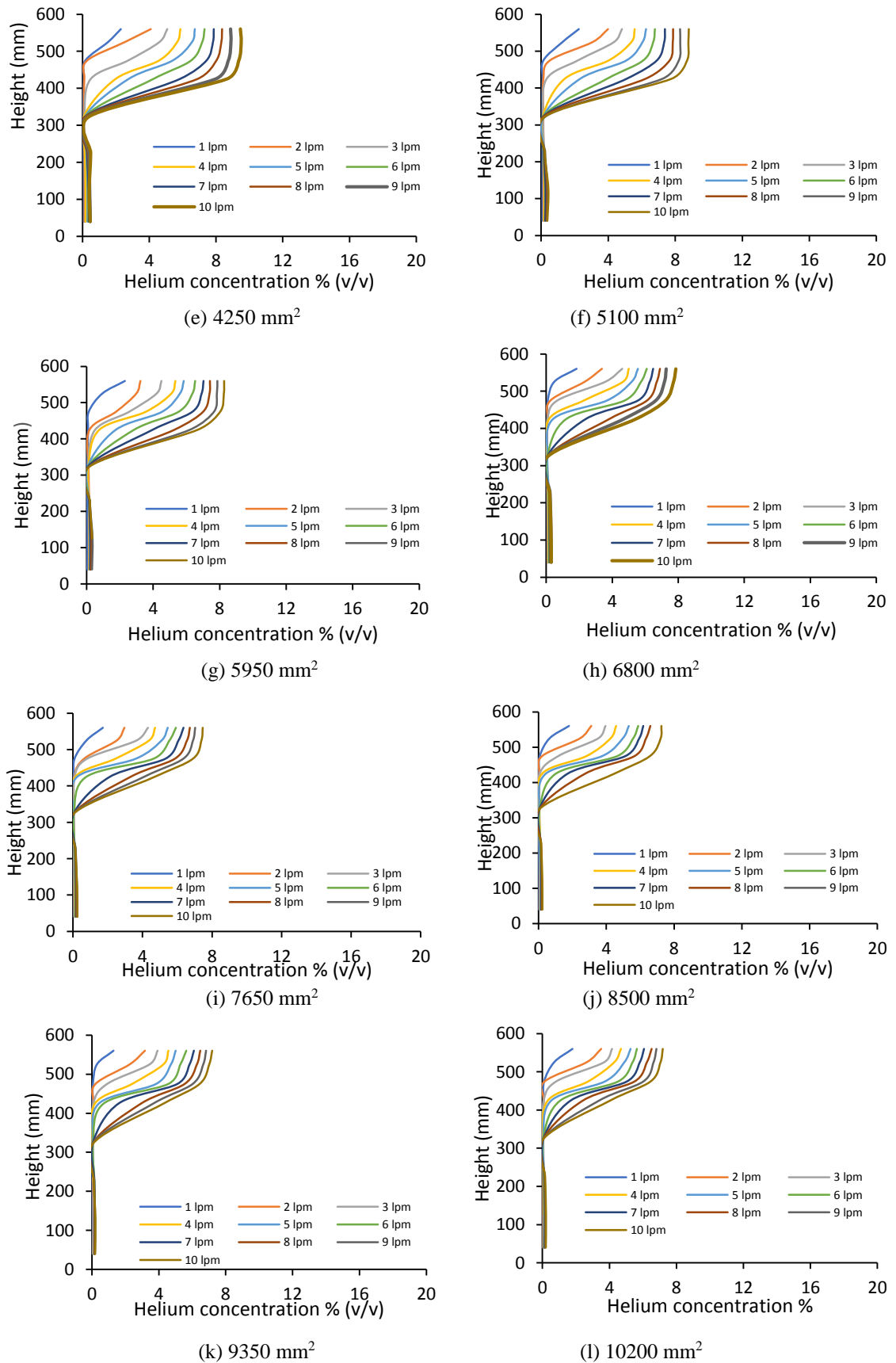


**Figure 4.21 Louvre vent results for all twelve vent areas**

The graphs in figure 4.21 show that as the number of louvre vents increases from one to twelve, helium concentration in the stratified zone decreases. Also apparent is that the stratified zone depth becomes shallower as louvre number increases. In graphs (a) to (g), with the higher leak rates, a layer is present at the top of the stratified zone with a consistent concentration. This is less evident in graphs (h) to (l) and at lower leak rates generally, where concentration increases with height through the stratified zone. As louvre vent number increases, passive ventilation volume flow increases. As a result, more helium is entrained in the flow and removed from the enclosure through the upper vents.

The results presented in Figure 4.21 are very similar to those shown in Figure 4.18 for the plain vent tests. The main differences are that for the higher leak rates the stratified zone is deeper and also the concentrations lower down in the enclosure are raised. This is most notable in Figure 4.21 (a) for the single louvre test where low level concentrations are increased at all leak rates. Peak concentrations in the stratified zones are also marginally higher than with the plain vents. The presence of the louvres has increased the flow resistance, but not to the level that was seen in the tests in section 4.4 with paper louvre extensions.

Figure 4.22 provides more detail using the 10 lpm data. There is a significant reduction in the size of the stratified zone and concentration when moving from the 850 mm<sup>2</sup> louvre to the 1700 mm<sup>2</sup> louvre opening. As the opening area increases at each step, the impact upon the depth of the stratified layer and the concentration present becomes less. The graphs for 9350 mm<sup>2</sup> and 10200 mm<sup>2</sup> are very close. This is because the vent area increase becomes proportionally less compared to the previous size, as the vent size increases.

The central position and shape of the openings allowing a degree of mixing to occur in the enclosure, not directly linked to the size of the louvre opening, but more to the enclosure volume and the leak rate. Of significance at this leak rate is that the LFL is reached above 400mm in the stratified zone for all louvre vent sizes. With the smallest opening size, half of the enclosure has a concentration in excess of 20%, a very dangerous situation as seen with the plain vents.

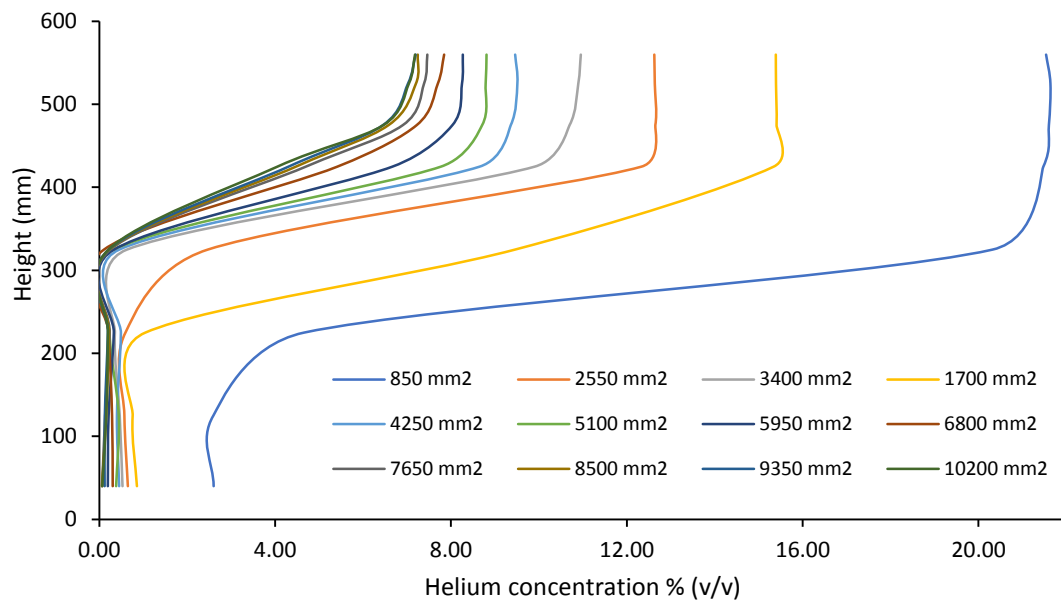


**Figure 4.22 Louvre vent results at 10 lpm for all opening sizes**

Figure 4.23 presents a comparison of plain and louvre vent enclosure concentrations at 10 lpm for the 850 mm<sup>2</sup> size openings. The lines are similar with a slightly higher concentration in the stratified zone for the louvre vent, which is also deeper. Concentrations lower in the enclosure are also higher with the louvre vent.

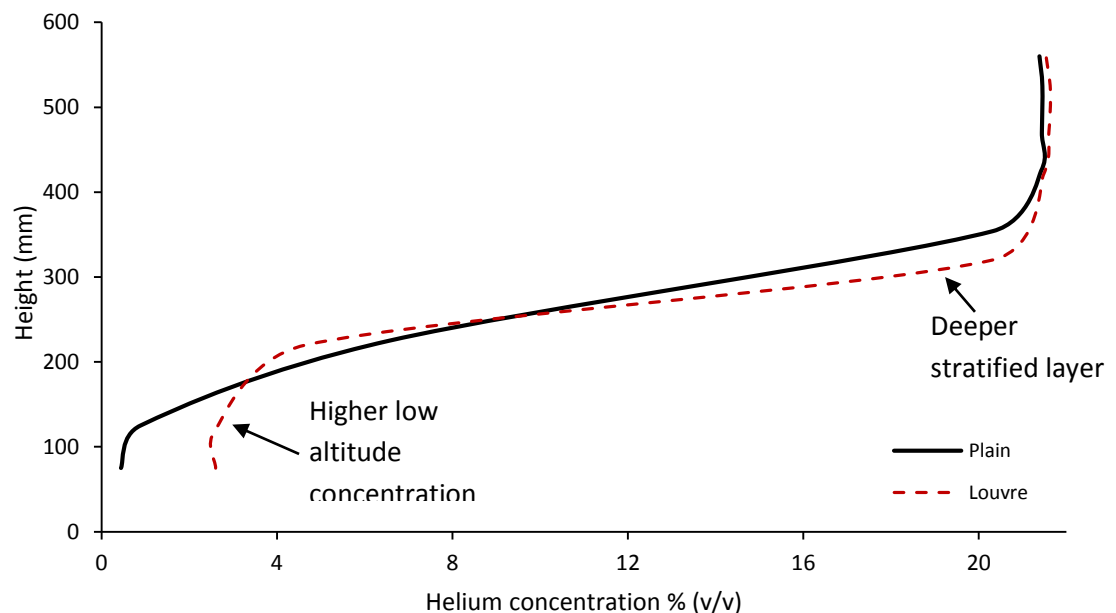


**Figure 4.23 Comparison plain and louvre vent concentrations at 10 lpm-850 mm<sup>2</sup>**

#### 4.6.2 High level louvre vents only

It has already been suggested that the vents on enclosures situated in the outdoors environment could be prone to blockages due for example to foliage. Lower vents will naturally be more susceptible to this. A set of tests was completed using only two upper opposing louvre vents. The vents comprised four rows of louvres with an opening area of  $3400 \text{ mm}^2$ . The results of the comparable cross flow ventilation test with four vents and four rows of louvres is shown in Figure 4.21 (d).

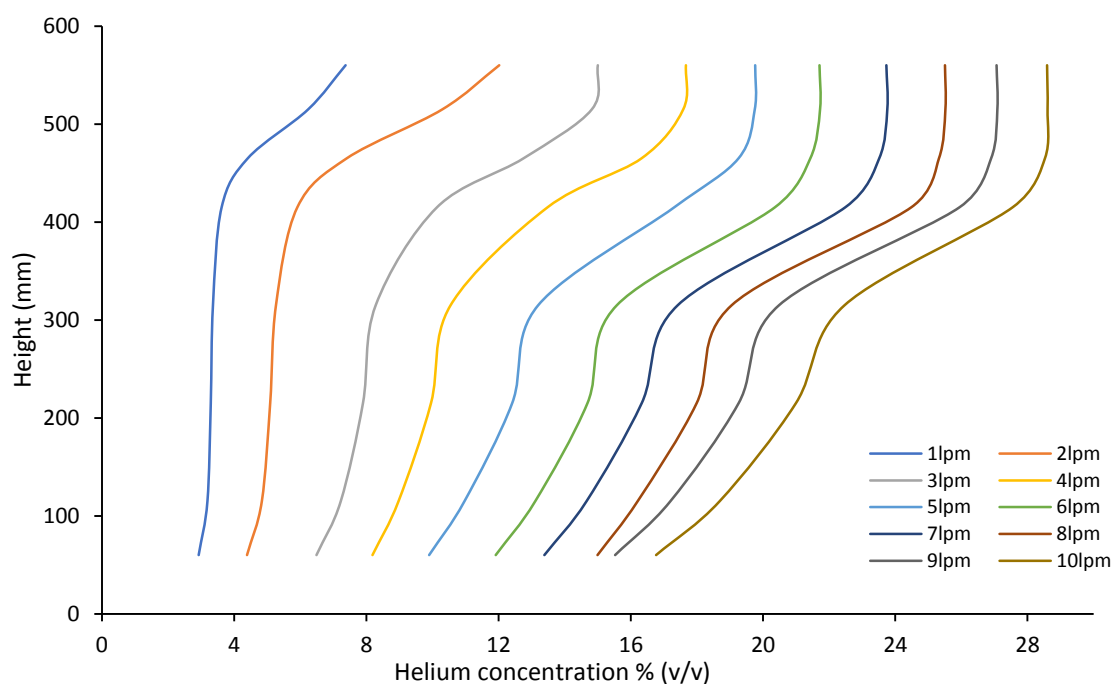


**Figure 4.24 Top louvre vent only results for  $3400 \text{ mm}^2$  vent opening area**

Figure 4.24 presents the results of top louvre vent tests. With only upper ventilation openings, the ventilation regime should change from displacement to mixing ventilation where a more uniformly distributed concentration develops as opposed to strongly stratified, as seen in earlier tests. Higher concentrations are present at all levels in the enclosure with all leak rates. A concentration gradient though is present with concentration increasing with height.

The gradient is more evident at the higher leak rates. Also evident as the leak rate increases, is a homogenous zone at the top of the enclosure. The LFL is breached at 1 lpm from about 500mm. At 2 lpm the LFL is breached throughout the enclosure. This is quite a worrying scenario as an explosive mixture has developed at the lowest leak rate. The

LFL has also been achieved in a relatively short space of time, just over 100 seconds at 1 lpm, as shown in Figure 4.25.

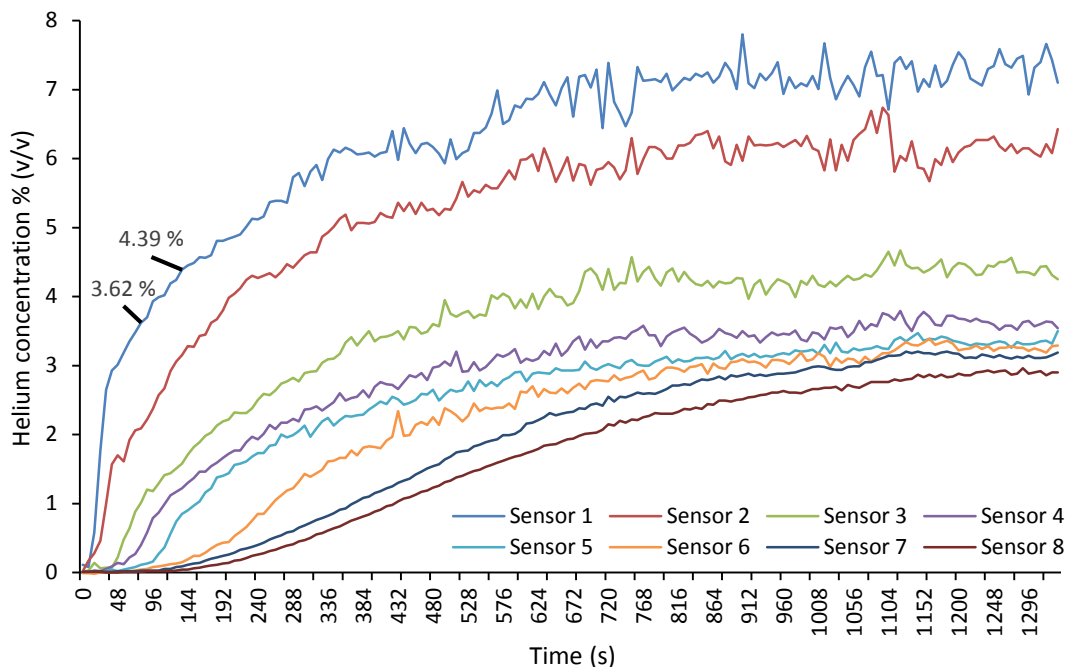


**Figure 4.25 Helium concentration with time-top louvre vents 3400mm<sup>2</sup> at 1 lpm**

The impact of blocking the two lower vents is quite significant on enclosure concentrations and also the distribution of buoyant gas vertically through the enclosure. Figure 4.26 compares helium concentration against enclosure height for the two and four vent (3400 mm<sup>2</sup>) schemes at 1 and 10 lpm. At 1 lpm with four vents the peak concentration at the top of the enclosure is just under 3 %. With two vents there is a homogenous mix up to about 450 mm of about 3.5%. Above this the LFL is breached and peaks at 7.37 %.

At 10 lpm the change is more significant. With four vents, below about 300 mm the concentration is below 0.5 %. Above 400 mm the LFL is exceeded and peaks at 10.9 %, with a clear stratified layer. With only two vents the concentration exceeds 16.75 % from 75 mm. The concentration increases steadily with height peaking at 28.6 % in a zone about 100 mm thick at the top of the enclosure. The blockage of lower vents has significant potential to increase buoyant gas concentrations to explosive levels.



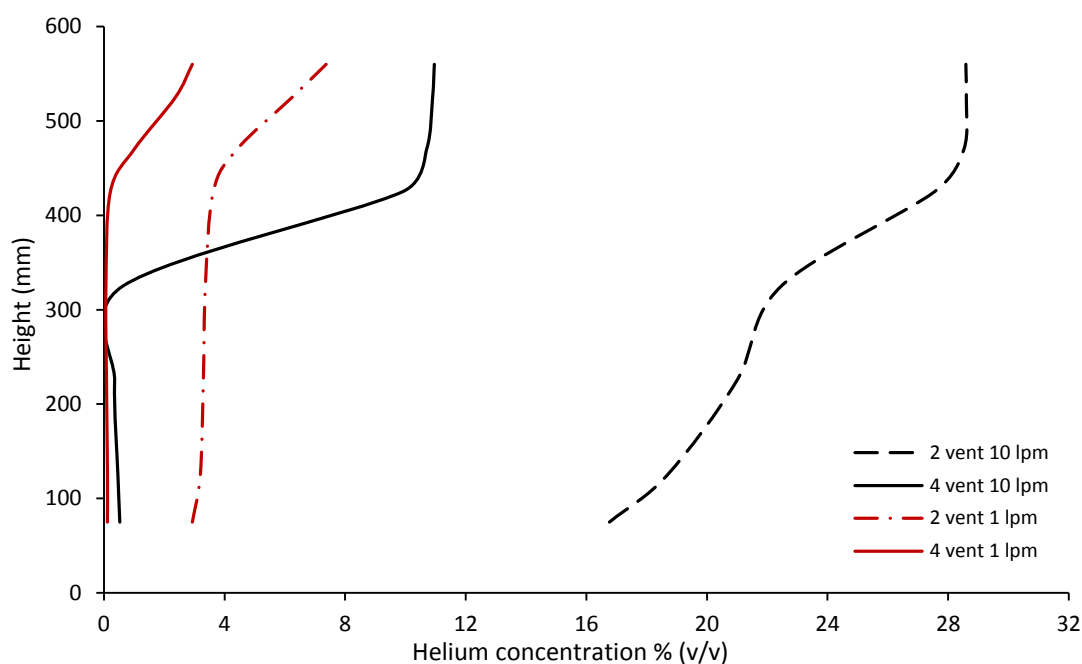


**Figure 4.26 Comparison two and four vent schemes (3400 mm<sup>2</sup>) at 1 and 10 lpm**

#### **4.7 Chimney ventilation [Roof mounted various heights]**

For this set of experimental tests, the standard enclosure was used, but the end panels were sealed, and chimney vents were installed on the roof. The end panels were sealed so that ventilation would only occur via the chimney openings. The chimney design was simple based upon a 64 mm diameter drainpipe. Tests were conducted with no rain lid, a flat rain lid and a China cap rain lid (Figure 4.27). Stacked sensor positions are used in all tests.

The area of the pipe opening was 3216 mm<sup>2</sup>, the opening area with a flat lid was 2168 mm<sup>2</sup> (approximately 2/3 of the pipe area) and the opening area with the China cap was 3255 mm<sup>2</sup>, (approximately the same as the pipe area). A number of chimney variations were tested (Tables 4.5 and 4.6). The tests in Table 4.5 are similar but vary the rain cap design. The tests in Table 4.6 all use the same configuration but vary the height on one chimney to investigate the effect. Sensor heights are as per previous tests.

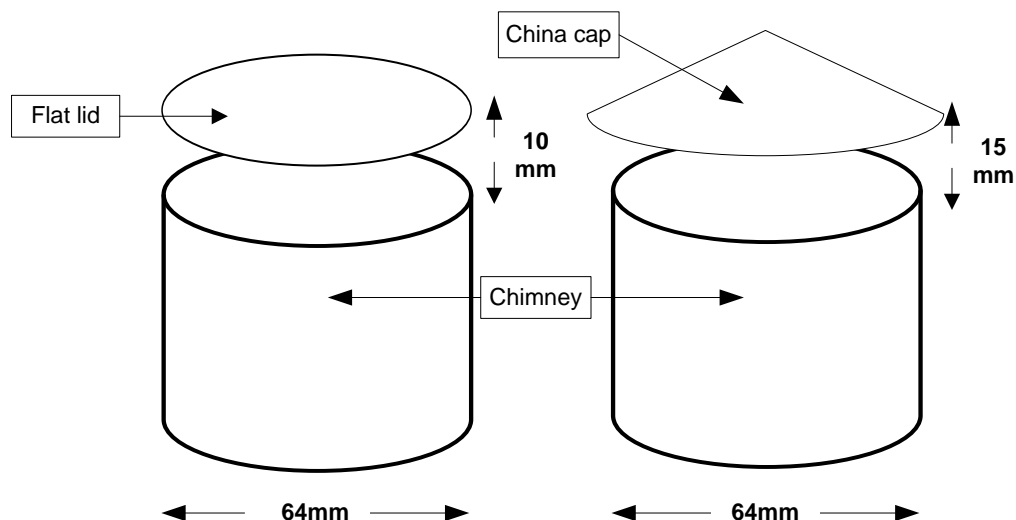


Figure 4.27 Chimney schematic showing flat and china caps [not to scale]

Table 4.5 Chimney vent configurations: Various arrangements

	<i>Test 1</i>	<i>Test 2</i>	<i>Test 3</i>	<i>Test 4</i>	<i>Test 5</i>	<i>Test 6</i>
<b>Chimneys Number</b>	1	1	2	2	2	2
<b>Chimney Height</b>	110mm	110mm	110mm	110mm	110mm	110mm
<b>Chimney Size</b>	64mm inner diameter	64mm inner diameter	64mm inner diameter	64mm inner diameter	64mm inner diameter	64mm inner diameter
<b>Vent area</b>	3216mm <sup>2</sup>	3216mm <sup>2</sup>	3216mm <sup>2</sup>	3216mm <sup>2</sup>	3216mm <sup>2</sup>	3216mm <sup>2</sup>
<b>Lid gap</b>	N/A	10mm	N/A	10mm	15mm	15mm
<b>Gap area</b>	N/A	2168mm <sup>2</sup>	N/A	2168mm <sup>2</sup>	3255mm <sup>2</sup>	3255mm <sup>2</sup>
<b>Chimney position</b>	Opposing end to sensors	Adjacent to sensors	Adjacent to end walls	Adjacent to end walls	Adjacent to end walls	Adjacent to end walls
	100mm in/180mm centred	100mm in/180mm centred	100mm in/180mm centred	100mm in/180mm centred	100mm in/180mm centred	100mm in/180mm centred
<b>Rain Cap</b>	None	None	None	Flat Cap 69mm diameter 10mm gap	Flat Cap 69mm diameter 15mm gap	China cap 15mm gap
<b>Leak rate</b>						0.25lpm
						0.5lpm
						0.75lpm
	1lpm	1lpm	1lpm	1lpm	1lpm	1lpm
						1.5lpm
					2lpm	2lpm

**Table 4.6 Chimney vent configurations: Increasing chimney height/obstruction**

	<i>Test 7</i>	<i>Test 8</i>	<i>Test 9</i>	<i>Test 10</i>	<i>Test 11</i>	<i>Test 12</i>
<i>Chimneys Number</i>	2	2	2	2	2	2
<i>1st Chimney Height</i>	110mm	110mm	0mm	0mm	0mm	0mm
<i>2nd Chimney Height</i>	110mm	220mm	420mm	630mm	840mm	1680mm
<i>Chimneys Diameter</i>	64mm	64mm	64mm	64mm	64mm	64mm
<i>Vent area</i>	3216mm <sup>2</sup>	3216mm <sup>2</sup>	3216mm <sup>2</sup>	3216mm <sup>2</sup>	3216mm <sup>2</sup>	3216mm <sup>2</sup>
<i>Lid gap</i>	15mm	15mm	15mm	15mm	15mm	15mm
<i>Gap area</i>	3255mm <sup>2</sup>	3255mm <sup>2</sup>	3255mm <sup>2</sup>	3255mm <sup>2</sup>	3255mm <sup>2</sup>	3255mm <sup>2</sup>
<i>Chimney position (adjacent to end walls)</i>	100mm in/180mm centred	100mm in/180mm centred	100mm in/180mm centred	100mm in/180mm centred	100mm in/180mm centred	100mm in/180mm centred
<i>Rain cap</i>	China cap 15mm Gap	China cap 15mm Gap	China cap 15mm Gap	China cap 15mm Gap	China cap 15mm Gap	China cap 15mm Gap
<i>Obstruction size</i>	255 x 278 x 316	255 x 278 x 316	255 x 278 x 316	255 x 278 x 316	255 x 278 x 316	255 x 278 x 316
<i>Leak rate</i>	0.25lpm	0.25lpm				
	0.5lpm	0.5lpm				
	0.75lpm	0.75lpm				
	1lpm	1lpm		1lpm		1lpm
	1.5lpm	1.5lpm				
	2lpm	2lpm	2lpm	2lpm	2lpm	2lpm
	3lpm	3lpm				
	4lpm	4lpm	4lpm	4lpm	4lpm	4lpm

#### 4.7.1 Analysis

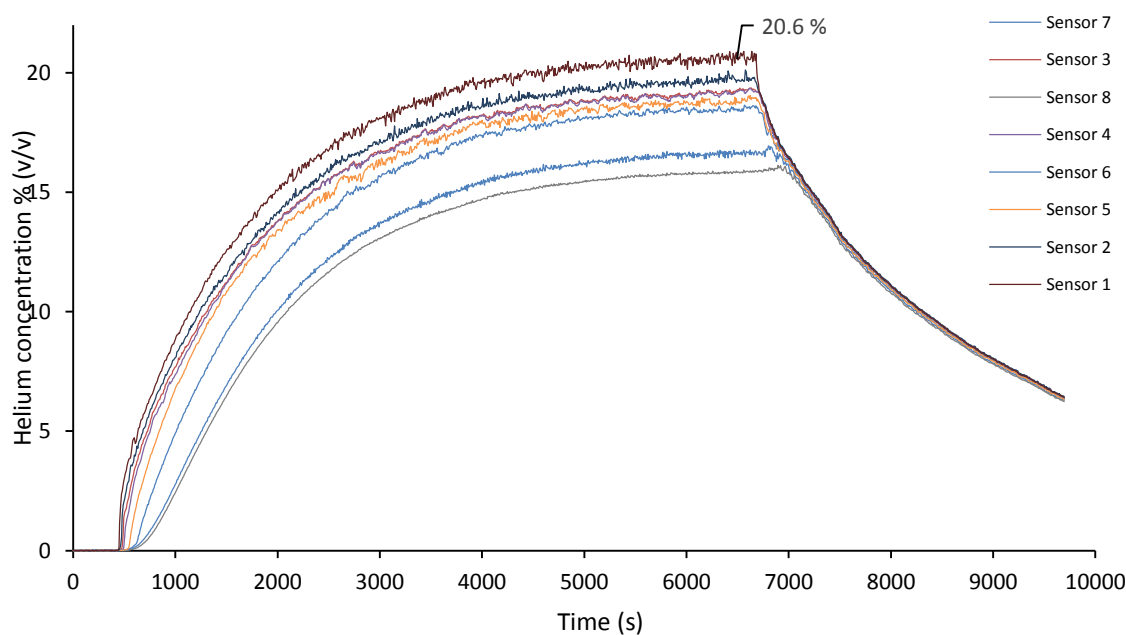
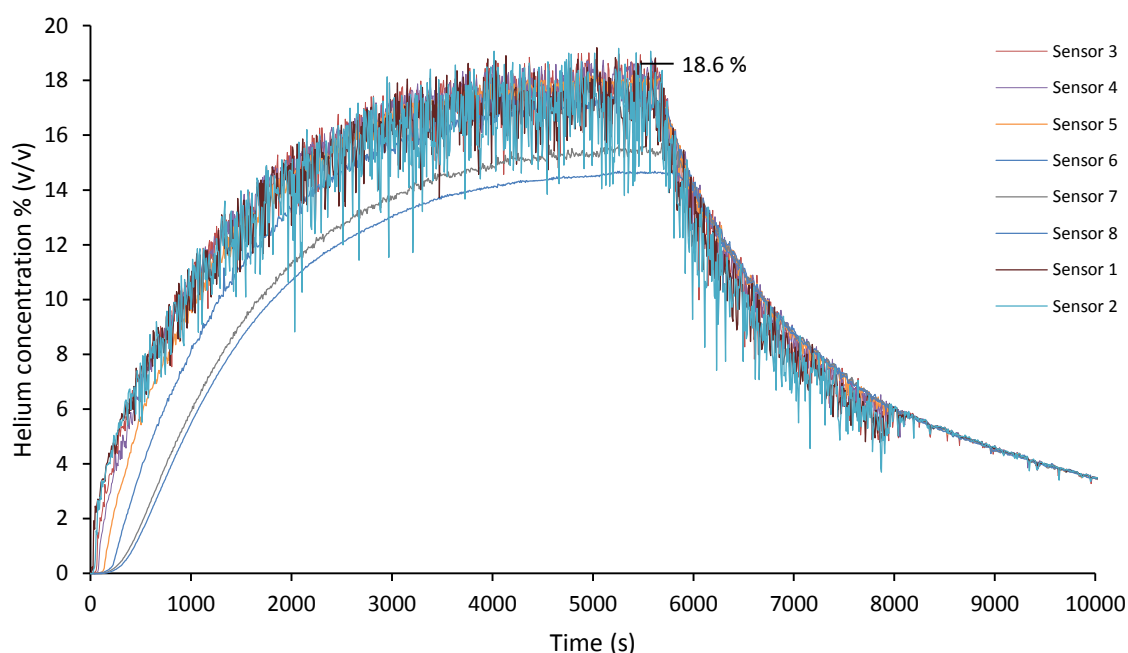
**Figure 4.28 Test 1: Single 110 mm chimney, no rain cap, at 1 lpm leak rate**

Figure 4.28 presents the results of Test 1 using a single 110 mm chimney. The graphs show a steady increase in concentration throughout the enclosure, leading to a steady state condition. On this test the sensors were at the opposing end to the position of the chimney. The vertical concentration gradient in the enclosure is fairly narrow, suggesting mixing has occurred, although the two lower sensors have not attained the concentrations achieved higher up, but given more time this may have changed. The peak concentration is over 20 %, at a leak rate of 1 lpm, and it does not fall below 15% at any level. With a single chimney, effectively half of the area will become an inlet and half an outlet, thus reducing the ventilation capability by 50 %.



**Figure 4.29 Test 2: Single chimney, no rain cap, 1 lpm, sensors adjacent to opening**

Figure 4.29 presents the results of test 2. This is the same scenario as test 1, but the sensor stack is now adjacent to the chimney opening. As can be seen in the graph, the readings from the sensors are a lot more unsteady, due to the more turbulent flow adjacent to the chimney. Concentrations below the opening are lower than at the other end of the enclosure (Test 1). This will be due to the two-way flow through the chimney (figure 4.30), with more fresh air being present in the vicinity of the chimney base.

This is effectively mixing ventilation, which should lead to a homogenous enclosure environment. This is not completely evident, with a concentration gradient present in the

enclosure. The graph has followed the track of test 1, with the two lower sensors recording lower concentrations. The peak concentration achieved near the chimney was 18.6 %, two percentage points lower than in test 1.

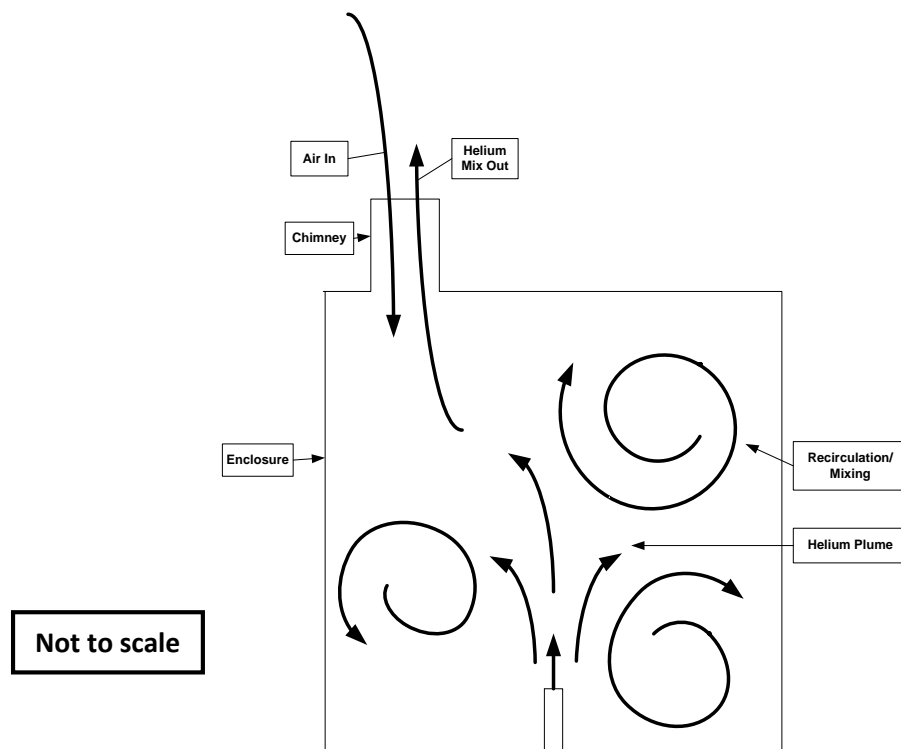
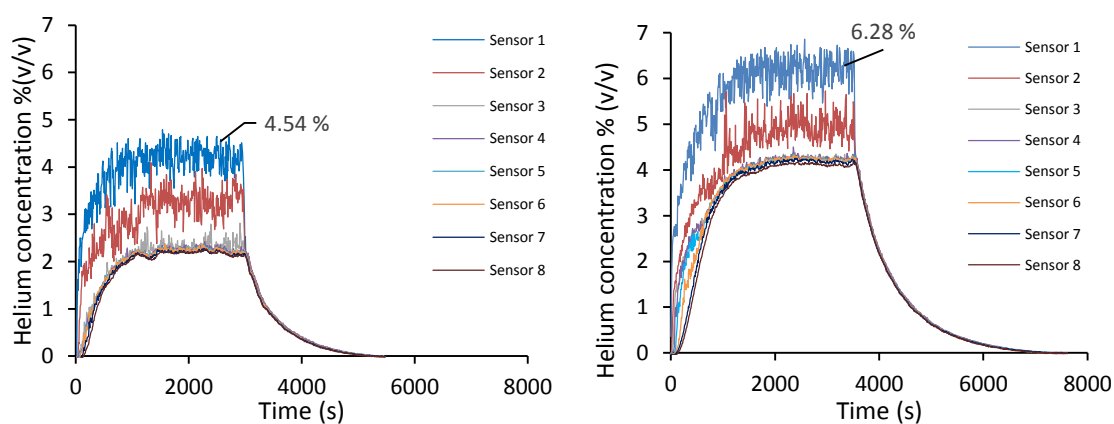


**Figure 4.30 Schematic showing two-way flow through the chimney and recirculation. Representation is 2D, whereas in reality flow is 3 dimensional**



**Test 3: Without rain cap**

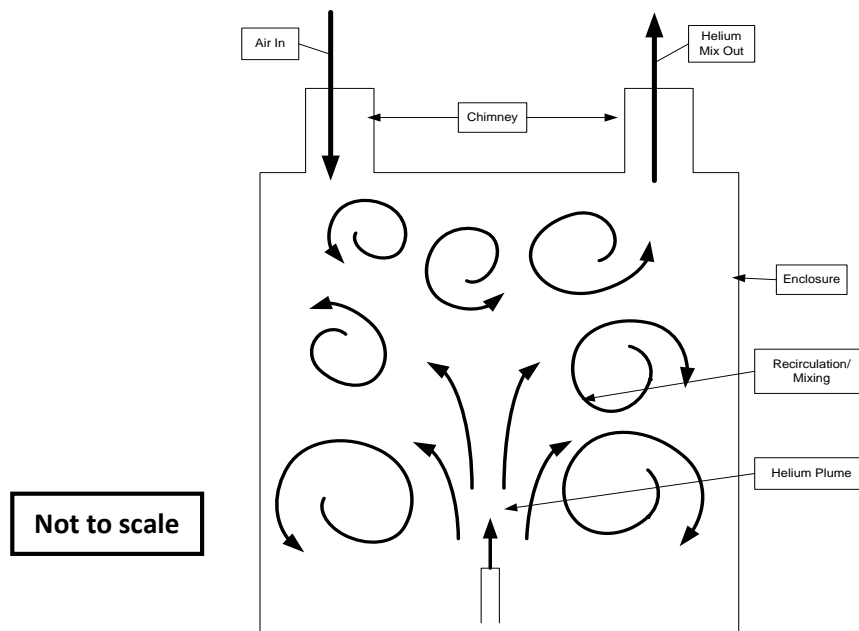
**Test 4: With rain cap**

**Figure 4.31 Tests 3 and 4 two chimneys, with and without flat lids at 1lpm**

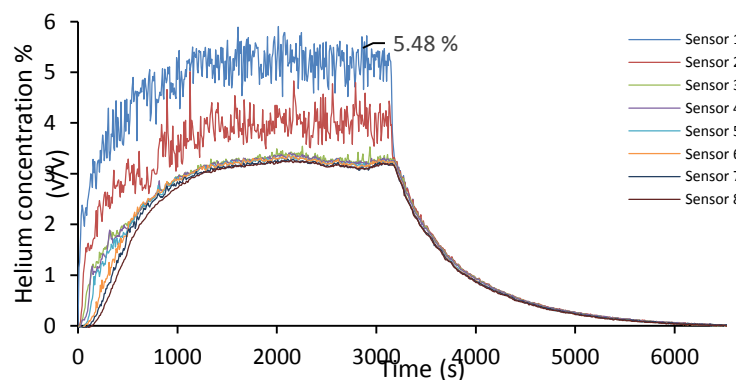
Tests 3 and 4 (Figure 4.31) are effectively the same but test 4 used a flat rain lid 10 mm above the top of the chimney. With two chimneys, a displacement ventilation regime will

be present (Figure 4.32) with one becoming an inlet and the other an outlet. A phenomenon that can occur is oscillating flow, where the inlet becomes an outlet and vice versa. This is usually caused by pressure differences due to for example wind and can lead to impaired flow performance and higher gas concentrations.

It can be seen from Test 4, that the addition of the rain lids has impeded flow through the enclosure and led to increased helium concentrations. The addition of the lid with a 10 mm gap has though effectively reduced the opening area by a third, which will have contributed to the reduced flow. The positioning of the rain lid above the chimney is clearly important. A stratified layer is apparent due to the displacement ventilation.

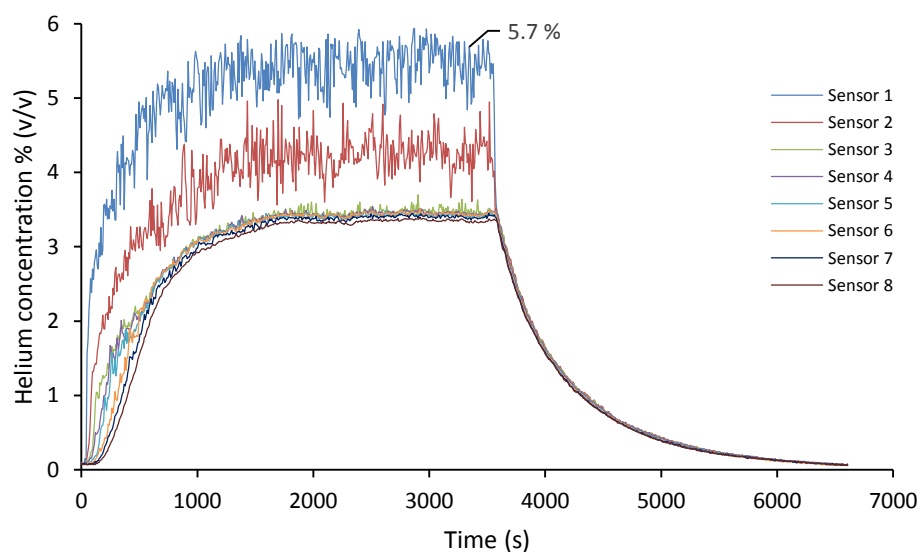


**Figure 4.32 Schematic showing displacement ventilation and recirculation with double chimney arrangement [not to scale]**



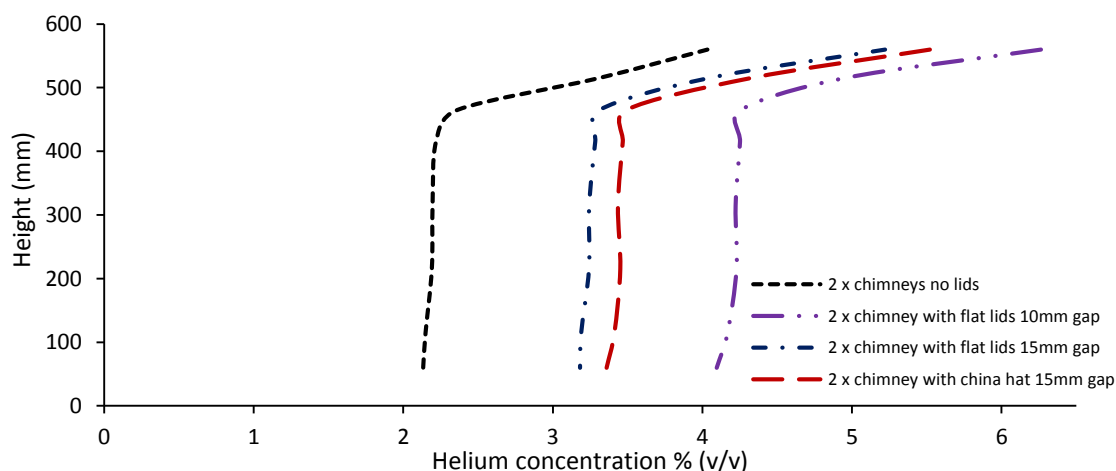
**Figure 4.33 Test 5 two chimneys, flat lids and 15 mm gap at 1lpm**

Figure 4.33 presents the results of test 5, where the lid has been positioned at 15 mm above the chimney opening, to produce an opening area of 3255 mm<sup>2</sup>, which is close to the chimney opening area of 3216 mm<sup>2</sup>. The difference being that with the lid, the opening is vertical, and with the chimney it is horizontal. The peak concentration achieved is still about one percentage point above that achieved without a lid in test 3. This does point towards the presence of a lid impeding flow. Also apparent in all of the tests is that a homogenous area is present up to sensor 6 at 465 mm height.



**Figure 4.34 Test 6 two chimneys, china hat lids, 15mm gap at 1lpm**

Test 6 uses the same set up as the previous tests but replaces the flat rain lids with china cap rain lids with a 15 mm ventilation gap. There has been a slight increase in peak concentrations in the stratified layer and also a slight increase in the homogeneous zone below 465 mm.



**Figure 4.35 Comparison of tests 3, 4, 5 and 6 at 1 lpm**

Figure 4.35 compares the results at 1 lpm for tests 3, 4, 5 and 6. It shows how the homogenous zone is at a similar height for all schemes, however the concentration achieved varies according to the type of rain lid fitted. The china cap lid appears to impede flow out of the chimney more than the flat lid, which could be due to the conical shape buffering flow (Figure 4.36).

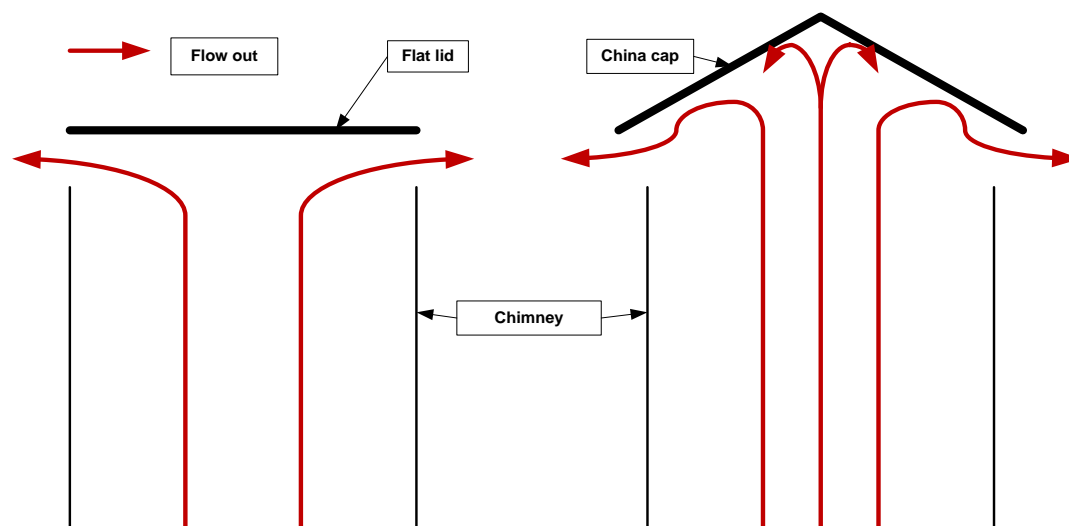


**Figure 4.36 Flow through chimney with flat lid and china cap [not to scale]**

#### 4.7.2 Effect of a tall chimney

Tests 7 to 12 use the standard enclosure with two roof openings. One opening is a 64 mm pipe, which approximately doubles in height with each test. The other opening is a 64 mm diameter circular opening, flush with the enclosure roof, in the same position as the second chimney in the earlier tests. The purpose of this is to maximise the pressure differential and to attribute changes in concentration to the increase in chimney height. The chimney and the circular opening were fitted with a china cap with a 15 mm gap. This series of tests will compare concentrations at a leak rate of 2 lpm.

Figure 4.37 presents the results from tests 7 to 12. As is shown in the graph, as the height of the chimney increases the concentration of helium in the enclosure reduces. With a chimney at 110 mm height clear stratification is present in the enclosure. As the chimney height increases, the level of stratification becomes less pronounced. As the chimney height increases, the pressure differential between the top of the chimney and the plain



opening increases (due to the rising atmospheric pressure difference), increasing the rate of flow through the chimney and sucking out more gas from the enclosure. This will displace the contents of the enclosure more effectively, introducing greater amounts of fresh air through the plain vent to mix with the helium entering the enclosure from the nozzle. A tall chimney is therefore very effective as means of passive ventilation. 2 lpm is a fairly low leak rate, however the LFL is exceeded even with the 840 mm tall chimney. A wider diameter chimney would increase gas flow, as would a chimney in conjunction with a louvre panel mounted low down on the enclosure side panel.

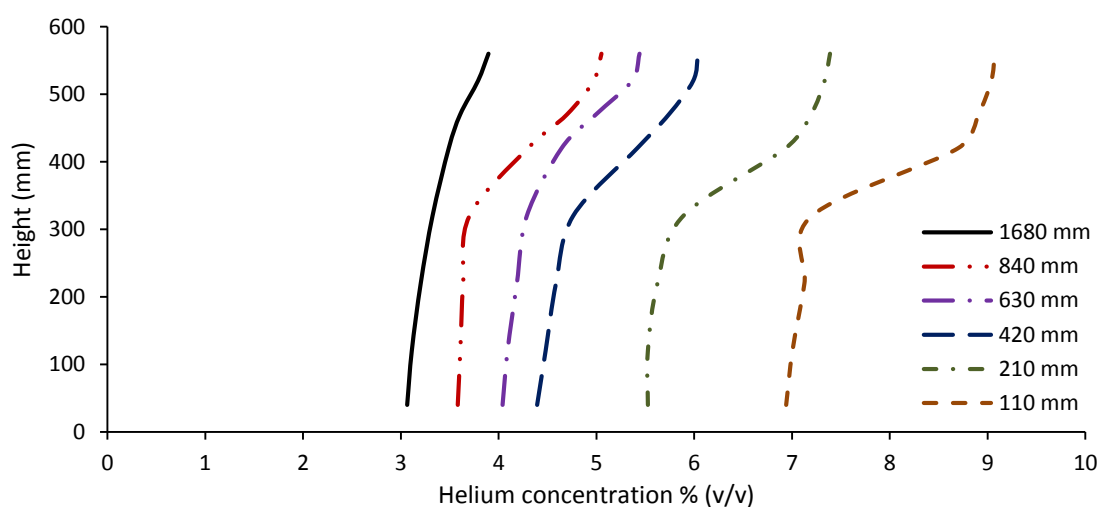


**Figure 4.37 Tests 7 to 12: Increasing chimney height at 2 lpm**

#### 4.8 Chimney test with internal obstruction [Simulated fuel cell]

In this test, the enclosure with two 110 mm chimneys was used. A Hymera fuel cell sized box was fixed internally to the sidewall of the enclosure. An operational enclosure would contain the fuel cell and supply pipes and potentially also a car battery for energy storage and associated electronics. This would make the inside of the enclosure very complex for effective passive ventilation flow paths to establish. As such there is the potential for concentrations to be higher than with an empty enclosure and the possibility of pockets of gas to become trapped.

The purpose of this simple test is to see whether the addition of the fuel cell itself into the enclosure has an effect on helium concentrations. The fuel cell box was 316 mm wide by 255 mm deep by 278 mm tall. It was fixed centrally 280 mm above the enclosure floor. Figure 4.38 provides a schematic diagram of the setup.

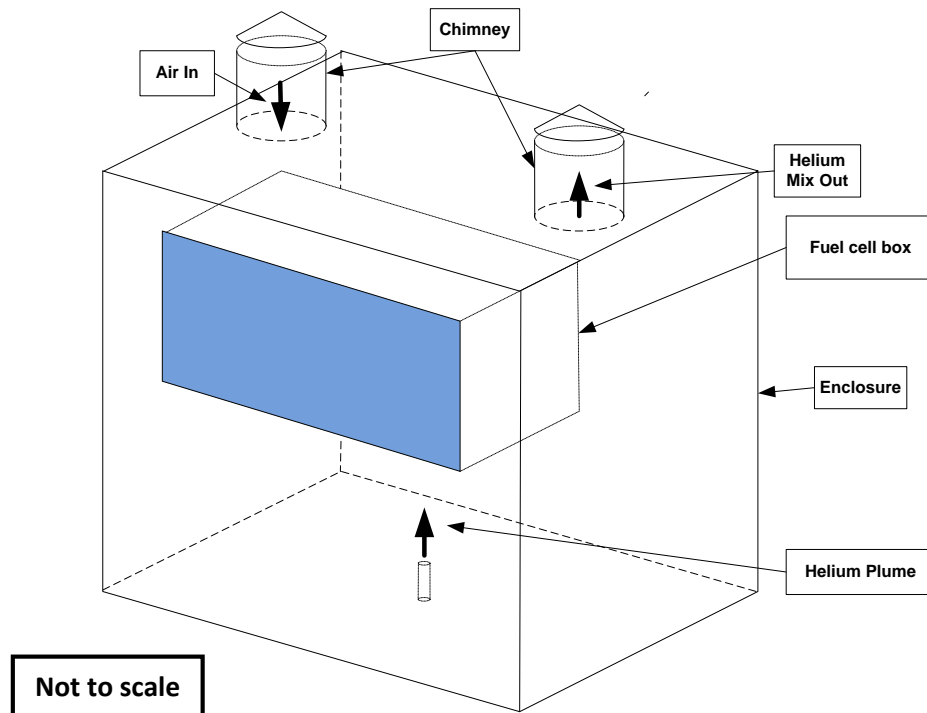


**Figure 4.38 Enclosure with two capped chimneys containing the fuel cell box**

Figure 4.39 provides a comparison of the results at 2 lpm. Without the obstruction there is a homogenous zone up to about 475 mm height and then a stratified layer where the concentration increases to a peak of about 8.5%. With the obstruction there is a homogenous zone up to about 300 mm height (just above the position of the fuel cell). The concentration then increases over a distance of about 120 mm before settling at about 9%. The obstructions have broadly increased the helium concentration in the enclosure and has also affected the distribution of the gas.

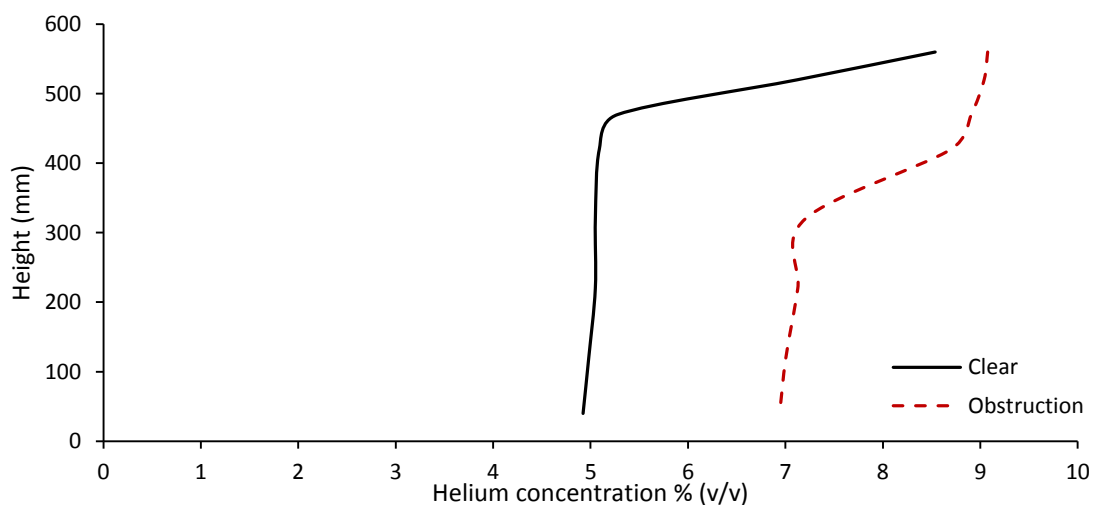


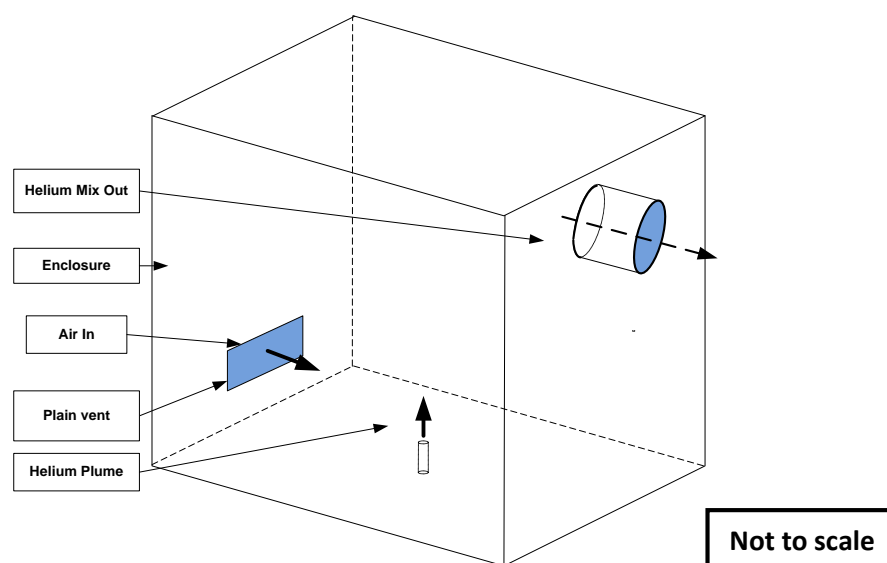
**Figure 4.39 Chimney x 2 china cap with and without obstruction at 2 lpm.**

## 4.9 Flue ventilation [Tubular side vent]

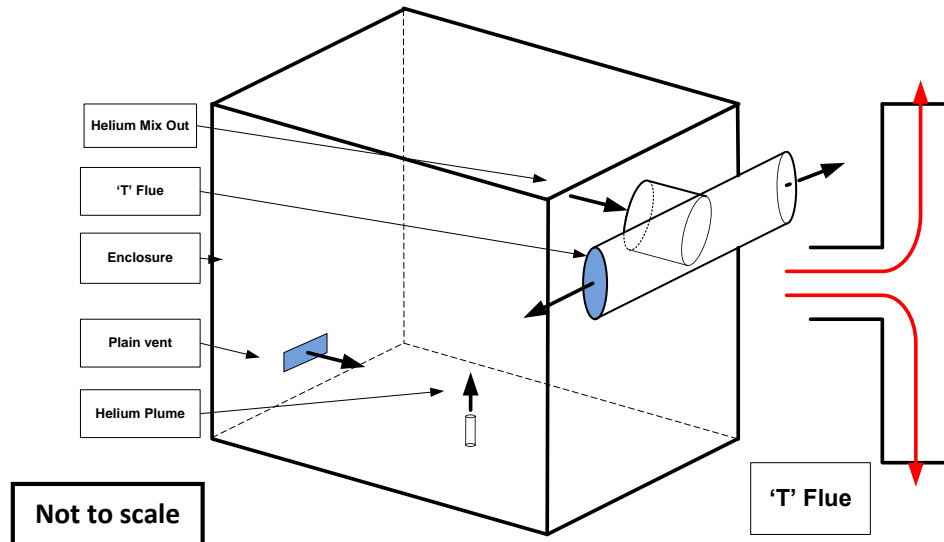
For some enclosures fixed to a wall, it may be necessary to pass a pipe through the wall to vent gas to the atmosphere. The following simple tests (Table 4.7) use a flue of the same diameter as that used for the chimney tests (64 mm) Figure 4.40. The final test uses a 64 mm diameter 'T' flue (Figure 4.41) to see if the increase in vent area improves flow. Test results are presented, but the 4 lpm results will be used for comparison.

**Table 4.7 Flue tests**

<i>Experiment</i>	1	2	3	4	5	6
<i>Flue length (mm)</i>	110	110	110	110	330	110
<i>Flue diameter (mm)</i>	64	64	64	64	64	64
<i>Flue opening area (mm<sup>2</sup>)</i>	3217	3217	3217	3217	3217	6434
<i>Flue position</i>	Side / top / centre	Side / top / centre	Side / top / centre	Side / top / centre	Side / top / centre	Side / top / centre
<i>Flue height (mm)</i>	550	550	550	550	550	550
<i>Flue design</i>	Single tube	Single tube	Single tube	Single tube	Single tube	"T" Tube
<i>Inlet vet [Y/N]</i>	N	Y	Y	Y	Y	Y
<i>Inlet vent dimensions (mm)</i>	No inlet vent	100 x 32	100 x 64	100 x 96	100 x 96	100 x 32
<i>Inlet vent area (mm<sup>2</sup>)</i>	N/A	3200	6400	9600	9600	3200
<i>Inlet vent position</i>	N/A	Opposing lower	Opposing lower	Opposing lower	Opposing lower	Opposing lower
<i>Flow rate (lpm)</i>	0.5	0.5	0.5	0.5		
<i>Flow rate (lpm)</i>		1	1	1	1	1
<i>Flow rate (lpm)</i>		2	2	2		
<i>Flow rate (lpm)</i>		4	4	4	4	4



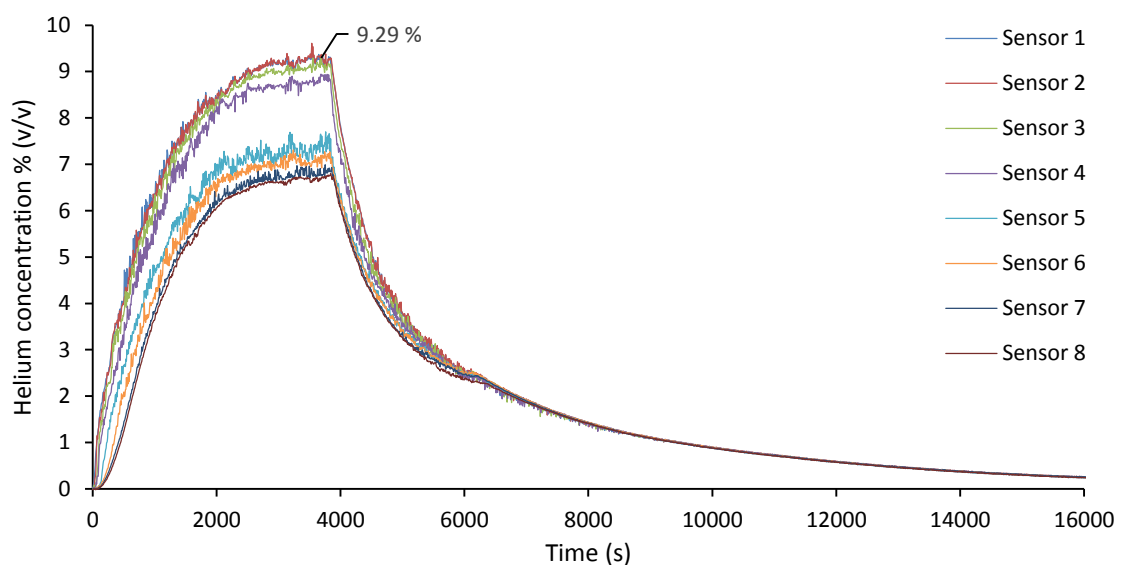
**Figure 4.40 Enclosure with flue and single side vent**



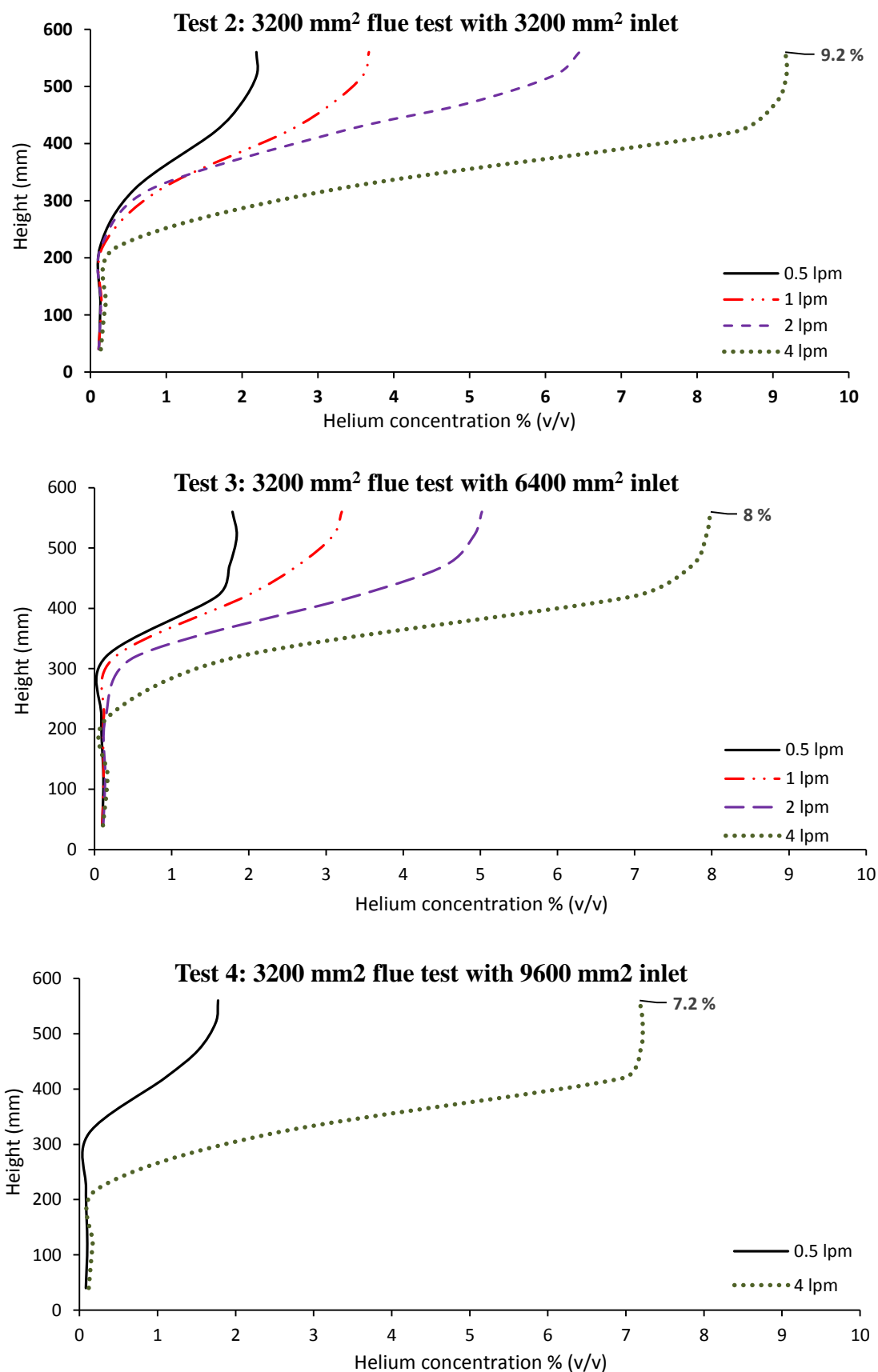
**Figure 4.41 Enclosure with T flue and single side vent**

#### 4.9.1 Analysis

Test 1 uses just the flue vent outlet and no inlet. This creates a mixing ventilation regime with two-way flow through the flue. A low leak rate of 0.5 lpm was used only for this test. Figure 4.42 shows that a peak concentration over 9 % was achieved in a layer at the top of the enclosure. Two distinct zones are present in the enclosure, an upper more concentrated layer around 9 % above 420 mm, and a zone below this at about 7 %. As the LFL was exceeded so quickly and at such a low leak rate, an opposing lower plain vent was added to the enclosure for subsequent tests. Three inlet sizes were tested.

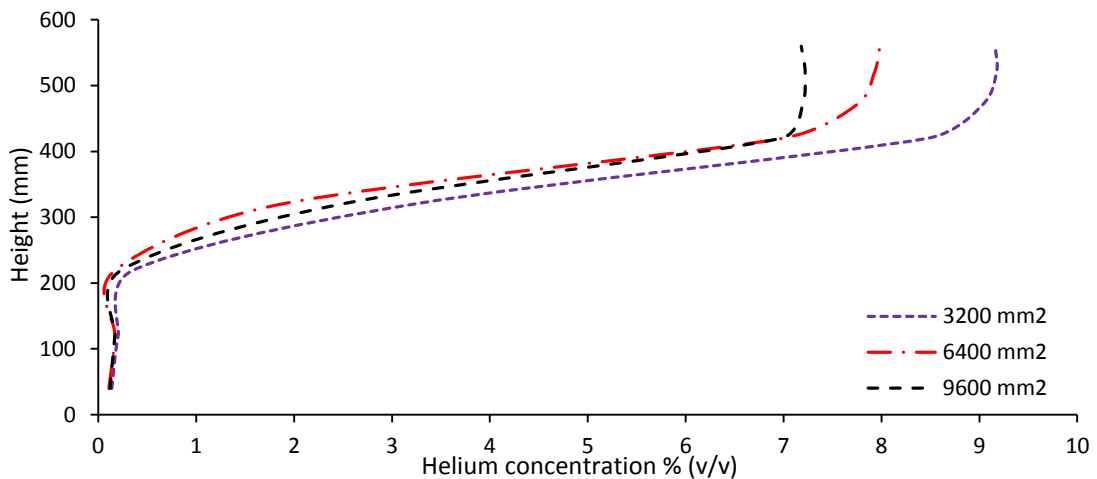


**Figure 4.42 Test 1 64 mm flue with no inlet at 0.5 lpm**

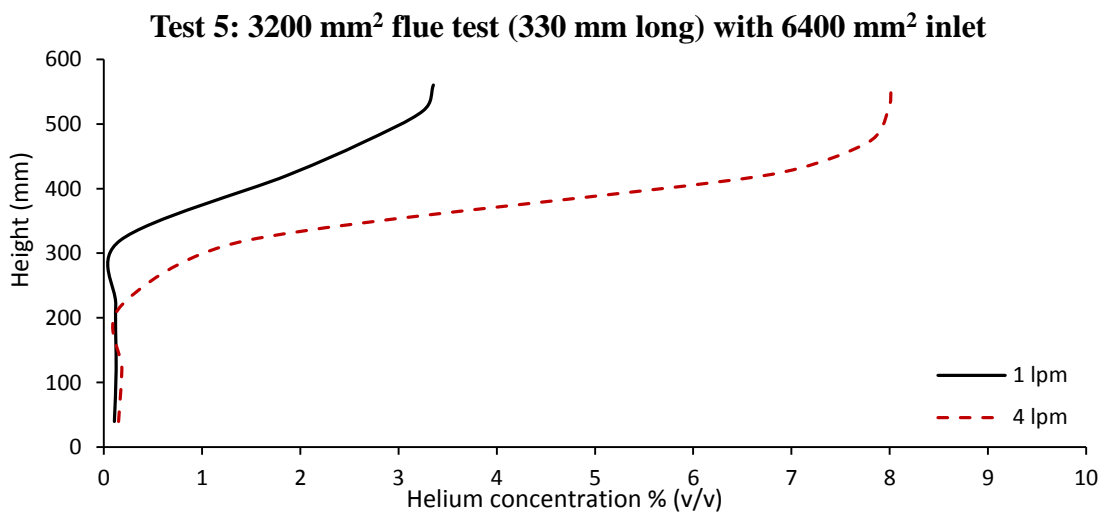


**Figure 4.43 Results of tests 2, 3 and 4: 110 mm flue with increasing inlet size**

Figure 4.43 presents the results for tests 2, 3 and 4 and figure 4.44 compares the results of the three tests at 4 lpm. Increasing the area of the plain vent opening has clearly led to an increase in the driving force for the passive ventilation mass flow through the enclosure as there has been a decrease in high level concentration as vent area increases. It is of interest that although there is a very slight reduction in the depth of the stratified layer, concentrations below 400 mm height are not significantly affected by the increased opening area.

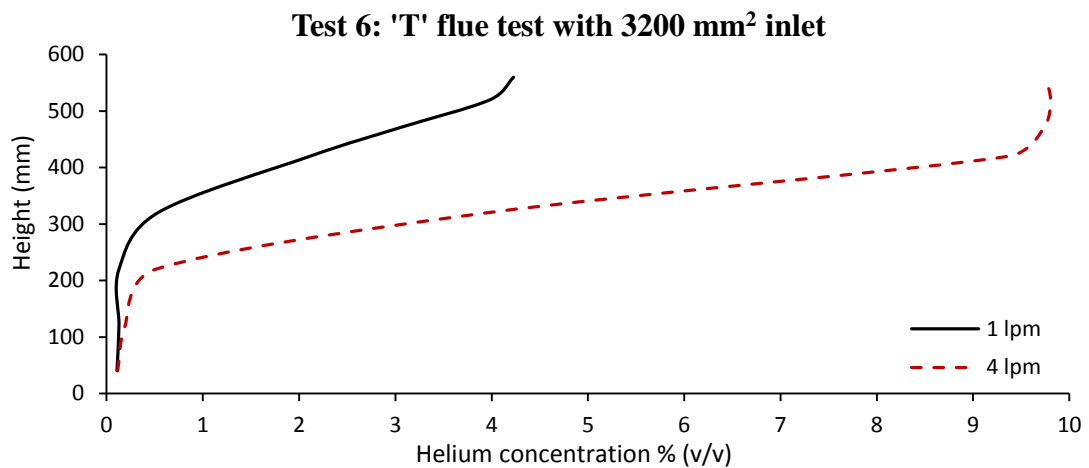


**Figure 4.44 Comparison of 4 lpm results for test 2, 3 and 4**



**Figure 4.45 Result of test 5: 330 mm long flue**

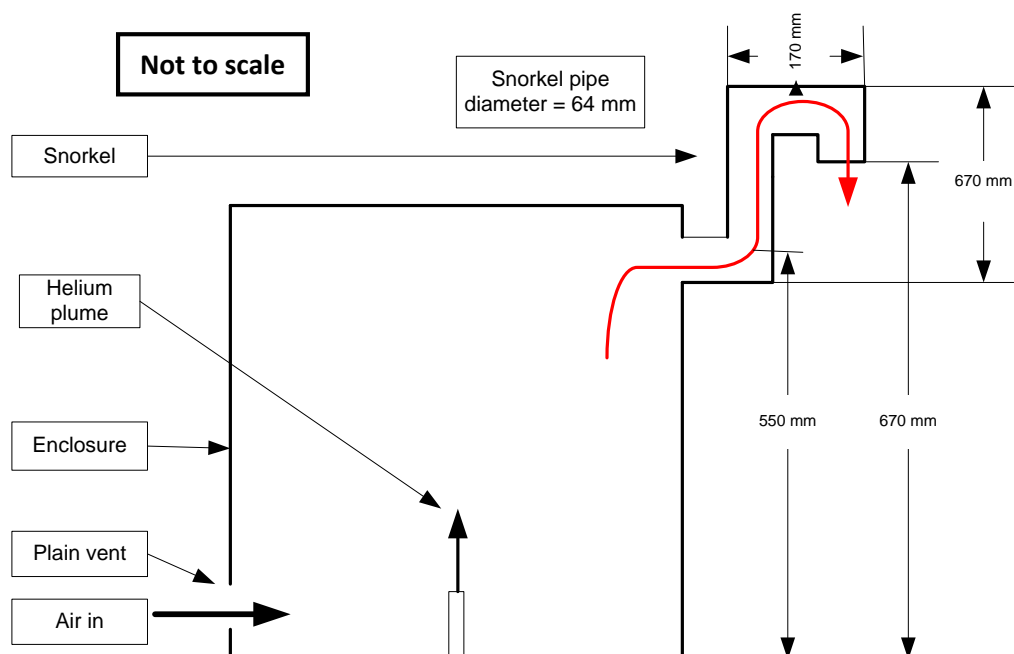
Figure 4.45 presents the results of the test where the flue was extended to 330 mm length. When compared to test 3, there has been no change in the test results. Extending the flue horizontally has no effect on the performance of the ventilation regime and it appears to function in the same way as with the short flue.



**Figure 4.46 Results of test 6: T flue test**

Figure 4.46 presents the results of the ‘T’ flue test. This test doubled the final outlet area to 64 mm<sup>2</sup>, to see whether the driving force was improved. When compared to test 2, it is found that the ‘T’ flue has led to an increase in concentrations in the enclosure. Rather than increase the driving force, the ‘T’ flue would appear to have increased the flow resistance. Its use in isolation would therefore not be beneficial. In environmental situations where a wind force may be present, passing through the ‘T’ section, enhanced flow may occur, but further testing would be needed to verify this.

#### 4.10 Snorkel ventilation [Inverted tubular side flue]



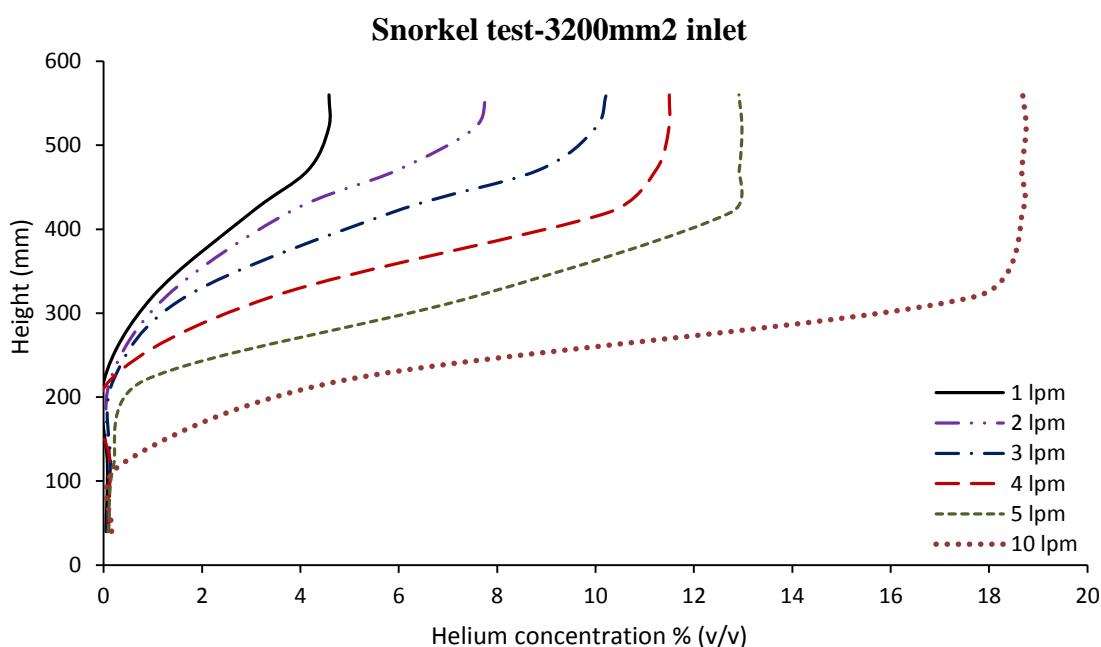
**Figure 4.47 Schematic of snorkel enclosure with low opposing side vent**

Figure 4.47 presents a schematic of the snorkel ventilation scheme. The snorkel raises the level of the outlet, but also inverts it to provide a measure of protection from outdoors weather conditions. The area of the plain vent inlet and the snorkel outlet were the same at  $3200 \text{ mm}^2$ . Helium leak rates from 1 to 10 lpm were tested.

#### 4.10.1 Analysis

Figure 4.48 presents the results of the snorkel test. The performance of this test will be compared with flue test 2, which used the  $3200 \text{ mm}^2$  plain vent at 4 lpm. In test 2 the peak helium concentration was 9.16 %. In the snorkel test the peak concentration at 4 lpm was 11.5 %. This is a significant increase in concentration and is also present with the other leak rates tested.

Adding complexity to the vent outlet appears to adversely affect the passive ventilation flow through the enclosure. The low driving forces present in the system are unable to cope with the shape of the snorkel. The stratified layer formed at the top of the enclosure begins at about the same height as found in test 2.



**Figure 4.48 Results of the snorkel test**



#### 4.11 Schlieren imaging: Helium release in the enclosure

A Schlieren system (see section 3.7) was set up in the laboratory (Figure 4.49) to obtain qualitative information about buoyant gas behaviour in the experimental enclosure. It was hoped to be able to view the helium emerging from the nozzle and see the type of plume/jet formed at the leak rates tested in this investigation (1 to 10 lpm). Due to the limitations of the available equipment, only a narrow field of view was possible, so a cross-section of the entire enclosure could not be achieved. It was therefore necessary to focus on specific areas

- Helium emerging from the nozzle
- The plume/jet rising (laminar/turbulent)
- Near ceiling (stratification/recirculation)
- Vent outlet

Previous tests have relied upon the sensors to provide a helium concentration for a fixed point in the enclosure and then inferring from this what is happening to the buoyant gas. This investigation is essentially about acquiring greater insight into how the helium is behaving in the enclosure by making it visible. This information will support the evidence from previous tests. It was not possible to recreate all of the enclosure ventilation regimes that have been tested, due to the limitations of the Schlieren equipment, available laboratory space and the time required.

The base case cross-flow scenario was chosen for testing as it is the simplest design and provides recirculation and stratification inside the enclosure for viewing. The sensors were not included in the rig for Schlieren testing as it was not feasible. The sensors require a USB connection to an adjacent PC, which the complex Schlieren set-up would not allow. The need to raise and lower the platform would add to this difficulty. The quality of the glass used in the rig plays a key role in image clarity. Although non-toughened glass was used on the rig, linear horizontal dark and light areas are visible on the Schlieren images, likely due to the glass manufacturing process. Also present was contamination from the lens surface as seen in Figure 4.50. As such the images have undergone a degree of processing using Photoshop CS (Adobe, 2008) to remove some of the flaws and improve the presentation of the helium flow. Appendix C contains thumbnail proofs of the original images for reference purposes.

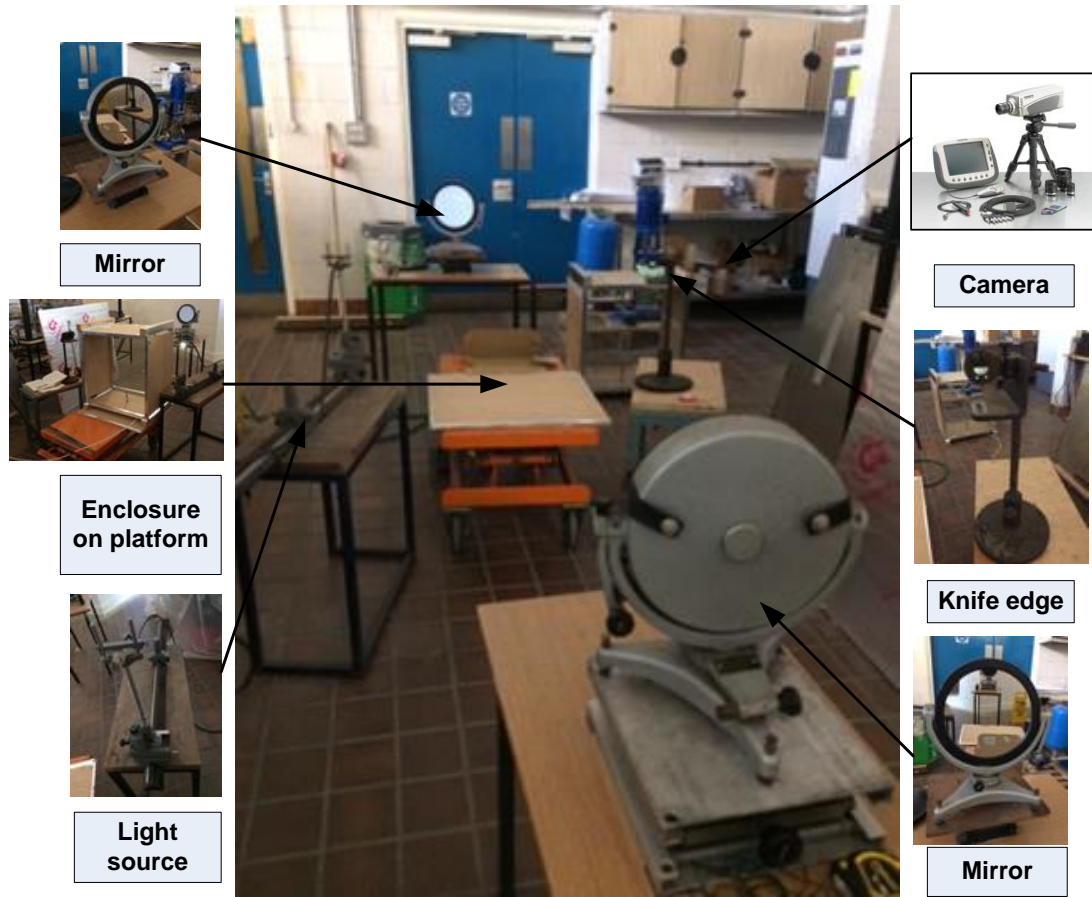


**Figure 4.49 Schlieren equipment laid out in the laboratory for the test**

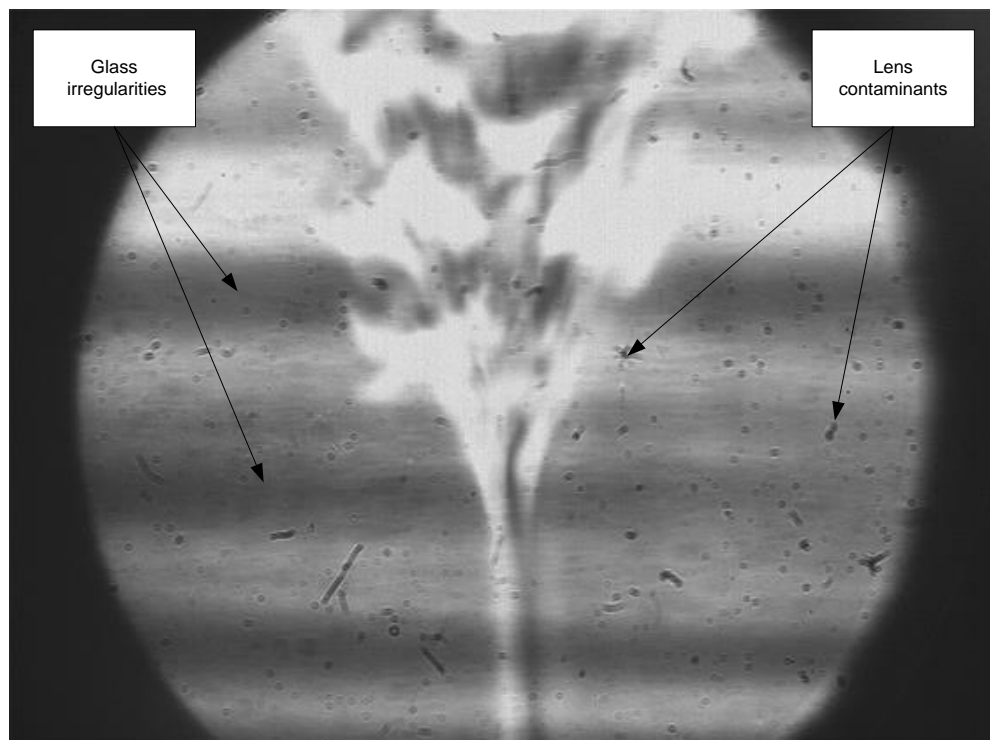


**Figure 4.50 Schlieren image lens contamination and glass irregularities.**

#### 4.11.1 Analysis

This analysis comprises a presentation of Schlieren images and an explanation of the buoyant gas behaviour observed. The first set of tests used the cross-flow enclosure scheme with plain vents and helium leaking from the central nozzle. Figure 4.51 presents a composite schlieren image of helium leaving the nozzle in the enclosure at 10 lpm. This equates to a Reynolds number of 483 ( $D=4\text{mm}$ ,  $v=13.3\text{ m/s}$ ,  $\rho=0.179\text{ kg/m}^3$ , dynamic viscosity =  $0.0000196\text{ Pa}\cdot\text{s}$ ) confirming laminar flow in the nozzle and on leaving, as the helium was observed to travel vertically upwards, for a period, in a narrow jet, similar to the width of the nozzle bore.

About 5 cm from the nozzle the jet begins to break up and become a turbulent plume. This is likely to be due to a reduction in the speed of the jet to air resistance. It is of interest to note from the observations of 10 tests that the point at which the break up occurs, becomes closer to the nozzle as the leak rate increases. The turbulent plume is seen to billow like a cloud of smoke from a fire. Figure 4.51 presents a much more turbulent condition in the enclosure than was assumed from the sensor data alone. The plume is well defined in the image, showing the helium rising in the central region. It was not possible to capture a clearly defined stratified layer through these tests. The sensor data, however, makes it clear that this does form at the top of the enclosure. The plume must rise to the enclosure roof and then circulate, either leaving through a top vent or mixing with air in the enclosure.

Figure 4.52 is a Schlieren image of helium leaving a plain vent at the top of the enclosure. A short plume is evident, rising from the vent opening, which quickly starts to disperse. There is a suggestion of moving gas at the top of the enclosure, which can just be seen, and possible stratification. Also tested was the pressed aluminium louvre vent. Four tests were run (1, 2, 3 and for louvres) to see how different the behaviour of gas leaving the louvre was, compared to the plain vent. Figure 4.53 presents a Schlieren image of helium leaving the enclosure through four louvre vents. The louvres have directed the helium plume downwards at an angle of about 45 degrees. The longest plume emerges from the top louvre and they get progressively smaller as they go down. This is markedly different behaviour than that found with the plain vent and provides valuable information about how louvre vents affect flow.

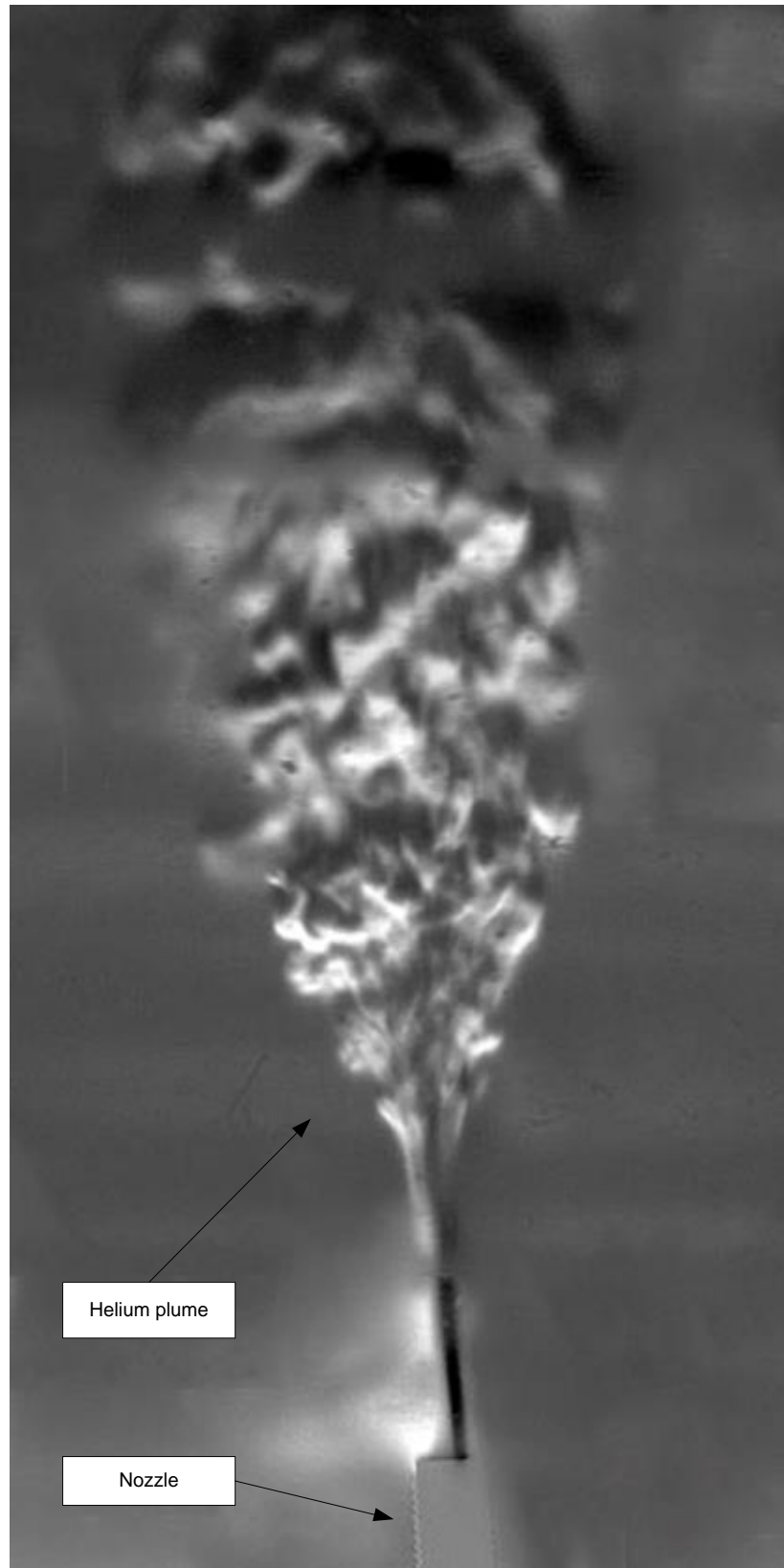


**Figure 4.51 Composite Schlieren helium plume in the enclosure at 10 lpm**

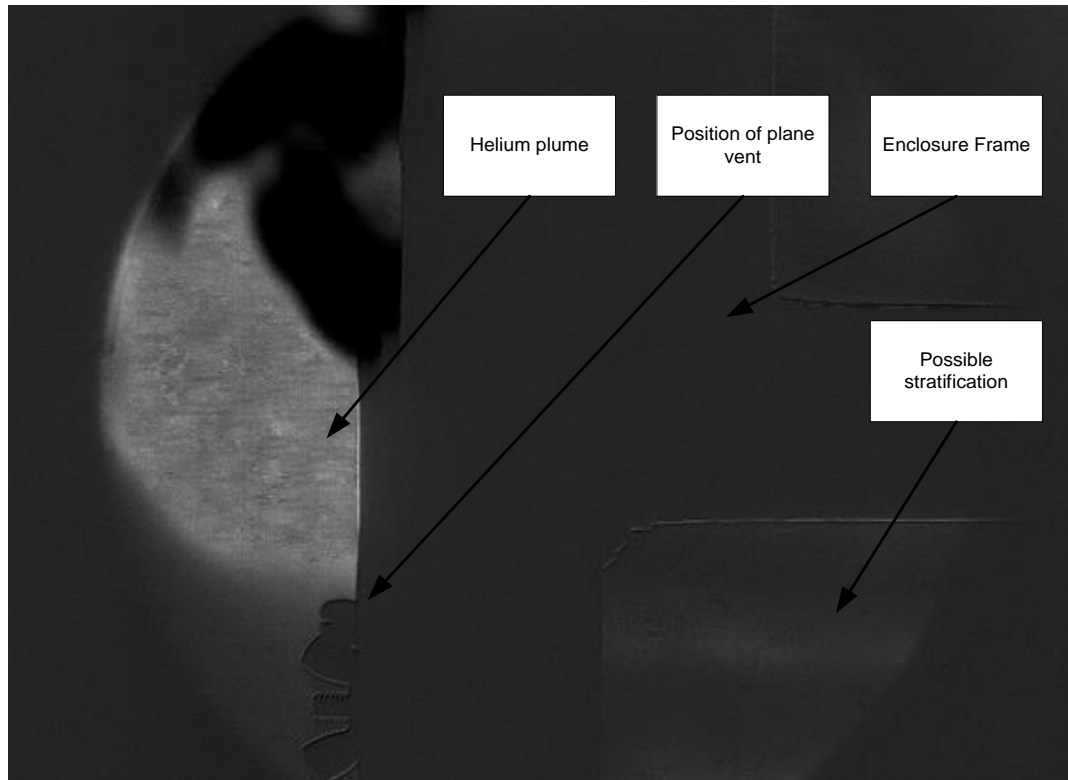


**Figure 4.52 Schlieren image of helium emerging from plain vent at 10lpm**

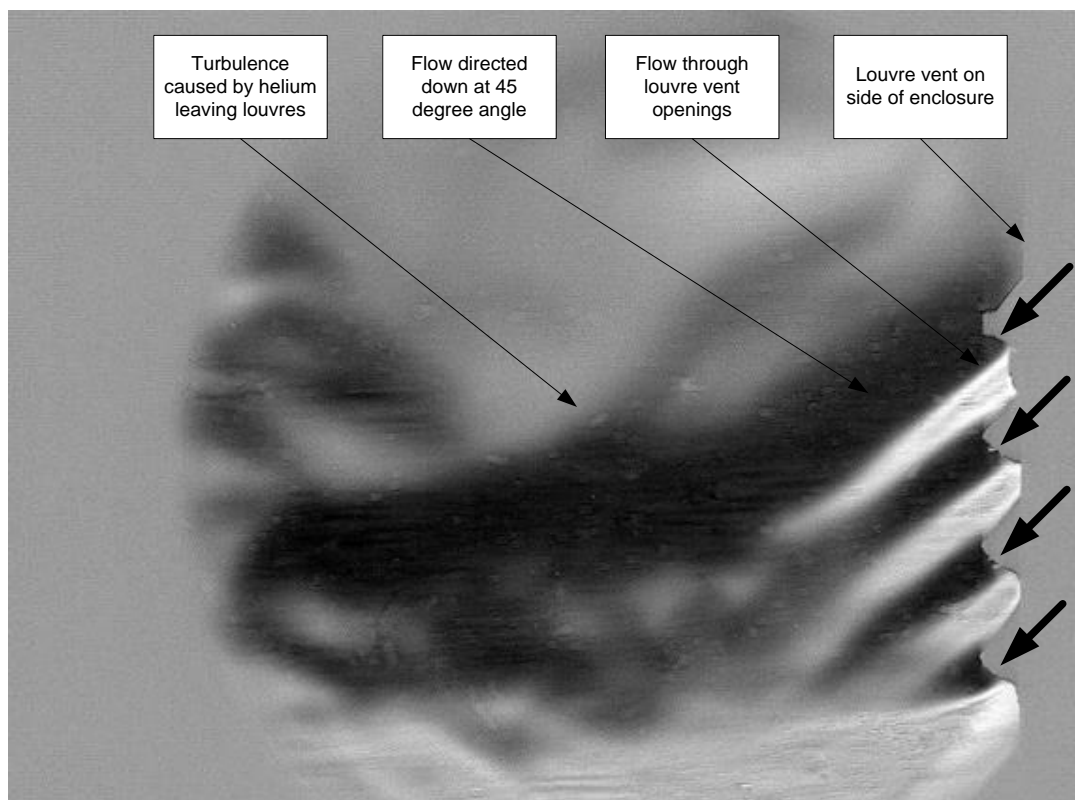


**Figure 4.53 Schlieren image of helium emerging from four louvre vents**

## 4.12 Conclusion

The series of tests conducted have determined helium concentration parameters for low leak rates up to 10 lpm. They have shown that ventilation adaption can impact on the flow regime in the enclosure and consequently the helium concentration in the upper stratified area in displacement ventilation scenarios. Some regimes lead to increased concentration lower down in the enclosure due to mixing ventilation, but generally a stratified regime develops with higher concentration found in the top of the enclosure. This is useful information for enclosure design to ensure inclusion of complementary systems.

The louvre tests were interesting because clearly louvre design and not just the presence of louvres on the vent affects enclosure air flow. The simple cardboard vents would have appeared to have restricted flow to a greater extent than the curved, downward facing aluminium vents. The position and width of the vents may also have had an impact. Regardless though, the presence of louvres does increase flow resistance and must be accounted for in enclosure design.

The Schlieren imaging has provided an amazing qualitative insight into this project. Sensor data has provided information on concentration gradients and the degree of stratification evident in the enclosure. It did not though provide information about what the plume looked like and how it develops or what may be happening at vents. Although there were limitations around what could be achieved the ability to observe an invisible gas has added a further dimension to this work.

What has been shown in these enclosure scenarios, is that the LFL can very quickly be exceeded, even at the lowest leak rate tested. The speed with which this can happen and also the high concentrations present give cause for concern. To optimise the flow through the enclosure a combination of ventilation techniques can be applied. This will carry an additional commercial cost, however thoughtful design in the application may well offset this, for example using a hollow lighting mast as a chimney vent. The design safety case will always be paramount, so the performance limits achieved in these tests should be noted when designing an enclosure.

## Chapter 5 Results and Analysis: CFD simulations

### 5.0 Introduction

This chapter presents the results and analysis of the SolidWorks Flow Simulation CFD investigation into passive ventilation schemes applied to the initial test rig and the BOC Ltd. specification fuel cell enclosure. Limitations on space mean not all simulation results are presented. The vent scenarios tested were;

- A. Initial test rig (Four sensor positions): SolidWorks Flow Simulation CFD
- B. Final test rig (Eight sensor positions): SolidWorks Flow Simulation CFD;
  - i. Simple plain vents – cross-flow setup
  - ii. Simple louvre tests – horizontal louvre extensions
  - iii. Plain vents equivalent to louvre opening areas
  - iv. Aluminium louvre tests
  - v. Chimney-Stack tests – roof mounted chimney
  - vi. Flue test – side mounted
  - vii. Snorkel tests – side mounted
  - viii. Internal obstruction test
  - ix. ANSYS: Fluent comparison exercise

Each SolidWorks CFD simulation was run to steady state conditions. SolidWorks Flow Simulation treats all analysis as transient. For a steady state analysis, no time dependency is set. This allows the solver to run the transient analysis and look for convergence in the flow field which means a steady state has been achieved (Dassault Systemes (2015 (c))). Once complete, helium sensor position point source data, (stacked or frame) was extracted from the results and plotted. ANSYS: Fluent CFD was used in a comparison exercise. Comparison was further made with the empirical and adjusted empirical results, which used the findings of the sensor calibration described in section 3.3.3.

**Mesh sensitivity study:** A mesh sensitivity study was undertaken for the SolidWorks Flow Simulation CFD investigations to achieve mesh independence, as explained in the methodology (Section 3.9.3). This was to assess the level of mesh refinement (number of cells in the mesh) necessary before consistent calculation results were achieved i.e. little change in results with further refinement.

The approach taken was based upon that used by Visser et al (2016) where [at least] three mesh levels (course, standard and fine) were tested. A mesh sensitivity study was completed for every enclosure ventilation configuration tested with fine meshes chosen in all instances. At the selected mesh level, the computational expense was low, with most calculations taking about an hour to complete. Where meshes that are more complex were tested, the complexity was often beyond the computational capability of the available computer.

Section 3.9.5 describes how ‘local meshes’ were used to refine the region of the plume and the stratified layer in the enclosure. This approach was used to add refinement to the standard and louvre vents as well as the chimneys, flues and snorkel. The region of buoyant gas flow adjacent to the vents was also refined in this way to resolve flow through the openings. ‘Solution adaptive meshing’ was selected to allow mesh refinement to change during the simulation. Table 5.1 provides additional detail concerning the SolidWorks Flow Simulation approach.

**Table 5.1 SolidWorks Flow Simulation studies CFD approach**

CFD Criteria	Detail
Computational Domain	1000 mm x 1000 mm x 2000 mm with the enclosure centrally positioned
Boundary Conditions	Helium volume flow rate set at nozzle face [1 to 10 lpm] Environmental parameters set for domain [STP] Initial Pressure 101325 Pa Initial Temperature 293.2 K
Turbulence model	Turbulent/Laminar (k-ε)
Mesh design optimisation	Rectangular parallelepiped [cells] Local initial mesh for plume, stratified region, vents, chimney, flues and snorkel Solution adaptive meshing selected
Discretisation scheme	Finite volume [control volumes]
Solution methods	SIMPLE (Dassault Systemes 2014)
Convergence criteria	Steady state [concentration]
Post processing	SW Flow Simulation analysis tools



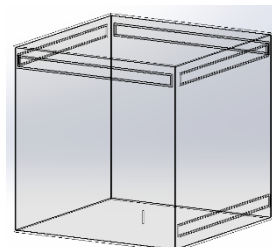
## 5.1 Initial test rig (four sensor positions)

Five simulations were run using SolidWorks Flow Simulation as shown in table 5.2.

Figure 5.1 presents the SolidWorks CAD model of the initial test rig.

**Table 5.2 Initial test rig configurations**

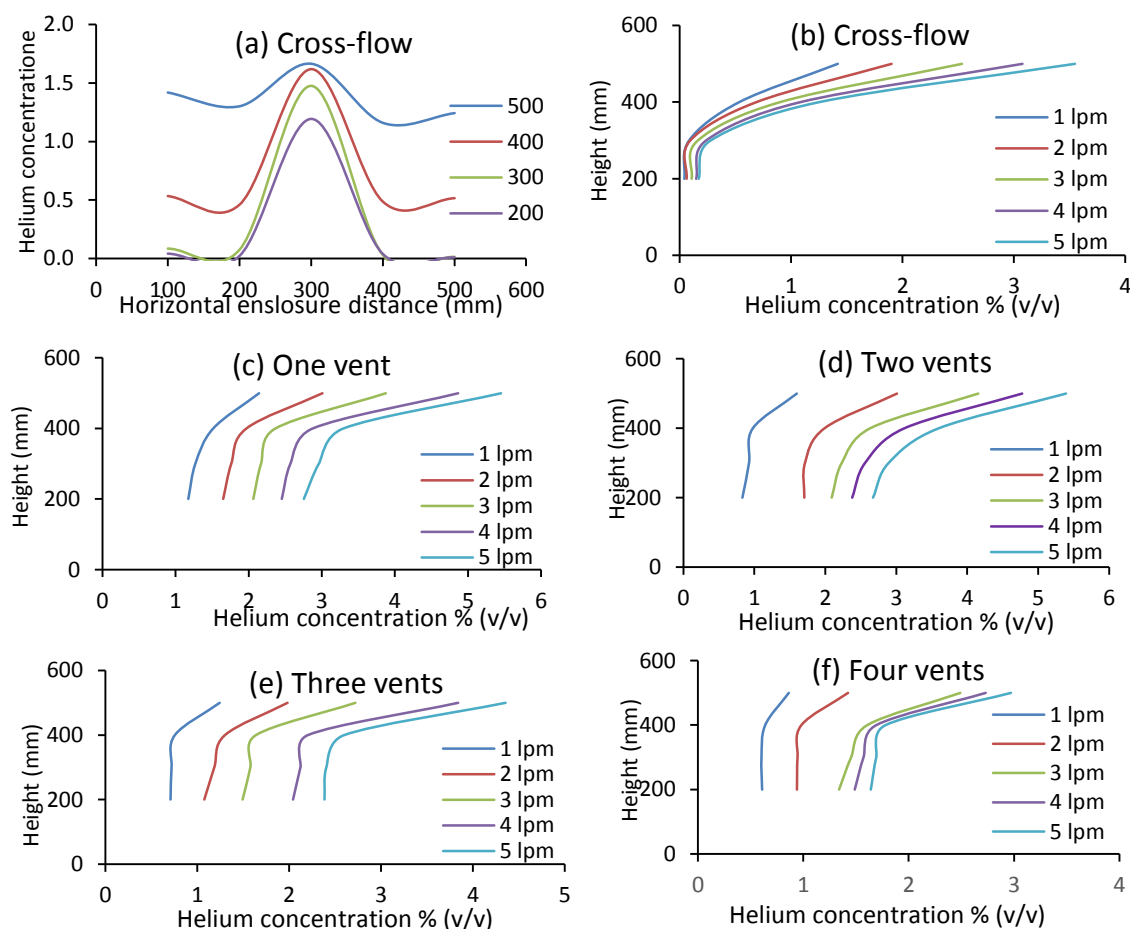
1	Two vent cross flow (one upper and one lower)
2	One top vent (no lower vent)
3	Two top vents (no lower vent)
4	Three top vents (no lower vent)
5	Four top vents (no lower vent)



**Figure 5.1 SolidWorks CAD model**

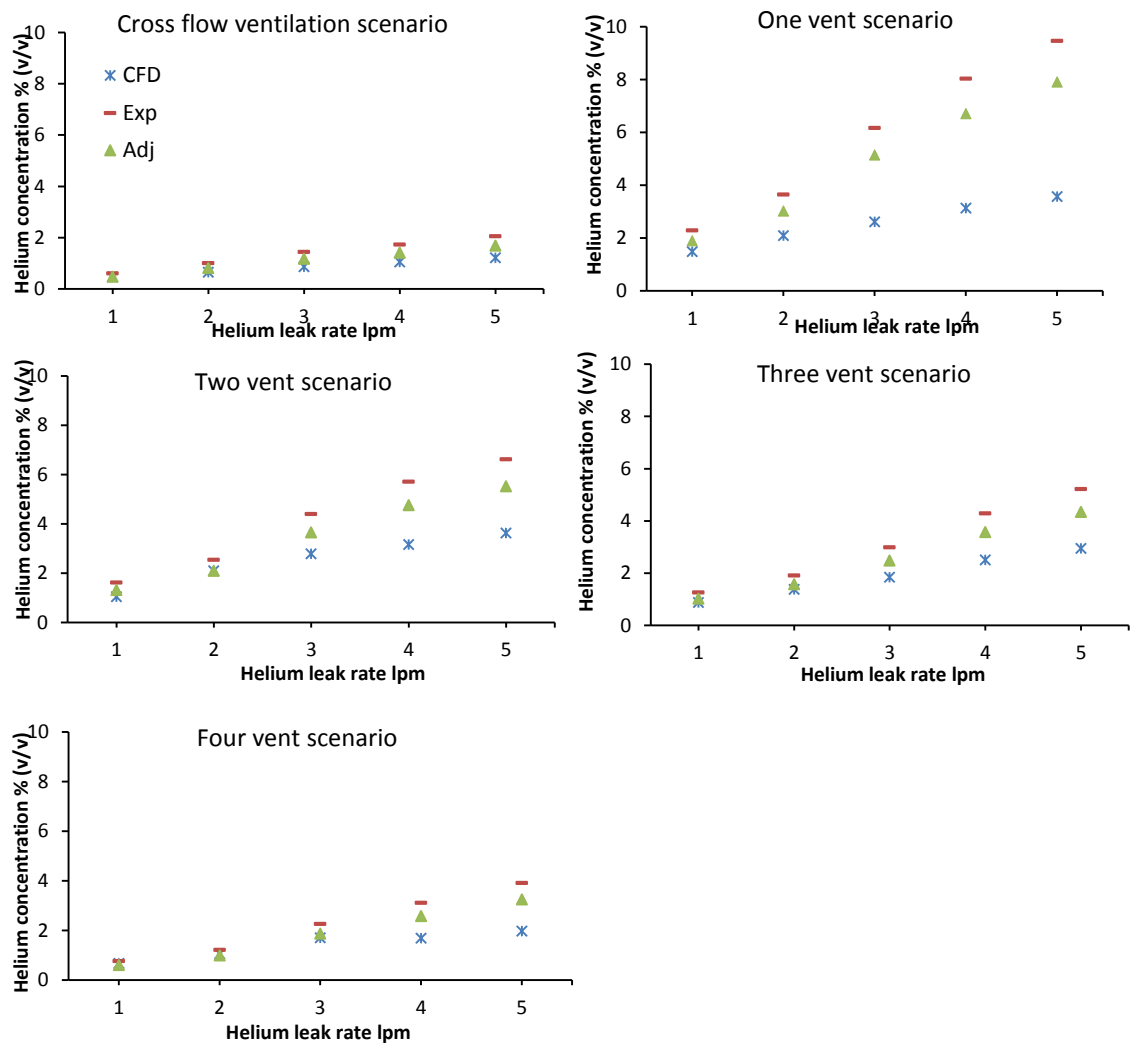
In the corresponding empirical test four sensors were suspended from the enclosure roof in a column (at heights of 0.2 m, 0.3 m, 0.4 m and 0.5 m above the enclosure floor).

Readings were taken at five positions across the centre of the enclosure (100 mm, 200 mm, 300 mm, 400 mm, 500 mm). Once the simulations had completed, point source concentration values were obtained for the twenty sensor positions described above.



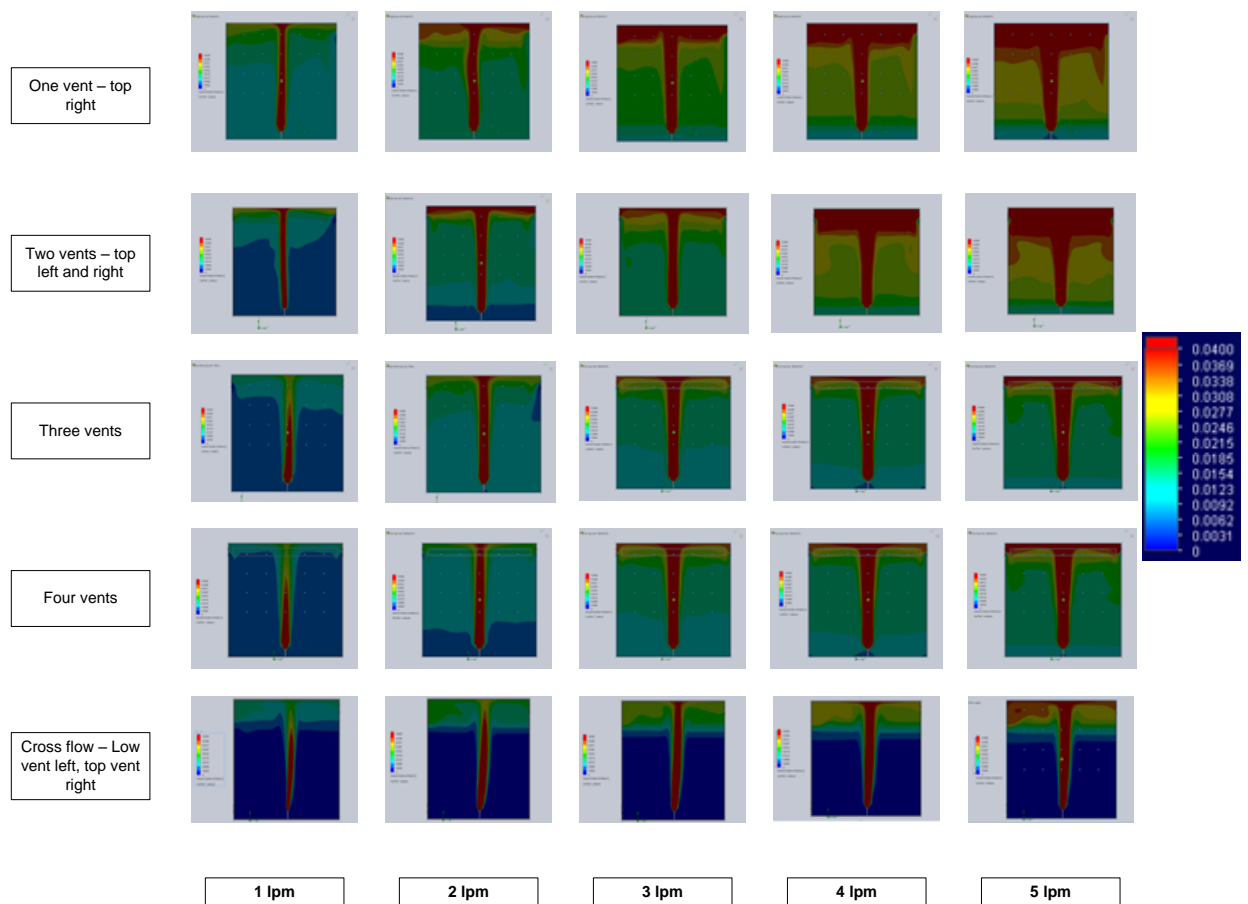
**Figure 5.2 SolidWorks Flow Simulation CFD data for the five scenarios tested**

Figure 5.2 presents the SolidWorks Flow Simulation CFD output for the five tests. Graph (a) shows helium concentration at the four sensor heights across the enclosure, for the cross-flow scenario. This example shows the effect of the helium plume, with higher concentrations at 300 mm than on either side. This position is in the path of the helium plume and the sensors report high concentrations. Graphs (b) to (f) present data for the top vent tests at the 100 mm vertical sensor position. As the number of vents increase the overall concentration at each leak rate decreases. A stratified layer is evident in all cases, with lower concentrations present below about 400 mm. The cross-flow scenario appears the most controlled with lower concentration below 400 mm and a smoother concentration gradient above this level. The graphs show the limitations of only four sensors in the stack, but are still informative on concentration variation.



**Figure 5.3 Average helium concentration (all sensor positions) vs leak rate (CFD and experimental data comparison)**

Figure 5.3 presents a comparison between the CFD prediction data and the data from the experimental tests for the initial test rig study. The graphs include the initial experimental sensor data and the processed data that accounts for the sensor error calculated in section 3.3.3. Correcting the sensor data has reduced the experimental concentration values (shown as Adj. for adjusted) bringing them closer to the CFD predictions. Many of the CFD values are less than the experimental sensor values, however in the cross-flow scenario and four-vent scenario the values are close, particularly at the lower leak rates. The single top vent scenario is the poorest performing of all the studies where even with the error adjustment the values diverge significantly with increasing leak rate. For all of the scenarios there is some divergence between the CFD and experimental values as the leak rate increases with the greatest difference found in the single vent study at 5 lpm. Aside from the divergence at higher leak rates there appears to be some conformity in the CFD results, but no full correlation with the experimental data.



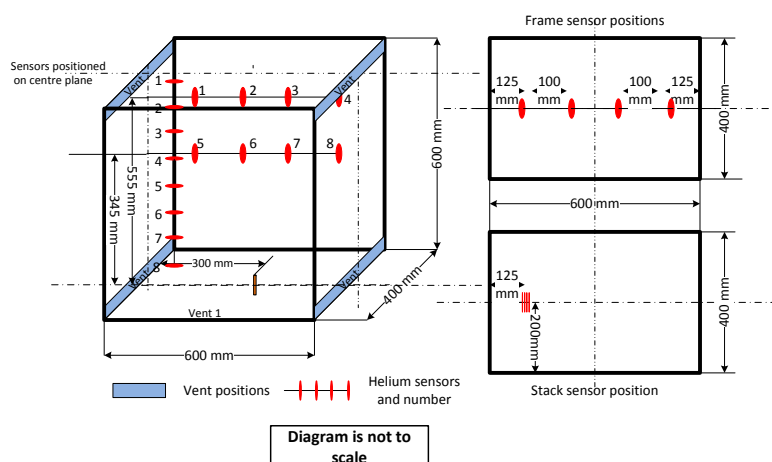
**Figure 5.4 SolidWorks cut plane images of steady state helium concentrations (0-4% v/v range) for each scenario at 1 to 5 lpm leak rates**

Figure 5.4 presents cut-plane images for all of the scenarios at all of the tested leak rates. The helium concentration range has been set to 0 – 4 %, with the red zones indicating a concentration of equal to or greater than 4 %. This qualitative information provides a strong visual insight into the behaviour of a buoyant gas in a small enclosure. The helium plume from the nozzle is evident and an increase in helium concentration in parts of the enclosure is clear as the leak rate increases. There is also strong visual evidence of stratification, particularly with the cross-flow scenario with displacement ventilation.

In the other four scenarios mixing ventilation should dominate and this is also evident with increased helium concentrations throughout the enclosure. Some stratification is evident also in the mixing scenarios, but this too makes sense as the plume is directed upwards, with the gas collecting near the roof, before leaving through a vent or mixing with incoming air and recirculation in the enclosure. Of note also is that the shape of the plume is at variance with that observed in the Schlieren test, where a narrow jet was present which fans out into a plume as it loses velocity, although CFD leak rates are lower.

## 5.2 Final test rig (eight sensors) simple plain vents (BOC Ltd enclosure)

This investigation uses the dimensions of the final test rig based upon the BOC Ltd., environmental enclosure (600 mm x 600 mm x 400 mm, with opposing upper and lower ventilation openings across the width of the enclosure and 20 mm high). A simplified CAD model was created in SolidWorks based upon the BOC Ltd. enclosure dimensions. In the empirical tests, the enclosure sat inside a 1 m x 1 m 2 m outer enclosure. These dimensions were chosen for the computational domain and an external simulation was selected so that flow through the enclosure could be observed.



**Figure 5.5 Helium sensor positions (stacked and frame sensors)**

Figure 5.5 is a schematic of the test rig showing the sensor positions that were used as data points when the simulations were complete. Two sets of data points were used, stacked sensors and frame sensors. This arrangement is used in the simple louvre tests also, but subsequent CFD investigations only use the stacked sensor arrangement to investigate the degree of stratification present.

### 5.2.1 Plain Vents-Frame sensors

Figure 5.6 (a) presents the frame sensor CFD concentration data. The overall trends in terms of increasing concentration with increased leak rate are similar to those found with the empirical test in section 4.3.1 (figure 4.11). The simulations have reproduced the flow behaviour but have not replicated the helium concentrations produced in the experimental tests. Notable differences are that CFD helium concentrations are higher than the empirical results, for the top frame sensor positions at low leak rates, and the CFD top sensor concentrations at higher leak rates are lower than with the empirical data. Figure 5.6 (b) presents the point source data for the top row. The concentration steadily increases with leak rate, with the outer sensors recording slightly higher values than the two in board sensor points. This correlates with the helium being drawn towards the top vents, a behaviour also seen with the empirical data.

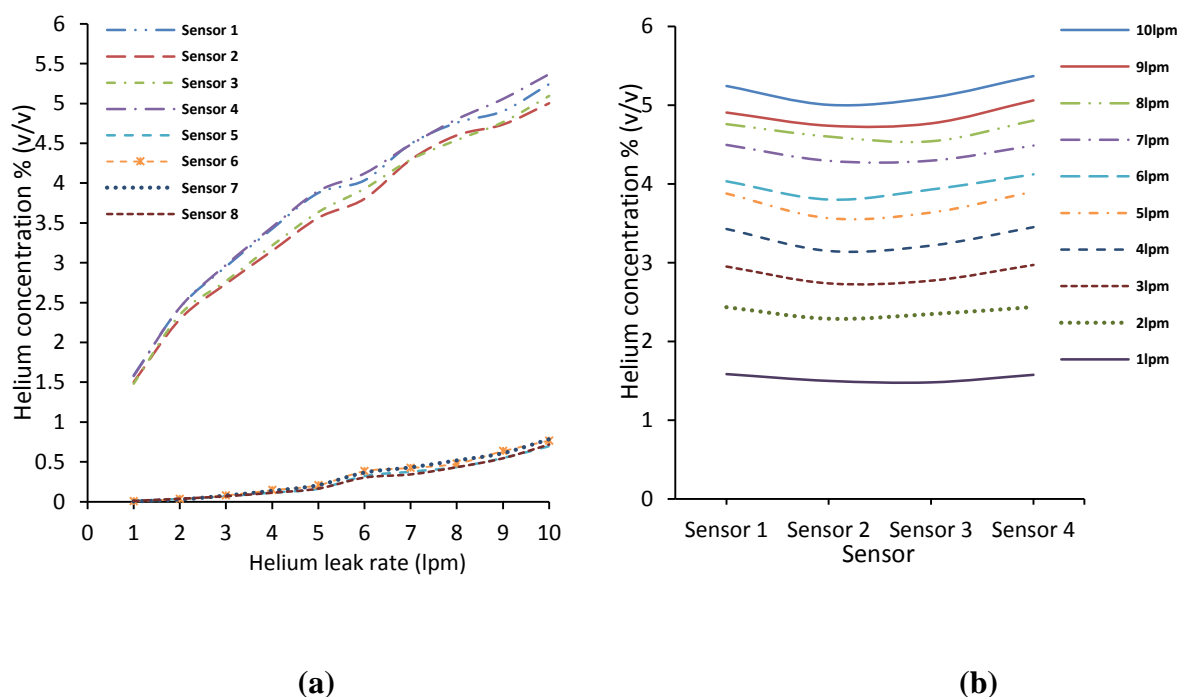


**Figure 5.6 Frame sensor helium concentrations (a) all sensors (b) at the 555 mm level**

### 5.2.2 Plain Vents-Stacked sensors

Figure 5.7 presents the plain vent enclosure CFD results with stacked sensors. The trends produced by the experimental data of increasing concentration with height are reflected in the CFD data. The LFL is not exceeded until 6lpm, which is the same as for the adjusted empirical data. The maximum concentration achieved is 5.29 % at 10 lpm compared to 5.59 % for the adjusted empirical data and the depth of the stratified layer is deeper across the leak rate range than with the empirical data. The 1 and 2 lpm data series also both exceed the 1 % (25 % of LFL) mark, whereas the empirical data did not.

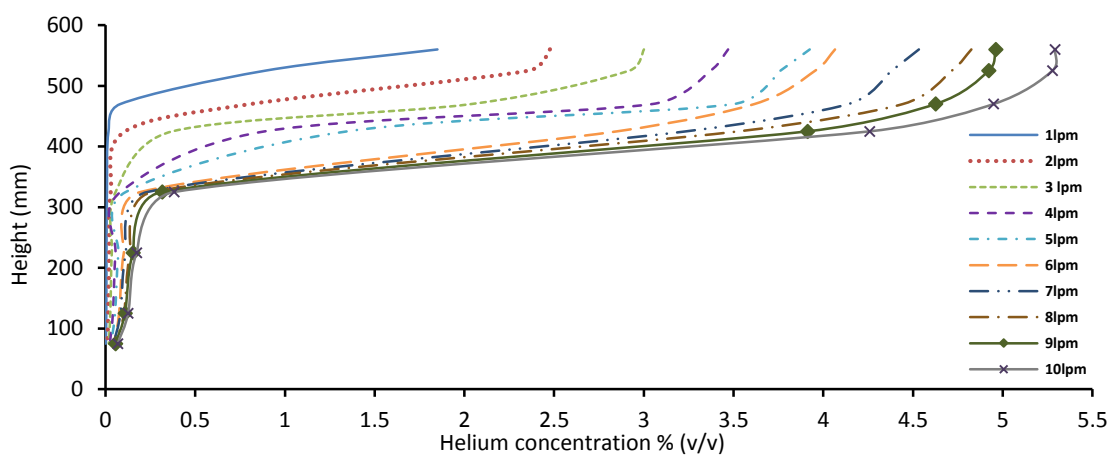


**Figure 5.7 Stacked sensor helium concentrations against height**

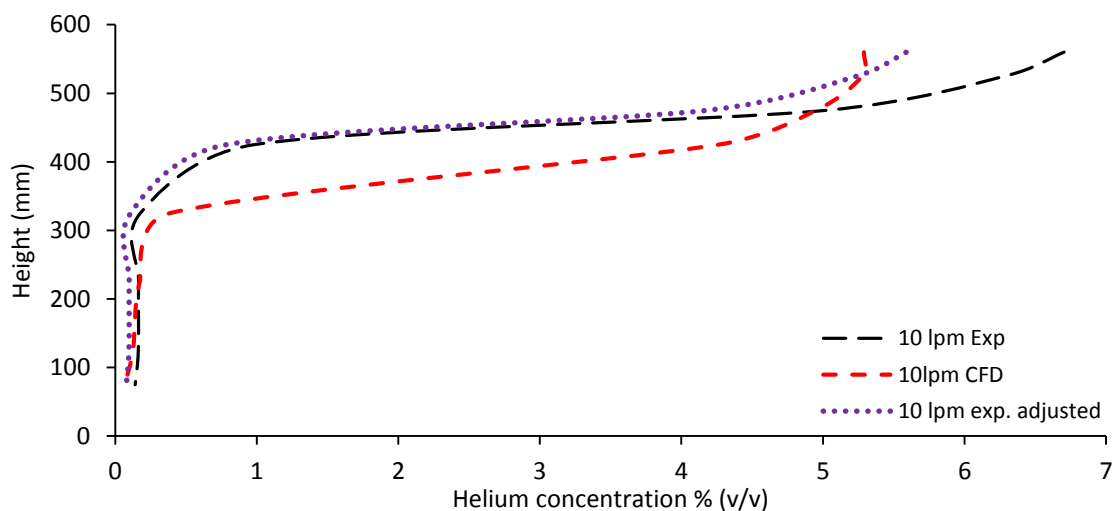


**Figure 5.8 Comparison of experimental, adjusted experimental and CFD at 10 lpm**

Figure 5.8 compares the original experimental result at 10 lpm with the adjusted experimental data and the CFD prediction. The adjusted data brings down the peak

concentration closer to that of the CFD prediction but reduces the thickness of the stratified layer slightly moving it away from the CFD line. The prediction of peak helium concentration is acceptable, and the determination of a stratified layer is correct, but the depth of the stratified area is slightly thicker

Figure 5.9 presents a cut-plane of the initial mesh and figure 5.10 a CFD image at the 200 mm mid-point. It shows the plume immersing from the nozzle and a stratified layer near the enclosure roof. Also visible are plumes of helium leaving the upper vents. This image provides an insight to the distribution of helium in the enclosure but does not provide information on the turbulent nature of the plume in the way that the Schlieren image does.

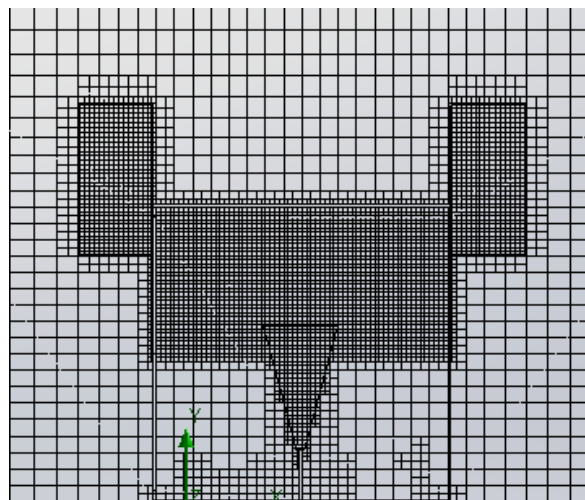


**Figure 5.9 Simple plain vent CFD cut plane of initial mesh with 318589 cells**

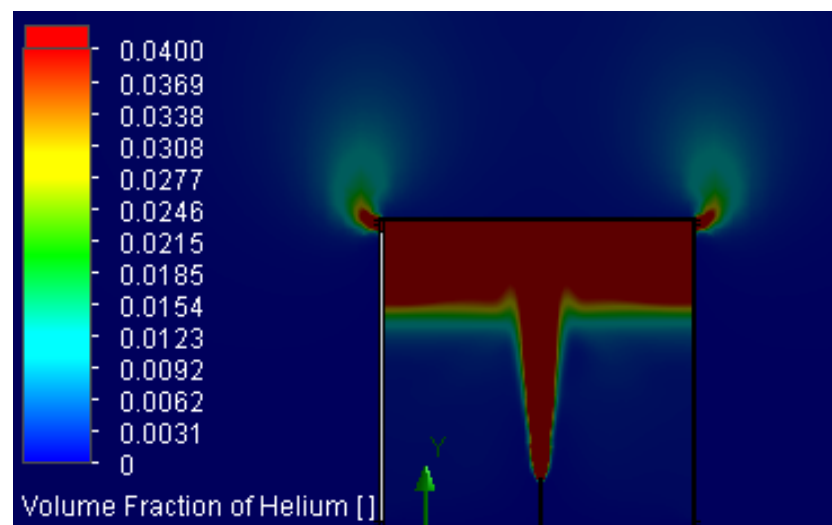
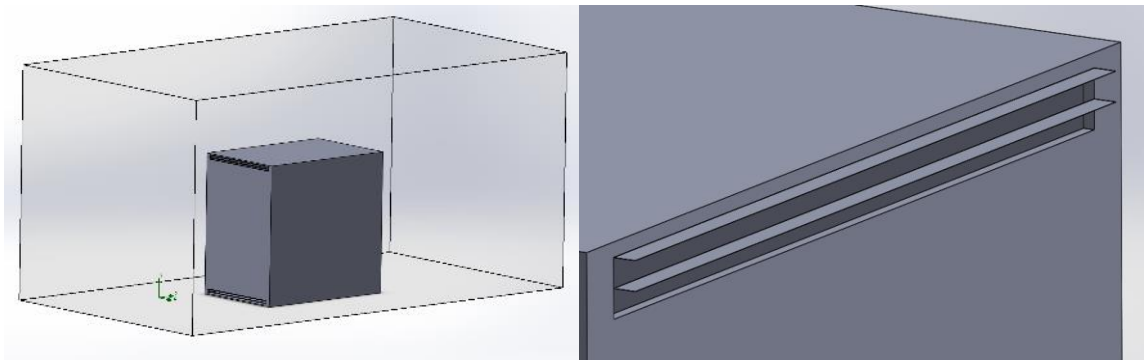


**Figure 5.10 Cut plane CFD image through the plume and vents at 10 lpm**

### 5.3 Simple louvre tests – horizontal louvre extensions

This CFD exercise uses the CAD design from section 5.2 but adds horizontal louvre extensions to the vent inlets and outlets as described in Figure 4.14. Frame and stacked sensor positions are used to collect data from the simulation output. Leak rates from 1 to 10 lpm are used. Figure 5.11 (a) shows the louvre vented enclosure within the



computational domain and 5.11 (b) shows a close up of the horizontal louvres. The empirical tests showed that adding the paper louvre extensions to the vent openings impeded flow through the vent leading to an increase in enclosure helium concentration. A similar effect should be evident with the CFD prediction data.

(a)

(b)

**Figure 5.11 SolidWorks (a) Enclosure and computational domain (b) louvres**

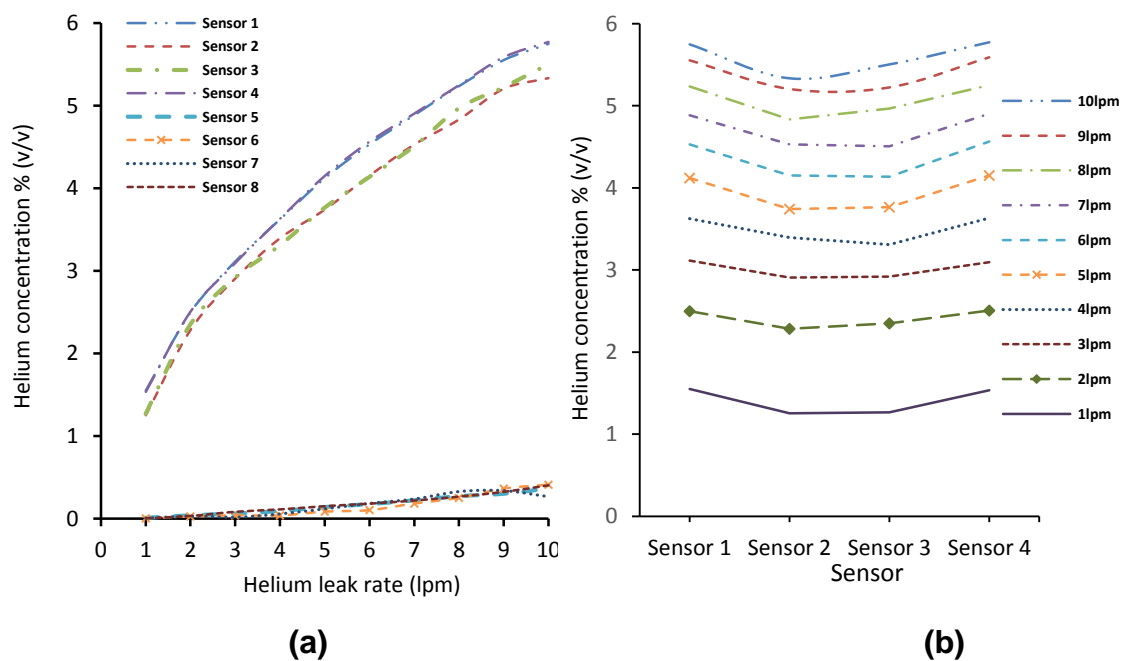
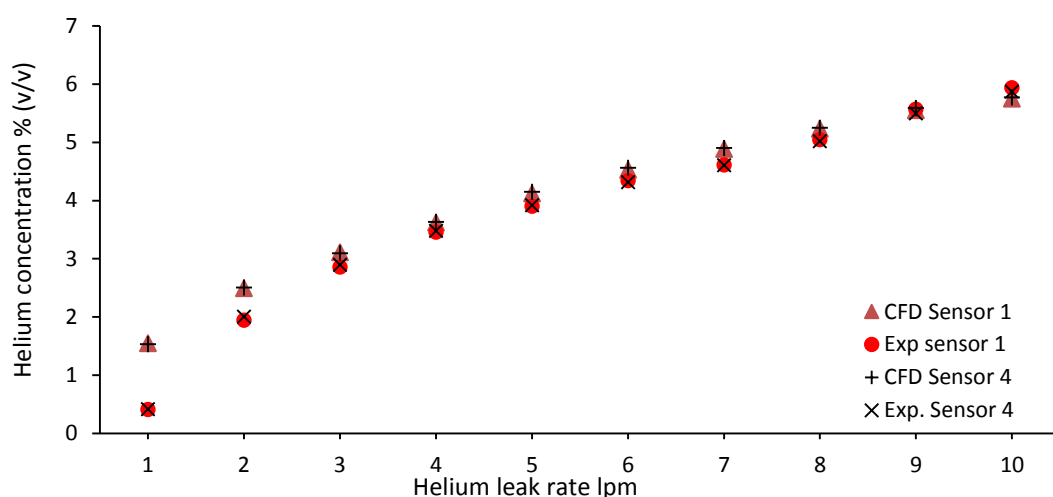


**Figure 5.12 Frame sensor helium concentrations (a) all sensors (b) at 555 mm**



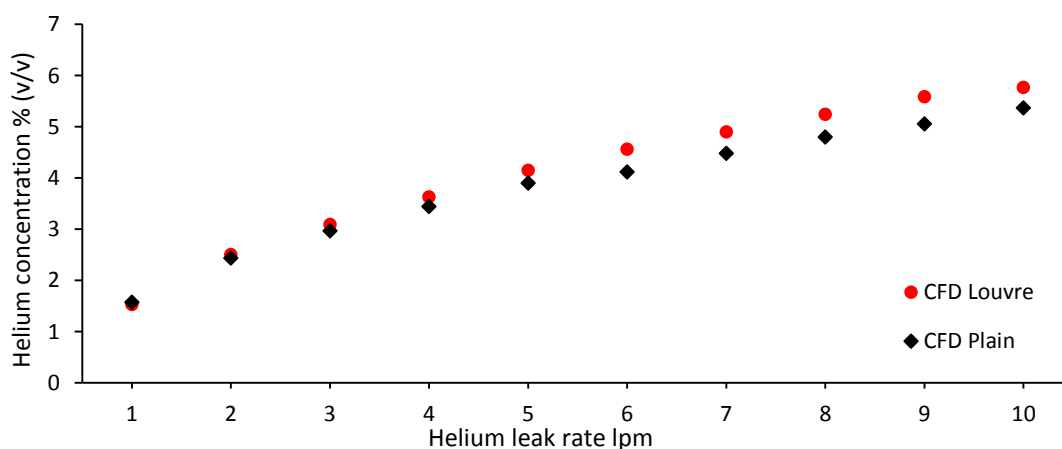
### 5.3.1 Louvre Vents-Frame sensors

Figure 5.12 (a) presents frame sensor CFD data for concentration against leak rate. The trends presented are similar to those found with the experimental data, with flow behaviour replicated, but broadly lower concentrations. The LFL is not exceeded by the top sensor positions until the 5 lpm point, which is a similar position with the adjusted experimental data. Figure 5.13 presents a comparison of the adjusted experimental and CFD data at sensor points one and four. The graphs correspond well at both points.



**Figure 5.13 A comparison of CFD and adjusted data at frame sensor points 1 and 4**

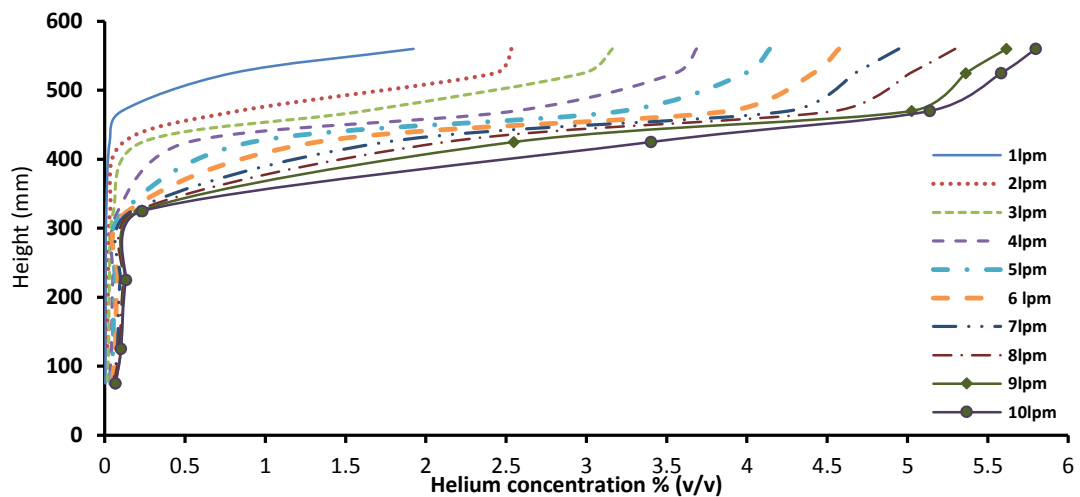
Figure 5.14 presents a comparison of the CFD sensor 4 data for plain and louvre vents. It can be seen that concentrations are higher with the louvre vent data, becoming more significant as the leak rate increases. This supports the findings from the empirical data and suggests that the SolidWorks CAD modelling of the louvres has been effective.



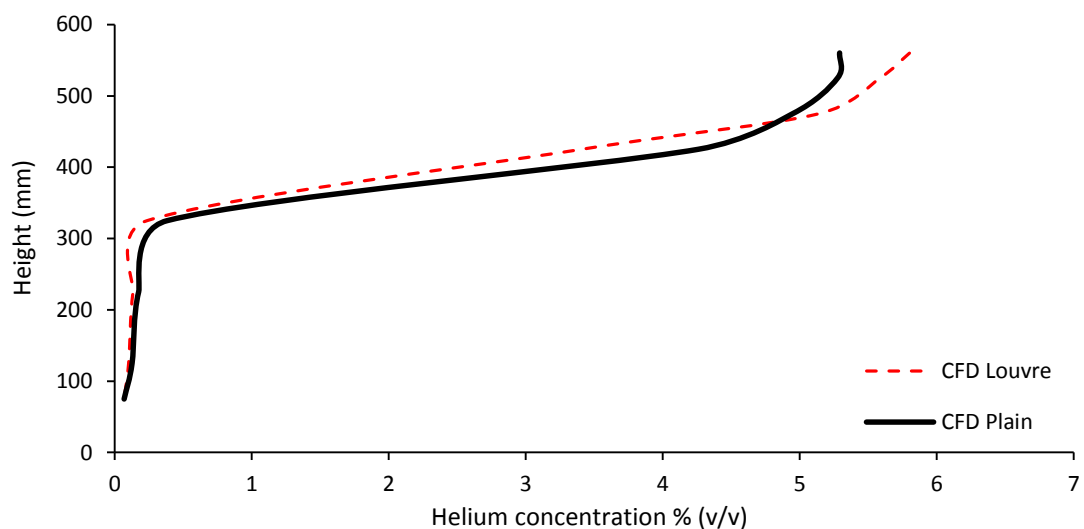
**Figure 5.14 A comparison of CFD plain and louvre vent data at sensor 4**

### 5.3.2 Louvre vents-stacked sensors

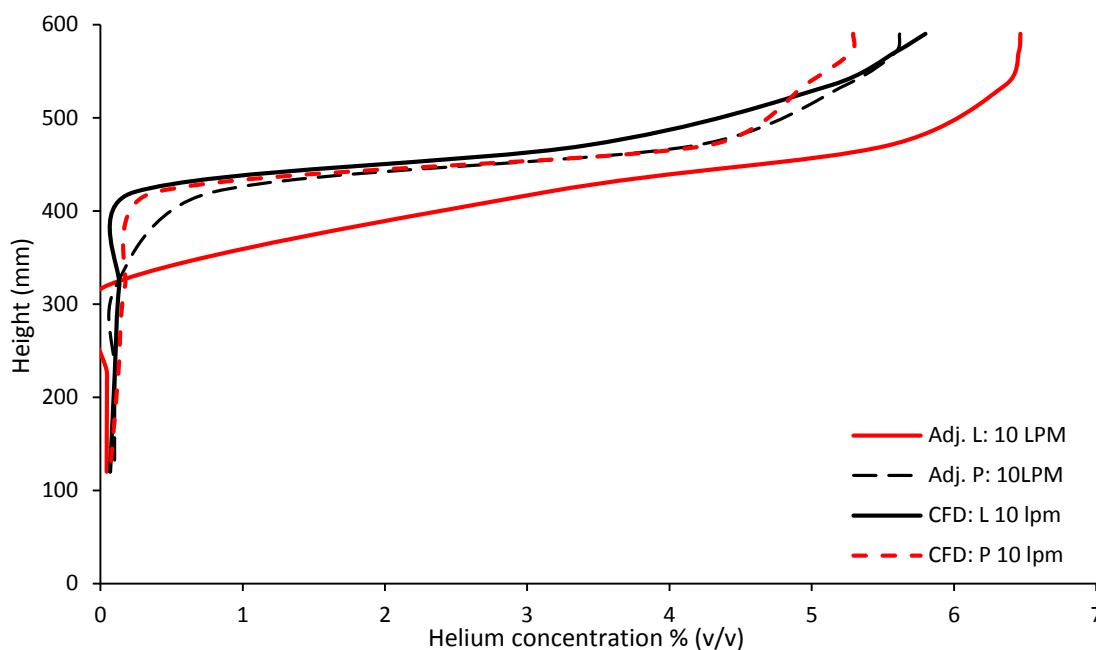
Figure 5.15 presents the stacked sensor helium concentrations for the louvre vent enclosure. The experimental trends of increasing concentration with height are present, but with lower concentrations. The LFL is now exceeded at 5lpm (6lpm for CFD plain vent tests). The depth of the stratified layer appears shallower than for the CFD plain vent data in figure in figure 5.7, which is not what was expected. Louvre vent resistance has led to an increase in concentration but has not increased the depth of the concentrated layer. This is demonstrated in figure 5.16 which compares plain, and louvre stacked sensor data at 10 lpm.



**Figure 5.15 Stacked sensor helium concentrations against height: Louvre vent**



**Figure 5.16 Stacked sensor plain and louvre CFD data at 10 lpm**



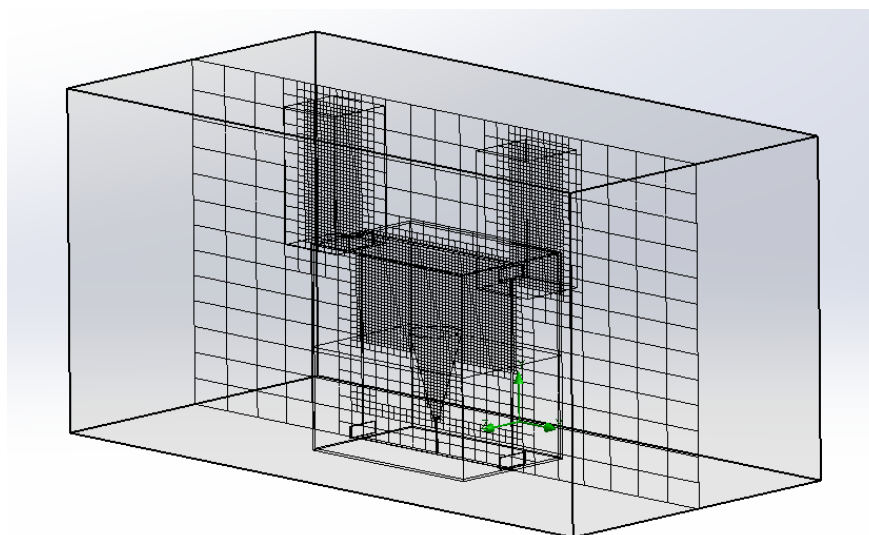
**Figure 5.17 Comparison of stacked sensor CFD and adj. Exp. data @ 10 lpm**

Figure 5.17 compares the 10 lpm CFD and adjusted experimental data. The plain vent results are very close and only deviate by a small amount at higher concentrations. The louvre vent CFD data follows a similar path to the experimental data but with greater variance at higher concentrations. This may be due to difficulty with effectively replicating the louvres in SolidWorks so that they provide realistic levels of flow resistance. Figure 5.14 though does provide evidence of flow resistance due to the louvres.

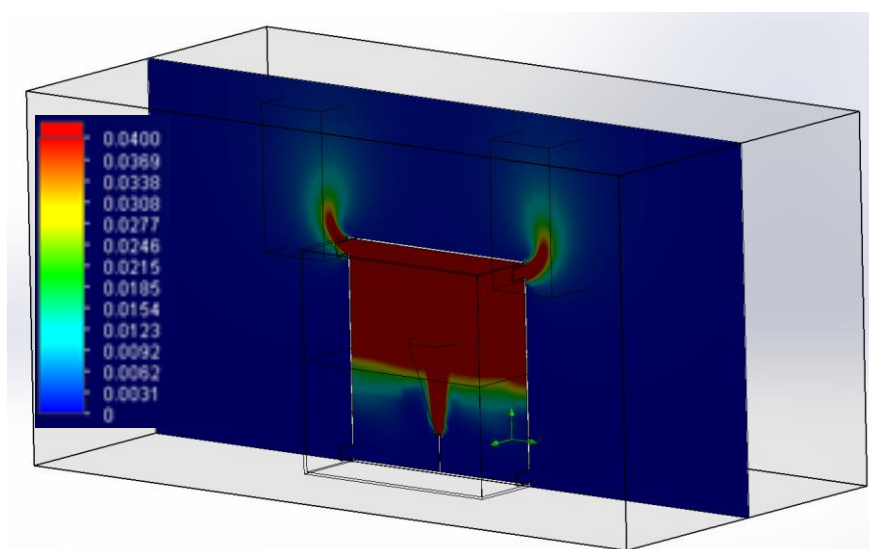
The louvre vents tested comprised a simple horizontal extension, whereas proprietary louvre vents more usually feature a horizontal near downward facing opening with curved ends, providing some wind protection, but which are likely to impede flow. Aluminium proprietary louvres were also tested. These louvres did not extend across the width of the enclosure but were centrally positioned. For comparison purposes rectangular plain vents were also tested in a central position with equal opening area to the aluminium vents. CFD simulations have been conducted using rectangular plane vents and also down facing louvres. These louvres were challenging to construct but offer a useful comparison. Plane louvres are the subject of section 5.4 and proprietary louvres, section 5.5.

#### 5.4 Plain vents (equivalent opening area to aluminium vents)

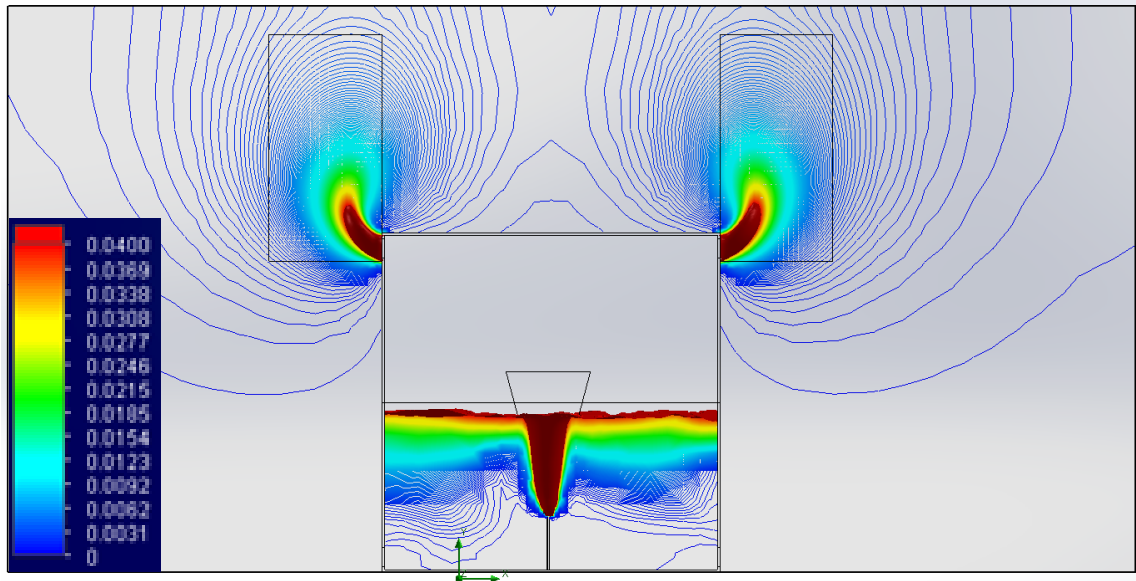
This investigation uses the dimensions of the BOC Ltd. enclosure with plain rectangular vents in a cross-flow regime, with opposing upper and lower vents. In the empirical tests twelve vent sizes were tested. To save on computational time only two vent sizes have been modelled,  $3400 \text{ mm}^2$  (100 mm x 34 mm) (four louvre equivalent) and  $10200 \text{ mm}^2$  (100 mm x 102 mm) (twelve louvre equivalent). This is the same position with the aluminium vent tests in section 5.6. Figure 5.17 shows the initial mesh for the plain vent enclosure ( $3400 \text{ mm}^2$ ). A cone over the plume and three cuboids have been added for additional refinement at the top of the enclosure and vent outlet area. Two leak rates are modelled, 10 lpm and 1 lpm.



**Figure 5.18 Plain vent CFD cut plain of initial mesh with refinement**



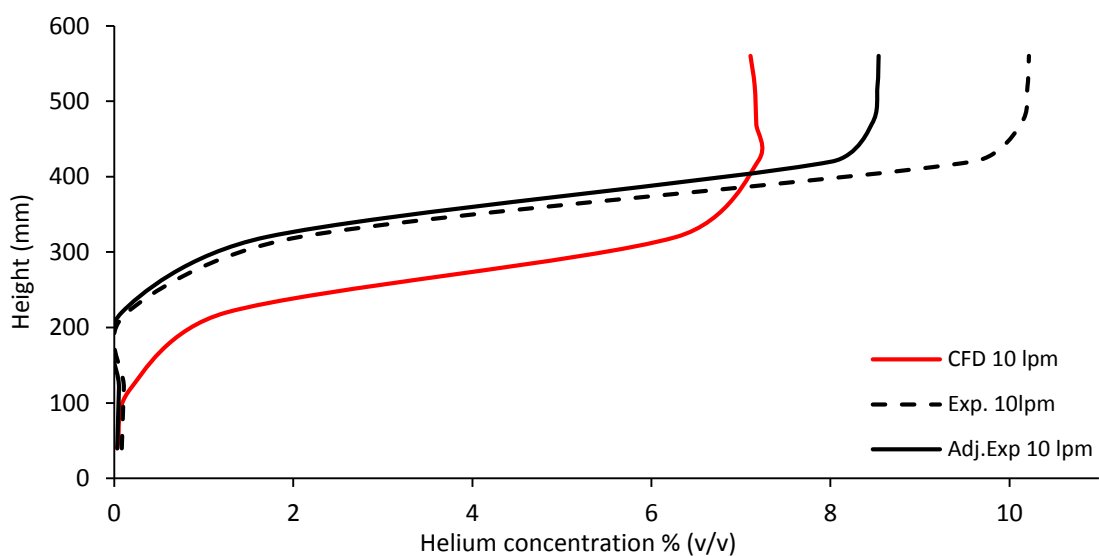
**Figure 5.19 Cut-plane conc. contour image of  $3400 \text{ mm}^2$  plain vent @ 10 lpm**



**Figure 5.20 Combined iso-surface/lines 0-4 % helium at 10 lpm 3400mm<sup>2</sup> plain vent**

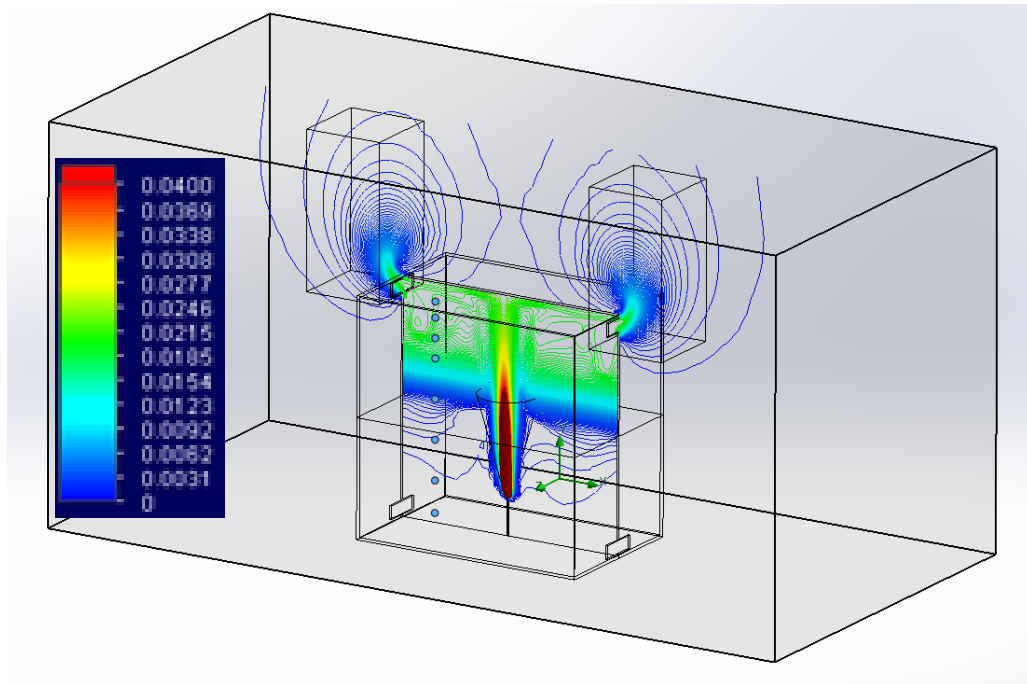
#### 5.4.1 Analysis: 3400 mm<sup>2</sup> opening area

Figure 5.19 presents a cut-plane image of concentration (0-4 % range) for the plain vent 3400 mm<sup>2</sup> enclosure at 10 lpm. It can be seen that helium at 4 % or greater has filled more than 50 % of the enclosure and helium at the LFL is leaving the enclosure through the upper vent. The vents are small, so flow will be restricted, so the deep layer is unsurprising. Figure 5.20 presents an iso-surface/line image showing the extent of helium concentrations within the enclosure and computational domain (0-4 %).



**Figure 5.21 Comparison of experimental and CFD 3400 mm<sup>2</sup> plain vent @ 10 lpm**

Figure 5.21 compares the CFD point source sensor data with the adjusted experimental data. The CFD has under predicted the peak concentration in the stratified zone, compared to the adjusted experimental data and has also predicted that the layer is thicker. Figure 5.22 presents an iso-surface/lines image of the 3400 mm<sup>2</sup> enclosure with a 1 lpm leak rate. Also visible are the sensor/data points. Due to the low leak rate the enclosure concentrations are much lower with the 4 % region confined to the plume from the nozzle.



**Figure 5.22 Combined iso-surface/lines 0-4 % helium at 1 lpm 3200mm<sup>2</sup> plain vent**

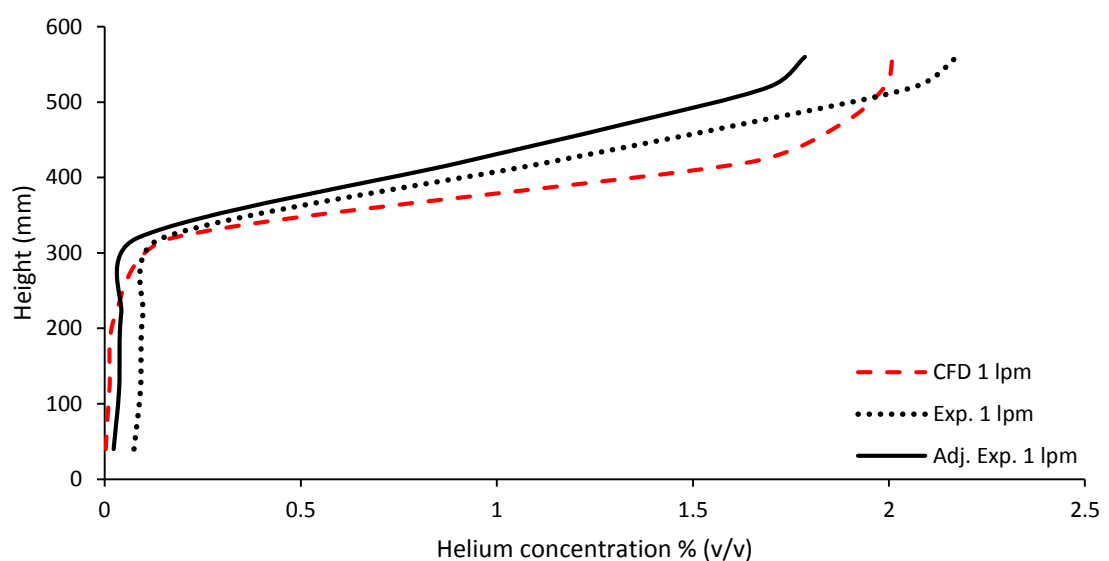
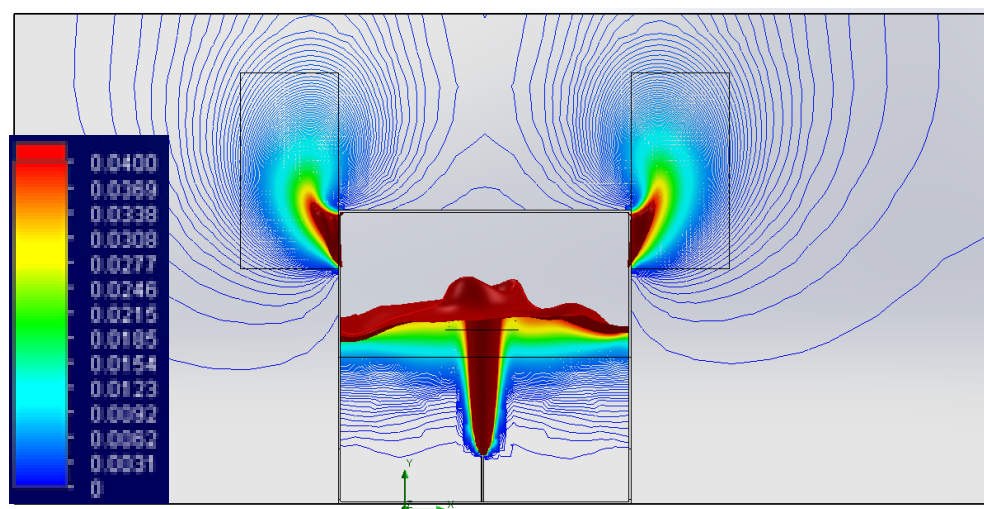


**Figure 5.23 Comparison of experimental and CFD 3400 mm<sup>2</sup> plain vent @ 1 lpm**

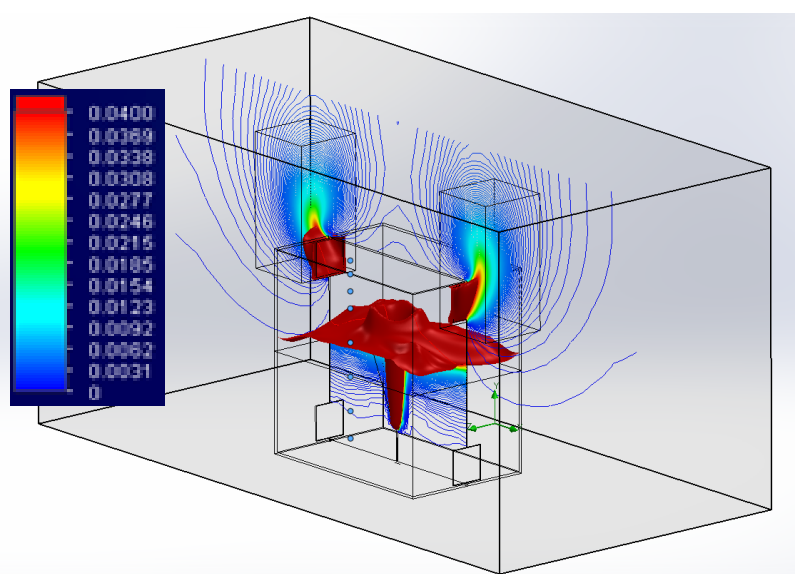
Figure 5.23 compares the CFD 1 lpm data with the adjusted experimental data. The stratified layer is deeper than with the adjusted experimental data, but on this occasion the CFD has over predicted the adjusted experimental peak concentration by a small amount.

#### 5.4.2 Analysis 10200 mm<sup>2</sup> opening area [388,916 cells in mesh]

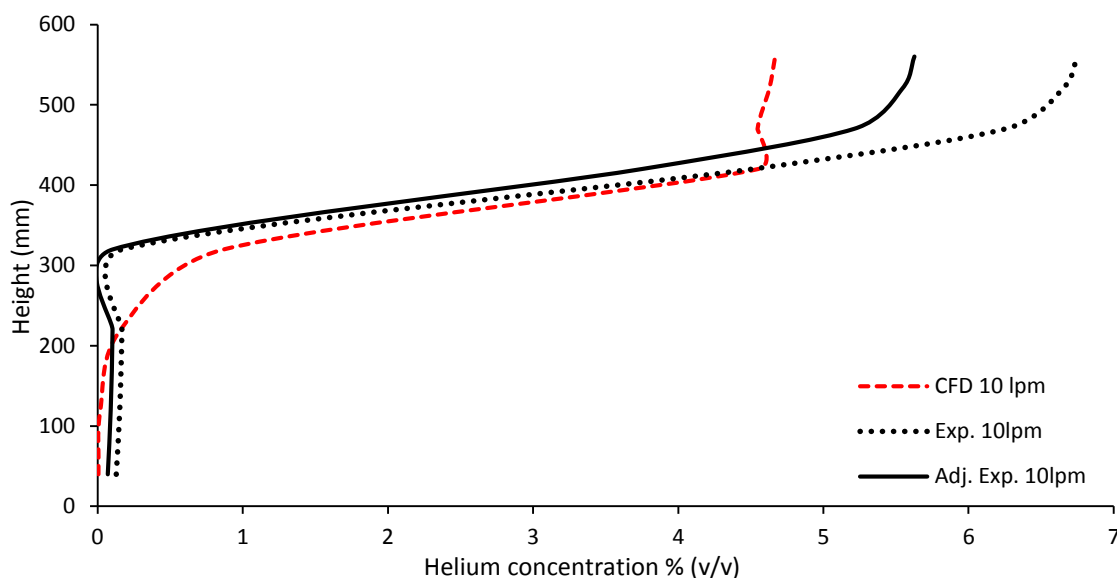
Figure 5.24 presents an iso-surface CFD image for the enclosure with the 10200 mm<sup>2</sup> openings at 10 lpm. The stratified layer is less deep than found with the smaller vent openings, but gas at or exceeding the LFL can be seen leaving the upper vents, though not to the same extent as found with the small vents. Figure 5.25 provides an isometric view of the iso-surface showing the boundary layer across the enclosure.



**Figure 5.24 Iso-surface/lines 0-4 % helium at 10 lpm 10200 mm<sup>2</sup> side view**

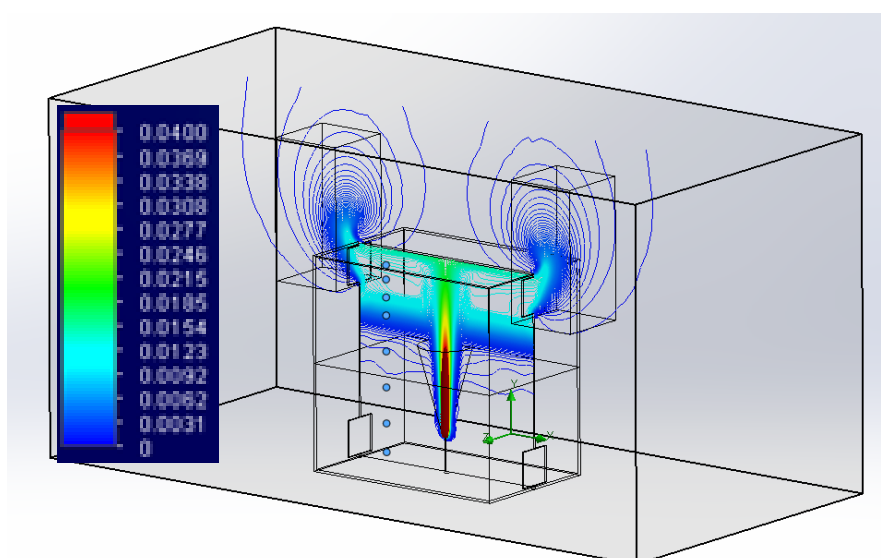


**Figure 5.25 Iso-surface/lines 0-4 % helium at 10 lpm 10200 mm<sup>2</sup> isometric view**



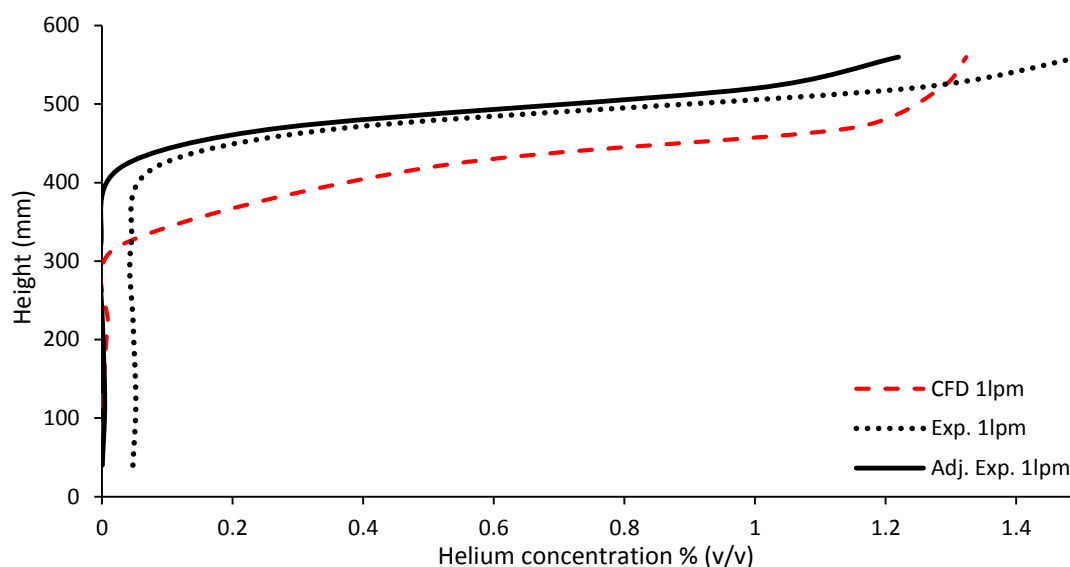
**Figure 5.26 Comparison of experimental and CFD 10200 mm<sup>2</sup> plain vent @ 10 lpm**

Figure 5.26 compares the CFD 10200 mm<sup>2</sup> plain vent data at 10 lpm with the experimental findings. The CFD has under predicted the peak helium concentration when compared to the experimental data, by about 1 %, however the CFD has closely predicted the thickness of the stratified layer. Figure 5.27 presents a concentration contour cut-plane at 1 lpm. Peak concentrations are confined to the plume and there is evidence of stratification. Figure 5.28 compares the 1 lpm CFD data with the experimental findings. The CFD has over predicted the adjusted experimental data and the depth of the stratified layer.



**Figure 5.27 Combined iso-surface/lines 0-4 % helium at 1 lpm 10200mm<sup>2</sup> plain vent**





**Figure 5.28 Comparison of experimental and CFD 10200 mm<sup>2</sup> plain vent @ 1 lpm**

### 5.5 Aluminium louvre vents [4 and 12 louvres]

The simplified vents (figure 5.29) are not the same shape as the real vents, although they do have the same opening area (850 mm<sup>2</sup>) and the same total opening area as the 3400 mm<sup>2</sup> plain vent. In much the same way as the plane vent tests, they have been positioned as far apart as possible to maximise the pressure differential and flow forces. Two louvre vent designs were tested, the one in figure 5.29 (a) (acute) and one in figure 5.29 (b) (obtuse) which better reflects the louvre angle in the aluminium vent.

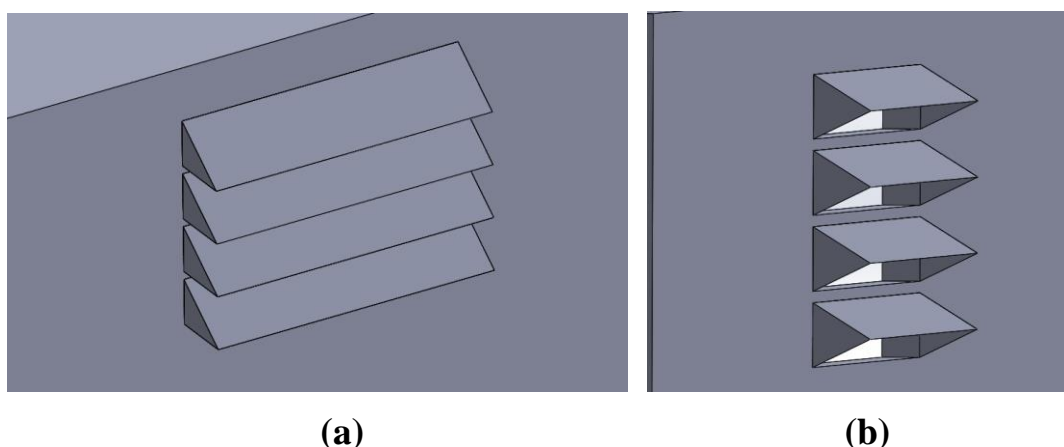
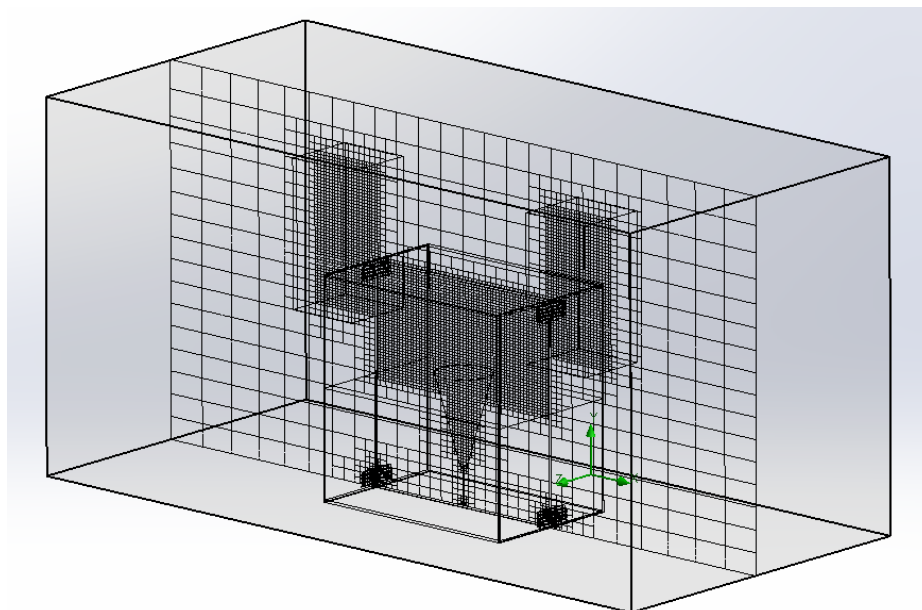


**Figure 5.29 SW simplified louvre vent CAD design (a) Acute (b) obtuse**

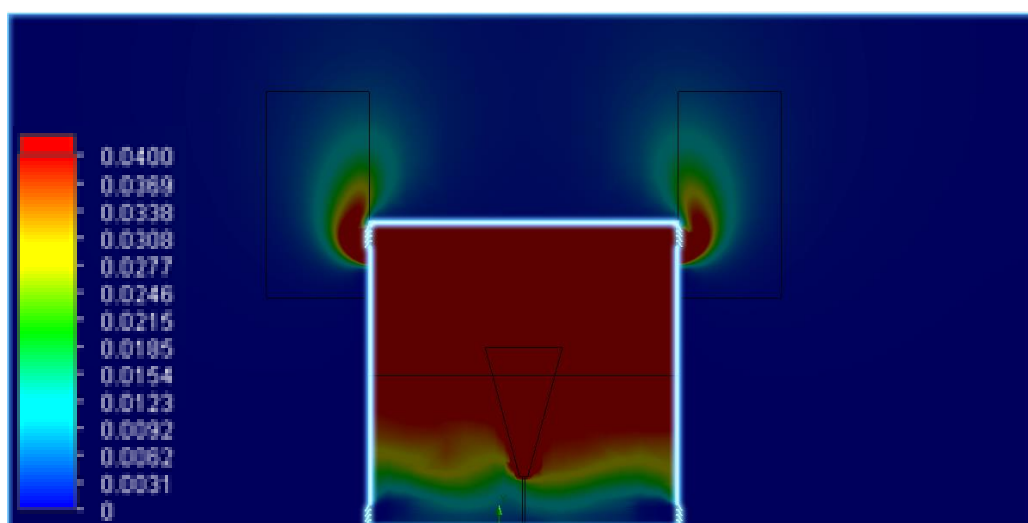
Figure 5.30 presents the meshed CAD model with 334,320 cells. Additional mesh complexity can be seen around the louvre vent openings.



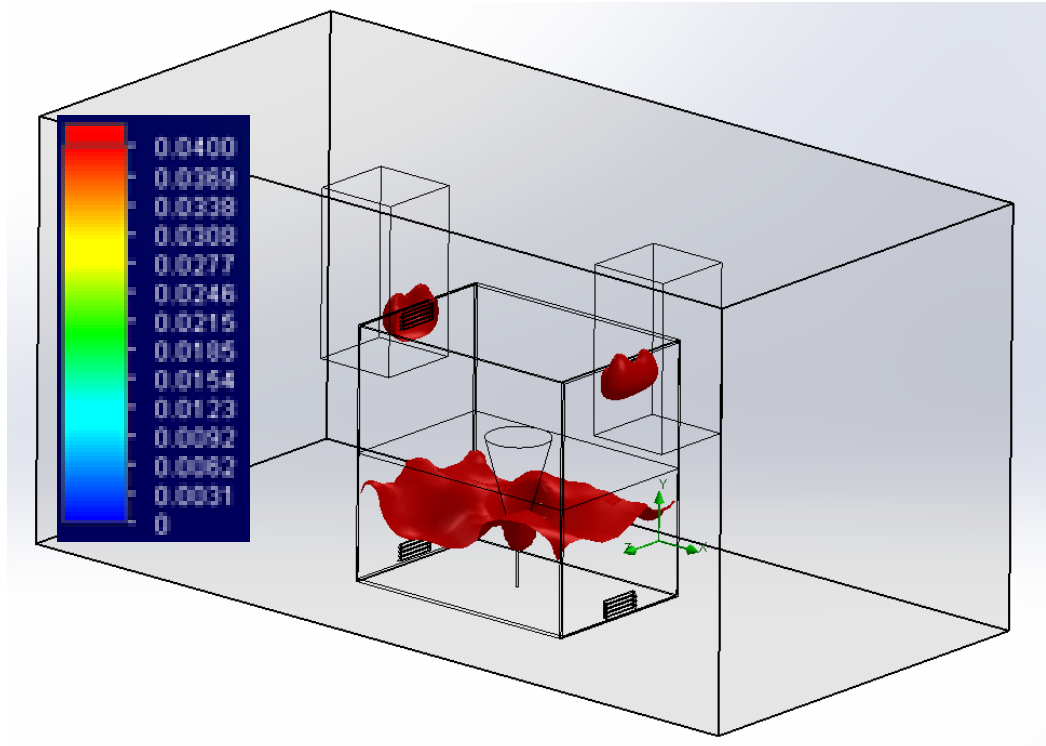
### 5.30 Four louvre initial mesh (acute louvres) (334,230 cells)

#### 5.5.1 Analysis 4 louvres

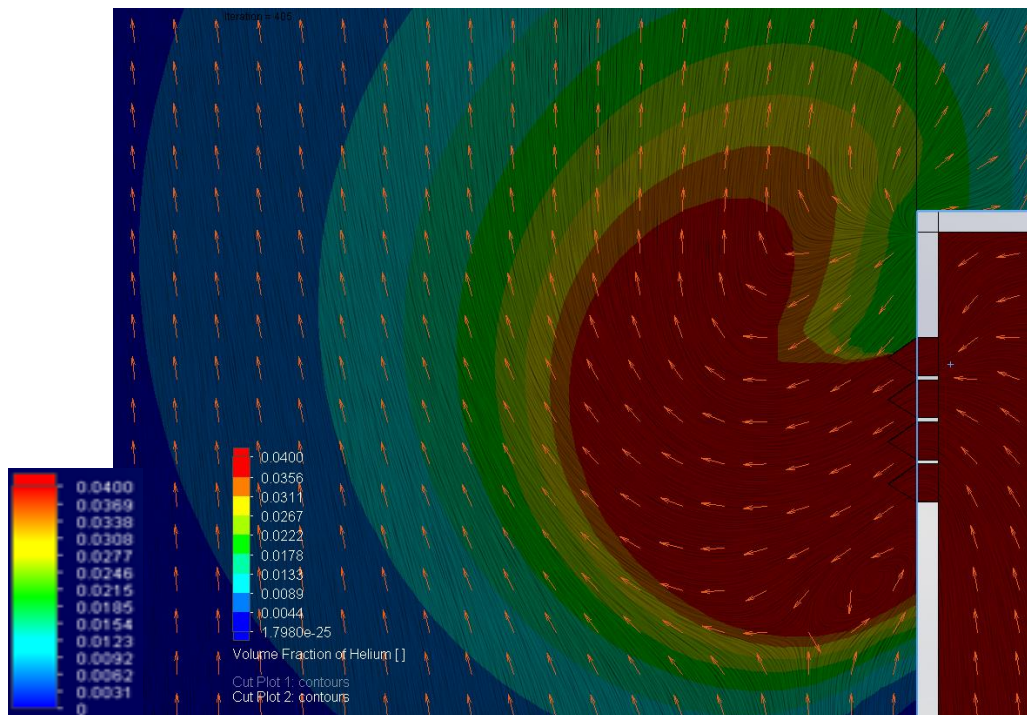
Figure 5.31 shows a concentration contour (0-4 %) central cut plane at 10 lpm, using the acute louvres. The concentrated layer is very thick and almost reaches the height of the nozzle. The iso-surface image in figure 5.32 shows the 4 % limits, which extend outside of the louvre vents. Figure 5.33 focuses in on the top left obtuse vent, with stream lines providing an indication of how the louvres have backed up the flow through the opening and also how the louvres direct the flow downwards out of the enclosure, in a similar way to that seen in the schlieren image (figure 4.53).



### 5.31 Four louvre (acute) cut plane concentration contour 0-4 %



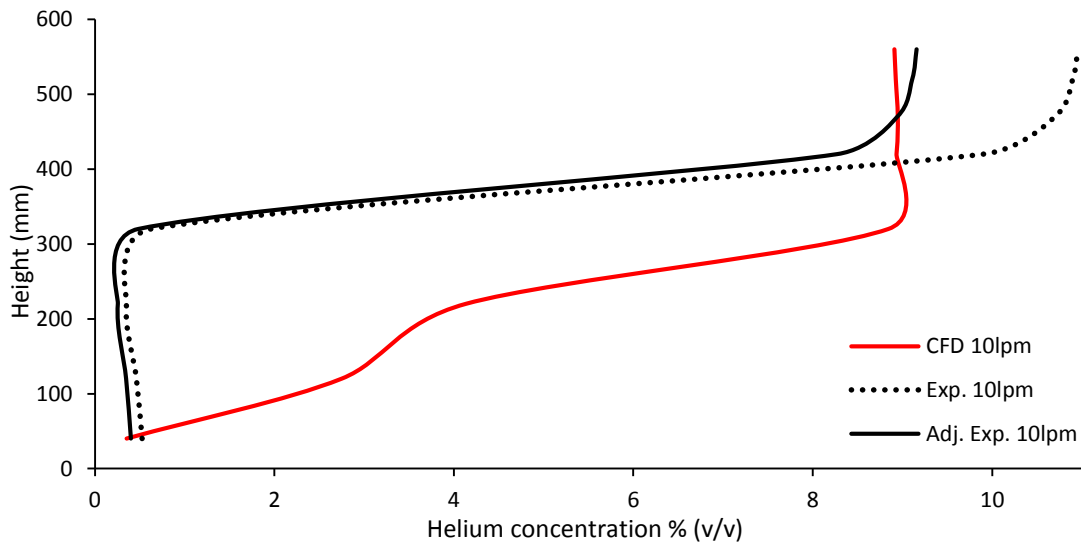
**5.32 Iso-surface at 4 % (10 lpm) acute louvre vents**



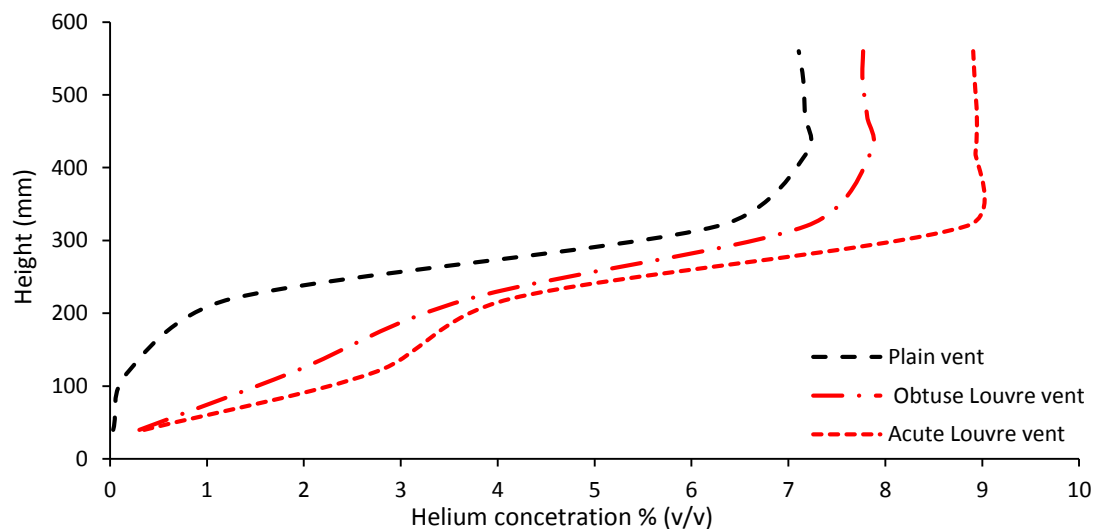
**5.33 Streamlines at top left louvre vent at 10 lpm**

Figure 5.34 compares the acute louvre CFD point source data with the experimental data. The CFD plot is at significant variance to the experimental findings below 400 mm where the helium concentration was predicted to be much higher. The CFD has predicted the

peak concentration well against the adjusted experimental data, however, it has over predicted the depth of the stratified layer and predicted higher concentrations throughout the rest of the enclosure. The CFD has correctly identified an increase in flow resistance but has over accounted for it. The design of the CAD louvres is different to the real louvres, which may have contributed to the over prediction. Figure 5.35 compares the plain and louvre vent (acute and obtuse) CFD predictions. The CFD has correctly accounted for the increased flow resistance due to the louvres. The acute louvres, where the louvre points down to a greater extent impedes flow more than the obtuse louvres and has significantly increased concentrations in the enclosure.



**Figure 5.34 Comparison of CFD and experimental data; 4 louvre vent at 10lpm**



**Figure 5.35 CFD comparisons of 4 louvre and 3400 mm<sup>2</sup> plain vent data; @ 10 lpm**

Figure 5.36 compares the 4 louvre (obtuse) 1 lpm CFD data with the experimental and adjusted experimental data. The CFD has under predicted the peak adjusted experimental helium concentration by about 0.5 % and has predicted higher concentrations lower down in the enclosure than was found in the experimental test. Figure 5.37 compares the louvre (obtuse) and plain vent CFD data at 1 lpm. The louvre data shows that the louvres have backed up the flow and increased the concentration lower down in the enclosure and to a smaller extent higher up.

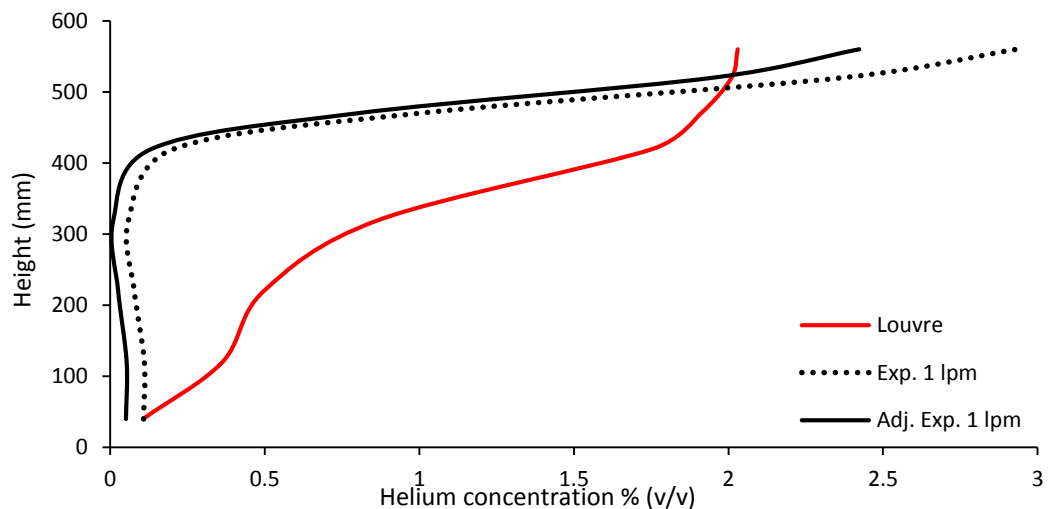


**Figure 5.36 Comparison of CFD and experimental data; 4 louvre vent at 1 lpm**

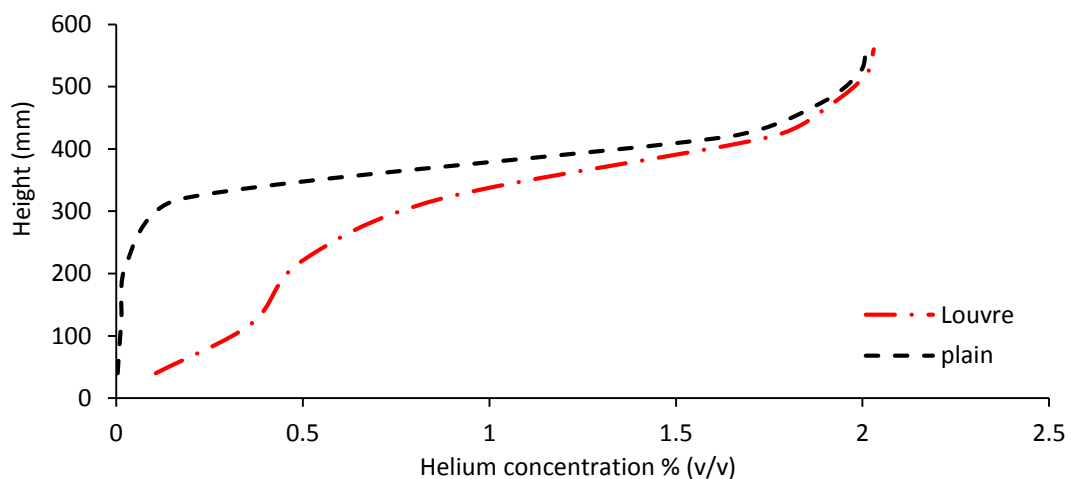


**Figure 5.37 CFD comparison of louvre and 3400 mm<sup>2</sup> plain vent data, @ 1 lpm**

### 5.5.2 Analysis 12 louvres

This analysis only uses the obtuse louvre CFD model as it best reflects the aluminium louvre design. Figure 5.38 presents the 12 louvre CAD model initial mesh and shows the

additional refinement around the louvre openings. Figure 5.39 presents two concentration contour images at 10 and 1 lpm. The stratified layer is visible in both images as is the plume of gas leaving through the upper vents.

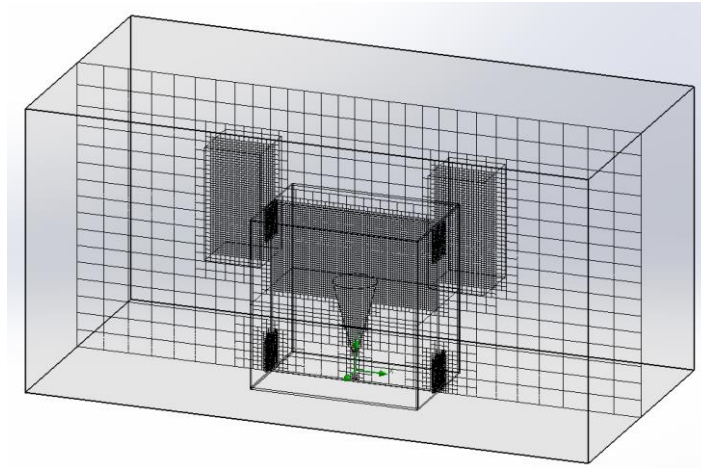


**Figure 5.38 12 louvre initial mesh (422,456 cells: additional louvre refinement)**

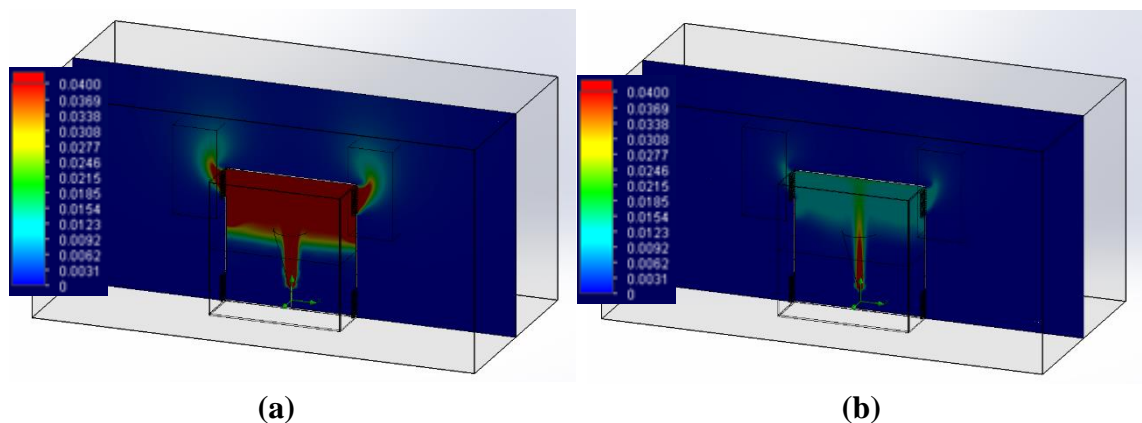


**Figure 5.39 Concentration contour images 12 louvre enclosure (a) 10 lpm (b) 1 lpm**

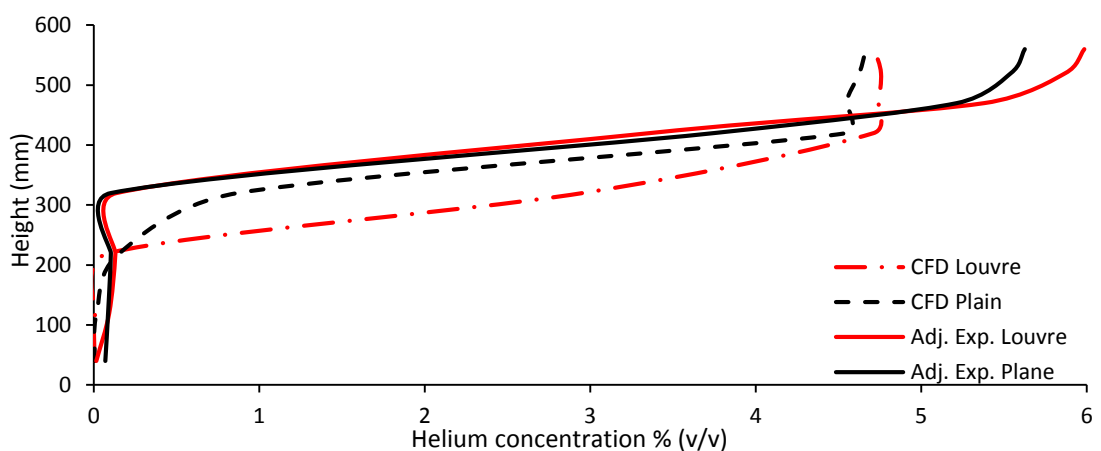


**Figure 5.40 12 louvre and 10200 mm<sup>2</sup> plain vent results 10 lpm: CFD and Exp.**

The graph in figure 5.40 compares the CFD and experimental data for plain and 12 louvre vents at a leak rate of 10 lpm. The CFD has under predicted the peak concentration by about 1 percentage point and shows a slightly higher helium concentration lower in the enclosure. The CFD has correctly reported the flow resistance of the louvre vents. The plain vent CFD plot stratification level is very close to the experimental results. Figure 5.41 compares the CFD plain and 12 louvre 1 lpm results. The CFD has again correctly reported the increase in flow resistance due to the louvres, leading to an increase in concentration and deeper stratified layer.

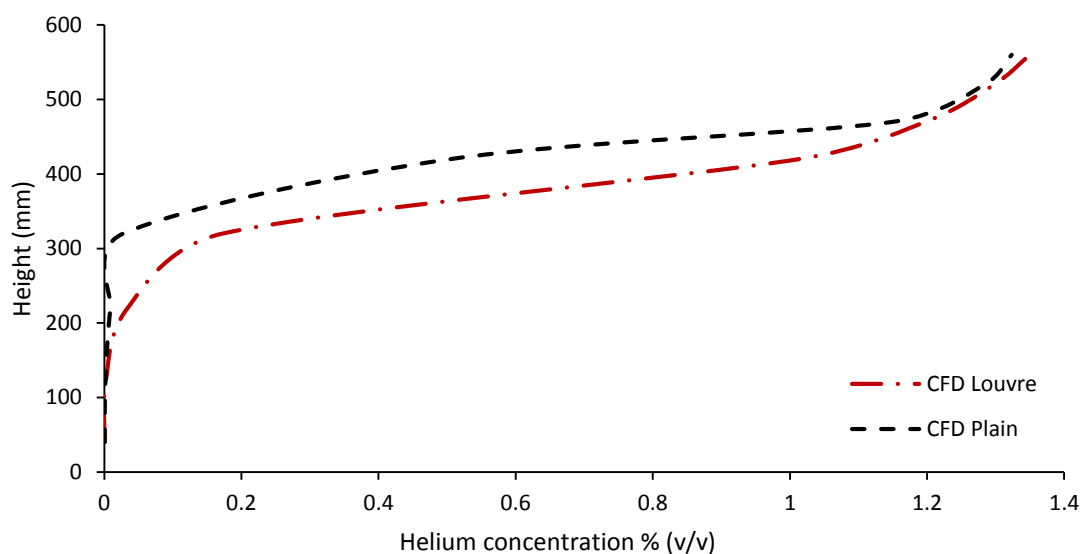


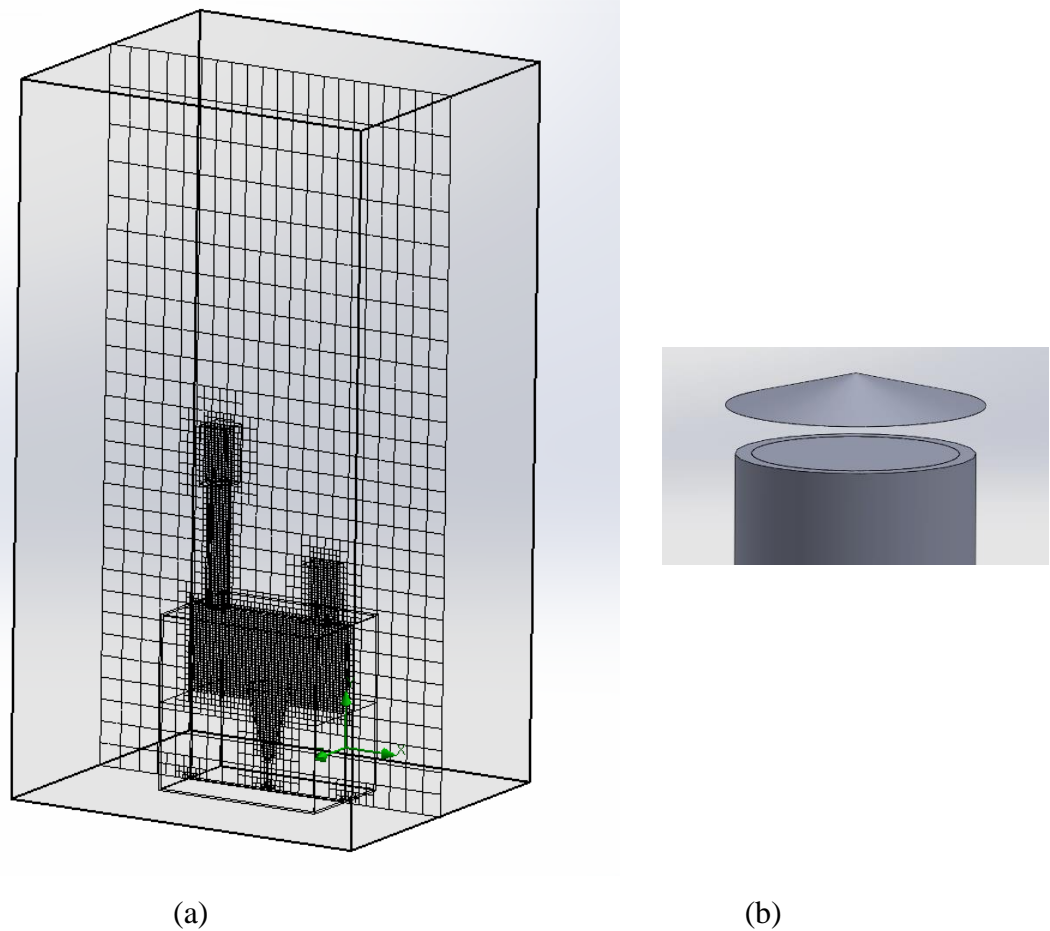
**Figure 5.41 Twelve louvre and 10200 mm<sup>2</sup> plain vent results 1 lpm**

## 5.6 Chimney ventilation [Roof mounted various heights]

This CFD investigation uses the dimensions of the BOC Ltd. enclosure with chimneys mounted on the roof and no side vents. Three chimney heights, 420 mm, 840 mm and 1680 mm are tested along with two leak rates, 2 and 4 lpm (apart from the 420 mm chimney where 1 and 10 lpm rates are also presented). CFD predictions are compared with the experimental findings. Figure 5.42 presents the meshed CAD model and the design of the chimney weather lid.

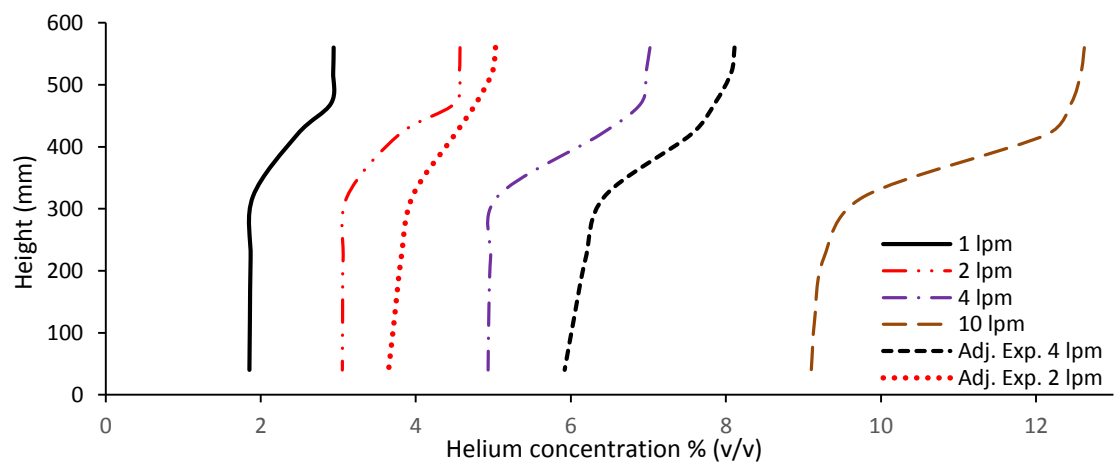
One of the vents is a 64 mm diameter chimney and the other is a 64mm diameter hole. The vents are positioned 100 mm in from the end of the enclosure and centred 200 mm in from the side panels. Two openings should develop a displacement ventilation regime, with the chimney being the outlet, due to the low pressure at the top and the hole becoming

an inlet as it is at higher pressure. Both vents are covered with an 80 mm diameter Chinese cap lid, positioned 15 mm above the vent opening.



**Figure 5.42 (a) Meshed 420 mm CAD model (241,334 cells) (b) chimney vent with lid**

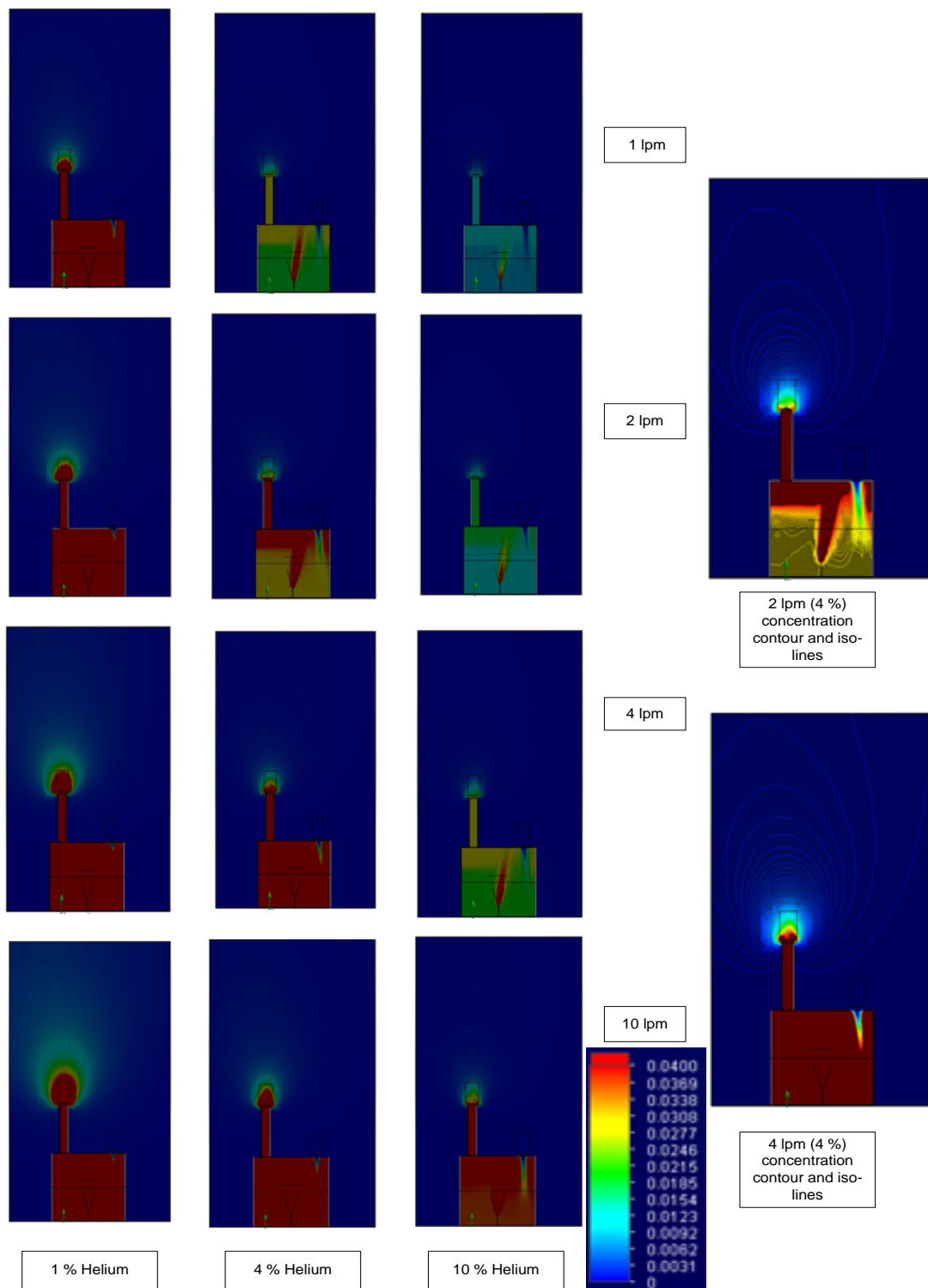
### 5.6.1 Analysis 420 mm chimney



**Figure 5.43 CFD data for the 420 mm chimney compared with Adj. Exp. data**

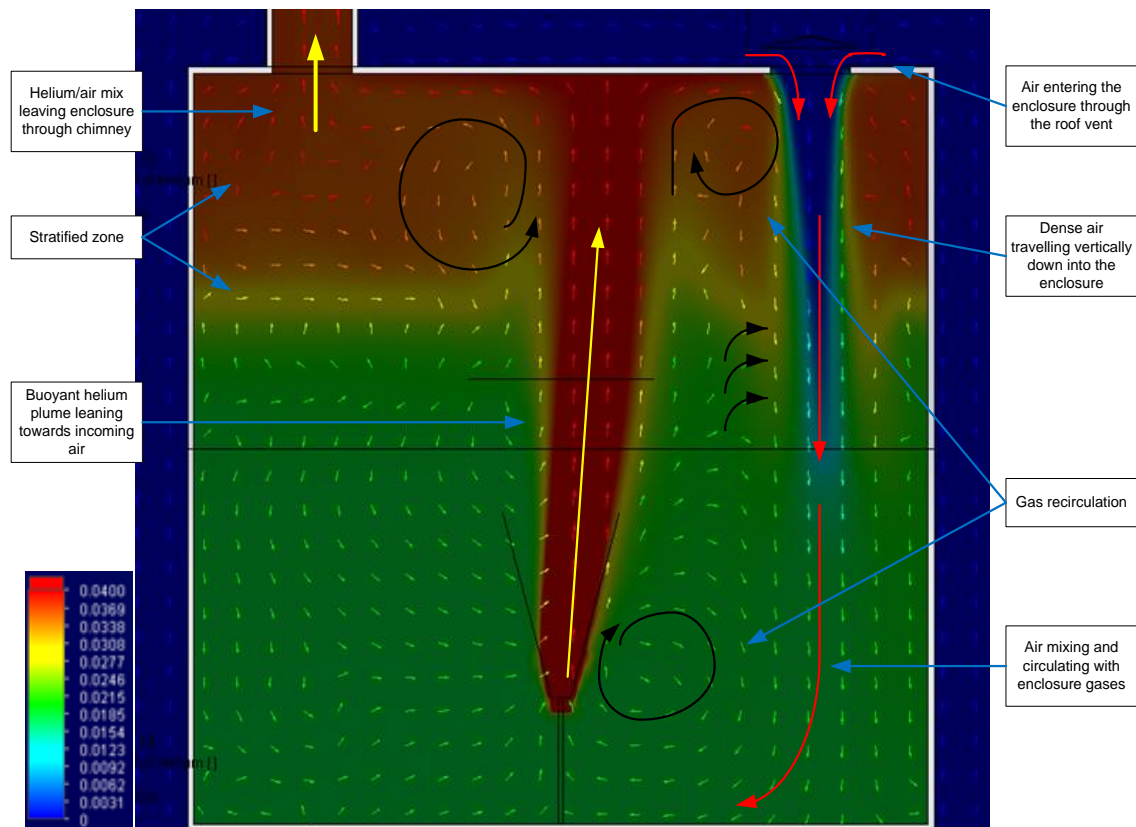


Figure 5.43 presents the 420 mm chimney predictions. The plots show a low concentration area below about 300 mm height which then increases up to about the 500 mm height point leading to a stratified zone above. This behaviour can be seen in the CFD cut planes presented in Figure 5.44.



**Figure 5.44 420 mm chimney CFD cut-plane images (@ 4 %) at 1, 2, 4 and 10 lpm**

Figure 5.43 also presents a comparison with the adjusted experimental data for 2 and 4 lpm. The 4 lpm adjusted data follows a similar profile to the CFD data but is about 1 % point higher at all levels. With the 2 lpm adjusted data the profile is slightly at variance, but the values are a lot closer to the CFD predictions. The CFD model is performing well but further mesh refinement may improve results further.



**Figure 5.45 Cut-plane image with velocity vectors describing enclosure circulation**

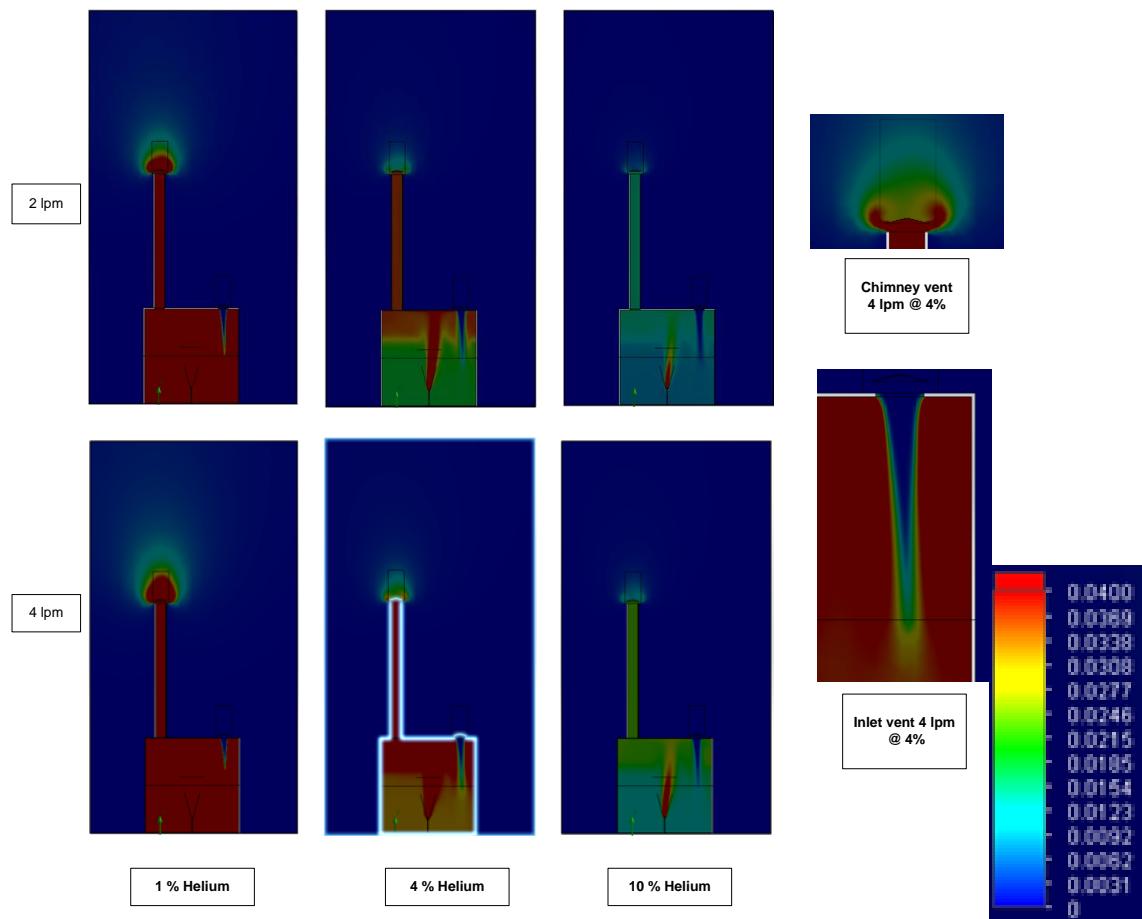
Figure 5.45 presents a cut plane concentration contour and velocity vector combination. This image is intended to provide an insight into the flow mechanisms taking place within the enclosure under a passive ventilation regime. The two-vent system in place is a displacement ventilation system where one vent becomes the inlet and the other an outlet, depending upon their height. The image shows the vent hole becoming the inlet for air into the enclosure and the tall chimney whose top is at lower atmospheric pressure becoming the outlet.

The dense air pours into the enclosure and travels down mixing with the enclosure gases. The momentum of the air causes recirculation and mixing to occur. The helium plume

can be seen emerging from the nozzle and leaning to the right towards the incoming air. This effect is probably due to the momentum of the downward travelling air displacing the plume over. Also visible is the stratified layer at the top of the enclosure containing higher concentration helium.

### 5.6.2 Analysis 840 mm chimney

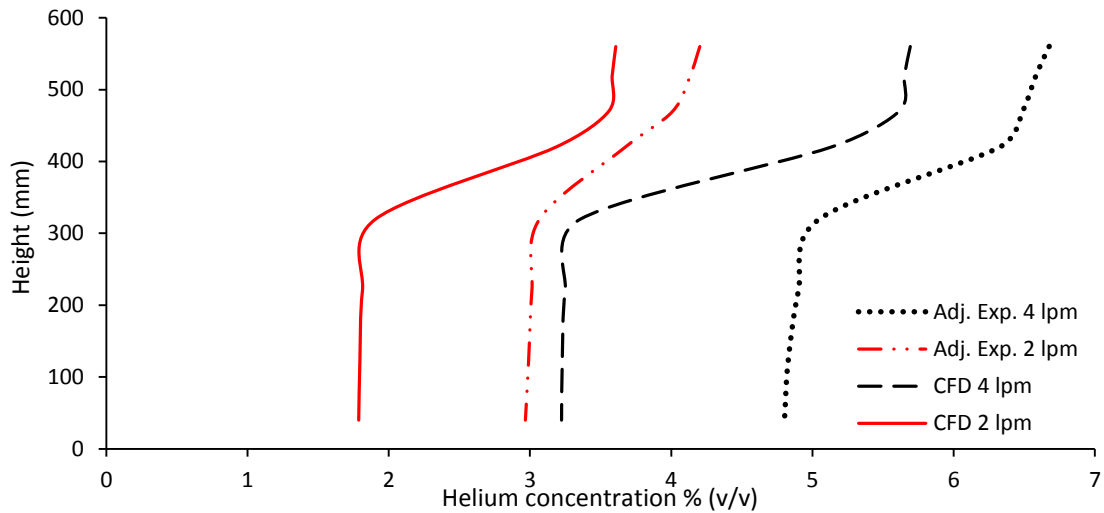
In this CFD study the chimney has been doubled in height to see how this affects the flow regime in the enclosure. Helium leaks rates of 2 and 4 lpm have been used. Figure 5.46 presents cut-plane concentration contour images at 1, 4 and 10 % helium concentration limits. The conditions in the enclosure appear similar to those found with the 420 mm chimney, but the concentrations across the system appear lower. Also shown is the chimney vent, where helium can be seen to curl around the edges of the Chinese hat lid.



**Figure 5.46 840 mm chimney cut-plane images (@ 4 %) at 2 and 4 lpm**

Figure 5.47 presents a comparison of the 2 and 4 lpm CFD data with the corresponding adjusted experimental data. Increasing the height of the chimney has led to a reduction in

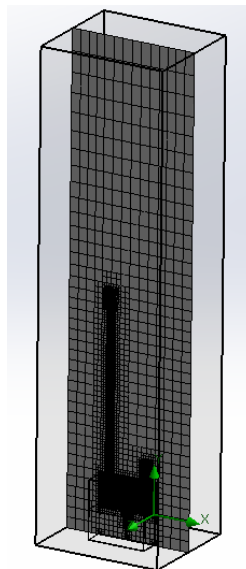
enclosure concentration as was found with the empirical tests. When compared with the adjusted experimental data the CFD has under predicted enclosure concentrations by over one percentage point but has identified the depth of the stratified layer. The increase in pressure differential has increased the mass flow rate as anticipated.



**Figure 5.47 CFD data for the 840 mm chimney compared with Adj. Exp. data**

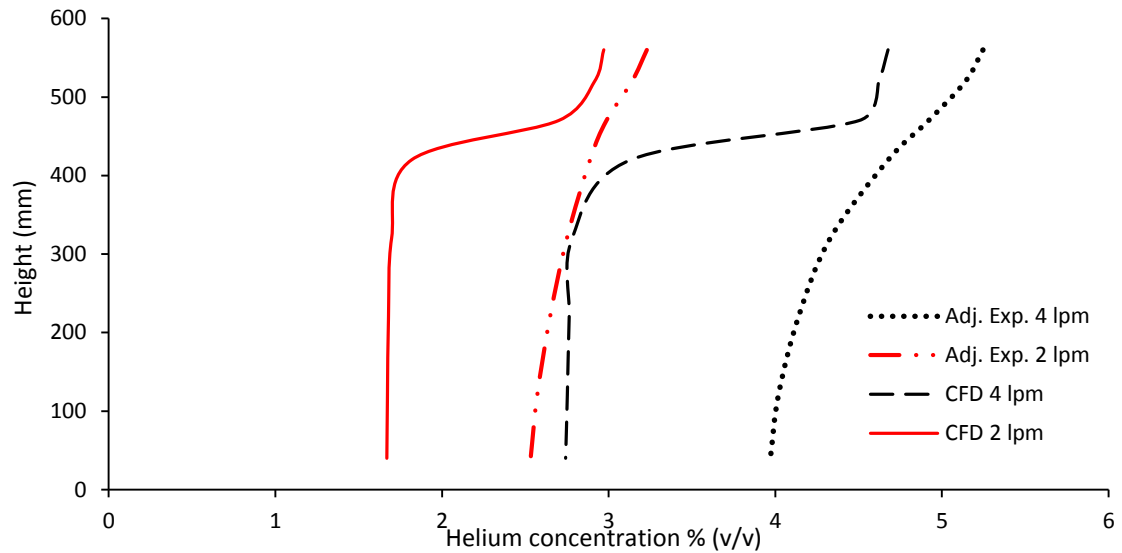
### 5.6.3 Analysis 1680 mm chimney

In this study the chimney has been doubled in height again to 1680 mm and leaks rates of 2 and 4 lpm tested. Figure 5.48 presents the meshed CAD model demonstrating the height of this chimney arrangement and the level of refinement present in the enclosure, chimney and vent areas.

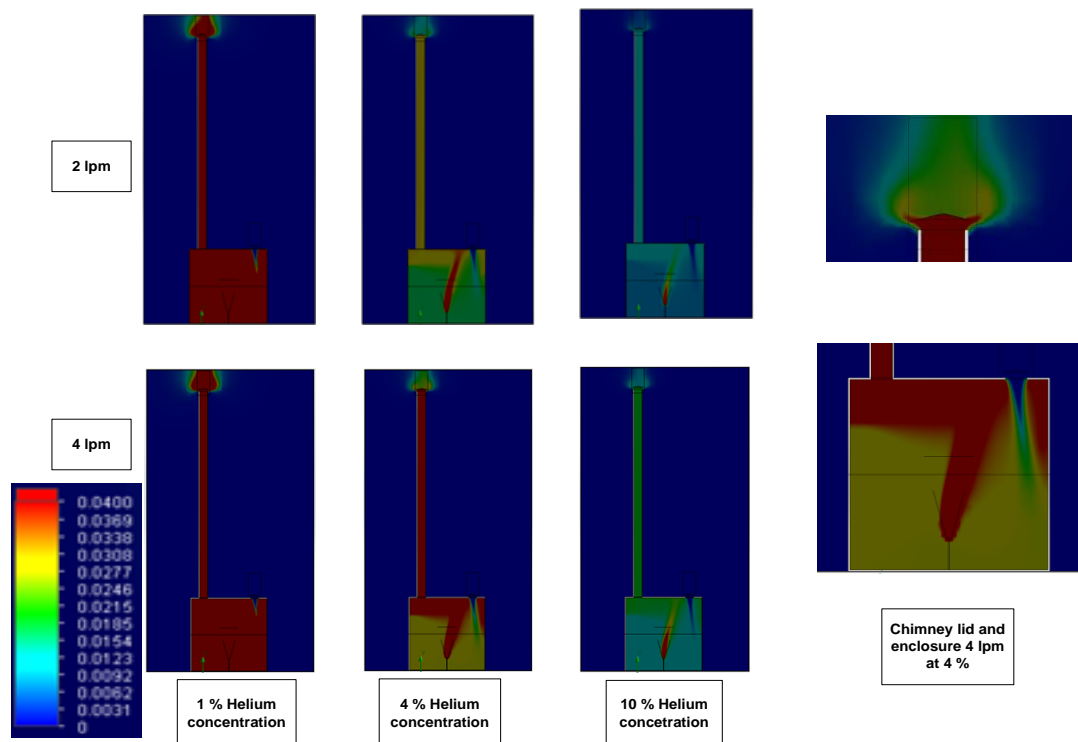


**Figure 5.48 Meshed 1680 mm chimney enclosure CAD model (442984 cells)**

Figure 5.49 presents the results of the 1680 mm chimney test. Compared to the 840 mm tests the concentrations are lower, albeit with the 2 lpm plot only slightly lower. A clear difference is that the stratified layer is shallower. The adjusted experimental results are interesting in that the range of concentration is lower suggesting a more homogenous mixture in the enclosure with the stronger driving force from the tall chimney pulling the gases through

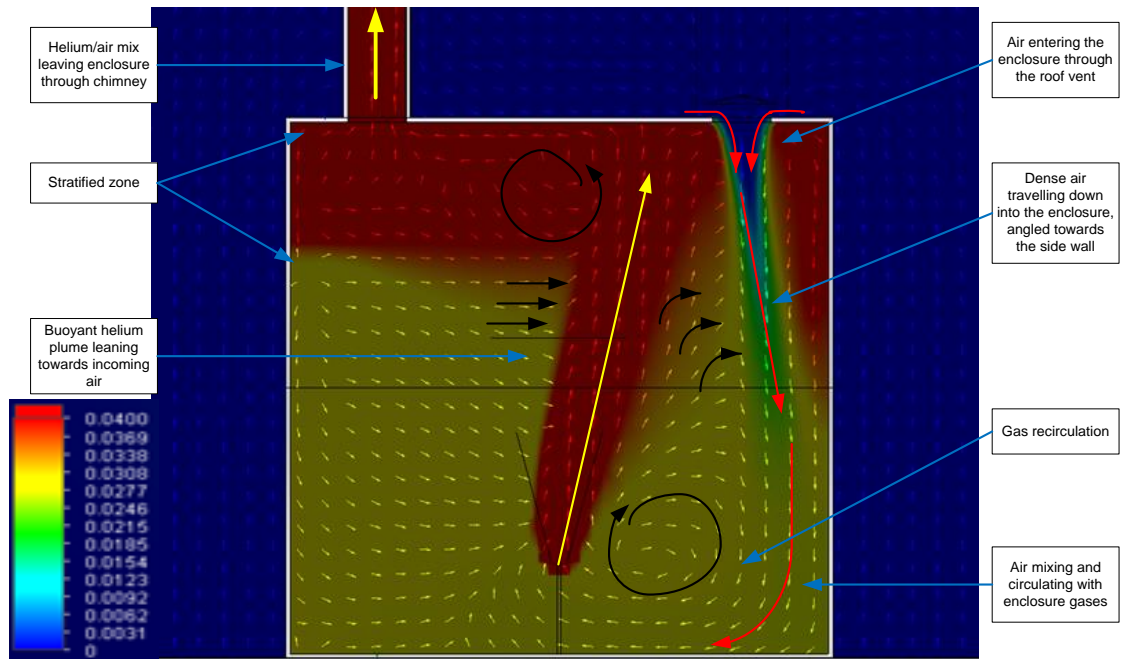


**Figure 5.49** CFD data for the 1680 mm chimney compared with Adj. Exp. data



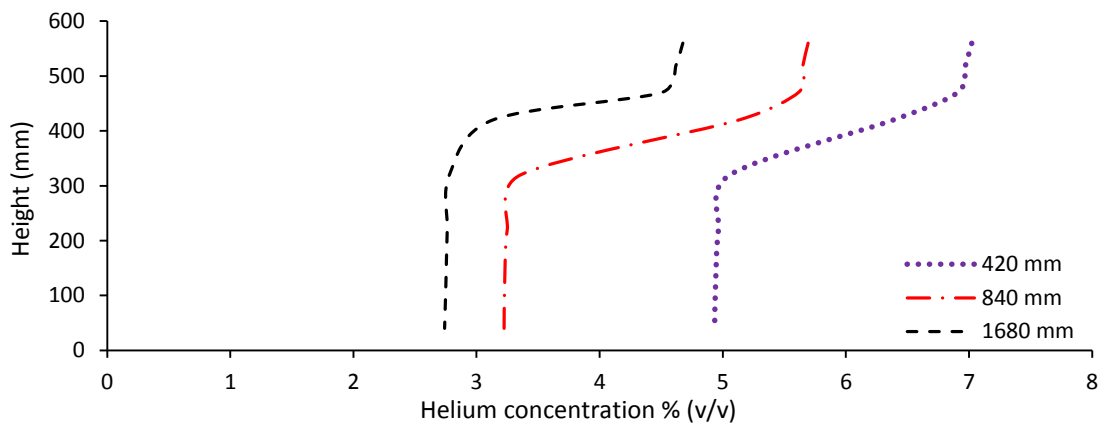
**Figure 5.50** 1680 mm chimney cut-plane images (@ 4 %) at 2 and 4 lpm

Figure 5.50 presents cut-plane concentration contour images at 2 and 4 lpm and at 1, 4 and 10 % helium concentration limits. It is noticeable that the plume is more deflected than in the earlier studies. Figure 5.51 (4 lpm at 4 %) shows this in more detail. Also visible is that the air flow into the enclosure has been deflected towards the wall.



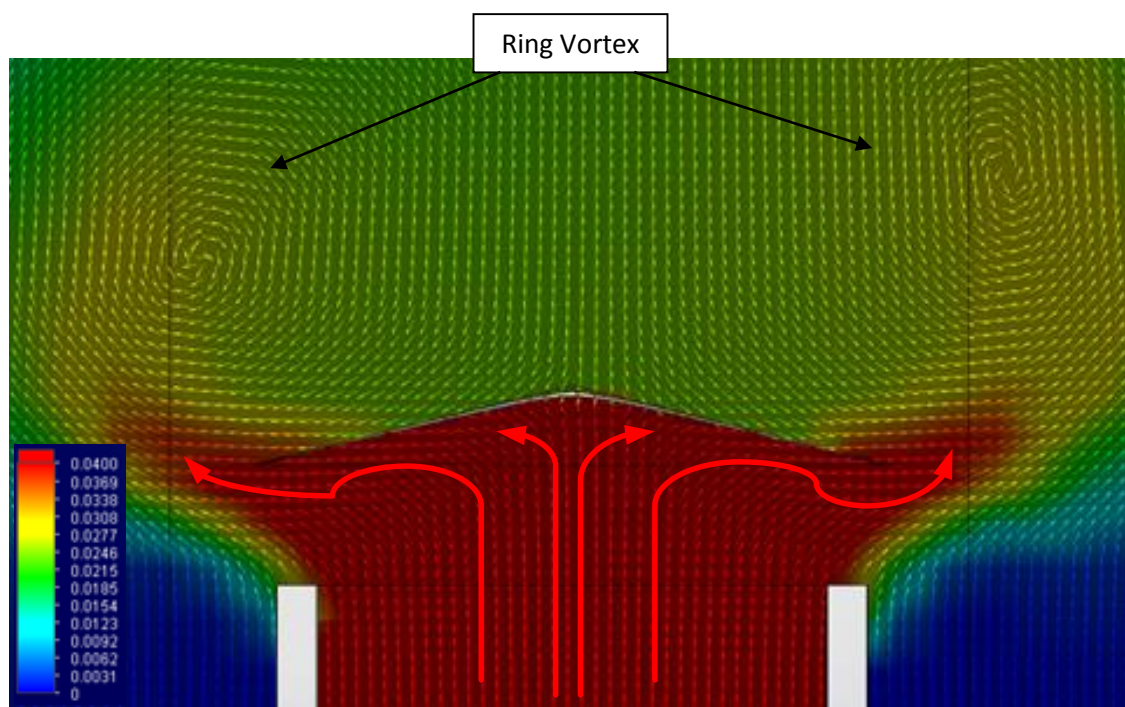
**5.51 Cut-plane image (@ 4 %) with velocity vectors describing enclosure circulation**

Figure 5.52 compares the 4 lpm CFD results at three chimney heights. The CFD has correctly predicted that increasing chimney height raises the driving force and consequently reduces enclosure concentration. However, it has not fully predicted the flow regime and has underpredicted concentrations and stratification levels when compared to the empirical data.



**Figure 5.52 Comparison 420, 840 and 1680 mm chimney CFD results (4 lpm)**

Figure 5.53 shows the velocity vectors at the Chinese cap. The cap is inducing a measure of flow resistance to the enclosure system. The cap is not identical to the empirical design (for example the supports are not present) and may be producing a different level of resistance, which may provide some variance from the empirical data. It is though behaving as predicted in figure 4.36, which also shows evidence of a ring vortex. This insight would assist with developing an improved weather lid.



**Figure 5.53 Cut-plane concentration contour (4 %) and iso vectors Chinese cap**

### **5.7 Flue ventilation [Tubular side vent / T Flue / Snorkel Flue]**

This series of studies uses the BOC Ltd. enclosure but with a range of side flues. The models tested are the BOC Ltd. enclosure with;

- Single top-level side flue 110 mm long
- Single top-level side flue 110 mm long with opposing 3200 mm<sup>2</sup> low vent
- Single top-level side flue 330 mm long with opposing 3200 mm<sup>2</sup> low vent
- Single T-flue 110 mm x 400 mm with opposing 3200 mm<sup>2</sup> low vent
- Single snorkel flue with opposing 3200 mm<sup>2</sup> low vent

The flue opening has an area of approximately 3200 mm<sup>2</sup> so is matched with the inlet where used. Leak rates tested are 0.5, 2, 4 and 10 lpm. Figure 5.54 presents the meshed 110 mm flue enclosure with (355925 cells).

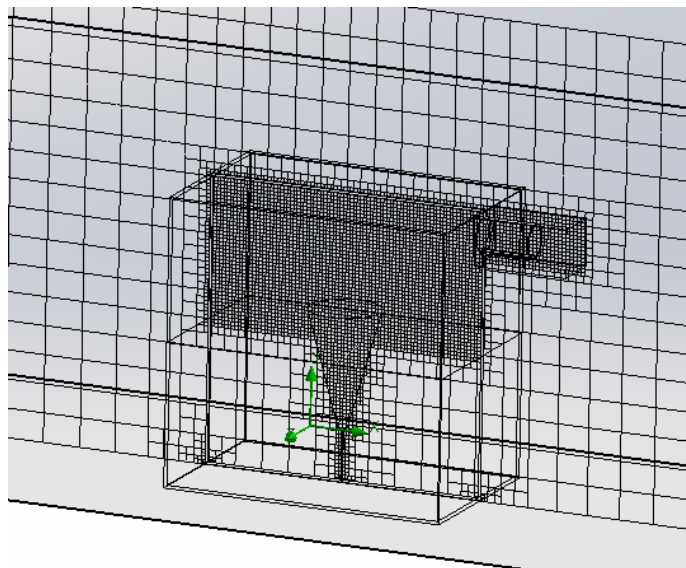


**Figure 5.54 Meshed 110 mm flue enclosure without inlet (355925 cells)**

### 5.7.1 Analysis standard enclosure with 110 mm straight flue no inlet

Figure 5.55 presents the results for the 110 mm flue enclosure with no inlet at leak rates of 0.5, 2 and 4 lpm. Unsurprisingly the enclosure concentrations are high as there is a mixing ventilation regime and effectively the vent is split into two. The CFD data at 2 and 4 lpm has followed the behaviour found with the 0.5 lpm experimental data with concentrations building up from about 300 mm height and then a stratified layer in the top 150 mm. The CFD data at 0.5 lpm only has a suggestion of this behaviour. It also over predicts the concentration below 400 mm and under predicts above this level, albeit by only about half a percentage point. As this is a mixing ventilation scenario it is valid to take an average of all sensor points. The CFD value is 6.9 % and the adjusted experimental value is 6.7 %. This is a good prediction of average enclosure concentration.

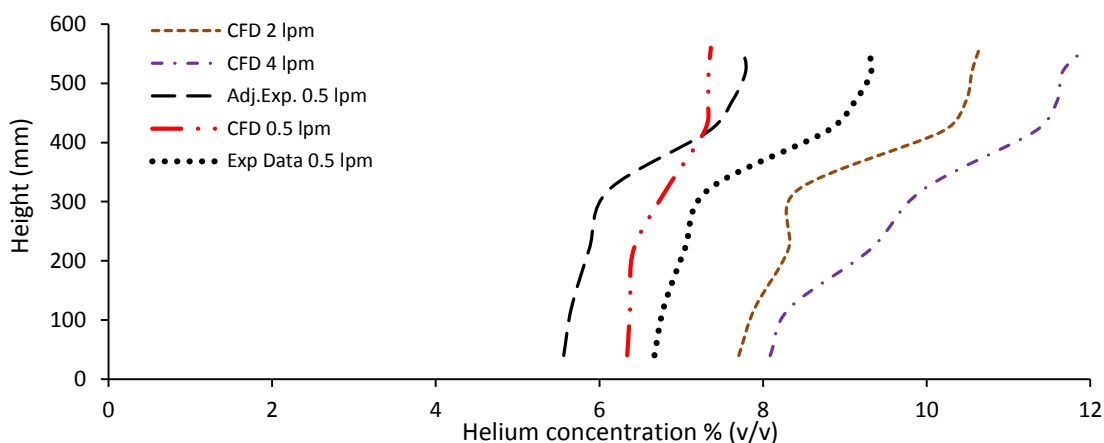


**Figure 5.55 Comparison of CFD and exp. data for 110 mm straight flu-no inlet**



### 5.7.2 Analysis: enclosure with 110 mm straight flue and 3200/6400/9600 mm<sup>2</sup> inlet

This study creates a cross flow displacement regime in the enclosure, with approximately equal inlet and outlet areas. Figure 5.56 compares the CFD results at 0.5 and 4 lpm with the corresponding adjusted experimental results. The CFD has produced good prediction results when compared to the experimental plots. At 0.5 lpm, the CFD has marginally over predicted enclosure concentrations. At 4 lpm, the CFD has predicted the depth of the stratified layer and has under predicted the peak concentration by about 0.4 %.

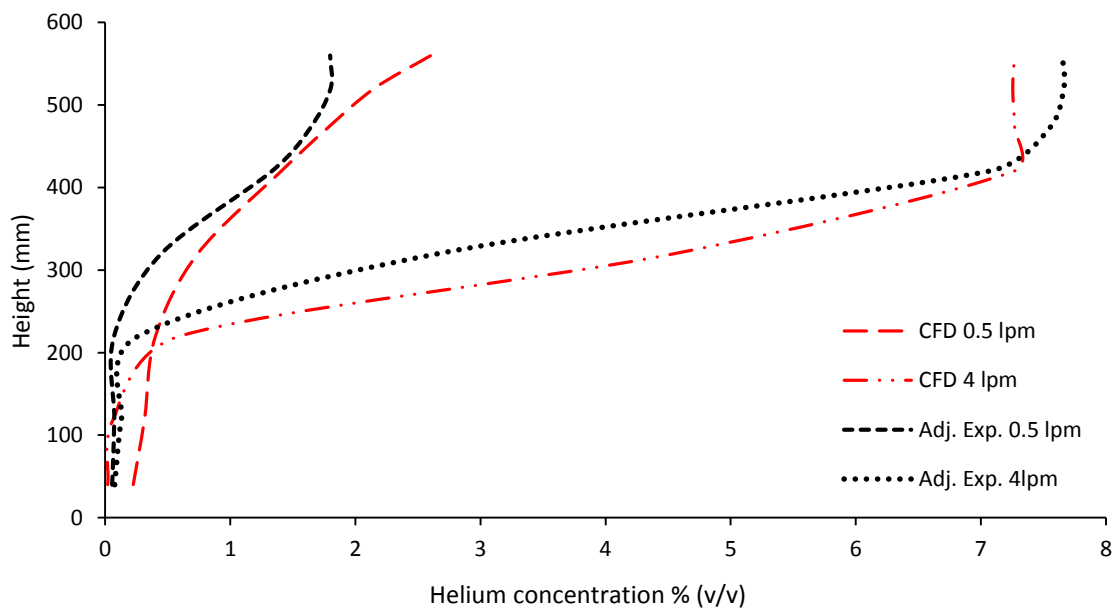


**Figure 5.56 Comparison: CFD and exp. data for 110 mm straight flue/ 3200 mm<sup>2</sup> inlet**

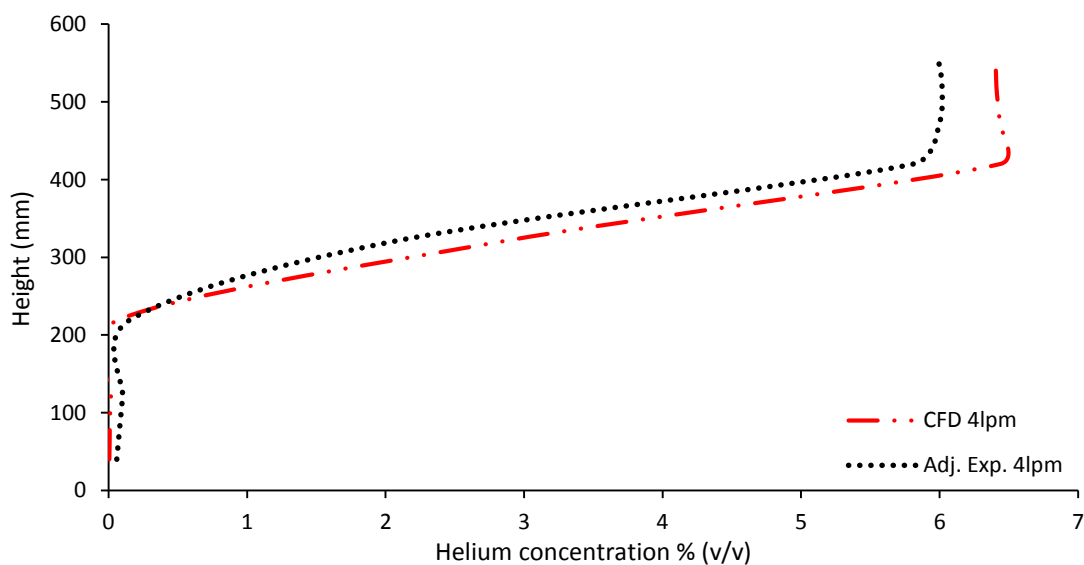
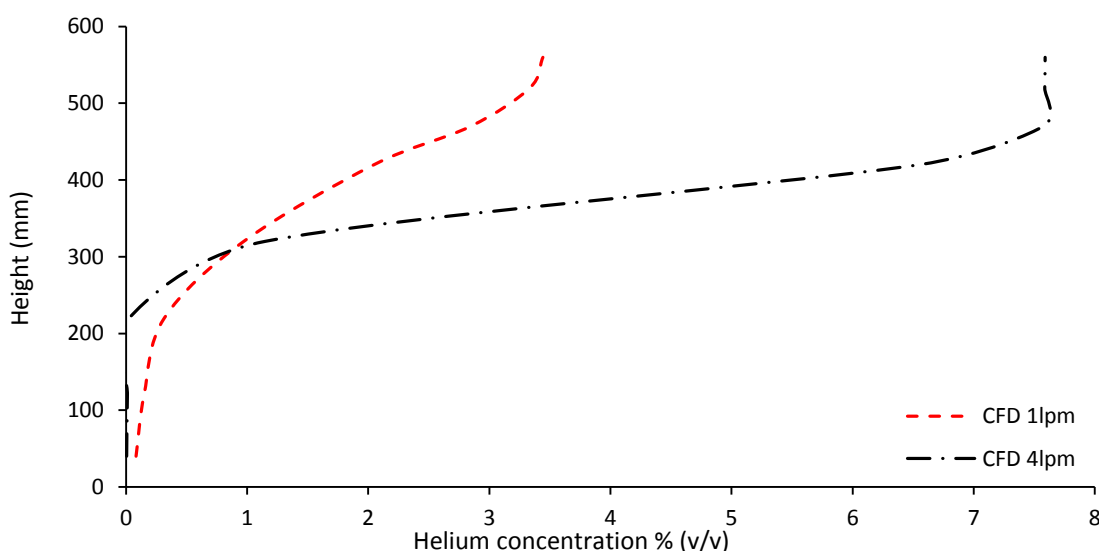


**Figure 5.57 Comparison: CFD and exp. data for 110 mm straight flue/ 9600 mm<sup>2</sup> inlet**

Figure 5.57 presents the 4 lpm results where the inlet has been increased to 9600 mm<sup>2</sup>. This should have the effect of increasing the available driving force through the enclosure as the vent area has been tripled. Figure 5.57 shows that in the case of both the CFD and the adjusted experimental data enclosure concentrations have been reduced when compared to the data in figure 5.56. The CFD has also closely predicted the adjusted experimental results, over predicting the peak concentration by about 0.4 % and a slightly deeper stratified zone. Increasing the lower vent area therefore has a positive effect upon mass flow in the enclosure.

### 5.7.3 Analysis standard enclosure 330 mm straight flue and 9600/6400 mm<sup>2</sup> inlet

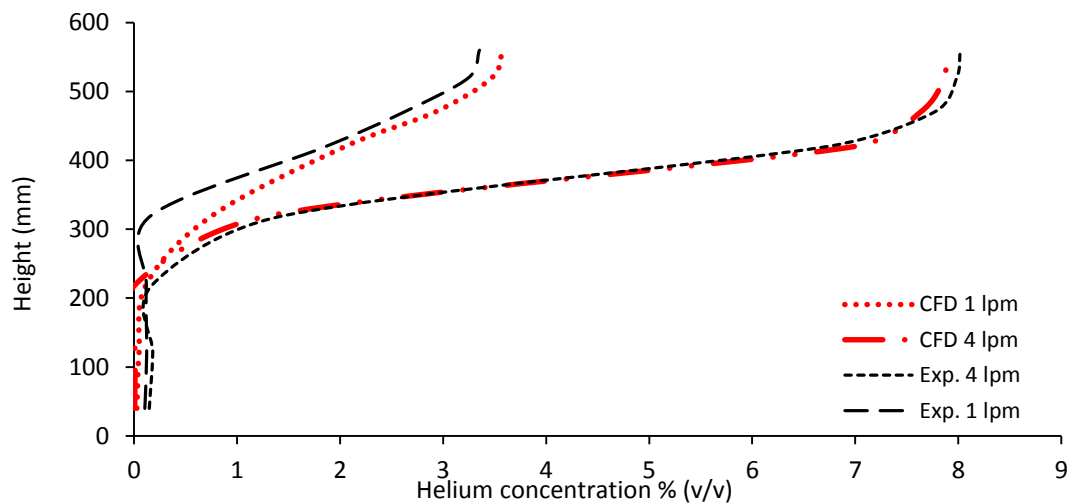
In this test the length of the flue outlet is increased three-fold to see how this effects flow through the enclosure and resultant concentrations. As the flue is horizontal there may not be any net increase in driving force, as occurs with an increase in length with a chimney, so concentrations may remain as in the previous study. Figure 5.58 presents the CFD results for the 330 mm long flue with the 9600 mm<sup>2</sup> inlet. The CFD has predicted an increase in enclosure concentration over the 110 mm flue with the same inlet area (See Figure 5.57 for comparison). This may be due to the CFD seeing the longer flue as having increased flow resistance.



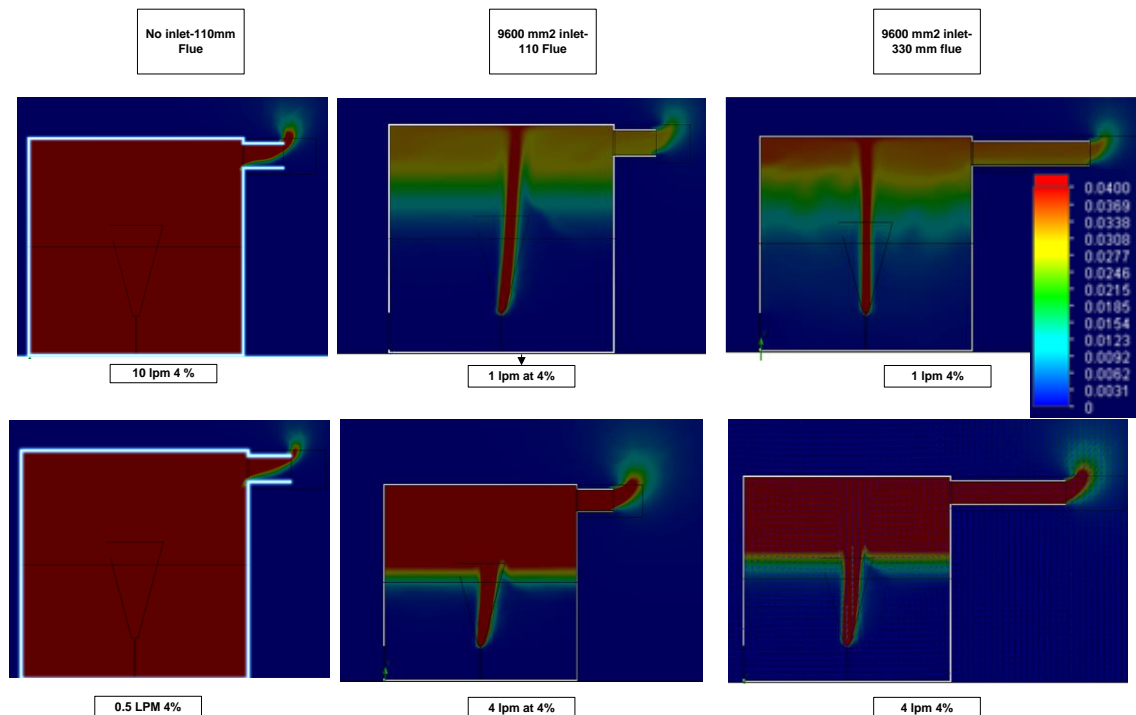
**Figure 5.58 CFD data for the 330mm flue with the 9600 mm<sup>2</sup> inlet**

Figure 5.59 presents a comparison of CFD and experimental data for the 3300 mm straight flue with the 6400 mm<sup>2</sup> inlet. The CFD prediction at 4 lpm correlates extremely well with the experimental data. With the 1 lpm leak rate the CFD has very slightly over predicted

the enclosure concentrations but closely follows the experimental plot. Figure 5.60 presents concentration contour cut-plane images for the no inlet scenario and the 110 mm and 330 mm flues with inlets. The increase in concentration is apparent with the 330 mm flue. In the no inlet images it can be seen that the outflow of buoyant gas appear to be greater than the inflow of air. If this is correct it would accord with the findings by Molkov et al that in a passive ventilation single vent scenario, the neutral plane in the vent opening is lower. A more detailed study would be required to confirm this position.



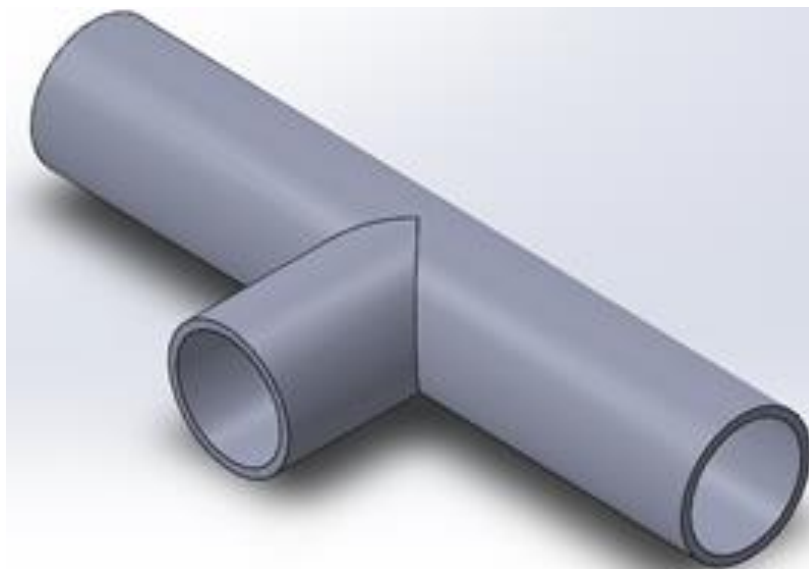
**Figure 5.59 Comparison: CFD and exp. data for 330 mm straight flue/ 6400 mm<sup>2</sup> inlet**



**Figure 5.60 Comparison of flue cut-plane images @ 4% concentration**

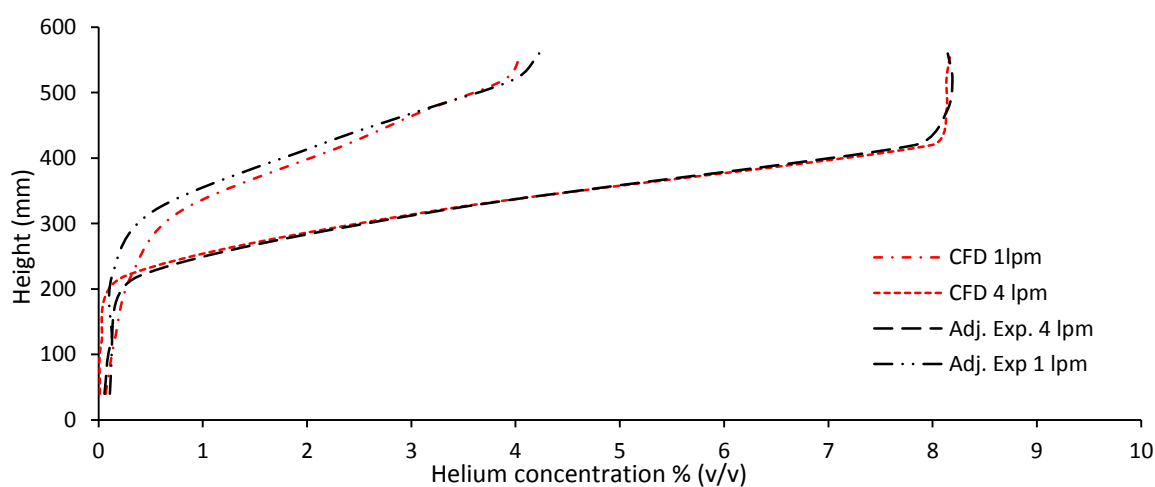
#### 5.7.4 Analysis: Standard enclosure ‘T’ flue with 3200 mm<sup>2</sup> inlet

In this study the 110 mm flue has been fitted with a cross T outlet (figure 5.61), effectively doubling the outlet area. It was seen in the previous section that increasing the inlet area led to an increase in driving force. This test investigates whether a similar phenomenon is apparent if the outlet area is increased and the inlet area remains the same.

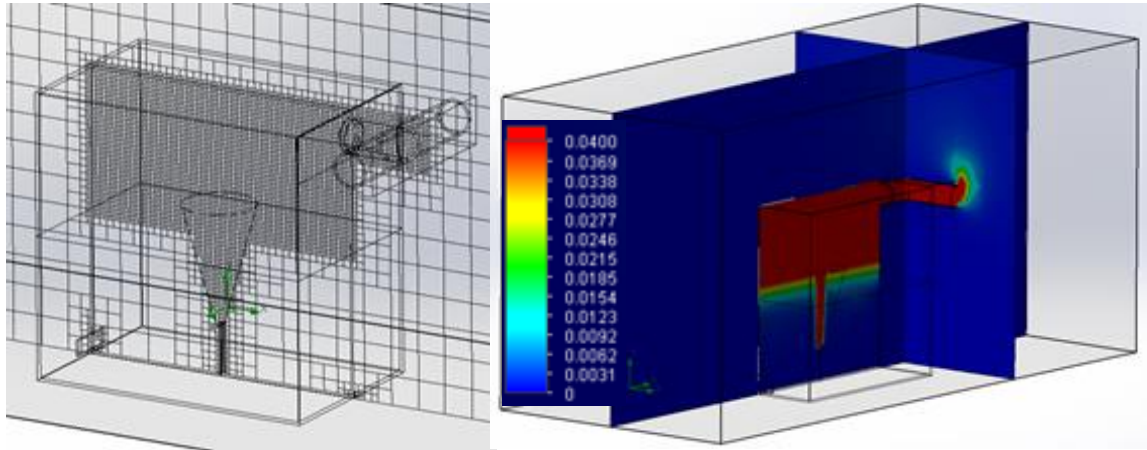


**Figure 5.61 CAD model of the T flue design**

Figure 5.62 presents a comparison of CFD and experimental data for the T flue study at 1 and 4 lpm. The CFD has produced impressive prediction results for this scenario, particularly with the 4lpm leak rate, where the plots are coincident. The 1 lpm plot is also very close and provides an acceptable result. Figure 5.63 presents the meshed CAD model and a cut-plane with trans-section through the T.



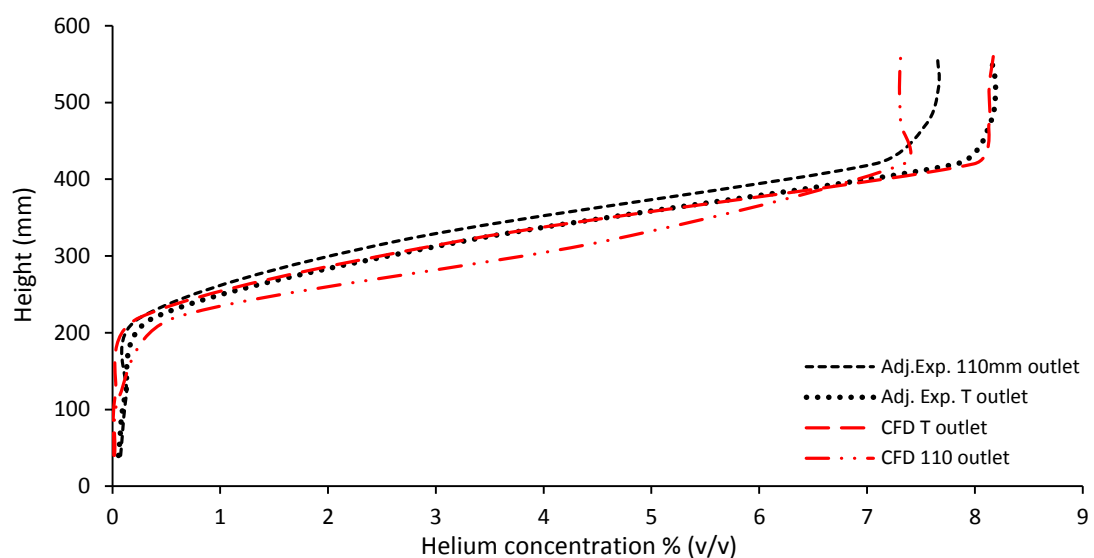
**Figure 5.62 Comparison of experimental and CFD T Flue data at 1 and 4 lpm**



**Figure 5.63 (a) T-Flue meshed CAD model (290,330 cells) (b) Cut-plane 4 lpm @ 4%**

Figure 5.64 presents CFD and adjusted experimental data for the 110 mm flue and T-flue at 4 lpm. It can be seen that the T-flue results have increased the helium concentration in the stratified zone, about 0.5 percent for the empirical data and 1.0 percent for the CFD.

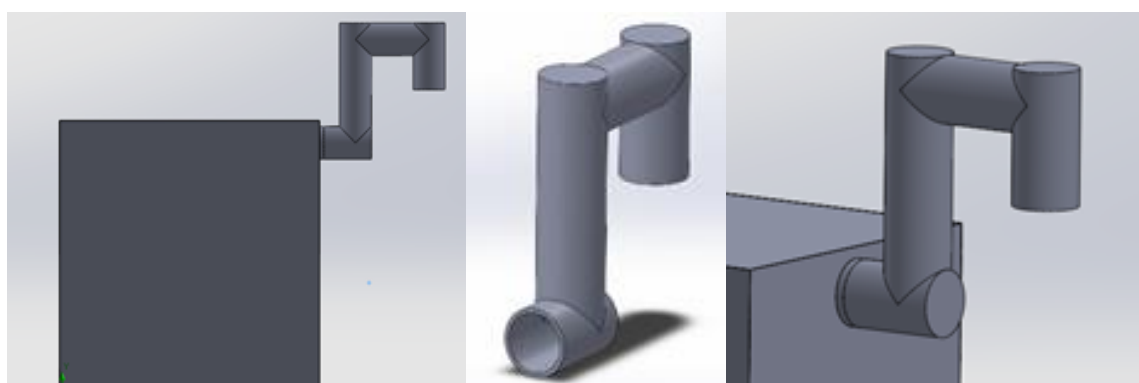
The CFD has correctly identified an increase in flow resistance due to the T-flue design but has under predicted the value for the 110 mm flue. This demonstrates that increasing the outlet area in this way actually impedes effective flow and would not be recommended, without a corresponding increase in inlet vent area. The CFD has performed well in this study and should produce good correlation results.



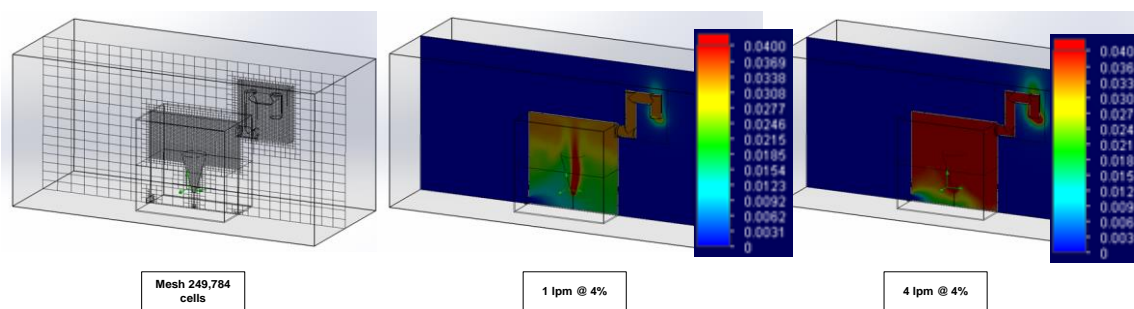
**Figure 5.64 Comparison of 110 mm flue and T flue at 4 lpm leak rate**

### 5.7.5 Analysis: Standard enclosure with snorkel vent [Inverted tubular side flue]

The snorkel flue is designed to take the buoyant gas away from the enclosure, slightly increase the differential pressure and also provide environmental protection. The CAD design is based upon the experimental test snorkel. As such it includes the 90-degree corners and is not a smoothed design. This is deliberate to assess the experimental model. Figure 5.65 presents the snorkel design and enclosure configuration. Figure 5.66 presents the meshed CAD model showing additional refinement around the snorkel and also two cut-plane concentration contours showing flow through the snorkel.



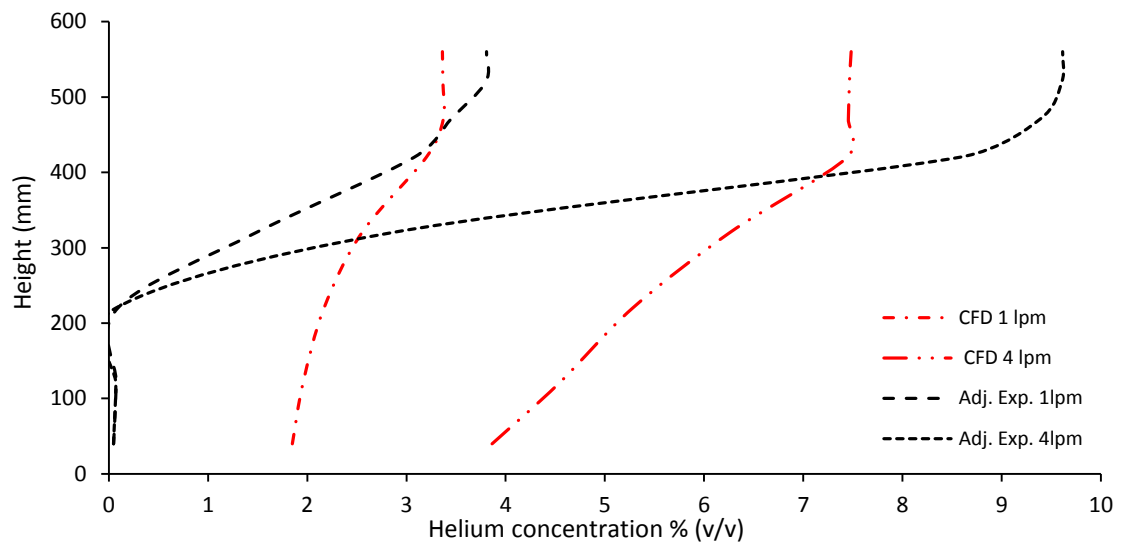
**Figure 5.65 CAD models showing Snorkel design and enclosure configuration**



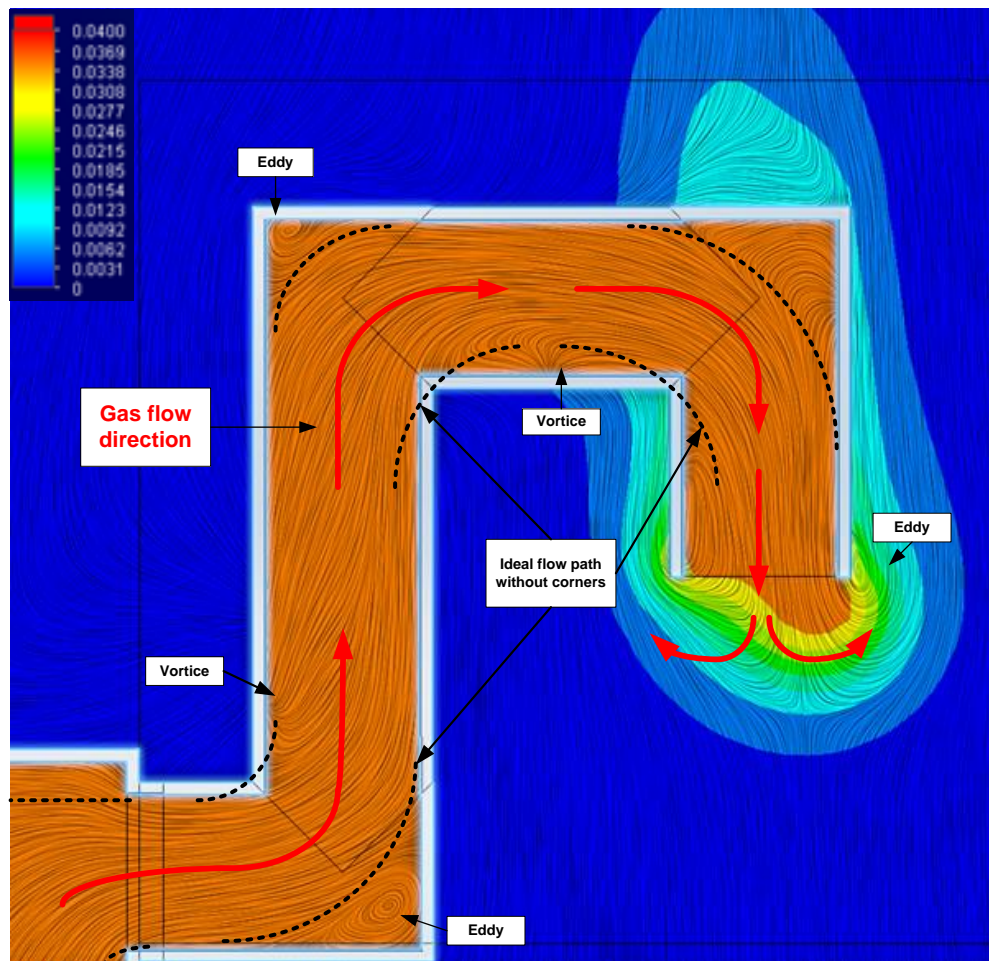
**Figure 5.66 Meshed CAD model and cut-planes at 1 and 4 lpm @ 4 % concentration**

Figure 5.67 presents the adjusted experimental and CFD data at 1 and 4 lpm. The CFD study has produced data that is at variance with the experimental data on this occasion. At 4 lpm it has under predicted the peak concentration by about 1 percent although the depth of the stratified zone is similar. The CFD has though predicted a higher concentration in the lower part of the enclosure. A similar trend is found with the 1 lpm study. The CFD would appear to have struggled with the flue design. Figure 5.68 presents a 2D image of streamlines in the snorkel on a central plane. In the outside corners of the

snorkel can be seen eddies and after the inside corners can be seen vortices. These phenomena all serves as flow resistance mechanisms reducing snorkel performance.



**Figure 5.67 Comparison of experimental and CFD snorkel data at 1 and 4 lpm**



**Figure 5.68 Flow lines in snorkel (2D image on central cut plane)**

The experimental results from the snorkel flue test were not as effective as had been hoped. The flue construction was basic, using available materials, however, its performance was not good. The CFD simulation results have revealed the flow conditions in the snorkel. Smoothing the snorkel construction to minimise eddies and vortices would reduce flow resistance and improve mass flow. Raising the height of the outlet would increase differential pressure and enhance the driving force. Also, as previously noted increasing the inlet area has a positive effect.

## 5.8 Internal obstruction [Simulated fuel cell]

The studies completed so far have used an empty enclosure. This has been to understand flow through the enclosure, bearing in mind that the contents will vary between deployments. Also the nuclear case would see flow through an empty ullage space. That said fuel cell enclosures will house the fuel cell and associated pipework as well as possibly a battery, so it is important to study the effect of internal obstacles which may add complexity to the flow through the enclosure. This study adds a fuel cell sized box attached to the side wall in the upper part of the enclosure (two 110 mm chimney vents).

### 5.8.1 Analysis: Internal obstruction

As with the empirical tests, in the CFD studies where the chimney vents are of equal height, it is not possible to predict which chimney will become an inlet or an outlet (of course if there is a variance in height between the chimneys, the taller chimney will become the outlet, due to lower pressure at the vent opening). Two sensor stack positions are therefore required for data abstraction from the CFD, under each of the chimneys. It can be seen in figures 5.69 and 5.70 that the inlets and outlets have reversed roles. This does not affect the simulation, only the results recovery location.

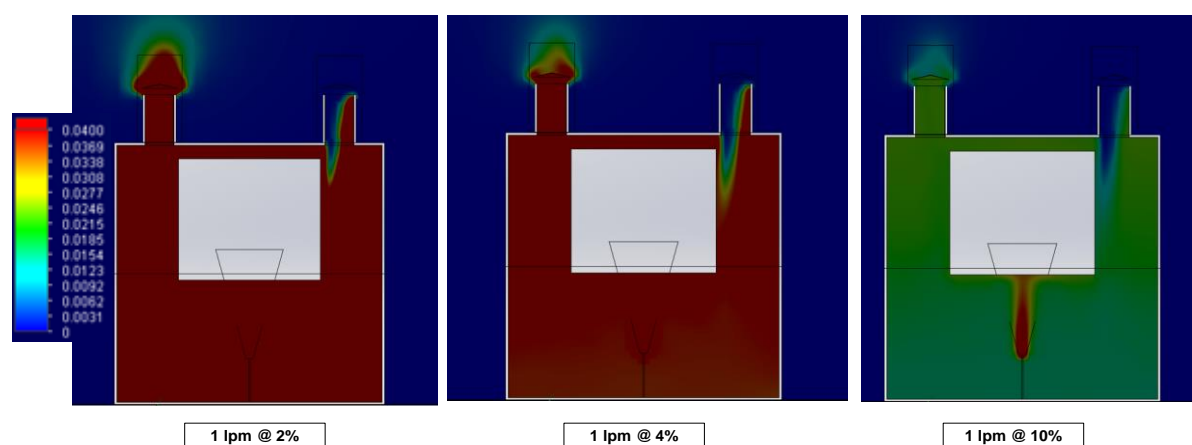


**Figure 5.69** Obstruction test cut-plane images at lpm



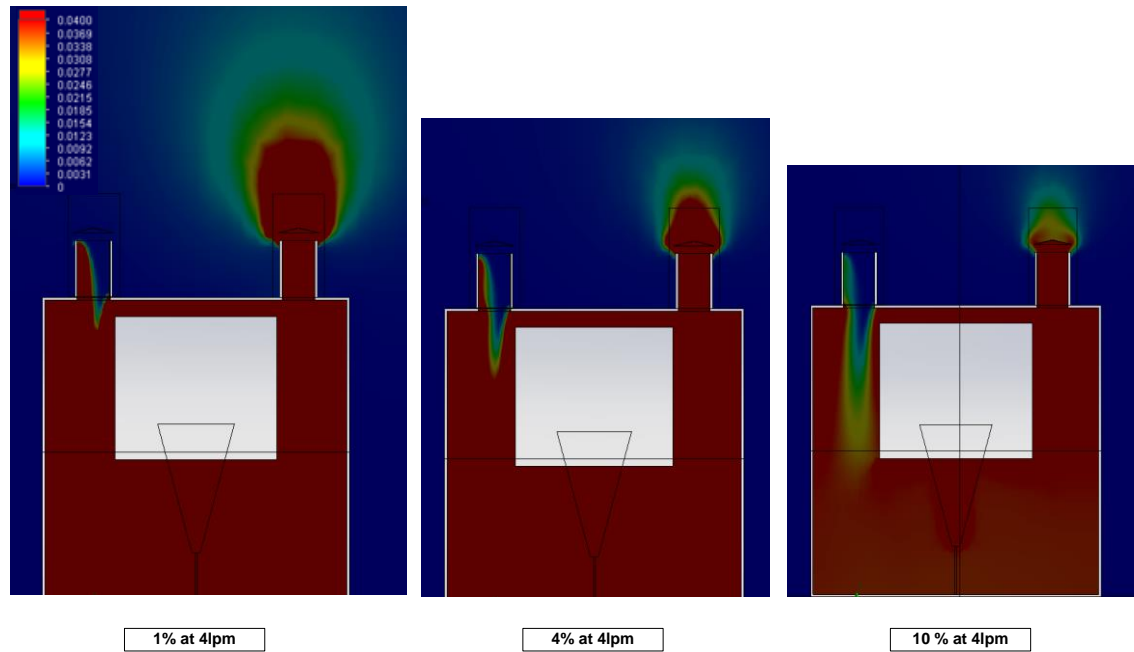


**Figure 5.70 Obstruction tests cut-plane images at 4 lpm**

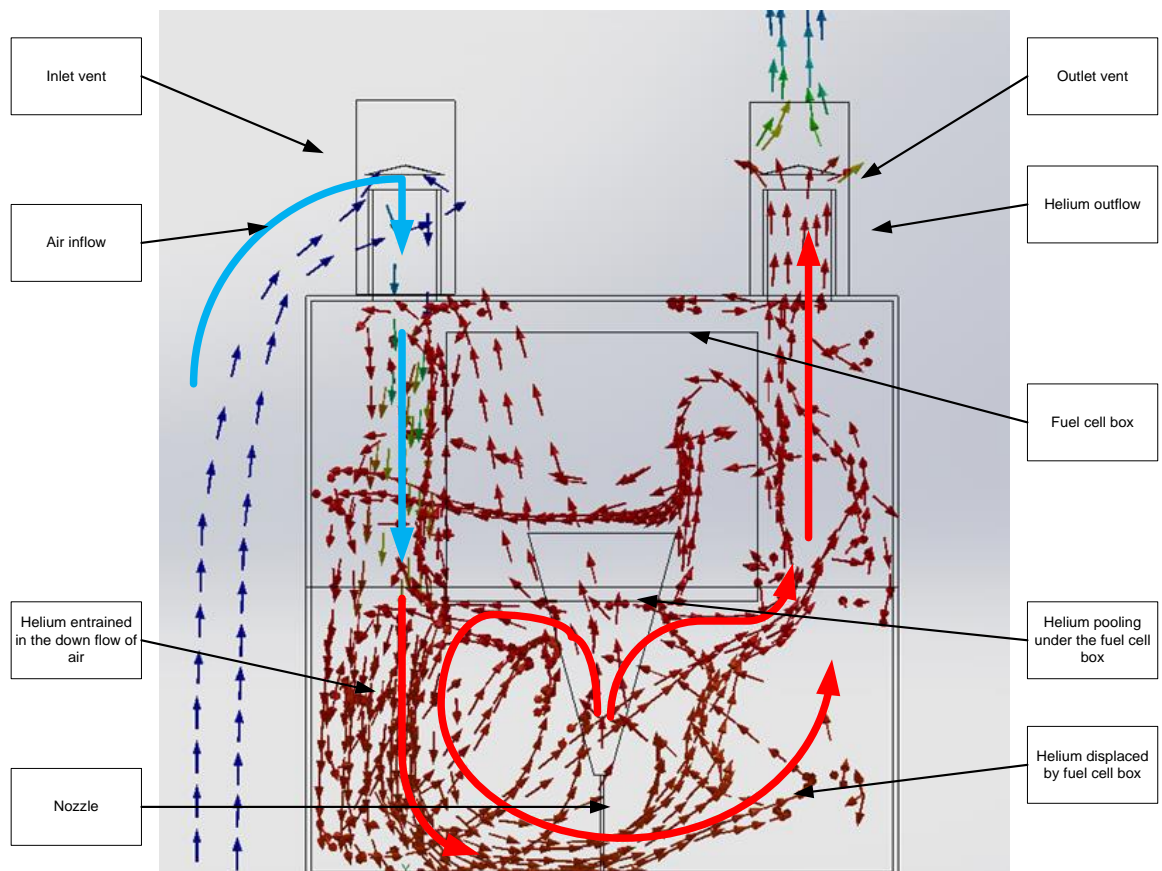


**Figure 5.71 Enclosure with HFC obstruction showing flow paths at 4 lpm**

Figure 5.71 presents a cut plane image with flow vectors. Understandably the flow path is complex. Helium can be seen to return on itself due to hitting the base of the fuel cell and be entrained in the flow of incoming air from the inlet chimney. The flow then travels towards the outlet chimney where it is sucked out into the atmosphere.

Figure 5.72 presents the experimental and CFD data at 1 and 4 lpm. Two sets of CFD data were collected to reflect sensor stack positions under the chimneys. This was necessary in order to identify whether the sensors in the experimental test were adjacent to an inlet or an outlet. The data in figure 5.72 shows this was successful and the experimental sensors were adjacent to the outlet chimney. The CFD has predicted the experimental position in a complex scenario. The two CFD plots adjacent to the inlet are also of interest. The 1 lpm plot actually has lower concentrations recorded from about 300mm height. This reflects the inflow of air through the inlet, which is visible in figure 5.70. With the 4 lpm study there is a slight reduction at the top of the enclosure, again reflecting the incoming air reducing the concentration.

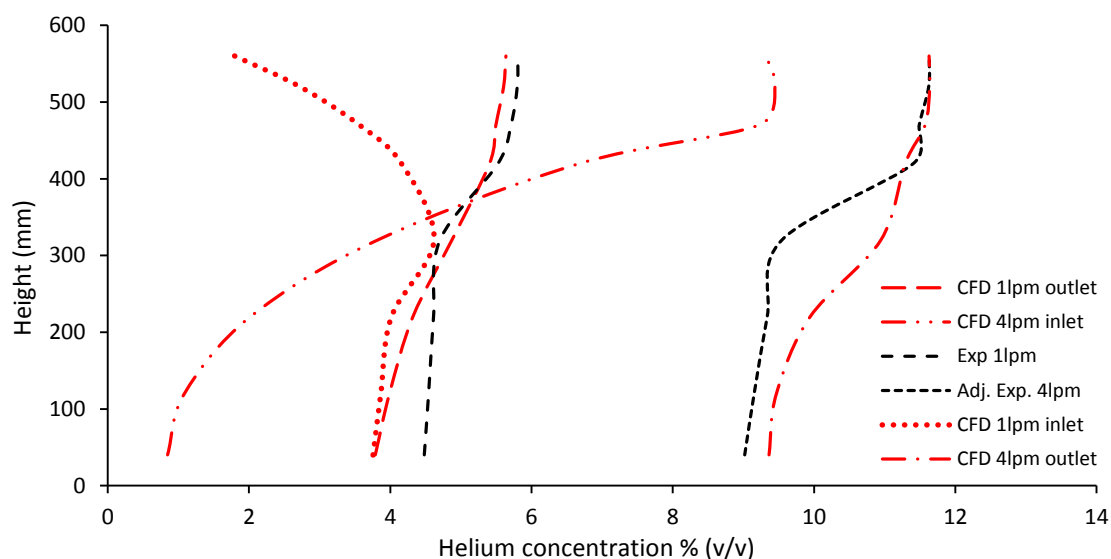


**Figure 5.72 Comparison of experimental and CFD obstruction data at 1 and 4 lpm**

## 5.9 ANSYS: Fluent comparison study

ANSYS: Fluent was used to test the performance of a second commercial CFD software package, applied to a buoyant gas leak small enclosure scenario. The BOC Ltd. base case enclosure with cross-flow upper and lower plain vents was chosen as the comparison model. The Fluent simulation predictions using this model were compared with SolidWorks Flow Simulation prediction and the empirical data. The CAD geometry was

prepared in SolidWorks (Figure 3.36) and the STEP file imported into an ANSYS: Fluid flow (Fluent) analysis system. ANSYS: Space-Claim was used to extract the fluid volume for the calculation in Fluent. ANSYS: Meshing created the mesh (Figure 5.73).

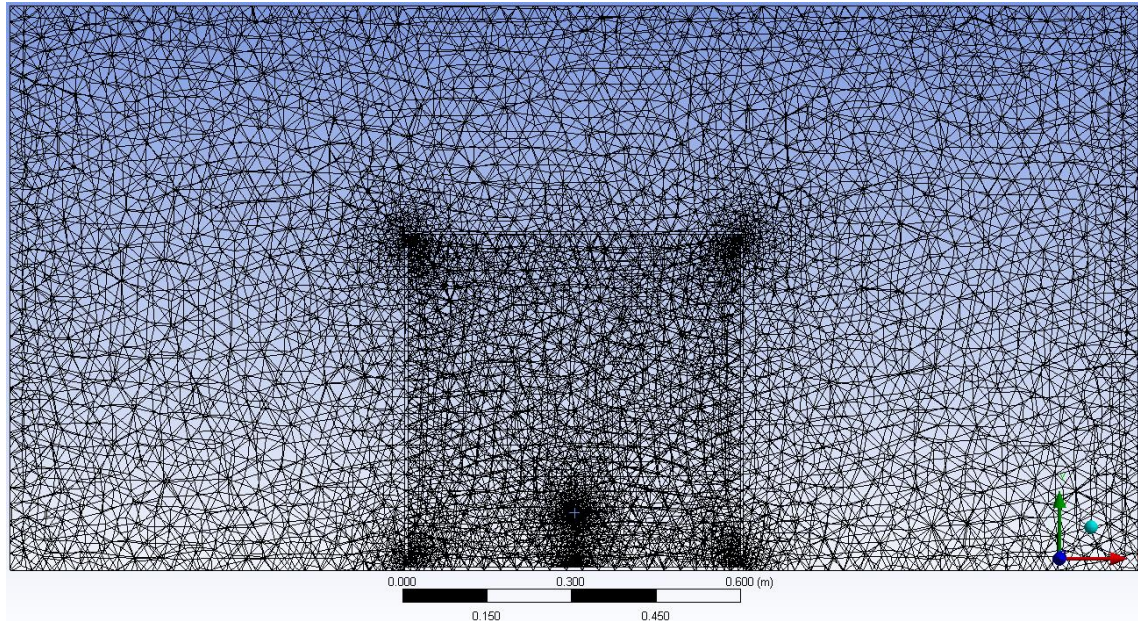


**Figure 5.73 ANSYS: Meshing: Mesh of the computational domain (511363 cells)**

To maximise available computer power and increase mesh density the model was split, and a symmetry plane boundary added. This domain (2m x 1m x 0.5 m) was meshed to 511363 cells. The same operating conditions as used in SolidWorks were used and a leak rate of 4 lpm ( $1.0833 \times 10^{-5}$  kg/s (Fluent)) applied. A range of turbulence model configurations available in Fluent were tested (see Appendix E) to understand how to optimise the model for best performance. The  $k-\varepsilon$  model was focused on for comparison with the SolidWorks predictions; however, a range of LES models was also tested. Simulations were run to steady conditions for the RANS models (transient for LES) and prediction data extracted for the sensor data point position from the experimental study.

Qualitative images provide an insight into how the solver behaved. Figure 5.74 presents a Fluent ( $k-\varepsilon$ , standard, standard wall function, standard buoyancy) model with a contour range up to 4 %. Flow through the enclosure is evident, with the plume and stratification nicely displayed. Of concern though is the helium attached to the side walls, which is unrealistic and highlights the near wall difficulties that can be experienced with some RANS model combinations. In this case the standard model alone has identified flow behaviour from the nozzle but has not been able to deal with near wall turbulence.

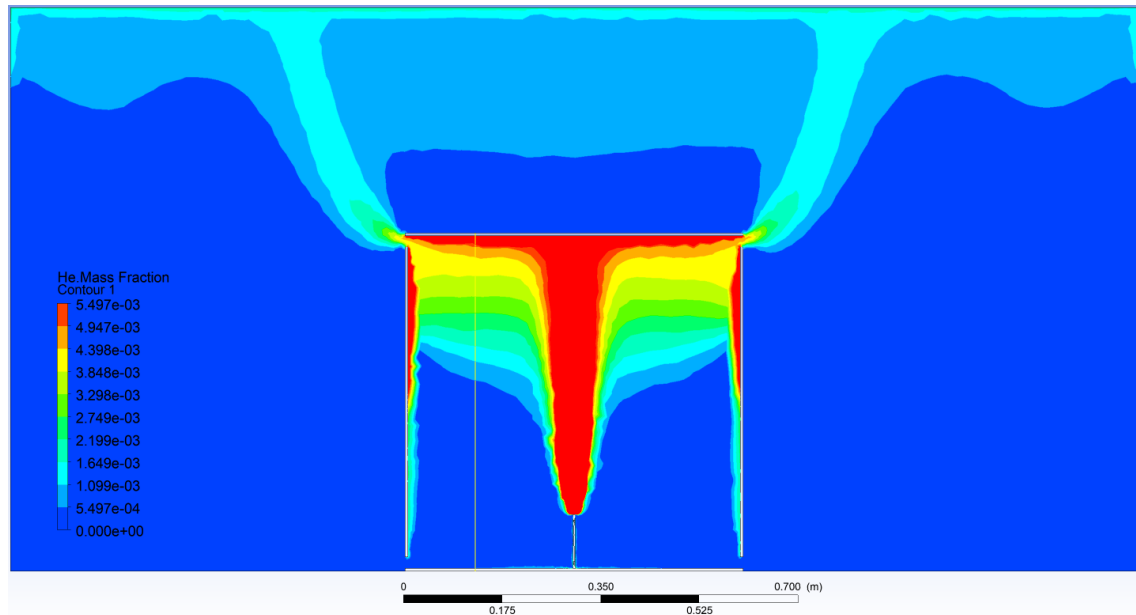


**Figure 5.74 ANSYS: Fluent cut-plane  $k\epsilon$  std., std. wall, std. buoyancy @ 4 lpm**

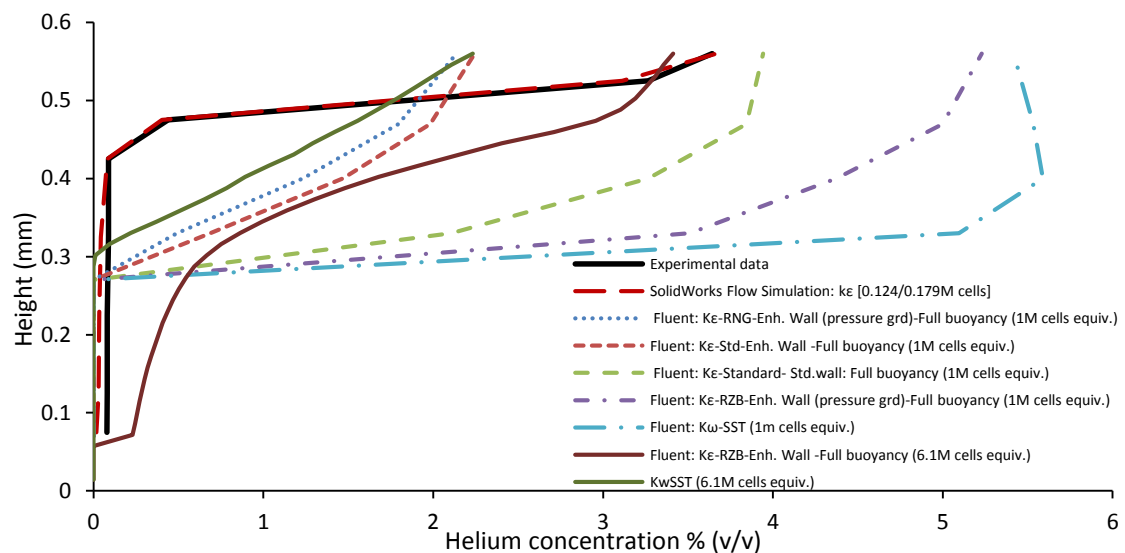


**Figure 5.75 ANSYS: Fluent- simulation predictions (with SW and empirical result)**

Figure 5.75 presents a range of ANSYS: Fluent RANS model predictions. None of the Fluent results presented could be considered a close correlation. The SolidWorks prediction in red has made a very good prediction particularly for stratified depth and peak concentration. All of the Fluent models predict deeper stratification than is present in reality, with two ( $k\epsilon$  RNG-enhanced wall/full buoyancy and  $k\epsilon$  standard-enhanced wall, full buoyancy) significantly under predicting the peak concentration and two ( $k\epsilon$ -Realizable-enhanced wall/full buoyancy and  $k\omega$ -SST) significantly over predicting the peak concentration. The  $k\epsilon$  standard/standard wall/full buoyancy model identifies the

peak concentration, but over predicts the depth of the stratified layer. The predictions show how well the damping functions perform in SolidWorks Flow Simulation (see section 3.9.5 equations 7 -14 for the damping functions and related equations).

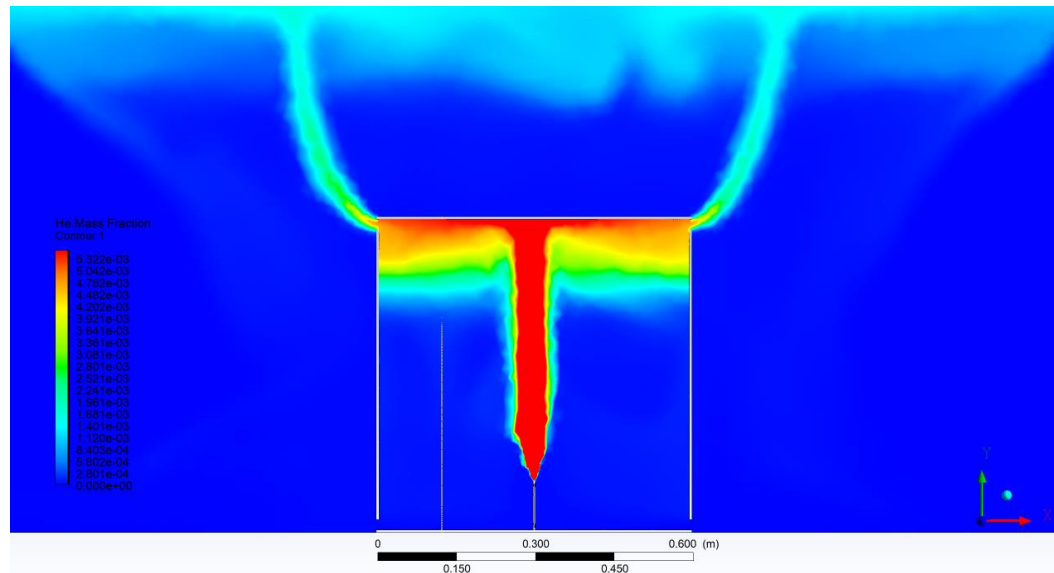


**Figure 5.76 ANSYS: Fluent cut-plane image. 4 lpm leak rate and 4 % range**

Large Eddy Simulation (LES) turbulence models are suitable for wall bounded turbulence conditions. ANSYS: Fluent provides a range of model variations, not available in SolidWorks. Figure 5.76 presents an ANSYS: Fluent cut-plane for a LES (Smagorinski-Lilly) model prediction. The dispersion behaviour is much more as expected, with no apparent wall difficulties. The LES model is known to have some difficulties with the use of a symmetry plane. Versteeg (2007) states the conditions at a symmetry boundary are;

- No flow or scalar flux across the boundary
- Initial normal velocities are set to zero at the symmetry boundary
- Property values outside the domain are equated to the nearest node value inside

Symmetry planes are used with RANS models to reduce computational time and provide reliable results. LES models are not generally used with symmetry planes as conditions imposed on the axis of symmetry alter the instantaneous flow field which is not symmetric across the geometry. Turbulence also is not symmetric and as velocity at the symmetry plane is zero, turbulence intensity will also be zero. In cases where there is no turbulence at the symmetry plane or the axis is not part of the flow, LES may be suitable (Schluter 2001). LES requires a fine mesh and is computationally expensive, but this should not be a major concern for modern computing. Interestingly, despite using a symmetry plane and the conditions noted by Versteeg the LES models tested have produced good

predictions. The small enclosure, dense mesh and symmetrical domain flow may have helped this. Despite the limitations, the result accords well with the experimental data.

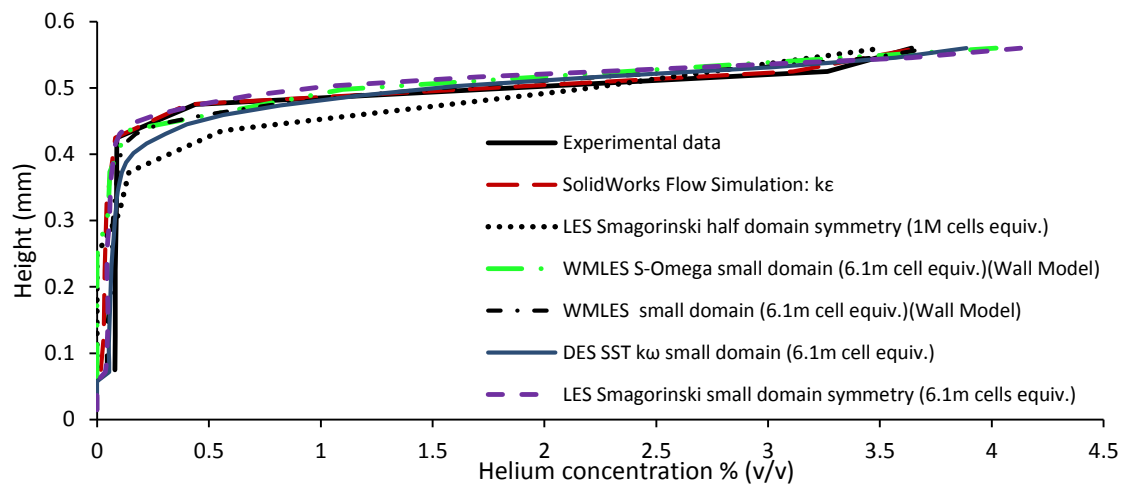


**Figure 5.77 ANSYS: Fluent-LES simulation predictions**

The result in Figure 5.76, was achieved with a domain mesh of 1 million cells. Figure 5.77 presents a range of LES results. The LES (Smagorinski-Lilly-1M cells) result is a close approximation, under predicting the peak concentration and suggesting a slightly thicker stratified layer. The mesh was further refined to a domain equivalent of 6.1 million cells (Figure 5.78.). The graph shows the results of four further predictions, all of which provide excellent correlations with the empirical data. Of particular note is the WMLES model, with the DES (detached eddy simulation) SST  $k-\omega$  and WMLES  $S-\omega$  also predicting well against the empirical dataset. It is interesting to note how well the SolidWorks  $k-\varepsilon$  model with a medium coarse mesh has performed in this simulation against the LES models with highly resolved meshes.

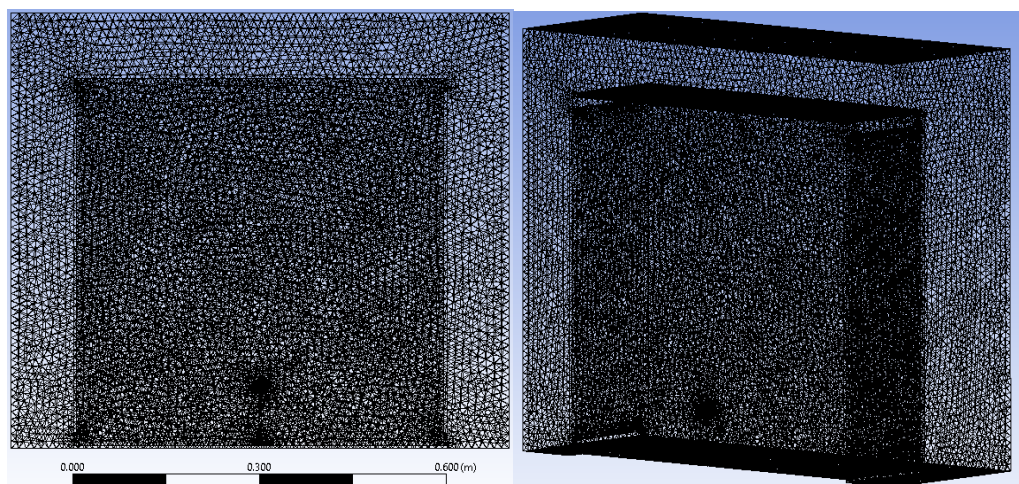


**Figure 5.78 Mesh at 6.1 million cells equivalent-small domain**

An interesting range of results has been produced in this comparison study. It highlights the need for validated cases to produce reliable CFD predictions and further supports the work in this thesis. The LES tests were the best performing. Molkov (2014) in an enclosure test CFD study found that the LES Smagorinsky-Lilly model provided good predictions, as it was able to simulate laminar and turbulent flows in one domain simultaneously, improved further with high CFL (Courant-Freidrich-Lewy) numbers.

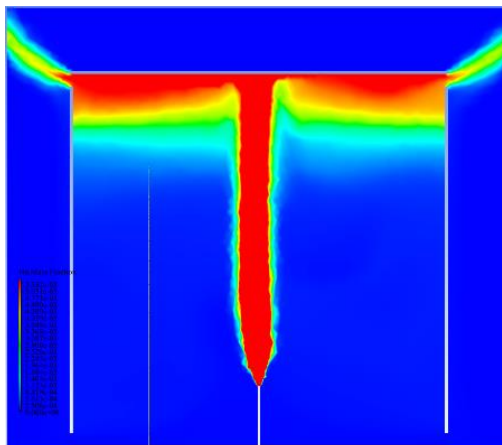


**Figure 5.79 ANSYS: DES cut plane contour image at 4 lpm (4 % conc. range)**

## 5.10 Conclusion

SolidWorks Flow Simulation CFD has been applied across the full range of passive ventilation empirical scenarios, producing very positive results in a number of cases, replicating test results well. The statistical measures detailed in section 6.5 provided the criteria for good agreement between the experimental and CFD results. Flow Simulation is not previously validated for the scenarios tested in this thesis, so the new datasets provide a valuable research resource. The comparison of test and CFD data provides the basis of the validation exercise with chapter six presenting the full correlation analysis. ANSYS: Fluent predictions have been presented to provide a second CFD perspective. A single test scenario was chosen with good Flow Simulation alignment with the test data. The ANSYS RANS model predictions proved inconsistent. Visser (2016) advises using the ‘Full buoyancy option’ with the  $k-\varepsilon$  model, [nuclear containment accident model] as does Toliás et al (2019). ANSYS: Fluent’s LES/DES variant performed well despite the use of a symmetry plane. ANSYS: Fluent’s range of models is advantageous if prior validation information is available, so that the correct settings can be chosen. The shortcomings of the  $k-\varepsilon$  predictions in Fluent demonstrate how effective the adaptations made (damping functions) to the model in SolidWorks are.

## Chapter 6 Discussion

### 6.0 Introduction

The use of hydrogen as an alternative energy source to fossil fuels is growing. It is used to power buses, vessels, cars, provide electricity to commercial buildings and domestic heat and power through CHP units. It is being added to natural gas in the gas grid, in trial areas in the UK, to provide cleaner domestic gas (Dodds et al 2013). Up to 20 % hydrogen is being added to the gas grid without the need to change domestic gas burners (Christopher et al 2018). The national gas grid is also a potential energy store for hydrogen, holding three times the energy of the power grid. Safe hydrogen venting is relevant to all of these applications.

When not being combusted for heat it can be used in a fuel cell to produce electricity and in some cases useable heat. A significant infrastructure is required to enable the growth of hydrogen as a source of energy, including its production, storage and transportation. Hydrogen's wide flammable range makes this a challenging endeavour, with safety a paramount consideration. Continued research and development is required in all of these areas to ensure that hydrogen can make a significant contribution to the growing global demand for energy and enable a reduction in fossil fuel dependence.

Small static fuel cells are housed in ventilated enclosures to protect the fuel cell, electronics and supply pipework. The ventilation manages temperature but will also need to displace any hydrogen that leaks from the system. Aside from catastrophic system failure of the hydrogen supply, extensively documented in the literature, which quickly releases a substantial volume of hydrogen, the more likely release scenario into a fuel cell enclosure is a low-level leak of hydrogen into the enclosure from a degraded supply component or the fuel cell itself. Such a leak will be at a low release rate, less than 10 lpm. Static fuel cells vary in size and power output, from large commercial MW installations to small kW and sub kW units. This thesis considers hydrogen safety in a sub kilowatt unit and its 0.144 m<sup>3</sup> enclosure.

Low leak rates into enclosures have not been widely tested in the literature and are worthy of investigation to assess the enclosure conditions that lead to explosive mixtures being attained. Such releases in confinement are also of interest in the nuclear industry, where



hydrogen producing waste is stored in boxes, which are then stacked in a waste store. The hydrogen produced diffuses through filters on the box lid and out via the narrow channel formed between the lid of the box and the bottom of the box located above it in the stack. This hydrogen is passively ventilated to remove it from the stack to ensure that flammable mixtures are not formed in the small confined spaces. The passive removal forces in operation in nuclear scenarios are the same as those found in small passively ventilated fuel cell enclosures (buoyancy, diffusion and convection), so the findings are of interest to both industries.

A series of empirical tests was undertaken in this research investigation to understand the passive ventilation performance of a 0.144 m<sup>3</sup> small fuel cell enclosure subject to a variety of passive ventilation schemes. This size was chosen as it meets the specification of the BOC Ltd. small fuel cell environmental enclosure. The simplicity of the enclosure design and test rig facilitated its adaption for the ventilation scenarios tested allowing the assessment of hydrogen safety parameters.

*Passive ventilation* describes the displacement of a buoyant gas leaking in air in a confined space such as a fuel cell enclosure, through density difference. The presence of the buoyant gas (e.g. hydrogen) changes the ventilation dynamics from those experienced with *natural ventilation* which involves only air with wind and convection the driving forces. For example, an electronics enclosure with a natural ventilation scheme for thermal management may not be suitable to house a fuel cell. A hydrogen leak in such an enclosure would change the flow dynamics at the vents as described in section 2.3 and could lead to flammable mixtures forming. The below research hypothesis was stated in chapter one on the basis that empirical tests will reveal leak rate levels that lead to the LFL being attained for passive ventilation scenarios.

***Research Hypothesis:*** *Safe, passive ventilation parameters can be determined that will manage hydrogen concentrations below the lower flammable limit, for hydrogen leak rates at or below 10 litres per minute in a passively ventilated 0.144 m<sup>3</sup> hydrogen fuel cell enclosure*

The empirical data sets have provided safety limits for the scenarios and leak ranges tested. The safety range varies with scenario, but in most cases a flammable mixture can

be attained in the enclosure at leak rates below 10 lpm. This is a design concern for small enclosures. The obvious passive solution is to enlarge the openings to increase air mass flow through the enclosure, but this can create other problems, such as exposure to environmental elements, requiring additional measures such as grills and wind stops, which can impede air flow or lead to flow reversal, potentially trapping pockets of hydrogen in the enclosure. With unit cost a major economic consideration for fuel cell manufacturers, design simplicity is important. Each installation will have its own particular requirements and the enclosure will need to be adaptable. For this reason a range of vents were tested, as it may be necessary to mix and match opening types to optimise the flow. The investigation using SolidWorks Flow Simulation CFD has proven helpful in demonstrating its predictive capabilities and further development will allow it to be used in CAE/CAM design processes to reduce production costs.

The empirical data documented in chapter four provides the data sets for the passive ventilation scenarios tested in this research. Chapter five documents the outcome of a series of SolidWorks Flow Simulation CFD exercises, based upon the experimental tests. This work provided a further set of data for comparison with the experimental data to verify how well the SolidWorks Flow Simulation CFD was predicting test outcomes.

This chapter critically discusses the effectiveness of the passive ventilation systems applied to the 0.144 m<sup>3</sup> at managing internal buoyant gas concentrations. It also considers the outcomes of the CFD studies. The results of analytical tests applied to the empirical and CFD data sets is presented with consideration on whether support can be given to CFD model validation. Also discussed are the effect of dynamic enclosure factors such as buoyancy, leak rate, diffusion, airflow and the neutral pressure level. It draws together the thesis findings and presents safety design parameters, as tested, for the BOC Ltd. enclosure that provide hydrogen concentrations below the LFL.

### **6.1 Small enclosure test performance**

Small fuel cell enclosures will vary in dimensions depending upon the size of the fuel cell and whether or not it additionally needs to house a battery, supplementary electronics, a hydrogen cylinder and the supply pipework. The enclosure location is also important. If housed inside a building, additional ventilation considerations are required for the internal building space. If located outside, environmental factors, become important such as,

- Wind (affecting ventilation flow through the enclosure)
- Rain (water ingress leading to electronics malfunction/corrosion)
- Solar radiation (heating the steel enclosure, increasing internal convective forces)
- Insects and animals (nesting, chewing wires/pipes, blocking vents)
- Foliage (blocking vents)
- Proximity to buildings (influence on external air flow, eddies and vortices)

This thesis has focused on a fixed size enclosure, informed by the design of the BOC Ltd. Hymera enclosure. This enclosure was designed with a cross-flow displacement ventilation scheme in mind, having opposed upper and lower vents. This is a fairly standard configuration for heat management in electrical enclosures and provides an off the shelf solution for the Hymera containment. For product certification though the enclosure must be shown to not only manage thermal output but also be effective at displacing any hydrogen from a low-level leak inside the enclosure. The empirical testing was designed to determine the capability of the enclosure, albeit using helium as a safe analogue for hydrogen in the laboratory.

As real enclosures will be deployed in a range of situations requiring adaptations to the ventilation scheme applied, a range of designs were tested. All ventilation schemes tested had the ability to displace the leaking helium from the enclosure and achieve a steady state condition for gas concentration. Testing established that the key factors determining the helium concentration reached were the helium leak rate and the vent opening area size. This is because the leak rate determines the amount of gas released into the enclosure and the vent area and its resistance determines the volume of air that can flow through the enclosure to entrain and displace the buoyant gas. As previously explained, it is important to manage down the vent opening area and this is in the control of the designer. The rate at which gas will leak in a real scenario is not foreseeable, but the enclosure can be designed to a leak rate limit by specifying appropriate ventilation opening sizes, for certification purposes. Figure 6.1 shows the leak rates at which the hydrogen LFL was achieved for selected tested scenarios. Comparisons were made for tests where designs with similar vent opening areas were used. Due to the constraints of the available equipment these areas are not identical but are sufficiently close for comparison.

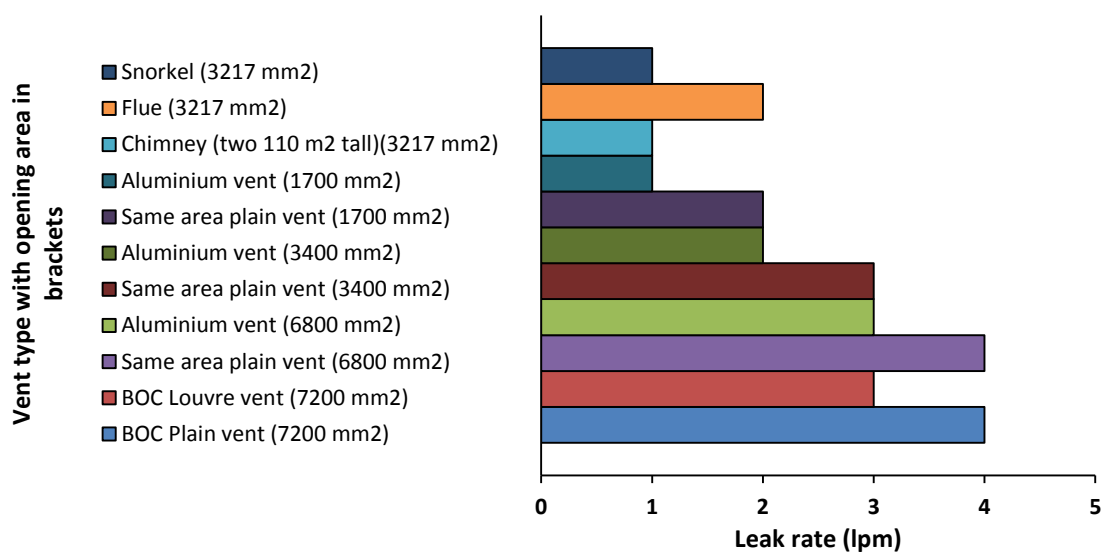


**Figure 6.1 leak rate hydrogen LFL (4%) was achieved for selected scenarios**

In the empirical tests a variety of vent opening sizes were used to determine the LFL limits. Figure 6.1 shows that the aluminium louvre and same area plain vent tests (6800 mm<sup>2</sup>) and the BOC Ltd. simple louvre and plain vent tests (7200 mm<sup>2</sup>) had the same LFL limits. The vent opening areas were similar, however wall position and vent shape was different. Comparing these two scenarios, it would appear that comparable vent areas in a cross flow scheme have created similar mass air flow through the enclosure achieving the same LFL limits.

The chimney, flu and snorkel scenarios used pipes with a 3217 mm<sup>2</sup> circular opening area. The flue and snorkel scenarios used an opposing plain vent of similar area. When compared to the 3400 mm<sup>2</sup> plain vent and aluminium vent scenarios, the pipe scenarios perform less well. However, there are four vents in these scenarios, so the opening area is twice that of the piped vent scenarios. When comparing the piped scenarios with the 1700 mm<sup>2</sup> plain and aluminium vents, the limits are closer. Although the tested regimes are different, the inference is that if the ventilation opportunity is the same in a displacement scenario, air displacement will take place at similar rates and the leak rate limits will be similar.

Mixing ventilation scenarios have also been tested. The initial test rig (section 5.1) was approximately 50% larger than the BOC Ltd. design and used a mixing ventilation regime with four variations of top vent openings. This replicates a condition where lower vents

may have become blocked. Figure 6.2 shows the leak rate at which the LFL was achieved for each scenario. As the number of vents increased so too did the leak rate required to attain the LFL by 1 lpm each time. This is due to the increase in air inflow at each stage.

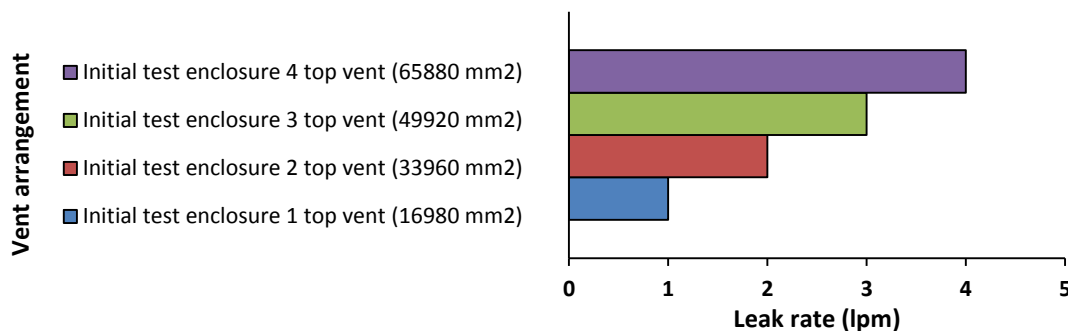


**Figure 6.2 Leak rate at which hydrogen LFL (4%) was achieved with initial test rig**

The area of each vent used on the initial test rig was larger (16890 mm<sup>2</sup>) than those used on the BOC Ltd. enclosure test rig scenarios. With mixing ventilation the vent effectively splits horizontally into two, the upper half being an outlet and the lower half an inlet (the position of the split will vary according to the buoyant gas concentration (see figure 2.21). The closest comparison with a crossflow test is the BOC Ltd. enclosure with two top and two bottom vents (7200 mm<sup>2</sup>) and the two top vent initial rig with mixing ventilation. For the crossflow test the total inlet and outlet size is 14400 mm<sup>2</sup>, whereas for the initial rig it is 16980 mm<sup>2</sup>. With the mixing regime, the LFL was achieved at 2 lpm and with the BOC Ltd. crossflow rig at 4 lpm. This suggests the crossflow is the more effective regime, albeit the enclosures were of different volumes.

A further safety consideration is the time that it could take for a flammable mixture to form after a leak has started in the enclosure. Hydrogen leaks can develop and worsen over a period of time, so the time that it can take to achieve a flammable mixture could be a crucial factor in explosion prevention. The tested scenarios have shown that it can take a relatively short time to reach the LFL in the enclosure. The effectiveness of any warning or shut down sensors used in a real fuel cell enclosure deployment is therefore very important. A number of scenarios have been studied in this investigation. It would be of interest to identify any differences in the time taken to achieve the LFL between a displacement and a mixing ventilation scheme. Figure 6.3 presents two plots of concentration against time at 5 lpm. One is for the initial test rig with a two top vent

mixing ventilation scheme and the other for the BOC Ltd. cross flow displacement ventilation scheme. The two schemes had comparable vent opening areas and the data is taken from the uppermost sensor close to the edge of the enclosure.

The displacement scheme sees the concentration rise quickly and settle to a steady state value just under 5 %. The LFL is achieved after about seven minutes. The mixing regime sees the concentration rise more slowly and achieve a steady state concentration of about 7 %, taking about twelve minutes to reach the LFL. This accords with the research findings that displacement ventilation is more effective than mixing ventilation at managing buoyant gas concentrations. That said, both schemes achieve 5 % at about the same time. Interestingly the LFL is reached more quickly with the displacement scheme possibly due to the upward air flow facilitating the creation of the concentrated top layer.

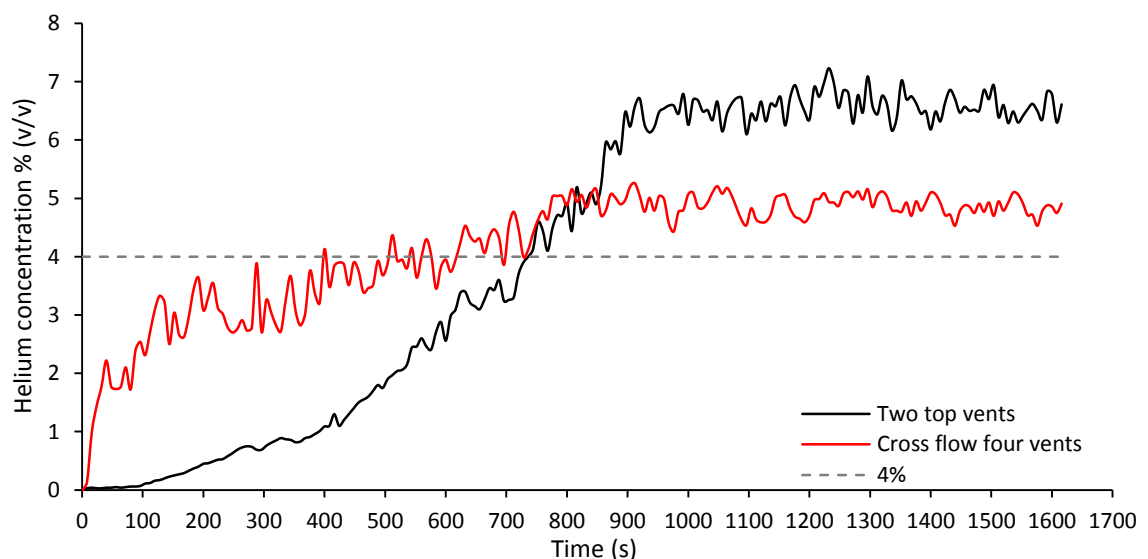


**Figure 6.3 Initial encl. mixing ventilation @ 5 lpm compared with BOC Ltd. encl. displacement ventilation @ 5 lpm: Conc. against time [highest sensor position]**

This is so particularly where there is air flow from a vent low down in the enclosure to one near the top. The leak is entrained in the air flow path and buoyant gas that does not immediately leave forms a stratified layer at the top of the enclosure. With mixing ventilation with high level vents, the dense air has to pour into the enclosure, travelling downwards whilst mixing with buoyant gas it meets. The flow path is not as defined as with displacement ventilation and this leads to a delay in achieving a steady state position. The entire volume of the enclosure becomes mixed, whereas with displacement schemes

this is not necessary as the flow is upwards and out, not just for the air flow, but the buoyant gas too. Also, with the displacement scheme the high concentration region is confined to the plume and the stratified layer at the top. With mixing ventilation the concentration is more uniform throughout the enclosure.

Small passively ventilated enclosure performance relates to its ability to manage internal buoyant gas concentrations below the LFL. The factors affecting performance are enclosure volume, ventilation scheme, ventilation opening area, whether the enclosure is inside a building or environmentally sited and the buoyant gas leak rate. These are all factors that can be influenced by the design engineer to optimise safety and reduce risk.

## **6.2 Passive ventilation performance**

Natural ventilation using environmental driving forces has been evident in building design for thousands of years. It is very effective at moving volumes of air through a space and is well suited to enclosure applications. As already discussed (section 2.3), passive ventilation in this field relates to the presence of a buoyant gas in the natural ventilation air flow adding a further driving force and factor to consider.

The buoyant nature of hydrogen is a positive factor as flow will be upwards, which should aid dispersal from the enclosure. As vents are generally vertically mounted on the side of the enclosure and not the roof, the flow path is not directly upwards and this is where the ventilation airflow helps to entrain the gas and direct it out. The position size and design of the vents determines how effective this flow is and the level of stratification that occurs at the top of the enclosure.

The two possible regimes of passive ventilation observed, displacement and mixing have both been studied in this thesis. Mixing ventilation is not an effective hydrogen venting safety solution. Having only top ventilation openings mounted on the side of the enclosure allows the dense air to pour into the enclosure and mix with the buoyant gas. There is no air flow entrainment helping to direct the gas out of the enclosure. The leaking gas will use its buoyancy to rise and leave through the high-level vents. There will be low level displacement as mixing occurs, which will reduce as the contents become more mixed.

The neutral pressure line position (see section 2.3) at the vent serves to limit two-way flow. The higher the leak rate, the less air will enter the enclosure. At the low-level leak rates dealt with in this thesis a buoyant gas/air mixture will form in the enclosure and remain at a steady level for the duration of the leak. This mixture could well be at a level in excess of the LFL. The studies have also shown that mixing regimes take longer to achieve steady state than displacement regimes and longer to disperse once the leak stops.

Displacement ventilation with vents vertically as far apart, horizontally as wide as feasible and sufficiently large to allow good volume air flow through the enclosure, is generally a more effective solution for buoyant gas management. However, it is still important to understand the effect of mixing ventilation on enclosure concentrations, as a displacement ventilation scheme could become a mixing ventilation scheme if a lower vent became blocked. The empirical tests have shown that stratified layers do form at the top of the enclosure in displacement ventilation tests and this is the area where gas concentrations can build. To study this aspect of behaviour a variety of vent designs were added to the enclosure. This was useful as enclosure installations may require alternative venting options to be considered, but still be effective. Vent arrangements tested included;

- Plain rectangular vents (vertically mounted)
- Louvre rectangular vents (vertically mounted)
- Flues and snorkel pipes (horizontal flues mounted on the vertical face)
- Chimney pipe vents (roof mounted)

All of the displacement regimes tested were effective at managing internal stratified concentrations, but only up to specific leak levels. Unless the vents are made extremely large, the LFL will be breached above 4 lpm in most regimes. The BOC Ltd. standard enclosure with plain vents just exceeds the LFL at 4 lpm with a vent opening size of 7200 mm<sup>2</sup> (28800 mm<sup>2</sup> total vent area). Twenty five percent of the LFL (1 %) is the safety ideal in many cases which would limit the design leak rate to a very low level. Figure 6.4 presents a plot of total enclosure vent area against peak helium concentration recorded for plain and louvre vent displacement ventilation tests at 4 lpm. With the exception of one large plain vent test, all breach the 4 % level. A total vent area exceeding 40,000 mm<sup>2</sup> would be required to be confident of not creating a flammable mixture at 4 lpm.



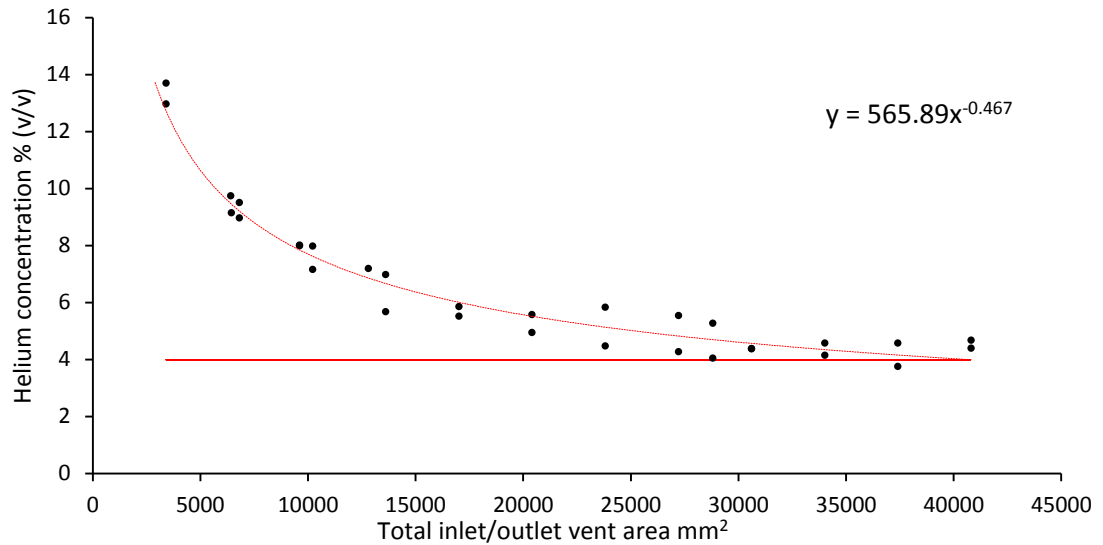


**Figure 6.4 Scatter plot: Total vent area vs peak conc. at 4 lpm for plain and louvre vents**

Figure 6.5 plots total vent area against peak helium concentration for non-louvre displacement tests, louvre tests and the mixing ventilation test. Although the mixing ventilation test had a larger internal volume, which should be accounted for, higher concentrations have been recorded than for the displacement tests. The plain and louvre tests have been separated out and the louvre concentrations can be seen to be slightly higher than for plain vents. The trend lines suggest that much larger total vent areas would be required if a design limit of 1 % were chosen.

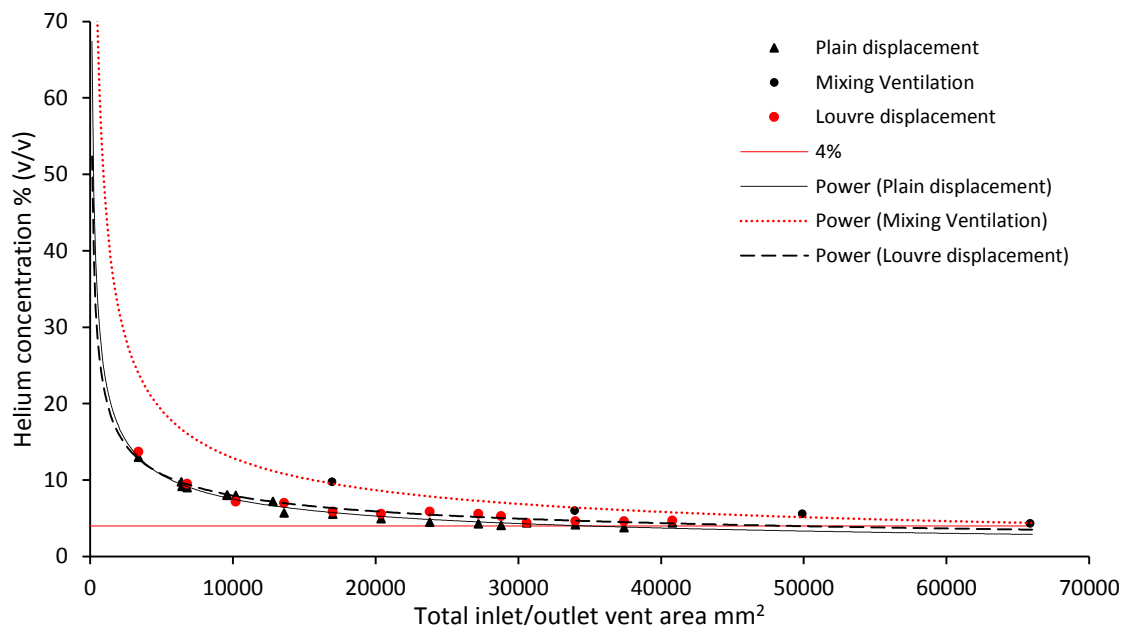


**Figure 6.5 Scatter plot: Vent area vs. peak concentration for three regimes at 4 lpm**

Figure 6.6 presents plots of the rectangular central plain vents and the BOC Ltd. wide vents at the 28800 mm<sup>2</sup> total vent area position. It confirms that the LFL is only achieved

at or below 4 lpm with 40800 mm<sup>2</sup> total vent area. None achieve 25% of the LFL. The BOC Ltd. wide vents (shown as circles at the 28800 position) do perform better than the centrally positioned rectangular plain vents. This is because the wide vents were positioned at the farthest points away from each other, maximising the air pressure driving force. Also, the vents were across the width of the enclosure allowing gas to escape across the width, as opposed to a smaller cross section in the middle of the end panel and also the vent abutted the roof panel, so the more concentrated stratified mixture at the top of the enclosure had a more direct route out, with less flow resistance.

Figure 6.6 demonstrates that the wide vents are better performers. 4 lpm is still the maximum leak rate for the LFL. Leak rates at 1 or 2 lpm would satisfy the 25% of the LFL requirement though. This analysis reveals the influence of vent position and shape. It also links the total vent area and the maximum leak rate that will not breach the LFL or preferably the 25% of the LFL point. The design leak rate for the BOC Ltd. enclosure would need to be reduced to at least 2 lpm with enlarged vents. This would allow for louvres to be applied and still keep within the leak rate limit.

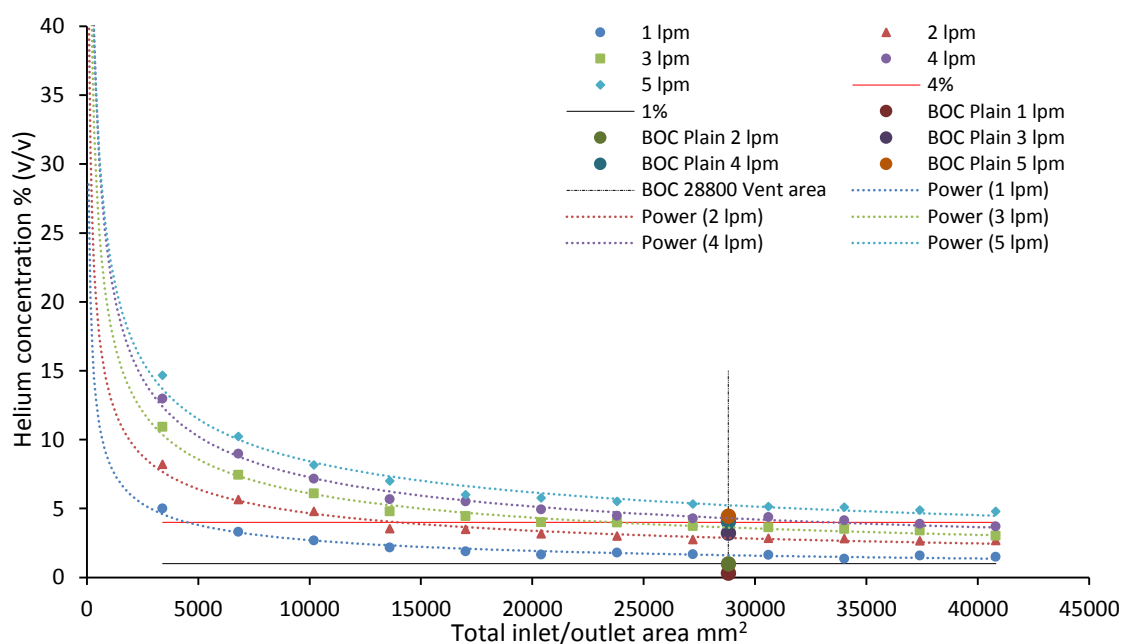


**Figure 6.6 Total vent area vs peak concentration for the rectangular plain vents with BOC wide plain vents overlaid; leak rates from 1 to 5 lpm.**

The chimney vents tested had a relatively small diameter (3216 mm<sup>2</sup>) and breached the LFL at 1 lpm. Increasing the height of the chimney improved its performance. A significantly wider chimney in conjunction with a low level plain or louvre vent should

produce a significant performance improvement. It would allow larger volumes of gas to flow upwards and out of the enclosure. It is of concern that the standard unmodified enclosure would need a design leak rate not exceeding 2 lpm, to be within 25 % of the LFL, which has an impact upon adaptations that increase flow resistance.

### **6.3 Safety guidance**

Small fuel cell enclosures of the type tested in this investigation are made commercially of thin wall pressed steel. The enclosures are robust, but lightweight. However, if an explosion were to occur within the enclosure the pressed and spot-welded construction may not hold together leading to fragments being scattered in the vicinity. It is therefore essential that the enclosure design provides adequate passive ventilation flow to dilute any leakage and mitigate the chance of a flammable mixture forming.

Swain and Swain in their works of 1992 and 1996 suggest that small hydrogen leaks are so buoyant that they are likely to disperse with minimal flammable volumes being formed even with enclosed passively ventilated conditions. This does though fail to consider the behaviour of a buoyant gas in confinement where a passive displacement ventilation scheme has been shown to result in a stratified condition with a high-level concentrated mixture. Although Swain and Swain are correct that hydrogen will readily disperse upwards, it does not account for hydrogen's behaviour in confinement, which with the advent of the hydrogen economy is a hydrogen safety research area. This thesis has shown that the LFL can be breached in passive ventilation conditions with low level leaks.

A further safety concern is the external buoyant plume emerging from the upper vents of the enclosure. It was recognised (ICI 1972) that where hydrogen is vented and able to mix with air, an ignition will occur at some point. There is the potential for hazardous areas to form around the vent exit (Long 1963) and as tests in this thesis have shown, a plume containing hydrogen at the LFL, albeit small, is evident near outlets at some leak rates. In many industrial hydrogen venting scenarios, the gas is flared, but this is not relevant for the small enclosure scenarios considered in this thesis, in the main due to the low volumes considered and the conditions of deployment.

Ignition of vent stacks, tested as chimneys in this thesis, is associated with weather conditions (ICI 1972), particularly thunderstorms. Sellers (1977) noted that higher stacks

had a higher frequency of ignitions. Also, frosty nights, or sleet or snow fall can additionally lead to ignitions due to the charge carried on ice particles (Camp 1976). Although the primary concern in this thesis has been conditions in the enclosure, ignition could initiate outside of the enclosure vent, particularly with environmentally sited plant. Astbury (2007) believes that due to hydrogen's low ignition energy (0.017 mJ), avoidance of ignition sources is almost impossible, but that ignition energies are associated with stoichiometric conditions which also need to be met.

Within the enclosure, concentrations above the LFL can form during a leak event. The HSE (1992) advise dilution with air to at least 25% of the LFL but acknowledge that flammable atmospheres will form at some point. Astbury (2007) suggests mechanical venting (fans) could be effective, but may not prevent flammable mixtures forming, likewise a purely passive system that failed due to a vent blockage would also lead to a loss of dilution and flammable mixtures forming. Low power fuel cells do not have capacity to run fans or other safety systems, such as nitrogen inerting. Passive venting with air dilution is seen as satisfactory, but only for very low-level leaks. Astbury's review of low-pressure hydrogen venting considered air dilution to be the last resort due to the large volumes of air required and inevitable transition through the flammable range.

The hazards associated with the fuel cell system are

- The hydrogen cylinder
- Regulator and gas connections
- Supply pipes
- The fuel cell
- Confinement in the enclosure
- Air flow paths
- Sources of ignition/battery storage
- Poor maintenance

With a small enclosure the cylinder would not normally be housed inside (Some mobile lighting installations do house a small cylinder (BOC Ltd. Genie) too). Cylinders and regulators that are well maintained are usually very reliable. The connecting pipework is a risk area. Connections should be kept to a minimum and the length of pipe as short as

possible. Installing the fuel cell onto the rear wall of the enclosure with pipe connections at the rear mean the enclosure itself will not contain supply pipes.

If the above are possible then the enclosure will contain the fuel cell, supporting electronics and maybe battery storage. This minimises the source of a hydrogen leak to the fuel cell itself (battery excluded). Mounting the fuel cell as high as possible will ensure that leaked gas has a short distance to travel to exit through the top vents. Minimising the contents of the enclosure will maximise the air volume available to dilute leaked hydrogen and also provide a more direct air flow path from inlet to outlet and prevent the chance of gas becoming trapped in pockets. A cross flow passive ventilation scheme is ideal as the upward flow of air works with the buoyant hydrogen to move the gas up and out of the enclosure. The addition of a chimney will further enhance flow.

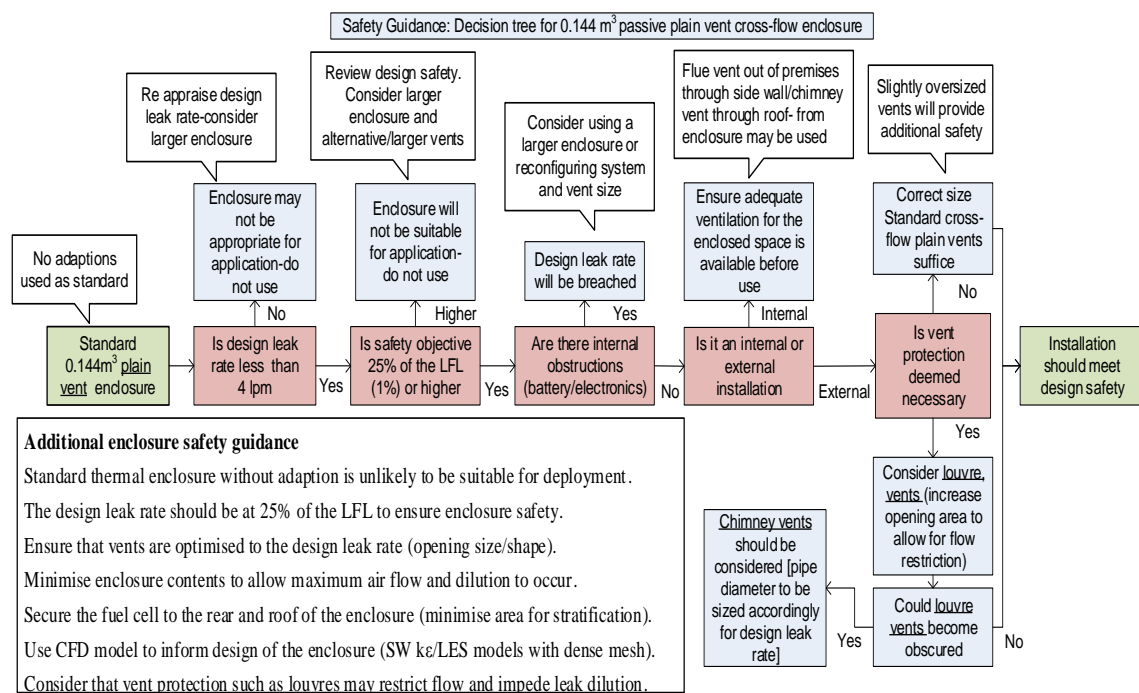


**Figure 6.7 Safety guidance: Decision tree standard 0.144 m<sup>3</sup> enclosure deployment**

In the above scenario the only leak source should be the fuel cell itself. The fuel cell will emit small amounts of hydrogen as part of normal operation, but degradation may lead to a more significant but still low level leak below 4 lpm for the standard enclosure. An effective displacement scheme is crucial, even if the other risks have been mitigated. The

designer will need to apply appropriate vent areas to the enclosure for the perceived leak rate risk. Figure 6.7 presents a decision tree for the deployment of the BOC Ltd. standard enclosure, where the safety goal would ideally be 25% of the LFL.

A further safety consideration is the weight that can be placed upon the predictions from numerical modelling. Much work has gone into CFD modelling of hydrogen systems and its practical application in engineering. To support the use of CFD for safety engineering design and assessment of fuel cell hydrogen (FCH) systems and infrastructure the EU supported the SUSANA (SUpport to SAfety aNAlYsis of Hydrogen and Fuel Cell Technologies) project.

SUSANA aimed to use the guidance on model evaluation protocols published by the ‘Model Evaluation Group’ (MEG, set up by the EC in the 1990s) (MEG 1994) to create a safety protocol for hydrogen use. SUSANA have produced a hydrogen model evaluation protocol (HYMEP) (Figure 6.8) as a safety reference document for CFD developers and users in academia and industry.

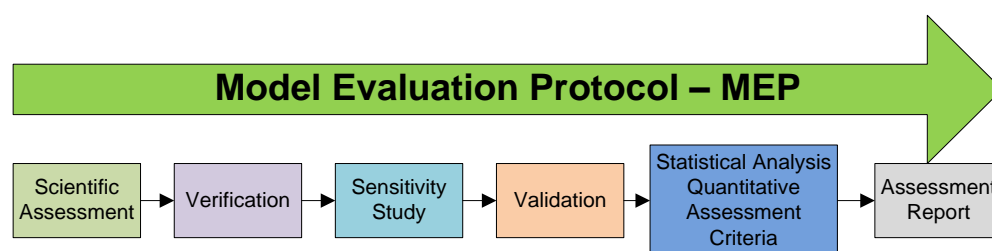


**Figure 6.8 Structure of the model evaluation protocol (HYMEP) (Baraldi et al 2016)**

The use of statistical performance measures to compare simulation and experimental results is included as a quantitative assessment criteria for target variables such as concentration. A range of statistical tests, as used in section 6.5 to analyse the data in this thesis, was recommended in the HYMEP with acceptable safety performance ranges.

#### **6.4 Factors affecting enclosure performance**

Vent design, shape and position as well as enclosure volume are key performance factors affecting displacement air flow. Environmental factors such as wind and solar heating will affect flow for external enclosures. The helium sensors used in the studies were also able to detect temperature and relative humidity. Before each test commences the

apparatus was switched on and allowed to stabilise for at least 30 minutes. It was interesting to observe that as the helium was introduced into the enclosure, the temperature would rise in accordance with the increase in helium concentration (Figure 6.9 BOC Ltd. plain vent test from 1 to 10 lpm) with potentially a small effect on convective flow.

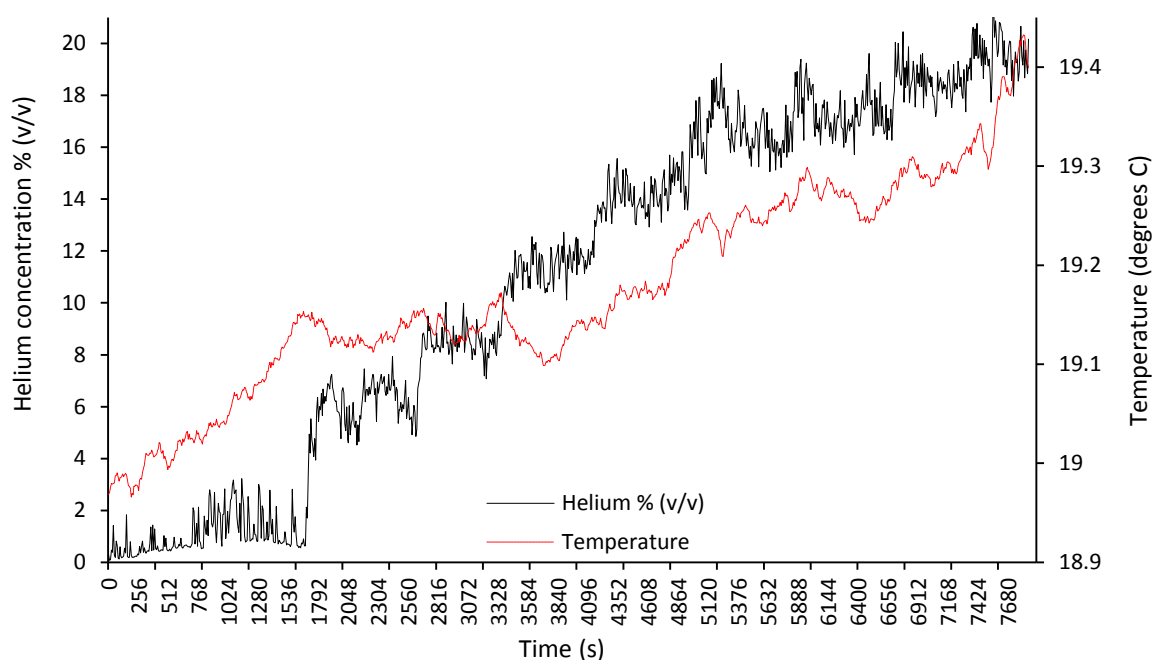


**Figure 6.9 BOC Ltd. Plain vent test helium concentration and temperature vs time**

In the same test it was also noticed that as the concentration increased the relative humidity in the enclosure decreased (figure 6.10). This may be due to the increasing helium volume displacing moist air or the flow having a slight drying affect. Draco (2019) in tests on the effect of moisture on buoyancy driven flow in an enclosed cavity, found that natural convection flows, and heat transfer were sensitive to humidity levels, which reduce with increasing temperature gradients. Draco also stated that humidity enhanced natural convection heat transfer in a greenhouse gas type effect, where it absorbs and emits radiant heat more than dry air. Yuanliang, L (2019) in studies looking at large scale LH2 spills observed that condensation of moisture in the gas cloud increased its buoyancy, but also that cloud temperature increases due to adsorption of heat released by condensation and turbulence created by the condensation. A low level, enclosure, hydrogen gas leak as studied in this thesis is of course a different phenomenon and buoyancy is not affected as with a LH2 spill.

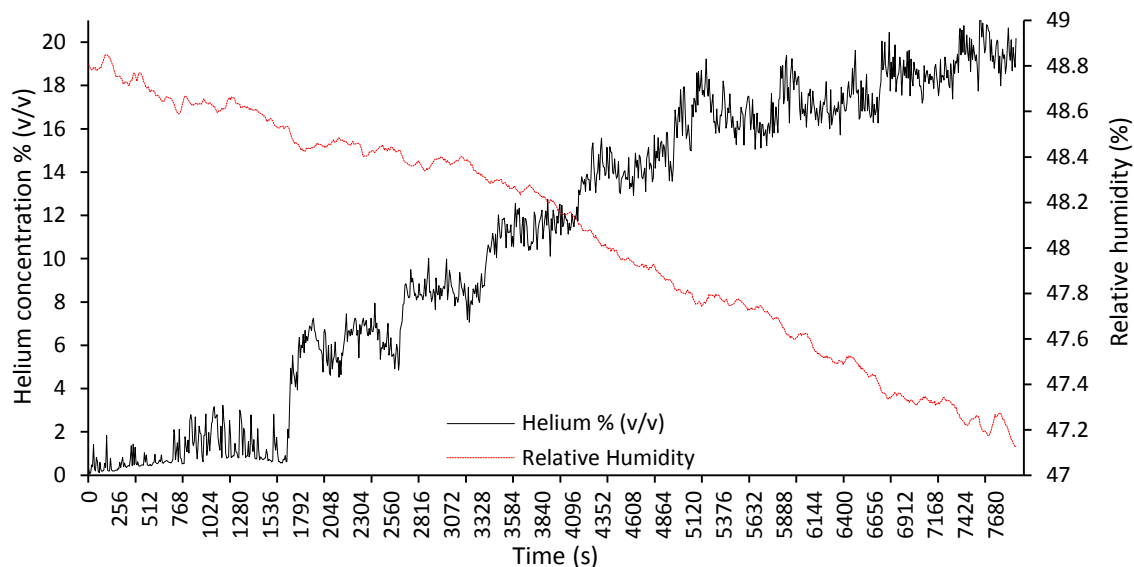


**Figure 6.10 BOC Plain vent test helium concentration and humidity vs time**

### 6.5 CFD and empirical data analytical comparison

As part of the CFD validation process statistical tests have been applied to 26 of the SolidWorks numerical predictions and the corresponding empirical results, to see how the data sets correlate. The data sets represented the majority of the enclosure variations used. Correlation is the quantitative measure of the association between observed and predicted values. The ratio of  $C_o$  (the observed experimental value) and  $C_p$  (the predicted concentrations) of a good model should not show large deviations from unity.

Four tests (explained in the methodology-section 3.10) have been applied to the data sets; Fractional Bias (FB), Normalised Mean Square Error (NMSE), Geometric Mean Bias (MG) and Geometric Mean Variance (VG). Table 6.1 provides the results for the test scenarios. Results within the test range limits are highlighted in green and those outside of the range in red. The tests measure ‘difference’ which is a quantitative assessment of the differences in the predicted and observed data and correlation, which is a measure of association between the data sets. Chang (2004), notes that a perfect model would produce MG and VG equal to 1 and FB and NMSE equal to 0 but that the perfect model is unlikely. Interpretation of analytical results follows the approach of Baraldi et al (2016) in their CFD benchmarking exercise comparing observed and predicted concentrations. NMSE and VG are measures of scatter, reflecting systematic and unsystematic (random) errors. FB and MG are measures of mean bias and indicate only systematic errors, which lead to always underestimate or overestimate the measured values.



**FB:** This is a measure of mean bias and indicates only systematic errors which lead to always underestimate or overestimate the measured values. FB is based on a linear scale and affected by extreme values in the data. The FB range is from -2 (extreme over-prediction) to +2 (extreme under-prediction). Baraldi (2016) states that an FB equal to +/- 0.67 is equivalent to over/under-prediction by a factor 2, that an FB equal to zero is equivalent to zero bias and absolute values below 0.3 can be considered a good model. Figure 6.11 presents the FB results for the 26 tests. All of the results are well within the +/- 0.67 range and with the exception of Test 1 all are below 0.3. On the basis of FB, the selected data sets all accord well.

**Table 6.1 Analysis results-empirical and SolidWorks data sets**

	Test Scenario	Fractional Bias (FB (-2 to 2))	Normalised mean square error (NMSE (0 - 0.5))	Geometric mean bias (MG (0.75 - 1.25))	Geometric mean variance (VG (0.75 - 1.25))
		FB	NMSE	MG	VG
1	BOC enclosure cross flow: Louvre vents 10 lpm	0.314	0.101	1.173	1.375
2	BOC enclosure cross flow: Louvre vents 4 lpm	0.289	0.085	1.238	1.533
3	BOC enclosure cross flow: Plain vents 10 lpm	0.056	0.003	1.076	1.157
4	BOC enclosure cross flow: Plain vents 4 lpm	-0.454	0.217	0.582	0.339
5	BOC enclosure Aluminium 4 louvre 10 lpm	-0.334	0.114	0.384	0.148
6	BOC enclosure Aluminium 4 louvre 1 lpm	-0.546	0.323	0.188	0.035
7	BOC enclosure Aluminium 12 louvre 10 lpm	-0.047	0.002	1.190	1.415
8	BOC enclosure Aluminium 12 Louvre 1 lpm	-0.567	0.349	1.075	1.157
9	BOC enclosure Plain vent 3400mm <sup>2</sup> 10 lpm	-0.027	0.001	0.552	0.305
10	BOC enclosure Plain vent 3400 mm <sup>2</sup> 1 lpm	-0.270	0.074	1.211	1.466
11	BOC enclosure Plain vent 10200 mm <sup>2</sup> 10 lpm	0.053	0.003	1.305	1.703
12	BOC enclosure Plain vent 10200 mm <sup>2</sup> 1 lpm	-0.519	0.288	0.292	0.085
13	BOC enclosure 840 mm tall chimney 4 lpm	0.260	0.069	1.331	1.101
14	BOC enclosure 840 mm tall chimney 2 lpm	0.277	0.078	1.377	1.145
15	BOC enclosure 1680 mm tall chimney 4 lpm	0.263	0.070	1.334	1.110
16	BOC enclosure 1680 mm tall chimney 2 lpm	0.282	0.081	1.368	1.139
17	BOC enclosure with 110 mm flue 0.5 lpm	-0.284	0.082	0.485	0.235
18	BOC enclosure with 110 mm flue 4 lpm	-0.037	0.001	1.096	1.201
19	BOC enclosure with 330 mm flue 1 lpm	-0.114	0.013	1.047	1.095
20	BOC enclosure with 330 mm flue 4 lpm	0.023	0.001	1.021	1.043
21	BOC enclosure with T flue 1 lpm	-0.032	0.001	0.876	0.768
22	BOC enclosure with T flue 4 lpm	0.005	0.000	1.001	1.112
23	BOC enclosure with snorkel 1 lpm	-0.318	0.104	0.274	0.075
24	BOC enclosure with snorkel 4 lpm	-0.212	0.046	0.201	0.040
25	BOC enclosure internal obstruction 1 lpm	0.052	0.003	1.007	1.120
26	BOC enclosure internal obstruction 4 lpm	-0.159	0.025	0.756	0.572

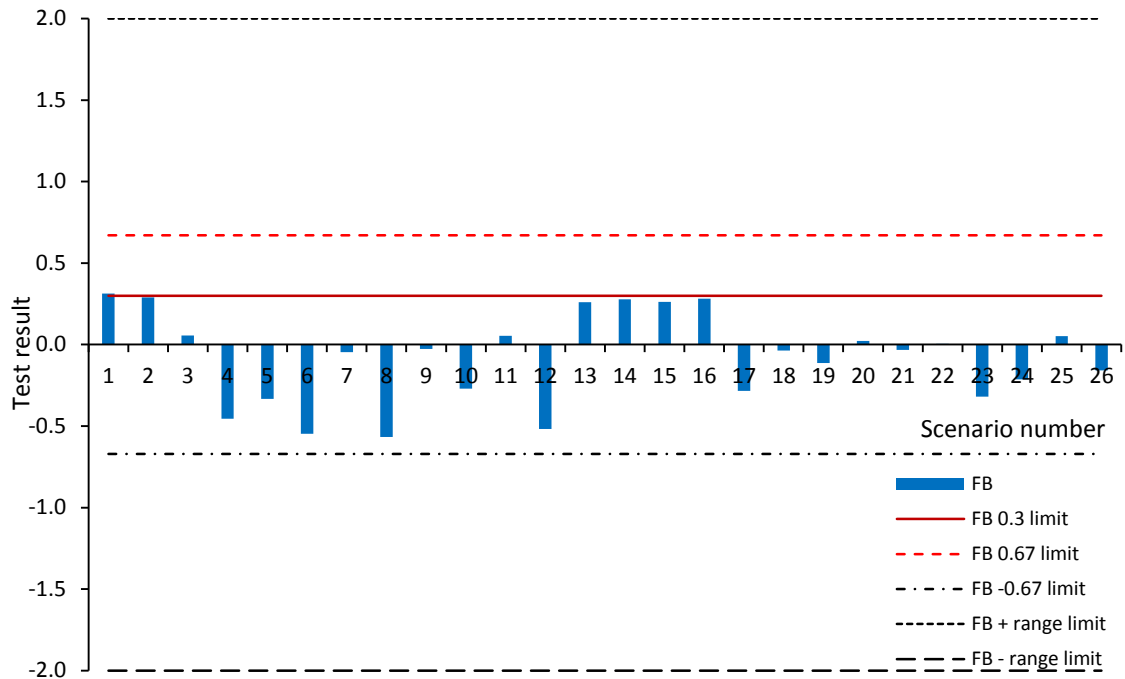


**Figure 6.11 Fractional bias (FB) test results**

**NMSE:** Values of 0.5 correspond to an equivalent factor of 2 mean bias without providing information on under or over prediction. Figure 6.12 shows that all of the values are below 0.5, with some close to the ideal of 0, notably the tests involving chimneys and flues, which similarly were the best performers for FB. The data has broadly performed well with good correlation in the majority of tests.

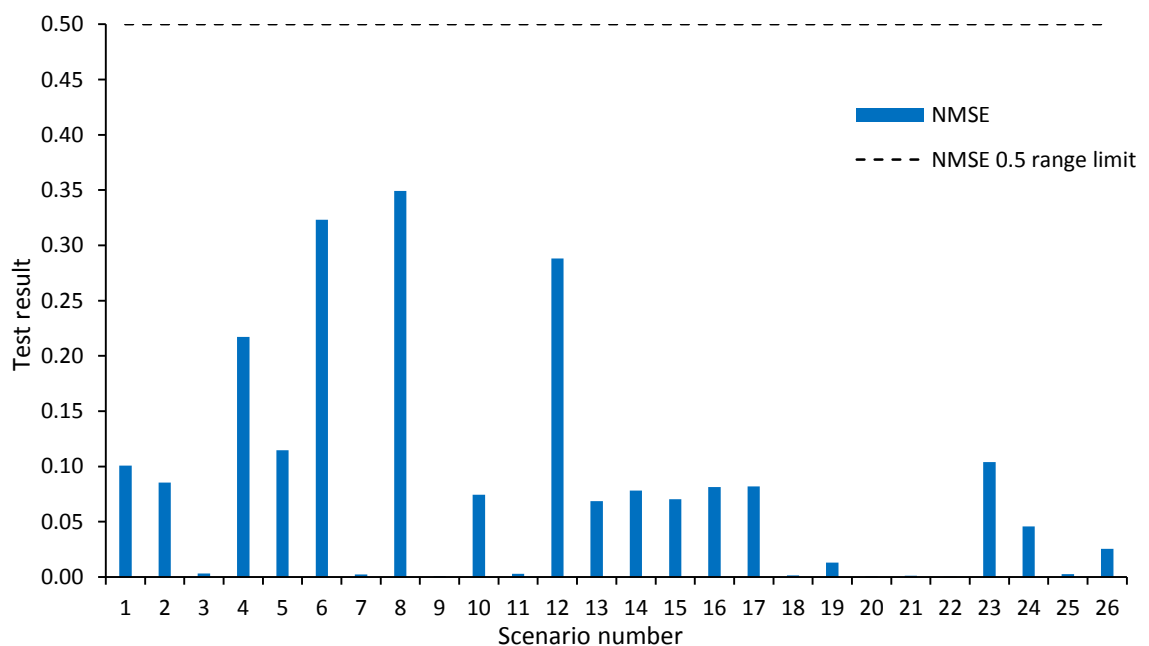


**Figure 6.12 Normalised mean square error (NMSE) results**

**MG:** Values between 0.7 and 1.3 can be considered a good model (Baraldi 2016). Figure 6.13 presents the results and shows that sixteen of the values fall within this range and ten are outside. The snorkel tests, chimney tests and one flue test fell outside of the range. There is some conflict with the FB result.

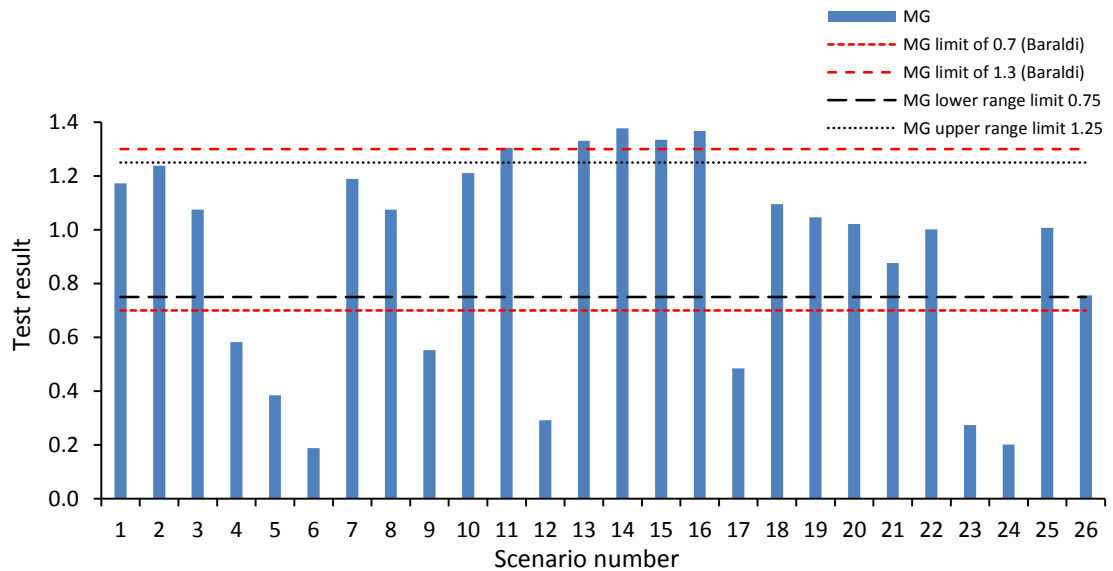


**Figure 6.13 Geometric mean bias (MG) results**

**VG:** This is a measure of scatter and reflects systematic and unsystematic (random) errors. Figure 6.14 presents the results. The graph follows a similar pattern to that shown for MG, but with more values falling outside of the target range. Fourteen tests fell outside, but not all the same as those seen with MG.

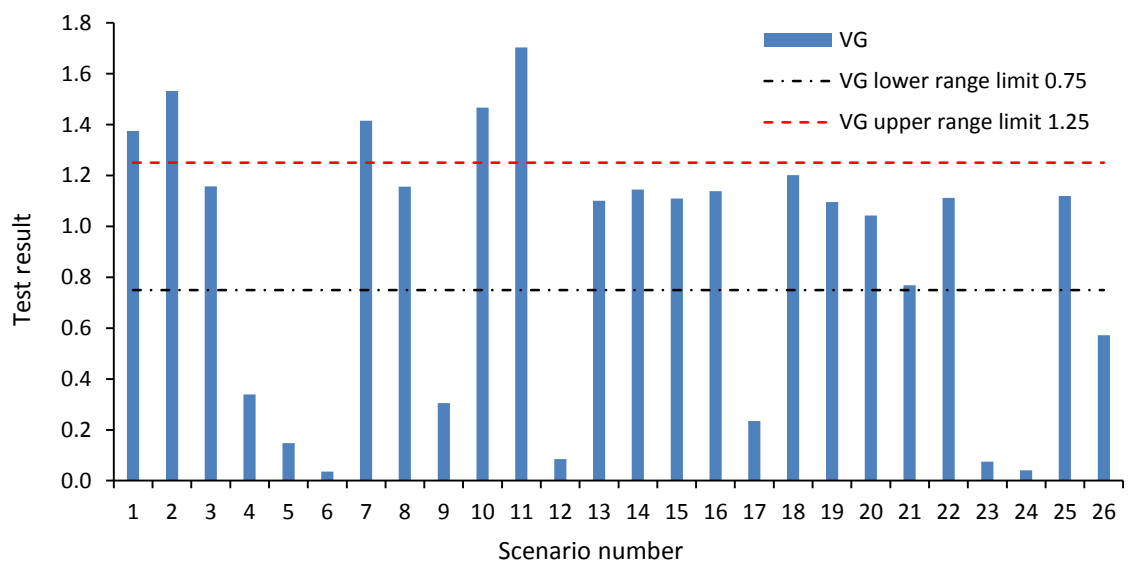


**Figure 6.14 Geometric mean variance (VG) results**

For FB all of the results are closer to zero than the extremes of the range, the most extreme value being -0.567. For NMSE, figure 6.6 shows that most of the results are near to zero with only a few approaching the 0.5 limit, the highest being 0.349. For MG and VG, the analytical test results are less consistent with 50% of the results are outside of the required range. The tests have broadly produced good results, suggesting that the CFD predictions correlate well with the empirical test results, however it is not perfect and the scenarios that produced MG and VG results outside of the desired criteria require further development, particularly with mesh refinement. It is interesting that Toliyas et al (2019) recommend only FB and NMSE for statistical analysis of dispersion models. This is because they are effective at indicating under or over predictions and scatter in the data. Figure 6.15 presents a scatter plot of the observed and predicted peak concentrations for the models tested in this section. Points that lay above the  $x=y$  line indicate a model over prediction and those below a model under prediction. All of the points are broadly in the vicinity of the line albeit the majority are below and represent under predictions. This does highlight a theme with some SolidWorks models and is an area for caution and further model development. Experimental error is a further important consideration.

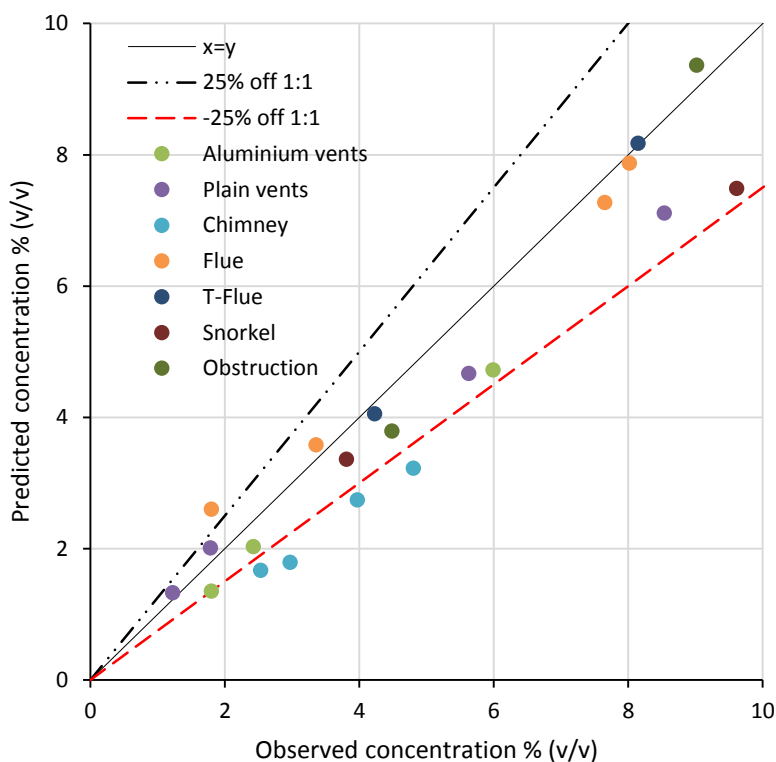


**Figure 6.15 Scatter plot of the observed versus the predicted peak enclosure concentrations for all the models tested in this section. [ $\pm 25\%$  off 1:1 shown]**

## 6.6 Experimental Error

Experimental error (or uncertainty) is defined as the difference between a measured or estimated value for a quantity and its true value and is inherent in all measurements. Accuracy is a measure of how close the measured value is to the true value. (Cornell, 2019). Errors can include human errors, data entry mistakes, faults with the experimental design and random errors caused by environmental conditions (e.g. draughts in the laboratory). Accuracy of the experimental equipment must be considered with a complex rig potentially increasing the level of error. This study involved gas flow metering and concentration measurement, so error could arise, amongst other factors, from the;

- Gas supply regulator,
- Mass flow meter (+/- 1.0% flow accuracy),
- Gas sensors (-1.1 %/%),
- Sensor height/position in the enclosure,
- Environmental condition variations (temp., humidity, atmos. pressure, draughts).

Error is also present with CFD simulations, with accuracy depending upon a number of factors including; model error and uncertainties, discretisation or numerical error, iteration or convergence error, round-off error, code errors and application uncertainties. User errors include CAD related errors, grid generation errors, inappropriate setting of solver and boundary conditions and post-processing errors (Gungor K. et al 2015).

**Table 6.2 Example experimental error calculations**

Data	Test	Leak rate (lpm)	Peak concentration experimental (%)	Peak concentration CFD (%)	Difference (%)	Experimental error (%)
Figure 5.17	Simple plain vent	10	5.62	5.29	0.33	6.24
Figure 5.17	Simple louvre vent	10	6.47	5.79	0.68	11.74
Figure 5.40	12 louvre aluminium vent	10	5.98	4.72	1.26	26.69
Figure 5.40	10200mm <sup>2</sup> plain vent	10	5.63	4.67	0.96	20.56
Hypothetical result at LFL			5	4	1	25.00

Experimental [percentage] error is the difference between an experimental and theoretical value divided by the theoretical value and multiplied by 100 to give percent. (thoughtco 2019). Table 6.2 presents experimental error calculations for some of the test scenarios. There is wide variation in the results but more significantly, what appear to be small differences in values are actually significant experimental errors. The hypothetical 1% difference at the hydrogen LFL equates to 25% experimental error. Accounting for error is an important element of experimental investigations. Error cannot be completely excluded from the tests but is an important consideration when making data comparisons.

### 6.7 Computational fluid dynamics comment

The CFD element of this thesis reflects the direction of contemporary engineering research. Engineering has become heavily computer based, used for design, development and analysis. Computer aided engineering (CAE) and computer aided manufacturing (CAM), particularly with the progress made in additive manufacturing are becoming industry norms. CFD provides further engineering insight that can save development costs. The use of CAD and CFD in this research supports fuel cell industry enclosure [safety] development and is informative in nuclear waste storage safety scenarios.

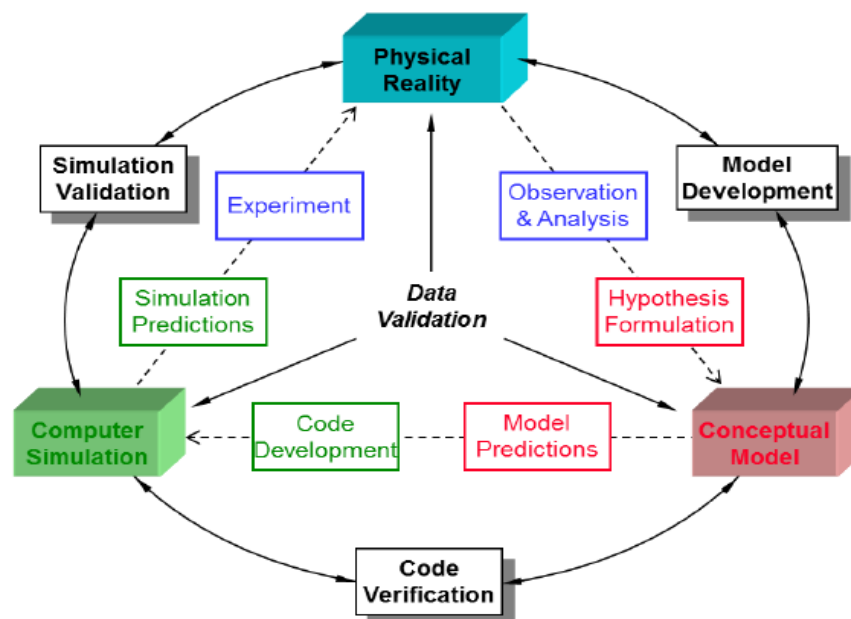


**Figure 6.16** CFD validation and verification process (Meroney et al (2016))

Although not a new discipline, CFD is a field of ongoing development and learning, with many shortcomings (Tolias et al (2019)). CFD predictions are just that and should be used informatively in conjunction with real world knowledge. CFD simulations also benefit from realistic boundary conditions, appropriate turbulence equations and preparation of the model, all of which takes time to achieve. The availability of a wide range of empirical datasets allows for the validation and verification of CFD codes for specific test scenarios to provide the basis of a reference library. This thesis adds to the range by presenting new empirical data sets that can be used for CFD validation. Figure 6.16 presents the scientific validation method proposed in Meroney R. et al's 'CFD Modelling Guidelines' (2016), the outer circle proposing technical processes required for model credibility. The method usefully presents the complexity of associating real world activity with numerical prediction. The work required for a satisfactory CFD outcome is often underestimated.

Two commercial CFD applications are tested in this thesis, primarily SolidWorks: Flow Simulation and also ANSYS: Fluent. SolidWorks is the engineering choice of BOC Ltd., who provided access to the software. Some of the empirical datasets from this thesis were used to validate SolidWorks CFD models. ANSYS: Fluent is widely used in industry and academia in a range of applications and has been used in hydrogen dispersion studies as detailed in the literature review. It was used in this thesis in a comparison study, with the Flow Simulation predictions, for the base case crossflow passive ventilation test.

The two systems are quite different in their approach. ANSYS has developed and evolved over a number of years, with additional software codes added on. ANSYS, although offering the components of a multi-physics system, requires separate pieces of software to be correctly set up before moving onto the next part of the process. The development history of the software is present in the code allowing a wide choice of turbulence models and settings to be applied. This can be useful from an academic perspective if particular detail is required. ANSYS applications are also widely used in many engineering sectors.

The complexity of the model variations available in ANSYS means that the availability of a validated similar case can aid progress by providing the turbulence settings. If one is not available, the literature may be advisory, but if not, it may be necessary to test a range of options to find the best fit, requiring an empirical dataset for comparison. As there was no prior comparable case (other than the SolidWorks prediction), a variety of turbulence model compositions was applied to find the best comparable prediction for the plain vent base case test. Conversely, Flow Simulation provides a modern user interface allowing transit from CAD design, to meshing to CFD solution, in what SolidWorks refers to as CAD embedded CFD (Dassault (2014)).

SolidWorks could be criticized for not offering model options for the engineer to choose from. ANSYS's range of options allows for adjustment of variables to suit the problem under investigation but requires prior knowledge to avoid inconsistency in *variable* application, leading to inconsistent prediction results. SolidWorks avoids such issues by only offering the  $k-\varepsilon$  model. The  $k-\varepsilon$  model in isolation has been known to have some limitations in reflecting flow behaviour in some scenarios; however, SolidWorks has made bespoke adaptations that cater for a wide range of engineering problems. As noted in

section 3.9.5 SolidWorks uses a modified  $k-\varepsilon$  turbulence model with damping functions, developed by Lam and Bremhorst (1981).

The correlation analysis, for the SolidWorks predictions in this thesis, as presented in Section 6.6 suggests that broadly there would be support for model validation, particularly with FB and NMSE, the tests recommended for validation exercises in Toliás et al (2019). Completing the two additional analytical tests MG and VG provides further evidence, but also highlights the models that would benefit from model developments such as further mesh refinement. In the experimental tests, stratification was a key flow feature, with the degree of stratification and helium concentration gradient in the layer the subject of discrepancies in the CFD. So how could CFD predictions be enhanced?

Toliás et al (2019), in their CFD Best Practice Guidance review, recommend a number of CFD modelling strategies arising from the SUSANA project. Key recommendations are; Turbulence model; The model used determines the level of mesh resolution. LES requires a fine grid in the turbulent area. RANS models [ $k-\varepsilon$ ] cope with coarser meshes.

Mesh sensitivity study: Grid independence should be achieved through progressively denser grids, until convergence is achieved. If density is prohibitively dense (computationally expensive), it can be confined to the areas of interest and high gradient.

Mesh refinement: Focused on areas of specific interest or where steep concentration gradients are anticipated. In dispersion tests, refinement should be made near the release point where high concentrations and gradients are expected. Parameters to consider are expansion factor, cell aspect ratio, cell skewness.

Domain size sensitivity study: The domain limits should be far away enough away from areas of interest to minimise impact on flow and boundary conditions.

Time-step sensitivity study: A constant time step can be used or Courant–Friedrichs–Lewy (CFL) number can be imposed to define the maximum time step. At least one simulation with a factor of two smaller time step/CFL number is recommended to ensure that the predictions remain the same. When LES is used, small time-step sizes corresponding to  $CFL \leq 1$  are recommended.

Buoyant gas: More mesh refinement is recommended near to the enclosure ceiling.

Gas inlets: A source area approach for the gas inlet provides a more realistic implementation of the inlet boundary, as opposed to a volumetric source approach.



These are all sensible recommendations, most of which were accounted for with the Flow Simulation studies. The main limiting factor is the computational resource available. The  $k-\varepsilon$  model is widely used, robust and has a low computational cost. It has been shown to provide good predictions, particularly when additional buoyancy terms are applied. LES can produce more accurate predictions in wall bounded studies but requires a fine mesh and small time-steps, making it computationally expensive. With regards the CFD studies undertaken in this thesis there are areas that would be addressed in future studies.

Vent openings: The vent openings are important to the flow regime through the enclosure. It is important to ensure adequate mesh resolution in these areas.

Upper enclosure zone: Ensure that the mesh is more refined in the areas where buoyant gas may pool, particularly in RANS tests. This could be the stratified layer at the top of the enclosure, or places where gas could become trapped e.g. under the fuel cell.

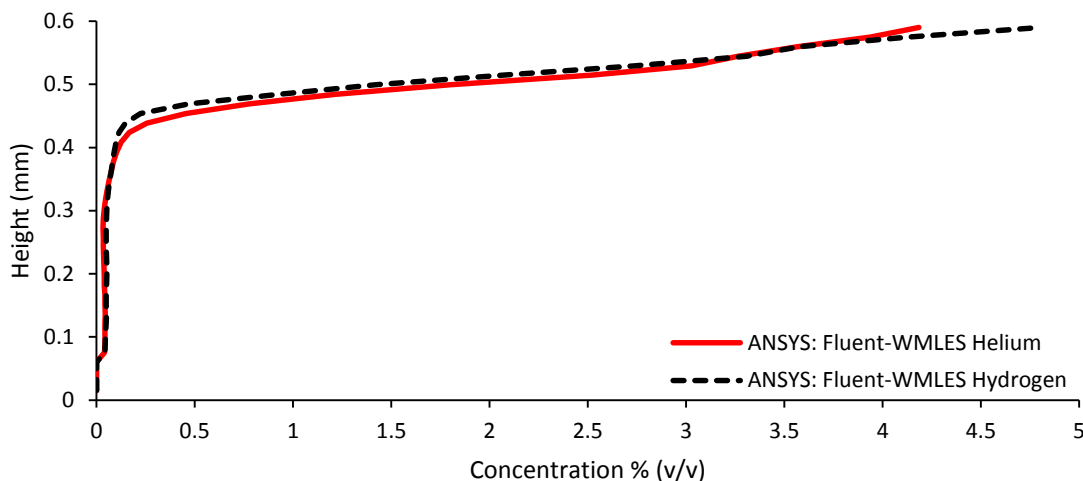
Domain boundary: The domain boundary in the simulations reflected the size of the outer enclosure on the test rig. A wider area may have been beneficial, but it would have been computationally expensive. The LES/DES tests used in the ANSYS study used a small but refined mesh. The outer boundaries of the domain were set as pressure outlets, which allowed the simulation to develop unhindered with very good test outcomes.

Chimney tests: The deeper stratified zone produced may be due to mesh resolution and the size of the computational domain. Other studies from the literature have found that the  $k-\varepsilon$  model can under predict concentrations (Giannissi et al (2015), Barley and Gawlik (2009)). This has been the case in several of the SolidWorks studies.

What appears to be a simple airflow model through a small enclosure is actually quite complex when it comes to numerical calculations. The crossflow scenario with airflow from two directions coupled with flow through the wider domain with the addition of a buoyant gas, clearly poses some challenges for the RANS models. Based on this review it appears SolidWorks Flow Simulation is suited to the dispersion modelling in this thesis.

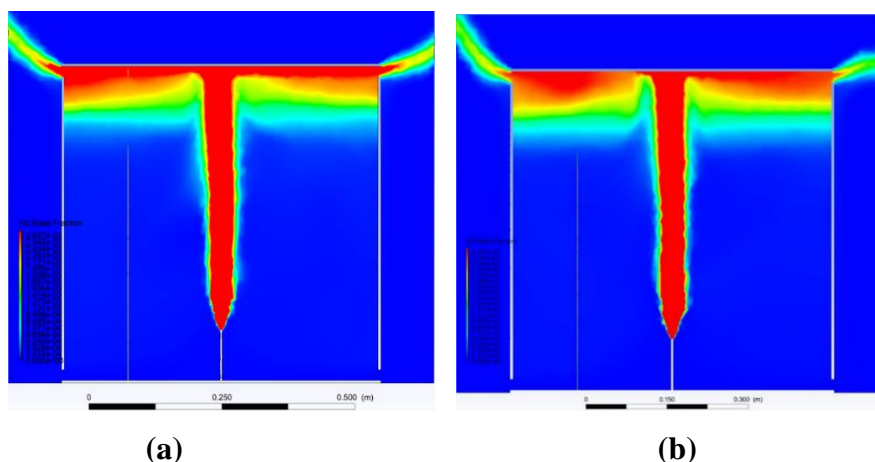
It is important to remember that although the CFD prediction studies in this thesis have used helium so that a direct comparison with the helium empirical data could be made, a safety engineer would want to know that the helium predictions were relevant and applicable to hydrogen scenarios when developing an enclosure. The literature review presented evidence that the properties of helium were close enough to hydrogen for it to

be used as a test analogue. To be sure that this is the case in the CFD studies in this thesis, comparison studies have been run in ANSYS: Fluent and SolidWorks Flow Simulation, using the cross-flow model applied to the ANSYS comparison study.



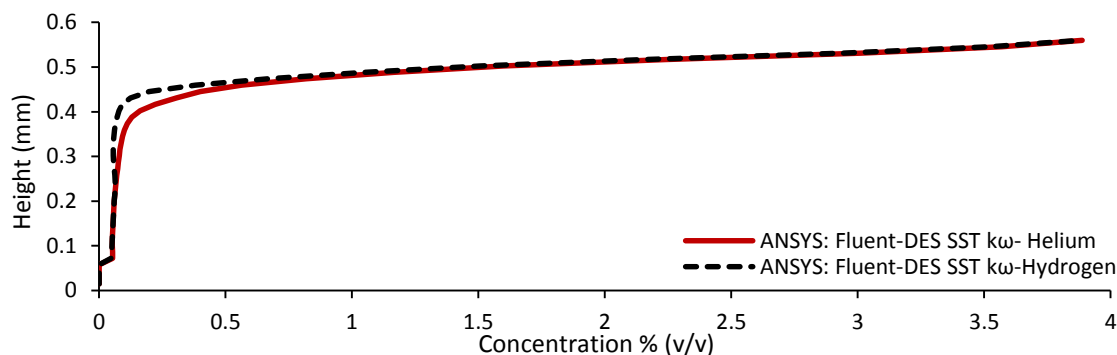
**Figure 6.17 CFD comparison of helium and hydrogen-ANSYS: Fluent [WM LES]**

Figure 6.17 presents a graph comparing the CFD predictions of two ANSYS: Fluent WMLES studies, one using helium and one hydrogen. It can be seen that there is a good correlation in the predictions except for the values at the top of the enclosure, where the hydrogen study predicts a higher concentration. This effect was found by Barley and Gawlik (2009) but with a garage sized enclosure. They did report though that Swain and Swain (2003), in their assessment of CFD models (using helium/hydrogen ratio), found that with simple vented enclosures (garage sized) that the concentration of hydrogen and helium were the same for areas of bulk flow near the ceiling, but not near the leak origin or vent, for steady state conditions. The flow conditions presented in figure 6.17 are not at garage scale, but there is accord with the findings of Barley and Gawlik.



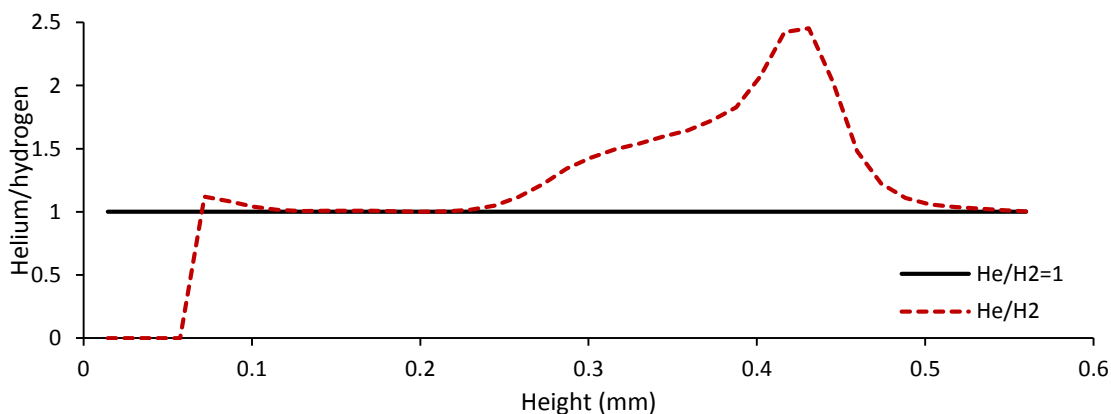
**Figure 6.18 ANSYS: Fluent (a) WM LES [hydrogen] (b) DES SST  $k\omega$  [hydrogen]**

Figure 6.18 presents a cut-plane image for (a) the ANSYS: Fluent WMLES study using hydrogen and (b) the DES SST  $k-\omega$  study. It provides information on how the model is dealing with the flow and it is clearly similar to that found with helium in figure 5.76 in the ANSYS comparison study.



**Figure 6.19 CFD comparison helium and hydrogen-ANSYS: Fluent [DES SST  $k-\omega$ ]**

Figure 6.19 compares the CFD predictions for hydrogen and helium using the ANSYS: Fluent-DES SST  $k-\omega$  settings. On this occasion there is closer accordance with the Swain et al (2003) findings, with diversion of the predictions at the mid enclosure level and both predicting the same peak concentration. Figure 6.20 uses the Swain et al ratio method for checking correlation showing good accordance at the ceiling and lower down in the enclosure. Swain et al observed that for simple geometries [enclosures] it was possible to directly interpret helium release data and for areas of bulk flow near the ceiling the concentrations of hydrogen and helium were the same but not in proximity to vents or the release source. The reduced gravity values  $g'$  for helium and hydrogen (using equation 12, chapter 2) are  $8.38 \text{ m s}^{-2}$  and  $9.09 \text{ m s}^{-2}$  respectively. This difference would be more apparent in regions of lower concentration such as near the vents. It is important to note that there is a difference, but that many studies have found helium to be a good analogue.



**Figure 6.20 Ratio of helium and hydrogen values against height**

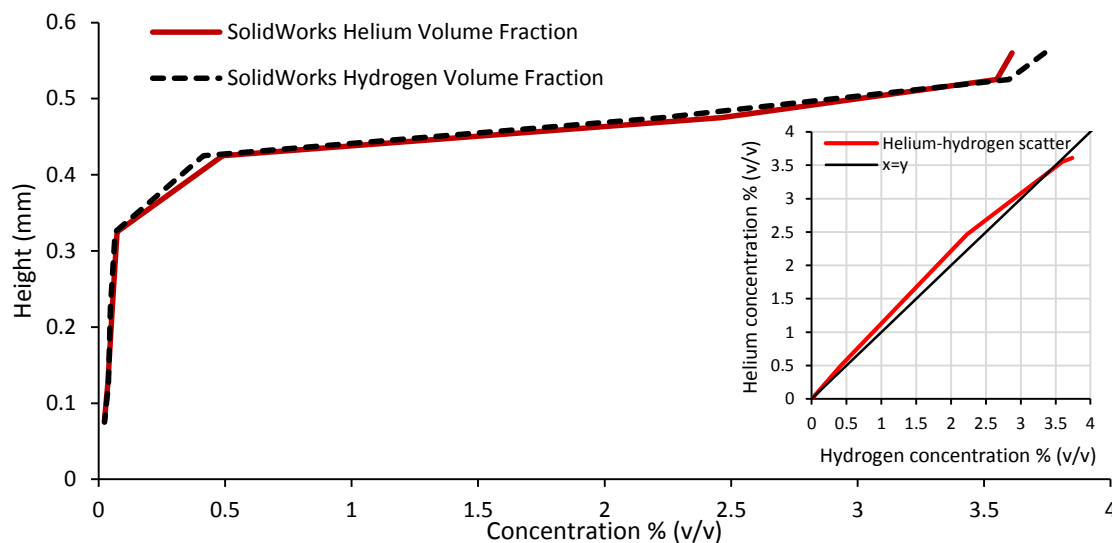


**Figure 6.21 CFD Comparison helium and hydrogen-SolidWorks [k-ε]**

Figure 6.21 presents the predictions from the same crossflow scenario but with SolidWorks Flow Simulation using the  $k-\epsilon$  model. The domain contained a well refined mesh of approximately 1.2 million cells, which included localised refinement added as described in chapter 3 to ensure that the plume, stratified area and the vents are more resolved. The comparison graph, as with the ANSYS studies show the predictions follow closely, except the middle and peak value where hydrogen is higher as in Barley and Gawlik. The inset scatter plot suggests good correlation. Figure 6.22 shows a similar gas distribution to that seen in the ANSYS cut-plane images.

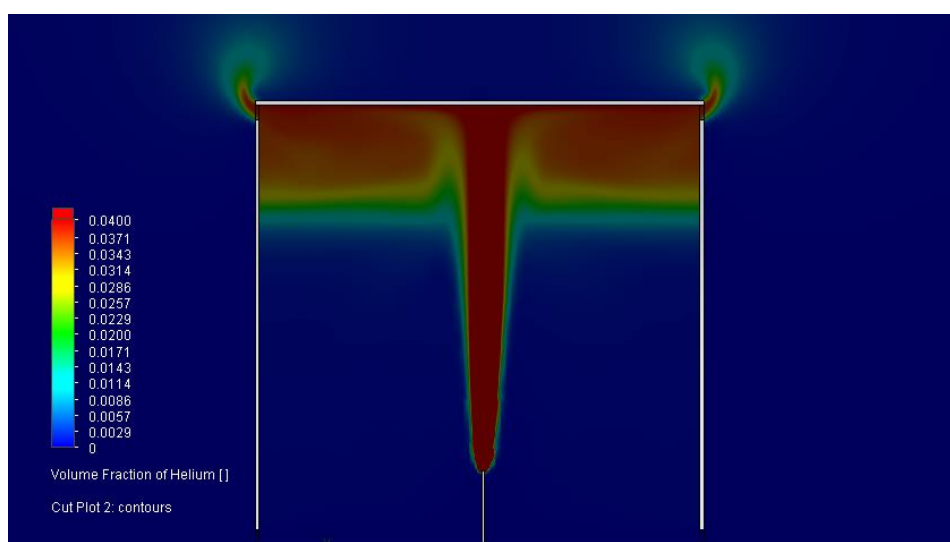


**Figure 6.22 SolidWorks cut-plane image at 4 lpm**

It is also worth noting the SolidWorks mesh sensitivity process. Refinement is generally added in specific areas through the addition of additional geometry which is disabled.

Further refinement levels can be set with detail around curvature and small channels if required. ‘Solution adaptive meshing’ if selected will automatically adapt the mesh in regions with high flow gradients (e.g. pressure, velocity and concentration). Figure 6.23 presents the results of an example mesh sensitivity test on the crossflow scenario. It shows that the initial coarse mesh under predicted and that the well refined meshes over predicted the stratified layer depth. A medium sized mesh produced a good prediction on this occasion. This process has shown how the  $k-\varepsilon$  model, unlike LES can cope with a coarser mesh and indicates the importance of this CFD step. It is important to note that mesh quality is not just about the number of cells, but how and where the detail is applied and in accordance with the turbulence model selected.

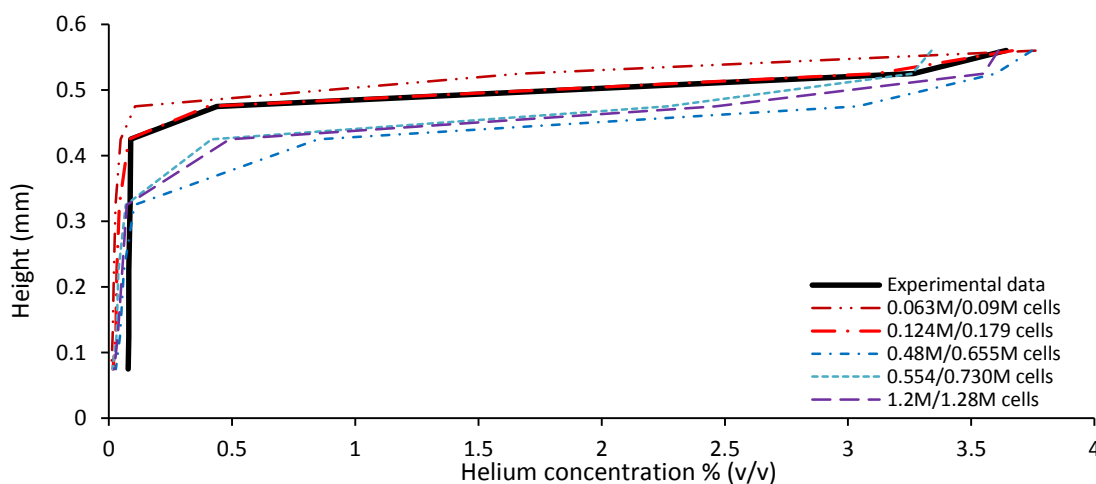


**Figure 6.23 SolidWorks mesh sensitivity study [initial and final meshes shown]**

The ANSYS: Fluent comparison study provided further insight into what CFD can offer in this field of study. The ANSYS RANS studies broadly failed to predict the empirical results, which was disappointing. Giannissi (2014) found over predictions could be attributed to overestimated diffusivity that leads to more diffused results and that LES models produced better outcomes. Piomelli (2008) found that wall bounded [turbulent] flow systems are particularly affected by near wall treatment in their calculations, with RANS simulations involving high Reynolds numbers having poor accuracy. LES were better able to deal with these conditions, particularly when coupled with ‘wall model’ equations, albeit with additional computational expense. It is also important to bear in mind that although helium is a close analogue for hydrogen, there are some differences in behaviour between hydrogen and helium in the CFD predictions that should be accounted for by design and safety engineers.

## 6.8 Small enclosure design safety

Swain and Swain (2003) advise that for leaks into partially enclosed spaces or structures with vents, both the total volume of hydrogen released, and the flow rate of the leak are integral to the resultant risk. Other important safety design parameters are the volume of the enclosure, leak location, the position, shape, number and size of the vent openings and the peak concentration achievable given the other variables. Ideally, vents positioned at the bottom and top of the enclosed space should allow air to flow through the space and entrain the leak. The type of vent opening applied to the enclosure can affect flow resistance as was found with the application of louvres to plain vent openings, so should be accounted for. Barilo (2013) supports this position recommending ‘the development of a technical basis for creating prescriptive and performance based requirements for enclosures used for hydrogen systems’. Barilo adds to the safety variables;

- Leak rate, a function of hydrogen pressure and enclosure components
- Leak probability, accounting for equipment degradation, improper installations
- Ventilation required to prevent flammable hydrogen ceiling layer developing
- Explosion protection measures other than leak prevention and ventilation
- Damage or injuries that might result from a leak
- Necessary separation distances between enclosures and other exposures

The level of the likely leak rate is difficult to predict. This is partly because the technology is young with limited historical accident data with statistical significance. Garage sized and larger enclosure tests are well represented in the literature. Small enclosure test data is more limited in the literature particularly in the leak range tested in this thesis. Also vent arrangements tested are limited, in some cases to single vents. The BOC Ltd. criteria was for a sub. 10 lpm leak rate in the enclosure to be tested. The evidence from this research suggests the design leak rate for the enclosure should be sub. 4 lpm for the scenarios tested, in order to fall below the LFL. To aid the design process it is helpful to know the likely peak enclosure concentration when assigning a vent size and design leak rate. To investigate this, the plain vent (Section 4.3) data has been processed to see if this is possible for the range between 1 and 5 lpm. Five sets of concentration data (1 to 5 lpm) were plotted against  $\text{Area}/\text{Volume}^{2/3}$  (Figure 6.24 (a)) and fourth order polynomial trend lines added. The five coefficients from the trend line equations (a to e) were then plotted against leak rate (Figures 6.24 b-f). To predict a peak concentration for a chosen leak rate

and vent area, the coefficients are read from the graphs (more practical on a spreadsheet) and inserted along with the vent area ( $A/V^{2/3}$  in this instance) into the fourth order polynomial equation ( $y = ax^4 + bx^3 + cx^2 + dx + e$ ). This could be applied to the other thesis data sets, but of course the calculation is unique to the enclosure tested. A spreadsheet will process this, but a nomogram would be more convenient.

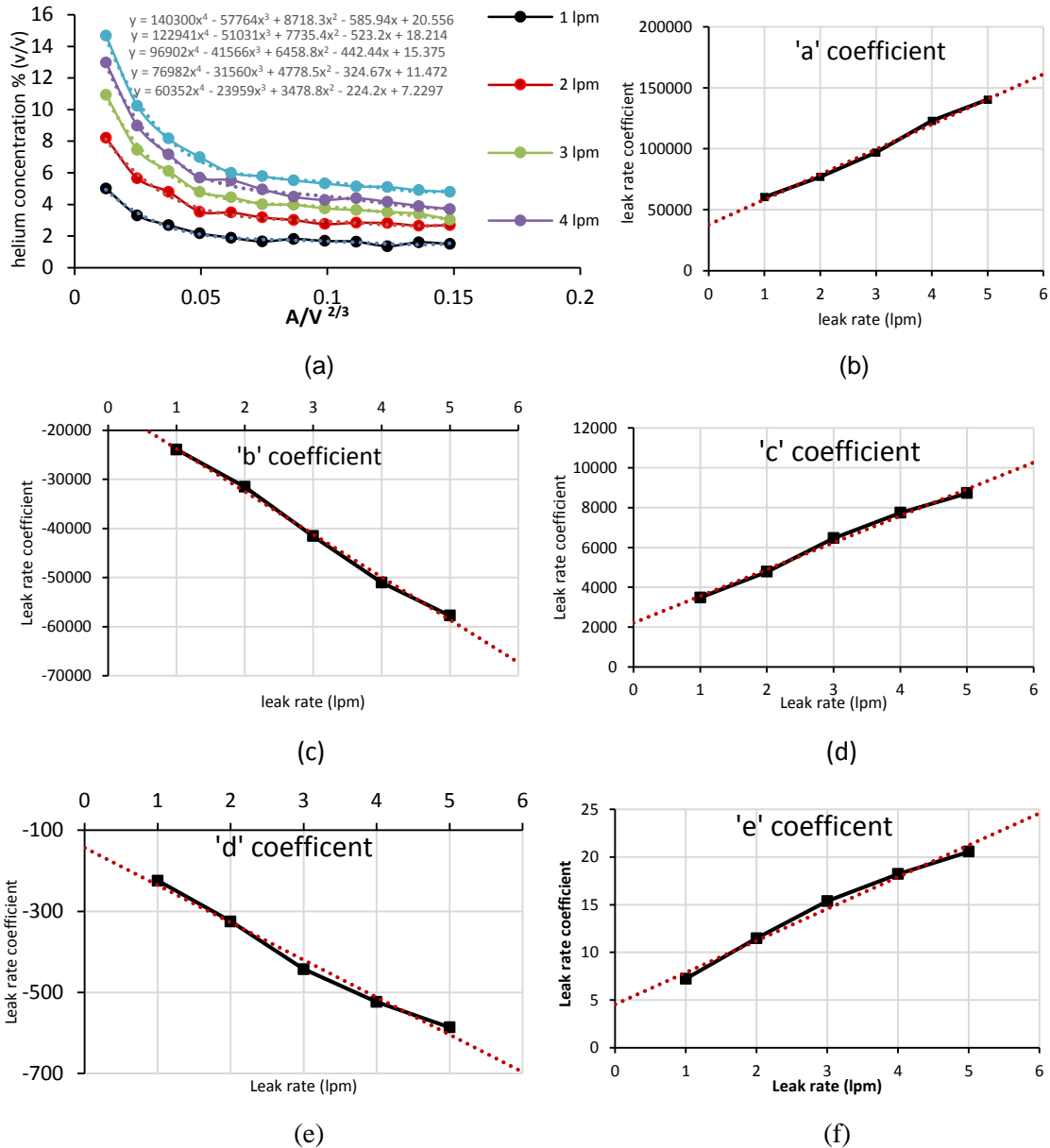


**Figure 6.24 Concentration prediction analysis: (a) helium concentration vs  $A/V^{2/3}$  (b) a coefficient vs leak rate (c) b coefficient vs leak rate (d) c coefficient vs leak rate (e) d coefficient vs leak rate (f) e coefficient vs leak rate**

It would be helpful if the data could be linked to the data from different enclosure volumes, as this would provide a useful design tool. Molkov (2014) provides three data

points for a 1 m<sup>3</sup> enclosure [1.6 % at 5.4 lpm (162000 mm<sup>2</sup> vent), 4.6 % at 5.38 lpm (32400 mm<sup>2</sup> vent) and 8.5 % at 5.436 lpm 31500 mm<sup>2</sup> vent] which is 7.5 times larger than the enclosure tested in this thesis. A difficulty with this approach is that Molkov determined that vent shape affects internal mixing and enclosure concentration.

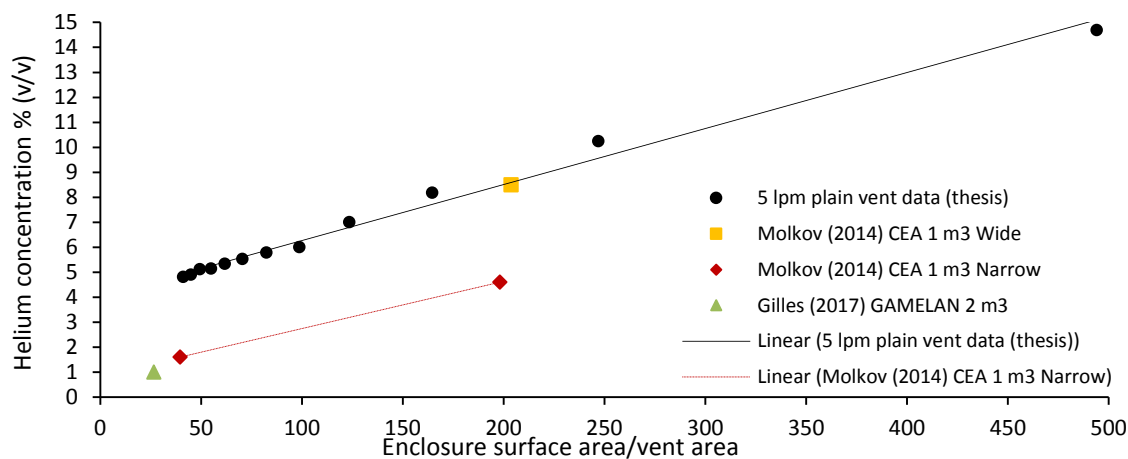


**Figure 6.25 Enclosure surface area/vent area against helium % at 5 lpm**

Figure 6.25 attempts to investigate a relationship between enclosures of different sizes. Using a dimensionless scale produces a straight line for the 5 lpm plain vent data. One of Molkov's data points fits the line (the widest vent 900 mm) and two do not (narrow vents both 180 mm). A data point from Gilles (2017) [2m<sup>3</sup> enclosure. 372400mm<sup>2</sup> vent at 5lpm], lays close to Molkov's two narrow vent points. Further data points would be required to establish a relationship with enclosure volume.

## 6.9 Conclusion

In enclosure scenarios hydrogen, due to its buoyancy, will accumulate near the enclosure roof or in a cluttered enclosure, can become trapped in pockets under the fuel cell or the supply plant. Similarities with the small spaces between nuclear storage boxes and the complexity of storage silos present the same hydrogen safety concerns. The standard plain vent enclosure tested in this thesis would fail to manage concentrations below the LFL at leak rates above 4 lpm, a significant restriction, with louvres further reducing flow. SolidWorks Flow Simulation CFD has demonstrated the capability to predict release and dispersion outcomes. ANSYS: Fluent performed well using LES/DES solvers despite the application of a symmetry plane, which is not recommended for these applications (see section 5.9). There is the potential to use the thesis data to develop engineering prediction tools for use in determining likely peak concentrations for given leak rates and vent areas.



## Chapter 7 Conclusion

### 7.0 Introduction

The focus of this thesis is improving safety in small enclosed spaces subject to low-level hydrogen leaks, using passive ventilation. Passive ventilation of leaked hydrogen is relevant to many safety engineering applications, in particular nuclear waste storage, nuclear decommissioning and the hydrogen economy. Passive ventilation of a buoyant gas is a different phenomenon to natural ventilation of air, so further research in this field is necessary to fully understand the safety and design implications.

The presence of a buoyant gas in a confined but ventilated system alters the flow dynamics in the space, due to the presence of the buoyant gas. Although now defined as ‘passive ventilation’ (Molkov 2014), there has not been extensive research into the effects in small enclosures, with a deficit of empirical data sets for CFD validation purposes. The hypothesis for this research, restated below, was to establish such datasets. This also supports BOC Ltd. with their enclosure safety case and provides useful hydrogen safety insight to Sellafield Ltd. in support of their nuclear decommissioning endeavours.

**Research hypothesis:** *Safe, passive ventilation parameters can be determined that will manage hydrogen concentrations below the lower flammable limit, for hydrogen leak rates at or below 10 litres per minute in a passively ventilated 0.144 m<sup>3</sup> hydrogen fuel cell enclosure.*

### 7.1 Overview

This research project has successfully produced a range of datasets for small enclosure passive ventilation scenarios. The datasets reveal the hydrogen leak rate limits that breach the LFL, linking the scenario tested to the total vent opening area and the enclosure volume. In some cases within the range tested, the LFL is exceeded and the enclosure environment would not be safe. These limits provide guidance to design engineers as well as offering a range of vent applications for different deployment scenarios. The SolidWorks Flow Simulation CFD validation exercise has shown that the RANS equations it uses coupled with wall damping functions produced creditable results in the scenarios tested. Analytical tests applied as part of the benchmarking process showed that there was a good correlation for FB and NMSE tests. The ANSYS: Fluent comparison

study highlighted some of the weaknesses of the RANS models in wall bounded flow studies. It also demonstrated the superior capability of LES/DES models in such studies, particularly when coupled with ‘Wall Model’ functions.

## 7.2 Conclusion

Passive ventilation is a no energy solution to buoyant gas management that if correctly specified can provide reliable venting and concentration management, but there are engineering limitations with the regards to leak rates and vent opening sizes. CFD can be used in the design and development of enclosure scenarios. The SolidWorks RANS model producing good results across a range of studies and ANSYS LES/DES models providing excellent results in the one case considered. The conditions in nuclear installations are unsurprisingly complex, with plenty of opportunities for hydrogen to become confined. The findings presented in this thesis provide valuable insight into passive ventilation management. In addition, a bespoke enclosure design methodology may prove more successful than applying adaptations to off the shelf thermal enclosures. In conclusion, the research hypothesis has been answered (see below) and data sets compiled. Passive ventilation is a viable solution for small confined spaces where the leak rate is very low. Ventilation openings on enclosures used outside cannot be too large as they would allow rain to enter and be vulnerable to animal intrusion. In some cases, mechanical backup may be the only solution to cater for situations where concentrations rise to or exceed the LFL.

**Research hypothesis response:** *This thesis has produced data sets for passive ventilation regimes in a 0.144 m<sup>3</sup> enclosure. This has allowed the safety parameters to be determined that produce concentrations that fall below the LFL. In some cases, the LFL is achieved at a leak rate well below the 10 lpm limit specified in the hypothesis, in most cases this is around the 4 lpm point. This fact demonstrates the importance of this work as minor leaks can lead to devastating consequences.*

**Thesis originality:** *This body of work including all experimental testing and CFD simulation studies is the original work of the author. This work and the completion of this thesis has been undertaken by the author, but under the professional guidance of the academic supervisory team.*

## **Chapter 8 Recommendations for Future Work**

### **8.0 Introduction**

The use of small vented enclosures to house hydrogen fuel cells provides for a diversity of use scenarios, from domestic CHP units to commercial application. The range of applications will broaden as the commercial and domestic markets grows. As such, future research will very much depend on market direction. However, as the UK market stands now, small stationary applications are at the forefront with domestic fuel cell CHP on the horizon, particularly with current testing of hydrogen in the gas grid. The venting of hydrogen in these scenarios will be an engineering safety concern.

Hydrogen venting in the nuclear industry will always be a safety concern. Passive ventilation techniques are preferable, so data sets relating to passive ventilation scenarios supports the nuclear safety case. Further research that focuses on the dispersal of evolved hydrogen from nuclear installations is necessary, particularly in accident scenarios. The use of CFD modelling in the field of nuclear safety is particularly relevant due to the complexity of the real life scenarios and difficulties with empirical testing.

### **8.1 Ideas for further research**

This research investigation has focused upon small stationary hydrogen fuel cell applications. In particular those contained in small steel enclosures which incorporate passive ventilation schemes to remove buoyant gas that may be present. Many of these installations are sited in the environment and as such exposed to the elements. The impact of heat and wind on enclosure performance is therefore relevant and worthy of investigation. Humidity too may affect ventilation performance and will vary widely in outdoor conditions and should be considered for further investigation.

The tests in this investigation mainly used an empty enclosure; however, in reality it will of course house the fuel cell, associated electronics, supply pipework and possibly a battery for energy storage. This reduction in internal space and the complexity of the equipment may lead to the possibility of pockets of buoyant gas being trapped due to the lack of a good airflow path. Ways to overcome this should be investigated. Further, the

effect of heat generated by the fuel cell and electronics on ventilation flow are an area also worthy of investigation.

**Future research investigations in this field should consider;**

- The effect of environmental conditions on passive ventilation flow e.g.
  - wind,
  - temperature and
  - humidity
- The effect of solar heating on a metal enclosure
  - Solar chimney flow enhancement
- The effect of internal heat generation on flow
- Enclosure/vent design modifications e.g.
  - Venturi effect: An enclosure with an adapted roof design that uses wind forces to create negative pressure in the vent area thereby increasing the enclosure ventilation driving force
  - New enclosure design methodology
- Schlieren tests
  - incorporating helium sensors to determine concentration
  - widening the field of view
  - investigating observed CFD behaviour
- Computational fluid dynamics
  - Further validation and verification investigations
  - Improve on SolidWorks prediction outcomes
  - ANSYS: Fluent validation and verification with LES/DES
- Development of a nomogram relating leak rate, vent size, concentration and enclosure volume.

## 8.2 Conclusion

The ability to enhance natural airflow, turbulence and gas mixing in the enclosure has been suggested by the investigation in this thesis. Further work in the areas above may aid the design of an efficient and cost effective to produce enclosure that meets the safety needs of the small fuel cell industry. The development of an engineering nomogram would also be a beneficial design safety tool, useful to nuclear and fuel cell industries.

## References

- Adobe Photoshop CS2 Version 9.0: [www.adobe.com](http://www.adobe.com)
- Anon, 1972, Imperial Chemical Industries Petrochemicals Division Safety Newsletter 72/3, p. 2.
- ANSYS: Fluent; ANSYS 18.2; ANSYS, Inc., Southpointe, 2600 ANSYS Drive, Canonsburg, PA 15317, USA; <https://www.ansys.com>
- Ashtead Technology; Ion Science Gas Check 3000 Gas Leak Detector data sheet; [www.ashtead-technology.com](http://www.ashtead-technology.com); [Accessed November 2017]
- Astbury G.R. (2007); Venting of low pressure hydrogen gas- a critique of the literature: Journal of Process Safety and Environmental Protection; Volume 84 (B4), pp 289-304
- Bachelierie, E.; Arnould, F.; Auglaire, M.; de Boeck, B.; Braillard, O.; Eckardt, B.; Ferroni, F.; Moffett R. (2003); Generic approach for designing and implementing a passive autocatalytic recombiners PAR-system in nuclear power plant containments; Journal of Nuclear Engineering and Design; 221, pp. 151–165.
- Baer S. (1996); Two means for riddance of hydrogen; Research Department, Zomeworks Corporation, Post Office Box 25805 Albuquerque, NM 87125 USA
- Baraldi et al (2016); Development of a model evaluation protocol for CFD analysis of hydrogen safety issues the SUSANA project; International Journal of Hydrogen Energy 42; 7633 – 7643; Elsevier 2016
- Baines, W.D., Turner, J.S. (1969), Turbulent Bouyant convection from asource in a confined region; Journal of Fluid mechanics; 37; 51-80
- Barilo, N. F. (2013); Safety of Hydrogen Systems Installed in Outdoor Enclosures; Pacific Northwest National Laboratory; U.S Department of Energy; Office of Scientific and Technical Information; Tennessee
- Barley C.D and Gawlik K. (2009): Buoyancy-driven ventilation of hydrogen from buildings: Laboratory test and model validation; International Journal of Hydrogen Energy; Volume 34 (2009), pp 5592-9903
- Bernard-Michel, G., Houssin-Agbomson, D (2016); Comparison of helium and hydrogen releases in 1m<sup>3</sup> and 2m<sup>3</sup> two vent enclosures: concentration measurements at different flow rates and for two diameters of injection nozzle; IJHE; 1-9; Elsevier
- BOC (2016): Hymera and Genie cylinder image; BOC Ltd, Customer Service Centre, Priestley Road, Worsley, Manchester M28 2UT, United Kingdom
- BOC Limited (2014); HYMERA™, Hydrogen fuel cell power generator data sheet; [http://www.boconline.co.uk/internet.lg.lg.gbr/en/images/Hymera-II-Data-Sheet410\\_138254.pdf](http://www.boconline.co.uk/internet.lg.lg.gbr/en/images/Hymera-II-Data-Sheet410_138254.pdf)
- Brennan S., et al (2011); Hydrogen and fuel cell stationary applications: Key findings of modelling and experimental work in the HYPER project; International Journal of Hydrogen Energy; Volume 36 (2011); pp 2711-2720

Brooks Instruments (2017); Brooks® GF100 Series High Purity/Ultra-High Purity Digital Thermal Mass Flow Device, Installation and operation manual; Brooks Instruments; 407 West Vine Street, Hatfield, PA, 19440-0903 USA

Brown W.G., Solvason K. R (1962); Natural convection through rectangular openings in partitions (Part 1 Vertical partitions and Part 2 Horizontal partitions); International Journal of Heat and mass Transfer; Vol 5 pp 859-878; Pergamon Press.

BS EN 60529 (1992):1992+A2:2013: Degrees of protection provided by enclosures (IP code); © British Standards Institution 2018

Camp, P.R., 1976, Charge, morphology and pH of natural snow, J Geophysical Research, 81(9): 1589–1592.

Cariteau et al (2011); Experimental results on the dispersion of buoyant gas in a full-scale garage from a complex source; IJHE; Volume 36, pp 2489-2496; Elsevier

Cariteau et al (2011); Experiments on the distribution of concentration due to buoyant gas low flow rate release in an enclosure; IJHE; Volume 36, pp 2505-2512; Elsevier

Cariteau et al (2012); Experimental study of the concentration build-up regimes in an enclosure without ventilation; IJHE; Volume 37 (2012); pp 17400-17408; Elsevier

Cariteau (2013); Experimental study of the effects of vent geometry on the dispersion of a buoyant gas in a small enclosure; IJHE; Volume 38, Issue 19, 27 June 2013, Pages 8030-8038; Elsevier.

Chang, J.C., Hanna, S.R. (2004): Air quality model performance evaluation; Journal of Meteorology and Atmospheric Physics; 87, 167-196; Springer Verlag (2004)

Chen Qingyan (2007); Design of natural ventilation with CFD; Sustainable urban housing in China, principle ventilations and case studies for low energy design; Springer

Chen, Qingyan (2009); Ventilation performance prediction for buildings: A method overview and recent applications; Building and Environment, 44, 4, 848-858

Christopher, J et al (2018) Power to gas for injection into the gas grid: What can we learn from real life projects, economic assessments and systems modelling? Journal of renewable and sustainable energy reviews; 98, 302-316; Elsevier.

Cogen-Europe (2015); the benefits of micro-CHP; Delta Energy and Environment; COGEN Europe [<http://www.cogeneurope.eu>]

Cook M.J; Lomas, K.J. (1979); Guidance on the use of computational fluid dynamics for modelling buoyancy driven flows; DE Montfort University; Leicester

Cornell (2019); [https://courses.cit.cornell.edu/virtual\\_lab/LabZero/Experimental\\_Error.shtml](https://courses.cit.cornell.edu/virtual_lab/LabZero/Experimental_Error.shtml) [Accessed October 2019]

Dadashzadeh (2016); Dispersion modelling and analysis of hydrogen fuel gas released in an enclosed area: A CFD-based approach; Journal of Fuel, Vol. 184 (2016) 192–201; Elsevier

Dalziel SB, Lane-Serff GF (1991); The hydraulics of doorway exchange flows. *Journal of Buildings and Environment*; Volume 26(2); pp121-135.

Dassault Systemes (2014)); Numerical basis of CAD embedded systems; Dassault Systemes SolidWorks Corporation, Waltham, MA 02451 USA.

Dassault Systemes (2015 (a)); Technical Reference; SOLIDWORKS Flow Simulation 2015; Dassault Systemes SolidWorks Corporation, Waltham, MA 02451 USA.

Dassault Systemes (2015(b)); Solving Engineering Problems; SolidWorks Flow Simulation 2015; Dassault Systemes SolidWorks Corporation, Waltham, MA 02451 USA

Dassault Systemes (2015(c)); SOLIDWORKS Flow Simulation; SolidWorks 2015 Training; Dassault Systemes SolidWorks Corporation, Waltham, MA 02451 USA.

Department for communities and local government (2010); English housing survey: Homes 2010; Annual report on England's housing stock; Department for communities and local government; Crown Copyright; ISBN: 978-1-4098-3472-4; July 2012

Deri E, Cariteau B (2010); Air fountains in the erosion of gaseous stratifications; *International Journal of Heat and Fluid Flow*; Volume 31, pp 935-941; Elsevier

Dodds, P. et al (2013); Conversion of the UK gas system to transport hydrogen; *International Journal of Hydrogen Energy*; 38, 7189-7200; Elsevier

Dodds, P. et al (2015); Hydrogen and fuel cell technologies for heating: A Review; *International Journal of Hydrogen Energy*; Volume (2015) 1-19

Draco I, et al (2019); Numerical investigation of the effect of moisture on buoyancy-driven low turbulence flow in an enclosed cavity; *International journal of heat and mass transfer*; Volume 136, June 2019, Pages 543-554; Elsevier

Driss et al (2014); Numerical simulation and experimental validation of the turbulent flow around a small incurved Savonius wind rotor; *Energy* Volume 74, 1 September 2014, Pages 506-517

E4tech. The fuel cell industry review 2014, November 2014. Available at <<http://www.e4tech.com/fuelcellindustryreview/>> [accessed on May 2017].

Ekins, P., Hughes, N., (2009). The prospects for a hydrogen economy; *Hydrogen futures; Technol; Anal Strateg. Manag.* 21, 783–803.

Epstein M. (1988); Buoyancy-driven exchange flow through small openings in horizontal partitions; *Journal of Heat Transfer*; November 1988; Volume 110/885

Epstein M., Kenton M. A. (1989); Combined natural convection and forced flow through small openings in a horizontal partition, with special reference to flows in multicompartment enclosures.

Epstein M. and Burelbach J.P. (1999); Transient mixing by natural convection in a wide layer; *International journal of heat and mass transfer*; Volume 43 (2000); pp 321-325; Pergamon.

FCH.europa (2015); HYPER Project; <http://www.fch.europa.eu/project/integrated-hydrogen-power-packs-portable-and-other-autonomous-applications>[Accessed 03.01.2017]

FCH-JU: [www.fch.europa.eu](http://www.fch.europa.eu)

- Flickr.com (2016); Image of Iranian Badgir wind catcher; [Accessed April 2016]
- Friedrich et al (2011); HYPER experiments on catastrophic hydrogen releases inside a fuel cell enclosure: *International Journal of Hydrogen Energy*; Volume 36, pp 2678-2687
- Giannissi, S. et al (2015); CFD benchmark on hydrogen release and dispersion in a ventilated enclosure: Passive ventilation and the role of an external wind; *International Journal of Hydrogen Energy*, Volume 40, Issue 19, 25 May 2015, Pages 6465-6477
- Giannissi et al (2015); Passive ventilation and the role of an external wind; *International Journal of Hydrogen Energy*; Volume 40, pp 6465 to 6477
- Giannissi et al (2016); Mitigation of buoyant gas releases in single-vented enclosure exposed to wind: Removing the disrupting wind effect; *International Journal of Hydrogen Energy*; Volume 41, Issue 6, 19 February 2016, Pages 4060-4071
- Giannissi et al (2018); Study of key parameters in modelling liquid hydrogen release and dispersion in open environment; *International Journal of Hydrogen Energy*; V 43, pp 455 to 467
- Groves, W. R. (1838); A New Voltaic Combination; London and Edinburgh Philosophical Magazine and Journal of Science; December 1938 Edition
- Gungor et al (2015); Sources of errors for indoor air CFD simulations; Norman Disney and Young. Semantic Scholar
- Hamri, O. et al (2010); Software environment for CAD/CAE integration; *Advances in Engineering Software* 41 1211-1222
- Hanna, S.R. (1989); Confidence limits for air quality model evaluations as estimated by bootstrap and jack-knife resampling methods; *Journal of Atmospheric environments*; 23: 1385-98
- Hargather M. et al (2012); A comparison of three quantitative Schlieren techniques; *Optics and Lasers in Engineering* 50 (2012) 8–17; Elsevier 2012
- Hawksworth S.J., Hedley D, et al (2014): Large scale passive ventilation trials of hydrogen; *International Journal of Hydrogen Energy* 39 (2014) 20325-20330; Elsevier
- Health and Safety Executive (HSE), 1992, Flame arresters and explosion reliefs, Health & Safety Booklet (HSG) 11, 4<sup>th</sup> impression.
- Health and Safety Laboratory (2009): Installation permitting guidance for hydrogen and fuel cell stationary applications: UK version; Health and Safety Laboratory, Harpur Hill, Buxton, Derbyshire, SK17 9JN
- Hedley D. et al (2014); Large scale passive ventilation trials of hydrogen; *International Journal of Hydrogen Energy*; V39, Iss 35, 3.12 2014, Pages 20325-20330; Elsevier
- Hindenburg image (airships.net) [Accessed December 2017]
- Holborn, P. et al (2012); A review of hydrogen dispersion modelling: Revision 2: Explosion and Fire Research Group, London South Bank University, SE1 0AA.
- Hooker P, Willoughby DB, Royle M. (2011); Experimental releases of liquid hydrogen. In: 4th ICHS; 12e14 September 2011. San Francisco, USA, paper 160.



Hübert, T (2011). Hübert, T.; Boon-Brett, L.; Black, G.; Banacha, U. (2011); Hydrogen sensors – A Review; Journal of Sensors and Actuators B: Chemical; 157, pp. 329–352

Hunt G. R., Linden P.F. (1999); The fluid mechanics of natural ventilation – displacement ventilation by buoyancy-driven flows assisted by wind; Journal of Building and Environment; Volume 34 (1999); pp 707-720; Pergamon Press.

H2FC Supergen: <http://www.h2fcsupergen.com/about/>

H<sub>2</sub>FC European Research Infrastructure: <http://www.h2fc.eu/portal.html>

HyIndoor Project: <http://www.hyindoor.eu/>

HYPER project (2015); Installation Permitting Guidance for Hydrogen and Fuel Cells Stationary Applications (HYPER) [www.hyperproject.eu](http://www.hyperproject.eu); European Commission; [www.fch.europa.eu](http://www.fch.europa.eu) [Accessed 02/06/2015]

HYSAFE: <http://www.hysafe.info/http://www.HySafe.org> [Accessed 10/06/2015]

HySAFER: <https://www.ulster.ac.uk/research/institutes/built-environment/centres/hydrogen-safety-engineering/people>

IEA. Energy balance flows. Paris, France: International Energy Agency; 2014.

Ingram J. et al (2015); Dispersion of hydrogen releases from a liquid surface and surface bursting behaviour; Journal of Hydrogen Energy; Volume 40, Issue 14, Pages 4898-4913; Elsevier 2015

Jiang Y, Chen Q (2003); Buoyancy driven single-sided natural ventilation in buildings with large openings; Journal of Heat and Mass Transfer; 45: 973-988

Jiaqing He et al (2016); Assessment of similarity relations using helium for prediction of hydrogen dispersion and safety in an enclosure; International Journal of Hydrogen Energy; 41 (2016) 1538 to 1539; Elsevier 2016

Krakovich A., Bieder U. (2015); Analysis of the interaction of round jets with stratified light gas layers with a simple turbulence model; Proceedings of ICAPP May 03-06, 2015 - Nice (France) Paper 15056

Lam, C.K.G. and Bremhorst, K.A. (1981) Modified Form of Model for Predicting Wall Turbulence, ASME Journal of Fluids Engineering, Vol.103, pp. 456-460.

Launder and Spalding (1972); The Numerical computation of turbulent flows; Paper 38; Numerical prediction of flow, heat transfer, turbulence and combustion, p96-116

Launder, B.E. and Spalding, D.B. (1974), The numerical computation of turbulent flows: Computational methods in applied mechanical engineering, 3, 269-289

Liddament, M.W. (1996); A Guide to Energy Efficient Ventilation; Air Infiltration and Ventilation Centre, IEA Energy Conservation in Buildings and Community Systems Programmed; Coventry

Linden P.F. et al (1989); Emptying filling boxes: the fluid mechanics of natural ventilation; Journal of Fluid Mechanics (1990); Volume 212, pp 309-335

Liu Pei-Chun, Lin, Hsien-Te, Chou, KJung-Hua (2009); Evaluation of buoyancy driven ventilation in atrium buildings using computational fluid dynamics and reduced scale air models; Building and Environment; 44 1970-1979

Long, V.D., 1963, Estimation of the extent of hazard areas round a vent, IChemE Second Symposium on Chemical Process Hazards,6–14.

Marbán, G., Valdés-Solís, T., (2007). Towards the hydrogen economy; *International Journal of Hydrogen of Energy* 32, 1625–1637

Merilo (2011); Experimental study of hydrogen release accidents in a vehicle garage; *International Journal of Hydrogen Energy*; Volume 36; pp 2436-2444; Elsevier.

Meroney, R. et al (2016); Review of CFD guidelines for dispersion modeling; *Multi-Disciplinary Digital Publishing Institute (MDPI)*; <https://doi.org/10.3390/fluids1020014>.

Middha, P.; Hansen, R. (2009); Validation of CFD-model for hydrogen dispersion; *Journal of loss prevention in the process industries*; 22, pp.1034-1038

Model Evaluation Group (MEG) (1994). Model evaluation protocol. European Communities Directorate, General XII Science Research and Development; 1994.

Molkov V. (2012); *Fundamentals of hydrogen safety engineering*. eBook (search hydrogen), [www.bookboon.com](http://www.bookboon.com); October 2012.

Molkov (2014); Passive ventilation of a sustained gaseous release in an enclosure with one vent; *International Journal of Hydrogen Energy* Volume 39, Issue 15, 15 May 2014, Pages 8158-8168; Elsevier

Moreno-Benito M., Antonucci P., Papa Georgiou L. (2017); Towards a sustainable hydrogen economy; *Optimisation-based framework for hydrogen infrastructure development*; *Computers & Chemical Engineering*, V102, 12 July 2017, Pages 110-127

NASA (2018): [https://www.nasa.gov/centers/glenn/technology/fuel\\_cells.html](https://www.nasa.gov/centers/glenn/technology/fuel_cells.html) [Accessed 2018]

National Aeronautics and Space Administration (2005), *Hydrogen and Hydrogen Systems; Guidelines for hydrogen system design, materials selection, operations, storage and transportation*; Office of Safety and Mission Assurance Washington, DC 20546; NSS 1740.16

Neverpaintagain.co.uk (2018): <http://www.neverpaintagain.co.uk/blog/does-anyone-still-use-their-garage-to-store-their-car/>

Nolan, D.C. et al (2015); Defining Simulation Intent; *Jrnl of Computer-aided Design*; 59; 50-63

Papanikolaou E., Venetsanos A.G et al (2011); CFD Simulations on small hydrogen releases inside a ventilated facility and assessment of ventilation efficiency; *International Journal of Hydrogen Energy*; Volume 36 (2011), pp 2597-2605; Elsevier.

Patankar, S.V. and Spalding, D.B. (1972); A calculation procedure for heat, mass and momentum transfer in three dimensional parabolic flows; *International Journal of Heat and Mass Transfer*, 15, 1787

Piomelli (2008); Wall-layer models for large eddy simulation; *Progress in aerospace sciences*; V44, Iss.6, 437-446; August 2008; Elsevier.

Prasad, K. Pitts, W.M. Fernandez, M. Yang, J.I. (2012); Natural and forced ventilation of buoyant gas released in a full-scale garage: Comparison of model predictions and experimental data; *International Journal of Hydrogen Energy* 37 (2012) 17436-17445

RAC (2006): RAC Report on motoring 2006; The future of motoring: A clear road map or collision course; ISBN 0 – 9549364 –1 – 8; ISBN 978 – 0 – 9549364 – 1 – 9 (from January 2007); RAC, 8 Surrey Street, Norwich, NR1 3NG; Website: rac.co.uk

Reinecker E. (2011); Integration of experimental facilities: A joint effort for establishing a common knowledge base in experimental work on hydrogen safety; International Journal of Hydrogen Energy; Volume 36 (2011); pp 2700-2710; Elsevier.

Renewable energy use 1960 to 2015 (OECD data 2016);  
<https://data.oecd.org/energy/renewable-energy.htm>

Rifkin, J (2002), The Hydrogen Economy; The creation of the worldwide energy web and the redistribution of power on Earth-The next great economic revolution; ISBN 1-58542-193-6; Penguin Group (USA) Inc.

Rothleder, Mark (2017); Net base load electricity generation 2012 through 2015 (California ISO-2012); <https://www.eia.gov/conference/2016/pdf/presentations/> [Accessed Jan18]

Saad, Y. (2003) Iterative methods for sparse linear systems; Society for Industrial and Applied Mathematics; Philadelphia (PA)

Schefer, R.W., Houf, W.G. and Williams, T.C. (2008); Investigation of small-scale unintended releases of hydrogen; Buoyancy effects; International Journal of Hydrogen Energy; Volume 33, pp 4702-4712

Schluter J (2001); Influence of Axisymmetric Assumptions on Large Eddy Simulations on a Confined Jet and a Swirl Flow; Stanford University, Center for Turbulence Research, Bldg. 500, Stanford, CA, 94305-3030, USA, Jorg.Schluter@stanford.edu

Sellafield (2018); <https://www.gov.uk/government/organisations/sellafield-ltd> [Accessed 2018]

Settles G.S. (2001); Schlieren and shadowgraph techniques. Visualising phenomena in transparent media. Springer-Verlag, Berlin Heidelberg New York (2006)

Shaw B.H. and Whyte, W (1974); Air movement through doorways. The influence of temperature and its control by forced airflow. Building service engineering. Vol 42 (12); pp 210-218

SolidWorks Flow Simulation (2017): Dassault Systemes SolidWorks Corporation; 175 Wyman Street, Waltham, MA 02451, United States; <https://www.solidworks.com>

Srinivasa et al (2014); CFD code benchmark against the air/helium tests performed in the MISTRA facility; Annals of Nuclear Energy; Volume 69, pp 37–43

Staffell, I et al (2013); The cost of domestic fuel cell micro CHP systems; International Journal of Hydrogen Energy; Volume 38, issue 2, 1088-1102; Elsevier

Swain, M. R., & Swain, M. N (1992). A comparison of H<sub>2</sub>, CH<sub>4</sub> and C<sub>3</sub>H<sub>8</sub> fuel leakage in residential settings. International Journal of Hydrogen Energy, 17(10), 807-815. DOI: 10.1016/0360-3199(92)90025-R

Swain M.R. (1996); Passive Ventilation Systems for the Safe use of Hydrogen; International Journal of Hydrogen Energy; Volume 21, pp 823-835; Elsevier.

Swain M.R. et al (2002), Hydrogen leakage into simple geometric enclosures; International Journal of Hydrogen Energy; Volume 28, pp 229-248; Pergamon.

SUSANA: <http://www.fch.europa.eu/project/support-safety-analysis-hydrogen-and-fuel-cell-technologies>

Thakur, A et al (2009); A survey of CAD model simplification techniques for physics based simulation applications; *Journal of Computer Aided Design*; 41; 65-80

The Federation of British Historic Vehicle Clubs Vaughan B and Hows R (2010); An Overview of the Development of IP-2 ISO Freight Containers in the UK; Patram 2010

Thoughtco (2019); <https://www.thoughtco.com/how-to-calculate-percent-error-609584> [Accessed October 2019]

Tolias, I. C. et al (2019); Best practice guidelines in numerical simulations and CFD benchmarking for hydrogen safety application; *International Journal of Hydrogen Energy*; 44, 9050-9062; Elsevier; <https://h2tools.org/bestpractices/passive-ventilation>

US Energy Information Administration (2016); Fossil fuel use – Projection; <https://www.eia.gov/todayinenergy/detail.php?id=26912>

Versteeg H.K., (2007); An introduction to Computational Fluid Dynamics [The finite volume method] 2<sup>nd</sup> edition; ISBN: 978-0-13-127498-3 Pearson Education Limited, UK.

Venetsanos et al (2010); On the use of hydrogen in confined spaces: Results from the internal project InsHyde; *International Journal of Hydrogen Energy*; Volume 36 (2011), pp 2693-2699; Elsevier.

Visser et al (2012); Validation of a FLUENT CFD model for hydrogen distribution in a containment; *Nuclear Engineering and Design*; 245 (2012) 161– 17; Elsevier

Volkart, K et al (2017); Europe’s Energy Transition – Insights into Policymaking; pp 189-205;

Vudumu, S.; Koylu, U. (2009); Detailed simulations of the transient hydrogen mixing, leakage and flammability in air in simple geometries; *IJHE*; 34, pp. 2824-2833

Weiner S.C. (2014); Advancing the hydrogen safety knowledge base; *International Journal of Hydrogen Energy*; 39 (2014) 20357-20361

Wilson D. J. and Kiel D. (1990); Gravity driven counter flow through an open door in a sealed room. *Building and environment*. Vol 25 (4). Pp 379-388

Wyman, O (2016); World Energy trilemma: World Energy Council Definition - <https://www.worldenergy.org/work-programme/strategic-insight/assessment-of-energy-climate-change-policy/>

XEN-TGC 3880 Data Sheet; <http://www.xensor.nl/pdf/files/sheets/xen-tcg3880.pdf> [Accessed 02/06/2015]

Xensor Integration (2017); Thermal Conductivity Gauge, TCG 3880; Data sheet; <http://www.xensor.nl/pdf/files/sheets/xen-tcg3880.pdf>

Yang et al (2013); Measurements of effective diffusion coefficients of helium and hydrogen through gypsum; *International journal of hydrogen energy*; Volume 8 pp 8125 to 8131

Yuanliang L. (2019); Modelling the development of hydrogen vapor cloud considering the presence of air humidity; *International Journal of Hydrogen Energy*; Volume 44, Issue 3, 15 January 2019, Pages 2059-2068; Elsevier

## Appendix A: Posters and Publications [Front page only]

Conference abstract: H2FC Supergen Conference Bath 2015 [Presented September 2015]

<b>Presenter Name</b>	Tara Singh Ghatauray
<b>Type of Presentation</b> (Oral, Poster and/or 3MT)	Poster presentation
<b>Topic Area</b> <i>Select from list or Other</i>	Hydrogen Safety
<b>Email</b>	ghataurt@lsbu.ac.uk
<b>Authors of Abstract</b>	Tara Singh Ghatauray Dr James Ingram, Dr Paul Holborn

### Abstract

#### Experimental and CFD study into cross-flow passive venting in small Fuel Cell enclosures

An experimental and Computational Fluid Dynamics (CFD) study is presented on Helium dispersion in a 0.216 m<sup>3</sup> ‘cross-flow’ passively ventilated enclosure at low release rates (1-5 L/min), to simulate a Hydrogen leak in a small fuel cell (FC) enclosure. The Helium, (a safe analogue for Hydrogen), was released from a centrally positioned vertical 5mm diameter nozzle. Observations of Helium dispersal behaviour and concentration were made, subject to variations in vent area and leak rate. SolidWorks ‘Flow Simulation’ CFD, studies, of the scenarios were undertaken, with the empirical data used to validate the CFD model.

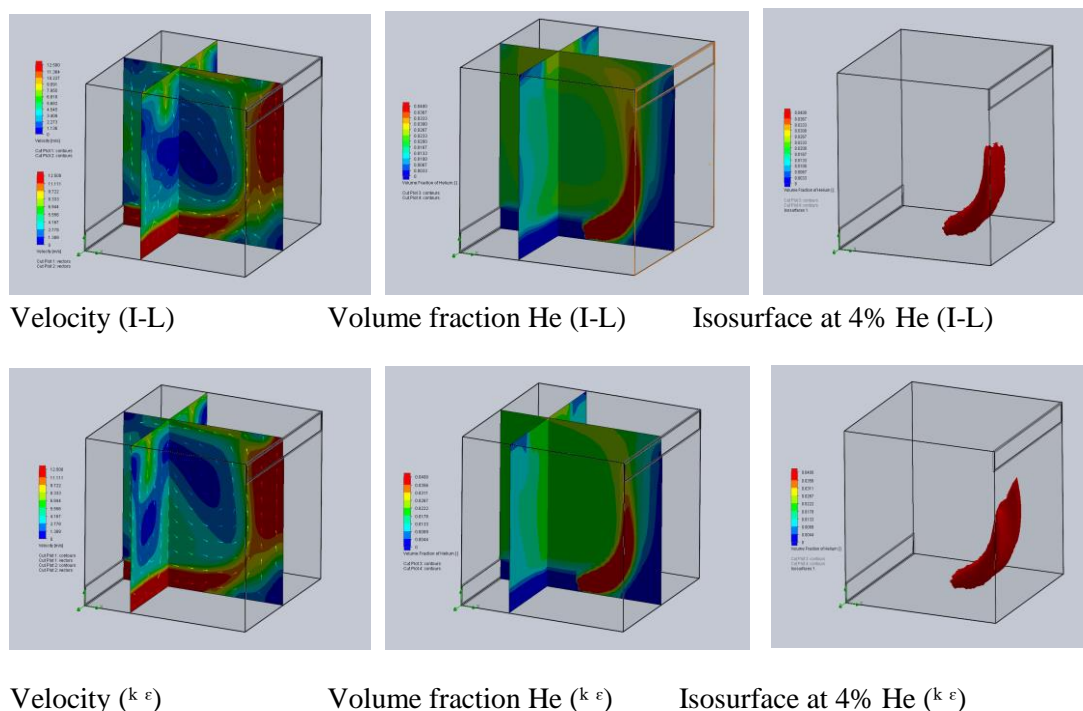
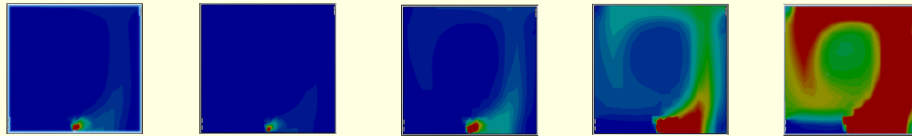


Figure 1 Examples of SolidWorks ‘Flow Simulation’ CFD output

## Poster: H2FC Supergen Conference Bath 2015 [Presented September 2015]

## Experimental and CFD Study of Buoyant Gas Dispersion, Through Passive Ventilation in a Small Fuel Cell Enclosure

Tara Singh Ghatauray, Paul Holborn, James Ingram  
 'Explosion and Fire Research Group'  
 School of Engineering, London South Bank University

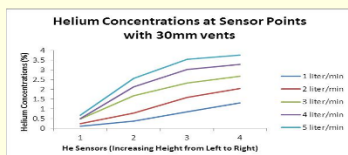


CFD images of Helium dispersal in a cuboid enclosure

### INTRODUCTION

With the emergence of a 'Hydrogen Economy', fuel cell (FC) deployment in small enclosures will become common place. However, hydrogen's wide flammable range (4-74%) poses a significant safety concern. Without adequate ventilation, a hydrogen gas leak from a FC could create flammable mixtures in the enclosure, and hence the potential for an explosion. Traditionally, a mechanical ventilation system would be employed in an enclosure to ensure Hydrogen gas is removed and prevent a flammable concentration forming. However, in many applications (e.g. low power and remote installations) mechanical ventilation is undesirable, since it would drain the FC output and its operation would be vulnerable to any power failures that may occur. In such situations, it is therefore desirable to be able to employ a passive ventilation system to remove the hydrogen gas from the FC enclosure.

### EXPERIMENTAL DATA



### STUDY POSITION

- Experimental data is being produced for a number of cases
- Simulation refinement is working towards validation
- Determination of optimal turbulence model is unclear at this point

### NEXT STEPS

- Further experimental work with various vent arrangements and sizes
- Continue to investigate SolidWorks Flow Simulation modelling solutions to validate the software for this study
- Apply variations in nozzle height and release direction
- To replicate these studies on ANSYS CFD

### REFERENCES

- Cariteau, B., Tkatschenko, I. (2012); Experimental study of the effects of vent geometry on the dispersion of a buoyant gas in a small enclosure; International Journal of Hydrogen Energy; 38 (2013) 8030-8038
- Giannisi, S.G., Molkov, V. et al (2015); CFD benchmark on hydrogen release and dispersion in confined, naturally ventilated space with one vent; International Journal of Hydrogen Energy; 40 (2015) 2415-2429
- Molkov, V., Shentov, V (2014); Numerical and physical requirements to simulation of gas release and dispersion in an enclosure with one vent; International Journal of Hydrogen Energy; 39 (2014) 13328-13345
- Xensor Integration by-Suppliers of Helium sensors  
 SolidWorks- Flow Simulation software

### ACKNOWLEDGEMENTS

The authors would like to acknowledge Sellafeld Ltd for their financial support of this project and BOC for training in and the use of their SolidWorks application.

### PASSIVE VENTILATION

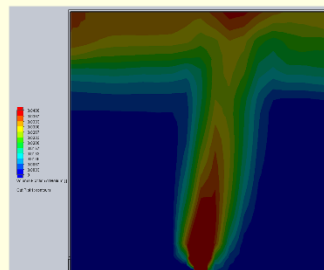
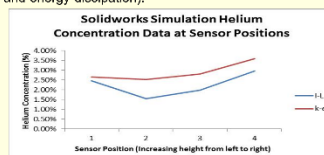
Passive ventilation relies upon buoyancy and internal/external pressure and temperature differences to drive flow through a containment. The size, shape and position of ventilation openings is critical for producing predictable flows and maintaining low gas concentrations.

### OBJECTIVES

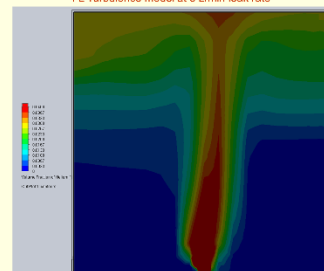
- To obtain experimental and simulation data to support the validation of the SolidWorks Flow Simulation software in a new application scenario
- To obtain data to support the development of a predictive model for passive ventilation schemes

### CFD SIMULATION DATA

SOLIDWORKS TURBULENCE MODELS: Two models are available within the application. I-L (Turbulence intensity and length) and standard k-e (kinetic energy and energy dissipation).



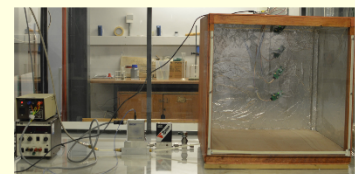
I-L Turbulence model at 5 L/min leak rate



k-e Turbulence model at 5 L/min leak rate

### EXPERIMENTAL/SIMULATION SCENARIO

A small cuboid enclosure incorporating a simple cross-flow ventilation scheme is used to assess its ability to manage buoyant gas concentrations in a leak scenario. Helium, (a safe analog for Hydrogen), is released from a 4mm diameter tube in a central position on the enclosure floor. Leak rates from 1-5 liters per minute are tested.



### XENSOR HELIUM SENSORS

Gas concentrations are recorded at positions through the enclosure using static 'mini-katharometer' Helium sensors. The sensors are Xensor 'XEN-TCG3880' connected via a XEN-8500 USB read-out to a PC running 'LabVIEW'. Sensors positioned at 20, 30, 40 and 50mm centrally.



### CFD MODELLING

A Computational Fluid Dynamics (CFD) simulation is run on a CAD model of the test rig with boundary conditions replicating the experimental tests. SolidWorks Flow Simulation CFD is used. The system allows selection of turbulence models to suit the modelling scenario.

### CFD BOUNDARY CONDITIONS

- Environmental pressure at the vents
- Leak rates 1,2,3,4,5 litres per minute
- Adiabatic wall conditions
- Gravity in y direction
- Vent pressure - environmental



### GAS DELIVERY

A Brooks GF125 High purity digital thermal mass controller manages the Helium delivery using the 'Brooks Expert Support Tool' to change the flow 'set-point', through a USB connection.



London South Bank  
 University

Conference Paper: ICHEME HAZARDS 26 Conference Edinburgh [Presented May 2016]

**Title:**

*A comparison study into the dispersion of buoyant gas using plain and louvre vent passive ventilation schemes in a small fuel cell enclosure at low leak rates*

**Ghatauray, T.S.<sup>1</sup>, Ingram, J.M. and Holborn, P.G.**

**<sup>1</sup> Explosion and Fire Research Group, London South Bank University, Borough Road, London, SE1 0AA, UK, ghataurt@lsbu.ac.uk**

The development of a 'Hydrogen Economy' will see hydrogen fuel cells used in transportation and the generation of power for buildings as part of a decentralised grid, with low power units used in domestic and commercial environmental, situations. Low power fuel cells will be housed in small protective enclosures, which must be ventilated to prevent a build-up of hydrogen gas, produced during normal fuel cell operation or a supply pipework leak. Hydrogen's flammable range (4-75%) is a significant safety concern. With poor enclosure ventilation, a low-level leak (below 10 lpm) could quickly create a flammable mixture with potential for an explosion. Mechanical ventilation is effective at managing enclosure hydrogen concentrations but drains fuel cell power and is vulnerable to failure. In many applications (e.g. low power and remote installation) this is undesirable and reliable passive ventilation systems are preferred. Passive ventilation depends upon buoyancy driven flow, with the size and shape of ventilation openings critical for producing predictable flows and maintaining low gas concentrations. Environmentally installed units use louvre vents to protect the fuel cell, but the performance of these vents compared to plain vertical vents is not clear. Comparison enclosure (0.144m<sup>3</sup>) tests of 'same opening area' louvre and plain vents, with leak rates from 1 to 10 lpm, were conducted. A displacement ventilation arrangement was installed on the test enclosure with upper and lower opposing openings. Helium gas was released from a 4mm nozzle at the base of the enclosure to simulate a hydrogen leak. The tests determined that louvre vents increased average enclosure hydrogen concentrations by approximately 2% across the leak range but regulated the flow. The test data was used to validate a SolidWorks CFD simulation model of the enclosure. The model provided a good qualitative representation of the flow behaviour but under predicted average concentrations.

**Keywords:** hydrogen safety, helium, passive venting, louvre vent, fuel cell enclosure

## **1.0 INTRODUCTION**

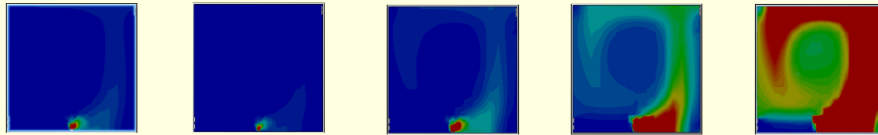
### **1.1 Background to the investigation**

The impact of climate change, the depletion of fossil fuels and the global policy drive towards carbon reduction has led to a technology push for renewable forms of energy, improved energy efficiency and decentralised generation which aims to achieve social, economic and environmental sustainability. The concept of a Hydrogen Economy is gathering momentum as a means to achieve these objectives. Hydrogen, the most abundant element in the universe, can be used as an energy carrier, able to release its energy usefully in a number of ways. It can be combined with other gaseous fuels to improve combustion and reduce carbon emissions in boilers and engines. It can also be burnt in isolation as a clean fuel producing only water as a by-product. A popular choice is its use in Hydrogen fuel cells to generate electricity, again producing water as a by-product.

Poster: LSBU Research Conference 2016 [Presented July 2016]

# London South Bank University Study into buoyant gas dispersion using passive ventilation in a small fuel cell enclosure

Tara Singh Ghatauray, Paul Holborn, James Ingram  
 'Explosion and Fire Research Group'  
 School of Engineering, London South Bank University



CFD images of Helium dispersal in a cuboid enclosure

**INTRODUCTION**

With the emergence of a 'Hydrogen Economy', fuel cell (FC) deployment in small enclosures will become common place. However, hydrogen's wide flammable range (4-74%) poses a significant safety concern. Without adequate ventilation, a hydrogen gas leak from a FC could create flammable mixtures in the enclosure, and hence the potential for an explosion. Traditionally, a mechanical ventilation system would be employed in an enclosure to ensure Hydrogen gas is removed and prevent a flammable concentration forming. However, in many applications (e.g. low power and remote installations) mechanical ventilation is undesirable, since it would drain the FC output and its operation would be vulnerable to any power failures that may occur. In such situations, it is therefore desirable to be able to employ a passive ventilation system to remove the hydrogen gas from the FC enclosure.

**PASSIVE VENTILATION**

Passive ventilation relies upon buoyancy and internal/external pressure and temperature differences to drive flow through a containment. The size, shape and position of ventilation openings is critical for producing predictable flows and maintaining low gas concentrations.

**OBJECTIVES**

- To obtain experimental and simulation data to support the validation of SolidWorks Flow Simulation
- To obtain data to support the development of a predictive model for passive ventilation schemes

**STUDY POSITION**

- Experimental data is being produced for a number of cases
- Simulation refinement is working towards validation
- Determination of optimal turbulence model is unclear at this point

**EXPERIMENTAL/SIMULATION SCENARIO**

A small cuboid enclosure incorporating a simple cross-flow ventilation scheme and variants is used to assess its ability to manage buoyant gas concentrations in a leak scenario. Helium, (a safe analogue for Hydrogen), is released from a 4mm diameter tube in a central position on the enclosure floor. Leak rates from 1-5 litres per minute are tested.

**CFD MODELLING**

A Computational Fluid Dynamics (CFD) simulation is run on a CAD model of the test rig with boundary conditions replicating the experimental tests. SolidWorks Flow Simulation CFD is used. The system allows selection of turbulence models to suit the modelling scenario.

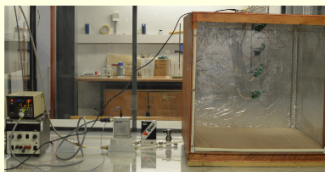
**CFD BOUNDARY CONDITIONS**

- Environmental pressure at the vents
- Leak rates 1,2,3,4,5 litres per minute
- Adiabatic wall conditions
- Gravity in y direction
- Vent pressure - environmental

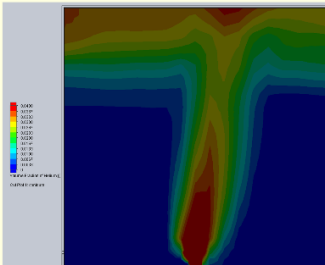
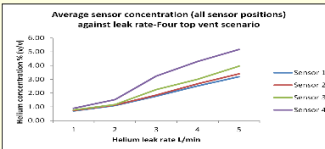
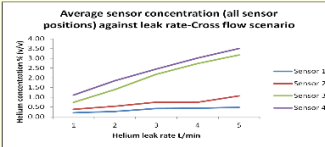
**SOLIDWORKS TURBULENCE MODELS:** Two models are available within the application. I-L (Turbulence intensity and length) and standard k-e (kinetic energy and energy dissipation).

**NEXT STEPS**

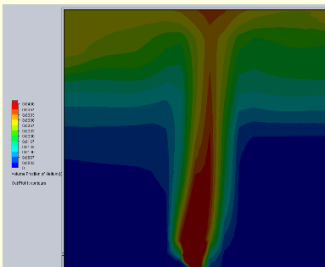
- Environmental effects on enclosure performance
- Vent, stack, flue arrangements
- CFD Benchmarking



**EXPERIMENTAL DATA**



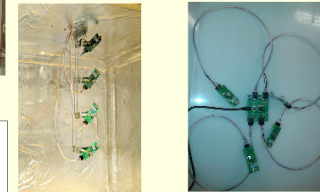
I-L Turbulence model at 5 L/min leak rate



k-e Turbulence model at 5 L/min leak rate

**XENSOR HELIUM SENSORS**

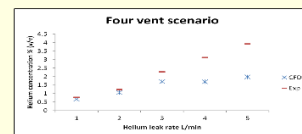
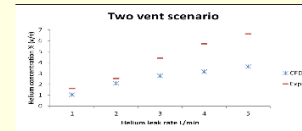
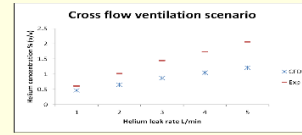
Gas concentrations are recorded at positions through the enclosure using static 'mini-kathometer' Helium sensors. The sensors are Xensor 'XEN-TCG3980' connected via a XEN-8500 USB read-out to a PC running 'LabVIEW'. Sensors positioned at 20, 30, 40 and 50mm centrally.



**GAS DELIVERY**

A Brooks GF125 High purity digital thermal mass controller manages the Helium delivery using the 'Brooks Expert Support Tool' to change the flow 'set-point', through a USB connection.

**CFD/experimental data comparison**



**REFERENCES**

Cariteau, B., Tkatschenko, I. (2012); Experimental study of the effects of vent geometry on the dispersion of a buoyant gas in a small enclosure; International Journal of Hydrogen Energy; 38 (2013) 8030-8038  
 Giannissi, S.G., Molkov, V. et al (2015); CFD benchmark on hydrogen release and dispersion in confined, naturally ventilated space with one vent; International Journal of Hydrogen Energy; 40 (2015) 2415-2429  
 Molkov, V., Shentov, V (2014); Numerical and physical requirements to simulation of gas release and dispersion in an enclosure with one vent; International Journal of Hydrogen Energy; 39 (2014) 13328-13345  
 Xensor Integration by- Suppliers of Helium sensors  
 SolidWorks- Flow Simulation software



**ACKNOWLEDGEMENTS**

The authors would like to acknowledge Sellafeld Ltd for their financial support of this project and BOC for training in and the use of their SolidWorks application.



Poster: LSBU Research Conference 2016 [Presented July 2016]

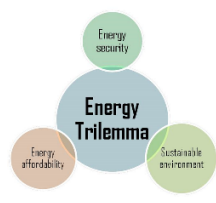
**London South Bank University**

# Retrofitting Dwellings to Achieve Near Zero Energy Buildings

Tara Singh Ghatauray  
School of Engineering, London South Bank University

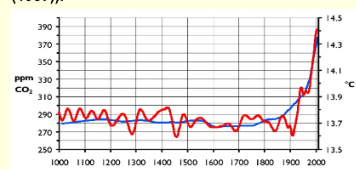
### Environmental position

Threats to Energy Security, Environmental Sustainability and Energy affordability (fuel poverty) arising from fossil fuel exploitation and dependence requires assertive action to mitigate harm and reduce greenhouse gas emissions. EU buildings consume 40% of energy and emit 36% of our CO<sub>2</sub>. Domestic properties contribute about 27% of UK CO<sub>2</sub> emissions. With 35% of EU buildings over 50 years old, there is significant scope to reduce consumption and emissions.



### Sustainable Development

Atmospheric carbon dioxide levels have risen since the industrial revolution, increasing greenhouse effect. Consequences are rising temperatures, melting glaciers, droughts, floods and weather extremes. Impact on world economies and migration are global issues. Countering these problems requires a shift towards 'sustainable development', defined as "meeting the needs of the present, without compromising the needs of future generations" (The Brundtland Report (1987)).



**Near Zero Energy Retrofit (NZEB) rational**  
There is a strong environmental and economic case for the NZEB retrofit of old and inefficient housing stock. Legislation and growing concern is driving improved energy performance in buildings

### Regulations Relevant to NZEB Retrofit

- The 1992 Rio 'Earth Summit'
- 2015 Paris UN Climate Change Conference set limits for global warming to 2%.
- UK Climate Change Act 2008 set carbon emissions target of 80% below 1990 levels by 2050 (with a 34% reduction by 2020)
- EU set goals of 20% reduction in greenhouse gasses, 20% increase in energy efficiency and a 20% increase in renewable energy by 2020.
- UK Zero Carbon Standard (2007) required;
  - Reduced energy demand through fabric energy efficiency
  - Fabric performance, heating, cooling, lighting and ventilation to meet Carbon Compliance limit
  - CO<sub>2</sub> emissions from regulated energy reduced to zero.
- The Energy Performance in Buildings Directive (EPBD) 2010,
- The Building Regulations 2010 - Conservation of Fuel and Power and Part F Ventilation

### Incentives available to domestic retrofits

**Renewable energy feed-in tariff (REFIT)** is a tariff paid for surplus electricity generated and exported back to the grid. It is available for Solar PV and wind installations of 50kW or less.

**The domestic renewable heat incentive (RHI)** provides quarterly payments for up to seven years for installed renewable heat systems such as;

- Biomass boilers/pellet stoves
- Air/Ground source heat pumps
- Solar thermal panels

### Retrofit aims and objectives

- To reduce energy use and carbon emissions by
  - Reducing fabric heat loss
  - Improving ventilation/infiltration/air tightness
  - Replacing space/water heating
  - Minimising lighting and appliance energy
  - Improve glazing
  - Applying low carbon technologies
  - Improve the thermal comfort



### Retrofit technologies

- Insulation:
  - Internal/external/cavity wall
  - Loft / floor
- Glazing: Double/triple (coated)
- Ventilation: Mechanical with heat recovery
- Heating and Hot Water:
  - Air Source Heat Pump (ASHP)
  - Ground source heat pump
  - Solar Thermal
- On site generation
  - Solar Photovoltaic
  - CHP/Fuel cell
  - Wind
- Lighting: LED lamps
- Appliances: A+ (or better) rated

### Multi-disciplinary Team

- A multi-disciplinary team is required for an NZEB project, including
- Architect/designer /project manager
  - Housing authority
  - Resident
  - Contractor s/Installers



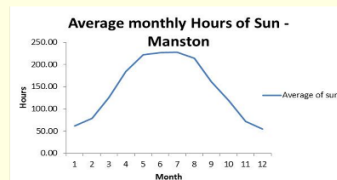
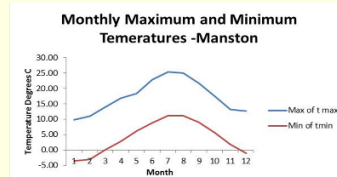
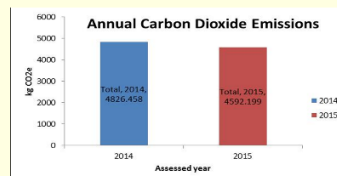
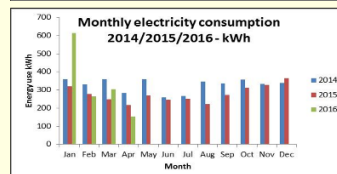
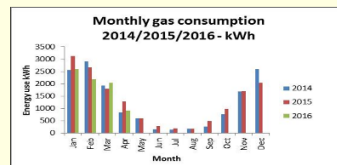
### Standard Assessment Procedure SAP

The SAP is the governments recommended methodology for determining the energy performance of dwellings (SAP (2012)). Performance indicators associated with energy costs for space heating, ventilation, water heating and lighting are;

- Energy consumption per unit floor area,
- Dwelling CO<sub>2</sub> Emission Rate (DER),
- Environmental Impact rating based on CO<sub>2</sub> emissions (the EI rating-1-100)

### Case Study

Average 1960s unrestored detached dwelling



Month	Jan	Feb	Mar	Apr	May	Jun	Jul	Aug	Sep	Oct	Nov	Dec
Heating Degree Days	293	285	287	205	119	50	18	13	60	114	148	150

Environmental impact rating (EI)	2015	Retrofit
CF (Carbon factor)	34.79	1.49
EI (1-100)	53.56	98.00
Rating band (SAP 2012 BRE)	E	A

### Conclusions

An unmodified home requires the maximum of regulated energy to run. Regulated energy will produce a massive amount of CO<sub>2</sub>. An NZEB retrofit will produce radical results and can achieve BRESAP A ratings. There is a significant financial cost and payback periods of twenty-five years are common.

### REFERENCES

- Craig-dea.co.uk / gregolis.en-global warming
- SAP 2012
- Tohoku-indonesia.com



**Conference Paper: LSBU Research Conference 2017 [Presented July 2017]**

**Title:** *Changing the future with hydrogen*

**Author:** Ghatauray, T.S.

**Explosion and Fire Research Group, London South Bank University, Borough Road, London, SE1 0AA**

**Abstract:**

What do the following have in common? Pollution, poor air quality, eutrophication, war, water shortages, population explosion, migration, climate change, global warming, sea level rise, deglaciation, resource depletion, social inequality, energy shortage and insecurity, economic instability, loss of habitat, eco-system damage, species extinction, cancer. They are all linked to fossil fuel use since the industrial revolution.


In a few short years, anthropogenic environmental damage has been extraordinary, and in the main irreparable. Damage mitigation is required to ameliorate the harm. Moving away from fossil fuel exploitation and towards renewable and sustainable energy sources is the only short-term way to reduce carbon emissions, slow atmospheric warming and ease planetary damage.

There is an alternative, in the form of hydrogen, the most abundant element in the universe. Hydrogen can be safely produced from water and when used to generate heat or electricity, returns the water to us. A new hydrogen economy can fulfill heat and power needs and be produced from renewables such as wind and solar PV.

Hydrogen fuel cells (HFC) produce electricity, heat and water. They can power buildings, run domestic combined heat and power units, replace remote diesel generators and replace vehicle drive trains. In Japan and Korea hundreds of thousands of units have been sold. However, UK sales are slow, partly due to hydrogen safety concerns.

HFCs are housed in protective enclosures, requiring venting to eliminate any leaked hydrogen. Hydrogen is a buoyant gas with a wide flammable range (4-74%), needing careful management in confinement. Reliable passive ventilation schemes, particularly in small enclosures will raise consumer confidence and speed market up take. Success will reduce carbon emissions, improve air quality, provide energy independence, and start to heal the world.

Poster: LSBU Research Conference 2017 [Presented July 2017]



**London South Bank University**  
EST 1892

**Hydrogen Economy-Fuel Cell Future?**  
**Societal and Economic Benefits**  
Tara Singh Ghatauray, Dr James Ingram, Dr Paul Holborn  
School Of Engineering [Explosion and Fire Research Group]

**CHOOSE YOUR ELEMENT PATH WISELY!**


**“BOTH ARE ENERGY GIFTS FROM THE SUN”**

**HYDROGEN FUTURE**

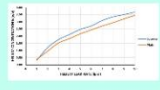
hydrogen  
**H**  
1.0079

Available now!!

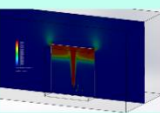
**‘H<sub>2</sub>’ Safety Research : Passive Hydrogen Venting**  
Using natural forces of buoyancy to remove hydrogen from small HFC enclosures



Investigating the effect of vent design upon enclosure hydrogen concentration



Using CFD prediction modelling to improve enclosure design



**CARBON FUTURE**

**C**<sup>12</sup><sub>6</sub>

Explosive power!!

**Petroleum Research: How can we get more oil out of the planet!!!!!!**

- We still need fossil fuels during the transition to hydrogen
- Fossil fuel research is aimed at enhanced production
- Hydrogen will be produced from fossil fuels
- Hydrogen can be mixed with natural gas in the gas network for domestic and commercial heat
- Fuel cells can be run on methane or steam reformed at point of use to produce hydrogen
  - **Fossil fuel production must stop soon if we are to create a sustainable planet!**

**STOP Fracking**

Poisoning of water courses is killing eco-systems

Plastics do not degrade

**“BUT DON’T FOCUS ON THE PRESENT THINK ABOUT THE FUTURE”**

**“DO NOT GET IT WRONG”**

**Conference Paper: HYSAFE 2017 Hamburg [Presented October 2017]**

*Title: A comparison study into low leak rate buoyant gas dispersion in a small fuel cell enclosure using plain and louvre vent passive ventilation schemes*

**Ghatauray, T.S.<sup>1</sup>, Ingram, J.M.<sup>1</sup> and Holborn, P.G.<sup>1</sup>**

**<sup>1</sup> Explosion and Fire Research Group, London South Bank University, Borough Road, London, SE1 0AA, UK, ghataurt@lsbu.ac.uk; ingramja@lsbu.ac.uk; p.holborn@lsbu.ac.uk**

**Abstract**

The development of a ‘Hydrogen Economy’ will see hydrogen fuel cells used in transportation and the generation of power for buildings as part of a decentralised grid, with low power units used in domestic and commercial environmental, situations. Low power fuel cells will be housed in small protective enclosures, which must be ventilated to prevent a build-up of hydrogen gas, produced during normal fuel cell operation or a supply pipework leak. Hydrogen’s flammable range (4-75%) is a significant safety concern. With poor enclosure ventilation, a low-level leak (below 10 lpm) could quickly create a flammable mixture with potential for an explosion. Mechanical ventilation is effective at managing enclosure hydrogen concentrations but drains fuel cell power and is vulnerable to failure. In many applications (e.g. low power and remote installation) this is undesirable and reliable passive ventilation systems are preferred. Passive ventilation depends upon buoyancy driven flow, with the size and shape of ventilation openings critical for producing predictable flows and maintaining low buoyant gas concentrations. Environmentally installed units use louvre vents to protect the fuel cell, but the performance of these vents compared to plain vertical vents is not clear. Comparison small enclosure tests of ‘same opening area’ louvre and plain vents, with leak rates from 1 to 10 lpm, were conducted. A displacement ventilation arrangement was installed on the test enclosure with upper and lower opposing openings. Helium gas was released from a 4mm nozzle at the base of the enclosure to simulate a hydrogen leak. The tests determined that louvre vents increased average enclosure hydrogen concentrations by approximately 10% across the leak range tested but regulated the flow. The test data was used in a SolidWorks CFD simulation model validation exercise. The model provided a good qualitative representation of the flow behaviour but under predicted average concentrations.

Keywords: hydrogen safety, helium, passive venting, louvre vent, fuel cell enclosure

**Nomenclature**

nlp	Normal litre per minute
lpm	Litre per minute
stp	Standard temperature and pressure
LFL	Lower flammable limit (4%)
$C_d$	Discharge coefficient

**1.0 INTRODUCTION****1.1 Background to the investigation**

The impact of climate change, the depletion of fossil fuels and the global policy drive towards carbon reduction has led to a technology push for renewable forms of energy, improved energy efficiency and decentralised generation which aims to achieve social, economic and environmental sustainability. The concept of a Hydrogen Economy is gathering momentum to achieve these objectives. Hydrogen, the most abundant element in the universe, can be used as an energy carrier, able to release its energy usefully in many ways. It can be combined with other gaseous fuels to improve combustion and reduce carbon emissions in boilers and engines.

**Journal Paper: International Journal of Hydrogen Energy [Submitted April 2018]**

**Title:**

*A comparison study into low leak rate buoyant gas dispersion in a small fuel cell enclosure using plain and louvre vent passive ventilation schemes*

**Authors:** Ghatauray, T.S. \*, Ingram, J.M., Holborn, P.G.

Explosion and Fire Research Group, School of Engineering, London South Bank University (LSBU), Borough Road, London, SE1 0AA, UK,

**Abstract**

Hydrogen, producing electricity in fuel cells, is a versatile energy source, but with risks associated with flammability. Fuel cells use enclosures for protection which need ventilating to remove hydrogen emitted during normal operation or from supply system leaks. Passive ventilation, using buoyancy driven flow is preferred to mechanical systems. Performance depends upon vent design, size, shape, position and number. Vents are usually plain rectangular openings, but environmentally situated enclosures use louvres for protection. The effect of louvres on passive ventilation is not clear and has therefore been examined in this paper. Comparison ‘same opening area’ louvre and plain vent tests were undertaken using a 0.144 m<sup>3</sup> enclosure with opposing upper and lower vents and helium leaking from a 4 mm nozzle on the base at rates from 1 to 10 lpm, simulating a hydrogen leak. Louvres increased stratified level helium concentrations by a minimum of 15 %. The empirical data obtained was also used in a validation exercise with a SolidWorks: Flow Simulation CFD model, which provided a good qualitative representation of flow behaviour but under predicted average concentrations.

**Keywords**

- Hydrogen safety,
- Passive ventilation
- Buoyant gas
- Louvre vent
- Helium
- SolidWorks CFD

**Nomenclature and units**

nlpn	Normal litre per minute
lpm	Litre per minute
$C_d$	Discharge coefficient

**Abbreviations**

STP	Standard temperature and pressure
LFL	Lower flammable limit (Hydrogen = 4%)
CFD	Computational fluid dynamics

**1.0 Introduction**

There is a global move away from fossil fuel dependence and its replacement with a distributed energy system based upon renewable sources of energy. A ‘Hydrogen Economy’ is being promoted as a transition measure that will support a new energy infrastructure based upon renewables. The hydrogen economy though will only succeed if issues around hydrogen production, storage, transportation and safe conversion to a viable energy source are resolved.

## Published Journal Paper: International Journal of Hydrogen Energy

## ARTICLE IN PRESS

INTERNATIONAL JOURNAL OF HYDROGEN ENERGY XXX (2018) 1–10

Available online at [www.sciencedirect.com](http://www.sciencedirect.com)

ScienceDirect

journal homepage: [www.elsevier.com/locate/hydro](http://www.elsevier.com/locate/hydro)

## A comparison study into low leak rate buoyant gas dispersion in a small fuel cell enclosure using plain and louvre vent passive ventilation schemes

T.S. Ghatauray\*, J.M. Ingram, P.G. Holborn

Explosion and Fire Research Group, School of Engineering, London South Bank University (LSBU), Borough Road, London, SE1 0AA, UK

## ARTICLE INFO

## Article history:

Received 30 April 2018  
 Received in revised form  
 2 August 2018  
 Accepted 9 August 2018  
 Available online xxx

## Keywords:

Hydrogen safety  
 Passive ventilation  
 Buoyant gas  
 Louvre vent  
 Helium  
 SolidWorks: Flow Simulation CFD

## ABSTRACT

Hydrogen, producing electricity in fuel cells, is a versatile energy source, but with risks associated with flammability. Fuel cells use enclosures for protection which need ventilating to remove hydrogen emitted during normal operation or from supply system leaks. Passive ventilation, using buoyancy driven flow is preferred to mechanical systems. Performance depends upon vent design, size, shape, position and number. Vents are usually plain rectangular openings, but environmentally situated enclosures use louvres for protection. The effect of louvres on passive ventilation is not clear and has therefore been examined in this paper. Comparison 'same opening area' louvre and plain vent tests were undertaken using a 0.144 m<sup>3</sup> enclosure with opposing upper and lower vents and helium leaking from a 4 mm nozzle on the base at rates from 1 to 10 lpm, simulating a hydrogen leak. Louvres increased stratified level helium concentrations by typically in excess of 15%. The empirical data obtained was also used in a validation exercise with a SolidWorks: Flow Simulation CFD model, which provided a good qualitative representation of flow behaviour and close empirical data correlations.

© 2018 Hydrogen Energy Publications LLC. Published by Elsevier Ltd. All rights reserved.

## Introduction

There is a global move away from fossil fuel dependence and its replacement with a distributed energy system based around renewable energy sources. A 'Hydrogen Economy' is promoted as a transition measure that will support the development of the new renewable energy infrastructure. The hydrogen economy though will only succeed if concerns relating to hydrogen production, storage, transportation and safe conversion to a viable energy source are resolved.

Hydrogen fuel cells are a key part of the initiative being used at a variety of scales to provide distributed energy. Low power fuel cells, housed in small protective enclosures, are likely to become widely used in domestic and commercial applications. However, because fuel cells emit small amounts of hydrogen and there is the possibility of a leak from supply pipes, the enclosures represent a potential hydrogen confinement hazard. Hydrogen's wide flammable range (4–75%) means that explosive mixtures can quickly develop, so effective ventilation is needed to maintain safe

Abbreviations: STP, Standard Temperature and Pressure; LFL, Lower Flammable Limit (Hydrogen = 4%); CFD, Computational Fluid Dynamics.

\* Corresponding author.

E-mail address: [ghataurt@lsbu.ac.uk](mailto:ghataurt@lsbu.ac.uk) (T.S. Ghatauray).<https://doi.org/10.1016/j.ijhydene.2018.08.065>

0360-3199/© 2018 Hydrogen Energy Publications LLC. Published by Elsevier Ltd. All rights reserved.

Please cite this article in press as: Ghatauray TS, et al., A comparison study into low leak rate buoyant gas dispersion in a small fuel cell enclosure using plain and louvre vent passive ventilation schemes, International Journal of Hydrogen Energy (2018), <https://doi.org/10.1016/j.ijhydene.2018.08.065>

Conference Paper: HYSAFE 2019 Adelaide

## VISUALISING BUOYANT GAS DISPERSION IN A PASSIVELY VENTILATED SMALL FUEL CELL ENCLOSURE

Ghatauray, T.S.<sup>1</sup>, Ingram, J.M.<sup>1</sup>, Battersby, P.<sup>1</sup> and Holborn, P.G.<sup>1</sup>

<sup>1</sup> Explosion and Fire Research Group, London South Bank University, Borough Road, London, SE1 0AA, UK, ghataurt@lsbu.ac.uk; ingramja@lsbu.ac.uk; batterpa@lsbu.ac.uk; p.holborn@lsbu.ac.uk

### Abstract

Helium is a colourless, odourless, buoyant gas used as a safe analogue for hydrogen in empirical tests. Hydrogen is used in fuel cells to produce electricity, however there are risks associated with its flammability. Fuel cells are protected by enclosures which are ventilated to remove leaked hydrogen. Many empirical investigations into buoyant gas dispersal in enclosures used fixed gas sensor matrixes to infer gas behaviour. Computational fluid dynamics (CFD) is used for concentration predictions and graphically adds qualitative insight into gas dispersal. However, visualising a helium leak in real time during an empirical test is the most informative. The Schlieren system provides a means to visualise gases of different densities and refractive index gradient. As refractive index is proportional to density, helium as a light gas, is ideally suited. An investigation was conducted into buoyant gas dispersal in a 0.144m<sup>3</sup> fuel cell enclosure, incorporating a cross-flow ventilation scheme using louvre vents and glass side panels. A general purpose, two mirror, Z-type Schlieren system was installed around the enclosure. A low-level gas leak was simulated at the enclosure base and a high-speed camera recorded the test. The limited field of view allowed only small sections of the enclosure to be viewed at a time. However, helium behaviour was observed during the test and qualitative images of the helium plume and gas transition through the louvre vents, where the louvres can be seen to direct the flow downwards, were achieved. This information informs enclosure safety design and inferences drawn from CFD graphics.

Keywords: hydrogen safety, helium, louvre vent, buoyant gas, Schlieren, CFD

### Nomenclature and abbreviations

CHP	Combined heat and power
CFD	Computational fluid dynamics
lpm	Litre per minute

### 1.0 Introduction

The use of hydrogen as an alternative source of energy to fossil fuels is increasing around the world. Hydrogen is used to power buses, vessels, cars, provide electricity to commercial buildings and supply domestic heat and power through CHP units. It is being added to natural gas in the gas grid, in trial areas in the UK, to provide cleaner domestic gas. When not being combusted for heat it can be used in a fuel cell to produce electricity and in some cases useable heat. A significant infrastructure is required to enable the use of hydrogen, including its production, storage and transportation. Hydrogen's wide flammable range makes this a challenging endeavour, with safety a paramount consideration. Ongoing research and development is required in all of these areas to ensure that hydrogen can make a significant contribution to the current and growing global demand for energy and enable reduced fossil fuel dependence.

Conference paper: HYSAFE 2019 Adelaide

## AN INVESTIGATION INTO THE EFFECT OF PRESSED METAL LOUVRE VENT PASSIVE VENTILATION ON LOW LEAK RATE BUOYANT GAS DISPERSION IN A SMALL FUEL CELL ENCLOSURE

Ghatauray, T.S.<sup>1</sup>, Ingram, J.M.<sup>1</sup> and Holborn, P.G.<sup>1</sup>

<sup>1</sup> Explosion and Fire Research Group, London South Bank University, Borough Road, London, SE1 0AA, UK, [ghataurt@lsbu.ac.uk](mailto:ghataurt@lsbu.ac.uk); [ingramja@lsbu.ac.uk](mailto:ingramja@lsbu.ac.uk); [p.holborn@lsbu.ac.uk](mailto:p.holborn@lsbu.ac.uk)

### Abstract

Hydrogen is used in fuel cells to produce electricity in a variety of applications, however there are risks associated with flammability. Fuel cells are housed in protective enclosures which require ventilating to remove hydrogen that may have leaked from the system. Passive ventilation schemes are preferred for reliability, but they require vent design insight (e.g. shape, size, position) to optimise air flow. The effect of simple louvre vents (horizontal louvre vanes on the opening) was shown in earlier tests to increase stratified level buoyant gas concentrations by in excess of 15%. More commonly used on enclosures are pressed metal louvres (vanes cut into the metal side wall) producing horizontal vanes that are angled down with some curvature. A series of tests was undertaken to investigate their effect on buoyant gas dispersal in a 0.144 m<sup>3</sup> enclosure. Aluminium pressed louvre vents were installed on the enclosure in a cross-flow passive ventilation arrangement. Helium was released from a 4mm nozzle at the base of the enclosure to simulate a hydrogen leak at rates from 1 to 10 lpm and concentrations recorded in the enclosure using an eight gas-sensor array. Comparison tests using centrally positioned rectangular plain vent openings were also undertaken. Pressed aluminium louvre vents produced marginally higher helium concentrations in the stratified layer which was also slightly deeper and higher concentrations lower down in the enclosure. The empirical data was used in a validation exercise with a CFD model produced using SolidWorks: Flow Simulation CFD.

### Keywords:

- Hydrogen safety,
- Helium,
- Passive ventilation,
- Louvre vent,
- Buoyant gas
- SolidWorks: Flow Simulation CFD

### Nomenclature

n <sub>lpm</sub>	Normal litre per minute
lpm	Litre per minute
STP	Standard temperature and pressure
LFL	Lower flammable limit (hydrogen = 4%)
CFD	Computational fluid dynamics
$C_d$	Discharge coefficient

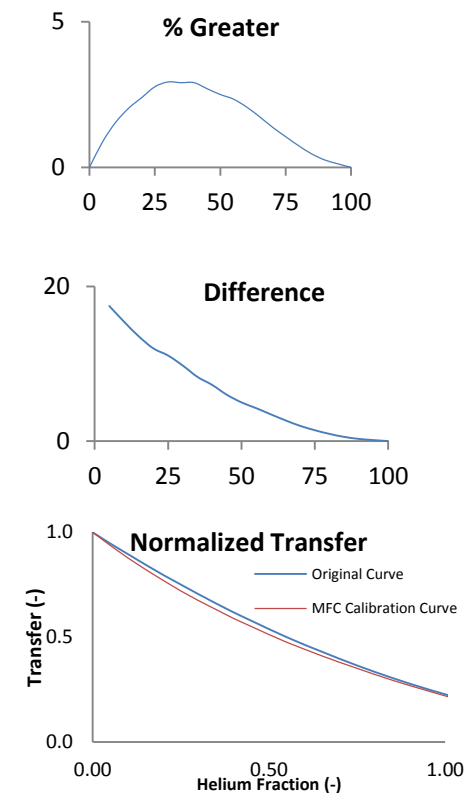


## Appendix B: Helium Sensor Manufacturers Calibration Data

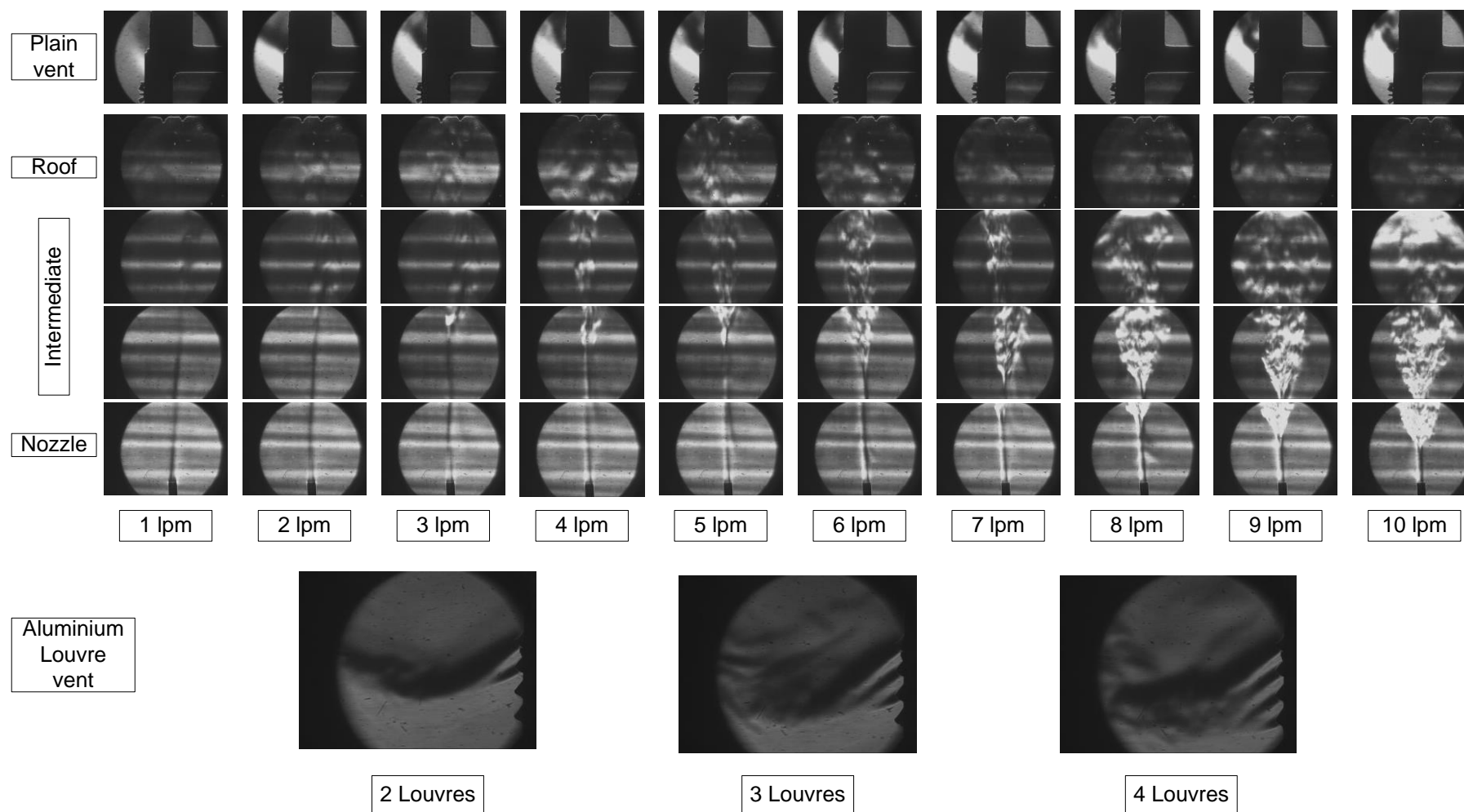
Analysis of the measurements on devices with the original helium curve, when using MFC calibration data: Source Sensor Integration

Helium concentration by MFC	XEN-5320	MFC table
-0.05	1.054	1.06
0.00	1.000	1.00
0.05	0.947	0.94
0.10	0.896	0.88
0.15	0.846	0.82
0.20	0.798	0.77
0.25	0.751	0.72
0.30	0.705	0.67
0.35	0.662	0.63
0.40	0.619	0.59
0.45	0.578	0.55
0.50	0.539	0.51
0.55	0.501	0.48
0.60	0.465	0.44
0.65	0.430	0.41
0.70	0.397	0.38
0.75	0.365	0.35
0.80	0.334	0.32
0.85	0.306	0.30
0.90	0.278	0.27
0.95	0.252	0.24
1.00	0.228	0.22
1.05	0.205	0.20

Deviation Chart Helium-Air			
Helium concentration by MFC	Indicated using original curve	% Greater	difference
0	0.00		0
5	5.87	17.46	0.87
10	11.54	15.44	1.54
15	17.03	13.55	2.03
20	22.40	11.98	2.40
25	27.77	11.06	2.77
30	32.93	9.77	2.93
35	37.91	8.31	2.91
40	42.91	7.27	2.91
45	47.70	6.00	2.70
50	52.50	5.00	2.50
55	57.34	4.26	2.34
60	62.08	3.46	2.08
65	66.74	2.68	1.74
70	71.38	1.97	1.38
75	76.06	1.41	1.06
80	80.74	0.93	0.74
85	85.46	0.54	0.46
90	90.25	0.28	0.25
95	95.12	0.13	0.12
100	100.00	0.00	0.00



## Appendix C: Schlieren image thumbnails (unprocessed)



## Appendix D Aluminium vent data

MAP Hardware (Selecthardware.com)

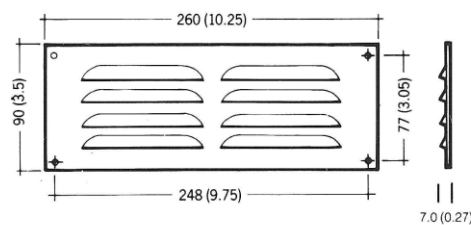
Surface mounted satin anodised aluminium louvre vent

# MAP

### GAS VENTS

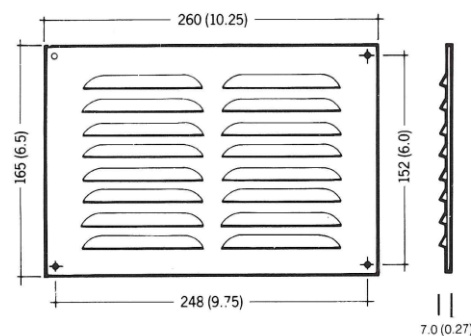
#### Louvre Range only

These vents meet current requirements for gas installations.



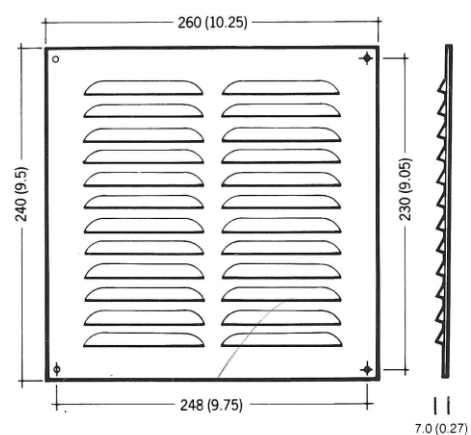
#### 953/963

For openings up to  
229 x 76 (9 x 3)  
Free airspace (mm<sup>2</sup>/in<sup>2</sup>)  
3,400 (5.26)



#### 956/966

For openings up to  
229 x 152 (9 x 6)  
Free airspace (mm<sup>2</sup>/in<sup>2</sup>)  
6,800 (10.53)



#### 959/969

For openings up to  
229 x 229 (9 x 9)  
Free airspace (mm<sup>2</sup>/in<sup>2</sup>)  
10,200 (15.8)

## Appendix E CFD Configuration Comparison Table

BOC Cross-Flow Geometry								
	Software	Domain Mesh size	Turbulence model	Additional	Wall function	Options	Conditions	Leak rate
1	Fluent	1M	LES	Smag/Lily	Dynamic stress	Time Step =1	300K/1bar/g	4 lpm
2	Fluent	1M	LES	Smag/Lily	Standard	Time Step =1	300K/1bar/g	4 lpm
3	Fluent	512k	K- $\epsilon$ (2 eqn)	RNG	Enhanced/pres grad	Full buoyancy	300K/1bar/g	4 lpm
4	Fluent	512k	K- $\epsilon$ (2 eqn)	Std	Enhanced	Full buoyancy	300K/1bar/g	4 lpm
5	Fluent	512k	K- $\epsilon$ (2 eqn)	Std	Std	Full buoyancy	300K/1bar/g	4 lpm
6	Fluent	512k	K- $\epsilon$ (2 eqn)	RZB	Enhanced/pres grad	Full buoyancy	300K/1bar/g	4 lpm
7	Fluent	512k	SST	N/A	N/A	N/A	300K/1bar/g	4 lpm
8	Fluent	6.1M	LES	WALE	Wall adapting	N/A	300K/1bar/g	4 lpm
9	Fluent	6.1M	LES	WM	S-Omega	N/A	300K/1bar/g	4 lpm
10	Fluent/Hydrogen	6.1M	LES	WM	N/A	N/A	300K/1bar/g	4 lpm
11	Fluent	6.1M	LES	WM	N/A	N/A	300K/1bar/g	4 lpm
12	Fluent	6.1M	DES	SST K $\omega$	Enhanced	delayed	300K/1bar/g	4 lpm
13	Fluent/Hydrogen	6.1M	DES	SST K $\omega$	Enhanced	delayed	300K/1bar/g	4 lpm
14	Fluent	6.1M	LES	Smag/Lily	Std	Std	300K/1bar/g	4 lpm
15	Fluent	6.1M	K- $\epsilon$ (2 eqn)	RZB	Enhanced	buoyancy	300K/1bar/g	4 lpm
16	Fluent	6.1M	Transition K $\omega$	N/A	N/A	N/A	300K/1bar/g	4 lpm
17	Fluent	6.1M	K- $\epsilon$ (2 eqn)	RNG	Enhanced/pres grad	Full buoyancy	300K/1bar/g	4 lpm
18	Fluent	6.1M	K- $\epsilon$ (2 eqn)	Std	Enhanced	Full buoyancy	300K/1bar/g	4 lpm
19	Fluent	6.1M	K- $\epsilon$ (2 eqn)	Std	Std	Full buoyancy	300K/1bar/g	4 lpm
20	Fluent	6.1M	K- $\epsilon$ (2 eqn)	RZB	Enhanced/pres grad	Full buoyancy	300K/1bar/g	4 lpm